TESIS DOCTORAL

UNIVERSIDAD DE BURGOS

"Investigación sobre propiedades de nuevos fluidos industriales de bajo impacto ambiental como sustitutivos de gases fluorados para reducción del cambio climático."

NATALIA MUÑOZ RUJAS

DIRECTOR:

Dr. Fernando Aguilar Romero

TUTOR:

Dr. Eduardo Montero García

Burgos, 2018

UNIVERSIDAD DE BURGOS
DEPARTAMENTO DE INGENIERÍA ELECTROMECÁNICA

FERNANDO AGUILAR ROMERO, Profesor Titular del Área de Máquinas y Motores Térmicos del Departamento de Ingeniería Electromecánica, de la Universidad de Burgos,

CERTIFICA

Que la presente memoria "Investigación sobre propiedades de nuevos fluidos industriales de bajo impacto ambiental como sustitutivos de gases fluorados para reducción del cambio climático" ha sido realizada bajo mi dirección por Dña. NATALIA MUÑOZ RUJAS en el programa de doctorado de Investigación en Ingeniería Termodinámica de Fluidos (interuniversitario) de la Universidad de Burgos y constituye su Tesis para optar al grado de Doctor por la Universidad de Burgos. Esta memoria cuenta con mi informe favorable.

Y para que conste y en cumplimiento de la legislación vigente, firmamos el presente certificado en Burgos a 1 de Diciembre de 2017

Fdo.: Fernando Aguilar Romero

Dedicatoria

A mamá y a Antonio

Y que la ola esencial, y el vendaval,
me lleven donde estáis, me lleven donde estáis.
Os quiero aquí, os quiero aquí, os quiero aquí, os quiero aquí.
Estáis aquí, estáis aquí, ahora mismo estáis aquí,
no puedo veros pero sé que estáis aquí.
Estáis aquí, estáis aquí, en Buenos Aires y en Berlín,
estáis callados pero sé que estáis aquí.

(Sidonie, Estáis aquí, 2015).

Agradecimientos

A todos. A todas las personas que me han acompañado durante el camino que ha llevado a esta Tesis Doctoral, y durante el camino de mi vida. De todas esas personas he aprendido algo. Gracias.

Muy en especial a mi familia: a los que están, papá, mi hermano John, y a los que se han ido, mamá, mi hermano Antonio, sin vosotros no hubiera llegado hasta aquí. A mis cuñados, Ana, Carlos, a mi sobrino, Rodrigo, y cómo no, a tí, César, por ayudarme tanto, en lo bueno y en lo malo. Mil gracias, os debo todo.

A mis abuelos; me encantaría que hubiesen podido acompañarme en este momento, os echo de menos. A mis tíos y a mis primos.

A mis amigos, los de verdad, los que siempre han estado ahí. A todos los alumnos a los que he tenido la oportunidad de enseñar durante este tiempo, especialmente a mis alumnos de TFG, porque yo también he aprendido con ellos.

A mi tutor de tesis, Dr. Eduardo Montero García, y a mi director, Dr. Fernando Aguilar Romero, por ser excelentes profesionales y mejores personas, por ayudarme tanto, por guiarme, por comprenderme, por su calidad humana, y por demostrarme que las buenas personas existen.

A todo el personal de la Escuela Politécnica Superior, profesores, compañeros de doctorado y PAS que me han acompañado, ayudado, y enseñado.

También deseo agradecer a los doctores D. Christian Boned, D. Jean Luc Daridon y D. Guillaume Galliero, por permitirme realizar la estancia en el Laboratoire des Fluides Complexes de la Universidad de Pau, y especialmente a D. Jean Patrick Bazile, por tanta ayuda prestada durante la estancia. Gracias también a todo el personal con el que tuve la oportunidad de trabajar en el Laboratoire des Fluides Complexes: a Bertrand, Djamel, Matthieu, y como no, a Lidia, por brindarme su amistad. *Merci beaucoup à tous.*

Deseo manifestar mi admiración y agradecimiento a la ciencia, y a la termodinámica en particular, por darme tantas alegrías, por permitirme cada día conocerla un poquito más, y a mi hermano Antonio por haberme inculcado este amor tan profundo desde muy pequeña.

Por último, agradecer al lector que esté haciendo buen uso de esta Tesis Doctoral; espero que sea útil, que con ella pueda contribuir, aunque sea un poquito, a hacer de este mundo un lugar mejor.

Muchas, muchísimas gracias a todos.

Índice

INTRODUCCIÓN

Introducción.

El conocimiento de las propiedades termodinámicas de los fluidos puros y de sus mezclas es de gran interés en cualquier sector de la industria. En aplicaciones como la refrigeración se hace necesario conocer la temperatura de ebullición del fluido, así como su cambio en densidad con la presión y temperatura; en ámbitos como el de la limpieza de precisión, conocer la viscosidad o la tensión superficial es de suma importancia. Asimismo, la caracterización de un azeótropo, su composición a una determinada presión y temperatura, es de gran utilidad en muchas de las aplicaciones industriales en las que el fluido transite del estado líquido al de vapor. En este campo de los fluidos industriales, la problemática medioambiental ha aparecido como un nuevo requisito a cumplir para los ampliamente utilizados fluorocarbonos: CFCs (clorofluorocarbonos), HCFCs (hidroclorofluorocarbonos), HFCs (hidrofluorocarbonos), PFCs (perfluorocarbonos) y PFPEs (perfluoropoliéteres), entre otros. Algunos de ellos tenían un gran potencial de destrucción de la capa de ozono, mientras que otros mostraban también un elevado potencial de calentamiento global. Asimismo, sus largos tiempos de vida en la atmósfera les hacían prolongar su dañino efecto sobre el medio ambiente.

A raíz de los Protocolos de Montreal (1978) y Kyoto (1997), así como del Acuerdo de París (2016), se han ido proponiendo varias alternativas a estos fluidos de uso industrial: los hidrocarburos, los HFCs (hidrofluorocarbonos), las HFOs (hidrofluoroolefinas), los HFEs (hidrofluoroéteres), etc., los cuales buscan sustituir a los anteriormente empleados CFCs, HCFCs, PFCs y PFPEs. En la literatura, varios autores recogen en sus publicaciones datos y comparativas en cuanto a aplicaciones y efectos sobre el medio ambiente de estos nuevos fluidos.

Se hace necesario, por tanto, caracterizar las propiedades termodinámicas de estos fluidos industriales, muchos de ellos comenzados a sintetizar recientemente, a fin de poder diseñar las redes de distribución, almacenamiento y maquinaria que trabajará con estos compuestos.

Este trabajo se ha enfocado hacia los hidrofluoroéteres (HFEs) como fluidos industriales de bajo impacto ambiental. Los HFEs han sido considerados como alternativa de reemplazamiento de los CFCs, HCFCs, PFCs, PFPEs, e incluso de los HFCs, debido a que poseen valores de sus propiedades termo-físicas y químicas muy similares a las de los anteriores fluorocarbonos, incluyendo alta volatilidad, baja conductividad térmica, baja tensión superficial, índice ODP (índice de destrucción de la capa de ozono; Ozone Depletion Potential) nulo, baja toxicidad, y baja o nula inflamabilidad. Algunos de ellos tienen un GWP (potencial de calentamiento global; Global Warming Potential) bajo (<150) y otros elevado, pero la presencia de un éter en su molécula tiende a reducir apreciablemente su tiempo de vida media en la atmósfera con respecto a los fluorocarbonos a los que sustituyen, por lo que pueden ser considerados medioambientalmente valiosos. Por ejemplo, los HFEs de peso molecular bajo son candidatos a sustituir a numerosos refrigerantes (HFE-125, HFE-134, HFE-143a, HFE-227me,

HFE-245mf, HFE-245-mc), mientras que los de peso molecular alto son considerados alternativas como disolventes en la industria electrónica y aeronáutica (HFE-7000, HFE-7100, HFE-7200, HFE-7300, HFE-7500). Estos fluidos de alta densidad tienen además valores de GWP por debajo de 150 o ligeramente superiores. Son por tanto fluidos con un gran interés industrial y medioambiental. Algunos de ellos son propuestos también como fluidos de transferencia de calor y para ciclos de Rankine orgánicos.

Los objetivos generales en el desarrollo de esta Tesis han sido: i) la determinación del comportamiento termodinámico de las fases líquida y vapor (presión de vapor, composición de ambas fases) de las mezclas de algunos de los HFEs para resolver problemas de transporte y almacenamiento, ii) la determinación de la densidad y la velocidad del sonido a altas presiones y temperaturas a fin de caracterizar el comportamiento fluido de los HFEs puros y sus mezclas en las fases de producción, distribución y uso, y iii) la determinación de la viscosidad a altas presiones y temperaturas para poder caracterizar el comportamiento de los HFEs puros y sus mezclas durante las fases de transporte y bombeo de los mismos.

Actividades realizadas durante el desarrollo de la Tesis Doctoral.

Al inicio de esta Tesis Doctoral, durante los meses de enero y febrero de 2014, he disfrutado de un contrato de cooperación educativa entre la Universidad de Burgos y la Fundación General de la Universidad de Burgos para la realización de las tareas de investigación propias del desarrollo de la Tesis Doctoral. A partir de marzo de ese mismo año, he disfrutado de un contrato predoctoral, enmarcado dentro de la convocatoria de contratos predoctorales de la Universidad de Burgos de 2013, durante un periodo de aproximadamente 4 años. A lo largo de este tiempo se han llevado a cabo los trabajos experimentales y de tratamiento de datos que suponen los resultados de la misma, y que han conducido a la redacción de distintos artículos científicos, algunos de ellos ya publicados en revistas científicas con un alto índice de impacto, y a otros que en el momento de presentación de esta Tesis Doctoral aún se encuentran en proceso de revisión. Se tiene previsto publicar sucesivamente el resto de artículos que ya se encuentran redactados.

Asimismo, durante los cuatro años en los que se ha desarrollado la Tesis Doctoral, he realizado numerosas contribuciones, tanto en formato póster como oral, en distintos congresos nacionales e internacionales, muy consolidados en el dominio de la Termodinámica de Fluidos.

A lo largo del segundo año de realización de esta Tesis, he disfrutado de una estancia predoctoral por un periodo de 5 meses, (de febrero a junio 2015), en el Laboratoire des Fluides Complexes et leurs Réservoirs de la Universidad de Pau, en Francia. Durante esta estancia utilicé distintas técnicas experimentales (densidad a alta presión, viscosidad a alta presión, y velocidad del sonido a alta presión), las cuales contribuyeron a ampliar mi conocimiento de propiedades termofísicas de los hidrofluoroéteres y sus mezclas.

En el tercer año de la Tesis, concretamente en octubre de 2016, he impartido dos actividades formativas, orientadas a alumnos de máster y doctorado, en la École Nationale des Sciences Appliquées d'El Jadida, perteneciente a la Université Chouaib Doukkali, en Marruecos. La primera de estas actividades estuvo enfocada a presentar los nuevos fluidos refrigerantes capaces de sustituir a CFCs, HCFCs, y HFCs, mientras que la segunda de las sesiones fue una actividad práctica enmarcada dentro del aprendizaje basado en problemas, en el cual se estudiaba el fenómeno de la transmisión de calor.

Estructura de la presente memoria.

La memoria de Tesis que se presenta a continuación se ha estructurado en ocho capítulos y seis anexos, cada uno de los cuales recoge una parte específica del trabajo realizado.

- En el Capítulo 1, Hipótesis de partida y objetivos, se describe el contexto general en el que se encuentran los gases fluorados, y se explica cuál es el panorama para los fluidos seleccionados como objeto de estudio en la tesis, los HFEs.

- En el Capítulo 2, Termodinámica de sistemas fluidos multicomponentes, se presenta una revisión de los fundamentos teóricos de la termodinámica clásica de los sistemas fluidos multicomponentes.

- En el Capítulo 3, Determinación experimental del equilibrio líquido-vapor isóbaro, se hace una descripción de la técnica de medida del equilibrio líquido-vapor isóbaro empleada, así como de la técnica auxiliar de densimetría utilizada, y se expone el método de ajuste de los datos experimentales, empleo de modelos, y estudio de la consistencia termodinámica.

- En el Capítulo 4, Determinación experimental de la densidad a alta presión, se expone la técnica de determinación de la densidad a alta presión, se describen los dos densímetros de tubo vibrante empleados, así como su proceso de calibración, y el ajuste de los datos experimentales.

- En el Capítulo 5, Determinación experimental de la viscosidad a alta presión, se hace una descripción del viscosímetro de caída de cuerpo empleado para determinar la viscosidad dinámica de una de las mezclas binarias estudiadas. Asimismo se trata el ajuste de los datos experimentales, y la calibración del aparato.

- En el Capítulo 6, Determinación experimental de la velocidad del sonido a alta presión, se explica la técnica para la determinación de esta propiedad física, se detalla el procedimiento de ajuste de los datos experimentales y se describe el procedimiento auxiliar empleado para la determinación de la capacidad calorífica, dato necesario para calcular la densidad a alta presión a partir de los datos de velocidad del sonido obtenidos.

- En el Capítulo 7, Resultados experimentales, se presenta la breve descripción de los trabajos realizados durante el desarrollo de la Tesis Doctoral.

- En el Capítulo 8, Conclusiones, se recogen las conclusiones más relevantes a las que se han llegado tras la finalización de los estudios llevados a cabo en esta Tesis Doctoral.

- El Anexo I recoge los distintos artículos resultantes de los trabajos desarrollados durante la Tesis. Algunos de estos artículos ya están publicados en revistas con un alto índice de impacto, otros se encuentran en proceso de revisión, y el resto se encuentran redactados, a fin de ser enviados para su publicación.

- En el Anexo II se incluyen las distintas comunicaciones presentadas en congresos nacionales e internacionales durante el periodo de desarrollo de la Tesis.

- En el Anexo III se adjunta el contrato de cooperación educativa suscrito entre la Universidad de Burgos y la Fundación General de la Universidad de Burgos, del cual se ha disfrutado durante los meses de enero y febrero de 2014.

- En el Anexo IV se incluye el contrato predoctoral obtenido de acuerdo con la convocatoria de contratos predoctorales de la Universidad de Burgos de julio de 2013, del cual se disfruta desde el mes de marzo de 2014, y que ha tenido una duración de 4 años.

- El Anexo V recoge tanto la carta de invitación para realizar una estancia predoctoral de cinco meses en la Universidad de Pau (Francia), durante el periodo 02/02/2015 al 30/06/2015, así como el certificado de realización de dicha estancia.

- En el Anexo VI se encuentra el certificado de presentación de las actividades formativas impartidas en la École Nationale des Sciences Appliquées d'El Jadida (Marruecos), en octubre de 2016.

INTRODUCTION

Introduction.

The knowledge on thermodynamic properties of pure fluids and their mixtures is of common interest in any industrial area. In applications such as refrigeration, it is necessary to well know the boiling temperature of the fluid, as well as its change on density with pressure and temperature. In fields as high precission cleaning, the knowledge of viscosity or surface tension are of utmost importance. In the same way, the characterization of an azeotrope, its composition at a fixed pressure and temperature, has utility in most of industrial applications in which the fluid changes from liquid to vapor state.

In the field of industrial fluids, the environmental issue has grown as a new requirement that has to be fulfilled for commonly used fluorocarbons: CFCs (chlorofluorocarbons), HCFCs (hydrochlorofluorocarbons), HFCs (hydrofluorocarbons), PFCs (perfluorocarbons) and PFPEs (perfluoropolyethers), among others. Some of these fluorocarbons had great ozone depletion potentials (ODP), while others shown high global warming potentials (GWP). Also, their long atmospheric lifetimes (ALT) made them extend their harmful effect over the years on the environment.

As a result of the Montreal Protocol (1987), the Kyoto Protocol (1997), as well as the Agreement of Paris (2016), many alternatives for these industrial fluids have been proposed: hydrocarbons, HFCs (hydrofluorocarbons), HFOs (hydrofluoroolefins), HFEs (hydrofluoroethers), etc., in order to substitute the previously used CFCs, HCFCs, PFCs, and PFPEs. Some authors have published data and comparatives concerning the applications and effects on the environments for these new fluids.

Many of these new fluids have started to be synteshized recently. Then, it is necessary to characterize their thermophysical properties, in order to well design distribution networks, storage tanks, and machinery involved in the use of these fluids.

The aim of this work is focused on hydrofluoroethers (HFEs), as new industrial fluids with low environmental effect. HFEs have been considered as good alternative in the replacement of CFCs, HCFCs, PFCs, PFPEs, and even HFCs, due to they exhibit values of thermophysical and chemical properties similar as the previously used fluorocarbons, including high volatility, low thermal conductivity, low surface tension, zero or near zero ODP, low toxicity, being most of them non-flammable. Some these HFEs have low GWP (<150), while others exhibit higher GWP, but the presence of an ether group in the molecule tends to reduce its atmospheric lifetimes with respect to other fluorocarbons, which make them environmentally valuable. As an example, low molar weight HFEs are very good candidates to substitute most of the commonly used refrigerants: (HFE-125, HFE-134, HFE-143a, HFE-227me, HFE-245mf, HFE-245-mc), while high molecular weight HFEs are considered as an alternative to solvents used in electronics and aeronautics industry: (HFE-7000, HFE-7100, HFE-7200, HFE-7300, HFE-7500). These high

density fluids have also low GWP (less than 150), being then environmentally friendly fluids with interest in the industry. Some of them have been also proposed as heat transfer fluids, and as fluids in organic Rankine cycles (ORC).

The general targets on the development of this Doctoral Thesis have been: i) the determination of the thermodynamic behaviour of liquid and vapor phases (vapor pressure, mole compositions of both phases), for some HFEs mixtures, in order to solve transport and storage problems, ii) determination of the density and the speed of sound at high pressures and temperatures, in order to characterize the behaviour of the pure components and their mixtures in the production, distribution and utilization of these fluids, and iii) viscosity determination at high pressures and temperatures, to well characterize the behaviour of pure HFEs, and their mixtures during transport and pumping operations.

Activities implemented during the development of the Doctoral Thesis.

At the beginning of this Doctoral Thesis, during January and February of 2014, I took advantage of an educational cooperation contract between the University of Burgos and the Fundación General de la Universidad de Burgos, to develop the research tasks involving the Doctoral Thesis. From March 2014, I am tooking advantage of a predoctoral grant, in the framework of the University of Burgos predoctoral grants of 2013, during an approximate period of 4 years. During this time, experimental measurements and data treatment have been carried out, constituting the results of the Doctoral Thesis. Some of these results have already been published in high impact scientific journals, while others are still in revision. It is planned to successively publish the rest of the results of this Thesis, which are already written.

On the other hand, during these four years, many contributions in poster and oral formats were presented. These contributions were presented in national and international consolidated Conferences on the field of Thermodynamics.

In the second year, I had a 5 months predoctoral stay (from February to June 2015), at the Laboratoire des Fluides Complexes et leurs Réservoirs, of the University of Pau, in France. During this stay, I had the opportunity to perform several experimental techniques (high pressure density, high pressure viscosity, and high pressure speed of sound), which contributed to broad my knowledge on thermophysical properties of hydrofluoroethers and their mixtures.

In October 2016, (third year of the Doctoral Thesis), I provided training in two activities at the École Nationale des Sciences Appliquées d'El Jadida, of the University Chouaib Doukkali, in Morocco. Both activities were oriented to master and doctorate students, and were focused on the presentation of new environmentally friendly refrigerant fluids the first one, and the second one was a problem-based learning practice concerning heat transfer.

Structure of this report.

This Thesis report is structurated in eight chapters and six annexes, gathering each one of them a specific topic of the work that has been carried out.

- In Chapter 1, Starting hypothesis and objectives, the general context of fluorinated gases is described. An explanation concerning the general context of these fluids is also given, as well as an overview for the selected fluids that have been studied on this Thesis, the hydrofluoroethers (HFEs).

- In Chapter 2, Multicomponent fluid systems thermodynamics, a review on theorethical principles of classical thermodynamics for multicomponent fluid systems was introduced.

- In Chapter 3, Experimental determination of isobaric vapor-liquid equilibrium, a description of the experimental technique involved on isobaric vapor-liquid equilibrium (VLE), was done. Moreover, the description of the auxiliary technique employed in the determination of VLE data, atmospheric pressure densimetry, was done, as well as the fitting methods for the experimental results, by using several mathermatical models. Also, the thermodynamic consistency calculations are explained.

- In Chapter 4, Experimental determination of high pressure density, a presentation of the technique involved on the determination of high pressure density data was done. A description of the two vibrating tube densitometers employed was also carried out, as well as the calibration method, and the fitting to the experimental data.

- In Chapter 5, Experimental determination of high pressure viscosity, the description of the falling body viscometer employed to determine the dynamic viscosity was carried out. In the same way, experimental data fitting and the calibration of the apparatus have been explained.

- In Chapter 6, Experimental high pressure speed of sound, an explanation of the measuring principle is detailed. Also, the experimental data fitting, and the additional technique employed to determine heat capacities at constant pressure, which was necessary to calculate high pressure density data from high pressure speed of sound data, were described.

- In Chapter 7, Experimental results, a brief description of the results obtained during the development of this Doctoral Thesis can be seen.

- In Chapter 8, Conclusions, some of the most relevant conclusions obtained for this Doctoral Thesis are presented.

- The Annex I gathers the papers concerning the results of this Thesis. Some of them were already published in several journals with high impact factor, while others are currently in revision. The rest of the results are already written, and prepared to be sent.

- In Annex II, all the communications presented to several national and international conferences during the development of this Thesis are included.

- In Annex III, the contract signed with the University of Burgos, and the Fundación General de la Universidad de Burgos, from which I took advantage during January and February 2014, is attached.

- In Annex IV, the predoctoral contract obtained in March 2014, in accordance with the predoctoral grants of the University of Burgos 2013 framework, is included.

- Annex V gathers the invitation letter for the five months research stay at the University of Pau (France), during the period from 02/02/2015 to 06/30/2015, as well as the certification of this stay.

- In Annex VI, the certification of presentation for the activities taught at the École Nationale des Sciences Appliquées d'El Jadida (Morocco), in October 2016, is attached.

Capítulo 1

HIPÓTESIS DE PARTIDA Y OBJETIVOS

1.1 Contexto general de los gases fluorados.

En 1974, los trabajos de los científicos Molina y Rowland dieron cuenta, en un artículo publicado en la revista Nature [1], de los resultados de sus investigaciones sobre el destino de algunas partículas químicas inertes derivadas de procesos industriales, los clorofluorocarbonos (CFC). Los átomos de cloro producidos por la descomposición de los CFCs destruían las moléculas de ozono mediante una reacción fotoquímica, suponiendo esto una amenaza creciente para la capa de ozono en la estratosfera.

Los CFCs habían sido empleados, desde su creación en 1930, en numerosos usos industriales con excelentes resultados dadas sus propiedades termofísicas: demostraban ser muy buenos refrigerantes en ciclos de compresión, podían ser utilizados como agentes de limpieza de precisión dado que no dejaban residuos, como propelentes de aerosoles, y para fabricar aislantes térmicos, entre otros muchos usos.

Tomada conciencia de la problemática de estos fluidos, en 1983 se definió el término ODP (Ozone Depletion Potential), Potencial de Destrucción de la capa de Ozono, como la *cantidad relativa de degradación de la capa de ozono que un fluido puede causar, tomando el triclorofluorometano, o CFC-11, como referencia con un ODP = 1.0.*

A raíz del descubrimiento de la destrucción de la capa de ozono por parte de estos fluidos, en 1985 se aprobó el Convenio de Viena [2], que tenía como objetivo fundamental impulsar la investigación, fomentar la cooperación entre los países y facilitar el intercambio de información en torno a la reducción de las emisiones de estos fluidos. El Convenio de Viena sentó un importante precedente, ya que por primera vez las naciones acordaron hacer frente a un problema medioambiental global, antes incluso de que se comprobasen científicamente sus impactos. Ese mismo año, Farman *et al.* ratificaron ésta problemática publicando otro artículo, también en Nature [3], el cual notificaba una reducción considerable del espesor de la capa de ozono sobre la Antártida.

De esta manera se potenció el uso de nuevas alternativas a expensas del protocolo de Montreal (1987), [4] el cual promovía la reducción progresiva en el uso y fabricación de los compuestos con átomos de cloro en su molécula (CFCs, fin de producción y uso situado en 1995, y HCFCs, hidroclorofluorocarbonos, con un fin de producción y uso situado en 2010). Asimismo, los HFCs (hidrofluorocarbonos) eran propuestos como fluidos de reemplazamiento a los anteriores CFCs y HCFCs.

Simultáneamente, durante los años 80, se comienza a advertir que la curva de temperatura media anual global está aumentando, lo cual promueve que comience a hablarse de la teoría sobre el calentamiento global, teoría que ya había sido proclamada anteriormente (1896) por el científico Arrhenius [5], quien aseguraba que los combustibles fósiles podrían dar lugar o acelerar el calentamiento de la Tierra. Esta hipótesis fue reiterada por Schneider (1976) [6], quien predijo

que el calentamiento global estaba comenzando a tener lugar como resultado de la actividad humana. Después de los descubrimientos de Arrhenius se había olvidado el tema durante un tiempo. En este tiempo se pensaba que la influencia de las actividades humanas eran insignificantes comparadas con las fuerzas naturales, como la actividad solar, o los movimientos circulatorios de agua en el océano. En 1988 se reconoce finalmente que el clima había sido más caliente que antes de 1880. La teoría del efecto invernadero fue tomando fuerza y se estableció el Panel Intergubernamental sobre el Cambio Climático (IPCC) por el Programa Medioambiental de las Naciones Unidas y la Organización Mundial Meteorológica. El propósito de este Panel era predecir el impacto de los gases de efecto invernadero teniendo en cuenta modelos predictivos sobre el clima e información científica actualizada.

Con todo esto, se define el término GWP (Global Warming Potential), Potencial de Calentamiento Global, como la *medida relativa de cuánta cantidad de calor es capaz de retener cierto gas de efecto invernadero en la atmósfera.* Este término compara la cantidad de calor atrapada por cierta masa de gas con la cantidad de calor retenida por una masa de CO_2 similar. De esta manera, se toma el CO_2 como referencia, con un GWP = 1.0.

En 1997, el Protocolo de Kyoto [7], surgido a partir de la Convención Marco de las Naciones Unidas sobre el Cambio Climático (CMNUCC), incorpora medidas más concretas, cuantificables y jurídicamente vinculantes, orientadas a reducir las emisiones causantes del incremento global de la temperatura. Este Protocolo promueve como objetivo reducir las emisiones de seis gases de efecto invernadero que causan el calentamiento global: dióxido de carbono (CO_2), metano (CH_4), óxido nitroso (N_2O), y los gases industriales HFCs (hidrofluorocarbonos), PFCs (perfluorocarbonos), y SF_6 (hexafluoruro de azufre), en un porcentaje aproximado de, al menos, un 5% dentro del periodo que va desde 2008 a 2012. Estudios científicos previos habían demostrado que estos gases, una vez eran liberados a la atmósfera, retenían parte de la energía que la superficie terrestre emite al haber sido calentada por la radiación solar.

En lo que concierne a los HFCs, algunos de ellos mostraban un GWP extremadamente elevado, caso del R-23, con un GWP = 11700, o del R-404a, con un GWP = 3260, y de igual manera sucedía con los ampliamente utilizados perfluorocarbonos (PFCs) y perfluoropoliéteres, (PFPEs).

Para poner en marcha los compromisos del Protocolo de Kyoto, en el año 2006 la Unión Europea publicó el Reglamento (UE) nº 842/2006, de 17 de mayo, sobre determinados gases fluorados de efecto invernadero, que regulaba el uso de los HFCs, los PFCs y el SF_6, todos ellos con un potencial de calentamiento global, GWP entre 120 y 22200 veces superior al del dióxido de carbono (CO_2) [8]. Este Reglamento impulsaba la recuperación y gestión de estos gases, así como la minimización de las fugas a la atmósfera durante su empleo. Asimismo recogía un ambicioso programa de certificación del personal involucrado en la instalación, mantenimiento,

control de fugas y recuperación de sistemas frigoríficos fijos, así como de sistemas de extinción de incendios fijos, que utilizasen los gases fluorados enumerados en su Anexo I. También establecía requisitos para la recuperación de estos gases en otra serie de aplicaciones como son los aparatos que contengan disolventes, equipos de conmutación de alta tensión, y aplicaciones móviles, estableciendo procedimientos claros de control de fugas. Este documento sería posteriormente derogado a fin de publicar el nuevo Reglamento (UE) nº 517/2014, de 16 de abril, el cual conservaría los mismos principios, pero ajustando plazos para finalizar la producción y comercialización de ciertos gases, así como para el uso de los equipos que los empleen. Por ejemplo, se expone que a partir de 1 de enero de 2020 queda prohibida la comercialización de aparatos portátiles de aire acondicionado para espacios cerrados que contengan HFCs con un GWP igual o superior a 150, así como a partir del 1 de enero de 2025 se prohíbe la comercialización de sistemas partidos simples de aire acondicionado que contengan menos de 3 kg de gases fluorados de efecto invernadero, o cuyo funcionamiento dependa de ellos, con un GWP igual o superior a 750.

De la misma forma, este Reglamento recoge la obligación, para todos los productores, importadores y exportadores de gases fluorados de efecto invernadero, de presentar ante la Comisión, anualmente, y antes del 31 de marzo, un informe de todas sus actividades.

La Directiva 2006/40/CE de 17 de mayo, relativa a emisiones procedentes de sistemas de aire acondicionado en vehículos a motor, regula del mismo modo parte del sector de la automoción en lo que se refiere a gases fluorados.

Con respecto a los fluidos que agotan la capa de ozono, la Unión Europea publicó el Reglamento (CE) nº 1005/2009 del Parlamento Europeo y del Consejo, el cual sustituye al anterior Reglamento (CE) nº 2037/2000, con el objetivo de eliminar progresivamente estas sustancias, y proteger la salud humana y el medio ambiente, y que sería de aplicación a partir del 1 de enero de 2010.

De esta manera, a nivel europeo tenemos que, por ejemplo, el empleo del fluido R-134a en los sistemas de aire acondicionado de los automóviles (recarga y nuevos modelos) ha sido prohibido desde 2013, y que en países como Dinamarca, Austria o Suiza, ya se han prohibido muchos de los usos de los HFCs.

A nivel nacional, a fin de adaptar los requerimientos derivados de la normativa europea a la legislación española, a partir del día 26 de junio del 2010 es de aplicación el Real Decreto 795/2010, de 16 de junio, por el que se regula la comercialización y manipulación de gases fluorados y equipos basados en los mismos, así como la certificación de los profesionales que los utilizan. Este Real Decreto complementa la reglamentación existente en esta materia, cuyo objetivo es minimizar las emisiones de fluidos organohalogenados. La norma, además, establece una serie de medidas adicionales que desarrolla la Ley 34/2007 de 15 de noviembre, de calidad del aire y protección de la atmósfera, en lo que se refiere al control de las emisiones.

El reciente Acuerdo de París [9], negociado durante la XXI Conferencia sobre el Cambio Climático (COP 21) en diciembre de 2015, y abierto para firma el 22 de abril de 2016, es un acuerdo dentro del marco de la Convención Marco de las Naciones Unidas sobre el Cambio Climático que establece medidas para la reducción de las emisiones de gases de efecto invernadero a través de la mitigación, adaptación y resiliencia de los ecosistemas a efectos del Calentamiento Global. La aplicabilidad de este acuerdo comenzaría en el año 2020, año para el cual finaliza la vigencia del Protocolo de Kyoto. Los puntos principales de este acuerdo, en lo que a mitigación de emisiones de efecto invernadero se refiere, son los siguientes:

1. Se propone el objetivo a largo plazo de mantener el aumento de la temperatura media mundial muy por debajo de 2ºC sobre los niveles preindustriales.
2. Se limitará dicho aumento a 1.5ºC, lo cual reducirá considerablemente los riesgos y el impacto del cambio climático.
3. Aplicación de rápidas reducciones basadas en los mejores criterios científicos disponibles.

A este efecto, ya en marzo de 2015 la Unión Europea fue la primera gran economía en presentar su contribución prevista al nuevo Acuerdo. De hecho, la UE ya está tomando medidas para alcanzar su objetivo de reducir las emisiones un 40% como mínimo en 2030.

En resumen, a lo largo de los últimos 40 años se han ido desarrollando nuevas alternativas a los gases fluorados que mostraban esta problemática medioambiental. Se hacía necesario introducir nuevos fluidos industriales con las mismas aplicaciones que sus predecesores, mismas o similares propiedades termofísicas, alta eficiencia operacional, bajas tasas de fuga, y con un ODP cercano o igual a cero, así como con reducidos valores de GWP. Algunos de los candidatos propuestos han sido los llamados "refrigerantes naturales" (NH_3, CO_2, hidrocarburos, etc), algunos de ellos ampliamente utilizados en la industria (caso del NH_3 en procesos de refrigeración por absorción y compresión), pero con la característica común de la media-alta inflamabilidad y menor eficiencia en su aplicación en ciertos procesos en relación con otros fluidos. Otra propuesta han sido los HFCs con bajo GWP, como el R-430a (GWP = 104) o el R-32 (GWP = 675). Estos fluidos poseen muy bajos o nulos ODP y buena eficiencia en su uso, pero la mayoría de ellos presentan una inflamabilidad media. Las hidrofluoro-olefinas (HFOs) son fluidos de reciente sintetización, que provienen de los alquenos (olefinas). Estos fluidos presentan muy bajos GWP (por ejemplo el R-1234-yf presenta un GWP = 4) dado que el doble enlace que poseen les otorga de tiempos de permanencia en la atmósfera (ALT, Atmospheric Lifetime) de unos pocos días, GWP muy bajos y ODP nulos. Por el contrario, su elevado precio y baja eficiencia energética penaliza su uso a día de hoy. Los hidrofluoroiodocarbonos (HFICs) también han sido propuestos como alternativa, pero muchos de ellos presentan una elevada toxicidad, elevado precio y ODP >

0. Por último, otra de las alternativas propuestas han sido los HFEs (hidrofluoroéteres). Estos fluidos, líquidos a temperatura y presión ambientales, se comenzaron a sintetizar en la década de los años 90 como alternativa a los HFCs, PFCs y PFPEs entre otros, dado que mostraban similares valores sus propiedades termofísicas, y el oxígeno del grupo éter proveía a la molécula de bajos tiempos de vida en la atmósfera (ALT), bajos GWP, y nulos o casi nulos ODP. Los HFEs presentan una toxicidad muy baja, prácticamente nula inflamabilidad, y una buena relación coste-efectividad. Los HFEs de elevado peso molecular (HFE-7000, HFE-7100, HFE-7200, HFE-7300, HFE-7500) son excelentes disolventes en numerosos procesos industriales. De la misma forma los HFE-7000 y HFE-7100 puros o sus mezclas azeotrópicas con algunos alcoholes pueden ser empleadas en la industria de la refrigeración o en Ciclos Rankine Orgánicos (ORC).

1.2 Panorámica de los hidrofluoroéteres (HFEs).

Como ya se dijo en la sección anterior, los hidrofluoroéteres comenzaron a ser sintetizados en la década de los 90 en la búsqueda de nuevos fluidos capaces de reemplazar a los ampliamente utilizados CFCs, HCFCs, HFCs, PFCs y PFPEs, pero siendo medioambientalmente amigables. Estos fluidos no se encuentran de forma natural sino que son sintetizados empleando distintos métodos. En general, estos métodos se basan en la fluoración de los éteres o en la adición de alcoholes a fluoro-olefinas, alquilación electrofílica de aniones polifluorados con reactivos como pueden ser el sulfato de dimetilo $(CH_3)_2SO_4$, o adición de éteres a fluoro-olefinas. Otras técnicas comprenden la condensación de éteres polifluorados y de fluoroetilenos empleando como catalizador pentafluoruro de antimonio [10].

Existen gran variedad de HFEs, de forma que su rendimiento y aplicaciones pueden variar ampliamente [11]. Sus propiedades termofísicas varían de unos a otros, lo cual les hace poder ser empleados en numerosas aplicaciones. Basándonos en los HFEs de alto peso molecular, algunos de los cuales han sido objeto de estudio en esta tesis, tenemos que, por ejemplo, los fluidos HFE-649, HFE-7000, e incluso el fluido HFE-7100 en algunos casos, son particularmente adecuados para su uso en Ciclos Rankine Orgánicos (ORC) [12], que requieren bajas o medias temperaturas de ebullición, una buena estabilidad térmica del fluido de trabajo, no inflamabilidad y un elevado peso molecular, que contribuye a reducir el régimen de giro de la turbina.

Las mezclas azeotrópicas de HFE-7100 y HFE-7200 con alcoholes son especialmente interesantes en el campo de la limpieza de precisión donde se requieren disolventes altamente polares. Estas mezclas sustituyen a los anteriores CFC-113, HCFC-141b y HCFC-225ca/cb en todas sus aplicaciones: limpieza de grasas, huellas dactilares, aceites de silicona, lubricantes etc., ya sea mediante su uso en aerosoles, o en paño [13]. HFE-7100 también puede ser utilizado como

compuesto puro en la industria médica, en sustitución de los anteriormente mencionados CFC-113 y HCFC-141b, como agente de reducción de la fricción en cuchillas de bisturíes, o como agente anticoagulante en las bolsas de recogida de sangre.

El HFE-7300 es un muy buen agente de limpieza de componentes electrónicos en sus mezclas ternarias con alcoholes y trans-1,2-dicloroetileno, así como también puede ser usado como agente de recubrimiento, como lubricante, y como fluido de transferencia de calor.

El HFE-7500 puede sustituir a muchos PFCs y PFPEs dado el bajo valor de su constante dieléctrica entre otras propiedades. También puede ser empleado como refrigerante de componentes electrónicos; en contacto directo puede refrigerar superordenadores y electrónica militar de alta sensibilidad, así como refrigerar transformadores de alta tensión y refrigeración de reactores en la industria farmacéutica [14].

Estos HFEs son inertes ante la mayoría de los metales y polímeros, y para su utilización muchas veces se requieren pequeñas modificaciones de los equipos que los van a emplear.

Teniendo en cuenta el efecto medioambiental, diversos estudios han constatado los cortos tiempos de vida en la atmósfera de algunos de los HFEs [15, 16]: en la troposfera los radicales hidroxilo presentes rompen rápidamente las moléculas de HFE, resultando esto en cortos tiempos de vida en la atmósfera (ALT), y bajos GWP.

En cuanto a su seguridad y toxicidad, los HFEs poseen un perfil más seguro que sus predecesores [17], mostrando unos límites de explosión en el aire iguales a cero en cuanto a inflamabilidad se refiere, y límites de exposición muy altos (del orden de miles de ppm) para producir algún tipo de efecto negativo sobre el cuerpo humano.

Quizás uno de los puntos más críticos en la introducción del uso de los HFEs sean los costes. Estos disolventes son más caros que sus predecesores, por lo cual se imponen políticas de conservación y recuperación del fluido mediante procesos de destilación una vez ha sido usado. Por ejemplo, la empresa 3M provee de un servicio de recogida para el reciclaje de HFEs posterior a su uso, que de momento sólo está disponible en los Estados Unidos.

En general puede verse que, para los HFEs, el balance entre seguridad, toxicidad, aplicaciones, rendimiento, efecto medioambiental y coste es bueno.

1.3. Objetivos de la Tesis Doctoral.

Por todo lo anterior, el objetivo de esta Tesis Doctoral ha sido llevar a cabo la caracterización de las propiedades termofísicas de algunos HFEs de alto peso molecular, dado su potencial de sustitución de muchos de los fluorocarbonos en numerosos procesos industriales. A la hora de seleccionar tanto los fluidos a utilizar, ya sea puros como en mezcla, y las técnicas a emplear, se ha hecho una revisión bibliográfica del estado del arte, a fin de conocer, por un lado,

cuáles eran los fluidos o mezclas potencialmente interesantes y, por otro, conocer cuáles eran los datos ya publicados de propiedades de estos fluidos. Por otra parte, a la hora de determinar qué técnicas experimentales se iban a emplear, se ha tenido en cuenta la compatibilidad de los distintos HFEs con los materiales de los aparatos disponibles (juntas, sellos, etc.). En los siguientes apartados se describe cómo se ha llevado a cabo la selección de los HFEs y las mezclas a medir, así como cuáles han sido las técnicas empleadas con cada uno de ellos.

1.3.1 Selección de los HFEs y sus mezclas.

Respecto a las referencias bibliográficas disponibles para los HFEs y sus mezclas, en cuanto a caracterización de propiedades termodinámicas se refiere, actualmente son escasas, si bien es sabido que la industria necesita el conocimiento preciso de las mismas para el uso de estos fluidos en los procesos industriales. La Tabla 1 recoge las referencias encontradas en la literatura que caracterizan algunas propiedades termodinámicas para los HFEs de alto peso molecular objeto de estudio en esta tesis (HFE-7100, HFE-7200, HFE-7300 y HFE-7500). Estas referencias aportan datos de medidas hechas en fluidos puros o en mezclas, teniendo en cuenta distintas técnicas (densidad, viscosidad, equilibrio líquido-vapor, curva de presión de vapor, equilibrio líquido-líquido y velocidad del sonido).

Tabla 1. Relación de HFEs y sus mezclas cuyas propiedades termodinámicas se han medido en esta tesis, o de las cuales se encuentran datos en la literatura.

HFE	Propiedad	ρ[a]	η[b]	P^{sat}[c]	E.L.L.[d]	E.L.V.[e]	c[f]
HFE-7100	FLUIDO PURO						
		[Este trabajo], [18], [19], [20], [21], [22]	[20]	[Este trabajo], [23]			[24]
	MEZCLAS						
	+ 1-propanol (Propuesta en [13] *y* [25])	[Este trabajo]					
	+ 2-propanol (Propuesta en [13] *y* [25])	[Este trabajo]		[Este trabajo]		[Este trabajo]	
	+ n-hexano	[26]					
	+ perfluorohexano + tolueno + 1,4 dioxano ó dimetilformamida				[27]		
	+ 1-etil-3-metilimizadolio				[28]		
HFE-7200	FLUIDO PURO						
		[Este trabajo], [20], [29], [30], [31], [32]	[20], [33]				
	MEZCLAS						
	+ 2-propanol (Propuesta en [13])	[Este trabajo]					[Este trabajo]
	+ n-hexano	[34]					
	+ 1-etil-3-metilimizadolio				[28]		
HFE-7300	FLUIDO PURO						
		[Este trabajo], [20]	[20]				[Este trabajo]
	MEZCLAS						
	+ 1-etil-3-metilimizadolio				[28]		
HFE-7500	FLUIDO PURO						
		[Este trabajo], [20], [29], [30], [35], [36], [37]	[Este trabajo, [20], [33]	[Este trabajo]			[Este trabajo], [36]
	MEZCLAS						
	+ diisopropil éter	[Este trabajo]	[Este trabajo]			[Este trabajo]	[Este trabajo]
	+ 1-etil-3-metilimizadolio				[28]		

[a] ρ = *densidad.*
[b] η = *viscosidad.*

[c] *P^{sat} = curva de presión de vapor.*
[d] *E.L.L. = equilibrio líquido-líquido.*
[e] *E.L.V. = equilibrio líquido-vapor.*
[f] *c = velocidad del sonido.*

Se encuentran pocos datos referentes a mezclas de estos HFEs con otros compuestos. Para el fluido HFE-7100, las referencias [26 - 28] reportan datos experimentales para distintas mezclas. En el caso de la referencia [26], se presentan datos de densidad para la mezcla binaria HFE-7100 + *n*-hexano. En la referencia [27] se reportan datos de equilibrio líquido-líquido para la mezcla HFE-7100 + perfluorohexano + tolueno + 1,4 dioxano ó dimetilformamida, así como también se presentan datos de equilibrio líquido-líquido para la mezcla HFE-7100 + 1-etil-3-metilimidazolio [28]. En el caso del HFE-7200, se han encontrado dos referencias en la literatura, las cuales reportan datos de densidad a alta presión para la mezcla binaria HFE-7200 + *n*-hexano, en el caso de la referencia [34], y datos de equilibrio líquido-líquido para la mezcla HFE-7200 + 1-etil-3-metilimidazolio, referencia [28]. Esta última referencia proporciona también datos de equilibrio líquido-líquido para la mezcla binaria HFE-7300 + 1-etil-3-metilimidazolio.

Para los fluidos puros se encuentran más referencias y más técnicas. El HFE-7100 se ha medido en densidad a presión atmosférica y a alta presión por varios autores [18 - 22], mientras que la referencia [20] aporta datos de viscosidad a presión atmosférica. Para este mismo fluido la referencia [23] aporta datos de la curva de presión de vapor, y la referencia [24] proporciona medidas de la velocidad del sonido a alta presión. La densidad del fluido HFE-7200 también ha sido determinada tanto a presión atmosférica como a alta presión por las referencias [20], [29 - 32]. La viscosidad de este componente se ha medido también a presión atmosférica por Rausch *et al.* [20], y a altas presiones por Hu *et al.* [33]. Para el HFE-7300 puro, la referencia [20] reporta datos a presión atmosférica tanto de densidad como de viscosidad. Por último, el fluido HFE-7500 ha sido medido en densidad a presión atmosférica y a alta presión por las referencias [20], [29 y 30], [35 - 37]. Las otras propiedades que se han determinado para este fluido puro han sido la viscosidad a presión atmosférica [20] y a alta presión [33], y la velocidad del sonido a alta presión, determinada por Lafitte *et al.* [36].

La Tabla 1 también muestra cuáles han sido las mezclas y técnicas medidas en este trabajo. Respecto a los fluidos puros, aunque en algunos casos se han repetido técnicas que algunas referencias en la literatura habían empleado, se ha ampliado el rango de datos, ya sea en presión, temperatura, o ambas. A la hora de elegir qué mezclas y técnicas se iban a emplear, se tuvo en cuenta lo anteriormente publicado en la literatura, y de igual manera se buscaron referencias que indicaran cuáles de ellas eran de interés, ya sea por su aplicación en la industria, ya sea por su posibilidad de sustitución de fluorocarbonos que fuesen ampliamente utilizados en

procesos industriales, pero cuyo uso estuviera prohibido o en vías de prohibirse debido a su impacto ambiental.

A fin de establecer una clasificación, en cuanto a su posible interés de utilización, en relación a los HFEs y sus mezclas de interés propuestos en la literatura, tenemos los siguientes grupos:

a) *HFEs puros*
b) *HFE + alcohol*
c) *HFE + otros componentes*

a) *HFEs puros:* Teniendo en cuenta los HFEs puros, según la referencia [13], el HFE-7100 podría emplearse como sustituto del HCFC-141b en algunos usos. La referencia [11] propone tanto al HFE-7100, como al HFE-7200 y HFE-7500, en fluido puro, como sustitutos de algunos perfluorocarbonos (PFCs). Varias patentes [38 - 40] indican al HFE-7300 como fluido de utilidad en su empleo como disolvente y agente de limpieza de componentes electrónicos.

b) *HFE + alcohol:* De acuerdo con las mezclas propuestas en la literatura, la referencia [13] indica algunas mezclas binarias de HFEs como interesantes: HFE-7100 + (1-propanol o 2-propanol o metanol o etanol), así como HFE-7200 + (etanol o 2-propanol), dado que pueden sustituir a otros fluorocarbonos anteriormente utilizados. En concreto, las mezclas HFE-7200 + (etanol o 2-propanol) sustituirían al HCFC-225ca/cb, mientras que las mezclas HFE-7100 + (etanol o 2-propanol) se indican como buenos sustitutos del CFC-113. La referencia [25] indica la mezcla azeotrópica de HFE-7100 + 2-propanol como sustituta del fluido HCFC-141b en sus aplicaciones. De la misma manera también son interesantes las mezclas azeotrópicas de HFE-7100 + 1-propanol y HFE-7200 + 2-propanol.

   La referencia [39] propone la mezcla binaria HFE-7300 + 1-metoxi-2-propanol. Esta mezcla podría ser empleada en aplicaciones de limpieza de componentes electrónicos, y como fluido de transferencia de calor.

c) *HFE + otros componentes:* La referencia [13] propone las mezclas HFE-7100 + alcano (ciclohexano o metil ciclohexano o heptano) como buenas sustitutas del HCFC-225ca/cb y del CFC-113.

   Por otra parte las referencias [38 - 40] son patentes, las cuales recogen mezclas binarias y ternarias de HFE-7300: HFE-7300 + (trans-1,2-dicloroetileno + alcanol) en el caso de [38], y HFE-7300 + isobutil acetato en la referencia [40].

El diisopropil éter es ya de por sí un buen agente de limpieza, aunque inflamable. La adición del HFE-7500 a este compuesto reduce su inflamabilidad, por tanto esta mezcla puede ser empleada en limpieza de precisión de componentes electrónicos, o de material militar de alta sensibilidad, como disolvente, además de en procesos de deposición química de vapor (CVD por sus siglas en inglés).

Con base en las consideraciones anteriores, se determinó emplear como fluidos puros cuatro HFEs (HFE-7100, HFE-7200, HFE-7300 y HFE-7500), y como mezclas las siguientes binarias:

- HFE-7100 + 1-propanol,
- HFE-7100 + 2-propanol,
- HFE-7200 + 2-propanol,
- HFE 7500 + diisopropil éter.

1.3.2 Técnicas experimentales disponibles.

A la hora de emplear las distintas técnicas de medida disponibles tanto en el Laboratorio de Ingeniería Energética de la Universidad de Burgos, como las disponibles en el Laboratoire des Fluides Complexes de la Universidad de Pau, ha sido necesario tener en cuenta la compatibilidad de los materiales de los equipos con los HFEs.

Aunque, según las referencias, la compatibilidad de los HFEs con otros materiales en general es buena [14], y los HFEs serían inertes ante la mayoría de metales y polímeros [11], por ejemplo esta misma referencia indica que las juntas y sellos en contacto con los HFEs deberían estar hechas de fluoroelastómeros que contengan bajas cantidades de plastificante, y que hayan demostrado no tener problemas previamente con el uso de PFCs. Esto es debido a que los HFEs pueden disolver estos materiales plastificantes, que son comúnmente añadidos a los elastómeros. Como ejemplos de materiales que pueden ser problemáticos en su empleo con los HFEs se pueden mencional el nitrilo, el butilo, la goma natural, el EPDM [41], y, en algunos casos, el Vitón, mientras que el polietileno, el ABS, y el PVC, entre otros, no generarían problemas en su uso con HFEs. Para el HFE-7100, el HFE-7200, y el HFE-7500, las hojas de datos técnicos proporcionadas por 3M^{TM} [14], [43 y 44], indican que todos ellos pueden ser absorbidos tanto por el Teflón (PTFE), como por la silicona. En el caso de reacción / absorción del HFE con alguno de los materiales, se podría producir contaminación del fluido así como obstrucción de conductos y filtros.

En el caso de este trabajo se descartó la determinación de la viscosidad a presión atmosférica con el viscosímetro Stabinger disponible en el Laboratorio de Ingeniería Energética de la Universidad de Burgos al tener éste juntas de Vitón. Tampoco se pudo determinar la velocidad del sonido a presión atmosférica para el HFE-7500 con el dispositivo situado en el Laboratoire des Fluides Complexes de la Universidad de Pau dado que este aparato tenía un sello de silicona, la cual absorbía gran parte del HFE-7500 en contacto con ella, derivando esto en grandes errores en las medidas.

Por tanto, basándonos en las recomendaciones hechas en la literatura sobre las mezclas y técnicas a utilizar, lo ya publicado en la literatura, y la compatibilidad con los materiales, además de la disponibilidad temporal para llevar a cabo la determinación de las propiedades, se ha seguido el siguiente esquema de trabajos:

A. Determinación de las curvas de presión de vapor y de los datos de equilibrio líquido-vapor mediante el empleo de un ebullómetro isóbaro. Adicionalmente se ha empleado la técnica de la densimetría (a presión atmosférica) para la determinación de las composiciones. Se han obtenido estos datos para las mezclas binarias que se enumeran a continuación:

    1) *x* HFE-7500 + (1-*x*) Diisopropil éter; en las presiones: 101.3 y 200.0 kPa.

    2) *x* HFE-7100 + (1-*x*) 2-Propanol; en las presiones: 50.0, 101.3 y 200.0 kPa.

    Asimismo se ha realizado la reducción de datos y posterior ajuste a modelos matemáticos (NRTL, Wilson, UNIQUAC) así como a modelos predictivos (UNIFAC). Estos trabajos se desarrollaron íntegramente en el Laboratorio de Ingeniería Energética de la Universidad de Burgos.

B. Determinación de la densidad a alta presión y a alta temperatura. A este efecto se han empleado dos densímetros de tubo vibrante, uno situado en el Laboratorio de Ingeniería Energética de la Universidad de Burgos, y el otro situado en el Laboratoire des Fluides Complexes de la Universidad de Pau, Francia. Los fluidos puros y mezclas estudiados han sido:

    1) *x* HFE-7500 + (1-*x*) Diisopropil éter; en el rango de presiones (0.1 – 140) MPa, y en el rango de temperaturas (293.15 – 393.15) K. Laboratoire des Fluides Complexes de la Universidad de Pau.

2) *x* HFE-7100 + (1-*x*) 2-Propanol; en el rango de presiones (0.1 – 140) MPa, y en el rango de temperaturas (298.15 – 393.15) K. Laboratorio de Ingeniería Energética de la Universidad de Burgos.

3) *x* HFE-7100 + (1-*x*) 1-Propanol; en el rango de presiones (0.1 – 70) MPa, y en el rango de temperaturas (298.15 – 393.15) K. Laboratorio de Ingeniería Energética de la Universidad de Burgos.

4) *x* HFE-7200 + (1-*x*) 2-Propanol; en el rango de presiones (0.1 – 140) MPa, y en el rango de temperaturas (293.15 – 393.15) K. Laboratorio de Ingeniería Energética de la Universidad de Burgos.

5) *x* HFE-7300; en el rango de presiones (0.1 – 140) MPa, y en el rango de temperaturas (293.15 – 393.15) K. Laboratorio de Ingeniería Energética de la Universidad de Burgos.

Los fluidos puros y las mezclas medidas se han ajustado posteriormente a la ecuación de Tamman-Tait, y se han determinado las propiedades derivadas (compresibilidad isotérmica y expansividad isobárica) así como los volúmenes de exceso de las mezclas.
La determinación de la densidad a alta presión en la mezcla (1), HFE-7500 + diisopropil éter, sería de utilidad en la posterior determinación de la viscosidad a alta presión, y en la determinación de la densidad a alta presión a partir de los datos de velocidad del sonido (comparación de los datos obtenidos en los cálculos con los experimentales).

C. Determinación de la viscosidad a alta presión y a alta temperatura empleando para ello un viscosímetro de caída de cuerpo. Las medidas se realizaron en el Laboratoire des Fluides Complexes et leurs Réservoirs de la Universidad de Pau en Francia. La mezcla medida fue la siguiente:

1) *x* HFE-7500 + (1-*x*) Diisopropil éter; en el rango de presiones (0.1 – 100) MPa, y en el rango de temperaturas (293.15 – 353.15) K.

Para la determinación de la viscosidad dinámica fueron necesarios los datos de densidad a alta presión medidos previamente para esta mezcla. El ajuste de estos datos se hizo mediante la ecuación Vogel-Fulcher-Tamman (VFT).

D. Determinación de la velocidad del sonido a altas presiones y temperaturas con un aparato que emplea la técnica impulsional. Estos trabajos fueron llevados a cabo en el Laboratoire des Fluides Complexes et leurs Réservoirs de la Universidad de Pau en Francia. La mezcla empleada fue la siguiente:

    1) *x* HFE-7500 + (1-*x*) Diisopropil éter; en el rango de presiones (0.1 – 100) MPa, y en el rango de temperaturas (293.15 – 353.15) K.

Los datos experimentales se han correlacionado con ecuaciones, y se ha empleado un método para determinar la densidad a alta presión a partir de los datos de velocidad del sonido a alta presión. Para poder llevar a cabo esta determinación se ha medido experimentalmente la capacidad calorífica de los fluidos puros y sus mezclas con una técnica de calorimetría diferencial.

E. Determinación de la velocidad del sonido a presión atmosférica. Para ello se ha empleado un analizador de densidad y velocidad del sonido que utiliza la técnica basada en el fenómeno de la resonancia, situado en el Laboratorio de Ingeniería Energética de la Universidad de Burgos. Los fluidos medidos han sido los siguientes:

    1) *x* HFE-7200 + (1-*x*) 2-Propanol; en el rango de temperaturas (293.15 – 333.15) K.

    2) *x* HFE-7300; en el rango de temperaturas (293.15 – 333.15) K.

Para la mezcla (1), *x* HFE-7200 + (1-*x*) 2-Propanol, recomendada por la referencia [13], la determinación de la velocidad del sonido brindaría la posibilidad de determinar la capacidad calorífica y la compresibilidad isoentrópica, de importancia en los fluidos de transferencia de calor, así como en el caso del fluido puro HFE-7300.

1.4 Referencias.

[1] M.J. Molina, F.S. Rowland, Nature 249 (1974) 810-812.

[2] Convenio de Viena, 22 de marzo (1985). https://treaties.un.org/doc/Treaties/1988/09/19880922%2003-14%20AM/Ch_XXVII_02p.pdf

[3] J.C. Farman, B.G. Gardiner, J.D. Shanklin, Nature 315 (1985) 207-210.

[4] Protocolo de Montreal, 16 de septiembre (1987). http://ozone.unep.org/es/manual-del-protocolo-de-montreal-relativo-las-sustancias-que-agotan-la-capa-de-ozono/31974

[5] S. Arrhenius, Phys. Mag. J. Sci. 41 (1896) 237-276.

[6] S. Schneider, T. Gal-Chen, J. Appl. Meteor. 15 (1976) 1050-1056.

[7] Protocolo de Kyoto, 11 de diciembre (1997). http://unfccc.int/resource/docs/convkp/kpspan.pdf

[8] Unión Europea. Reglamento (CE) 842/2006 del Parlamento Europeo y del Consejo de 17 de mayo (2006).

[9] Acuerdo de París, 12 de diciembre (2015). http://unfccc.int/files/essential_background/convention/application/pdf/spanish_paris_agreement.pdf

[10] V.A. Petrov, J. Fluor. Chem. 112 (2001) 117-121.

[11] P. Tuma, L. Tousingnant, SEMI Tech, Symp. (2001). http://multimedia.3m.com/mws/media/122381O/reducing-emissions-of-pfc-heat-transfer-fluids.pdf

[12] 3M™ Novec™ Engineered Fluids for ORC. http://multimedia.3m.com/mws/media/569866O/3mtm-novectm-fluids-for-organic-rankine-cycle-systems.pdf

[13] J. B. Durkee II, Cleaning with Solvents: Science and Technology, 1st ed. Elsevier B.V., Oxford (2014).

[14] 3M™ Novec™ Engineered Fluids. HFE-7500 technical data. http://multimedia.3m.com/mws/media/65496O/3mtm-novectm-7500-engineered-fluid.pdf

[15] A. Rodríguez, D. Rodríguez, A. Moraleda, I. Bravo, E. Moreno, A. Notario, Atm. Env. 96 (2014) 145-153.

[16] M. Goto, Y. Inoue, M. Kawasaki, A.G. Guschin, L.T. Molina, M.J. Molina, T.J. Wallington, M.D. Hurley, Environ. Sci. Technol. 36 (2002) 2395-2402.

[17] J. Kehren, datatech; http://www.solvents.net.au/index_htm_files/71IPA%20Engineered%20Fluid.pdf

[18] M.M. Piñeiro, D. Bessières, J.L. Legido, H. Saint-Guirons, Int. J. Thermophys. 24 (2003) 1265-1276.

[19] H. Qi, D. Fang, X. Meng, J. Wu, J. Chem. Thermodyn. 77 (2014) 131-136.

[20] M.H. Rausch, L. Kretschmer, S. Will, A. Leipertz, A.P. Fröba, J. Chem. Eng. Data 60 (2015) 3759-3765.

[21] T. Minamihounoki, T. Takigawa, K. Tamura, S. Murakami, J. Chem. Thermodyn. 33 (2001) 189-203.

[22] G. Marchionni, P. Maccone, G. Pezzin, J. Fluor. Chem. 118 (2002) 149-155.

[23] B. An, Y. Duan, L. Tan, Z. Yang, J. Chem. Eng. Data 60 (2015) 1206-1210.

[24] M.M. Piñeiro, F. Plantier, D. Bessières, J.L. Legido, J.L. Daridon, Fluid Phase Equilib. 222-223 (2004) 297-302.

[25] F. Govaerts, D. D. Keane, Medical Device Technol. (2001). http://solutions.3mbelgie.be/3MContentRetrievalAPI/BlobServlet?lmd=1360239440000&locale=nl_BE&assetType=MMM_Image&assetId=1319247019271&blobAttribute=ImageFile

[26] J. Cendón, M.M. Piñeiro, D. Bessières, J. Vijande, J.L. Legido, J. Chem. Eng. Data 49 (2004) 1368-1372.

[27] K.W. Eum, H. Gu, T.G. Lee, J. Choe, K. Lee, K.H. Song, J. Chem. Eng. Data 58 (2013) 915-919.

[28] M.B. Shiflett, A. Yokozeki, J. Chem. Eng. Data 52 (2007) 2413-2418.

[29] D. Fang, Y. Li, X. Meng, J. Wu, J. Chem. Thermodyn. 69 (2014) 36-42.

[30] D. Fang, Y. Li, X. Meng, J. Wu, J. Chem. Thermodyn. 83 (2015) 123-125.

[31] J. Murata, S. Yamashita, M. Akiyama, J. Chem. Eng. Data 47 (2002) 911-915.

[32] P. Warrier, A.S. Teja, J. Chem. Eng. Data 56 (2011) 4291-4294.

[33] X. Hu, X. Meng, K. Wei, W. Li, J. Wu, J. Chem. Eng. Data 60 (2015) 3562-3570.

[34] J. Cendón, J. Vijande, J.L. Legido, M.M. Piñeiro, J. Chem. Eng. Data 51 (2006) 577-581.

[35] S.L. Outcalt, J. Chem. Eng. Data 59 (2014) 2087–2094.

[36] T. Lafitte, F. Plantier, M.M. Piñeiro, J.L. Daridon, D. Bessières, Ind. Eng. Chem. Res. 46 (2007) 6998–7007.

[37] M.O. McLinden, C. Lösch-Will, J. Chem. Thermodyn. 39 (2007) 507–530.

[38] J.G. Owens, Patente: US/12/557,610 (2012).

[39] J.G. Owens, Patente: US 11/782,783 (2010).

[40] P.E. Rajtar, J.G. Owens, Patente: US 10/739,231 (2003).

[41] 3M™ Novec™ Thermal Management Fluids. https://multimedia.3m.com/mws/media/65495O/3mtm-thermal-management-fluids.pdf

[42] 3M™ Novec™ Engineered Fluids. HFE-7100 technical data. https://multimedia.3m.com/mws/media/199818O/3mtm-novectm-7100-engineered-fluid.pdf

[43] 3M™ Novec™ Engineered Fluids. HFE-7200 technical data. https://multimedia.3m.com/mws/media/199819O/3mtm-novectm-7200-engineered-fluid.pdf

Chapter 1

STARTING HYPOTHESIS AND OBJECTIVES

1.1 General context of fluorinated gases.

In 1974, Molina and Rowland's scientific works reported, in a paper published in Nature [1], their research results concerning the destination of some chemical particles derivated from industry processes, named chlorofluorocarbons (CFCs). Chlorine atoms resulting from CFCs decomposition were destroying ozone molecules through a photochemical reaction, this being an increasing threat to the ozone layer in the stratosphere.

Since their creation, in 1930, CFCs have been employed with excellent results for several uses thanks to their thermophysical properties: they demonstrated to be good refrigerants in compression based cycles, they could be used as high-precision cleaning solvents, due to they were non-residue fluids, as aerosol propellents, and to manufacture thermal insulators, among others.

As scientists become aware of these fluids' problematic, in 1983 the term ODP, Ozone Depletion Potential, was defined as *the relative amount of degradation to the ozone layer a fluid can cause, with trichlorofluoromethane, or CFC-11, being fixed at an ODP = 1.0.*

As a result of discovering that the CFCs were destroying the ozone layer, in 1985 the Vienna Convention was approved. Its fundamental objectives were to boost the research, to encourage the cooperation between the parties, and to facilitate the information exchange concerning emissions reduction [2]. The Vienna Convention set an important precedent, because, for the first time, nations agreed to fight against a global environmental problem, even before its impact was scientifically proven. The same year, Farman *et al.* confirmed the problem publishing a paper, also in Nature [3], which notified a considerable reduction of the ozone layer thickness over Antarctica.

In this way, the use of new alternatives to chlorofluorocarbons was boosted following the Montreal Protocol (1987), [4] which promoted the progressive reduction in the use and production of chlorine-atom-based fluids (CFCs, end of use and production situated in 1995, and HCFCs, hydrochlorofluorocarbons, with an usage and production end situated in 2010). In the same way, HFCs (hydrofluorocarbons) were proposed as replacement fluids for commonly used CFCs and HCFCs.

Simultaneouslly, during the '80s, experts began to notice that the average annual temperature was increasing, which promoted to start speaking about the global warming theory, which had been previously proposed in 1896 by the Swedish scientific Arrhenius [5], who ensured that fossile fuels could lead to or accelerate global warming. This hypothesis was reiterated by Schneider (1976) [6], who predicted that the global warming was starting to take place as a result of the human activity. After Arrhenius' discovery, this subject was forgotten, and during this time, it was thought that the influence of human activities was insignificant compared to those of the natural forces, such as solar activity, or the ocean currents. In 1988, it was finally recognized that

the climate was warmer than before 1880. The global warming theory was getting strong, and the Intergubernamental Panel on Climate Change (IPCC), was established by the United Nations Environment Programme and the World Meteorological Association. The proposal of this Pannel was to predict the impact of the greenhouse gases, taking into account predictive models about climate and up-to-date scientific information.

Then, the term Global Warming Potential (GWP), was defined as t*he relative measure of how much heat a greenhouse gas traps in the atmosphere*. This term compares the amount of heat trapped by a certain mass of gas with the amount of heat trapped by a similar mass of CO_2. In this way, CO_2 is being fixed as reference, with a GWP = 1.0.

In 1997, the Kyoto Protocol [7], implemented following the United Nations Framework Convention on Climate Change (UNFCCC), added more precise actions, which were quantificable and legally binding, oriented to reduce the global-warming emissions. The main goal of the Kyoto Protocol was to reduce the emissions of six greenhouse effect gases: carbon dioxide (CO_2), methane (CH_4), nitric oxide (N_2O), and the industry gases HFCs (hydrofluorocarbons), PFCs (perfluorocarbons), and SF_6 (sulphur hexafluoride), in an approximated percentage of 5% in the period from 2008 to 2012. Previous scientific works demonstrated that these gases, once released to the atmosphere, were able to trap part of the energy emmited by the Earth's surface after it was warmed by the solar radiation.

Concerning HFCs, some of them exhibited extremely high GWP, as was the case of R-23, with a GWP = 11700, or the case of R-404a, with a GWP = 3260. The same problem was observed with the widely used perfluorocarbons (PFCs) and perfluoropoliethers (PFPEs).

To implement the targets of the Kyoto Protocol, in 2006, the European Union published the Regulation (CE) nº 842/2006, of 17 May 2006, concerning some fluorinated gases with greenhouse effect, which regulates the use of HFCs, PFCs, and SF_6, all of them with a global warming potential, GWP between 120 and 22200 times higher than carbon dioxide (CO_2) [8]. This Regulation boosted the recovery and control of these gases, as well as the minimization of leakage to the atmosphere during their use. In the same manner, it resulted in an ambicious program of certification for the personnel involved in the installation, maintenance, leakage control and recovery of refrigerating systems, as well as fire extinghishing media which included fluorinated gases in its composition, listed in the Annex I of the Regulation. It established also a requirement for the recovery of the gases employed in other applications such as any equipment containing these solvents, high voltage equipment, mobile devices, etc., establishing clear procedures for leakage control. This document was subsequently repealed, in order to publish the new Regulation (EU) nº 517/2014, of 16 April, where the same principles would remain, but adjusting the deadlines in order to put an end to the production and commercialization of certain gases, as well as the utilization of any equipment using that kind of fluids. As an example, it is stated that from 1st January 2020, the commercialization of portable air conditioning equipment

for closed spaces containing HFCs with a GWP equal to or higher than 150 will be prohibited. The same occurs from 1st January 2025, date from which the commercialization of simple split air conditioning systems containing less than 3 kg of fluorinated gases with greenhouse effect, having a GWP higher than 750, will be forbidden.

In the same way, this Regulation establishes the duty for all producers and traders of greenhouse gases to present an annual activity report to the Commision before the end of March of the following year.

The Directive 2006/40/CE, of 17 May, relative to the emissions that come from mobile air conditioners, regulates, in the same way, the part of the automotive field which is related to fluoriated gases.

With respect to the ozone-depleting fluids, the European Union published the Regulation (CE) nº 1005/2009, of the European Parliament and the Council, which susbstitutes the previous Regulation (CE) nº 2037/2000, with the objectives of progressively eliminating eliminate these substances, and to protecting human health and the environment, which will be of application since 1st January 2010.

Taking this into account, at European level we find that, for example, the use of fluid R-134a in mobile air conditioning systems (recharge and new models), has been banned since 2013, and that in countries like Denmark, Austria and Switzerland, most of the uses of HFCs have been banned.

At a national level, in order to adapt to the European requirements, since the 26th June 2010, the Royal Decree 795/2010, of 16 June, which regulates the commercialization and handling of fluorinated gases, the use of the equipment that contains that kind of fluids, as well as the certification of the professionals involved in its utilization, is applicable. This Royal Decree complements the existing regulations on this matter, which main goal is to minimize the organohalogenated emissions. Moreover, the regulation establishes several further actions, which are contained in the Law 34/2007, of 15 November, of air quality and atmosphere protection, referred to emissions control.

The recent Paris Agreement [9], negotiated during the XXI Conference on Climate Change (COP 21) in December 2015, and signed the 22nd April 2016, is an agreement within the framework of the United Nations Framework Convention that sets specific actions intended to reduce the greenhouse gas emissions dealing with their mitigation, adaptation and finance starting in the year 2020, year in which Kyoto Protocol expires. The main objectives for this agreement, referring greenhouse gas emissions, are the following ones:

1. Holding the increase in the global average temperature to well below 2ºC above pre-industrial levels.

2. To pursue efforts to limit the temperature increase to 1.5ºC above pre-industrial levels, recognizing that this would significantly reduce the risks and impacts of climate change.
3. Making finance flows consistent with a pathway towards low greenhose gas emissions and climate-resilient development.

To this effect, in Mach 2015, the European Union was the first economy which presented its contribution to the new Agreement. The fact is that the EU is now taking actions in order to meet the requirements of reducing greenhouse gas emissions by at least 40%, before 2030.

In short, along the last 40 years, new alternatives to fluorinated gases have been developed. It was necessary to introduce new industry fluids with the same applications than their predecesors, with the same or similar thermophysical properties, high operational efficiency, low leakage rates, and with an ODP near o equal to zero, also having low GWP values. A kind of these candidates are the so called "natural refrigerants", (NH_3, CO_2, hydrocarbons, etc). Some of these natural refrigerants are widely used in the industry, as is the case of NH_3 in absorption or compression-based refrigeration cycles. These fluids exhibit, as a common feature, a medium to high flammability, and less effectiveness on its applications compared to other fluids. Other kind of replacement fluids are the low GWP HFCs, as is the case of R-430a (GWP = 104) or R-32 (GWP = 675). These fluids have low or zero ODP, and a good efficiency in their use, but most of them exhibit medium flammability rates. Hydrofluoro-olefins (HFOs), are a class of recently synthesized fluids coming from the olefins. These fluids present very low GWP (for example, R-1234-yf presents a GWP = 4), mainly due to the double bond present in the olefin, which allows them to exhibit short atmospheric lifetimes (ALT), in the order of a few days, low GWP, and zero ODP. On the other hand, nowadays their high price and low efficiency rates penalize their utilization. Hydrofluoroiodocarbons (HFICs) have also been proposed as an alternative, but most of them show high toxicity rates, high prices, and ODP > 0. Finally, another proposed alternative are the hydrofluoroethers (HFEs). These fluids, in a liquid state at room temperature, started being synthesized at the begining of the '90s as an alternative to commonly used HFCs, PFCs and PFPEs, among others, because they exhibited similar thermophysical properties, and the oxygen atom located on the ether group provided the molecule with short atmospheric lifetimes (ALT), low GWP, and zero or near zero ODP. HFEs present very low toxicity, they are practically non-flammable, and they have a good cost-effectiveness reatio. HFEs with high molecular weight (HFE-7000, HFE-7100, HFE-7200, HFE-7300, HFE-7500), are excellent solvents in a wide range of industrial applications. In the same manner, HFE-7000 and HFE-7100, as pure compounds or as azeotropic mixtures with some alcohols, could be used in the refrigeration industry or in Organic Rankine Cycles (ORC).

1.2 Overview of hydrofluoroethers (HFEs).

As already stated, hydrofluoroethers began to be synthesized during the 1990s decade while searching for new fluids suitable to replace the widely used CFCs, HCFCs, HFCs, PFCs and PFPEs, but being environmentally friendly. These fluids don't occur naturally; they are synthesized using different methods. Generally, these methods are based on ethers fluorination or in alcohols addition to fluoro-olefins, electhophillic alkylation of polyfluorated anions with several solvents as dimethyl sulphate $(CH_3)_2SO_4$, or ethers addition to fluoro-olefins. Other techniques are based on polyfluorated ethers and fluoroethylenes condensation, employing antimonium pentafluoride as catalyst [10].

There are a broad variety of HFEs, so their performance and applications can vary widely [11]. Their thermophysical properties differ from one to another, which make them suitable to be employed in lots of applications. Based on high molecular weight HFEs, some of them being studied in this Thesis, we have that, for example, HFE-649, HFE-7000 and even HFE-7100 in some cases, are particularly suitable to be used in Organic Rankine Cycles (ORC) [12], requiring low or medium boiling temperatures, a good thermal estability, non flammability, and a high molecular weight, which contributes to reduce the engine speed of the turbine.

Azeotropic mixtures of HFE-7100 and HFE-7200 with alcohols are of utmost interest on the high precission cleaning field, where high polar solvents are needed. These mixtures are able to substitute the previously used CFC-113, HCFC-141b and HCFC-225ca/cb in all of their applications: wax removal, fingerprints removal, silicone oils and lubricants removal, etc., whether used in spray aerosols, or in wipe cleaning [13]. HFE-7100 can also be used as pure compound in the medical industry, in substitution of the aforementioned CFC-113 and HCFC-141b, as friction-reduction agent on devices such as surgical knife blades, staples and hypodermic needles, as well as anti-clotting onto tubing and blood bags.

HFE-7300 is a very good cleaning agent for electronic components, as pure compound or in its ternary mixtures with alcohols and trans-1,2-dichloroethilene, and it can be used as well as coating agent, lubricant, and heat transfer fluid.

HFE-7500 can substitute most of PFCs and PFPEs, due to its low dielectric constant, among other desirable properties. Also, it can be used as electronic components cooling agent; in direct contact single-and two-phase cooling of supercomputers and high sensitivity military electronics, and to cool high voltage transformers and power electronics. Other uses include freeze drying and reactor cooling in the pharmaceutical industry [14].

These HFEs are inert to most metals and hard polymers, and employing them usually requires only minor modifications in the equipment.

Regarding the environmental effect, some scientific works report the short atmospheric lifetimes that most of the HFEs exhibit [15, 16]: the hydroxyl molecules present in the troposphere break the HFE molecules, resulting in short ALT and also in low GWP.

In terms of safety and toxicity, HFEs have a safety profile better than their predecessors [17], showing explosion limits in air equal to zero, referred to flammability, and very high exposition limits (in the order of thousands of ppm) to produce any negative effect on the human body.

Perhaps, one of the critical points in their utilization or introduction are the costs. These solvents are more expensive than their predecessors, whereby recycling and disposal policies using distillation techniques once used are needed. As an example, 3M Company provides a used fluid return program, which is nowadays only available in the U.S.A.

As summary, it can be seen that HFEs offer a good balance between safety, toxicity, applications, performance, environmental effect and costs.

1.3. Objectives of the Doctoral Thesis.

According to the aforementioned arguments, the objective of this Doctoral Thesis is to carry out the determination of the thermophysical properties of some high molecular weight HFEs, due to their potential to replace most of the commonly used fluorocarbons in a wide range of industrial applications. In order to choose the HFEs that were going to be used, either as pure compounds, or in mixture, as well as the measurement techniques, a literature revision was done, to decide which HFEs or their mixtures were of interest, and also to evaluate the already published property data for these fluids. On the other hand, to select the measurement techniques that will be used, the compatibility of the different HFEs with the materials of the available devices (O-rings, seals, etc.) was studied. In the following sections, we will present the detailed description on how the selection of the HFEs and their mixtures was carried out, as well as the techniques employed to measure their thermophysical properties.

1.3.1 Selection of the HFEs and their mixtures.

With respect to the available literature references for HFEs and their mixtures, concerning their thermophysical properties characterization, they are currently scarce, although it is well known that industry needs appropriate knowledge of these properties to implement the use of this kind of fluids. Table 1 gathers the references found in the literature characterizing some

thermophysical properties for the four high molecular weight HFEs studied in this Thesis (HFE-7100, HFE-7200, HFE-7300 and HFE-7500).

These references provide data for the pure compounds, and also for their mixtures, taking into account several properties (density, viscosity, liquid-vapor equilibrium, liquid-liquid equilibrium, vapor pressure curves, and speed of sound).

Not much data concerning the mixtures with other compounds were found. Concerning HFE-7100, references [26 - 28] report data for three different mixtures. High pressure density data for the binary mixture HFE-7100 + *n*-hexane are reported in reference [26], while liquid-liquid equilibrium data are reported in the other two references: for the mixture HFE-7100 + perfluorohexane + toluene + 1,4 dioxane or dimethylformamide in reference [27], and for the mixture HFE-7100 + 1-ethyl-imidazolium, in reference [28] respectively. In the case of HFE-7200, only two references for mixtures reporting high pressure density data were found in the literature. The data for the binary mixture HFE-7200 + *n*-hexane can be found in reference [34], while the data concerning the mixture HFE-7200 + 1-ethyl-3-methylimidazolium can be found in reference [28]. This last reference reports also data of liquid-liquid equilibrium for the mixture HFE-7300 + 1-ethyl-3-methylimidazolium.

For the pure compounds, more references and more techniques were found. Density for HFE-7100 was measured at atmospheric pressure and at high pressure by some authors [18 - 22], while reference [20] provides also viscosity data at atmospheric pressure. For this compound, reference [23] provides vapor pressure data, and reference [24] provides speed of sound measurements at high pressure. Density of HFE-7200 was determined at atmospheric pressure and at high pressure too by references [20], [29 - 32]. The viscosity of this compound was also measured at atmospheric pressure by Rausch *et al.* [20], and at high pressures by Hu *et al*. [33]. For pure HFE-7300, reference [20] reports data at atmospheric pressure both for density and for viscosity. Finally, the density of pure HFE-7500 was determined at atmospheric pressure and at high pressure by references [20], [29, 30], [35 - 37]. The other properties determined for this fluid were the viscosity at atmospheric pressure [20], and at high pressure [33], as well as the speed of sound at high pressure, which was determined by Lafitte *et al.* [36].

Table 1. Relation of HFEs and their mixtures which thermodynamic properties were measured in this Doctoral Thesis, and those that were found in the literature.

HFE	Property	ρ[a]	η[b]	P^{sat}[c]	L.L.E.[d]	V.L.E.[e]	c[f]
HFE-7100	PURE COMPOUND						
		[This work], [18], [19], [20], [21], [22]	[20]	[This work], [23]			[24]
	MIXTURES						
	+ 1-propanol (Proposed in [13] *and* [25])	[This work]					
	+ 2-propanol (Proposed in [13] *and* [25])	[This work]		[This work]		[This work]	
	+ n-hexane	[26]					
	+ perfluorohexane + toluene + 1,4 dioxane or dimethylformamide				[27]		
	+ 1-ethyl-3-methylimizadolium				[28]		
HFE-7200	PURE COMPOUND						
		[This work], [20], [29], [30], [31], [32]	[20], [33]				
	MIXTURES						
	+ 2-propanol (Proposed in [13])	[This work]					[This work]
	+ n-hexano	[34]					
	+ 1-ethyl-3-methylimizadolium				[28]		
HFE-7300	PURE COMPOUND						
		[This work], [20]	[20]				[This work]
	MIXTURES						
	+ 1-ethyl-3-methylimizadolium				[28]		
HFE-7500	PURE COMPOUND						
		[This work], [20], [29], [30], [35], [36], [37]	[This work, [20], [33]	[This work]			[This work], [36]
	MIXTURES						
	+ diisoprophyl ether	[This work]	[This work]			[This work]	[This work]
	+ 1-ethyl-3-methylimizadolium				[28]		

[a] ρ = *density.*
[b] η = *viscosity.*

[c] *P^{sat} = vapor-pressure curve.*
[d] *L.L.E = liquid-liquid equilibrium.*
[e] *V.L.E. = vapor-liquid equilibrium.*
[f] *c = speed of sound.*

Table 1 also shows which are the mixtures and techniques used in this work. For the pure fluids, even though some properties were already determined in the literature, the ranges in pressure or in temperature have been broadened. To decide which mixtures and techniques were the relevant ones, previously published data were taken into account. In the same manner, a search on non-published mixtures of interest was carried out, considering their applications, and their suitability to substitute other fluorocarbons which are commonly used in the industry, but not environmentally friendly.

To establish a classification, concerning the interest of use of the pure HFEs and of their mixures, we have the following groups:

a) *Pure HFEs*
b) *HFE + alcohol*
c) *HFE + other components*

a) *Pure HFEs:* Taking into account the pure HFEs, as stated in reference [13], HFE-7100 could be used as substitute of HCFC-141b for some applications. Reference [11] suggests HFE-7100, HFE-7200 and HFE-7500, as pure compounds, as substitutes for several perfluorocarbons (PFCs). Some patents [38 - 40] indicate HFE-7300 as a good solvent and as a good high precision cleaning agent for electronic components.

b) *HFE + alcohol:* According to the mixtures proposed in the literature, reference [13] points out to some binary mixtures of HFEs as interesting: HFE-7100 + (1-propanol or 2-propanol or methanol or ethanol), as well as HFE-7200 + (ethanol or 2-propanol), because they can substitute other previously used fluorocarbons. In particular, mixtures HFE-7200 + (ethanol or 2-propanol) could substitute HCFC-225ca/cb, while mixtures HFE-7100 + (ethanol or 2-propanol) are indicated as good substitutes for CFC-113. Reference [25] points out that the azeotropic mixture HFE-7100 + 2-propanol as a good replacement of fluid HCFC-141b in its applications. In the same way, azeotropic mixtures of HFE-7100 + 1-propanol and HFE-7200 + 2-propanol are also of interest.

Reference [39] reports the binary mixture HFE-7300 + 1-methoxi-2-propanol as a good option to be used in cleaning applications for electronic components, and as heat transfer fluid.

c) *HFE + other components:* Reference [13] suggests the binary mixtures HFE-7100 + alkanol (cyclohexane or methyl cyclohexane or heptane), as good substitutes of HCFC-225ca/cb and CFC-113.

On the other hand references [38 - 40] are patents, which gather binary and ternary mixtures of HFE-7300: HFE-7300 + (trans-1,2-dichloroethylene + alkanol) in the case of reference [38], and HFE-7300 + isobuthyl acetate in reference [40].

Diisopropyl ether is considered as a good cleansing agent, but flammable. The addition of HFE-7500 reduces its flammability, so this mixture can be used in electronic components precision cleaning, as well as in sentitive military electronics cleaning, as solvent, and also in chemical vapor deposition (CVD) processes.

For the aforementioned considerations, it was decided to use, four HFEs (HFE-7100, HFE-7200, HFE-7300 and HFE-7500), as pure compounds, and the following mixtures:

- HFE-7100 + 1-propanol,
- HFE-7100 + 2-propanol,
- HFE-7200 + 2-propanol,
- HFE 7500 + diisopropyl ether.

1.3.2 Experimental techniques.

In order to choose the different techniques available at the Laboratorio de Ingeniería Energética of the University of Burgos, Spain, and also the available ones at the Laboratoire des Fluides Complexes of the University of Pau, France, it was necessary to take into account the materials compatibility between the devices and the HFEs.

Although the compatibility of HFEs with other materials is good [14], and HFEs are inert to common metals and polymers. Reference [11], for example, indicates that O-rings and seals in direct contact with HFEs should be made of fluoroelastomers containing low plasticizer percentage, which have been demonstrated not to have problems in the use of PFCs. This is due to the fact that HFEs are able to dissolve this plasticizers, which are commonly added to elastomers in order to bring more flexibility. As examples of critical materials in their use with HFEs, we have that for nitrile, butyl, natural rubber, EPDM [41], and in some cases Viton, the

compatibility is not good, while poliethylene, ABS, and PVC, among others, will not generate problems in their use with HFEs. For HFE-7100, HFE-7200 and HFE-7500, technical data sheets supplied by 3M^{TM} [14], [43 y 44], point out that all of them could be absorbed by Teflon (PTFE) and by silicone. In the case of reaction / absorption of HFEs with some of the materials, contamination of the fluid can occur, as well as seals swelling and clogging of small fluid pipes and filters.

In this work, the determination of the viscosity at atmospheric pressure with the Stabinger viscometer available at the Laboratorio de Ingeniería Energética, at the University of Burgos, was discarded because its O-rings are made of Viton. Neither was possible to determine the speed of sound at atmospheric pressure for HFE-7500 with the available device at the Laboratoire des Fluides Complexes, at the University of Pau, because this apparatus had a silicone seal, which was able to absorb high amounts of HFE-7500 when in contact with it, leading to large errors in the measurements.

Thus, based on the recommendations found in the literature, concerning the mixtures and techniques which were of interest to be used, and taking into account the previously published in the literature, the materials compatibility, as well as the temporal availability to determine the thermophysical properties, the following schedule has been followed:

A. Determination of vapor pressure data and vapor-equilibria data by using an isobaric ebullometer. In additon, an experimental atmospheric pressure density technique was employed, in order to determine the compositions of the binary mixtures. These data were obtained for the following mixtures:

    1) *x* HFE-7500 + (1-*x*) Diisopropyl ether; at pressures: 101.3 and 200.0 kPa.

    2) *x* HFE-7100 + (1-*x*) 2-Propanol; at pressures: 50.0, 101.3 and 200.0 kPa.

    Furthermore, the data reduction and mathematical models fitting were done, by employing the NRTL, Wilson, and UNIQUAC models. The predictive model of UNIFAC was also employed. These works were all performed at the Laboratorio de Ingeniería Energética of the University of Burgos.

B. High pressure and high temperature density determination. For this purpose, two vibrating tube densitometers were used, one of them located at the Laboratorio de Ingeniería Energética of the University of Burgos, and the other one located at the Laboratoire des Fluides Complexes, of the University of Pau. The pure compounds and mixtures studied were:

1) *x* HFE-7500 + (1-*x*) Diisopropyl ether; in the pressure range (0.1 – 140) MPa, and in the temperature range (293.15 – 393.15) K. Laboratoire des Fluides Complexes, of the University of Pau.

2) *x* HFE-7100 + (1-*x*) 2-Propanol; in the pressure range (0.1 – 140) MPa, and in the temperature range (298.15 – 393.15) K. Laboratorio de Ingeniería Energética of the University of Burgos.

3) *x* HFE-7100 + (1-*x*) 1-Propanol; in the pressure range (0.1 – 70) MPa, and in the temperature range (298.15 – 393.15) K. Energy Engineering Laboratory, University of Burgos.

4) *x* HFE-7200 + (1-*x*) 2-Propanol; in the pressure range (0.1 – 140) MPa, and in the temperature range (293.15 – 393.15) K. Energy Engineering Laboratory, University of Burgos.

5) *x* HFE-7300; in the pressure range (0.1 – 140) MPa, and in the temperature range (293.15 – 393.15) K. Energy Engineering Laboratory, University of Burgos.

The pure fluids and their mixtures were correlated to a Tamman-Tait equation. The derivative properties, that is, the isothermal compressibility and the isobaric expansion, as well as the excess volumes, were also determined.

The high pressure density determination for the binary mixture (1), HFE-7500 + diisopropyl ether, was of interest for the subsequent determinations of high pressure viscosity data, and for the high pressure density determination from high pressure speed of sound data (comparison of the calculated data with the experimental ones).

C. High pressure and high temperature viscosity data determination. For this purpose, a falling body viscometer was used. The measurements were carried out at the Laboratoire des Fluides Complexes, University of Pau, France. The measured mixture was the following one:

1) *x* HFE-7500 + (1-*x*) Diisopropyl ether; in the range of pressures (0.1 – 100) MPa, and in the range of temperatures (293.15 – 353.15) K.

To determine the dynamic viscosity, the previously measured high pressure density data for this mixture were necessary. The fitting of the experimental data was carried out by using a Vogel-Fulcher-Tamman (VFT) equation.

D. High pressure and high temperature speed of sound determination, by using an apparatus which involves the impulsional technique. These works were carried out at the Laboratoire des Fluides Complexes of the University of Pau. The measured mixture was:

    1) *x* HFE-7500 + (1-*x*) Diisopropyl ether; in the pressure range (0.1 – 100) MPa, and in the temperature range (293.15 – 353.15) K.

The experimental data were correlated to equations, and a method to determine high pressure density data from speed of sound measurements was implemented. To carry out this determination, heat capacities of the pure compounds and of the mixture had to be determined. For this purpose, a differential scanning calorimetry (DSC), technique was applied.

E. Determination of speed of sound measurements at atmospheric pressure. To carry out the measurements, a density and sound velocity analyzer, which measuring principle is based on the resonance phenomenon, was used. The measurements were carried out at the Laboratorio de Ingeniería Energética of the University of Burgos, with the following fluids:

    1) *x* HFE-7200 + (1-*x*) 2-Propanol; in the temperature ranges (293.15 – 333.15) K.

    2) *x* HFE-7300; in the temperature ranges (293.15 – 333.15) K.

For the mixture (1), *x* HFE-7200 + (1-*x*) 2-Propanol, recommended by reference [13], the speed of sound determination brings the possibility to determine the heat capacities and the isentropic compressibilities, relevant properties in heat transfer fluids. The same occurs with the pure fluid HFE-7300.

1.4 References.

[1] M.J. Molina, F.S. Rowland, Nature 249 (1974) 810-812.

[2] Convenio de Viena, 22 de marzo (1985). https://treaties.un.org/doc/Treaties/1988/09/19880922%2003-14%20AM/Ch_XXVII_02p.pdf

[3] J.C. Farman, B.G. Gardiner, J.D. Shanklin, Nature 315 (1985) 207-210.

[4] Montreal Protocol, 16th september (1987). http://ozone.unep.org/en/handbook-montreal-protocol-substances-deplete-ozone-layer/27570

[5] S. Arrhenius, Phys. Mag. J. Sci. 41 (1896) 237-276.

[6] S. Schneider, T. Gal-Chen, J. Appl. Meteor. 15 (1976) 1050-1056.

[7] Kyoto Protocol, 11st december (1997). http://unfccc.int/resource/docs/convkp/kpeng.pdf

[8] European Union. Regulation (EC) 842/2006 of the European Parliament and the Council of 17 may (2006).

[9] Paris Agreement, 12th december (2015). http://unfccc.int/files/essential_background/convention/application/pdf/english_paris_agreement.pdf

[10] V.A. Petrov, J. Fluor. Chem. 112 (2001) 117-121.

[11] P. Tuma, L. Tousingnant, SEMI Tech, Symp. (2001). http://multimedia.3m.com/mws/media/122381O/reducing-emissions-of-pfc-heat-transfer-fluids.pdf

[12] 3M™ Novec™ Engineered Fluids for ORC. http://multimedia.3m.com/mws/media/569866O/3mtm-novectm-fluids-for-organic-rankine-cycle-systems.pdf

[13] J. B. Durkee II, Cleaning with Solvents: Science and Technology, 1st ed. Elsevier B.V., Oxford (2014).

[14] 3M™ Novec™ Engineered Fluids. HFE-7500 technical data. http://multimedia.3m.com/mws/media/65496O/3mtm-novectm-7500-engineered-fluid.pdf

[15] A. Rodríguez, D. Rodríguez, A. Moraleda, I. Bravo, E. Moreno, A. Notario, Atm. Env. 96 (2014) 145-153.

[16] M. Goto, Y. Inoue, M. Kawasaki, A.G. Guschin, L.T. Molina, M.J. Molina, T.J. Wallington, M.D. Hurley, Environ. Sci. Technol. 36 (2002) 2395-2402.

[17] J. Kehren, datatech; http://www.solvents.net.au/index_htm_files/71IPA%20Engineered%20Fluid.pdf

[18] M.M. Piñeiro, D. Bessières, J.L. Legido, H. Saint-Guirons, Int. J. Thermophys. 24 (2003) 1265-1276.

[19] H. Qi, D. Fang, X. Meng, J. Wu, J. Chem. Thermodyn. 77 (2014) 131-136.

[20] M.H. Rausch, L. Kretschmer, S. Will, A. Leipertz, A.P. Fröba, J. Chem. Eng. Data 60 (2015) 3759-3765.

[21] T. Minamihounoki, T. Takigawa, K. Tamura, S. Murakami, J. Chem. Thermodyn. 33 (2001) 189-203.

[22] G. Marchionni, P. Maccone, G. Pezzin, J. Fluor. Chem. 118 (2002) 149-155.

[23] B. An, Y. Duan, L. Tan, Z. Yang, J. Chem. Eng. Data 60 (2015) 1206-1210.

[24] M.M. Piñeiro, F. Plantier, D. Bessières, J.L. Legido, J.L. Daridon, Fluid Phase Equilib. 222-223 (2004) 297-302.

[25] F. Govaerts, D. D. Keane, Medical Device Technol. (2001). http://solutions.3mbelgie.be/3MContentRetrievalAPI/BlobServlet?lmd=1360239440000&locale=nl_BE&assetType=MMM_Image&assetId=1319247019271&blobAttribute=ImageFile

[26] J. Cendón, M.M. Piñeiro, D. Bessières, J. Vijande, J.L. Legido, J. Chem. Eng. Data 49 (2004) 1368-1372.

[27] K.W. Eum, H. Gu, T.G. Lee, J. Choe, K. Lee, K.H. Song, J. Chem. Eng. Data 58 (2013) 915-919.

[28] M.B. Shiflett, A. Yokozeki, J. Chem. Eng. Data 52 (2007) 2413-2418.

[29] D. Fang, Y. Li, X. Meng, J. Wu, J. Chem. Thermodyn. 69 (2014) 36-42.

[30] D. Fang, Y. Li, X. Meng, J. Wu, J. Chem. Thermodyn. 83 (2015) 123-125.

[31] J. Murata, S. Yamashita, M. Akiyama, J. Chem. Eng. Data 47 (2002) 911-915.

[32] P. Warrier, A.S. Teja, J. Chem. Eng. Data 56 (2011) 4291-4294.

[33] X. Hu, X. Meng, K. Wei, W. Li, J. Wu, J. Chem. Eng. Data 60 (2015) 3562-3570.

[34] J. Cendón, J. Vijande, J.L. Legido, M.M. Piñeiro, J. Chem. Eng. Data 51 (2006) 577-581.

[35] S.L. Outcalt, J. Chem. Eng. Data 59 (2014) 2087–2094.

[36] T. Lafitte, F. Plantier, M.M. Piñeiro, J.L. Daridon, D. Bessières, Ind. Eng. Chem. Res. 46 (2007) 6998–7007.

[37] M.O. McLinden, C. Lösch-Will, J. Chem. Thermodyn. 39 (2007) 507–530.

[38] J.G. Owens, Patent: US/12/557,610 (2012).

[39] J.G. Owens, Patent: US 11/782,783 (2010).

[40] P.E. Rajtar, J.G. Owens, Patent: US 10/739,231 (2003).

[41] 3M™ Novec™ Thermal Management Fluids. https://multimedia.3m.com/mws/media/65495O/3mtm-thermal-management-fluids.pdf

[42] 3M™ Novec™ Engineered Fluids. HFE-7100 technical data. https://multimedia.3m.com/mws/media/199818O/3mtm-novectm-7100-engineered-fluid.pdf

[43] 3M™ Novec™ Engineered Fluids. HFE-7200 technical data. https://multimedia.3m.com/mws/media/199819O/3mtm-novectm-7200-engineered-fluid.pdf

Capítulo 2

TERMODINÁMICA DE SISTEMAS FLUIDOS MULTICOMPONENTES

2.1 Introducción.

Para introducir los conceptos fundamentales de la termodinámica de sistemas multicomponentes, nos basaremos en las consideraciones de *Van Ness y Abbot* [1]. De esta obra de referencia extraeremos aquellos párrafos y ecuaciones que nos ayuden a sintetizar los conocimientos necesarios para la compresión de los siguientes capítulos de esta tesis. El propósito de este capítulo es mostrar cómo se pueden determinar las propiedades volumétricas y termodinámicas de interés en las mezclas de fluidos a partir de las medidas experimentales.

2.2 Equilibrio líquido-vapor en mezclas multicomponentes.

Cualquier cambio que perturbe el estado de equilibrio de un sistema *PVT* se va a reflejar como un cambio en las propiedades termodinámicas del fluido contenido en ese sistema. Como consecuencia del primer y segundo principio de la termodinámica en sistemas cerrados, tenemos una ecuación fundamental que relaciona los cambios en las propiedades molares primarias: energía interna (*U*), volumen (*V*), y entropía (*S*).

$$dU^t = TdS^t - PdV^t \tag{1}$$

Donde el superíndice *t* es el indicador del total del sistema.

De esta forma tenemos que, siendo *n* el número de moles:

$$d(nU) = Td(nS) - Pd(nV) \tag{2}$$

Al igual que la ecuación (1), la ecuación (2) se puede aplicar a un sistema cerrado multifase. A partir de la ecuación (2) podemos se puede deducir que:

$$\left[\frac{\partial(nU)}{\partial(nS)}\right]_{nV,n} = T \tag{3}$$

$$\left[\frac{\partial(nU)}{\partial(nV)}\right]_{nS,n} = -P \tag{4}$$

Tiene más interés el caso más general de una única fase en el que n_i varía, bien ya sea como resultado del intercambio de materia con los alrededores (en el caso de un sistema abierto), ya sea como resultado de una reacción química que tenga lugar en el sistema, o como consecuencia de ambos. En este caso se puede asumir que el valor de la energía interna, *nU*, es función de n_i, de la misma forma que sucede para *nV* y *nS*:

$$nU = f(nS, nV, n_1, n_2, ...) \tag{5}$$

La diferencial total de *nU* es entonces:

$$d(nU) = \left[\frac{\partial(nU)}{\partial(nS)}\right]_{nV,n} d(nS) + \left[\frac{\partial(nU)}{\partial(nV)}\right]_{nS,n} d(nV) + \sum \left[\frac{\partial(nU)}{\partial(n_i)}\right]_{nS,nV,nj} dn_i \tag{6}$$

El potencial químico, μ_i se puede expresar como:

$$\mu_i \equiv \left[\frac{\partial(nU)}{\partial(n_i)}\right]_{nS,nV,nj} \tag{7}$$

De esta forma, la ecuación (6) puede reescribirse como:

$$d(nU) = Td(nS) - Pd(nV) + \sum \mu_i dn_i \tag{8}$$

Esta ecuación, que relaciona las propiedades fundamentales, conecta las variables termodinámicas primarias para un sistema *PVT* con una única fase, ya sea este abierto o cerrado. Todas las demás ecuaciones que relacionan las propiedades de cada sistema van a derivar de esta ecuación. El cambio en el valor del potencial químico μ_i, propiedad definida en la ecuación (7), es la fuerza conductora para el cambio químico, de la misma forma que el gradiente de temperaturas lo es para la transferencia de calor.

Consideremos ahora un sistema fluido formado por dos o más fases en equilibrio. Cada una de las fases puede considerarse como un sistema abierto al que se puede aplicar la ecuación (8). El equilibrio entre fases supone, en primer lugar, la uniformidad de la presión, *P*, y la temperatura, *T*, en todas las fases. Por otro lado, el principio de conservación de la masa aplicado a la transferencia de masa entre fases en el equilibrio, exige que se cumpla la igualdad del potencial químico de cada especie *i*, en cada una de las fases.

$$\mu_i^{\alpha} = \mu_i^{\beta} = ... = \mu_i^{\pi} \qquad (i = 1,2,...,n) \tag{9}$$

Esta condición de equilibrio tiene más posibilidades de aplicación práctica cuando se expresa en términos de fugacidad, f_i, en lugar de potencial químico, mediante la relación existente entre ambas, tal y como se describe en la referencia [1].

$$f_i^{\alpha} = f_i^{\beta} = ... = f_i^{\pi} \qquad (i = 1,2,...,n) \tag{10}$$

La fugacidad posee unidades de presión, ya que esta propiedad reemplaza a la presión, *P*, en la función de Gibbs aplicada a sistemas fluidos en una sola fase a temperatura constante:

$$dG_i = RTd \ln f_i \tag{11}$$

Donde G_i es la energía libre de Gibbs, y *R* es la constante universal de los gases.
La ecuación (11) también puede escribirse de la forma:

$$d \ln f_i = \frac{V_i}{RT} dP \tag{12}$$

Sustrayendo el término *dP/P* (≡ *d* ln*P*) a ambos lados de la ecuación (12), llegamos a:

$$d \ln(f_i / P) = -\frac{1}{RT}\left(\frac{RT}{P} - V_i\right) dP \tag{13}$$

El término *RT/P* es el volumen molar del gas ideal, V_i', mientras que el volumen residual se define como: $\Delta V_i'$ ($\equiv V_i' - V_i$). Sustituyendo en la ecuación (13) tenemos que:

$$d \ln(f_i / P) = -\frac{\Delta V_i'}{RT} dP \tag{14}$$

Integrando a temperatura constante desde una presión arbitraria de referencia (P^o), respecto a la presión actual, la expresión queda como sigue:

$$d \ln(f_i / P) = \ln(f_i / P)^o - \frac{1}{RT} \int_{P^o}^{P} \Delta V_i' dP \tag{15}$$

Si establecemos que P^o=0, y $(f_i/P)^o$=1 ó $\ln(f_i/P)^o$=0, llegamos a que:

$$\lim_{P\to 0}(f_i / P) = 1 \tag{16}$$

Por tanto:

$$\ln(f_i / P) = -\frac{1}{RT}\int_0^P \Delta V_i^{'} dP \tag{17}$$

Las ecuaciones (11) y (16) constituyen la definición de fugacidad para un líquido puro *i*, mientras que la ecuación (17) describe cómo el valor numérico de f_i se tiene que calcular a partir de la información *PVT* del fluido, que puede obtenerse experimentalmente. En esta misma ecuación, al término adimensional f_i/P se le conoce como coeficiente de fugacidad del componente puro *i*:

$$\phi_i \equiv f_i / P \tag{18}$$

En el caso del equilibrio líquido-vapor, tendremos una mezcla de dos o más componentes, así como la coexistencia de dos fases, líquida, cuya composición se denotará como x_i, y vapor, y_i. Expresando la fugacidad de uno de los componentes, sea este el componente *i*, y tomando como referencia el gas perfecto en el caso de ambas fases, líquida y vapor, la fugacidad se puede expresar de la siguiente manera [2]:

$$\begin{aligned} \hat{f}_i^{\,l} &= \hat{\phi}_i^{\,l} x_i P \\ \hat{f}_i^{\,v} &= \hat{\phi}_i^{\,v} y_i P \end{aligned} \tag{19}$$

Donde $\hat{f}_i^{\,l}$ es la fugacidad del componente *i* en la fase líquida en un sistema multifase y multicomponente, y $\hat{\phi}_i^{\,l}$ es el coeficiente de fugacidad en la fase líquida del componente *i* considerando también un sistema multifase y multicomponente. Ídem para la fase vapor.
Ya que se cumple que: $\hat{f}_i^{\,l} = \hat{f}_i^{\,v}$, expresando estas ecuaciones en función de los coeficientes de fugacidad:

$$x_i\hat{\phi}_i^{\,l} = y_i\hat{\phi}_i^{\,v} \qquad (i = 1,2,...,n) \tag{20}$$

Para la fase líquida, es más conveniente expresar la fugacidad en términos del coeficiente de actividad, γ_i del componente puro, el cual se define como:

$$\gamma_i \equiv \frac{\hat{f}_i}{x_i f_i^{\circ}} \tag{21}$$

Por tanto, se puede decir que:

$$\hat{f}_i^{\,l} = \gamma_i x_i f_i^{\circ}$$
$$\hat{f}_i^{\,v} = \hat{\phi}_i \, y_i P \tag{22}$$

Donde $\hat{\phi}_i$ omite el superíndice *v*, el cual hace referencia a la fase vapor, y f_i^o es la fugacidad en el estado de referencia.

De esta manera se puede decir que:

$$y_i \Phi_i P = x_i \gamma_i P_i^{sat} \qquad (i = 1,2,..., n) \tag{23}$$

Donde:

$$\Phi_i \equiv \hat{\phi}_i \, \frac{P_i^{sat}}{f_i} \tag{24}$$

La ecuación (23) se emplea ampliamente en la determinación experimental del equilibrio líquido-vapor a bajas presiones, y recibe la denominación de "*aproximación Gamma/Phi*". El coeficiente de actividad γ_i da cuenta de la desviación existente entre la idealidad y la realidad.
En la ecuación (24), f_i es la fugacidad del líquido puro *i*, a la presión *P* y temperatura *T* del sistema, y P_i^{sat} es la presión de vapor del componente puro *i*, a la temperatura de equilibrio. A bajas presiones se puede asumir que $\Phi_i = 1$, de igual manera que se puede asumir que:

a) La fase vapor es un gas ideal,
b) La fugacidad de la fase líquida es independiente de la presión.

Así la ecuación (23) podría escribirse de la siguiente forma:

$$y_i P = x_i \gamma_i P_i^{sat} \qquad (i = 1,2,...,n) \tag{25}$$

En el caso de una disolución ideal, el valor del coeficiente de actividad es igual a la unidad, así pues la ecuación (25) quedaría como sigue:

$$y_i P = x_i P_i^{sat} \qquad (i = 1,2,...,n) \tag{26}$$

Expresión la cual recibe el nombre de *Ley de Raoult*, y que expresa las relaciones del equilibrio líquido-vapor cuando la fase vapor se trata como un gas ideal, y cuando la fase líquida es una disolución ideal.

En este estudio se considerará que tanto la fase líquida como la fase vapor tienen un comportamiento no ideal. El comportamiento real de las mezclas, para el caso de sistemas binarios, puede presentar distintos tipos de alejamiento de la idealidad; los diagramas de equilibrio pueden representar un mínimo o un máximo, denominado azeótropo, punto en el cual las fases líquida y vapor presentan la misma composición ($x_1 = y_1$). La causa de este alejamiento de la idealidad en sistemas a bajas presiones suele ser el comportamiento no ideal de la fase líquida. En la Figura 1 se representan las gráficas *Txy* de tres sistemas binarios; el primero de ellos se comporta de acuerdo a la Ley de Raoult, y los dos siguientes presentan desviaciones (azeótropos).

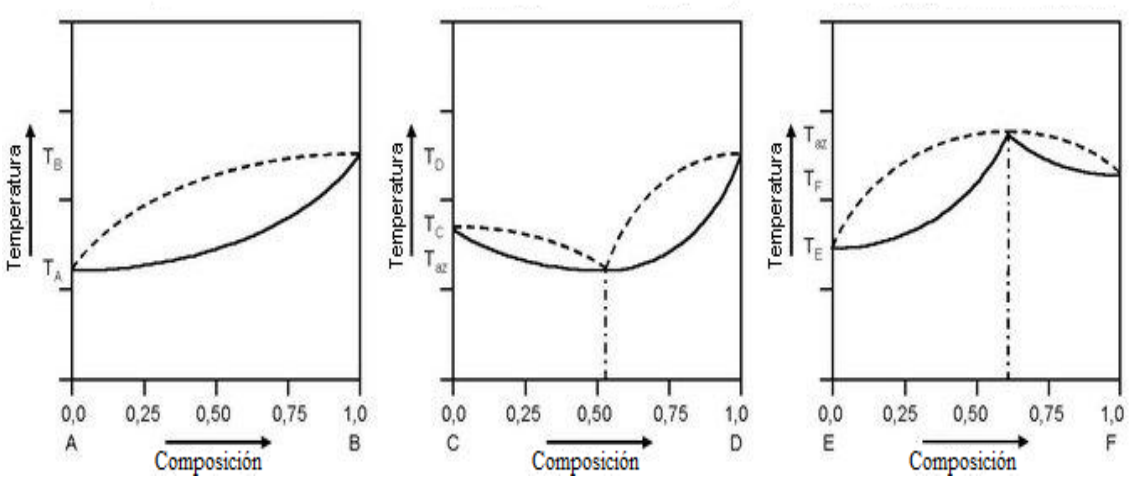

Figura 1. Diagramas temperatura composición. El primer diagrama por la izquierda muestra un comportamiento ideal, de acuerdo a la Ley de Raoult. El diagrama del centro muestra un azeótropo positivo o azeótropo de mínimo, mientras que el diagrama de la derecha muestra un azeótropo negativo o de máximo.

Así pues, partiendo de la ecuación (14), a temperatura constante, se puede establecer que:

$$d \ln f_i = \frac{V_i^L}{RT} dP \qquad (T \text{ constante}) \tag{27}$$

Donde V_i^L representa el volumen molar del componente puro *i*.

La integración desde el estado de líquido saturado al de líquido comprimido conduce a:

$$\ln \frac{f_i}{f_i^{sat}} = \frac{1}{RT} \int_{P_i^{sat}}^{P} V_i dP \tag{28}$$

Como V_i^L, el volumen molar de la fase líquida, es una función muy débil de *P* a temperaturas muy por debajo de la temperatura crítica, T_c, con frecuencia se obtiene una excelente aproximación cuando la evaluación de la integral se basa en la consideración de que V_i es constante e igual al valor para el líquido saturado. Sustituyendo $f_i^{sat} = \phi_i^{sat} P_i^{sat}$ y resolviendo para f_i ,se obtiene:

$$f_i = \phi_i^{sat} P_i^{sat} \exp \frac{V_i^L (P - P_i^{sat})}{RT} \tag{29}$$

Donde el término exponencial se conoce como el *factor de corrección de Poynting*.

Igualando las ecuaciones contenidas en (22), llegamos nuevamente a la ecuación (23), donde el coeficiente de fugacidad se puede expresar como:

$$\Phi_i = \frac{\hat{\phi}_i}{\phi_i^{sat}} \exp\left[- \frac{V_i^L (P - P_i^{sat})}{RT} \right] \tag{30}$$

En la ecuación (30), $\hat{\phi}_i$ es el coeficiente de fugacidad del componente *i* en cada fase, ϕ_i^{sat} es el valor del coeficiente de fugacidad a la temperatura de saturación, V_i^L es el volumen molar, P_i^{sat} es la presión de saturación, y *R* es la constante universal de los gases.

Los coeficientes de fugacidad $\hat{\phi}_i$ y ϕ_i^{sat} se determinan a partir de las siguientes ecuaciones:

$$\ln \hat{\phi}_i = \frac{P}{RT} \left[B_{ii} + \frac{1}{2} \sum_j \sum_k y_j y_k (2\delta_{ji} - \delta_{jk}) \right] \tag{31}$$

$$\ln \phi_i^{sat} = \frac{P^{sat}}{RT} B_{ii} \tag{32}$$

Donde B_{ii} son los segundos coeficientes del virial, y donde:

$$\delta_{ji} = 2B_{ji} - B_{jj} - B_{ii} \tag{33}$$

$$\delta_{jk} = 2B_{jk} - B_{jj} - B_{kk} \tag{34}$$

Despejando γ_i de la ecuación del equilibrio líquido-vapor, (23) tenemos que:

$$\gamma_i = \frac{y_i \Phi_i P}{x_i P_i^{sat}} \tag{35}$$

En el caso de una mezcla binaria, tenemos que la ecuación del equilibrio líquido-vapor viene dada por:

$$\ln \gamma_i = \ln \frac{y_i P}{x_i P_i^{sat}} + \frac{\left(B_{ii} - V_i^L\right)\left(P - P_i^{sat}\right)}{RT} + \frac{P}{RT}\left(1 - y_i\right)^2 \delta_{ji} \tag{36}$$

Que permite obtener:

$$\frac{(B_{ii} - V_i^L) \cdot (P - P_{sat})}{R \cdot T} + \frac{P}{R \cdot T} \cdot (1 - y_i)^2 \delta_{ji} = \ln \phi_i \tag{37}$$

La determinación de los segundos coeficientes del virial, B_{ii} *y* B_{jj}, que representan la interacción entre dos distintas moléculas, se ha llevado a cabo empleando el método de Tsonopoulos [3]. Este método emplea datos de propiedades críticas, factor acéntrico ω, el momento dipolar μ, y los parámetros de interacción polar *a* y *b*. Algunos de los datos necesarios no estaban disponibles en la literatura y han tenido que ser estimados mediante varios métodos, lo cual se describe en el apartado de resultados para el equilibrio líquido-vapor.

El segundo coeficiente de virial de la mezcla B_{ij}, se calcula según la metodología descrita en Assael *et al.* [4], donde el coeficiente cruzado de virial, B_{ij}=B_{ji}, es obtenido tras aplicar las reglas de mezcla de Lorentz-Berthelot a las propiedades críticas.

El volumen molar en las condiciones de líquido saturado del compuesto puro *i* V_i^L, se estima mediante la ecuación de Rackett [5], a partir de sus propiedades críticas:

$$V_i^{sat} = V_c Z_c^{(1-T/T_c)^{2/7}} \tag{38}$$

Donde V_c es el volumen crítico del componente, y Z_c es el valor del factor acéntrico para el componente estudiado. Una vez que la ecuación (35) permite evaluar, mediante los datos experimentales, los coeficientes de actividad de cada componente, la energía libre de Gibbs de exceso, G^E, se calcula a partir de estos valores de los coeficientes de actividad, y de las composiciones de la fase líquida:

$$\frac{G^E}{RT} = x_i \ln \gamma_i + x_j \ln \gamma_j \tag{39}$$

2.3 Propiedades de exceso.

El comportamiento termodinámico de las mezclas de fluidos suele estudiarse mediante las denominadas funciones de exceso. Estas funciones corresponden a las variaciones con respecto a un comportamiento ideal que muestran las propiedades físicas en una mezcla. Este "exceso" es el resultado de las interacciones moleculares que tienen lugar en el seno de la mezcla y que vienen dadas a su vez por los tipos de enlaces de las moléculas, por las fuerzas electrostáticas, las fuerzas de dispersión y repulsión, etc., que no tienen en cuenta los modelos de idealidad. Es imprescindible el conocimiento de estas propiedades de exceso y cómo éstas varían con la presión y la temperatura, y asimismo cómo pueden variar con respecto a cambios en la composición de alguno de los componentes. Esta información es crucial para el diseño de muchos de los sistemas de almacenamiento, transporte y utilización de fluidos industriales.

Si tomamos *M* como designación general de cualquiera de las propiedades termodinámicas, ya que la variación de estas propiedades está afectada por la composición, presión y temperatura, es mejor utilizar las cantidades en forma molar. De esta manera, cada una de estas propiedades debería escribirse en función de *nM*, donde *n* es el número de moles totales presentes en el sistema, y *M* es la propiedad molar general del fluido en el sistema. De esta manera, las funciones de exceso molares se pueden expresar como:

$$M_m^E = M_m^R - M_m^{id} \tag{40}$$

Donde M^E_m denota la propiedad molar de exceso, M^R_m es el valor de la propiedad de la mezcla real, y M^{id}_m es el valor de la propiedad en una mezcla ideal. El modo de definir la mezcla ideal varía según la propiedad de interés. Si, por ejemplo, $M^{id}_m = V^{id}_m$, el volumen molar de la mezcla ideal será [6]:

$$V^{id} = \sum_{i=1}^{n} x_i V_i \tag{41}$$

Donde V_i, es el volumen molar del componente *i*. El volumen de exceso se puede definir entonces a partir de la siguiente ecuación:

$$V^E = \sum_{i=1}^{n} x_i Mw_i \left(V - V_i\right) \tag{42}$$

Donde Mw_i, es la masa molar del componente *i*, *V*, es el volumen de la mezcla, y V_i, es el volumen molar del componente *i*.

De la misma manera se pueden definir otras propiedades termodinámicas de exceso, algunas de ellas representadas en la Tabla 1.

Además de las propiedades anteriores, también son de interés otras conocidas como propiedades derivadas. La determinación experimental de los datos *ρPT,* bien en componentes puros, bien en mezclas, se puede utilizar para determinar las anteriormente mencionadas propiedades termodinámicas derivadas: compresibilidad isoterma, κ_T, y expansividad isobárica, α_P, a partir de las siguientes expresiones [7]:

$$\kappa_T = -\frac{1}{V}\left(\frac{\partial V}{\partial T}\right)_T = \frac{1}{\rho}\left(\frac{\partial \rho}{\partial P}\right)_T \tag{43}$$

$$\alpha_P = \frac{1}{V}\left(\frac{\partial V}{\partial T}\right)_P = \frac{1}{\rho}\left(\frac{\partial \rho}{\partial T}\right)_P \tag{44}$$

Tabla 1. Relación de funciones termodinámicas para disoluciones. Extraído de [1].

M_i	H_i	$\ln f_i$	G_i
$\bar{M}_i$	$\bar{H}_i$	$\ln(\hat{f}_i / x_i)$	$\bar{G}_i \equiv \mu_i$
$M = \sum x_i \bar{M}_i$	$H = \sum x_i \bar{H}_i$	$\ln f = \sum x_i \ln(\hat{f}_i / x_i)$	$G = \sum x_i \bar{G}_i \equiv \sum x_i \mu_i$
$\bar{M} = M_i + m(x_i)$	$\bar{H}_i^{id} = H_i$	$\ln(\hat{f}_i^{id} / x_i) = \ln f_i$	$\bar{G}_i^{id} = G_i + RT \ln x_i$
$M_i^{id} = \sum x_i \bar{M}_i^{id}$	$H^{id} = \sum x_i H_i$	$\ln f^{id} = \sum x_i \ln f_i$	$G^{id} = \sum x_i G_i + RT \sum x_i \ln x_i$
$\Delta\bar{M}_i = \bar{M}_i - M_i$	$\overline{\Delta H}_i = \bar{H}_i - H_i$	$\overline{\Delta \ln f_i} = \ln(\hat{f}_i / x_i) - \ln f_i \equiv \ln \gamma_i$	$\Delta\bar{G}_i = \bar{G}_i - G_i \equiv RT \ln a_i$
$\Delta M = \sum x_i \overline{\Delta M}_i$	$\Delta H = \sum x_i \Delta\bar{H}_i = H - H_i^{id}$	$\Delta \ln f^{id} = 0$	$\Delta G = \sum x_i \overline{\Delta G}_i = RT \sum x_i \ln a_i$
$\overline{\Delta M}_i^{id} = \bar{M}_i^{id} - M_i$	$\overline{\Delta H}_i^{id} = 0$	$\Delta \ln f = \sum x_i \ln \gamma_i$	$\overline{\Delta G_i^{id}} = RT \ln x_i$
$\Delta M_i^{id} = \sum x_i \overline{\Delta M}_i^{id}$	$\Delta H^{id} = 0$	$\Delta \ln f^{id} = 0$	$\Delta G_i^{id} = RT \sum x_i \ln x_i$
$\bar{M}^E = \bar{M}_i - \overline{M_i^{id}}$	$\bar{H}_i^E = \bar{H}_i - H_i = \overline{\Delta H}_i$	$\left[\ln(\hat{f}_i / x_i)\right]^E = \ln(\hat{f}_i / x_i) - \ln f_i \equiv \ln \gamma_i$	$\bar{G}_i^E = RT \ln \gamma_i$
$M^E = \sum x_i \bar{M}_i^E$	$H^E = \sum x_i \overline{\Delta H}_i = \Delta H$	$\left(\ln f^E\right) = \Delta \ln f = \sum x_i \ln \gamma_i$	$G^E = RT \sum x_i \ln \gamma_i$

Para las propiedades termodinámicas derivadas, se define la mezcla ideal a partir de los valores de las propiedades de los componentes puros:

$$\kappa_T^{id} = \sum_{i=1}^{n} \phi_i \kappa_T, i \tag{45}$$

$$\alpha_P^{id} = \sum_{i=1}^{n} \phi_i \alpha_P, i \tag{46}$$

Donde:

$$\phi_i = \frac{x_i V_i}{\sum_{i=1}^{n} x_i V_i} \tag{47}$$

Los valores de las propiedades derivadas de exceso se pueden obtener directamente a partir de los valores del volumen molar de exceso, utilizando las siguientes ecuaciones:

$$\kappa_T^E = \left[\left(\frac{\partial V^E}{\partial P} \right)_T - V^E \sum_{i=1}^{n} \phi_i \kappa_T, i \right] / V \tag{48}$$

$$\alpha_P^E = \left[\left(\frac{\partial V^E}{\partial T} \right)_P - V^E \sum_{i=1}^{n} \phi_i \alpha_P, i \right] / V \tag{49}$$

Donde *V*, es el volumen molar de la mezcla.

En cuanto al resto de propiedades, y a modo de resumen, se puede indicar que los efectos de la presión a temperatura constante sobre la función energía libre de Gibbs de exceso, ΔG^E, la contribución entrópica a la función de exceso de Gibbs, $T\Delta S^E$, y la entalpía molar de exceso, ΔH^E, se pueden evaluar a partir de los datos de volumen molar de exceso:

$$\Delta G^E = G^E(T, P, x_i) - G^E(T, P^o, x_i) = \int_{P^o}^{P} V^E(T, P, x_i) dP \tag{50}$$

$$T\Delta S^E = TS^E(T, P, x_i) - TS^E(T, P^o, x_i) = \int_{P^o}^{P} -T(\partial V^E / \partial T)_P \, dP \tag{51}$$

$$\Delta H^E = H^E(T, P, x_i) - H^E(T, P^o, x_i) = \int_{P^o}^{P} \left[V^E - T\left(\partial V^E / \partial T\right)P \right] dP \tag{52}$$

Donde P^o es la presión de referencia.

1.4 Definiciones termodinámicas de la velocidad del sonido.

En la sección anterior se definieron las propiedades termodinámicas derivadas, compresibilidad isoterma, κ_T, y expansividad isobárica, α_P, en las ecuaciones (43) y (44) respectivamente. Estas propiedades pueden ser determinadas a partir de datos experimentales de ρPT, e igualmente pueden ser obtenidas a partir de los datos experimentales de velocidad del sonido, *c*, mediante integración. La relación entre la velocidad del sonido y estas propiedades derivadas comprende un conjunto de ecuaciones diferenciales parciales de segundo orden [8],

que, para el caso de los líquidos, permite obtener una solución particular a partir de medidas experimentales directas de propiedades volumétricas y de capacidades caloríficas [9].

Otra propiedad derivada es la compresibilidad isoentrópica, κ_S, propiedad que indica los cambios que experimenta el volumen cuando la presión cambia mientras la entropía permanece constante, y que se expresa como:

$$\kappa_S = -\frac{1}{v}\left(\frac{\partial v}{\partial P}\right)_S = \frac{1}{\rho}\left(\frac{\partial \rho}{\partial P}\right)_S \tag{53}$$

La compresibilidad isoentrópica está relacionada con la velocidad a la que las ondas de sonido viajan en la sustancia considerada, así pues, la medida de dicha velocidad es útil para determinar la compresibilidad isoentrópica. Esta velocidad, denominada velocidad del sonido, *c*, se puede determinar a partir de la ecuación (54):

$$c = \sqrt{-v^2\left(\frac{\partial P}{\partial v}\right)_S} = \sqrt{\left(\frac{\partial P}{\partial \rho}\right)_S} \tag{54}$$

La velocidad del sonido está a su vez relacionada con la compresibilidad isoentrópica, κ_S. Teniendo en cuenta que:

$$\left(\frac{\partial P}{\partial v}\right)_S \left(\frac{\partial v}{\partial P}\right)_S = 1 \tag{55}$$

De acuerdo con lo expuesto en las ecuaciones (53 - 55), a través de la siguiente expresión es posible obtener la relación entre la velocidad del sonido y la compresibilidad isoentrópica:

$$c = \frac{1}{\sqrt{\rho \cdot \kappa_S}} \tag{56}$$

Las propiedades derivadas también están relacionadas con otras propiedades termodinámicas, como son las capacidades caloríficas a presión constante, c_p, y a volumen constante, c_v. De acuerdo con la referencia [10], se puede establecer lo siguiente:

$$(c_p - c_V)dT = T\left(\frac{\partial P}{\partial T}\right)_V dv + T\left(\frac{\partial v}{\partial T}\right)_P dP \tag{57}$$

Considerando que $P = P(T,v)$, la diferencial de P se puede expresar de la siguiente manera:

$$dP = \left(\frac{\partial P}{\partial T}\right)_V dT + \left(\frac{\partial P}{\partial v}\right)_T dv \tag{58}$$

Si se elimina dP, y se agrupan los términos, obtenemos que:

$$\left[(c_p - c_V) - T\left(\frac{\partial v}{\partial T}\right)_P \left(\frac{\partial P}{\partial T}\right)_V dP\right] dT = T\left[\left(\frac{\partial v}{\partial T}\right)_P \left(\frac{\partial P}{\partial v}\right)_T + \left(\frac{\partial P}{\partial T}\right)_V\right] dV \tag{59}$$

Temperatura y volumen específico varían independientemente, por tanto, los coeficientes de las diferenciales en esta expresión han de anularse:

$$c_p - c_V = T\left(\frac{\partial P}{\partial T}\right)_V \left(\frac{\partial v}{\partial T}\right)_P \tag{60}$$

$$\left(\frac{\partial P}{\partial T}\right)_V = -\left(\frac{\partial v}{\partial T}\right)_P \left(\frac{\partial P}{\partial v}\right)_T \tag{61}$$

Sustituyendo la ecuación (61) en (60) llegamos a la siguiente expresión:

$$c_p - c_V = -T\left(\frac{\partial P}{\partial v}\right)_T \left(\frac{\partial v}{\partial T}\right)_P^2 \tag{62}$$

Esta ecuación se puede relacionar con la compresibilidad isotérmica, κ_T, descrita en la ecuación (43), y con la expansividad isobárica, α_P, expresada en la ecuación (44), de forma que la diferencia de calores específicos se pueda expresar como:

$$c_p - c_V = v\frac{T\alpha_P^2}{\kappa_T} \tag{63}$$

A su vez, los calores específicos están relacionados con la velocidad del sonido. Tomando la ecuación (54), y ayudándonos de la siguiente relación termodinámica [10] y [11]:

$$\left(\frac{\partial P}{\partial \rho}\right)_S = \frac{c_P}{c_V}\left(\frac{\partial P}{\partial \rho}\right)_T \tag{64}$$

La ecuación (54) pasaría a expresarse como:

$$c = \sqrt{\frac{c_P}{c_V}\left(\frac{\partial P}{\partial \rho}\right)_T} \tag{65}$$

En el caso de disponer únicamente de datos de capacidad calorífica a presión constante, c_P, a partir de la ecuación (62) se puede extraer el término c_V:

$$c_V = c_P - T\left(\frac{\partial P}{\partial v}\right)_T\left(\frac{\partial v}{\partial T}\right)_P^2 \tag{66}$$

Sustituyendo la ecuación (66) en (65), tenemos que la expresión para el cálculo de la velocidad del sonido queda de la siguiente manera:

$$c = \sqrt{\left(\frac{\partial P}{\partial \rho}\right)_T - \frac{c_P T}{\rho^2}\left(\frac{\partial P}{\partial T}\right)_\rho^2} \tag{67}$$

De este modo, con los datos experimentales ρPT, y C_p, se puede calcular la velocidad del sonido, c.

1.5 Referencias.

[1] H.C. Van Ness, M.M. Abbott, Classical thermodynamics for nonelectrolite solutions with applications to phase equilibria, 1st ed. McGraw-Hill, USA (1982).

[2] L. Contat, A. Vallés, A. Ribes, Cuaderno guía 4: equilibrio líquido-vapor en sistemas multicomponentes, ed. UPV, Valencia (2003).

[3] C. Tsonopoulos, AIChE Journal, 20 (1974) 263-272.

[4] M.J. Assael, J.P.M. Trusler, T.F. Tsolakis, Thermophysical properties of fluids. An introduction to their prediction, Imperial College Press, London (1996).

[5] H.G. Rackett, J. Chem. Eng. Data 15 (1970) 514.

[6] J.V. Sengers, R.F. Kayser, C.J. Peters, H.J. White Jr., Equations of state for fluids and fluid mixtures, Part 1. Ed. Elsevier, Amsterdam (2000).

[7] E. Wilhelm, T. Letcher, Volume properties: liquids, solutions and vapours, 1st ed. Royal Society of Chemistry, Cambridge, U.K. (2015).

[8] J.P.M. Trusler, Physical acoustics and metrology of fluids, Adam Hilger, Bristol, U.K. (1991).

[9] M. Bijedić, S. Begić, J. Thermodyn. 2016 (2015) 1-8.

[10] M.J. Moran, H.N. Shapiro, Fundamentos de termodinámica técnica, ed. Reverté, Barcelona, España (1995).

[11] M. Bijedić, S. Begić, J. Thermodyn. 2014 (2014) 1-5.

Capítulo 3

DETERMINACIÓN EXPERIMENTAL DEL EQUILIBRIO LÍQUIDO-VAPOR ISÓBARO

3.1 Introducción.

La determinación del equilibrio líquido-vapor, ELV por sus siglas en inglés, (Vapor-Liquid Equilibrium), tiene una de sus su principales aplicaciones en el diseño de equipos de separación como por ejemplo las columnas de fraccionamiento, en las que se pone en contacto una fase líquida y una vapor, y también en el diseño de plantas de refrigeración, donde el fluido refrigerante, ya sea un compuesto puro, o una mezcla zeotrópica o azeotrópica, cambia de estado a lo largo de su ciclo de trabajo, ya sea por compresión o por absorción.

Para poder determinar los datos de equilibrio líquido-vapor es necesario conocer la presión, P, y temperatura, T, a las que sucede el equilibrio termodinámico, así como la composición de las fases líquida (x_1) y vapor (y_1). A partir de estos datos se determinan los coeficientes de actividad (γ_1 y γ_2) de los distintos fluidos que toman parte en el equilibrio líquido-vapor, los coeficientes de fugacidad (ϕ_1 y ϕ_2), así como el valor de la energía libre de Gibbs, G^E, la cual da cuenta de la espontaneidad de los procesos.

La determinación del equilibrio líquido-vapor puede hacerse a través de varios métodos, dependiendo del tipo de datos de equilibrio que se quieran obtener (isobáricos o isotérmicos), del rango de presiones y temperaturas de trabajo, y de la propia naturaleza del sistema del que se quieren obtener los datos de equilibrio. Los principales métodos se enumeran a continuación:

1. Método de destilación.
2. Método de flujo.
3. Método estático.
4. Método dinámico o de circulación.

El método de destilación se basa en destilar una pequeña cantidad de líquido de un matraz destilador que contiene una cantidad grande de mezcla líquida de composición conocida, de forma que la composición de la mezcla líquida permanezca prácticamente constante. El análisis del destilado dará la composición del vapor en equilibrio con la mezcla introducida inicialmente en el matraz destilador.

En el método de flujo una corriente estacionaria de líquido en ebullición y otra de vapor sobrecalentado de composición conocida y constante se introducen en una celda de equilibrio donde se procede a su separación y análisis.

En el método estático de determinación del equilibrio líquido-vapor, la mezcla se carga o se prepara directamente en un recipiente cerrado al que previamente se le ha hecho el vacío. El recipiente está inmerso en un baño termostático y se agita hasta que se establece el equilibrio entre

el líquido y el vapor. Es el método más utilizado para la obtención de datos de equilibrio líquido-vapor isotérmicos.

Por último, el método dinámico o de circulación se basa en la circulación del vapor que se ha formado en un matraz hacia otro matraz en el que condensa completamente. Una vez en este segundo matraz, el condensado volverá al primer matraz, donde mediante una fuente de calor volverá a la fase vapor. Este proceso continuará hasta que se alcance el estado estacionario, en el cual las composiciones de vapor del primer matraz (y_1) la líquida del segundo (x_1) permaneciesen invariantes.

Este último método es el que se ha empleado en la determinación de los equilibrios líquido-vapor en el Laboratorio de Ingeniería Energética de la Universidad de Burgos: método de circulación en el que la determinación de la composición de las fases líquida y vapor (x_1 e y_1) se hace a una presión fija (método isóbaro), obteniéndose por tanto distintas temperaturas de ebullición, T_b, para cada dato de composición.

3.2 Técnica experimental de medida del equilibrio líquido-vapor isóbaro.

El equipo destinado a la determinación del equilibrio líquido-vapor isóbaro es un ebullómetro de la marca Fischer GmbH, modelo VLE Labodest 602S, el cual a su vez posee varios elementos de control, medida y regulación. Este aparato permite realizar medidas en el rango de presiones (0.1 - 300) kPa, y en el rango de temperaturas (273.15 - 523.15) K. La Figura 1 muestra una imagen de conjunto del equipo experimental para la determinación del equilibrio líquido-vapor.

Figura 1. Equipo experimental para la determinación del equilibrio líquido-vapor Fischer Labodest 602S.

El equipo, como se dijo en la sección anterior, emplea el método dinámico o de circulación para la determinación de la temperatura de ebullición a cada composición (x, y) a una presión fija. En la Figura 2 se puede ver un esquema del ebullómetro en sí, con cada uno de sus componentes.

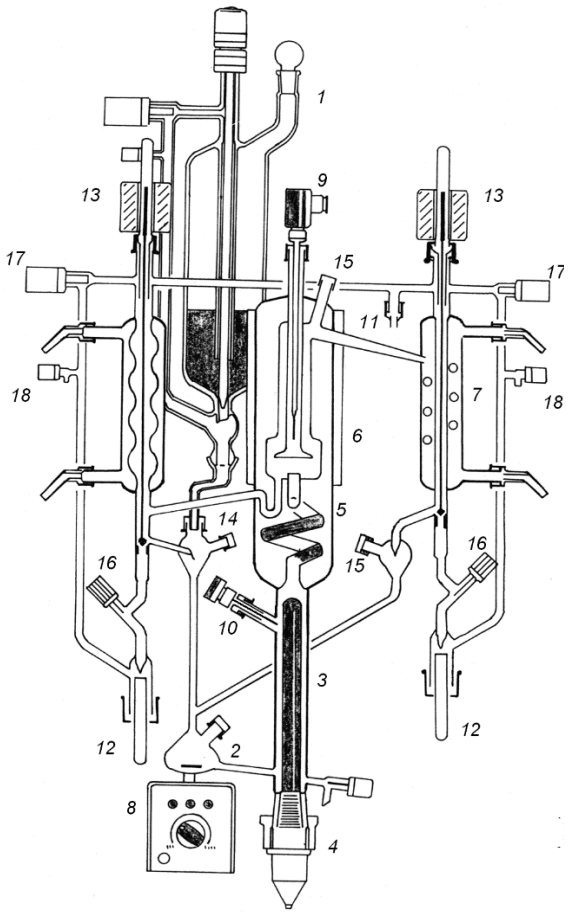

1. Depósito de alimentación
2. Matraz mezclador
3. Tubo de vidrio
4. Resistencia eléctrica
5. Bomba Cottrell
6. Pantalla deflectora
7. Condensador
8. Agitador magnético
9. Termoresistencia Pt100 (fase vapor)
10. Termoresistencia Pt100 (fase líquida)
11. Rosca de vidrio
12. Viales recogida muestras
13. Válvulas magnéticas
14. Tapón recogida muestras fase líquida
15. Tapón recogida muestras fase vapor
16. Llaves de cierre
17. Laves para equilibrado de presiones
18. Llaves de venteo

Figura 2. Esquema del ebullómetro VLE Fischer Labodest 602S.

En este dispositivo, el reservorio de alimentación (1) se llena con el fluido a medir, más o menos unos 150 cm^3, y mediante la llave de vaciado que posee en su parte inferior se deja que llene a su vez las zonas correspondientes al matraz mezclador (2) y el tubo de vidrio (3), hasta una altura determinada, intentando no embeber la bomba Cottrell (5). Gracias a una resistencia eléctrica (4), el fluido se calienta. En este punto, uno de los dispositivos de regulación permite determinar la potencia de la misma, a fin de llevar el fluido a su temperatura de ebullición. Cuando el fluido llega a esta temperatura, empieza a generarse vapor, el cual arrastra parte del líquido hacia la bomba Cottrell (5), donde se va a producir un contacto íntimo entre las fases líquida y

vapor. Una vez estas fases están en equilibrio, se separan en una cámara que contiene una pantalla deflectora (6) para prevenir el arrastre de gotas de líquido con la fase vapor. El vapor asciende hasta el condensador (7) situado a la derecha. Una corriente de agua fría, impulsada por un baño termostático Julabo modelo F12-ED, circula por la parte interior del serpentín del condensador (7), haciendo que el vapor pase a la fase líquida, y por gravedad descienda y pase nuevamente al matraz mezclador (2). Las muestras se podrán recoger una vez se haya llegado al equilibrio, por un lado la muestra de la fase vapor (derecha), y por el otro la de la fase líquida (izquierda). Para efectuar la recogida el sistema dispone de sendas válvulas magnéticas de apertura (13), las cuales abren el circuito para permitir la circulación del fluido hasta los viales recogemuestras (12).
El equipo dispone también de una manta calefactora envolviendo la bomba Cottrell y el circuito de retorno a fin de mantener la temperatura cuando se trabaja con sustancias con un alto punto de fusión.

La temperatura se mide gracias a dos sondas Pt100, situadas una de ellas cerca del tubo de vidrio (3), en contacto con la muestra en fase líquida, y otra en la parte superior de la bomba Cotrell (5), manteniendo contacto con la fase vapor. Estas dos sondas proporcionan por tanto las temperaturas de las fases líquida y vapor. Las dos sondas están conectadas a 4 hilos a un sistema de control, y poseen una incertidumbre en la medida de la temperatura de ±0.03 K.

La Figura 3 muestra una imagen de los sistemas de regulación del ebullómetro. En la parte superior derecha se observa el sistema de control Fischer, desde el cual puede realizarse la lectura de temperatura de las dos sondas Pt100. Este mismo sistema es el que permite realizar la regulación de la potencia de la resistencia eléctrica. En la parte inferior derecha de la imagen puede observarse el sistema de regulación de temperatura de las dos mantas calefactoras, mientras que a la izquierda se sitúa el equipo de presurización marca Mensor, modelo CPC 3000. Mediante este sistema se selecciona la presión a la cual se desean realizar las medidas. La medida de la presión es realizada por dos sensores de presión, uno barómetrico WIKA CPC 3000 (en el rango 80 - 120 kPa abs, resolución 0.01 kPa, incertidumbre 0.010%) y otro manométrico CPC 3000 (rango 0 - 500 kPa, resolución 0.001 kPa, incertidumbre 0.025%). Para trabajos a presiones inferiores a la atmosférica el sistema dispone de una conexión con una bomba de vacío; el sistema regula en todo momento de forma automática la presión para que se mantenga estable. De la misma forma, a fin de trabajar a presiones superiores a la atmosférica el sistema de presurización está conectado con una toma que proporciona un flujo de N_2 hacia el ebullómetro el cual generará la presión suficiente en el sistema.

Figura 3. Dispositivos de regulación y control de presión y temperatura del ebullómetro.

3.2.1 Técnica auxiliar: densimetría a presión atmosférica.

Una vez son recogidas las muestras de ambas fases, líquida y vapor, se desconoce la composición de las mismas y, por tanto, ésta se ha de determinar. En este caso, la determinación se hace de forma indirecta, esto es, determinando la composición a partir de la medida de alguna propiedad del fluido, como por ejemplo la densidad. La densidad de ambas fases, considerando la misma temperatura y presión, variará en función de la composición; la fase vapor será más rica en el componente más volátil, mientras que la fase líquida lo será en el componente con una temperatura de ebullición más alta.

El aparato aquí empleado para la determinación de la densidad es un densímetro de tubo vibrante (VTD) Anton Paar DSA 5000. En este tipo de densímetro la determinación del valor de la densidad se hace a partir del periodo de oscilación de un tubo en forma de U que contiene el fluido. La masa del tubo, junto con la masa de la muestra vibrarán en una frecuencia determinada, cuyo inverso es el periodo. La frecuencia de vibración natural del tubo en U será entonces:

$$f = \frac{1}{2\pi}\sqrt{\frac{K}{m}} \tag{1}$$

Donde f es la frecuencia de resonancia, m es la masa del oscilador y K es la constante elástica.

La masa del oscilador es la del tubo en U y la de la muestra del líquido contenida en él.

$$m = m_o + \rho \cdot V \tag{2}$$

Siendo m_o la masa del tubo oscilante, ρ la densidad del líquido y V el volumen del tubo en forma de U.

Sustituyendo en la ecuación (1) tenemos que:

$$f = \frac{1}{2\pi}\sqrt{\frac{K}{m_o + \rho \cdot V}} \tag{3}$$

A partir de la cual se puede obtener la densidad:

$$\rho = -\frac{m_o}{V} + \frac{K}{4\pi^2 V}\tau^2 \tag{4}$$

Donde τ es el periodo de oscilación del tubo con la muestra. A partir de aquí podemos decir que:

$$A = \frac{K}{4\pi^2 V} \tag{5}$$

$$B = \frac{m_0}{V} \tag{6}$$

De esta forma, la densidad será:

$$\rho = A(T,P) \cdot \tau^2 + B(T,P) \tag{7}$$

Donde *A(T, P)* y *B(T, P)* son los parámetros de calibración del aparato.

El tubo en U está hecho de vidrio de borosilicato el cual a su vez se encuentra en un cilindro de vidrio. Entre este cilindro y el tubo en U hay un gas con una elevada conductividad térmica y una baja densidad, a fin de no ocasionar amortiguamiento en las oscilaciones del tubo. El rango de medida de densidades de este aparato es de (0 – 3) gr·cm^{-3}, con una resolución de 10^{-6} gr·cm^{-3}, y con una precisión ± $2 \cdot 10^{-5}$ gr·cm^{-3}. Una imagen del mismo puede verse en la Figura 4.

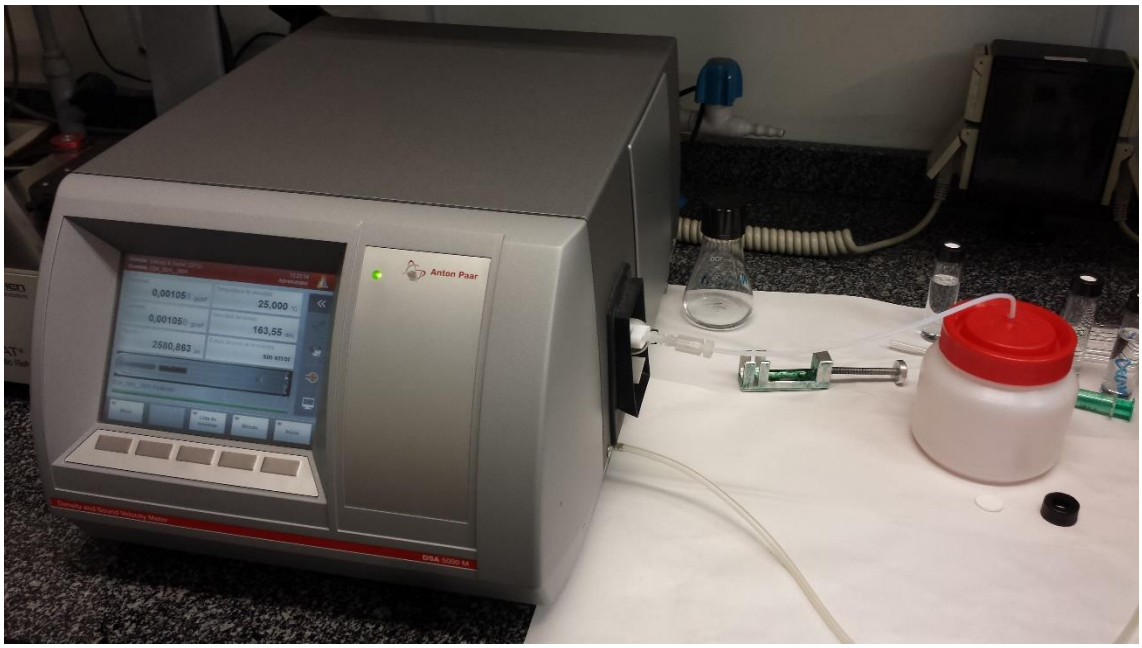

Figura 4. Densímetro de tubo vibrante Anton Paar DSA 5000.

La medida de la temperatura la proporciona una sonda Pt100 directamente inserta en el tubo de medida, mientras que el sistema de regulación de la misma proporciona una estabilidad en temperatura mejor que 0.01 K.

Este aparato es capaz también de proporcionar el dato de la velocidad del sonido, *c*, de la muestra introducida a la vez que determina la densidad empleando el mismo principio; a partir de la excitación producida en el tubo vibrante por una señal acústica es posible determinar la frecuencia de resonancia del fluido. Este método, denominado de determinación de la velocidad del sonido a partir de fenómenos de resonancia, obtiene el valor de *c* teniendo en cuenta la geometría del tubo, y la propagación de la onda en el fluido. La precision en la medida de la velocidad del sonido de este aparato es de ±0.5 $m \cdot s^{-1}$, mientras que su incertidumbre se estima en ±1 $m \cdot s^{-1}$.

La calibración del aparato, para poder determinar las constantes *A(T, P)* y *B(T, P)* se realiza una vez por semana con aire ambiental y agua bidestilada (miliQ), ya que la densidad de estos dos fluidos es bien conocida en los rangos de temperatura y presión medidos. A fin de comparar los resultados, se utilizan los proporcionados por la referencia [1].

3.3 Procedimiento experimental de medida.

El primer paso para comenzar con la experimentación corresponde al llenado del reservorio de alimentación con un volumen de unos 150 cm^3 de fluido, dejando pasar unos 75 cm^3

al interior del ebullómetro. Se comienza con los fluidos puros, determinando la curva de saturación para cada uno de ellos. Para ello se determina la temperatura de ebullición T_b del fluido puro a distintas presiones en un intervalo suficiente como para tener un amplio conjunto de datos experimentales. Tras haber finalizado las medidas completas con el fluido puro, se hace necesario vaciar el aparato y hacer vacío durante al menos una hora o hasta que la presión "de vacío" sea lo suficientemente baja, aproximadamente de 5 mbar. Después se vuelve a llenar el aparato con algún fluido de limpieza como puede ser 2-Propanol o con el mismo que se va a medir, a fin de hacer una homogeneización, se lleva a ebullición durante una media hora, se deja enfriar, y se vacía nuevamente. Posteriormente se hace vacío una vez más, y ya se rellena el reservorio con el compuesto a medir. Cuando lo que se desea es determinar el equilibrio líquido-vapor de una mezcla, comenzamos llenando todo el reservorio con el fluido puro 1, e iremos adicionando poco a poco el segundo fluido, 2. El sistema de refrigeración por agua estará conectado, así como los controles de presión y temperatura, y la potencia de la resistencia será la suficiente como para asegurar que el fluido llega a la ebullición. El aparato dispone de un imán agitador en el matraz mezclador encargado de mezclar los dos (o más) componentes que se encuentran en la mezcla. Una vez empezamos a tener generación de fase vapor, se espera unos 30 minutos a llegar al estado estacionario. Una vez alcanzado éste, debe existir un flujo pulsante continuo en el retorno de la fase líquida al matraz mezclador y producción de condensado de la fase vapor de 1-2 gotas por segundo, dependiendo de la viscosidad y tensión superficial del fluido.

Cuando la temperatura de la fase vapor esté estable, se esperan unos 15 minutos hasta proceder a tomar las muestras, para lo cual se disponen los dos viales (líquido y vapor) en la parte inferior del ebullómetro. El paso de la recogida de muestras es crítico, ya que habitualmente se tiende a recoger antes la fase líquida (flujo en chorro) que la de vapor (goteo). En este punto es importante que la temperatura permanezca constante; si ésta varía, lo hará también la composición de las fases. El volumen de muestras que se recoge es de unos 3 cm^3 por cada vial.

Después de tomar las muestras, la potencia de la resistencia se reduce a cero, y se recarga nuevamente el aparato con más fluido procedente del reservorio. Al alcanzar una concentración del 50%, es necesario eliminar totalmente el contenido del equipo mediante la llave de vaciado, limpiar, realizar vacío y volver a llenar, empezando con el segundo compuesto puro.

Las muestras se dejan enfriar, se desgasifican durante 10 minutos y posteriormente se introducen en el densímetro DSA 5000, donde se determinará su densidad a la presión atmosférica y a 298.15 K.

La determinación de la concentración de las muestras extraídas de las fases líquida y vapor se realiza a partir de las ecuaciones de calibrado y de la densidad con respecto a la concentración resultante de las medidas sobre el mismo sistema que se han hecho previamente. El ajuste de las curvas se ha realizado por el método de mínimos cuadrados a una función polinómica de la forma:

$$\rho(x_1) = A_0 + A_1 x_1 + A_2 x_1^{\,2} + A_3 x_1^{\,3} + ... \qquad (8)$$

El número de parámetros A_i, a emplear se optimiza empleando el test-F [2]. Para cada sistema binario se midieron las densidades de los fluidos puros y de sus mezclas preparadas a diversas concentraciones. Cada mezcla se preparó inmediatamente antes de su medida, mediante pesadas de cada uno de los componentes en viales de vidrio de 15 cm^3 de volumen, llenos y herméticamente cerrados a fin de evitar evaporaciones. Para medir la masa se ha utilizado una balanza Mettler Toledo modelo MS-204S, con resolución de 10^{-4} g, y con una incertidumbre de ±0.0001 gr. La incertidumbre estimada en fracción molar de estas muestras es de ±0.00005.

3.4 Ajuste de los datos experimentales.

Los datos experimentales proporcionados por el equilibrio líquido-vapor nos dan la presión a la que se han realizado las medidas *P*, las composiciones tanto de la fase líquida como de la fase vapor de los dos componentes en el caso del ELV binario, x_1, x_2, y_1, y_2, y las temperaturas de ebullición correspondientes a cada par de composiciones, líquida y vapor. A partir de estos datos experimentales es posible correlacionar los mismos, caso de las presiones de vapor, así como es posible determinar otros datos de interés como son los coeficientes de actividad (γ_1 y γ_2), los coeficientes de fugacidad (ϕ_1 y ϕ_2), y la energía libre de Gibbs de exceso G^E.

En el caso de la obtención de las presiones de vapor de los compuestos puros, se ha establecido una correlación a partir de la ecuación de Antoine, la cual estima el valor de la presión de saturación, P^{sat} a partir de la temperatura de ebullición T_b del fluido, y de los parámetros *A, B* y *C* obtenidos aplicando el método de los mínimos cuadrados a partir de los datos experimentales. La ecuación es la siguiente:

$$\log P^{sat} = A - \frac{B}{T_b + C} \qquad (9)$$

Para la determinación tanto de los coeficientes de actividad, γ como los coeficientes de fugacidad, ϕ se ha considerado que tanto la fase vapor como la fase líquida no tienen un comportamiento ideal, siguiéndose el procedimiento descrito en la Sección 2.2 del Capítulo 2.

Los datos experimentales se han correlacionado a distintos modelos matemáticos de composición local, como son los de NRTL (Non-Random Two Liquids), [3], Wilson, [4], y

UNIQUAC (UNIversal QUAsi Chemical), [5]. Así mismo, en una de las mezclas binarias que se han estudiado (*x* HFE-7500 + (1-*x*) Diisopropil éter), se ha aplicado el modelo predictivo de UNIFAC (UNIQUAC Functional-group Activity Coefficients), [6] al estar disponibles en la literatura los datos de todos los grupos funcionales necesarios para aplicarlo. Este método de contribución de grupos considera que la molécula está dividida en grupos funcionales donde las interacciones molécula-molécula se estiman por medio de sumas de interacciones grupo-grupo.
Para la determinación de las correlaciones, en el modelo de NRTL, el cálculo de la energía libre de Gibbs es como sigue:

$$\frac{G^E}{RT} = x_i x_j \left(\frac{\tau_{ji} G_{ji}}{x_i + x_j G_{ji}} + \frac{\tau_{ij} G_{ij}}{x_j + x_i G_{ij}} \right) \tag{10}$$

Mientras que los coeficientes de actividad se calculan a partir de:

$$\ln \gamma_i = x_j^2 \left[\tau_{ji} \left(\frac{G_{ji}}{x_i + x_j G_{ji}} \right)^2 + \frac{\tau_{ij} G_{ij}}{(x_j + x_i G_{ij})^2} \right] \tag{11}$$

$$\ln \gamma_j = x_i^2 \left[\tau_{ij} \left(\frac{G_{ij}}{x_j + x_i G_{ij}} \right)^2 + \frac{\tau_{ji} G_{ji}}{(x_i + x_j G_{ji})^2} \right] \tag{12}$$

Donde τ_{ij}, τ_{ji}, G_{ij} y G_{ji} son los parámetros ajustables.

En el modelo de Wilson, la energía libre de Gibbs y los coeficientes de actividad se calculan a partir de:

$$\frac{G^E}{RT} = -x_i \ln(x_i + \Lambda_{ij} x_j) - x_j \ln(x_j + \Lambda_{ji} x_i) \tag{13}$$

$$\ln \gamma_i = -\ln(x_i + \Lambda_{ij} x_j) + x_j \left(\frac{\Lambda_{ij}}{x_i + \Lambda_{ij} x_j} - \frac{\Lambda_{ji}}{\Lambda_{ji} x_i + x_j} \right) \tag{14}$$

$$\ln \gamma_j = -\ln(x_j + \Lambda_{ji} x_i) + x_i \left(\frac{\Lambda_{ij}}{x_i + \Lambda_{ij} x_j} - \frac{\Lambda_{ji}}{\Lambda_{ji} x_i + x_j} \right) \tag{15}$$

Donde Λ_{ij} y Λ_{ji} son los parámetros ajustables.

La determinación de la energía libre de Gibbs en el modelo de UNIQUAC tiene dos contribuciones: la parte combinatoria que intenta describir la contribución entrópica dominante, y la parte residual, debida principalmente a las fuerzas intermoleculares, las cuales son responsables de la entalpía de mezcla:

$$\frac{G^E}{RT} = \left(\frac{G^E}{RT}\right)_{combinatorio} + \left(\frac{G^E}{RT}\right)_{residual} \tag{16}$$

$$\left(\frac{G^E}{RT}\right)_{combinatorio} = x_i \ln\frac{\phi_i^*}{x_i} + x_j \ln\frac{\phi_j^*}{x_j} + \frac{z}{2}\left(x_i q_i \ln\frac{\theta_i}{\phi_i^*} + x_j q_j \ln\frac{\theta_j}{\phi_j^*}\right) \tag{17}$$

$$\left(\frac{G^E}{RT}\right)_{residual} = -x_i q_i' \ln\left(\theta_i' + \theta_j' \tau_{ji}\right) - x_j q_j' \ln\left(\theta_j' + \theta_i' \tau_{ij}\right) \tag{18}$$

Mientras que los coeficientes de actividad se calculan a partir de:

$$\begin{aligned} \ln\gamma_i &= \ln\frac{\phi_i^*}{x_i} + \frac{z}{2} q_i \ln\frac{\theta_i}{\phi_i^*} + \phi_j^*\left(l_i - \frac{r_i}{r_j} l_j\right) \\ &- q_i' \ln\left(\theta_i' + \theta_j' \tau_{ji}\right) + \theta_j' q_i'\left(\frac{\tau_{ji}}{\theta_i' + \theta_j' \tau_{ji}} - \frac{\tau_{ij}}{\theta_j' + \theta_i' \tau_{ij}}\right) \end{aligned} \tag{19}$$

$$\begin{aligned} \ln\gamma_j &= \ln\frac{\phi_j^*}{x_j} + \frac{z}{2} q_j \ln\frac{\theta_j}{\phi_j^*} + \phi_i^*\left(l_j - \frac{r_j}{r_i} l_i\right) \\ &- q_j' \ln\left(\theta_j' + \theta_i' \tau_{ij}\right) + \theta_i' q_j'\left(\frac{\tau_{ij}}{\theta_j' + \theta_i' \tau_{ij}} - \frac{\tau_{ji}}{\theta_i' + \theta_j' \tau_{ji}}\right) \end{aligned} \tag{20}$$

Donde ϕ_i, $^*\phi_j$, $^*\theta_i$, θ_j, θ_i, $'\theta_j'$, τ_{ij}, τ_{ji}, l_i y l_j son los parámetros ajustables, según la referencia [11]. A fin de determinar el valor de los parámetros ajustables de los tres modelos se ha empleado la siguiente función objetivo:

$$F.O. = \sum\left(\frac{\gamma_1^{\exp} - \gamma_1^{cal}}{\gamma_1^{\exp}}\right)^2 + \sum\left(\frac{\gamma_2^{\exp} - \gamma_2^{cal}}{\gamma_2^{\exp}}\right)^2 \tag{21}$$

Donde el superíndice *exp* hace referencia a los datos experimentales, mientras que el superíndice *cal* hace referencia a los datos calculados con el modelo.

3.5 Consistencia termodinámica de los resultados.

Los datos de equilibrio líquido vapor se suelen mostrar como la composición de la fase líquida (x_1) en función de la temperatura si el procedimiento es isóbaro, como en este caso, o en función de la presión si estamos ante el caso isotermo. De acuerdo con la regla de las fases, esta información es suficiente para caracterizar el sistema y de esta forma poder determinar la composición de la fase vapor (y_i). Si la información que proveen los datos experimentales incluye la composición de la fase vapor (y_i), esa información extra puede ser utilizada para comprobar si los datos cumplen con la consistencia termodinámica [7].

Existen varios métodos para determinar la consistencia termodinámica de los resultados. Algunos de ellos, como es el caso del test de áreas descrito por primera vez por Herington [8] y por Redlich-Kister [9], es exclusivo de datos isotermos, no resultando adecuado para el caso isobárico.

En la evaluación de la consistencia termodinámica de los sistemas estudiados en esta tesis se han empleado dos métodos: el test punto por punto de Fredenslund, y el método de Wisniak, que comprende un test punto por punto, y el test por área.

El método de Fredenslund se basa en la regla de las fases. Tomando en cuenta la forma general de la ecuación de Gibbs-Duhem tenemos que:

$$\sum x_k d \ln \gamma_k = -\frac{V^E}{RT} dP + \frac{H^E}{RT^2} dT \qquad (22)$$

Los datos experimentales se consideran termodinámicamente consistentes cuando la desviación absoluta promedio de las composiciones de la fase vapor (AADy) es menor que 0.01. El test de Fredenslund [7] para la evaluación de la consistencia termodinámica emplea los polinomios de Legendre, los cuales se expresan como:

$$\ln \gamma_1 = g + x_2 g' \qquad g \equiv G^E/RT$$
$$\ln \gamma_2 = g + x_1 g' \qquad g' \equiv (dg / dx_1)_\sigma \qquad (23)$$

Donde:

$$g = \frac{G^E}{RT} = x_1(1-x_1)\sum^{k} a_k L_k(x_1) \qquad k = 0,1,\ldots,n \tag{24}$$

$$L_k(x_1) = \{(2k-1)(2x_1-1)L_k\text{-}1(x_1)-(k-1)L_{k-2}(x_1)\}/k$$
$$L_0(x_1) = 1$$
$$L_1(x_1) = 2x_1-1 \tag{25}$$

Donde σ significa "a lo largo de la línea de saturación", $L_k(x_1)$ es la expression para los polinomios de Legendre, n es el grado del polinomio empleado, y a_k es el parámetro del polinomio de Legendre.

En el caso del equilibrio líquido-vapor isóbaro, es posible eliminar el término $V^E/RT\ dT$ de la ecuación (22). Normalmente también se elimina el término $H^E/RT^2\ dT$ en la ecuación de Gibbs-Duhem debido a la dificultad para determiner la entalpía de exceso en la mezcla si no se dispone de datos experimentales, lo que suele conllevar a resultados de AAD*y* ligeramente mayores a 0.01.

Debido a esto, y a que la evaluación de la consistencia termodinámica mediante el test punto por punto de Fredenslund no considera la dependencia de la temperatura, se ha determinado emplear adicionalmente otro test para su evaluación. Se ha escogido el método de Wisniak [10], el cual evalúa la consistencia mediante dos tests: punto por punto, y por área.

El método de Wisniak relaciona la función de Gibbs de exceso, G^E con la temperatura de ebullición, aplicando la ecuación de Clausius-Clapeyron:

$$\ln\frac{P}{Pi^{\circ}} = \frac{\Delta H_i{}^{\circ}(T_i{}^{\circ}-T)}{RT_i{}^{\circ}T} = \frac{\Delta S_i{}^{\circ}(T_i{}^{\circ}-T)}{RT} \tag{26}$$

Se considera que los datos son termodinámicamente consistentes cuando los valores de D_W son menores que 3-5. El límite mayor se propone para el caso en el que las entalpías de vaporización tengan que ser estimadas si no se dispone de datos experimentales sobre su valor.

El test se expresa como sigue:

$$D_W = 100\frac{|L-W|}{L+W} \tag{27}$$

Donde L y W se definen como:

$$L = \int_0^1 L_n dx_i = \int_0^1 W_n dx_i = W \tag{28}$$

Siendo:

$$L_n = \frac{T^o{}_i \; x_{i,n}\Delta S^o{}_{i,n} + T^o{}_j \; x_{j,n}\Delta S^o{}_{j,n}}{x_{i,n}\Delta S^o{}_{i,n} + x_{j,n}\Delta S^o{}_{j,n}} - T_n \tag{29}$$

$$W_n = \frac{RT_n\left[\left(x_{i,n}\ln\gamma_{i,n} + x_{j,n}\ln\gamma_{j,n}\right) - w_n\right]}{x_{i,n}\Delta S^o{}_{i,n} + x_{j,n}\Delta S^o{}_{j,n}} \tag{30}$$

T_n es la temperatura experimental para cada punto, T_i^o y T_j^o son las temperaturas de ebullición de los componentes *i* y *j*, y $\Delta S^o_{i,n}$ y $\Delta S^o_{j,n}$ son las entropías de vaporización de los componentes *i* y *j*. w_n y $\Delta S^o_{i,n}$ se definen como:

$$w_n = \sum x_{i,n} \ln(y_{i,n} / x_{i,n}) \tag{31}$$

$$\Delta S^o{}_{i,n} = \frac{\Delta H^o{}_i}{T^o{}_i} \tag{32}$$

Donde ΔH^o_i es la entalpía de vaporización del componente *i*.

3.6 Incertidumbre en la medida.

La determinación de la incertidumbre en las medidas se ha realizado de acuerdo con el documento EA-4/02, que es la guía para el cálculo de incertidumbres de medida del Bureau Internacional de Pesas y Medidas BIPM, Comisión Electrotécnica Internacional IEC, Unión Internacional de Química Pura y Aplicada IUPAC, Federación Internacional de Química Clínica FICC, Organización Internacional de Normalización ISO, Organización Internacional de Metrología Legal OIML, Unión Internacional de Física Pura y Aplicada IUPAP (1999; EA4-02 1999), [11]. Los resultados de la determinación de la misma pueden observarse en la Tabla 1.

Tabla 1. Cálculo de las incertidumbres en las medidas realizadas en el equilibrio líquido vapor de acuerdo al documento EA-4/02 [11].

		Unidad	Estimación	Divisor	U(x)
u(T)	Calibración	K	0.03	2	0.02
	Resolución		0.01	$2\sqrt{3}$	
	Repetibilidad		0.02	$\sqrt{3}$	
u(p)	Calibración	kPa	0.09	2	0.05
	Resolución		0.01	$2\sqrt{3}$	
	Repetibilidad		0.02	1	
U(T)		K		k=2	0.04
U(p)		kPa		k=2	0.10

La Tabla 2 muestra el cálculo de la incertidumbre en densidad para el densímetro Anton Paar DSA 5000.

Tabla 2. Cálculo de las incertidumbres en la medida de la densidad experimental de acuerdo al documento EA-4/02.

		Unidad	Estimación	Divisor	U(x) $kg \cdot m^{-3}$
u(T)	Calibración	K	0.025	2	$4 \cdot 10^{-3}$
	Resolución		0.001	$2\sqrt{3}$	
	Repetibilidad		0.008	$\sqrt{3}$	
u(τ)	Resolución	ms	$1 \cdot 10^{-6}$	$2\sqrt{3}$	$3 \cdot 10^{-3}$
	Repetibilidad		$3 \cdot 10^{-6}$	1	
u(A)		$kg \cdot m^{-3} ms^{-2}$	$2 \cdot 10^{-1}$	2	$1 \cdot 10^{-1}$
u(B)		$kg \cdot m^{-3}$	$3 \cdot 10^{-2}$	2	$1.5 \cdot 10^{-2}$
u(ρ_w)		$kg \cdot m^{-3}$	0.1	$\sqrt{3}$	$6 \cdot 10^{-2}$
u(ρ)		$kg \cdot m^{-3}$		k=1	$1 \cdot 10^{-1}$
U(ρ)		$kg \cdot m^{-3}$		k=2	$2 \cdot 10^{-1}$
U(ρ)		$kg \cdot m^{-3}/kg \cdot m^{-3}$		k=2	$2 \cdot 10^{-4}$

La incertidumbre de la fracción molar x_1 obtenida a partir de las medidas realizadas en la balanza de las masas de los compuestos puros, m_1 y m_2, se calcula mediante la expresión:

$$u(x_1) = \frac{x_1 \cdot (M_1 \cdot \Delta m_2) + (1 - x_1) \cdot (M_2 \cdot \Delta m_1)}{m_1 \cdot M_2 + m_2 \cdot M_1} \quad (33)$$

El valor de la incertidumbre calculada es ±0.00004, con un coeficiente de recubrimiento k=2, mientras que la estimación de la incertidumbre en la determinación de la composición de las muestras de la fase líquida y vapor, para fracciones molares en el entorno de x_1 = 0.5 a partir de las medidas de la densidad es U(x_1) = ±0.0003.

3.7 Referencias.

[1] TRC, Thermodynamic Tables, Texas A & M University, College Station, 1996.

[2] P.R. Bevington, D.K. Jobinson, Data reduction and error analysis for the physical sciences, McGraw-Hill 2nd ed. U.S.A. (1992).

[3] H. Renon, J.M. Prausnitz, AIChE J. 14 (1968) 135-144.

[4] G.M. Wilson, J. Am. Chem. Soc. 86 (1964) 127-130.

[5] D.S. Abrams, J.M. Prausnitz, AIChE J. 21 (1975) 116–128.

[6] A. Fredenslund, R.L. Jones, J.M. Prausnitz, AIChE J. 21 (1975) 1086-1100.

[7] A. Fredenslund, J. Gmehling, P. Rasmussen, Vapor-liquid equilibria using UNIFAC, 1st ed. Elsevier, New York (1977).

[8] E.F.G. Herington, Nature 160 (1947) 610.

[9] O. Redlich, A.T. Kister, Ind. & Eng. Chem. 40 (1948) 345-348.

[10] J. Wisniak, Ind. Eng. Chem. Res. 32 (1993) 1531-1533.

[11] Expression of the Uncertainty of Measurement in Calibration, European Cooperation for Accreditation, EA-4/02 (1999).

Capítulo 4

DETERMINACIÓN EXPERIMENTAL DE LA DENSIDAD A ALTA PRESIÓN

4.1 Introducción.

La densidad es una de las propiedades físicas cuyo conocimiento es de vital importancia en ciencia e ingeniería, ya que partiendo de ella es posible determinar otras propiedades derivadas. La determinación de la densidad a alta presión se lleva a cabo tanto para las sustancias puras como para las mezclas de dos o más de ellas, aportando información precisa para el diseño de compresores, redes de abastecimiento, tanques de almacenamiento, etc. de dichas sustancias. De la misma forma, resulta de importancia conocer no solo cómo varía esta propiedad con respecto a la variación en la presión, sino que también los cambios en temperatura influirán en su valor.
Como bien es sabido, la densidad ρ, se puede expresar de acuerdo con la ecuación (1):

$$\rho = \frac{m}{V} \tag{1}$$

Donde m se corresponde con la masa del fluido, y V con el volumen que éste ocupa.
Por tanto, el conocimiento de la densidad ρ (P, T) aporta datos valiosos para el posterior diseño de maquinaria o redes de transporte, así como para la determinación de otras propiedades físicas, como son la compresibilidad isoterma, κ_T, la cual se puede definir como el cambio en volumen que experimenta un fluido en respuesta a un cambio en la presión mientras la temperatura permanence constante, y la expansividad isobárica, α_P, definida como la medida de la respuesta del volumen de un sistema a un incremento en la temperatura del mismo, a una presión dada.
Además de estas dos propiedades derivadas, también es de importancia la determinación del cambio real de volumen que sufre una mezcla con respecto al cambio de volumen ideal que sufriría teniendo en cuenta únicamente las densidades de los dos compuestos puros, propiedad que se denomina volumen de exceso, y que se representa como V^E. Lo anteriormente dicho se puede expresar a partir de la siguiente ecuación:

$$V^E = \sum_{i=1}^{n} x_i M_i \left[\left(1/\rho \right) - \left(1/\rho_i \right) \right] \tag{2}$$

Donde M_i es la masa molar del componente puro i, x_i es la fracción molar del componente i en la mezcla, ρ es la densidad de la mezcla, y ρ_i se corresponde con la densidad del compuesto puro i.

El valor de esta propiedad, así como su signo, depende en gran medida de las interacciones entre las moléculas que forman la muestra, así como de los grupos funcionales que las forman. Por ejemplo, un valor positivo de volumen de exceso puede venir dado por la

expansión que tiene lugar en el seno de la mezcla debido a la aproximación de diferentes moléculas con tamaños moleculares distintos. De la misma forma, moléculas polares como los alcoholes desarrollarán interacciones fuertes entre ellas, lo cual derivará en un mayor efecto de empaquetamiento, y por tanto en valores de V^E menores.

La determinación de la densidad se puede realizar mediante distintas técnicas, pero comúnmente se hace una clasificación con base en dos grandes familias: métodos directos y métodos indirectos.

Los métodos directos se basan en la medición del volumen que ocupa un determinado fluido, realizándose una comparación posterior con el volumen ocupado por líquidos conocidos, mientras que los métodos indirectos relacionan propiedades de la materia con la densidad, por lo cual van a requerir de sustancias patrón para su calibrado. La Tabla 1 enumera algunas de las técnicas asociadas a cada método.

Tabla 1. Técnicas de medida de la densidad, ρ.

Métodos Directos	**Métodos Indirectos**
- Picnómetro	- Densímetros de oscilación mecánica
- Densimetría de flotador	- Refractómetros
- Balanza hidrostática	

Cuando se requiere determinar la densidad a altas presiones se emplean distintas técnicas como la picnometría o las celdas de volumen variable, pero sin duda la más empleada es la densimetría de oscilación mecánica. Ésta técnica basa su principio de funcionamiento en la medida de la frecuencia de resonancia de un oscilador mecánico excitado electrónicamente que contiene en su interior el fluido cuya densidad se desea determinar. Su amplia utilización viene dada por su rapidez en la medida y precisión en la determinación de los datos $\rho\ (P, T)$.

En las siguientes secciones se describe la técnica de medida de la densidad a alta presión mediante el empleo de dos densímetros de oscilación mecánica, en concreto densímetros de tubo vibrante, situados el primero de ellos en el laboratorio de Ingeniería Energética de la Universidad de Burgos, y el segundo en el Laboratoire des Fluides Complexes de la Universidad de Pau, en Francia.

4.2 Técnica experimental de medida de la densidad a alta presión.

Dentro de los densímetros de oscilación mecánica, los densímetros de tubo vibrante, VTD, por sus siglas en inglés, son los más ampliamente utilizados. El primero de ellos fue diseñado por Stabinger *et al.* [1]. Existen en la actualidad una gran variedad de densímetros de tubo vibrante [2], pero básicamente la configuración de un VTD comprende un tubo en forma de U, ya sea de vidrio borosilicatado, o metálico de distintas aleaciones como Hastelloy, o Inconel, unido por sus dos extremos a un bloque aislante que los sujeta y aísla de vibraciones externas. Este tubo se halla en el interior de un cilindro de pared doble; entre este tubo, también llamado oscilador, y la pared interna del cilindro se encuentra un gas con una alta conductividad térmica así como baja densidad para no ocasionar amortiguamiento en las oscilaciones. A fin de producir la vibración armónica del tubo con la muestra existen distintas configuraciones, como puede observarse en la Figura 1, si bien el modelo utilizado tanto en la Universidad de Burgos como en la Universidad de Pau (Anton Paar DMA HPM) tiene en su configuración dos imanes montados en la parte libre del tubo, así como dos bobinas en la base del densímetro que se prolongan hasta los imanes.

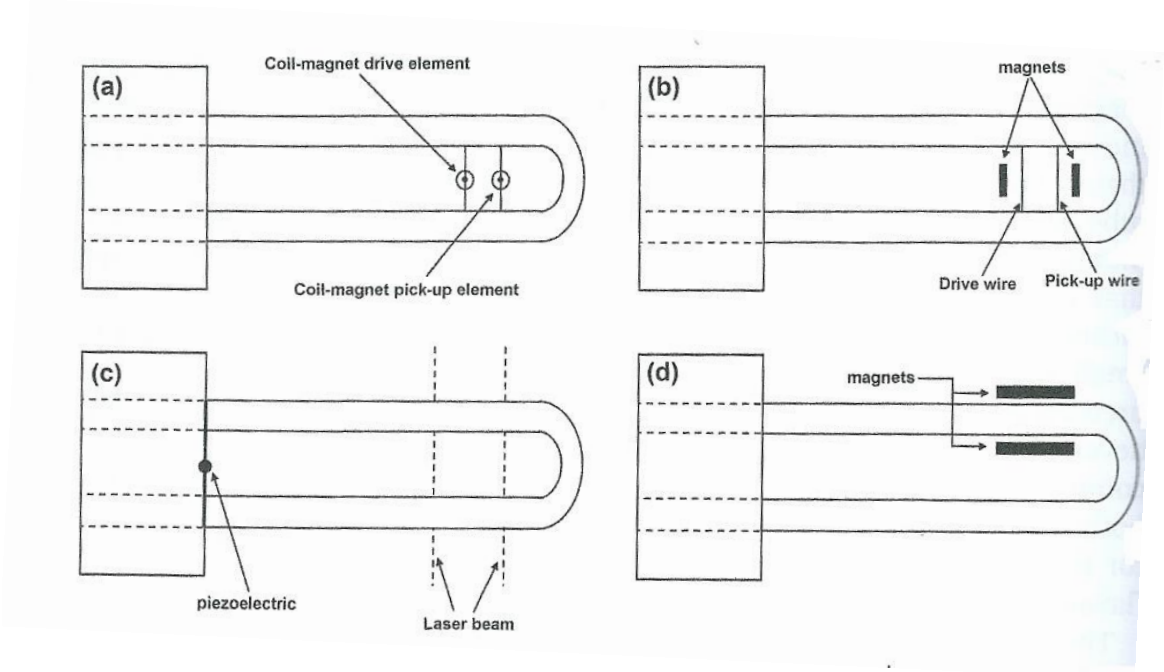

Figura 1. Diagramas de distintos tubos en U de un VTD. Con dos imanes fijos a la parte final del tubo (a), con dos cables, uno que conduce la vibración y otro que recoge la señal unidos al tubo (b), con un elemento piezoeléctrico encargado de generar la vibración (c), y con dos imanes en el cual una corriente pasa a través del tubo generándose una vibración armónica como resultado de la fuerza creada por el campo magnético a su vez generado por la corriente (d). Tomado de referencia [2].

Una de las dos bobinas se activa mediante una fuente de energía, y aplica una fuerza en uno de los imanes haciendo que el tubo vibre. La vibración del tubo hace que a su vez el segundo imán vibre entrando y saliendo de la segunda bobina, induciendo este movimiento una frecuencia de oscilación que variará en función de la masa del fluido que esté contenida en el tubo.

La oscilación que tiene lugar se puede expresar mediante la siguiente ecuación:

$$\frac{d^2y}{dt^2} + \frac{bdy}{mdt} + \frac{K}{m}y = \frac{F_0}{m}cos(\omega t) \tag{3}$$

Donde *y* es el desplazamiento con respecto a la posición de equilibrio, *b* es la constante de amortiguamiento, *K* es la constante elástica, F_0 es la amplitud de la fuerza externa, ω es la frecuencia, *m* la masa, y *t* el tiempo.

La solución general para la ecuación (3) es de la forma:

$$y(t) = A_0 \cdot cos(\omega t - \delta) \tag{4}$$

Donde A_0 es la amplitud de la oscilación y δ es el cambio de fase entre la fuerza externa y la oscilación *y(t)*.

La frecuencia natural del oscilador adopta la forma:

$$\omega = \omega_0 = \sqrt{\frac{K}{m}} \tag{5}$$

A partir de la ecuación (5), la relación entre ω_0 con el periodo natural de vibración τ, será:

$$\omega_0 = \frac{2\pi}{\tau} \tag{6}$$

Con la ecuación (6), y conociendo la masa *m*, cuya contribución será la de la masa del tubo vacío, m_0, y la masa debida al fluido contenido en el tubo, ρV, se llega a la siguiente ecuación:

$$\rho = \frac{K}{4\pi^2 V}\tau^2 - \frac{m_0}{V} = A\tau^2 + B \tag{7}$$

Donde ρ es la densidad de la muestra, *V* es el volumen del tubo en U, y *A* y *B* son las constantes de calibración. De esta forma tenemos que:

$$A = \frac{K}{4\pi^2 V} \tag{8}$$

$$B = \frac{m_0}{V} \tag{9}$$

Teniendo en cuenta que las principales variables que influyen en la densidad son la presión *P*, y la temperatura, *T*, se puede concluir que:

$$\rho(T, P) = A(T, P)\tau^2 - B(T, P) \tag{10}$$

De esta manera, conociendo los parámetros *A(T, P)* y *B(T, P)* y el periodo de vibración cuando el sistema está en resonancia es posible determinar la densidad del líquido contenido en el tubo en forma de U. Ya que el dato que provee el densímetro es el del periodo de vibración, este método de determinación de la densidad es considerado como indirecto.

4.2.1 Descripción del densímetro del Laboratorio de Ingeniería Energética de la Universidad de Burgos.

Como ya se dijo anteriormente, el densímetro de alta presión utilizado en el Laboratorio de Ingeniería Energética de la Universidad de Burgos se corresponde con un densímetro de tubo vibrante (VTD) Anton Paar DMA HPM, que puede realizar mediciones de densidad en el rango (0 – 3) $g \cdot cm^{-3}$ con una resolución de 10^{-5} $g \cdot cm^{-3}$, en el rango de temperaturas (263.15 – 473.15) K y hasta una presión máxima de 140 MPa. En este caso el tubo en U está fabricado en Hastelloy C-276. Para realizar las tareas de llenado, vaciado y limpieza, medida y control de la presión así como medida y control de la temperatura, y el registro y almacenamiento de los datos obtenidos el densímetro posee una serie de elementos que se pueden observar en la Figura 2.

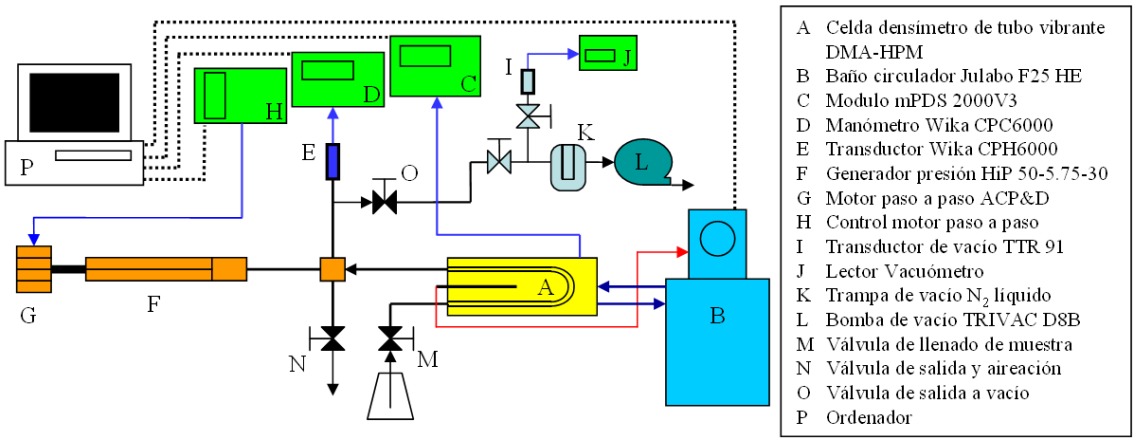

Figura 2. Elementos del sistema de medida de densidad a alta presión en el Laboratorio de Ingeniería Energética de la Universidad de Burgos.

Como se describió en la sección anterior, la medida que realmente realiza el densímetro es la del periodo de vibración del tubo en U con la muestra (A), por tanto, es necesaria una unidad de evaluación para medir ese periodo de vibración. La unidad mPDS 2000V3 (C) es la encargada de medir ese dato con una incertidumbre de $1 \cdot 10^{-6}$ m·s, además de recoger el dato de temperatura interior del densímetro, y de comunicar con un PC a través de una conexión RS232. La adquisición de datos al PC se hace mediante el entorno de programación Agilent VEE-Pro 7.0. Para realizar la medición de la temperatura, se dispone de una sonda Pt100 de cuatro hilos directamente inserta en el densímetro, cuya incertidumbre en la medida de la temperatura (k = 2) es de 30 mK. A fin de mantener la temperatura deseada en la muestra se dispone de un baño termostático Julabo F25 HE (B) que hace circular aceite de silicona por la camisa interna de la celda de medida.

Para llevar a la muestra a la presión requerida se dispone de un generador de presión marca HiP (F), con una presión máxima de trabajo de 200 MPa conectado directamente a un motor paso a paso ACP&D (G) provisto de una caja de cambios reductora. Como sistema de medida de presión se utiliza un manómetro WIKA CPC 6000 (D), con resolución de 0.0001 MPa, conectado a un calibrador WIKA CPH 6000 (E).

Para proceder al llenado y vaciado del sistema se dispone de dos válvulas de aguja para alta presión (M, N). El llenado se hace realizando previamente el vacío del sistema mediante una bomba (L); de esta forma se hace limpieza de todo producto que pudiera existir en el interior del aparato, y posteriormente se facilitará el llenado con la nueva muestra, que entrará al sistema por succión. Teniendo en cuenta las incertidumbres en la temperatura, presión, el periodo de oscilación medido para el agua y el vacío, así como la incertidumbre en densidad de los sistemas

medidos, la incertidumbre expandida (k = 2) se corresponde con un valor de ±0.7 kg·m^{-3}. Una imagen de conjunto del sistema de medida de densidad a alta presión se observa en la Figura 3.

Figura 3. Vista general de los elementos para la medida de la densidad a alta presión en el Laboratorio de Ingeniería Energética de la Universidad de Burgos.

4.2.1.1 Procedimiento Experimental de Medida.

Previo a la realización de las medidas de densidad, los fluidos se mantienen alejados de la luz y sin contacto con el aire. Si el fluido a medir es puro, se procede al llenado de un vial de 21 cm^3 y posteriormente se desgasifica mediante un baño de ultrasonidos durante al menos 15 minutos, para después introducirlo en el sistema mediante succión. Para preparar las mezclas, a partir de los datos de masa molar de cada uno de los componentes, teniendo en cuenta el volumen del vial (21 cm^3), y la fracción molar x, que se desea conseguir, se pipetea el volumen pertinente de cada uno de los compuestos puros, se vierte al vial, y se homogeneiza. Posteriormente las muestras se tratan igual que los compuestos puros, se desgasifican y se introducen en el sistema de medida de densidad a alta presión. La Figura 4 muestra las válvulas que conforman el sistema de llenado y de vaciado.

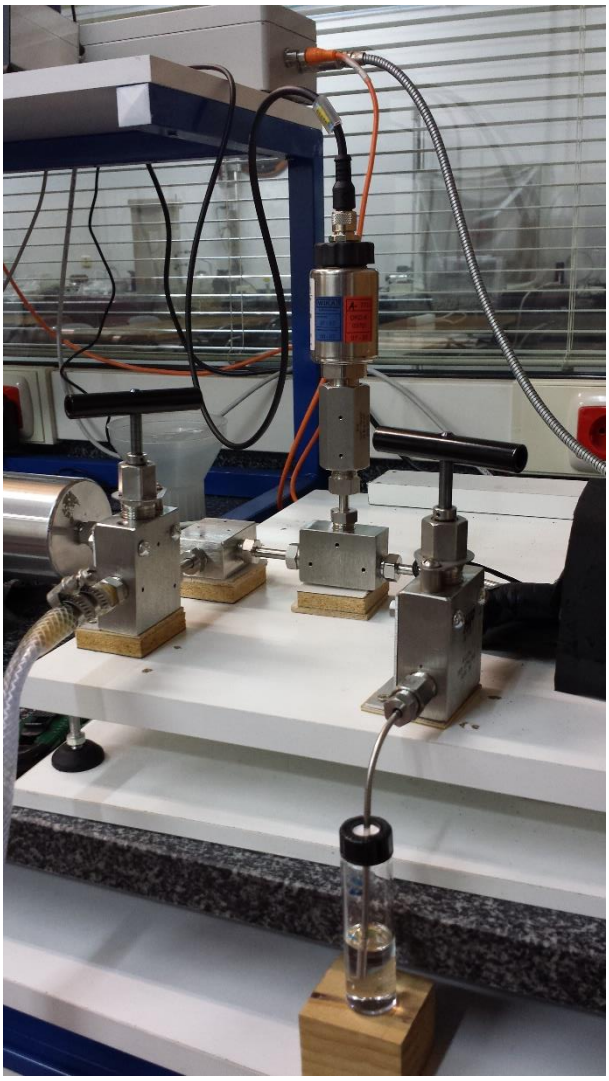

Figura 4. Sistema de llenado y vaciado del densímetro de alta presión. La válvula de la derecha (con el vial) corresponde al llenado, mientras que la de la izquierda está conectada a la bomba de vacío. Se observa al fondo el sensor de presión.

La incertidumbre expandida en la composición de la mezcla es de $\pm 4 \cdot 10^{-5}$ en fracción molar, con un coeficiente de recubrimiento $k = 2$. Una vez lleno el sistema con el fluido, se cierra la válvula de llenado, y se lleva a la temperatura requerida. Las presiones que van a ser medidas están previamente programadas en el software Agilent, por tanto el proceso de medida comienza en 0.1 MPa, toma el dato de presión cada 5 MPa hasta 65 MPa, y desde 70 MPa hasta 140 MPa lo hace cada 10 MPa. La rampa de medida finaliza bajando progresivamente desde 140 MPa hasta 50 MPa, 10 MPa y 0.1 MPa. El cambio de temperatura en el baño se hace de forma manual.

4.2.2 Descripción del densímetro del Laboratoire des Fluides Complexes de la Universidad de Pau.

El densímetro situado en el Laboratoire des Fluides Complexes es similar al situado en el Laboratorio de Ingeniería Energética de la Universidad de Burgos (Anton Paar DMA HPM), siendo únicamente distintos los elementos que conforman el sistema de medida. Un esquema del mismo se puede observar en la Figura 5, mientras que la Figura 6 muestra una vista general del sistema de medida de densidad a alta presión.

Este densímetro, al igual que el de la Universidad de Burgos, posee una sonda Pt100 directamente inserta en el densímetro (A), a fin de proveer del dato de temperatura, en este caso con una incertidumbre de ±0.05 K. La temperatura se alcanza gracias a la circulación de aceite de silicona el cual es bombeado por un baño termostático Julabo Polystat 36 (E), que permite la regulación de la temperatura con una estabilidad mejor que 0.01 K. El periodo de vibración del tubo con la muestra es registrado gracias a la unidad mPDS 2000v3 (C).

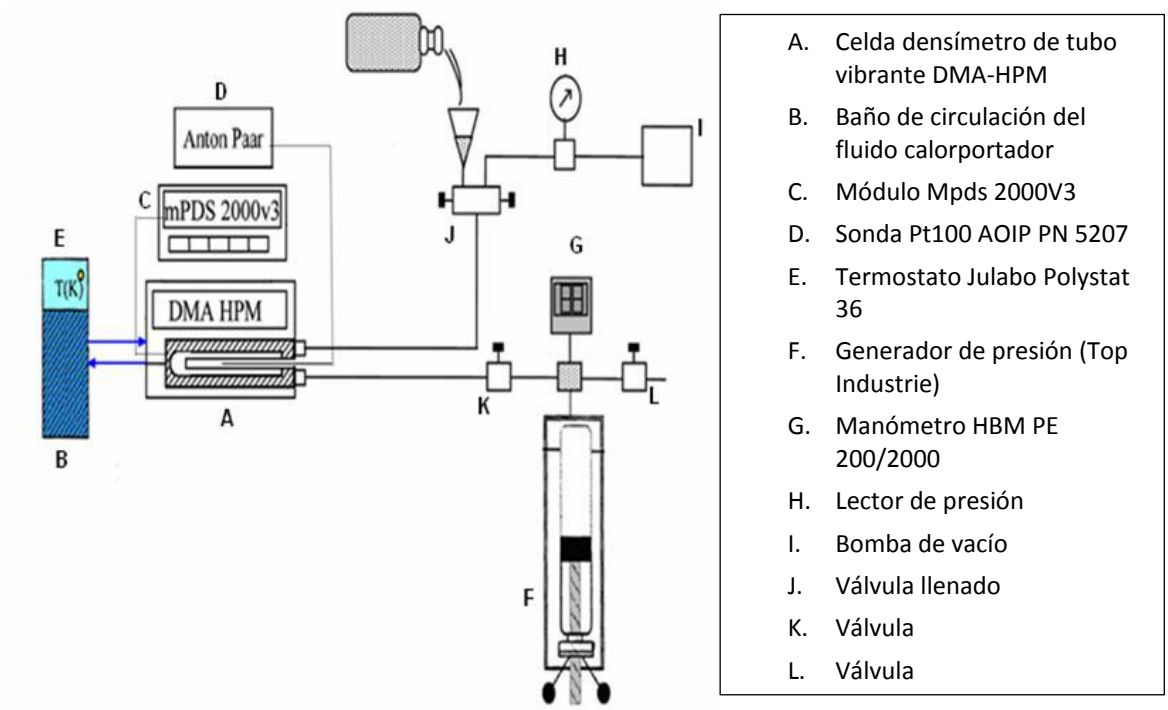

Figura 5. Elementos del sistema de medida de densidad a alta presión en el Laboratoire des Fluides Complexes de la Universidad de Pau.

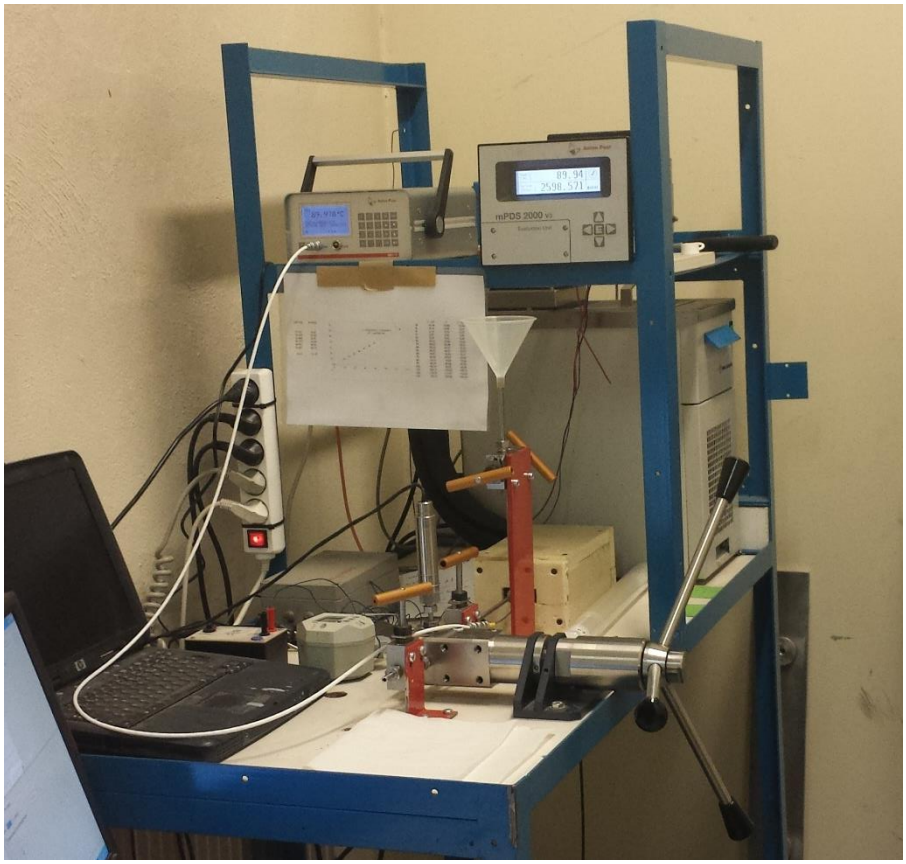

Figura 6. Vista general del sistema de medida de la densidad a alta presión en el Laboratoire des Fluides Complexes de la Universidad de Pau.

En este caso el sistema para generación de presión consiste en una bomba manual, marca Top Industrie (F), con un volumen máximo de 12 cm^3 y capaz de llegar a una presión de 200 MPa. La presión se mide con un transmisor de presión digital Presens 63 Precise Gold Plus (H), con una incertidumbre de 0.015 MPa, mientras que la lectura de la misma se hace mediante el software LAbview.

Teniendo en cuenta la incertidumbre de la temperatura, la presión, el período de oscilación de medición de agua, vacío y los sistemas estudiados, y la exactitud de la densidad del agua, (calibración) la incertidumbre experimental total de los valores de densidad obtenidos se estima en ± 0.5 kg·m-3.

Las válvulas de llenado y vaciado, marca Top Industrie, soportan una presión máxima de 200 MPa.

4.2.2.1 Procedimiento Experimental de Medida.

En este caso, previamente a realizar las medidas de densidad, los fluidos se mantienen alejados de la luz y sin contacto con el aire. Una vez realizado el vacío en el sistema, el fluido entra al mismo por succión así como por gravedad; la válvula de llenado dispone de un embudo que se llena con el fluido, posteriormente se abre la válvula y el fluido entra hasta llenar el sistema.

El fluido, si es puro, se vierte directamente desde su botella. Si es una mezcla, ésta se prepara en viales de 250 cm^3 mediante pesada de las cantidades requeridas de cada uno de los fluidos, teniendo en cuenta su masa molar y la fracción molar que se desee obtener. La incertidumbre expandida (k = 2) en la composición de la mezcla es de $\pm 6 \cdot 10^{-5}$ en fracción molar.

Una vez lleno el sistema con el fluido, se cierra la válvula de llenado, y se lleva a la temperatura a la que se desea medir. La presión se alcanza gracias al uso de la bomba manual midiendo en el intervalo desde 0.1 MPa hasta 140 MPa en escalones de 10 MPa. El cambio de temperatura en el baño se hace de forma manual.

4.3 Calibración.

El método de calibración más empleado en este tipo de densímetros consiste en la medición del periodo de vibración de dos sustancias de referencia, de las cuales se conoce con mucha exactitud su densidad a ciertas presiones y temperaturas. A partir de estos datos se realizará la determinación de los parámetros *A(T, P)* y *B(T, P)*. En las ecuaciones (11) y (12) se puede observar el procedimiento de cálculo para estos dos parámetros.

$$A(T,P) = \frac{\rho_1(T,P) - \rho_2(T,P)}{\tau_1^2(T,P) - \tau_2^2(T,P)} \tag{11}$$

$$B(T,P) = A(T,P)\tau_2^2(T,P) - \rho_2(T,P) \tag{12}$$

Donde los subíndices 1 y 2 hacen referencia a cada uno de los fluidos empleados en la calibración. Determinado el valor de *A(T, P)* y *B(T, P)* es posible conocer la densidad de cualquier fluido en el mismo rango de presiones y temperaturas. En los casos en que la temperatura de ebullición de la muestra cuya densidad se desea determinar sea menor de 373.15 K a 0.1 MPa, los fluidos de calibración que se emplean son el vacío y agua, de acuerdo al procedimiento descrito por Comuñas *et al.* [3], el cual es una modificación del anteriormente propuesto por Lagourette *et al.* [4]. A temperaturas superiores a 373.15 K y presión de 0.1 MPa, hay que emplear

otro fluido de calibración, en este caso *n*-decano, tomando como referencia los datos de densidad para este fluido contenidos en la referencia [5]. En el caso del agua, los datos de densidad se obtuvieron a partir de la referencia [6]. El mismo procedimiento de calibración se emplea para los dos densímetros de alta presión, el situado en el Laboratorio de Ingeniería Energética de la Universidad de Burgos, y el situado en el Laboratoire des Fluides Complexes de la Universidad de Pau. Ambos densímetros se calibran previamente a cada campaña de medidas.

4.4 Ajuste de los datos experimentales.

Los datos de densidad a las diferentes presiones y temperaturas medidas se han ajustado a la ecuación de estado de Tamman-Tait, que ha demostrado tener una gran precisión en la reproducción de datos de densidades a alta presión [7]. Esta ecuación es de gran utilidad ya que a partir de ella es posible determinar las propiedades termodinámicas derivadas que se expondrán en la siguiente sección. En concreto, en este trabajo se ha empleado la ecuación de Tamman-Tait modificada, la cual ha sido propuesta en distintos trabajos por Cibulka [8 - 10], y que se expresa como sigue:

$$\rho(T,P) = \frac{\rho_0(T)}{1 - C\ln\left(\frac{B(T) + P}{B(T) + 0.1\ MPa}\right)} \tag{13}$$

Donde:

$$\rho_0(T) = A_0 + A_1 T + A_2 T^2 + A_3 T^3 \tag{14}$$

$$B(T) = B_0 + B_1 T + B_2 T^2 \tag{15}$$

Los parámetros A_i, B_i y C se obtienen correlacionando simultáneamente los datos experimentales de densidad en función de la presión y temperatura a la que han sido medidos. En este caso, para la determinación de los mismos se ha empleado el software Table Curve 3D [11].

4.5 Propiedades derivadas.

Como se ha dicho en la sección anterior, a partir de la ecuación de Tamman-Tait modificada se pueden obtener las denominadas propiedades derivadas, esto es, la compresibilidad isoterma, κ_T, y la expansividad isobárica, α_P. La primera de ellas, compresibilidad isoterma, describe el efecto de la presión en la densidad a una temperatura fija de acuerdo a la expresión:

$$\kappa_T = \left(\frac{1}{\rho}\right)\left(\frac{\partial \rho}{\partial p}\right)_T = \frac{C}{\left(1 - C\ln\left(\frac{B(T)+P}{B(T)+0.1MPa}\right)\right)\left(B(T)+P\right)} \tag{16}$$

En el caso de la expansividad isobárica, que da cuenta del efecto de la temperatura sobre la densidad a una determinada presión, la expresión para su cálculo se obtiene derivando analíticamente la ecuación de Tamman-Tait, quedando la expresión como sigue:

$$\alpha_P = -\left(\frac{1}{\rho}\right)\left(\frac{\partial \rho}{\partial T}\right)_P \tag{17}$$

Algunos autores [12] y [13], señalan que la expansividad isobárica depende de ambas funciones *B(T)* y $\rho_0(T)$. De la misma forma, Jaquemin *et al.* [14] notifica que las diferencias que a veces se pueden encontrar para los valores de α_P en la literatura con respecto a los valores experimentales se deben a la diferencia en los valores de densidad, siendo también función de las ecuaciones de ajuste empleadas. De esta manera se propone derivar la expansividad isobárica a partir de las densidades isobáricas. Así, a cada presión podemos suponer que:

$$\rho_P = a_0 + a_1 T + a_2 T^2 \tag{18}$$

Consecuentemente tenemos que:

$$\left(\frac{\delta \rho}{\delta T}\right)_P = a_1 + 2a_2 T \tag{19}$$

Para cada presión se obtiene un conjunto de valores (a_0, a_1, a_2) mediante un ajuste por mínimos cuadrados. Insertando la densidad diferenciada $\rho_P(T)$ y las densidades calculadas en la ecuación (17) llegamos a la expresión que permite calcular la expansividad isobárica:

$$\alpha_p = -\frac{a_1 + 2a_2 T}{a_0 + a_1 T + a_2 T^2} \tag{20}$$

4.6 Incertidumbre en la medida.

El cálculo de la incertidumbre se ha realizado de acuerdo al documento EA-4/02 [15], que es la guía para el cálculo de incertidumbres de medida del BIPM, IEC, IUPAC, FICC, ISO OIML, IUPAP *(1999)*. En el caso de la densidad, la ecuación de partida para la determinación de la incertidumbre es la (21), pero hay que tener en cuenta también las dos constantes de calibración, *A(T)* y *B(T, P)*. La ley de propagación de incertidumbres aplicada en base a estas expresiones permite calcular la incertidumbre en ambas constantes, así como la incertidumbre de la densidad, de la siguiente manera:

$$\rho(T,P) = \rho_w(T,P) + \frac{\rho_w(T,\,0.1)}{\tau_w^2(T,\,0.1) - \tau_v^2(T)}\left[\tau^2(T,P) - \tau_w^2(T,P)\right] \tag{21}$$

En el caso del coeficiente *A(T)*:

$$A(T) = \frac{\rho_w(T, 0.1\,\mathrm{MPa})}{\tau_w^2(T, 0.1\,\mathrm{MPa}) - \tau_0^2(T)} \tag{22}$$

La incertidumbre expandida (k = 2) es:

$$U(A(T)) = 2\left[\left(\frac{\partial A(T)}{\partial \rho_w}\right)^2 u(\rho_w)^2 + \left(\frac{\partial A(T)}{\partial \tau_w}\right)^2 u(\tau_w)^2 + \left(\frac{\partial A(T)}{\partial \tau_0}\right)^2 u(\tau_0)^2\right]^{1/2}$$

$$U(A(T)) = 2\left[\left(\frac{A(T)}{\rho_w}\right)^2 u(\rho_w)^2 + \left(\frac{-2A^2(T)\tau_w}{\rho_w}\right)^2 u(\tau_w)^2 + \left(\frac{2A^2(T)\tau_0}{\rho_w}\right)^2 u(\tau_0)^2\right]^{1/2} \tag{23}$$

En donde ρ_w y τ_w están evaluados en (T, 0.1MPa).

Para el coeficiente *B(T, P)*:

$$B(T,P) = \frac{\rho_w(T,0.1\,MPa)}{\tau_w^2(T,0.1\,MPa) - \tau_0^2(T)}\tau_w^2(T,P) - \rho_w(T,P) \tag{24}$$

La incertidumbre expandida (k = 2) es:

$$U(B(T,P)) = 2\left[\left(\frac{\partial B(T,P)}{\partial \rho_w}\right)^2 u(\rho_w)^2 + \left(\frac{\partial B(T,P)}{\partial \tau_w}\right)^2 u(\tau_w)^2 + \left(\frac{\partial B(T,P)}{\partial \tau_0}\right)^2 u(\tau_0)^2\right]^{1/2} \tag{25}$$

En donde:

$$\frac{\partial B(T,P))}{\partial \rho_w} = \frac{A(T)\tau_w^2(T,P)}{\rho_w(T,0.1MPa)} - 1 \tag{26}$$

$$\frac{\partial B(T,P))}{\partial \tau_w} = 2A(T)\tau_w(T,P)\left[1 - A(T)\frac{\tau_w(T,0.1MPa)\tau_w(T,P)}{\rho_w(T,0.1MPa)}\right] \tag{27}$$

$$\frac{\partial B(T,P)}{\partial \tau_0} = 2\frac{\tau_0(T)A^2(T)}{\rho_w(T,0.1MPa)}\tau_w^2(T,P) \tag{28}$$

La incertidumbre expandida (k = 2) de la densidad se calcula de la siguiente manera:

$$U(\rho(T,P)) = 2\left[\left(\frac{\partial \rho(T,P)}{\partial A(T)}\right)^2 u^2(A(T)) + \left(\frac{\partial \rho(T,P)}{\partial \tau(T,P)}\right)^2 u^2(\tau(T,P)) + \left(\frac{\partial \rho(T,P)}{\partial B(T,P)}\right)^2 u^2(B(T,P))\right]^{1/2} \tag{29}$$

$$U(\rho(T,P)) = 2\left[\left(\tau^2(T,P)\right)^2 u^2(A(T)) + \left(2A(T)\tau(T,P)\right)^2 u^2(\tau(T,P)) + u^2(B(T,P))\right]^{1/2} \tag{30}$$

En la Tabla 2 se observan las incertidumbres asociadas a las constantes de calibración, mientras que en la Tabla 3 se refleja la incertidumbre asociada con la medida de la densidad.

Para el densímetro Anton Paar DMA HPM situado en el Laboratorio de Ingeniería Energética de la Universidad de Burgos, la incertidumbre expandida con factor de cobertura k = 2 (nivel de confianza del 95% asumida distribución normal) en la medida de la densidad es $0.7 \cdot kg \cdot m^{-3}$. La mayor contribución a esta incertidumbre proviene del procedimiento de calibración a través de la incertidumbre de ambas constantes *A(T)* y *B(T, P)*. Sólo disponiendo de buenos datos de densidad de fluidos de referencia puede verse reducida la incertidumbre en la medida.

Tabla 2. Cálculo de la incertidumbre asociada a las dos constantes de calibración empleando el documento EA-4/02 [15], en el intervalo de temperaturas 298.15 - 343.15 K y presiones 0.1 - 140 MPa.

		Unidad	Estimación	Divisor	$u(x)$
					kg/m^3
$u(\rho_w)$	Referencia material	kg/m^3	0.01	$\sqrt{3}$	0.006
u(T)	Calibración	ºC	0.020	2	
	Resolución		0.010	$2\sqrt{3}$	0.0025
	Repetibilidad		0.005	1	
u(P)	Calibración	MPa	0.02	2	
	Resolucion		0.01	$2\sqrt{3}$	0.014
	Repetibilidad		0.01	1	
$u(\tau)$	Repetibilidad	µs	$5\ 10^{-4}$	1	$7.5\ 10^{-3}$
	Resolución		$1\ 10^{-3}$	$2\sqrt{3}$	
U(A(T))		$kg/m^3\mu s^2$		k=2	$7\ 10^{-8}$
U(B(T,P))		kg/m^3		k=2	0.5

Tabla 3. Cálculo de la incertidumbre asociada a la densidad experimental usando EA-4/02 [15], y la Tabla 2 en el intervalo de temperaturas 298.15 - 343.15 K y presiones 0.1 - 140 MPa.

		Unidad	Estimación	Divisor	$u(x)$
					kg/m^3
$u(\tau)$	Repetibilidad	µs	$5\ 10^{-4}$	1	$7.5\ 10^{-3}$
	Resolución		$1\ 10^{-3}$	$2\sqrt{3}$	
u(T)	Calibración	ºC	0.020	2	
	Resolución		0.010	$2\sqrt{3}$	0.0025
	Repetibilidad		0.005	1	
u(P)	Calibración	MPa	0.02	2	
	Resolución		0.01	$2\sqrt{3}$	0.014
	Repetibilidad		0.01	1	
u(A(T))	$kg/m^3\mu s^2$		$7\ 10^{-8}$	2	0.25
u(B(T,P))	kg/m^3		0.5	2	0.25
$u(\rho)$		kg/m^3		k=1	0.35
$U(\rho)$		kg/m^3		k=2	0.7
$U(\rho)$		$kg/m^3/kg/m^3$		k=2	$8\ 10^{-4}$

4.7 Referencias.

[1] H. Stabinger, Eingegangen am 17 Jänner 1967, 53 (1967) 2-4.

[2] E. Wilhem, T. Letcher, Volume Properties, Liquids, Solutions and Vapours, 1st ed. Royal Society of Chemistry, Cambridge (2015).

[3] M. J. P. Comuñas, J. Bazile, A. Baylaucq, C. Boned, J. Chem. Eng. Data 53 (2008) 986–994.

[4] H. Lagourette, B. Boned, C. Saint-Guirons, H. Xans, P. Zhou, Meas. Sci. Technol. 3 (1992) 699–703.

[5] TRC, Thermodynamic Tables, Texas A&M University, College Station (1996).

[6] W. Wagner, A. Pruß, J. Phys. Chem. Ref. Data 31 (2002) 387–535.

[7] J.H. Dymond, R. Malhotra, Int. J. Thermophys. 9 (1988) 942-951.

[8] I. Cibulka, M. Ziková, J. Chem. Eng. Data 39 (1994) 876.

[9] I. Cibulka, L. Hnedkovsky, J. Chem. Eng. Data 41 (1996) 657-668.

[10] I. Cibulka, T. Takagi, J. Chem. Eng. Data 44 (1999) 411-429.

[11] Table Curve 3D. Systat Software, U.S.A.

[12] C. A. Cerdeiriña, C. A. Tovar, D. González-Salgado, E. Carballo, L. Romaní, Phys. Chem. Chem. Phys. 3(2001) 5230–5236.

[13] J. Troncoso, D. Bessières, C. A. Cerdeiriña, E. Carballo, L. Romaní, Fluid Phase Equilib. 208 (2003) 141-154.

[14] J. Jacquemin, P. Husson, V. Mayer, I. Cibulka, J. Chem. Eng. Data 52 (2007) 2204–2211.

[15] Expression of the Uncertainty of Measurement in Calibration, European Cooperation for Accreditation, EA-4/02 (1999).

Capítulo 5

DETERMINACIÓN EXPERIMENTAL DE LA VISCOSIDAD A ALTA PRESIÓN

5.1 Introducción.

Dentro de las propiedades de transporte la viscosidad juega un papel muy importante ya que será un factor clave en el posterior diseño de redes de distribución para fluidos, bombas, etc. Esta propiedad se puede definir como la oposición de un fluido a las deformaciones tangenciales. La Ley de viscosidad de Newton establece que la fuerza por unidad de área es proporcional al gradient de velocidad, *v* con la distancia, *y*:

$$\tau_{x,y} = -\eta \frac{dv_x}{dy} = \frac{F_x}{A_y} \tag{1}$$

Donde $\tau_{x,y}$ se refiere al esfuerzo cortante (Pa), y la constante de proporcionalidad, η es la viscosidad dinámica (Pa·s), del fluido. Este esfuerzo cortante aparece porque existe una fuerza en la dirección *x*, F_x, actuando sobre una superficie perpendicular, A_y. A su vez, existirá un flujo de cantidad de movimiento en la dirección *x* que se va a transmitir en la dirección *y*.

Teniendo esto en cuenta, se puede establecer una clasificación de acuerdo con la relación entre la viscosidad y la dependencia respecto al gradiente de velocidad en dos tipos de fluidos, newtonianos y no newtonianos.

En los fluidos newtonianos la viscosidad absoluta del fluido no depende del gradiente de velocidad, es decir:

$$\tau_{x,y} = -\eta \frac{dv_x}{dy} \rightarrow \eta = cte \tag{2}$$

Algunos ejemplos de fluidos newtonianos son el agua, la glicerina y los hidrocarburos.

En el caso de los fluidos no newtonianos, el valor de la viscosidad es dependiente del gradiente de velocidad, de forma que:

$$\tau_{x,y} = -\eta \frac{dv_x}{dy} \rightarrow \eta = f\left(\frac{dv_x}{dy}\right) \tag{3}$$

Dentro de este grupo encontraríamos los pseudoplásticos, que son fluidos que disminuyen su viscosidad al aumentar la velocidad de deformación, y los dilatantes, en los cuales la viscosidad aumenta al aumentar la velocidad de deformación aplicada.

También se engloban dentro de los fluidos no newtonianos aquellos para los cuales la viscosidad cambia con el tiempo durante el esfuerzo, pudiendo estos ser tixiotrópicos (la

viscosidad disminuye con el tiempo) o reopécticos (el valor de la viscosidad aumenta con el tiempo). Ejemplos de fluidos no newtonianos son los geles, coloides, y las soluciones de polímeros. De la descripción de fluido no newtoniano se desprende que estos no tienen un valor de viscosidad definido y constante, por lo cual a la hora de caracterizarlos, aunque sería posible determinar la viscosidad empleando la técnica de la reometría, por la que se realizarían medidas a distintos gradientes de velocidad, es mejor emplear otras propiedades. La viscosidad, entendida como la resistencia de un líquido o gas a fluir, se determinará entonces en los fluidos newtonianos con un viscosímetro, que realizará medidas para un único gradiente de velocidad. El comportamiento de los fluidos empleados en esta tesis es newtoniano, por tanto la determinación de la viscosidad se realizará empleando viscosímetros. La Tabla 1 resume los principales tipos existentes.

La técnica de la viscosimetría ha sufrido un progreso muy importante en su desarrollo a lo largo de los años, derivando esto en una amplia variedad de técnicas de medida. Se puede establecer una clasificación general de los viscosímetros en la que encontramos cuatro grandes grupos atendiendo a la morfología de los mismos. En un primer grupo tenemos los viscosímetros de capilar, los cuales se encargan de caracterizar el flujo laminar del fluido a través de un capilar. Los viscosímetros de vibración caracterizan el comportamiento de un objeto inmerso en un fluido, el cual vibra o es torsionado. Los viscosímetros de rotación miden la respuesta de un fluido a un esfuerzo de torsión; un objeto axialmente simétrico suspendido de un eje oscila con respecto a ese eje en el seno del fluido cuya viscosidad se desea determinar [1]. Por último, los viscosímetros de cuerpo móvil basan su principio de funcionamiento en la medida de la velocidad de caída de un objeto en el seno del fluido.

El viscosímetro que se ha empleado en esta tesis ha sido el de tipo de Caída de Cuerpo, el cual basa su principio de funcionamiento en la Ley de Stokes, que hace referencia a la fuerza de fricción experimentada por un objeto moviéndose en el seno de un fluido en un régimen laminar. Conociendo las densidades del objeto que cae, la del líquido y la velocidad (o tiempo) de caída, se puede calcular la viscosidad a partir de de la Ley de Stokes (ecuación 4):

$$V_S = \frac{2}{9} \cdot \frac{r^2 g(\rho_S - \rho_L)}{\eta} \tag{4}$$

En esta ecuación, V_S es la velocidad de caída del cuerpo, r el radio equivalente, g es la aceleración de la gravedad, ρ_S es la densidad del cuerpo que cae, ρ_L es la densidad del líquido, y η es la viscosidad dinámica del fluido.

Complementariamente a esta técnica se ha empleado también el viscosímetro capilar de tipo Ubbelohde. Ambos viscosímetros se describen a continuación en las Secciones 5.2 y 5.3.

Tabla 1. Relación de los principales tipos de viscosímetros. A partir de [1].

• **Viscosímetros Capilares**	- Ostwald modificado	- *Cannon-Fenske* - *Zeitfuchs* - *Viscosímetro SIL* - *Cannon-Manning* - *BS/tubo en U* - *Viscosímetros miniatura* - *Pikenvitch*
	- Nivel suspendido	- *Ubbelohde* - *Cannon-Ubbelohde* - *Viscosímetro BS/IP/SL* - *Viscosímetro BS/IP/MSL* - *Fitz-Simmons* - *Atlántico*
	- Flujo inverso	- *Zeitfuchs cruzado* - *Cannon-Fenske* - *Lautz-Zeitfuchs* - *Viscosímetro BS/IP/RF tubo en U flujo inverso*
• **Viscosímetros de Vibración**	- Péndulo	
	- Hilo Vibrante	
• **Viscosímetros de Rotación**	- Viscosímetro de Couette	
	- Viscosímetro de Stabinger	
	- Viscosímetro de Plato y Cono	
	- Reogoniómetro de Weissenberg	
	- Viscosímetro de Brookfield	
• **Viscosímetros de Cuerpo móvil**	- Caída de Cuerpo	
	- Caída de Pistón	

5.2 Técnica experimental de medida de la viscosidad a alta presión.

El viscosímetro de caída de cuerpo empleado se encuentra en el Laboratoire des Fluides Complexes et leurs Réservoirs de la Universidad de Pau, Francia. Como se ha comentado anteriormente, este tipo de viscosímetros basan su funcionamiento en la caída de un cuerpo metálico cilíndrico, cuyas bases forman dos hemisferios, a través del espacio anular que contiene el fluido cuya viscosidad se desea determinar. Determinando el tiempo que tarda el cuerpo en pasar entre dos referencias fijas es posible determinar la viscosidad del fluido mediante el empleo de la siguiente ecuación:

$$\eta = K(\rho_S - \rho_L)\Delta t \tag{5}$$

La ecuación (5) relaciona la viscosidad dinámica, η, con la diferencia entre la densidad del cuerpo metálico, (ρ_S), y la del líquido, (ρ_L), y el tiempo que transcurre entre las dos detecciones del paso del cuerpo metálico, (Δt), siendo K un parámetro característico que depende del viscosímetro y del cuerpo metálico.

Este aparato está destinado al estudio tanto de líquidos como de gases bajo presión, pudiendo trabajar en un rango de (0.1 – 200) MPa para las presiones, y en un rango (293.15 – 393.15) K para las temperaturas. La descripción del mismo se detalla en la referencia [2].
Una vista general del mismo se puede observar en la Figura 1.

La celda de medida está compuesta por un tubo en el que se produce la caída del cuerpo metálico, el cual a su vez está contenido dentro de otra celda. El fluido rodea ambas caras interna y externa del tubo interior; esta configuración pretende minimizar las deformaciones geométricas en el tubo debido a la presión. La variación de presión se transmite a través de un pistón gracias a un fluido hidráulico cuyo reservorio está en otra celda situada al lado de la celda de medida, estando ambas conectadas entre sí. La presión se mide mediante el empleo de un manómetro HBM-P3M (con una incertidumbre de 0.2 MPa) conectado entre las dos celdas. Ya que las medidas se pueden realizar a diferentes temperaturas, un fluido circulante (aceite de silicona), que rodea toda la celda de medida, es bombeado mediante un baño de circulación. Inserta dentro de la celda de medida se encuentra una sonda Pt 100, que provee el dato de temperatura en el fluido con una incertidumbre de 0.05 K. Todo el conjunto que compone el viscosímetro se encuentra a su vez dentro de una cámara termorregulada por circulación de aire, que se cierra previamente a realizar las medidas, y que asegura que la temperatura seleccionada se mantenga constante en todo el dispositivo.

Figura 1. Vista general del viscosímetro de caída de cuerpo situado en el Laboraroire des Fluides Complexes et leurs Réservoirs de la Universidad de Pau (Francia).

Respecto al sistema de medida, el cuerpo metálico, que es de acero y toma diferentes morfologías y densidades dependiendo de la viscosidad del fluido a medir, se mueve libremente en el seno del fluido; además, el equipo está provisto de un sistema accionado neumáticamente que hace rotar la celda de medida, a fin de permitir el movimiento vertical del cuerpo. El tubo interior está provisto de dos pares de sensores eléctricos (primario, 60 Ω y secundario, 150 Ω) separados una distancia entre ellos de 150 mm, que detectan el paso del cuerpo metálico a partir de una variación en el campo magnético. Así se puede determinar el tiempo que emplea el mismo en caer.

Respecto al valor de la incertidumbre en la medida, teniendo en cuenta las incertidumbres en temperatura, presión, el tiempo que emplea el cuerpo en caer durante las medidas, así como la incertidumbre en la calibración (la cual se estudia más adelante), la incertidumbre expandida que se obtiene es del 2% para las medidas realizadas entre (0.1 – 100) MPa, y del 4% para las medidas hasta 200 MPa.

Un esquema de la celda de medida del viscosímetro se encuentra en la Figura 2.

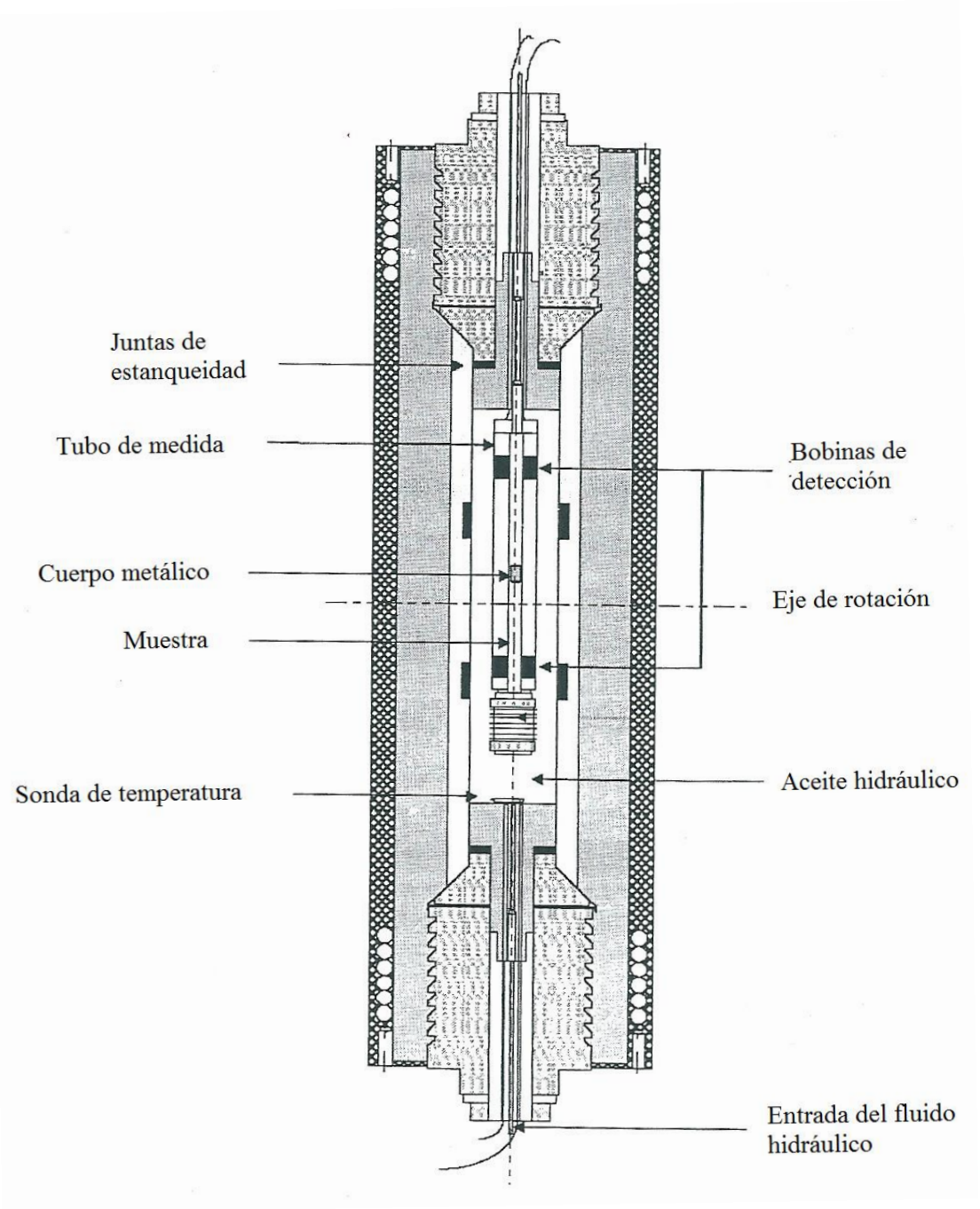

Figura 2. Esquema de la celda de medida del viscosímetro de caída de cuerpo. (tomada de: tesis G. Watson, referencia [3]).

5.3 Procedimiento experimental de medida.

Previamente a la realización de cualquier medida, se procede a hacer vacío en el interior de la celda de medida con una bomba de vacío, a fin de asegurar la correcta limpieza de la misma y prevenir contaminación con otros fluidos que se hubieran podido medir previamente.

Una vez hecho el vacío, el procedimiento de llenado se hace desde la parte superior de la celda de medida, donde se dispone de una válvula de apertura a la que se le incorpora un embudo para realizar el llenado. El fluido entra y rellena todo el espacio de la celda de medida, posteriormente se cierra la válvula de llenado y se llevará el sistema a la temperatura y presión deseadas. El fluido puro se introduce directamente, y si lo que se desea medir es una mezcla, esta se prepara en frascos en este caso de 250 cm^3 mediante pesada de las cantidades requeridas de cada uno de los fluidos, teniendo en cuenta su masa molar y la fracción molar que se desee obtener. La incertidumbre expandida en la composición de la mezcla es de $\pm 6 \cdot 10^{-5}$ en fracción molar.

Para tener una representación más fiable de los datos de tiempo que tarda en ser detectado el cuerpo entre un par de bobinas y otro, se repiten las medidas hasta en 6 ocasiones (reproducibilidad = 0.5%); como ya se dijo, el cilindro con la celda de medida puede rotar 180º a fin de permitir la caída del cuerpo metálico, y de homogeneizar la temperatura en el fluido a medir. El paso del cuerpo metálico entre los dos pares de sensores queda reflejado por la variación en la amplitud de la onda que es medida por un osciloscopio marca Tektronix TDS 1022B. A su vez, un software específico recoge los valores de los tiempos de caída del cuerpo en función de la presión y la temperatura del sistema, y lo envía a una hoja de Excel. En la Figura 3 se muestra la disposición del osciloscopio y la pantalla con el programa de captura de datos.

En el caso de este estudio, las medidas se realizaron en los intervalos de temperatura (293.15 – 353.15) K espaciados cada 20 K, y en el rango de presiones (0.1 – 100) MPa, cada 20 MPa.

Una vez realizas todas las medidas para cada compuesto puro o mezcla, se procede al vaciado y limpieza mediante vacío de todo el sistema.

Figura 3. Osciloscopio encargado de registrar el paso del cuerpo metálico a través de los pares de bobinas, y pantalla de captura de datos.

Hay que puntualizar que, para las medidas a 0.1 MPa, la viscosidad dinámica se determinó mediante el empleo de un viscosímetro capilar (Ubbelohde) a partir de la viscosidad cinemática. Para poder realizar las medidas a las distintas temperaturas, el viscosímetro capilar se sumerge en un baño termostático que utiliza agua como fluido calorportador, el cual proporciona un control de temperatura mejor que 0.1 K, y se conecta a un analizador de datos que reportará el tiempo que tarda en recorrer la muestra una determinada distancia, marca AVS350 Schott Geräte Analyzer.

La disposición del viscosímetro capilar en el baño, y conectado al analizador se muestra en la Figura 4.

La determinación de la viscosidad cinemática se hace teniendo en cuenta los parámetros de construcción del capilar de acuerdo a las ecuaciones (6) – (8):

$$E = \frac{1.66 \cdot \sqrt{V^3}}{L \cdot \sqrt{2 \cdot K \cdot R}} \tag{6}$$

Donde V es el volumen de medida en cm^3, L es la longitud del tubo capilar en cm, K es la constante del tubo en mm^2/s^2, y R es el radio del tubo capilar, en cm.

$$HC = \frac{E}{K \cdot t^2} \tag{7}$$

Donde E es el parámetro calculado en la ecuación (6), K es la constante del tubo capilar en mm^2/s^2, y t es el tiempo en segundos que tarda el fluido en recorrer una distancia especificada.

A partir de estos datos la viscosidad cinemática resulta ser:

$$\nu = T \cdot (t - HC) \tag{8}$$

Donde T, es la temperatura a la que se hace la medida, en grados Celsius, t, es el tiempo en segundos, y HC, es el parámetro calculado en la ecuación (7).

El dato de viscosidad dinámica se obtiene entonces a partir de la viscosidad cinemática proporcionada por el capilar, y a partir de los datos de densidad medidos previamente en el densímetro de tubo vibrante a la misma presión y temperatura de acuerdo con la ecuación (9):

$$\eta = \nu \cdot \rho \tag{9}$$

Donde η, es la viscosidad dinámica en mPa·s, ν es la viscosidad cinemática proporcionada por el viscosímetro capilar en cPs, y ρ es la densidad del fluido, en $g \cdot cm^{-3}$.

El dato de viscosidad dinámica obtenido arroja una incertidumbre menor al 1%.

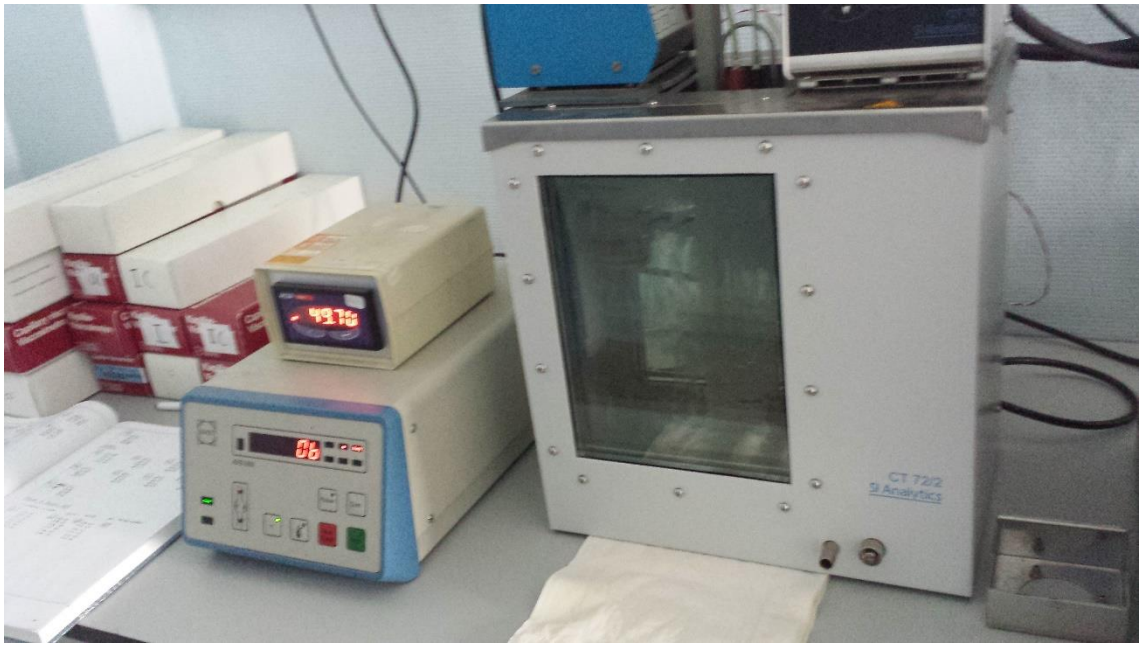

Figura 4. Situación del viscosímetro capilar, el baño termostático y el analizador en el Laboratoire des Fluides Complexes de la Universidad de Pau.

5.4 Calibración.

Como se dijo anteriormente, el valor de *K* en la ecuación (3) depende tanto de la configuración del viscosímetro (tubo interno) como de la del cuerpo de caída. Por tanto, para determinar este parámetro es necesario realizar una calibración con fluidos de referencia cuyos valores, tanto de viscosidad como de densidad, sean bien conocidos. En este caso la calibración se realizó con tolueno y *n*-decano en cada rango de presión y temperatura, tomando como referencia los datos publicados en la referencia [4] para el tolueno, y en la referencia [5] para el *n*-decano. El procedimiento de medida con ambos fluidos se repite varias veces para cada conjunto de *P* y *T*. La constante *K* se obtiene entonces representando gráficamente los valores de viscosidad de los dos fluidos de referencia en función de la relación $(\rho s - \rho_L)\Delta\tau$. En el caso del tolueno la incertidumbre experimental para la densidad es del 0.03%, mientras que la incertidumbre para la viscosidad es del 2% si las medidas se realizan en el rango de presiones (0.1 – 100) MPa, y del 4% entre (100 – 200) MPa. Para el *n*-decano, la incertidumbre experimental en densidad es del 0.01%, y la incertidumbre en viscosidad es la misma que en el caso del tolueno, 2%, si las medidas se realizan en el rango de presiones (0.1 – 100) MPa, y 4% a presiones entre (100 – 200) MPa.

5.5 Ajuste de los datos experimentales.

Los datos experimentales de viscosidad dinámica obtenidos se correlacionaron mediante la ecuación Vogel-Fulcher-Tamman (VFT) modificada, la cual se muestra como apta para realizar el ajuste de los datos de viscosidad a alta presión.

$$\eta = A\exp\left(a_1\Delta P + \frac{B + b_1\Delta P + b_2\Delta P^2}{T - C}\right) \tag{10}$$

Donde $\Delta P = P - P_{ref}$. *A, B, C* así como a_1, b_1 y b_2 son los parámetros ajustables de la ecuación, cuyo cálculo se ha realizado mediante el empleo del software Table Curve 3D. En la ecuación (10), 0.1 MPa es la presión de referencia, P_{ref}, de forma que cuando *P* es igual a 0.1 MPa, la ecuación (8) se puede expresar de la siguiente forma:

$$\eta = A\exp\left(\frac{B}{T - C}\right) \tag{11}$$

La correlación de los datos experimentales se lleva a cabo mediante el empleo de la ecuación VFT en los mismos rangos de *P* y *T* en los que se realizaron las medidas experimentales.

5.6 Incertidumbre en la medida.

La determinación de la incertidumbre para la viscosidad está relacionada por un lado con la variable independiente ($\Delta\rho\Delta t$), así como con la contribución de los parámetros de la calibración.

Al haberse empleado dos fluidos en el proceso de calibración (tolueno y *n*-decano), la ecuación (5) se transforma en:

$$\eta(T,P) = K_t(P,T) + K_d(P,T)\cdot(\rho_S - \rho_L)\Delta t \qquad (12)$$

Donde K_t es la constante de calibración del tolueno, y K_d es la del *n*-decano.

La Tabla 2 recoge los distintos valores de la incertidumbre en la determinación de la viscosidad, teniendo en cuenta que para la misma se han empleado tanto el viscosímetro capilar, en la determinación de la viscosidad a presión atmosférica, como el viscosímetro de caída de cuerpo, para la determinación de la viscosidad a alta presión.

Tabla 2. Cálculo de la incertidumbre asociada a la viscosidad experimental.

		Unidad	*u*(*x*)	*U(x)*
Presión		MPa	0.2	
Temperatura		K	0.05	
Densidad (ρ) Calibración	tolueno	kg·m^{-3}		$3\cdot10^{-4}$
	n-decano			$1\cdot10^{-4}$
Viscosidad (η) Calibración	tolueno	mPa·s		0.02
	n-decano			0.04
Composición (x)			$6\cdot10^{-5}$	
Viscosidad (η) Viscosímetro de caída cuerpo	(0.1 – 100) Mpa	mPa·s		0.02
	(101 – 200) Mpa			0.04
Viscosidad (η) Ubbelohde		mPa·s		0.01

5.7 Referencias.

[1] S.V. Gupta, Viscosimetry for liquids, calibration of viscometers, 1st ed. Springer, Switzerland (2014).

[2] C. Zéberg-Mikkelsen, A. Baylaucq, G. Watson, C. Boned, Int. J. Thermophys. 26 (2005) 1289-1302.

[3] G. Watson, Tesis doctoral: Masse volumique et viscosité dinamique sous haute pression de mélanges alcool + hydrocarbure et mise au point d'un conductimètre électrique haute pression, Université de Pau et des Pays de l'Adour, Pau, Francia (2007).

[4] M. J. Assael, J. H. Dymond, M. Papadaki, P. M. Patterson, Fluid Phase Equilibria 75 (1992) 245–255.

[5] M. L. Huber, A. Laesecke, H.W. Xiang, Fluid Phase Equilibria 224 (2004) 263-270.

Capítulo 6

DETERMINACIÓN EXPERIMENTAL DE LA VELOCIDAD DEL SONIDO A ALTA PRESIÓN

6.1 Introducción.

La velocidad del sonido se define como la velocidad de propagación de las ondas mecánicas longitudinales producidas por variaciones de presión en el medio. Esta velocidad variará dependiendo del medio en el que se realiza la propagación de la onda, por lo cual, variaciones en la temperatura o presión del medio en el cual se propaga generarán variaciones en el valor de la velocidad del sonido.

Para evitar que la velocidad de la onda acústica sea dependiente de la frecuencia con la cual se propaga en el fluido y, de la misma manera, evitar los fenómenos de relajación que conllevan los efectos dispersivos conducentes a una absorción energética de las ondas acústicas, las frecuencias deben responder a ciertos criterios [1]. Existen tres procesos responsables de la relajación: la viscosidad, la conducción térmica y las contribuciones moleculares; en el caso de los fluidos no asociados, como son los fluidos objeto de estudio en esta tesis, estos tres fenómenos están reservados al dominio de las longitudes de onda de varios centímetros (hiperfrecuencias), que están suficientemente lejos de nuestras condiciones de trabajo (3 MHz). Por lo tanto, se puede decir que nos encontramos en el dominio de las frecuencias nulas y que la velocidad de la propagación de la onda acústica es asimilable a la velocidad del sonido teórica de dicha onda.

La importancia de la determinación de esta propiedad en fluidos reside en la información que provee para, a partir de ella, determinar otras propiedades termodinámicas (valores de coeficientes de compresibilidad), así como brindar información sobre los procesos de relajación en fluidos. Así mismo, la velocidad del sonido está íntimamente ligada a propiedades como el calor específico.

Existen distintas técnicas experimentales para la determinación de esta propiedad, las cuales se pueden clasificar dentro de los métodos directos o de los métodos indirectos.

Los primeros basan su técnica en la medida directa de la velocidad del sonido utilizándose transductores que convierten una señal eléctrica en una onda acústica que se propaga en el fluido, la cual a su vez es captada por otro transductor, que transforma esa onda en una nueva señal eléctrica. Los métodos indirectos pueden basar la medida de la velocidad del sonido en la determinación de la frecuencia de resonancia de un fluido, o en la difracción de la luz que permite obtener la velocidad de la onda ultasonora. Algunas de estas técnicas se recogen en la Tabla 1.

Tabla 1. Relación de las distintas técnicas para la medida de la velocidad del sonido.

Métodos Directos	Métodos Indirectos
- Técnica impulsional	- Interferometría
	- Métodos ópticos
	- Métodos basados en fenómenos de resonancia.

En el caso de esta tesis, las determinaciones de velocidad del sonido a alta presión se hicieron empleando la técnica impulsional. Esta técnica utiliza dos transductores: uno funcionará como emisor y el otro como receptor. El primer transductor (emisor) está conectado a un generador de impulsos de tipo Dirac. A su vez este transductor está conectado a un osciloscopio que proporciona en tiempo real el tiempo que tarda la onda en viajar desde el transductor emisor al receptor, siendo este último el encargado de convertir la señal acústica recibida en señal eléctrica. De esta manera, la ecuación general de cálculo de la velocidad del sonido se expresa de la siguiente forma:

$$c = \frac{L(T,P)}{\Delta t} \tag{1}$$

Donde $L(T, P)$ es la distancia recorrida por la onda, la cual es función de la presión y la temperatura, y Δt es el tiempo que tarda la onda en viajar desde el emisor al receptor. En la siguiente sección se explica con detalle el dispositivo para determinación de la velocidad del sonido a alta presión situado en el Laboratoire des Fluides Complexes de la Universidad de Pau en Francia.

6.2 Técnica experimental de medida de la velocidad del sonido a alta presión.

El dispositivo empleado para la medida de la velocidad del sonido a alta presión se encuentra situado en el Laboratoire des Fluides Complexes de la Universidad de Pau, y emplea la técnica de medida por ecos sucesivos. Esta técnica se basa en llevar a cabo la medida del tiempo que tarda la onda en recorrer la distancia entre un transductor que actúa como emisor y otro que actúa como receptor. Una parte de la energía corresponde al primer eco mostrado en el osciloscopio, y es reflejada hacia el receptor antes de ser captada por el emisor que sirve a su vuelta como transductor receptor (distancia L_2) antes de que un nuevo tiempo sea medido sobre una nueva vuelta (distancia L_3). De esta manera, la eliminación del tiempo residual se hace como para una medida a distancia variable por ecos sucesivos de la onda ligada a la emisión de una

señal acústica a través del fluido. La Figura 1 muestra de forma esquemática el trayecto realizado por la onda visualizada en el osciloscopio.

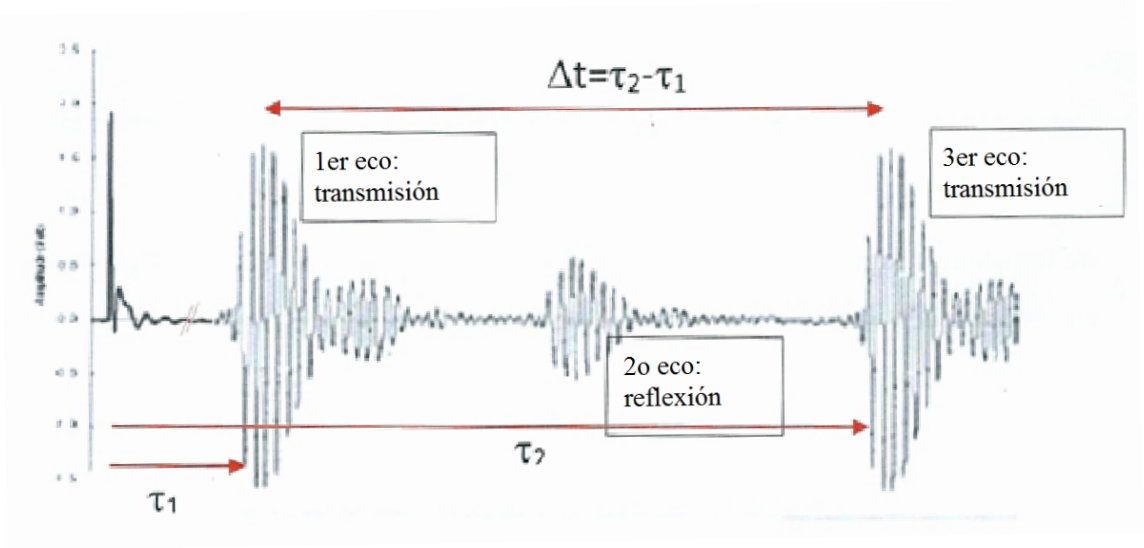

Figura 1. Trayecto de la onda acústica realizado el cual se visualiza en el osciloscopio durante la medición de la velocidad del sonido con la técnica de ecos sucesivos.

La ecuación de cálculo de la velocidad del sonido se expresa de la siguiente forma:

$$c = \frac{L(T,P)}{\Delta t} = \frac{L_3 - L_1}{\tau_2 - \tau_1} = \frac{2L_1}{t_{2,\,fluido} - t_{1,\,fluido}} \qquad (2)$$

Donde τ_1 es el primer intervalo de tiempo medido, que se corresponde con la longitud L_1, y τ_2, segundo intervalo de tiempo medido, que se corresponde con la longitud L_2.

La descripción precisa del aparato se hace en el artículo de Ndiaye *et al.* [2]. El mismo consiste en un sensor acústico realizado en acero inoxidable, que se encuentra completamente inmerso en el fluido. El sensor posee dos transductores piezoeléctricos (emisor y receptor) en contacto con el fluido, situados uno frente al otro, y cuya frecuencia natural es de 3 MHz. Los mismos se encuentran fijados en sus fondos a un soporte de acero inoxidable. La celda de medida de la velocidad del sonido es básicamente un cilindro cerrado en uno de sus lados por un tapón, en el cual se encuentran tres conectores eléctricos conectados al generador. A su vez, se dispone de dos conexiones a sendos indicadores de presión: uno de ellos proporciona el dato de presión entre (0.1 – 100) MPa, con una incertidumbre del 0.1%, mientras que el otro proporciona datos hasta 210 MPa, con una incertidumbre del 0.2%. La presión en el interior de la celda de medida se genera gracias a una bomba manual marca Top Industrie capaz de alcanzar 200 MPa. La celda está completamente sumergida en un baño termostático marca Huber que emplea aceite de

silicona como fluido portador de calor. El baño posee una estabilidad en temperatura de 0.02 K en el rango (283 – 403) K, mientras que una sonda Pt100 colocada en el interior de la celda de medida registra el dato de temperatura con una incertidumbre de 0.04%. La incertidumbre expandida en la medida de la velocidad del sonido que se reporta es del 0.2% en el rango de presiones (0.1 – 100) MPa y del 0.3% para el rango de presiones (0.1 – 210) MPa. Un esquema de la celda de medida puede observarse en la Figura 2.

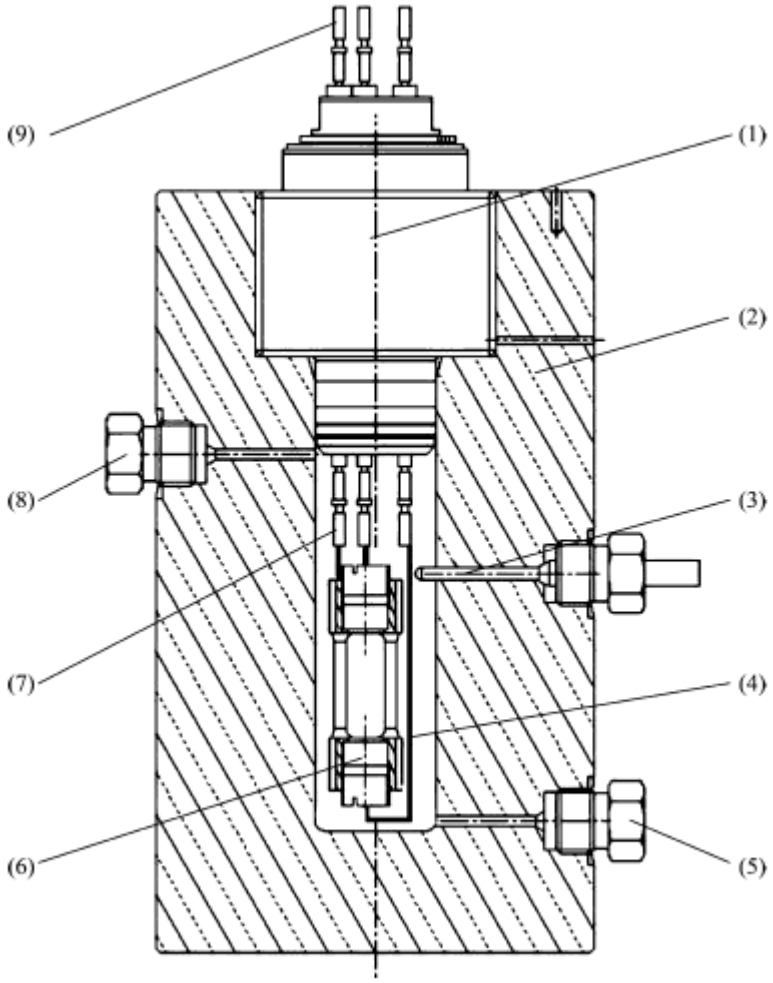

Figura 2. Celda de medida de la velocidad del sonido. (1) Tapón con conexiones eléctricas, (2) Cilindro de acero inoxidable, (3) Sonda Pt100, (4) Cable eléctrico, (5) Conexión para la entrada del fluido, (6) Sensor acústico inmerso en el fluido, (7) Conexiones eléctricas internas, (8) Conexión externa, (9) Conexiones eléctricas hacia el generador. Tomado de referencia [2].

La velocidad del sonido se mide empleando dos ecos sucesivos; el pulso producido por el generador es suministrado por uno de los transductores (emisor) a fin de generar la onda que viajará por el fluido. El primer y segundo ecos recibidos por el otro transductor (receptor) se muestran en un osciloscopio digital marca Tektronix TDS 1022B. El tiempo de vuelta se deduce

a partir de la medida del intervalo de tiempo entre estos dos ecos. La distancia o longitud teórica del trayecto *L*, se determina realizando una calibración a distintas temperaturas y presiones midiendo el tiempo de vuelo de la onda en un líquido cuya velocidad del sonido se conozca con precisión. Este procedimiento de describirá en la Sección 6.4, *Calibración*.

Una vista general del dispositivo para la medida de la velocidad del sonido a alta presión se puede ver en la Figura 3.

Figura 3. Situación del baño termostático en cuyo interior se encuentra la celda de medida de la velocidad del sonido a alta presión. Se observan en la parte superior del mismo los tres conectores eléctricos que conectan con el generador.

6.2.1. Técnica auxiliar: capacidad calorífica a presión constante.

En la Sección 6.5, *Ajuste de los datos experimentales*, se describirá la técnica empleada para determinar la densidad a alta presión a partir de los datos de velocidad del sonido. Con este fin se hace necesario conocer la capacidad calorífica a presión constante de las muestras, que se calcula a partir de los datos de *Cp* medidos a presión atmosférica ($Cp_{ref\ (T)}$). La determinación experimental de estas capacidades caloríficas se ha realizado con un calorímetro micro-DSC VII Evo de Setaram (*Differential Scanning Calorimeter*), instalado en el Laboratoire des Fluides Complexes et leurs Réservoirs de la Universidad de Pau. Una imagen del mismo puede observarse en la Figura 4.

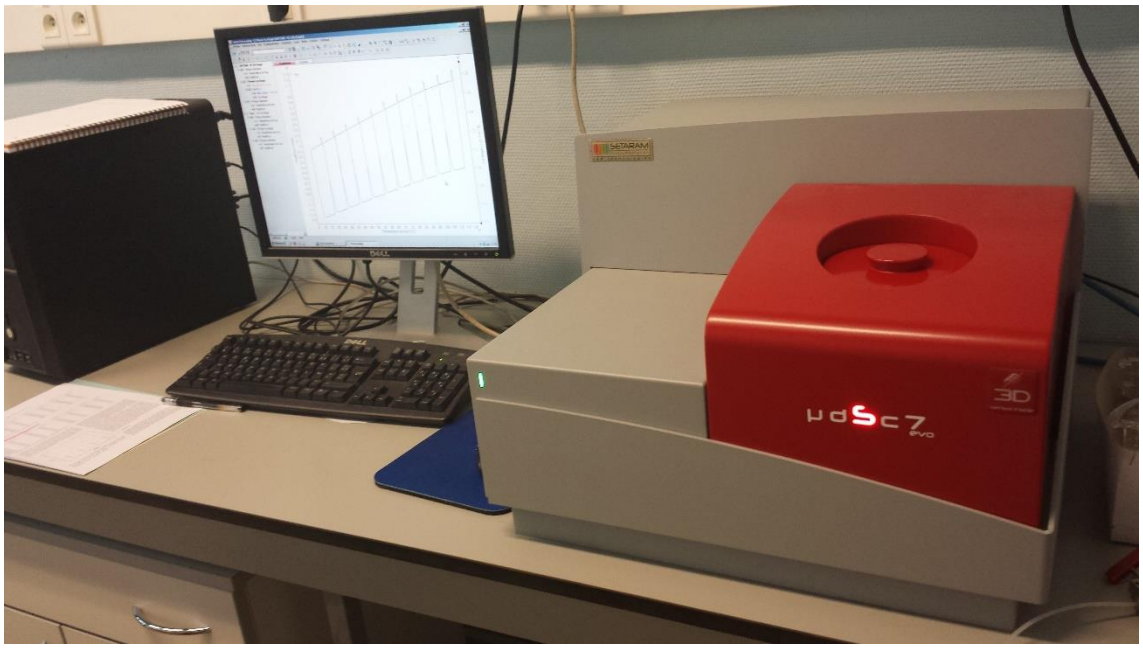

Figura 4. Calorímetro micro-DSC VII Evo de Setaram con el que se han determinado las capacidades caloríficas de las muestras a presión atmosférica.

Este tipo de calorímetro opera de acuerdo con el principio de Calvet: cuando dos termo-pilas equipadas con sus respectivas celdas son emparejadas y funcionan a la misma temperatura (en el mismo termostato), es posible determinar el flujo de calor diferencial entre esas dos termo-pilas [3]. El calorímetro micro-DSC VII Evo consiste esencialmente en un bloque cilíndrico metálico con una alta conductividad térmica que actúa como un termostato. En él se encuentran dos cavidades, una contiene la celda de medida, la otra la celda de referencia. Cada celda está rodeada por placas medidoras del flujo de calor (termo-pilas) de muy alta sensibilidad que procuran la conducción térmica con el bloque del calorímetro. La señal eléctrica de salida es proporcional al intercambio de calor que existe entre el contenedor de la muestra y el bloque. Por

la disposición de las dos termo-pilas, la de la celda de medida y la de referencia, en oposición, la interferencia común de ambas celdas es descontada. Así permiten la medida de los flujos de calor diferenciales entre las celdas de medida y de referencia resultantes de los pequeños cambios de temperatura en la celda de medida.

Este instrumento emplea un pequeño tamaño de muestra (1 cm^3 de capacidad de las celdas), y el circuito cerrado de líquido termostático que asegura que la estabilidad y homogeneidad en la temperatura del bloque es mejor que ±1 mK. El aparato está equipado con una circulación externa de agua como fluido de refrigeración alrededor de todo el bloque calorimétrico, asegurando un rango de temperaturas de trabajo entre 228.15 K y 393.15 K. La temperatura del calorímetro puede ser controlada y programada con una pendiente entre 0 y 1 $K \cdot min^{-1}$ tanto en los modos de calentamiento como de enfriamiento. La regulación de la temperatura se asegura mediante dos fases de elementos Peltier situadas alrededor de las celdas de referencia y de medida, y en el bloque calorimétrico. Esta disposición garantiza una menor inercia, un control preciso de la temperatura, y una alta sensibilidad en la señal de salida.

Para evitar la condensación de vapor sobre las paredes del calorímetro, fundamentalmente a baja temperatura, se emplea un barrido constante con nitrógeno seco con una pureza ≥ 99.995%. La conducción del gas está conectada a la cámara de experimentación que contiene las celdas y la caja de protección de los transductores.

La evolución del flujo diferencial de calor (± 0.005 mW), y de la temperatura (±0.01 K) frente al tiempo son monitorizados y analizados mediante el software Calisto Setaram.

Para llevar a cabo el proceso de medida, la temperatura del bloque se programa para que varíe linealmente en el tiempo con una pendiente determinada (*scanning rate*) un escalón (*step*), hasta que se produce un $\Delta T = T_2 - T_1$ de alrededor de 1 K. Los flujos de calor (*HF*) son registrados durante este incremento ΔT.

En un primer experimento, ambas celdas, de referencia y de muestra, se mantienen vacías a fin de obtener una línea de base del flujo de calor, lo cual se denomina "obtener un blanco". En el segundo experimento la celda de medida debe llenarse con un fluido de referencia, en este caso *n*-decano (pureza ≥ 99.0%). Este fluido se selecciona por el buen conocimiento que se tiene de su capacidad calorífica. Después se lleva a cabo un tercer experimento, en el que la celda de muestra se llena con una determinada cantidad del fluido cuyo *Cp* nos interesa determinar. Para conocer su masa, primero se pesa la celda de medida vacía, y posteriormente esta con el fluido empleando una balanza Ohaus Explorer E0RR80. Mientras, la celda de referencia debe mantenerse vacía. En todos los experimentos se hace un "pretratamiento" en el que la temperatura desciende por debajo del intervalo a medir. Después comienza la medida en los escalones de temperatura programados. Un esquema de cómo se realiza esta determinación del Cp_{ref} se puede ver en la Figura 5.

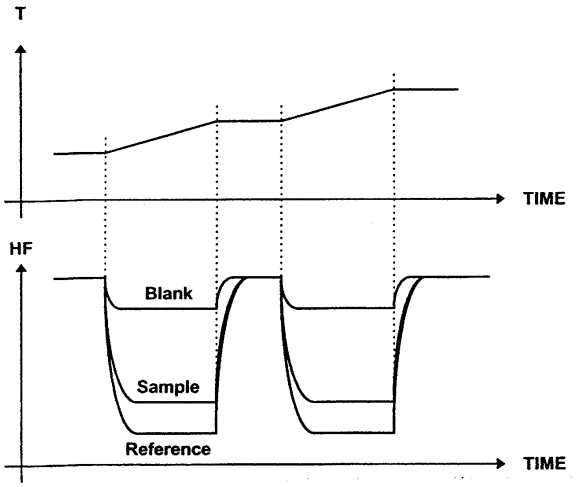

Figura 5. Determinación de Cp_{ref} a partir de los tres experimentos. En abscisas del segundo gráfico, HF hace referencia al flujo de calor.

La capacidad calorífica se calcula entonces a partir de la expresión:

$$Cp_{ref\,(T)} = \frac{HF_m - HF_v}{HF_r - HF_v} \cdot \frac{m_r}{m_m} \cdot Cp_R \qquad (3)$$

Donde *HF* hace referencia al flujo de calor diferencial, *m* a la masa, Cp_R es la capacidad calorífica del fluido referencia, y los subíndices *m*, *v* y *r* hacen referencia a muestra, vacío y referencia respectivamente.

La calibración del calorímetro micro-DSC VII Evo de Setaram se lleva a cabo midiendo la capacidad calorífica del *n*-dodecano (pureza mol% = 99.0%) en fase líquida, calculándose posteriormente la desviación promedio absoluta, AAD% (*Absolute Average Deviation*) con base en los datos proporcionados por el NIST [4] o por Zábranský *et al.* [5]

La incertidumbre expandida con un intervalo de confianza del 95% (k = 2) es, respectivamente, de 0.01 K para la temperatura, y 0.005 mW para el flujo diferencial de calor a partir de las estimaciones del fabricante del calorímetro. La incertidumbre expandida para la capacidad calorífica, con un nivel de confianza del 95% (k = 2) está estimada en un 0.5%.

6.3 Procedimiento experimental de medida.

Previamente a efectuar las medidas de velocidad del sonido, se procede a hacer el vacío en todo el circuito, para lo cual se conecta una bomba de vacío directamente a la celda de medida de la velocidad del sonido. La misma actúa durante al menos una hora a fin de asegurar la limpieza en el interior del aparato. Una vez hecho el vacío, el llenado se hace por succión llenando un embudo conectado a una válvula, como se puede observar en la Figura 6. Al abrirse la válvula, el fluido entra en el circuito. La bomba manual deberá estar en su posición de mínimo volumen, así en este punto se llevará a su posición de máximo volumen, para recoger el máximo fluido de muestra posible. El fluido puro se introduce directamente, y si lo que se desea medir es una mezcla, ésta se prepara en viales de 250 cm^3 mediante pesada de las cantidades requeridas de cada uno de los fluidos, teniendo en cuenta su masa molar y la fracción molar que se desee obtener. El volumen de muestra necesario para realizar las medidas es de 90 cm^3 aproximadamente. La incertidumbre expandida en la composición de la mezcla es de $\pm 6 \cdot 10^{-5}$ en fracción molar.

Figura 6. Dispositivo de llenado de la celda de medida de la velocidad del sonido a alta presión. En primer plano se aprecia la bomba manual, al fondo a la izauierda uno de los registradores de presión, y a la derecha el sensor de presión.

Una vez está el fluido en el circuito, se cierra la válvula de llenado, y se lleva a la temperatura y presión deseadas. Una vez alcanzadas, se realiza la medida del intervalo de tiempo entre los dos ecos sucesivos. El osciloscopio registra el trayecto la onda, mientras que gracias a un software específico es posible determinar el valor del intervalo de tiempo. Para realizar una determinación más correcta de este valor, se toma la media de entre tres mediciones sucesivas en las mismas condiciones de presión y temperatura. Las medidas realizadas en el marco de esta tesis se llevaron a cabo en los rangos de temperatura (273.15 – 353.15) K en isotermas espaciadas 10 K, y en el rango de presión (0.1 – 100) MPa cada 20 MPa.

La Figura 7 muestra el osciloscopio durante el proceso de medida de la velocidad del sonido. El cálculo de la distancia entre los dos ecos se realiza de acuerdo con la ecuación:

$$L(T,P) = \left(L_0\left(1 + a(T - T_0)\right)\left(1 + b(P - P_0)\right)\right) \tag{4}$$

Donde *L(T, P)* es la distancia en función de la presión y temperatura de la muestra, T_0 y P_0 son la temperatura y presión de referencia (293.15 K y 0.1 MPa), y L_0, *a* y *b* son los parámetros de calibración.

De esta manera la velocidad del sonido se determina de acuerdo a la ecuación (2).

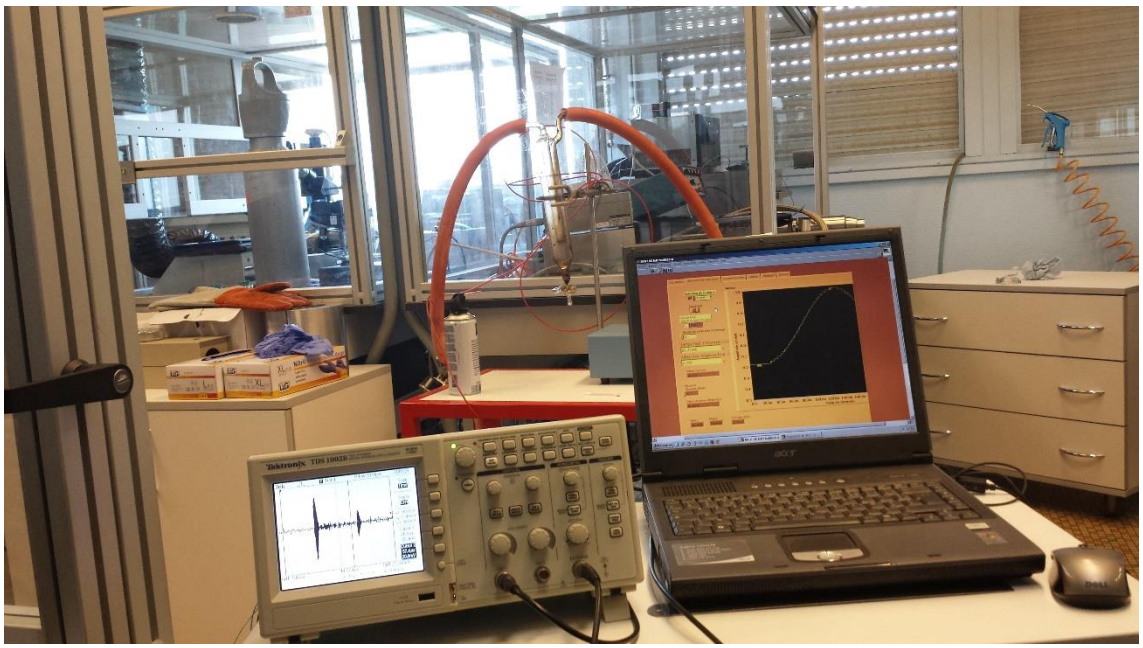

Figura 7. Osciloscopio durante el proceso de medida del tiempo entre dos ecos sucesivos y software de captura del dato de Δt.

6.4 Calibración.

A fin de determinar la distancia teórica *L(T, P)*, entre los dos transductores de acuerdo con la ecuación (4), se hace necesario llevar a cabo la calibración del aparato para poder determinar los parámetros L_0, *a* y *b*. Como fluidos de calibración se emplean el agua y el heptano, ya que existen datos fiables de velocidad del sonido a distintas presiones y temperaturas en la literatura. Para el caso del agua, se emplean los datos obtenidos en las referencias [6, 7], mientras que para el caso del heptano, se emplean los datos que proceden de la referencia [8]. El proceso de calibración consiste en determinar *L* a partir del dato de velocidad del sonido, a la presión y temperatura fijadas, obtenido en la literatura. De esta forma, una vez obtenidos los parámetros L_0, *a* y *b*, es posible determinar *L*, y con este dato, y el Δt medido, se calcula la velocidad del sonido del fluido de muestra según la ecuación (2). La incertidumbre en las medidas para el proceso de calibración es inferior al 0.2%.

6.5 Ajuste de los datos experimentales.

Los datos experimentales de velocidad del sonido se ajustaron a una función racional con nueve parámetros ajustables, que correlaciona $1/c^2$ en función de la presión y la temperatura:

$$\frac{1}{c^2} = \frac{A + BP + CP^2 + DP^3}{1 + ET + FP} \tag{5}$$

Donde:

$$A = A_0 + A_1 T + A_2 T^2 + A_3 T^3 \tag{6}$$

A partir de los datos experimentales de velocidad del sonido, es posible determinar tanto las propiedades derivadas, (compresibilidad isoentrópica, κ_S, compresibilidad isoterma, κ_T, y expansividad isobárica, α_P), así como la densidad a alta presión, ρ, a partir de un método basado en las relaciones de Newton-Laplace para el cálculo de la velocidad del sonido [9]. El procedimiento de cálculo comprende los siguientes pasos:

$$c = v\left(-\left(\frac{\partial v}{\partial P} \right)_T - \frac{T}{Cp}\left(\frac{\partial v}{\partial T} \right)_P^2 \right)^{0.5} \tag{7}$$

La compresibilidad isoentrópica κ_S, se determina a partir de la ecuación (8):

$$\kappa_S = -\frac{1}{v}\left(\frac{\partial v}{\partial P}\right)_T - \frac{T}{c \cdot Cp}\left(\frac{\partial v}{\partial T}\right)_P \tag{8}$$

La compresibilidad isoterma κ_T, se determina:

$$\kappa_T = -\frac{1}{v}\left(\frac{\partial v}{\partial P}\right)_T \tag{9}$$

Y la expansividad isobárica se calcula a partir de:

$$\alpha_P = \frac{1}{v}\left(\frac{\partial v}{\partial T}\right)_P \tag{10}$$

El objetivo es calcular las derivadas parciales de las ecuaciones (8), (9) y (10).

En las ecuaciones (7), (8), (9) y (10), v es el volumen específico ($1/\rho$), el cual se calcula a partir de:

$$v = v_{ref} - C(P - P_{ref}) + (BC - A)\ln\left(\frac{P + B}{P_{ref} + B}\right) \tag{11}$$

Donde:

$$A = A_0 + A_1 T + A_2 T^2 + A_3 T^3 \tag{12}$$

$$B = B_0 + B_1 T + B_2 T^2 \tag{13}$$

$$v_{ref} = v_0 + v_1 T + v_2 T^2 + v_3 T^3 \tag{14}$$

Los parámetros A_0, A_1, A_2, A_3, B_0, B_1, B_2, C, en las ecuaciones (12) y (13), así como v_0, v_1, v_2 y v_3 en la ecuación (14) se obtienen realizando un ajuste por mínimos cuadrados a partir de datos experimentales de densidad a alta presión.

En las ecuaciones (7) y (8) Cp, es la capacidad calorífica a presión constante a las distintas presiones, la cual se determina a partir de los datos de $Cp_{,ref}$ que se corresponden con las medidas hechas a presión atmosférica de la capacidad calorífica para cada muestra. Estas $Cp_{,ref}$ se expresan

como una función cuadrática o cúbica de la temperatura. *Cp* se determina entonces a partir de la ecuación (15):

$$Cp = Cp_{ref(T)} - T \cdot \frac{\partial^2}{\partial T^2} \int_{\Pr ef}^{P} v dP \tag{15}$$

La derivada del volumen con respecto a la presión se calcula como sigue:

$$\left(\frac{\partial v}{\partial P}\right)_T = -\frac{A + CP}{B + P} \tag{16}$$

Donde los parámetros *A*, *B* y *C* son los mismos que para las ecuaciones (11), (12) y (13). La derivada del volumen con respecto a la temperatura se obtiene operando:

$$\begin{aligned}\left(\frac{\partial v}{\partial T}\right)_P &= \left(\frac{\partial v_{ref}}{\partial T}\right)_P + \left(\left(\frac{\partial B}{\partial T}\right)C - \left(\frac{\partial A}{\partial T}\right)\right) \cdot \ln\left(\frac{P + B}{P_{ref} + B}\right) + \\ &+ (BC - A) \cdot \left(\frac{1}{P + B} - \frac{1}{P_{ref} + B}\right) \cdot \left(\frac{\partial B}{\partial T}\right)\end{aligned} \tag{17}$$

6.6 Incertidumbre en la medida.

En el caso de la velocidad del sonido, *c*, la determinación de la incertidumbre experimental está relacionada con la contribución de las constantes de la ecuación (4), L_0, *a* y *b*, obtenidas a partir de la calibración con dos fluidos de referencia: agua y heptano. De la misma forma, de acuerdo a la ecuación (2), la incertidumbre en el dato de velocidad del sonido depende de la distancia, *L*, entre el emisor y el receptor, la cual a su vez es función de la presión, *P*, y de la temperatura, *T*.

La Tabla 2 recoge los distintos valores de la incertidumbre en la determinación de la velocidad del sonido.

En el caso de la capacidad calorífica a presión constante, *Cp*, la incertidumbre es también función de los parámetros de calibración. La Tabla 3 muestra los valores de las distintas contribuciones a la incertidumbre para la capacidad calorífica a presión constante.

Tabla 2. Cálculo de la incertidumbre asociada a la velocidad del sonido experimental.

		Unidad	*u*(*x*)	*U*(*x*)
Presión	(0.1 – 100) Mpa	MPa	0.001	
	(101 – 210) MPa		0.002	
Temperatura		K	0.04	
Velocidad del sonido (c) Calibración	agua	$m \cdot s^{-1}$		0.002
	heptano			0.002
Composición (x)			$6 \cdot 10^{-5}$	
Velocidad del sonido (c)	(0.1 – 100) Mpa	$m \cdot s^{-1}$		0.002
	(101 – 210) MPa			0.003

Tabla 3. Cálculo de la incertidumbre asociada a la capacidad calorífica a presión constante.

	Unidad	*u*(*x*)	*U*(*x*)
Temperatura	K	0.01	
Flujo de calor (HF)	mW	0.005	
Composición (x)		$6 \cdot 10^{-5}$	
Capacidad calorífica (Cp)	$J \cdot K^{-1} \cdot kg^{-1}$		0.005

6.7 Referencias.

[1] M. Habrioux, Tesis doctoral: Caracterisation thermophysique des fluides sous pression a l'aide d'un dispositif unique de mesures acoustiques: application aux biodiesels, Université de Pau et des Pays de l'Adour, Pau, Francia (2015).

[2] E.H.I. Ndiaye, D. Nasri, J.L. Daridon, J. Chem. Eng. Data 57 (2012) 2667-2676.

[3] F. Aguilar, Puesta en marcha de dos técnicas de medida de alta precisión para la investigación termodinámica de mezclas de fluidos multicomponentes de interés industrial, técnica de medida de C_p (documento no publicado), (2002).

[4] E.W. Lemmon, M.O. McLinden, D.G. Friend. Thermophysical properties of fluid systems in WebBook of chemistry NIST. In: Linstrom P.J. Mallard, W.G. editors. Standard reference database NIST number 69. Gaither: National Institute of Standards and Technology (2013).

[5] M. Zábranský, Z. Kolská, V. Růžička, E.S. Domalski, J. Phys Chem Ref. Data 39 (2010).

[6] W.D. Wilson, J. Acoust. Soc. Am. 31 (1959) 1067-1072.

[7] E.H. Baltasar, M. Taravillo, V.G. Baonza, P.D. Sanz, B. Guignon, J. Chem. Eng. Data 56 (2011) 4800-4807.

[8] J.L. Daridon, A. Lagrabette, B. Lagourette, J. Chem. Thermodyn. 30 (1998) 607-623.

[9] J.L. Daridon, B. Lagourette, J.P. Grolier, Int. J. Thermophys. 19 (1998) 145-160.

Capítulo 7

RESULTADOS EXPERIMENTALES

7.1 Resultados experimentales

7.1 Resultados experimentales

Durante el desarrollo de esta Tesis Doctoral se han llevado a cabo una serie de trabajos (medidas experimentales, reducción de datos, aplicación de modelos matemáticos), los cuales quedan recogidos y redactados en formato de artículos de investigación, a modo de resultados, en el Anexo I. Como ya se explicó en el Capítulo 1, Hipótesis de partida y objetivos, se han empleado como fluidos puros cuatro hydrofluoroéteres (HFE-7100, HFE-7200, HFE-7300 y HFE-7500), así como dos alcoholes (1-propanol y 2-propanol), y un éter (diisopropil éter). Las mezclas estudiadas han sido las siguientes:

1) x HFE-7100 + (1-x) 1-propanol
2) x HFE-7100 + (1-x) 1-propanol
3) x HFE-7200 + (1-x) 2-propanol
4) x HFE-7500 + (1-x) diisopropil éter

Las técnicas experimentales utilizadas han ampliado el rango de datos previamente disponible en la literatura para los HFEs y sus mezclas, y se han basado en caracterizar distintas propiedades termofísicas tanto a altas presiones, como a altas temperaturas. Los equipos utilizados a tal fin son los siguientes:

a) Ebullómetro para equilibrio líquido-vapor isóbaro (Laboratorio de Ingeniería Energética de la Universidad de Burgos).
b) Densímetro de tubo vibrante para alta presión (Laboratorio de Ingeniería Energética de la Universidad de Burgos).
c) Densímetro y analizador de la velocidad del sonido a presión atmosférica (Laboratorio de Ingeniería Energética de la Universidad de Burgos).
d) Densímetro de tubo vibrante para alta presión (Laboratoire des Fluides Complexes de la Universidad de Pau).
e) Viscosímetro de caída de cuerpo (Laboratoire des Fluides Complexes de la Universidad de Pau).
f) Viscosímetro capilar de tipo Ubbelohde (Laboratoire des Fluides Complexes de la Universidad de Pau).
g) Equipo para la determinación de la velocidad del sonido a alta presión (Laboratoire des Fluides Complexes de la Universidad de Pau).
h) Calorímetro diferencial micro DSC, (Laboratoire des Fluides Complexes de la Universidad de Pau).

A continuación se recoge la secuencia de artículos publicados y/o redactados, los cuales se encuentran a texto completo en el Anexo I.

	Publicación	Nombre Artículo
1	Fluid Phase Equilibria 49 (2016) 281-292. DOI: 10.1016/j.fluid.2016.09.014	Liquid density of mixtures methyl nonafluorobutyl ether (HFE-7100) + 2-propanol at pressures up to 140 MPa and temperatures from 298.15 to 393.15 K.
2	Journal of Chemical Thermodynamics 112 (2017) 52-58. DOI: 10.1016/j.jct.2017.04.007	Speed of sound and derivative properties of hydrofluoroether fluid HFE-7500 under high pressure
3	Fluid Phase Equilibria 449 (2017) 148-155. DOI: 10.1016/j.fluid.2017.06.024	Speed of sound, density and derivative properties of diisopropyl ether under high pressure
4	(En revisión) Journal of Chemical Thermodynamics. Ref. JCT-17-546R1	Speed of sound, density and derivative properties of binary mixtures HFE-7500 + diisopropyl ether under high pressure
5	(En revisión) Journal of Chemical Thermodynamics.	High pressure density and speed of sound at atmospheric pressure of hydrofluoroether fluid 1,1,1,2,2,3,4,5,5,5-decafluoro-3-methoxy-4-(trifluoromethyl)-pentane (HFE-7300)
6		(P, V^E, T) measurements of mixtures methyl nonafluorobutyl ether (HFE-7100) + 1-propanol at pressures up to 70 MPa and at temperatures from 298.15 K to 393.15 K

7	Thermodynamics of binary mixtures 1-ethoxy-1,1,2,2,3,3,4,4,4-nonafluorobutane (HFE-7200) + 2-propanol: high pressure density, speed of sound and derivative properties.
8	High pressure viscosity measurements for the binary mixture HFE-7500 + diisopropyl ether
9	Isobaric vapor-liquid equilibrium at 50.0, 101.3, and 200.0 kPa, density and speed of sound at 298.15 K of binary mixtures HFE-7100 + 2-propanol.
10	Isobaric vapor-liquid equilibrium at 50.0, 101.3 kPa, density and speed of sound at 298.15 K of binary mixtures HFE-7500 + diisopropyl ether (DIPE).

Capítulo 8

CONCLUSIONES

8.1 Conclusiones.

8.1 Conclusiones.

La Tesis Doctoral "*Investigación sobre propiedades de nuevos fluidos industriales de bajo impacto ambiental como sustitutivos de gases fluorados para reducción del cambio climático*" ha sido realizada en su mayor parte en el Laboratorio de Ingeniería Energética de la Universidad de Burgos, junto con la estancia de cinco meses llevada a cabo en el Laboratoire des Fluides Complexes de la Universidad de Pau (Francia). La Tesis Doctoral centra su objeto de investigación en la caracterización de propiedades termofísicas de fluidos con interés industrial, en concreto aquellos denominados hidrofluoroéteres (HFEs), y sus mezclas con alcoholes y éteres, para sustitución de los compuestos fluorocarbonados con potencial de destrucción de la capa de ozono, y/o con un elevado índice de calentamiento global.

Las conclusiones que se enumeran a continuación exponen los objetivos alcanzados en la realización de los trabajos:

1. Se han seleccionado cuatro hidrofluoroéteres de alto peso molecular (HFE-7100, HFE-7200, HFE-7300 y HFE-7500), dos alcoholes (1-Propanol y 2-Propanol) y un éter (Diisopropil éter), como representativos de nuevos fluidos de bajo impacto ambiental que pueden sustituir a los actualmente utilizados fluorocarbonos.

2. Se han determinado las curvas de presión de vapor de cuatro componentes puros (HFE-7100, HFE-7500, 2-Propanol y Diisopropil éter), mediante un ebullómetro isóbaro, situado en el Laboratorio de Ingeniería Energética de la Universidad de Burgos, entre el rango de presiones (2.5 – 290) kPa.

3. Se han determinado experimentalmente los equilibrios líquido-vapor (ELV) de las mezclas binarias *x* HFE-7100 + (*1-x*) 2-propanol, y *x* HFE-7500 + (*1-x*) diisopropil éter, empleando el ebullómetro isóbaro del Laboratorio de Ingeniería Energética de la Universidad de Burgos, a distintas presiones (50.0, 101.3 y 200.0) kPa.

4. Se ha realizado la reducción de datos del equilibrio líquido-vapor, para las dos mezclas mencionadas, y se han correlacionado de acuerdo a distintos modelos matemáticos (NRTL, Wilson, UNIQUAC, y el modelo predictivo UNIFAC).

5. Se han medido las densidades a alta presión, empleando un densímetro de tubo vibrante, situado en el Laboratorio de Ingeniería Energética de la Universidad de Burgos, de cinco fluidos puros (HFE-7100, HFE-7200, HFE-7300, 1-propanol y 2-propanol), así como de tres mezclas binarias: *x* HFE-7100 + (*1-x*) 2-propanol, *x* HFE-7100 + (*1-x*) 1-propanol, y

x HFE-7200 + (*1*-*x*) 2-propanol, en el rango de presiones (0.1 – 140) MPa, y en el intervalo de temperaturas (293.15 – 393.15) K.

6. Se ha llevado a cabo la determinación de la densidad a alta presión, con un densímetro de tubo vibrante, situado en el Laboratoire des Fluides Complexes de la Universidad de Pau, en Francia, de los compuestos puros HFE-7500 y diisopropil éter (DIPE), y de su mezcla binaria, *x* HFE-7500 + (*1*-*x*) diisopropil éter, en el rango de presiones (0.1 – 140) MPa, y en el intervalo de temperaturas (293.15 – 393.15) K.

7. Los datos experimentales de densidad a alta presión se han correlacionado con una ecuación de tipo Tait, en los mismos rangos de presión y temperatura. Asimismo se han determinado los volúmenes de exceso de las mezclas, V^E, y las propiedades derivadas (compresibilidad isotérmica, κ_T, y expansividad isobárica, α_P).

8. Se han obtenido datos experimentales de viscosidad dinámica, empleando para ello un viscosímetro de caída de cuerpo, situado en el Laboratoire des Fluides Complexes de la Universidad de Pau (Francia), para los fluidos puros HFE-7500 y diisopropil éter (DIPE), así como para su mezcla binaria, en un intervalo de temperaturas (293.15 – 353.15) K, y en el rango de presiones (0.1 – 100) MPa.

9. Los datos experimentales de viscosidad a alta presión se han correlacionado con la ecuación Vogel-Fulcher-Tamman (VFT), en los mismos rangos de presión y de temperatura.

10. Se ha llevado a cabo la determinación de la velocidad del sonido a presión atmosférica para los cuatro HFEs seleccionados (HFE-7100, HFE-7200, HFE-7300 y HFE-7500), para el 2-propanol y para el diisopropil éter, así como para las siguientes tres mezclas binarias: *x* HFE-7500 + (*1*-*x*) diisopropil éter, *x* HFE-7100 + (*1*-*x*) 2-propanol, y *x* HFE-7200 + (*1*-*x*) 2-propanol, a distintas temperaturas dentro del rango (293.15 – 333.15) K, empleando un medidor de densidad y velocidad del sonido, situado en el Laboratorio de Ingeniería Energética de la Universidad de Burgos.

11. Se ha determinado el valor de la compresibilidad isoentrópica, κ_S, a partir de los datos de velocidad del sonido y de densidad a presión atmosférica, para los cuatro compuestos puros anteriormente mencionados (HFE-7100, HFE-7200, HFE-7300 y HFE-7500), para el 2-propanol y para el diisopropil éter, y para las tres mezclas binarias: *x* HFE-7500 + (*1*-*x*) diisopropil éter, *x* HFE-7100 + (*1*-*x*) 2-propanol, y *x* HFE-7200 + (*1*-*x*) 2-propanol, en los mismos rangos de temperatura que para la velocidad del sonido.

12. Se ha medido la velocidad del sonido a alta presión mediante un dispositivo que emplea la técnica impulsional, situado en el Laboratoire des Fluides Complexes de la Universidad de Pau, en Francia, para dos compuestos puros HFE-7500 y diisopropil éter, y su mezcla binaria, en el rango de presión (0.1 – 100) MPa, y en el rango de temperaturas (293.15 – 353.15) K.

13. Se han obtenido las capacidades caloríficas a presión constante en el rango de temperaturas (290.50 – 386.80) K, utilizando un calorímetro diferencial micro-DSC, situado en el Laboratoire des Fluides Complexes de la Universidad de Pau, para dos compuestos puros (HFE-7500 y diisopropil éter), así como para distintas fracciones molares de su mezcla binaria.

14. Se han correlacionado los datos de velocidad del sonido a alta presión a una ecuación, en el mismo rango de presiones y temperaturas.

15. Se ha realizado el cálculo de la densidad a alta presión a partir de los datos de velocidad del sonido a alta presión. Para ello se han empleado los datos de velocidad del sonido experimentales, así como los datos de capacidad calorífica de cada compuesto puro y de su mezcla binaria. También se han determinado las propiedades derivadas: compresibilidad isoentrópica, κ_S, compresibilidad isoterma, κ_T, y expansividad isobárica, α_P.

16. Por último, con esta investigación se ha aportado un corpus de datos sobre propiedades termofísicas que amplía la escasa bibliografía existente sobre los hidrofluoroéteres y sus mezclas como potenciales sustitutos de los fluorocarbonos. Los datos obtenidos a lo largo del trabajo realizado se han publicado en distintos congresos nacionales e internacionales, y en revistas con alto índice de impacto.

Chapter 8

CONCLUSIONS

8.1 Conclusions.

8.1 Conclusions.

The Doctoral Thesis entitled: *"Research on properties of new industrial fluids with low environmental impact as substitutes of fluorinated gases for climate change reduction"* has been carried out at the Laboratorio de Ingeniería Energética, of the University of Burgos, along with the five months research period at the Laboratoire des Fluides Complexes of the University of Pau, France. The research targets of this Doctoral Thesis are the thermophysical properties characterization of new industrial fluids, particularly those called hydrofluoroethers (HFEs), and their mixtures with alcohols and ethers, in order to substitute the commonly used ozone depleting and greenhouse effect fluorocabons.

The following conclusions present the achieved goals in the development of the research linked to this Doctoral Thesis:

1. Four high molecular weight hydrofluoroether fluids have been selected (HFE-7100, HFE-7200, HFE-7300 y HFE-7500), as well as two alcohols (1-propanol and 2-propanol) and an ether (diisopropyl ether), as representative substances of new industry fluids with low environmental impact, which are able to substitute the commonly used fluorocarbons.

2. Vapor pressure curves of four pure components have been determined (HFE-7100, HFE-7500, 2-propanol and diisopropyl ether), by using an isobaric ebullometer, placed at the Laboratorio de Ingeniería Energética of the University of Burgos, between the pressure ranges (2.5 – 290) kPa.

3. Vapor-liquid equilibria (VLE) of the two binary mixtures: x HFE-7100 + (1-x) 2-propanol, and x HFE-7500 + (1-x) diisopropyl ether, were determined, by using the isobaric ebullometer located at the Laboratorio de Ingeniería Energética, at the University of Burgos, at several pressures (50.0, 101.3 y 200.0) kPa.

4. Data reduction of vapor-liquid equilibrium data for the two binary mixtures has been carried out. Several mathematical models were employed for this purpose: (NRTL, Wilson, UNIQUAC, and the predictive model UNIFAC).

5. High pressure densities were determined by using a vibrating tube densitometer, situated at the Laboratorio de Ingeniería Energética, University of Burgos. Five pure components were studied: (HFE-7100, HFE-7200, HFE-7300, 1-propanol y 2-propanol), as well as three binary mixtures: x HFE-7100 + (1-x) 2-propanol, x HFE-7100 + (1-x) 1-propanol,

and *x* HFE-7200 + (*1*-*x*) 2-propanol, in the pressure range (0.1 – 140) MPa, and in the temperature interval (293.15 – 393.15) K.

6. High pressure density measurements were carried out by employing a vibrating tube densitometer, placed at the Laboratoire des Fluides Complexes, University of Pau, France, for the pure components HFE-7500 and diisopropyl ether (DIPE), and for the binary mixture, *x* HFE-7500 + (*1*-*x*) diisopropyl ether, in the pressure range (0.1 – 140) MPa, and in the temperature interval (293.15 – 393.15) K.

7. High pressure density data were correlated to a Tait type equation, in the same pressure and temperature ranges. Excess volumes, V^E, and the derivative properties, that is, the isothermal compressibility, κ_T, and the isobaric expansion, α_P, were also determined from high pressure density data.

8. High pressure dynamic viscosity measurements were carried out by using a falling body viscometer, situated at the Laboratoire des Fluides Complexes, at the University of Pau (France), for the pure components HFE-7500 and diisopropyl ether (DIPE), and for its binary mixture, in the temperature interval (293.15 – 353.15) K, and in the pressure range (0.1 – 100) MPa.

9. Experimental high pressure viscosity data were correlated to a Vogel-Fulcher-Tamman (VFT) equation, in the same pressure and temperature ranges.

10. Speed of sound data at atmospheric pressure were measured for the four selected HFEs (HFE-7100, HFE-7200, HFE-7300 y HFE-7500), for 2-propanol and for diisopropyl ether, as well as for the binary mixtures: *x* HFE-7500 + (*1*-*x*) diisopropyl ether, *x* HFE-7100 + (*1*-*x*) 2-propanol, and *x* HFE-7200 + (*1*-*x*) 2-propanol, at several temperatures whithin the range (293.15 – 333.15) K, by using a density and sound velocity analyzer, situated at the Laboratorio de Ingeniería Energética of the University of Burgos.

11. Isentropic compressibility κ_S values were determined from atmospheric pressure density data, and from atmospheric pressure speed of sound data, for the four HFEs: (HFE-7100, HFE-7200, HFE-7300 y HFE-7500), for 2-propanol and for diisopropyl ether, and for the three binary mixtures: *x* HFE-7500 + (*1*-*x*) diisopropyl ether, *x* HFE-7100 + (*1*-*x*) 2-propanol, and *x* HFE-7200 + (*1*-*x*) 2-propanol, in the same temperature and pressure ranges as for speed of sound measurements.

12. High pressure speed of sound measurements were carried out by employing an apparatus which uses the pulse-echo technique, placed at the Laboratoire des Fluides Complexes, University of Pau, for the pure components HFE-7500 and diisopropyl ether, and its binary mixture, in the pressure range (0.1 – 100) MPa, and in the temperature interval (293.15 – 353.15) K.

13. Isobaric heat capacities were measured in the temperature range (290.50 – 386.80) K, by employing a micro-DSC calorimeter, situated at the Laboratoire des Fluides Complexes, University of Pau, for the pure components HFE-7500 and diisopropyl ether, as well as for several mole compositions of its binary mixture.

14. High pressure speed of sound data were correlated by using a rational function, in the same pressure and temperature ranges.

15. High pressure density calculations were carried out from high pressure speed of sound data. For this purpose, experimental high pressure speed of sound and experimental heat capacity data were used. The derivative properties, isentropic compressibility, κ_S, isothermal compressibility, κ_T, and isobaric expansion, α_P, were also determined.

16. Finally, with this research, the set of new thermophysical data concerning hydrofluoroethers and their mixtures broadens the scarce literature references which are currently available. Data obtained along the development of this work were published in several national and international conferences, as well as in high impact factor journals.

Anexo I

Artículos de investigación

Fluid Phase Equilibria 429 (2016) 281–292

Contents lists available at ScienceDirect

Fluid Phase Equilibria

journal homepage: www.elsevier.com/locate/fluid

Liquid density of mixtures Methyl nonafluorobutyl ether (HFE-7100) + 2-propanol at pressures up to 140 MPa and temperatures from 298.15 K to 393.15 K

Natalia Muñoz-Rujas [a], Fernando Aguilar [a], Jean-Patrick Bazile [b], Eduardo A. Montero [a, *]

[a] Departamento de Ingeniería Electromecánica, Escuela Politécnica Superior, Universidad de Burgos, E-09006, Burgos, Spain
[b] Laboratoire des Fluides Complexes et leurs Réservoirs, CNRS-TOTAL, UMR 5150, Université de Pau, BP 1155, 64013, Pau Cedex, France

ARTICLE INFO

Article history:
Received 1 June 2016
Received in revised form
6 September 2016
Accepted 8 September 2016
Available online 10 September 2016

Keywords:
Methyl nonafluorobutyl ether
2-Propanol
Density
Isobaric thermal expansivity
Isothermal compressibility

ABSTRACT

This work reports experimental density data (1073 points) for the mixtures methyl nonafluorobutyl ether (HFE-7100) + 2-propanol along isotherms ranging from 298.15 to 393.15 K and at pressures from 0.1 to 140 MPa. To perform the measurements we used an Anton Paar vibrating tube densimeter, calibrated with an uncertainty of ±0.7 kg m^{-3}. The experimental density data were fitted with the Tait-like equation with low standard deviations. In addition, we derived the isobaric thermal expansivity and the isothermal compressibility from the Tait-like equation.

1. Introduction

Hydrofluoroether fluids (HFEs) have been investigated as an alternative to commonly used CFCs, HCFCs, HFCs and PFCs since the '90s. These fluids are an environmentally friendly alternative thanks to their near-zero ozone depletion potentials (ODP), low global warming potentials (GWP), and short atmospheric lifetimes [1]. HFEs possess many thermophysical properties similar to these fluorocarbons, so they can be used as substitutes for them for many of the same purposes. HFEs are also non-flammable fluids, have very low overall toxicity [2] and are inert to common metals and hard polymers [3].

The HFE selected as the subject of this work is methyl nonafluorobutyl ether, also known as HFE-7100. Its boiling point and low surface tension make it ideal for use as a cleaning solvent, low temperature heat transfer fluid, refrigerant, lubricant carrier, etc. as a pure compound or azeotropic component. HFE-7100 is a good option as a replacement for CFC-113, HCFC-14lb, HCFC-225ca/cb and 1,1,1-trichloroethane, especially its mixture HFE-7100 + 2-propanol, used in vapor degreasing and specialty cleaning. The exposure limits of this mixture are fairly high and it has no flash point, [2,4].

In this paper we present new $p\rho T$ experimental data for the binary mixture methyl nonafluorobutyl ether (HFE-7100) + 2-propanol at pressures from 0.1 MPa up to 140 MPa and temperatures between 298.15 K and 393.15 K. We also report isobaric thermal expansion coefficients and the isothermal compressibility coefficients for the pure components and for 6 mol fractions of the binary mixture.

2. Experimental

2.1. Materials

Methyl nonafluorobutyl ether or 1,1,1,2,2,3,3,4,4-nonafluoro-4-methoxybutane, also known as HFE-7100, consists of two inseparable isomers with essentially identical properties, with a mole fraction purity greater than 0.995 certified by the supplier 3M Company. 2-propanol was obtained from Sigma-Aldrich with 0.998 mol fraction purity and stored over molecular sieves type 0.4

* Corresponding author.
E-mail address: emontero@ubu.es (E.A. Montero).

http://dx.doi.org/10.1016/j.fluid.2016.09.014
0378-3812/

Table 1
Purity and related data of chemicals.

Compound	Source	Formula	Molar mass/g mol^{-1}	Stated purity[a]/mol%	CAS number
HFE 7100[b]	3M Company	$C_5H_3F_9O$	250.06	>99.5	163702-08-7/163702-07-6[c]
2-propanol	Sigma-Aldrich	C_3H_8O	60.096	>99.8[d]	67-63-0

[a] Determined by gas chromatography (GC).
[b] HFE 7100 = 1,1,1,2,2,3,3,4,4-nonafluoro-4-methoxybutane.
[c] Binary mixture of two isomers with mass ratio 0.5.
[d] The water content was checked to be less than 0.01% by titration method.

to prevent moisture. The two fluids were used without any further purification except careful degassing before use. Table 1 presents the specification of chemical samples.

2.2. Measurement technique. Experimental procedure

We used an Anton Paar DMA HPM high pressure vibrating tube densitometer to measure the experimental densities ρ as a function of pressure, p (from 0.1 up to 140 MPa) and temperature, T (from 298.15 to 393.15 K). The experimental setup was similar to the one described previously [5]. We performed the calibration of the densitometer according to the procedure described by Comuñas et al. [6] which is a modification of the procedure previously proposed by Lagourette et al. [7]. We used two reference fluids to perform the calibrations (vacuum and water). The density values of water were taken from the equation of state (EoS) reported by Wagner and Pruss [8]. At pressure equal to 0.1 MPa, no measurements were performed over 333.15 K, well below the boiling temperature of water. After filling the densitometer with the sample, it was brought to the desired temperature and pressure of interest and measured when the system reached both thermal and mechanical equilibrium.

The estimated expanded uncertainty of the measured temperature was ±0.03 K (Pt 100 calibrated probe), while the estimated expanded uncertainty of the measured pressure was ±0.04 MPa (pressure transducer WIKA CPH 6000). Both temperature and pressure sensors were periodically calibrated before and after the measurement campaign. The DMA HPM measuring cell is connected to the Anton Paar mPDS 2000V3 evaluation unit, which evaluates the oscillation period from the measuring cell filled with the sample. Taking into account the accuracy of the temperature, the pressure, the period of oscillation measurement for water, vacuum, and the studied systems, and the water density accuracy, the estimated expanded density uncertainty (k = 2) is ±0.7 kg m^{-3} (*i.e.* around ±0.07% for density close to water density), in accordance with the EA-4/02 document [9].

Pure fluids used in binary mixtures were degasified prior to the preparation of the samples. Degassing is carried out using an ultrasonic bath PSelecta, model Ultrason-H. Each mixture was prepared immediately before measuring, by weighing in glass vials sealed to prevent evaporation. For weighing, a Sartorius balance model BP 221S has been used, with resolution of 10^{-4} g, uncertainty ±0.0001 g. The estimated expanded uncertainty in the composition of the mixture is $\pm 4 \cdot 10^{-5}$ in mole fraction. Therefore, the excess molar volume should be accurate to within ±0.004 cm^3 mol^{-1}.

3. Results and discussion

We used several fitting parameters to compare the experimental density values with those obtained from the correlation considered in this work, such as the Absolute Average Deviation (AAD), the Maximum Deviation (MD), the Average Deviation (Bias), the standard deviation (σ), and the Root Mean Square Deviation (RMSD), which are defined as follows:

$$\mathrm{AAD} = \frac{100}{N}\sum_{i=1}^{N}\left|\frac{\rho_i^{\mathrm{exp}} - \rho_i^{\mathrm{calc}}}{\rho_i^{\mathrm{exp}}}\right| \tag{1}$$

$$\mathrm{MD} = \mathrm{Max}\left(100\left|\frac{\rho_i^{\mathrm{exp}} - \rho_i^{\mathrm{calc}}}{\rho_i^{\mathrm{exp}}}\right|\right) \tag{2}$$

$$\mathrm{Bias} = \frac{100}{N}\sum_{i=1}^{N}\frac{\rho_i^{\mathrm{exp}} - \rho_i^{\mathrm{calc}}}{\rho_i^{\mathrm{exp}}} \tag{3}$$

$$\sigma = \sqrt{\frac{\sum_{i=1}^{N}\left(\rho_i^{\mathrm{exp}} - \rho_i^{\mathrm{calc}}\right)^2}{N-m}} \tag{4}$$

$$\mathrm{RMSD} = \sqrt{\frac{\sum_{i=1}^{N}\left(\rho_i^{\mathrm{exp}} - \rho_i^{\mathrm{calc}}\right)^2}{N}} \tag{5}$$

where N is the number of experimental data ($N = 1073$) and m the number of parameters ($m = 8$ for our correlation).

3.1. Density

Table 2 reports the measured densities of HFE-7100, 2-propanol and its binary mixtures HFE-7100 + 2-propanol (molar compositions, $x = 0.1490, 0.3255, 0.5004, 0.6758, 0.7940$, and 0.8497) along the 6 isotherms ranging from 298.15 to 393.15 K and at pressures from 0.1 up to 140 MPa (23 isobars). No density measurements have been made at $p = 0.1$ MPa and T higher than 333.15 K for the pure 2-propanol due to its boiling point ($T = 355.39$ K) and at $p = 0.1$ MPa and T higher than 313.15 K for the pure HFE-7100 (boiling point, $T = 332.85$ K). Concerning the mixtures, no measurements have been taken at $p = 0.1$ MPa and at temperatures higher than 333.15 K. The reason is that under these conditions almost all of the binary mixtures are in the vapor phase.

3.2. Comparison with Cibulka's correlation

The experimental densities of pure 2-propanol were compared with the correlation equation proposed by Cibulka et al. [10]. The equation was obtained using different literature data and it is based on the Tait equation. This review covers papers published before 1987. The equation is valid within the temperature range 273.15–400 K and for pressures between 1 and 173.90 MPa. It should be noted that for temperatures higher than 348.15 K there are no references with pressure data above 50 MPa. Only reference

Table 2
Experimental Densities, ρ (g cm^{-3}), for the binary mixture x HFE-7100 + (1-x) 2-propanol at various Temperatures T and Pressures p.[a]

x	p/MPa	T/K					
		298.15	313.15	333.15	353.15	373.15	393.15
		ρ (g cm^{-3})					
0.0000	0.10	0.7814	0.7683	0.7495			
	1.00	0.7822	0.7692	0.7505	0.7298	0.7065	0.6802
	5.00	0.7857	0.7730	0.7550	0.7350	0.7127	0.6879
	10.00	0.7899	0.7776	0.7601	0.7410	0.7198	0.6966
	15.00	0.7938	0.7818	0.7649	0.7465	0.7262	0.7042
	20.00	0.7974	0.7859	0.7694	0.7516	0.7322	0.7111
	25.00	0.8010	0.7897	0.7737	0.7564	0.7377	0.7175
	30.00	0.8044	0.7933	0.7778	0.7610	0.7429	0.7234
	35.00	0.8076	0.7969	0.7817	0.7654	0.7476	0.7289
	40.00	0.8109	0.8001	0.7852	0.7693	0.7523	0.7339
	45.00	0.8139	0.8035	0.7889	0.7732	0.7566	0.7388
	50.00	0.8168	0.8066	0.7923	0.7770	0.7607	0.7434
	55.00	0.8197	0.8096	0.7954	0.7806	0.7646	0.7478
	60.00	0.8225	0.8125	0.7987	0.7839	0.7683	0.7520
	65.00	0.8253	0.8154	0.8018	0.7874	0.7721	0.7559
	70.00	0.8278	0.8182	0.8047	0.7906	0.7755	0.7598
	80.00	0.8328	0.8234	0.8104	0.7967	0.7822	0.7670
	90.00	0.8376	0.8284	0.8158	0.8025	0.7884	0.7737
	100.00	0.8422	0.8332	0.8209	0.8079	0.7943	0.7800
	110.00	0.8465	0.8378	0.8256	0.8131	0.7998	0.7861
	120.00	0.8508	0.8421	0.8304	0.8180	0.8050	0.7917
	130.00	0.8547	0.8463	0.8347	0.8229	0.8101	0.7970
	140.00	0.8587	0.8504	0.8391	0.8273	0.8149	0.8021
0.1490	0.10	0.9741	0.9546				
	1.00	0.9754	0.9560	0.9284	0.8984	0.8647	0.8268
	5.00	0.9809	0.9622	0.9358	0.9072	0.8757	0.8408
	10.00	0.9875	0.9694	0.9441	0.9171	0.8875	0.8556
	15.00	0.9934	0.9760	0.9518	0.9259	0.8980	0.8682
	20.00	0.9991	0.9822	0.9589	0.9340	0.9074	0.8792
	25.00	1.0045	0.9881	0.9655	0.9416	0.9161	0.8892
	30.00	1.0095	0.9936	0.9717	0.9485	0.9241	0.8982
	35.00	1.0144	0.9990	0.9775	0.9552	0.9313	0.9065
	40.00	1.0191	1.0038	0.9829	0.9612	0.9383	0.9142
	45.00	1.0236	1.0086	0.9883	0.9670	0.9447	0.9214
	50.00	1.0278	1.0132	0.9933	0.9726	0.9508	0.9282
	55.00	1.0320	1.0176	0.9980	0.9778	0.9566	0.9346
	60.00	1.0360	1.0218	1.0027	0.9828	0.9621	0.9407
	65.00	1.0399	1.0260	1.0071	0.9877	0.9674	0.9465
	70.00	1.0436	1.0300	1.0115	0.9925	0.9724	0.9520
	80.00	1.0507	1.0375	1.0197	1.0012	0.9820	0.9623
	90.00	1.0575	1.0447	1.0273	1.0095	0.9909	0.9719
	100.00	1.0640	1.0514	1.0345	1.0172	0.9992	0.9807
	110.00	1.0700	1.0579	1.0412	1.0246	1.0070	0.9892
	120.00	1.0760	1.0640	1.0480	1.0314	1.0144	0.9969
	130.00	1.0815	1.0698	1.0541	1.0381	1.0214	1.0044
	140.00	1.0870	1.0756	1.0601	1.0444	1.0282	1.0115
0.3255	0.10	1.1422	1.1161				
	1.00	1.1440	1.1182	1.0817	1.0421	0.9981	0.9482
	5.00	1.1518	1.1270	1.0924	1.0553	1.0147	0.9702
	10.00	1.1608	1.1370	1.1042	1.0696	1.0321	0.9921
	15.00	1.1690	1.1462	1.1150	1.0820	1.0471	1.0102
	20.00	1.1766	1.1548	1.1247	1.0933	1.0602	1.0257
	25.00	1.1839	1.1627	1.1338	1.1036	1.0721	1.0394
	30.00	1.1907	1.1701	1.1421	1.1131	1.0829	1.0517
	35.00	1.1972	1.1772	1.1500	1.1220	1.0928	1.0629
	40.00	1.2033	1.1837	1.1572	1.1302	1.1021	1.0732
	45.00	1.2092	1.1901	1.1643	1.1379	1.1106	1.0828
	50.00	1.2148	1.1962	1.1709	1.1452	1.1187	1.0916
	55.00	1.2203	1.2019	1.1772	1.1521	1.1263	1.1000
	60.00	1.2255	1.2075	1.1833	1.1587	1.1335	1.1080
	65.00	1.2305	1.2129	1.1892	1.1651	1.1406	1.1155
	70.00	1.2353	1.2181	1.1948	1.1713	1.1470	1.1227
	80.00	1.2446	1.2278	1.2054	1.1827	1.1595	1.1359
	90.00	1.2533	1.2371	1.2153	1.1933	1.1709	1.1483
	100.00	1.2616	1.2457	1.2245	1.2032	1.1815	1.1596
	110.00	1.2693	1.2539	1.2332	1.2127	1.1915	1.1703
	120.00	1.2769	1.2617	1.2417	1.2214	1.2009	1.1803
	130.00	1.2840	1.2692	1.2495	1.2299	1.2098	1.1897
	140.00	1.2909	1.2764	1.2571	1.2378	1.2183	1.1985
0.5004	0.10	1.2682	1.2370				

Table 2 (*continued*)

x	p/MPa	T/K					
		298.15	313.15	333.15	353.15	373.15	393.15
		ρ (g cm^{-3})					
	1.00	1.2705	1.2396	1.1961	1.1490	1.0966	1.0367
	5.00	1.2801	1.2507	1.2096	1.1659	1.1184	1.0665
	10.00	1.2911	1.2631	1.2244	1.1840	1.1407	1.0948
	15.00	1.3012	1.2744	1.2377	1.1996	1.1595	1.1176
	20.00	1.3105	1.2849	1.2497	1.2135	1.1758	1.1367
	25.00	1.3193	1.2945	1.2607	1.2262	1.1903	1.1536
	30.00	1.3276	1.3034	1.2709	1.2377	1.2035	1.1685
	35.00	1.3353	1.3120	1.2804	1.2484	1.2154	1.1820
	40.00	1.3427	1.3199	1.2892	1.2582	1.2266	1.1944
	45.00	1.3497	1.3275	1.2976	1.2675	1.2368	1.2057
	50.00	1.3564	1.3347	1.3055	1.2763	1.2464	1.2164
	55.00	1.3629	1.3416	1.3130	1.2846	1.2555	1.2263
	60.00	1.3690	1.3481	1.3203	1.2925	1.2641	1.2357
	65.00	1.3750	1.3545	1.3272	1.2999	1.2722	1.2445
	70.00	1.3807	1.3606	1.3339	1.3072	1.2800	1.2530
	80.00	1.3916	1.3722	1.3464	1.3206	1.2946	1.2686
	90.00	1.4018	1.3831	1.3580	1.3331	1.3080	1.2830
	100.00	1.4116	1.3931	1.3688	1.3448	1.3204	1.2962
	110.00	1.4206	1.4028	1.3790	1.3558	1.3321	1.3086
	120.00	1.4294	1.4119	1.3890	1.3660	1.3431	1.3202
	130.00	1.4376	1.4206	1.3979	1.3759	1.3534	1.3311
	140.00	1.4457	1.4290	1.4068	1.3851	1.3632	1.3414
0.6758	0.10	1.3694	1.3341				
	1.00	1.3721	1.3372	1.2880	1.2351	1.1764	1.1093
	5.00	1.3832	1.3501	1.3040	1.2553	1.2028	1.1457
	10.00	1.3960	1.3646	1.3214	1.2765	1.2292	1.1793
	15.00	1.4076	1.3776	1.3368	1.2948	1.2511	1.2060
	20.00	1.4183	1.3897	1.3506	1.3108	1.2699	1.2282
	25.00	1.4283	1.4007	1.3633	1.3254	1.2867	1.2475
	30.00	1.4377	1.4109	1.3749	1.3386	1.3018	1.2645
	35.00	1.4465	1.4206	1.3858	1.3508	1.3153	1.2798
	40.00	1.4549	1.4296	1.3957	1.3621	1.3280	1.2938
	45.00	1.4628	1.4381	1.4054	1.3725	1.3396	1.3066
	50.00	1.4704	1.4464	1.4143	1.3824	1.3504	1.3186
	55.00	1.4776	1.4541	1.4228	1.3919	1.3607	1.3297
	60.00	1.4846	1.4616	1.4310	1.4007	1.3703	1.3403
	65.00	1.4914	1.4687	1.4388	1.4091	1.3796	1.3502
	70.00	1.4977	1.4756	1.4462	1.4172	1.3883	1.3596
	80.00	1.5100	1.4885	1.4602	1.4324	1.4046	1.3771
	90.00	1.5214	1.5007	1.4733	1.4464	1.4196	1.3931
	100.00	1.5322	1.5120	1.4854	1.4593	1.4334	1.4078
	110.00	1.5423	1.5227	1.4968	1.4716	1.4464	1.4216
	120.00	1.5521	1.5329	1.5078	1.4831	1.4586	1.4344
	130.00	1.5613	1.5426	1.5179	1.4940	1.4701	1.4465
	140.00	1.5702	1.5519	1.5278	1.5043	1.4810	1.4579
0.7940	0.10	1.4270	1.3895				
	1.00	1.4299	1.3929	1.3409	1.2850	1.2236	1.1537
	5.00	1.4419	1.4069	1.3582	1.3071	1.2525	1.1936
	10.00	1.4557	1.4224	1.3770	1.3301	1.2810	1.2299
	15.00	1.4681	1.4365	1.3936	1.3498	1.3047	1.2584
	20.00	1.4795	1.4494	1.4085	1.3670	1.3249	1.2822
	25.00	1.4903	1.4612	1.4220	1.3827	1.3428	1.3027
	30.00	1.5002	1.4721	1.4345	1.3968	1.3589	1.3208
	35.00	1.5096	1.4825	1.4460	1.4098	1.3733	1.3371
	40.00	1.5186	1.4920	1.4567	1.4217	1.3868	1.3519
	45.00	1.5271	1.5012	1.4669	1.4329	1.3991	1.3656
	50.00	1.5350	1.5099	1.4765	1.4435	1.4107	1.3782
	55.00	1.5428	1.5182	1.4855	1.4534	1.4215	1.3900
	60.00	1.5502	1.5260	1.4942	1.4628	1.4318	1.4011
	65.00	1.5573	1.5337	1.5025	1.4718	1.4415	1.4116
	70.00	1.5641	1.5410	1.5105	1.4804	1.4507	1.4216
	80.00	1.5770	1.5547	1.5252	1.4964	1.4680	1.4400
	90.00	1.5892	1.5676	1.5391	1.5113	1.4838	1.4568
	100.00	1.6006	1.5795	1.5518	1.5250	1.4984	1.4723
	110.00	1.6113	1.5909	1.5639	1.5379	1.5121	1.4868
	120.00	1.6216	1.6016	1.5755	1.5500	1.5249	1.5003
	130.00	1.6313	1.6118	1.5862	1.5615	1.5370	1.5130
	140.00	1.6407	1.6216	1.5966	1.5723	1.5485	1.5250
0.8497	0.10	1.4520	1.4136				
	1.00	1.4549	1.4171	1.3641	1.3073	1.2450	1.1744
	5.00	1.4673	1.4315	1.3820	1.3300	1.2749	1.2158

(*continued on next page*)

Table 2 (*continued*)

x	p/MPa	T/K					
		298.15	313.15	333.15	353.15	373.15	393.15
		ρ (g cm^{-3})					
	10.00	1.4815	1.4476	1.4014	1.3539	1.3044	1.2529
	15.00	1.4943	1.4620	1.4185	1.3740	1.3286	1.2823
	20.00	1.5060	1.4753	1.4338	1.3918	1.3494	1.3066
	25.00	1.5171	1.4874	1.4477	1.4078	1.3677	1.3276
	30.00	1.5273	1.4986	1.4605	1.4223	1.3842	1.3461
	35.00	1.5369	1.5093	1.4723	1.4357	1.3990	1.3627
	40.00	1.5461	1.5191	1.4833	1.4479	1.4128	1.3779
	45.00	1.5548	1.5285	1.4938	1.4594	1.4254	1.3918
	50.00	1.5630	1.5375	1.5036	1.4702	1.4372	1.4047
	55.00	1.5710	1.5459	1.5128	1.4804	1.4483	1.4168
	60.00	1.5785	1.5539	1.5217	1.4900	1.4587	1.4282
	65.00	1.5858	1.5618	1.5301	1.4992	1.4687	1.4388
	70.00	1.5928	1.5692	1.5383	1.5080	1.4781	1.4490
	80.00	1.6061	1.5833	1.5534	1.5244	1.4958	1.4678
	90.00	1.6184	1.5964	1.5676	1.5395	1.5119	1.4850
	100.00	1.6301	1.6086	1.5807	1.5535	1.5268	1.5008
	110.00	1.6411	1.6203	1.5930	1.5667	1.5408	1.5156
	120.00	1.6516	1.6312	1.6048	1.5790	1.5538	1.5294
	130.00	1.6615	1.6417	1.6158	1.5908	1.5662	1.5423
	140.00	1.6710	1.6517	1.6263	1.6019	1.5779	1.5545
1.0000	0.10	1.5155	1.4759				
	1.00	1.5186	1.4796	1.4253	1.3677	1.3048	1.2339
	5.00	1.5318	1.4950	1.4444	1.3918	1.3361	1.2766
	10.00	1.5468	1.5120	1.4649	1.4169	1.3670	1.3153
	15.00	1.5603	1.5273	1.4830	1.4381	1.3924	1.3457
	20.00	1.5728	1.5413	1.4991	1.4568	1.4141	1.3710
	25.00	1.5844	1.5542	1.5138	1.4736	1.4333	1.3929
	30.00	1.5952	1.5660	1.5273	1.4888	1.4505	1.4122
	35.00	1.6054	1.5772	1.5397	1.5029	1.4660	1.4295
	40.00	1.6151	1.5876	1.5513	1.5157	1.4804	1.4453
	45.00	1.6243	1.5975	1.5623	1.5277	1.4936	1.4598
	50.00	1.6329	1.6068	1.5725	1.5390	1.5060	1.4732
	55.00	1.6413	1.6158	1.5822	1.5497	1.5175	1.4858
	60.00	1.6492	1.6242	1.5916	1.5597	1.5284	1.4977
	65.00	1.6569	1.6324	1.6005	1.5693	1.5388	1.5088
	70.00	1.6642	1.6403	1.6090	1.5786	1.5486	1.5194
	80.00	1.6781	1.6550	1.6249	1.5956	1.5671	1.5389
	90.00	1.6911	1.6688	1.6397	1.6115	1.5840	1.5569
	100.00	1.7035	1.6816	1.6534	1.6261	1.5995	1.5734
	110.00	1.7149	1.6938	1.6663	1.6400	1.6140	1.5889
	120.00	1.7260	1.7054	1.6786	1.6529	1.6276	1.6032
	130.00	1.7364	1.7163	1.6901	1.6651	1.6405	1.6167
	140.00	1.7464	1.7268	1.7012	1.6766	1.6527	1.6294

[a] Estimated expanded uncertainties (k = 2): temperature, $U(T) = \pm 0.03$ K, pressure, $U(p) = \pm 0.04$ MPa; mole fraction, $U(x) = \pm 0.00003$; density, $U(\rho) = \pm 0.7$ kg m^{-3}.

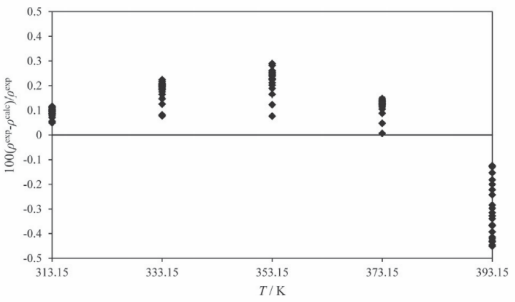

Fig. 1. Deviation between the measured values and the calculated densities for 2-propanol by using the correlation proposed in Ref. [10], (0.1 < p/MPa < 140; 298.15 < T/K < 393.15).

[11] covers a range of pressures higher than 50 MPa (173.90 MPa) which is in the temperature range 298.15–348.15 K. Regarding the temperature, only reference [12] covers temperatures over 348.15 K (up to 400 K).

For the data obtained in the range $298.15 \leq T \leq 353.15$ K and $0.1 \leq p \leq 140$ MPa ($N = 91$) the results quite agree with those obtained from the Cibulka correlation with an AAD of 0.13%, MD of 0.29%, Bias = 0.13% and with RMSD = $1.22 \cdot 10^{-3}$ g cm^{-3}. When the comparison is performed in all the temperature and pressure ranges of the experimental data used by Ref. [10] for their fitting procedure ($298.15 \leq T \leq 348.15$ K–$0.1 \leq p \leq 173.9$ MPa and $348.15 \leq T \leq 400$ K–$0.1 \leq p \leq 50$ MPa), the deviations obtained are AAD = 0.16%, MD of 0.45%, Bias = 0.06% and RMSD = $1.47 \cdot 10^{-3}$ g cm^{-3}. Fig. 1 shows the deviations obtained between our data and the calculated densities using the correlation proposed in Ref. [10] versus temperature. It can be seen that deviation values change from positive to negative as temperature increases. The highest temperature 393.15 K has the highest deviations, our data falling below Cibulka's prediction. Nevertheless, the maximum deviation falls within a narrow range of 0.35 to −0.45%, which shows good agreement with previous data.

3.3. New Tait representation

To correlate our values over our entire temperature and pressure ranges, in order to improve the previous representation (and consequently the evaluation of the derived properties), we use the following Tait-like equation, which has been used in our previous works [5,13,14],:

$$\rho(T,p) = \frac{\rho_0(T)}{1 - C \ln\left(\frac{B(T)+p}{B(T)+0.1\ \text{MPa}}\right)} \tag{6}$$

where

$$\rho_0(T) = A_0 + A_1 T + A_2 T^2 + A_3 T^3 \tag{7}$$

$$B(T) = B_0 + B_1 T + B_2 T^2 \tag{8}$$

The A_i, B_i and C parameters values were determined by correlating simultaneously all the experimental densities values versus pressure and temperature. Table 3 gives the Tait-correlation parameters and fitting parameters values obtained with this correlation for HFE-7100, 2-propanol and its binary mixtures.

It must be pointed out that all fitting deviations (the AAD, MD, Bias, the standard deviation σ and the RMSD), are lower than the experimental uncertainty. Fig. 2 shows the variation between the measured and calculated densities for each composition with Eqs. (6)–(8) as a function of temperature at (a) $p = 1$ and (b) at $p = 140$ MPa. Density decreases when temperature increases, as expected. This figure shows the non-linearity of density versus temperature, particularly at low pressures, when a sufficiently large temperature range is considered, which justifies the use of Eq. (6). Fig. 2 (c) and 2 (d) present the variation of density as a function of pressure at $T = (298.15$ and $393.15)$ K, which shows that density increases when pressure increases. At constant temperature the curves are concave, which is associated with a negative second order derivative. The shape of the isothermal curves of the density versus pressure is compatible with the logarithmic relationship used in the Tait-type density relation used to model the influence of pressure on density.

Table 3
Obtained Parameters and Deviations for Density Correlation by using Eqs. (6)–(8) for *x* HFE-7100 + (1-*x*) 2-propanol.

Parameters *X*	0.0000	0.1490	0.3255	0.5004	0.6758	0.7940	0.8497	1.0000
A_0/g cm^{-3}	1.293378	1.803993	2.271993	2.667433	2.867854	2.876196	2.833316	2.931883
A_1/g cm^{-3} K^{-1}	-3.768266×10^{-3}	-6.127384×10^{-3}	-8.345448×10^{-3}	-1.041220×10^{-2}	-1.098105×10^{-2}	-1.031916×10^{-2}	-9.604537×10^{-3}	-9.745889×10^{-3}
A_2/g cm^{-3} K^{-2}	1.088149×10^{-5}	1.742101×10^{-5}	2.361895×10^{-5}	2.953125×10^{-5}	3.089403×10^{-5}	2.856497×10^{-5}	2.621855×10^{-5}	2.621836×10^{-5}
A_3/g cm^{-3} K^{-3}	-1.341587×10^{-8}	-2.079992×10^{-8}	-2.794867×10^{-8}	-3.469516×10^{-8}	-3.661161×10^{-8}	-3.439072×10^{-8}	-3.200302×10^{-8}	-3.173991×10^{-8}
B_0/MPa	309.1025	316.6521	313.1853	307.2198	304.9220	302.9697	300.8068	290.3497
B_1/MPa K^{-1}	−0.9722444	−1.172846	−1.251741	−1.276610	−1.301264	−1.308858	−1.304396	−1.256549
B_2/MPa K^{-2}	6.601239×10^{-4}	1.054855×10^{-3}	1.241366×10^{-3}	1.324192×10^{-3}	1.391455×10^{-3}	1.419770×10^{-3}	1.421405×10^{-3}	1.367948×10^{-3}
C	0.08729084	0.08668191	0.08642419	0.0859960	0.08563579	0.08536951	0.08519084	0.08490464
AAD/(%)	0.01	0.01	0.02	0.02	0.02	0.02	0.02	0.01
MD/(%)	0.04	0.05	0.06	0.10	0.12	0.13	0.14	0.12
Bias/(%)	-2.01×10^{-6}	1.06×10^{-4}	1.98×10^{-5}	2.89×10^{-5}	1.52×10^{-4}	2.46×10^{-5}	-1.14×10^{-4}	4.13×10^{-5}
σ/(g cm^{-3})	1.15×10^{-4}	1.75×10^{-4}	2.22×10^{-4}	2.51×10^{-4}	2.83×10^{-4}	2.93×10^{-4}	2.99×10^{-4}	2.99×10^{-4}
RMSD/ (g cm^{-3})	1.11×10^{-4}	1.70×10^{-4}	2.15×10^{-4}	2.43×10^{-4}	2.75×10^{-4}	2.84×10^{-4}	2.90×10^{-4}	2.90×10^{-4}

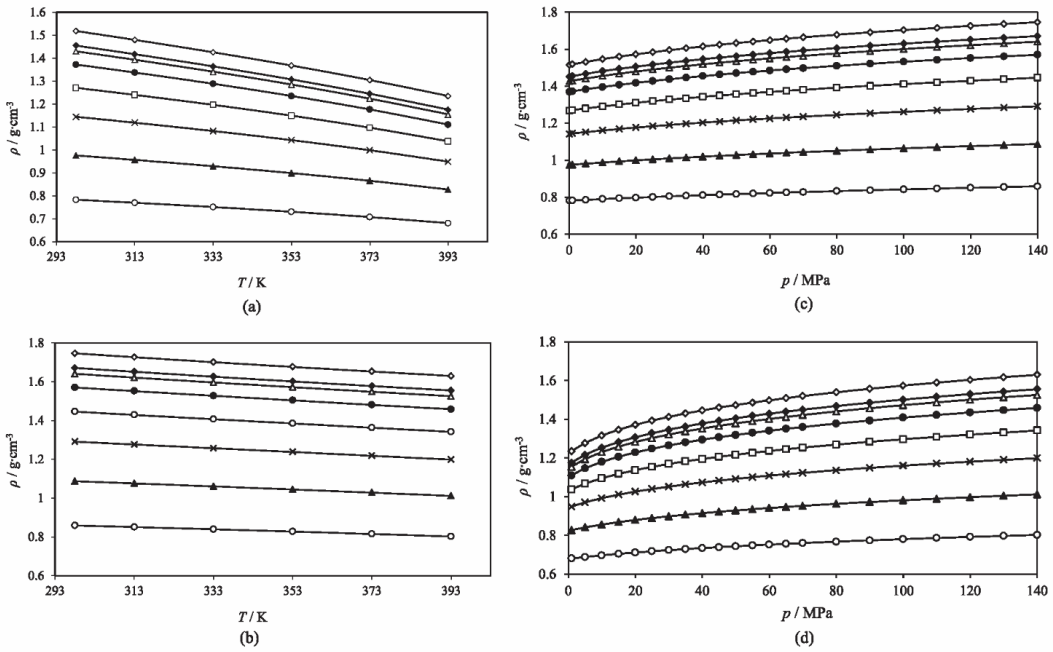

Fig. 2. Experimental values of densities, *ρ*, for different mole fractions of *x* HFE-7100 + (1-*x*) 2-propanol vs. (a) the temperature, *T* at 1 MPa, (b) the temperature, *T* at 140 MPa, (c) the pressure, *p* at 298.15 K and (d) the pressure, *p* at 393.15 K: ○, $x = 0$; ▲, $x = 0.1490$; x, $x = 0.3255$; □, $x = 0.5004$; ●, $x = 0.6758$; Δ, $x = 0.7940$; ◆, $x = 0.8497$; ◊, $x = 1$; (−), Tait Eq. (6).

Table 4
Comparison between the values generated by our correlation (Eqs. (6)–(8) and Table 3) at exactly the same experimental *p*, *T* sets given for HFE-7100 for several literature references.

Reference	Year	N_P	T_{min} (K)	T_{max} (K)	p_{min} (MPa)	p_{max} (MPa)	AAD (%)	MD (%)	Bias (%)	Density uncertainty
At atmospheric pressure										
Minamihounoki et al. [15]	2001	1	298.15	298.15	0.1	0.1	0.06	0.06	0.06	–
Marchionni et al. [16]	2002	1	298.15	298.15	0.1	0.1	1.35	1.35	−1.35	–
Rausch et al. [17]	2015	15	293.15	363.15	0.1	0.1	0.03	0.08	0.03	0.02%
At high pressure										
Piñeiro et al. [18]	2003	60	298.15	313.15	0.1	40	0.02	0.08	0.01	±10^{-4} g cm^{-3}
Qi et al. [19]	2014	124	293.23	362.79	0.1	100	0.12	0.39	−0.11	±0.036%

N_P Number of data points which are in our *p*, *T* ranges.

3.4. Comparison with literature data

We have found some literature data on density of the selected compounds, which can be used for comparison with the present work. In order to avoid any extrapolation, we performed a comparison with the values generated by our correlation (Eqs. (6)–(8) and Table 3) at exactly the same experimental p, T sets used in previous studies, subject to the p, T sets falling within our experimental ranges.

For pure HFE-7100, Table 4 presents a summary of literature data at atmospheric pressure [15–17] and at high pressure [18,19], while Table 5 presents the same for 2-propanol at atmospheric pressure [20–45] and at high pressure [11,12] and [46–53]. In both Tables 4 and 5 N_P represents the number of data points from each previous study which fall within our p, T ranges. No data were found for the binary mixture HFE-7100 + 2-propanol.

For HFE-7100 only two studies conducted at atmospheric pressure [15,16] were found, both of which give only one temperature-measuring point for each point. The reference [17] provides 15 points at atmospheric pressure from 293.15 K to 363.15 K. The highest deviation was found in the comparison established with reference [16], with an AAD = 1.35%. At high pressure the data given by the two references [18,19] show that the highest deviation was found when comparing with the data presented in Ref. [19], with an AAD of 0.12%. These data cover pressures of up to 100 MPa and temperatures from 293.23 to 362.79 K. For reference [18], the range of pressures covers from 0.1 MPa up to 40 MPa. We have considered a temperature range between (298.15–313.15) K, giving a deviation AAD = 0.02%.

Table 5 lists the different density data sets available at atmospheric pressure and at high pressure for 2-propanol published in the literature. Most data cover very limited temperature ranges, all below 343.15 K, except [20], which gave us the opportunity to compare our values up to 400 K.

At atmospheric pressure the highest deviations are found between our research and reference [42], as seen in Table 5. Comparison with this study gives us an AAD = 0.93% and high maximum deviation, with MD = 1.65%. Comparisons with all other studies show good agreement as AAD and MD are lower than the experimental uncertainty (0.1%), except for reference [36] where only its MD% deviation of 0.10% is slightly high.

Only reference [51] covers our entire pressure and temperature range while reference [53] covers a range of pressures from 0.1 MPa to 140 MPa and a range of temperatures from 313.15 K to 403.15 K. Reference [11] covers a range of temperatures from 298.15 K to 348.15 K and a range of pressures from 0.1 MPa to 138.9 MPa. Regarding pressure, all other authors provide data below 65 MPa.

Comparisons of data collected under high pressure conditions by different authors show a high degree of agreement. The highest deviations are found in Refs. [12,47–49] as seen in Table 5, with

Table 5
Comparison between the values generated by our correlation (Eqs. (6)–(8) and Table 3) at exactly the same experimental p, T sets given for 2-propanol for several literature references.

Reference	Year	N_P	T_{min} (K)	T_{max} (K)	p_{min} (MPa)	p_{max} (MPa)	AAD (%)	MD (%)	Bias (%)	Density uncertainty
At atmospheric pressure										
Hales et al. [20]	1976	7	298.15	400.00	0.1	0.1	0.06	0.10	−0.03	±0.15 kg m^{-3}
Aminabhavi et al. [21]	1993	3	298.15	308.15	0.1	0.1	0.05	0.05	−0.05	–
Cerdeiriña et al. [22]	1999	3	293.15	308.15	0.1	0.1	0.05	0.06	−0.05	–
González et al. [23]	2003	3	293.15	303.15	0.1	0.1	0.09	0.10	−0.09	±10^{-6} g cm^{-3}
Aralaguppi and Baragi [24]	2006	3	298.15	308.15	0.1	0.1	0.07	0.07	−0.07	±10^{-4} g cm^{-3}
González et al. [25]	2006	3	293.15	303.15	0.1	0.1	0.10	0.11	−0.10	±2 × 10^{-6} g cm^{-3}
Bhuiyan et al. [26]	2007	5	303.15	323.15	0.1	0.1	0.05	0.12	−0.04	–
Pang et al. [27]	2007	9	293.15	333.15	0.1	0.1	0.05	0.11	0.01	±1 × 10^{-5} g cm^{-3}
Li et al. [28]	2007	8	298.15	333.15	0.1	0.1	0.09	0.13	−0.09	±3 × 10^{-4} g cm^{-3}
Zarei et al. [29]	2007	6	293.15	343.15	0.1	0.1	0.08	0.10	−0.08	±5 × 10^{-5} g cm^{-3}
Awwad et al. [30]	2008	5	293.15	323.15	0.1	0.1	0.07	0.09	−0.07	±2 × 10^{-5} g cm^{-3}
Zarei et al. [31]	2008	7	293.15	343.15	0.1	0.1	0.08	0.10	−0.08	±5 × 10^{-5} g cm^{-3}
Dubey and Sharma [32]	2009	3	298.15	308.15	0.1	0.1	0.05	0.06	−0.05	±2 × 10^{-3} g cm^{-3}
Kao et al. [33]	2011	4	293.15	323.15	0.1	0.1	0.06	0.07	−0.06	±2 × 10^{-5} g cm^{-3}
Vercher et al. [34]	2011	4	298.15	328.15	0.1	0.1	0.08	0.09	−0.08	±7 × 10^{-3} kg m^{-3}
Kermanpour and Niakan [35]	2012	5	293.15	333.15	0.1	0.1	0.06	0.08	−0.06	±1 × 10^{-4} g cm^{-3}
Almasi [36]	2012	4	298.15	313.15	0.1	0.1	0.10	0.13	−0.10	±5 × 10^{-5} g cm^{-3}
Singh et al. [37]	2013	4	298.15	313.15	0.1	0.1	0.06	0.06	−0.06	±3 × 10^{-5} g cm^{-3}
Pal et al. [38]	2013	4	293.15	308.15	0.1	0.1	0.07	0.08	−0.07	±3 × 10^{-6} g cm^{-3}
González et al. [39]	2013	3	298.15	308.15	0.1	0.1	0.06	0.07	−0.06	±3 × 10^{-5} g cm^{-3}
González et al. [40]	2013	3	298.15	308.15	0.1	0.1	0.01	0.01	0.01	±3 × 10^{-5} g cm^{-3}
Almasi [41]	2013	4	298.15	313.15	0.1	0.1	0.08	0.08	−0.08	±5 × 10^{-5} g cm^{-3}
Sastry et al. [42]	2014	5	303.15	323.15	0.1	0.1	0.93	1.65	−0.72	±1 × 10^{-3} kg m^{-3}
Rodrigues Mesquita et al. [43]	2014	5	303.15	343.15	0.1	0.1	0.04	0.05	0.04	±5 × 10^{-4} g cm^{-3}
Lin and Tu [44]	2014	4	298.15	328.15	0.1	0.1	0.05	0.08	−0.03	±2 × 10^{-5} g cm^{-3}
Almasi [45]	2014	7	298.15	323.15	0.1	0.1	0.06	0.07	−0.06	±5 × 10^{-5} g cm^{-3}
At high pressure										
Golubev et al. [12]	1980	33	300.00	400.00	1.0	50	0.16	0.37	0.15	±0.1%
Kubota et al. [11]	1987	27	298.15	348.15	0.1	138.9	0.05	0.09	−0.02	0.09%
Yaginuma et al. [46]	1997	11	313.15	313.15	1.0	9.8	0.06	0.09	−0.06	±0.1 kg m^{-3}
Moha-Ouchane et al. [47]	1998	12	303.15	343.15	0.1	60	0.12	0.18	−0.12	±0.1 kg m^{-3}
Boned et al. [48]	2000	42	303.15	343.15	0.1	65	0.09	0.13	−0.09	±0.1 kg m^{-3}
Zuñiga-Moreno and Galicia-Luna [49]	2002	156	313.16	362.81	0.498	25.118	0.18	0.27	0.18	±0.05%
Stringari et al. [50]	2009	125	300.09	392.57	0.1867	9.8422	0.08	0.17	−0.05	±0.05%
Alaoui et al. [51]	2012	175	293,15	403,15	0.1	140	0.05	0.12	−0.05	±0.5 kg m^{-3}
Nourozieh et al. [52]	2013	20	302.9	323	0.1	10.02	0.04	0.07	0.02	±0.1 kg m^{-3}
Gómez-Álvarez et al. [53]	2014	185	313.15	403.15	0.1	140	0.04	0.13	−0.04	±0.05%

N_P Number of data points which are in our p, T ranges.

AAD = 0.16%, 0.12% and 0.18% respectively. In all other studies reported here the comparisons show an AAD less than 0.10%. We observed a high degree of agreement between our data and the data reported by Ref. [52].

3.5. Excess molar volumes

The excess molar volumes V^E were calculated from the equation,

$$V^E = \sum_{i=1}^{n} x_i M_i \left[\left({}^1/_{\rho} \right) - \left({}^1/_{\rho_i} \right) \right] \tag{9}$$

where n is the number of components; x_i is the mole fraction of component i in the mixture while M_i is its molar mass; ρ and ρ_i are the measured densities of the mixture and pure component i, respectively.

The calculated values of excess molar volumes show a regular trend with positive values for all compositions at the different temperatures and pressures measured. The positive values arise from a volume expansion which takes place in the mixture due to an approximation of different molecules with different molecular sizes. Moreover, the breaking of hydrogen bonds in the alcohol also contributes to the positive term. The hydrofluoroether is less polar than the alkanol, and this can lead to weak interactions between the two molecules. This translates into a low packing effect that results in high values of excess molar volumes. Fig. 3 shows the calculated excess molar volumes at both (a) 1 MPa and (b) 140 MPa for all the temperatures considered, (c) at both 298.15 K, and (d) at 393.15 K for pressures of 1 MPa, 35 MPa, 70 MPa, 110 MPa and 140 MPa. A systematic increase in V^E is noted when the temperature increases for all pressure ranges. It can be seen that when pressure increases, lower values of excess molar volumes are found since pressure increases the packing effect of the molecules. Fig. 3 shows also the fitting curves obtained for the binary systems by a Redlich-Kister polynomial of the type,

$$V^E = x(1-x) \sum_i z_i (2x-1)^{i-1} \tag{10}$$

where z_i are the adjustable parameters, and x is the mole fraction of HFE-7100. Table 6 presents the values of the adjustable parameters, z_i, and the standard deviations obtained by using Eq. (10) at different pressures for temperatures of 298.15 K and 393.15 K and for all the temperature measurements taken at 1.00 MPa, 70.00 MPa and 140.00 MPa.

3.6. The derived thermodynamic properties

Other relevant properties such as isothermal compressibility and isobaric expansivity are derived from the experimental densities. These properties can give valuable information on the dependence of the volumetric properties on temperature and pressure. The isothermal compressibility, κ_T, describes the effect of pressure on density based on the equation:

$$\kappa_T = \left(\frac{1}{\rho} \right) \left(\frac{\partial \rho}{\partial p} \right)_T = \frac{C}{\left(1 - C \ln \left(\frac{B(T)+p}{B(T)+0.1MPa} \right) \right) (B(T)+p)} \tag{11}$$

In a similar way, the isobaric thermal expansivity could also be obtained by differentiating Eq. (6) taking into account the temperature dependence of $\rho_0(T)$ and $B(T)$:

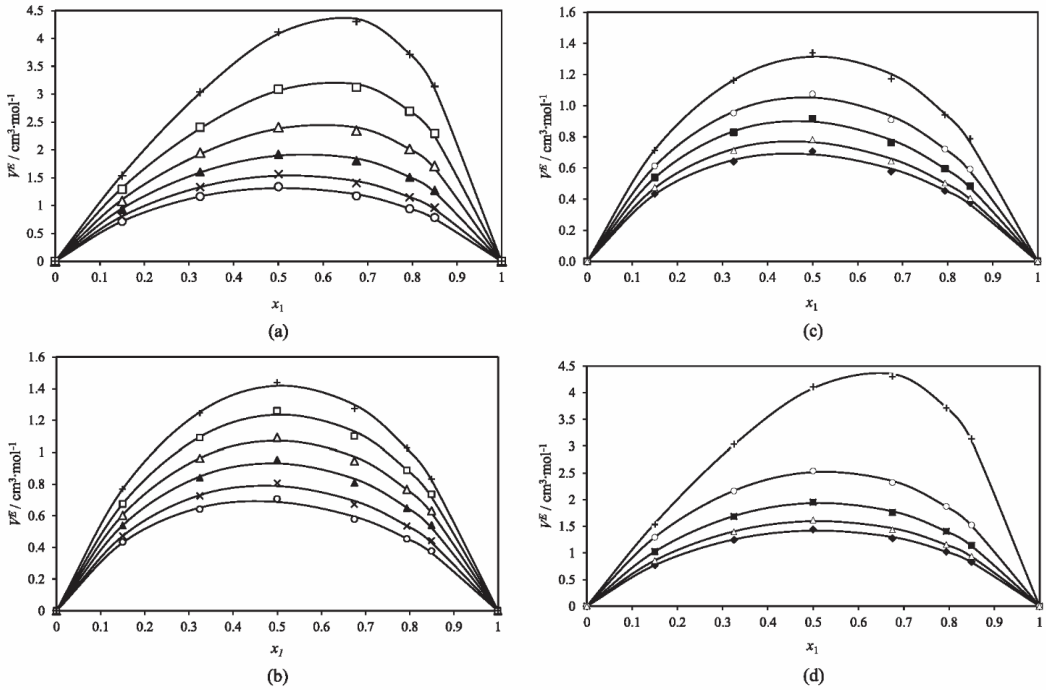

Fig. 3. Experimental values of excess molar volumes for the mixtures x HFE-7100 + (1-x) 2-propanol as a function of the mole fraction at different temperatures, (a) at 1 MPa, (b) at 140 MPa, where: ○, 298.15 K; ×, 313.15 K; ▲, 333.15 K; Δ, 353.15 K; □, 373.15 K; +, 393.15 K and (c) at T = 298.15 K and (d) at T = 393.15 K at various pressures, where: +, 1 MPa; ○, 35 MPa; ■, 70 MPa; Δ, 110 MPa; ◆, 140 MPa. (—), Redlich-Kister's Eq. (10).

Table 6
Values of parameters z_i of Eq. (10) and the corresponding standard deviation, σ, for binary mixtures at 298.15 K and 393.15 K for different pressures, and at 1.00 MPa, 70.00 MPa and 140.00 MPa for all the temperatures measured.

	z_1	z_2	z_3	σ (V^E)/cm^3·mol^{-1}
p/MPa	(T = 298.15 K)			
0.10	5.3159	0.2993	1.0974	0.02
1.00	5.2605	0.2475	1.1120	0.02
35.00	4.2063	−0.1948	0.9208	0.01
70.00	3.5896	−0.3645	0.7596	0.01
110.00	3.0627	−0.4105	0.7138	0.01
140.00	2.7490	−0.3718	0.7512	0.01
p/MPa	(T = 393.15 K)			
1.00	16.3360	8.6471	3.8754	0.03
35.00	10.0703	1.1965	1.8830	0.01
70.00	7.7430	0.5800	1.4382	0.01
110.00	6.3834	0.3895	1.2630	0.01
140.00	5.6738	0.2962	1.1566	0.01
T/K	(p = 1.00 MPa)			
298.15	5.2605	0.2475	1.1120	0.02
313.15	6.1457	0.7031	1.4126	0.02
333.15	7.5903	1.6322	2.0211	0.02
353.15	9.5250	3.1198	2.7624	0.03
373.15	12.2565	5.1803	3.4769	0.03
393.15	16.3360	8.6471	3.8754	0.03
T/K	(p = 70.00 MPa)			
298.15	3.5896	−0.3645	0.7596	0.01
313.15	4.1193	−0.2078	0.9722	0.01
333.15	4.8738	0.0535	1.1277	0.01
353.15	5.7275	0.3583	1.3743	0.01
373.15	6.6947	0.4382	1.5111	0.02
393.15	7.7430	0.5800	1.4382	0.01
T/K	(p = 140.00 MPa)			
298.15	2.7490	−0.3718	0.7512	0.01
313.15	3.1514	−0.2412	0.7837	0.01
333.15	3.7209	−0.0956	0.9080	0.01
353.15	4.2900	0.0537	1.0137	0.01
373.15	4.9461	0.2204	1.0417	0.02
393.15	5.6738	0.2962	1.1566	0.01

$$\alpha_p = -\left(\frac{1}{\rho}\right)\left(\frac{\partial\rho}{\partial T}\right)_p \tag{12}$$

Nevertheless, the estimated isobaric thermal expansivity depends on the form of functions $B(T)$ and $\rho_0(T)$ as pointed out by Refs. [54,55]. Therefore, it is better to derive the isobaric thermal expansivity from the isobaric densities. So for each pressure we assume that $\rho_p(T) = a_0 + a_1T + a_2T^2$ and consequently $(\partial\rho/\partial T)_p = a_1 + 2a_2T$. For each pressure we get a set (a_0, a_1, a_2).

By inserting the differentiated density and the calculated densities $\rho_p(T)$ into $\alpha_p = -(1/\rho(\partial\rho/\partial T)_p$ the isobaric thermal expansivity under different T, p conditions has been derived:

$$\alpha_p = -\frac{a_1 + 2a_2T}{a_0 + a_1T + a_2T^2} \tag{13}$$

As mentioned, the method used to evaluate the isobaric thermal expansion coefficient may affect the accuracy of the values. The differences that are sometimes found for the values of this coefficient in the literature are due not only to differences in density values but also to the fitting equations, as stated in Ref. [56].

The isobaric thermal expansivity, α_p, and the isothermal compressibility, κ_T, were calculated from the above procedures. Following [9], the estimated uncertainty is 1% for the isothermal compressibility and around 3% for the isobaric thermal expansivity, as recently indicated in similar high-pressure density studies

Table 7
Isothermal compressibility. 10^4 κ_T for x HFE-7100 + (1-x) 2-propanol as function of pressure p. and at different temperatures T.

x	p/MPa	T/K					
		298.15	313.15	333.15	353.15	373.15	393.15
		κ_T.10^4/MPa^{-1}					
0.0000	0.10	11.2	12.6	14.9			
	1.00	11.1	12.4	14.7	17.8	22.3	29.3
	5.00	10.6	11.8	13.9	16.6	20.4	26.1
	10.00	10.0	11.1	12.9	15.3	18.5	23.0
	15.00	9.5	10.5	12.1	14.2	16.9	20.6
	20.00	9.1	10.0	11.4	13.2	15.6	18.7
	25.00	8.7	9.5	10.8	12.4	14.4	17.1
	30.00	8.3	9.1	10.2	11.7	13.5	15.8
	35.00	8.0	8.7	9.7	11.0	12.6	14.7
	40.00	7.7	8.3	9.3	10.5	11.9	13.7
	45.00	7.4	8.0	8.9	9.9	11.2	12.9
	50.00	7.1	7.7	8.5	9.5	10.7	12.1
	55.00	6.9	7.4	8.2	9.1	10.2	11.5
	60.00	6.7	7.1	7.9	8.7	9.7	10.9
	65.00	6.4	6.9	7.6	8.3	9.3	10.4
	70.00	6.3	6.7	7.3	8.0	8.9	9.9
	80.00	5.9	6.3	6.8	7.5	8.2	9.1
	90.00	5.6	5.9	6.4	7.0	7.6	8.4
	100.00	5.3	5.6	6.0	6.5	7.1	7.8
	110.00	5.0	5.3	5.7	6.2	6.7	7.3
	120.00	4.8	5.1	5.4	5.8	6.3	6.8
	130.00	4.6	4.8	5.2	5.5	6.0	6.5
	140.00	4.4	4.6	4.9	5.3	5.7	6.1
0.1490	0.10	14.2	16.4				
	1.00	14.1	16.1	19.7	24.8	32.3	44.4
	5.00	13.3	15.1	18.2	22.5	28.5	37.5
	10.00	12.4	14.0	16.7	20.1	24.9	31.5
	15.00	11.7	13.1	15.3	18.3	22.1	27.2
	20.00	11.0	12.2	14.2	16.7	19.9	24.0
	25.00	10.4	11.5	13.3	15.4	18.1	21.5
	30.00	9.9	10.9	12.4	14.3	16.6	19.4
	35.00	9.4	10.3	11.7	13.4	15.4	17.8
	40.00	9.0	9.8	11.1	12.6	14.3	16.4
	45.00	8.6	9.4	10.5	11.8	13.4	15.2
	50.00	8.3	8.9	10.0	11.2	12.6	14.2
	55.00	7.9	8.6	9.5	10.6	11.9	13.4
	60.00	7.6	8.2	9.1	10.1	11.3	12.6
	65.00	7.4	7.9	8.7	9.6	10.7	11.9
	70.00	7.1	7.6	8.4	9.2	10.2	11.3
	80.00	6.6	7.1	7.8	8.5	9.3	10.3
	90.00	6.2	6.6	7.2	7.9	8.6	9.4
	100.00	5.9	6.2	6.8	7.3	8.0	8.7
	110.00	5.6	5.9	6.4	6.9	7.4	8.1
	120.00	5.3	5.6	6.0	6.5	7.0	7.6
	130.00	5.0	5.3	5.7	6.1	6.6	7.1
	140.00	4.8	5.1	5.4	5.8	6.2	6.7
0.3255	0.10	17.1	20.1				
	1.00	16.9	19.7	24.8	32.2	43.5	62.4
	5.00	15.7	18.2	22.5	28.3	36.8	49.5
	10.00	14.6	16.6	20.1	24.7	31.0	39.6
	15.00	13.5	15.3	18.2	22.0	26.8	33.1
	20.00	12.7	14.2	16.7	19.8	23.7	28.5
	25.00	11.9	13.2	15.4	18.0	21.2	25.1
	30.00	11.2	12.4	14.3	16.5	19.2	22.4
	35.00	10.6	11.7	13.3	15.3	17.6	20.3
	40.00	10.1	11.0	12.5	14.2	16.2	18.6
	45.00	9.6	10.5	11.8	13.3	15.1	17.1
	50.00	9.2	10.0	11.2	12.5	14.1	15.9
	55.00	8.8	9.5	10.6	11.8	13.2	14.8
	60.00	8.4	9.1	10.1	11.2	12.5	13.9
	65.00	8.1	8.7	9.6	10.7	11.8	13.1
	70.00	7.8	8.3	9.2	10.2	11.2	12.4
	80.00	7.2	7.7	8.5	9.3	10.2	11.2
	90.00	6.8	7.2	7.8	8.6	9.3	10.2
	100.00	6.3	6.7	7.3	7.9	8.6	9.4
	110.00	6.0	6.3	6.9	7.4	8.0	8.7
	120.00	5.7	6.0	6.5	7.0	7.5	8.1
	130.00	5.4	5.7	6.1	6.6	7.1	7.6
	140.00	5.1	5.4	5.8	6.2	6.7	72
0.4996	0.10	19.4	23.0				

Table 7 (*continued*)

x	p/MPa	T/K					
		298.15	313.15	333.15	353.15	373.15	393.15
		$\kappa_T 10^4$/MPa^{-1}					
	1.00	19.0	22.5	28.8	38.3	53.2	78.8
	5.00	17.6	20.5	25.7	33.0	43.5	59.4
	10.00	16.1	18.6	22.7	28.2	35.6	45.7
	15.00	14.9	16.9	20.3	24.7	30.2	37.3
	20.00	13.8	15.6	18.4	21.9	26.3	31.6
	25.00	12.9	14.4	16.9	19.8	23.3	27.5
	30.00	12.1	13.5	15.6	18.0	21.0	24.4
	35.00	11.4	12.6	14.4	16.6	19.1	21.9
	40.00	10.8	11.9	13.5	15.4	17.5	19.9
	45.00	10.2	11.2	12.7	14.3	16.2	18.3
	50.00	9.7	10.6	11.9	13.4	15.1	16.9
	55.00	9.3	10.1	11.3	12.6	14.1	15.8
	60.00	8.9	9.6	10.7	11.9	13.2	14.7
	65.00	8.5	9.2	10.2	11.3	12.5	13.9
	70.00	8.2	8.8	9.7	10.7	11.8	13.1
	80.00	7.6	8.1	8.9	9.8	10.7	11.8
	90.00	7.1	7.6	8.2	9.0	9.8	10.7
	100.00	6.6	7.1	7.7	8.3	9.0	9.8
	110.00	6.2	6.6	7.2	7.7	8.4	9.1
	120.00	5.9	6.2	6.7	7.2	7.8	8.5
	130.00	5.6	5.9	6.3	6.8	7.3	7.9
	140.00	5,3	5.6	6.0	6.4	6.9	7.5
0.6758	0.10	21.0	25.2				
	1.00	20.6	24.6	32.0	43.2	61.1	91.9
	5.00	18.9	22.3	28.2	36.5	48.6	66.5
	10.00	17.2	20.0	24.6	30.7	38.9	49.8
	15.00	15.8	18.1	21.8	26.6	32.6	40.1
	20.00	14.6	16.5	19.6	23.4	28.1	33.6
	25.00	13.6	15.3	17.9	21.0	24.7	29.0
	30.00	12.7	14.2	16.4	19.0	22.1	25.6
	35.00	12.0	13.2	15.2	17.4	20.0	22.9
	40.00	11.3	12.4	14.1	16.1	18.3	20.8
	45.00	10.7	11.7	13.2	15.0	16.9	19.0
	50.00	10.1	11.1	12.4	14.0	15.7	17.6
	55.00	9.7	10.5	11.7	13.1	14.6	16.3
	60.00	9.2	10.0	11.1	12.4	13.7	15.2
	65.00	8.8	9.5	10.6	11.7	12.9	14.3
	70.00	8.5	9.1	10.1	11.1	12.2	13.5
	80.00	7.8	8.4	9.2	10.1	11.0	12.1
	90.00	7.3	7.8	8.5	9.2	10.1	11.0
	100.00	6.8	7.2	7.9	8.5	9.3	10.1
	110.00	6.4	6.8	7.3	7.9	8.6	9.3
	120.00	6.0	6.4	6.9	7.4	8.0	8.7
	130.00	5.7	6.0	6.5	7.0	7.5	8.1
	140.00	5.4	5.7	6.1	6.6	7.1	7.6
0.7940	0.10	21.9	26.3				
	1.00	21.4	25.7	33.6	45.6	64.8	97.4
	5.00	19.6	23.1	29.4	38.2	50.9	69.3
	10.00	17.8	20.6	25.5	31.9	40.4	51.4
	15.00	16.3	18.6	22.5	27.4	33.6	41.1
	20.00	15.0	17.0	20.2	24.1	28.8	34.3
	25.00	13.9	15.7	18.3	21.5	25.3	29.6
	30.00	13.0	14.5	16.8	19.5	22.6	26.0
	35.00	12.2	13.5	15.5	17.8	20.4	23.3
	40.00	11.5	12.7	14.4	16.4	18.6	21.1
	45.00	10.9	11.9	13.5	15.2	17.2	19.3
	50.00	10.3	11.3	12.7	14.2	15.9	17.8
	55.00	9.8	10.7	11.9	13.3	14.8	16.5
	60.00	9.4	10.2	11.3	12.5	13.9	15.4
	65.00	9.0	9.7	10.7	11.9	13.1	14.5
	70.00	8.6	9.3	10.2	11.2	12.4	13.6
	80.00	7.9	8.5	9.3	10.2	11.2	12.2
	90.00	7.4	7.9	8.6	9.4	10.2	11.1
	100.00	6.9	7.3	8.0	8.6	9.4	10.2
	110.00	6.5	6.9	7.4	8.0	8.7	9.4
	120.00	6.1	6.5	7.0	7.5	8.1	8.8
	130.00	5.8	6.1	6.6	7.0	7.6	8.2
	140.00	5.5	5.8	6.2	6.6	7.1	7.7
0.8497	0.10	22.2	26.8				
	1.00	21.7	26.1	34.2	46.4	66.0	99.0
	5.00	19.9	23.5	29.8	38.8	51.6	70.1
	10.00	18.0	20.9	25.8	32.3	40.8	51.8

Table 7 (*continued*)

x	p/MPa	T/K					
		298.15	313.15	333.15	353.15	373.15	393.15
		$\kappa_T 10^4$/MPa^{-1}					
	15.00	16.5	18.9	22.8	27.7	33.9	41.3
	20.00	15.2	17.2	20.4	24.3	29.0	34.5
	25.00	14.1	15.8	18.5	21.7	25.5	29.7
	30.00	13.1	14.6	16.9	19.6	22.7	26.1
	35.00	12.3	13.6	15.6	17.9	20.5	23.3
	40.00	11.6	12.8	14.5	16.5	18.7	21.1
	45.00	11.0	12.0	13.6	15.3	17.2	19.3
	50.00	10.4	11.3	12.7	14.3	16.0	17.8
	55.00	9.9	10.7	12.0	13.4	14.9	16.5
	60.00	9.4	10.2	11.3	12.6	14.0	15.4
	65.00	9.0	9.7	10.8	11.9	13.1	14.5
	70.00	8.6	9.3	10.3	11.3	12.4	13.6
	80.00	8.0	8.5	9.4	10.2	11.2	12.2
	90.00	7.4	7.9	8.6	9.4	10.2	11.1
	100.00	6.9	7.4	8.0	8.7	9.4	10.2
	110.00	6.5	6.9	7.4	8.0	8.7	9.4
	120.00	6.1	6.5	7.0	7.5	8.1	8.8
	130.00	5.8	6.1	6.6	7.1	7.6	8.2
	140.00	5.5	5.8	6.2	6.7	7.1	7.7
1.0000	0.10	22.7	27.3				
	1.00	22.2	26.6	34.7	46.8	66.0	97.6
	5.00	20.3	23.9	30.2	39.1	51.6	69.3
	10.00	18.3	21.2	26.1	32.5	40.8	51.3
	15.00	16.7	19.1	23.0	27.8	33.8	41.0
	20.00	15.4	17.4	20.6	24.4	29.0	34.2
	25.00	14.2	16.0	18.6	21.8	25.4	29.5
	30.00	13.3	14.8	17.0	19.7	22.6	25.9
	35.00	12.4	13.7	15.7	17.9	20.4	23.2
	40.00	11.7	12.9	14.6	16.5	18.7	21.0
	45.00	11.1	12.1	13.6	15.3	17.2	19.2
	50.00	10.5	11.4	12.8	14.3	15.9	17.7
	55.00	10.0	10.8	12.0	13.4	14.8	16.4
	60.00	9.5	10.3	11.4	12.6	13.9	15.3
	65.00	9.1	9.8	10.8	11.9	13.1	14.4
	70.00	8.7	9.3	10.3	11.3	12.4	13.6
	80.00	8.0	8.6	9.4	10.2	11.2	12.2
	90.00	7.4	7.9	8.6	9.4	10.2	11.0
	100.00	7.0	7.4	8.0	8.6	9.4	10.1
	110.00	6.5	6.9	7.5	8.0	8.7	9.4
	120.00	6.1	6.5	7.0	7.5	8.1	8.7
	130.00	5.8	6.1	6.6	7.0	7.6	8.1
	140.00	5.5	5.8	6.2	6.6	7.1	7.6

[5,57,58], which used the same methods.

Tables 7 and 8 report the isothermal compressibility, κ_T, and the isobaric thermal expansivity, α_p, respectively. Values of κ_T increase with increasing temperature and decrease with increasing pressure. Similarly, the values of α_p increase with increasing temperature and decrease with increasing pressure.

4. Conclusions

Experimental densities in the compressed liquid state for the binary mixture methyl nonafluorobutyl ether (HFE-7100) + 2-propanol are presented. The measurements have been performed in a pressure range from 0.1 to 140 MPa, and in a temperature range between (298.15 and 393.15) K. The data obtained represent an extension of the ρpT data available for the pure compound HFE-7100, and opens up a source of new data for binary mixture compositions. The experimental densities were correlated with a Tait-type equation, showing a good agreement with the data obtained, with AAD lower than 0.02%. The densities of the pure compounds were compared with the literature data available at

Table 8
Isobaric thermal expansion coefficient. $10^4\ \alpha_p$. for x HFE-7100 + (1-x) 2-propanol as a function of pressure p and at different temperatures T.

x	p/MPa	T/K					
		298.15	313.15	333.15	353.15	373.15	393.15
		$\alpha_p.10^4/K^{-1}$					
0.0000	0.10	10.3	11.7	13.5			
	1.00	10.2	11.5	13.4	15.4	17.5	19.9
	5.00	9.9	11.1	12.7	14.5	16.4	18.5
	10.00	9.8	10.8	12.2	13.8	15.4	17.2
	15.00	9.5	10.4	11.7	13.1	14.6	16.2
	20.00	9.3	10.1	11.3	12.5	13.8	15.3
	25.00	9.0	9.8	10.9	12.0	13.2	14.5
	30.00	8.8	9.5	10.5	11.6	12.7	13.9
	35.00	8.6	9.3	10.2	11.2	12.2	13.4
	40.00	8.5	9.1	9.9	10.8	11.8	12.8
	45.00	8.3	8.8	9.7	10.5	11.4	12.4
	50.00	8.1	8.6	9.4	10.2	11.1	12.0
	55.00	8.0	8.5	9.2	9.9	10.7	11.5
	60.00	7.9	8.4	9.0	9.7	10.4	11.2
	65.00	7.7	8.2	8.8	9.5	10.2	11.0
	70.00	7.6	8.0	8.6	9.3	10.0	10.7
	80.00	7.3	7.7	8.3	8.9	9.5	10.2
	90.00	7.1	7.5	8.0	8.6	9.1	9.7
	100.00	6.9	7.3	7.8	8.3	8.8	9.3
	110.00	6.8	7.1	7.5	8.0	8.4	8.9
	120.00	6.6	6.9	7.3	7.8	8.2	8.7
	130.00	6.4	6.7	7.1	7.5	7.9	8.4
	140.00	6.3	6.6	6.9	7.3	7.7	8.2
0.1490	0.10	12.8	14.3				
	1.00	12.2	13.7	15.7	17.9	20.4	23.2
	5.00	12.0	13.2	14.9	16.7	18.7	20.9
	10.00	11.7	12.7	14.0	15.5	17.1	18.8
	15.00	11.3	12.1	13.3	14.5	15.9	17.3
	20.00	11.0	11.7	12.7	13.8	14.9	16.2
	25.00	10.6	11.3	12.2	13.1	14.1	15.2
	30.00	10.3	10.8	11.7	12.5	13.5	14.5
	35.00	10.1	10.6	11.3	12.1	12.9	13.7
	40.00	9.9	10.3	10.9	11.6	12.3	13.1
	45.00	9.6	10.1	10.6	11.2	11.9	12.6
	50.00	9.4	9.8	10.3	10.9	11.5	12.1
	55.00	9.3	9.6	10.1	10.6	11.1	11.6
	60.00	9.1	9.4	9.8	10.3	10.8	11.3
	65.00	8.9	9.2	9.6	10.0	10.5	10.9
	70.00	8.7	9.0	9.4	9.8	10.2	10.7
	80.00	8.4	8.6	9.0	9.4	9.7	10.1
	90.00	8.1	8.4	8.7	9.0	9.3	9.7
	100.00	7.9	8.1	8.4	8.7	8.9	9.3
	110.00	7.7	7.9	8.1	8.3	8.6	8.9
	120.00	7.5	7.6	7.9	8.1	8.3	8.6
	130.00	7.3	7.4	7.6	7.8	8.1	8.3
	140.00	7.1	7.2	7.4	7.6	7.8	8.0
0.3255	0.10	14.3	16.6				
	1.00	13.7	15.4	17.8	20.4	23.3	26.6
	5.00	13.4	14.7	16.6	18.6	20.8	23.3
	10.00	13.0	14.0	15.4	17.0	18.7	20.5
	15.00	12.5	13.3	14.5	15.7	17.1	18.6
	20.00	12.0	12.7	13.7	14.8	15.9	17.1
	25.00	11.6	12.2	13.1	14.0	15.0	16.0
	30.00	11.3	11.8	12.5	13.3	14.1	15.1
	35.00	10.9	11.4	12.0	12.7	13.5	14.3
	40.00	10.6	11.0	11.6	12.2	12.9	13.6
	45.00	10.4	10.7	11.3	11.8	12.4	13.0
	50.00	10.1	10.4	10.9	11.4	12.0	12.5
	55.00	9.9	10.2	10.6	11.1	11.5	12.0
	60.00	9.7	10.0	10.3	10.7	11.2	11.6
	65.00	9.4	9.7	10.1	10.5	10.9	11.3
	70.00	9.2	9.5	9.8	10.2	10.6	11.0
	80.00	8.8	9.1	9.4	9.7	10.1	10.4
	90.00	8.6	8.8	9.0	9.3	9.6	9.9
	100.00	8.3	8.5	8.7	9.0	9.2	9.5
	110.00	8.0	8.2	8.4	8.6	8.9	9.1
	120.00	7.8	8.0	8.1	8.3	8.6	8.8
	130.00	7.8	7.9	8.0	8.0	8.1	8.2
	140.00	7.6	7.7	7.7	7.8	7.9	8.0
0.4996	0.10	15.3	18.0				

Table 8 (*continued*)

x	p/MPa	T/K					
		298.15	313.15	333.15	353.15	373.15	393.15
		$\alpha_p.10^4/K^{-1}$					
	1.00	14.9	16.7	19.2	22.0	25.2	28.8
	5.00	14.6	15.9	17.7	19.7	21.9	24.4
	10.00	14.1	15.0	16.3	17.7	19.3	21.0
	15.00	13.5	14.2	15.2	16.3	17.5	18.7
	20.00	13.0	13.6	14.4	15.2	16.1	17.1
	25.00	12.5	13.0	13.6	14.3	15.0	15.8
	30.00	12.1	12.5	13.0	13.6	14.2	14.8
	35.00	11.7	12.0	12.5	13.0	13.5	14.0
	40.00	11.4	11.7	12.0	12.4	12.8	13.2
	45.00	11.1	11.3	11.6	12.0	12.3	12.7
	50.00	10.8	11.0	11.3	11.5	11.8	12.1
	55.00	10.6	10.7	10.9	11.2	11.4	11.7
	60.00	10.3	10.4	10.6	10.8	11.0	11.3
	65.00	10.1	10.2	10.4	10.5	10.7	10.9
	70.00	9.8	9.9	10.1	10.2	10.4	10.6
	80.00	9.5	9.5	9.6	9.8	9.9	10.0
	90.00	9.1	9.2	9.2	9.3	9.4	9.5
	100.00	8.8	8.9	8.9	9.0	9.0	9.0
	110.00	8.5	8.6	8.6	8.6	8.7	8.7
	120.00	8.3	8.3	8.3	8.3	8.4	8.4
	130.00	8.1	8.1	8.1	8.1	8.1	8.1
	140.00	7.9	7.9	7.9	7.9	7.8	7.8
0.6758	0.10	15.9	19.0				
	1.00	15.5	17.3	20.0	23.0	26.4	30.3
	5.00	15.3	16.5	18.3	20.3	22.5	24.9
	10.00	14.7	15.6	16.8	18.1	19.5	21.1
	15.00	14.1	14.7	15.6	16.5	17.5	18.6
	20.00	13.5	14.0	14.7	15.3	16.1	16.9
	25.00	13.0	13.4	13.9	14.4	15.0	15.6
	30.00	12.5	12.8	13.2	13.6	14.1	14.5
	35.00	12.1	12.3	12.7	13.0	13.3	13.7
	40.00	11.8	11.9	12.2	12.4	12.7	12.9
	45.00	11.4	11.5	11.7	11.9	12.1	12.3
	50.00	11.1	11.2	11.4	11.5	11.6	11.8
	55.00	10.8	10.9	11.0	11.1	11.2	11.4
	60.00	10.6	10.6	10.7	10.8	10.8	10.9
	65.00	10.3	10.4	10.4	10.5	10.5	10.6
	70.00	10.1	10.1	10.1	10.2	10.2	10.2
	80.00	9.7	9.7	9.7	9.7	9.7	9.6
	90.00	9.3	9.3	9.3	9.2	9.2	9.2
	100.00	9.0	9.0	8.9	8.9	8.8	8.7
	110.00	8.7	8.7	8.6	8.5	8.5	8.4
	120.00	8.4	8.4	8.3	8.3	8.2	8.1
	130.00	8.2	8.2	8.1	8.0	7.9	7.8
	140.00	8.0	7.9	7.8	7.8	7.7	7.6
0.7940	0.10	16.2	19.4				
	1.00	16.0	17.8	20.3	23.2	26.4	30.2
	5.00	15.5	16.7	18.4	20.4	22.5	24.9
	10.00	15.0	15.8	16.9	18.0	19.3	20.7
	15.00	14.3	14.9	15.6	16.4	17.3	18.3
	20.00	13.7	14.1	14.7	15.2	15.9	16.5
	25.00	13.2	13.5	13.9	14.3	14.7	15.2
	30.00	12.6	12.9	13.2	13.5	13.8	14.2
	35.00	12.2	12.4	12.6	12.8	13.1	13.3
	40.00	11.9	12.0	12.1	12.3	12.4	12.6
	45.00	11.5	11.6	11.7	11.8	11.9	12.0
	50.00	11.2	11.2	11.3	11.3	11.4	11.5
	55.00	10.9	10.9	10.9	11.0	11.0	11.0
	60.00	10.6	10.6	10.6	10.6	10.6	10.6
	65.00	10.4	10.4	10.3	10.3	10.3	10.2
	70.00	10.1	10.1	10.1	10.0	10.0	9.9
	80.00	9.7	9.7	9.6	9.5	9.4	9.3
	90.00	9.3	9.3	9.2	9.1	9.0	8.9
	100.00	9.0	9.0	8.8	8.7	8.6	8.5
	110.00	8.7	8.6	8.5	8.4	8.3	8.1
	120.00	8.5	8.4	8.3	8.1	8.0	7.8
	130.00	8.2	8.1	8.0	7.9	7.7	7.6
	140.00	8.0	7.9	7.8	7.6	7.5	7.3
0.8497	0.10	16.3	19.5				
	1.00	16.2	17.9	20.4	23.2	26.3	29.9
	5.00	15.6	16.8	18.4	20.3	22.3	24.6
	10.00	14.9	15.7	16.8	18.0	19.3	20.8

Table 8 (*continued*)

x	p/MPa	T/K					
		298.15	313.15	333.15	353.15	373.15	393.15
		α_p.10^4/K^{-1}					
	15.00	14.4	14.9	15.6	16.3	17.1	17.9
	20.00	13.8	14.1	14.6	15.1	15.6	16.2
	25.00	13.2	13.5	13.8	14.1	14.5	14.9
	30.00	12.7	12.9	13.1	13.3	13.6	13.9
	35.00	12.2	12.4	12.5	12.7	12.9	13.1
	40.00	11.9	11.9	12.0	12.1	12.2	12.3
	45.00	11.5	11.5	11.6	11.6	11.7	11.7
	50.00	11.2	11.2	11.2	11.2	11.2	11.2
	55.00	10.9	10.9	10.9	10.8	10.8	10.8
	60.00	10.6	10.6	10.5	10.5	10.4	10.4
	65.00	10.4	10.3	10.3	10.2	10.1	10.0
	70.00	10.1	10.1	10.0	9.9	9.8	9.7
	80.00	9.7	9.6	9.5	9.4	9.3	9.1
	90.00	9.3	9.3	9.1	9.0	8.8	8.7
	100.00	9.0	8.9	8.8	8.6	8.5	8.3
	110.00	8.7	8.6	8.5	8.3	8.1	7.9
	120.00	8.5	8.4	8.2	8.0	7.8	7.6
	130.00	8.2	8.1	7.9	7.8	7.6	7.4
	140.00	8.0	7.9	7.7	7.5	7.3	7.1
1.0000	0.10	16.0	19.3				
	1.00	15.8	17.4	19.8	22.5	25.4	28.8
	5.00	15.4	16.4	18.0	19.6	21.5	23.5
	10.00	14.6	15.3	16.3	17.4	18.5	19.8
	15.00	13.9	14.4	15.1	15.8	16.6	17.4
	20.00	13.3	13.6	14.1	14.6	15.1	15.7
	25.00	12.7	13.0	13.3	13.7	14.1	14.5
	30.00	12.4	12.5	12.7	12.8	13.0	13.2
	35.00	11.9	12.0	12.1	12.2	12.3	12.4
	40.00	11.6	11.6	11.6	11.7	11.7	11.7
	45.00	11.2	11.2	11.2	11.2	11.2	11.2
	50.00	10.9	10.9	10.8	10.8	10.7	10.7
	55.00	10.6	10.6	10.5	10.4	10.3	10.2
	60.00	10.3	10.3	10.2	10.1	10.0	9.8
	65.00	10.1	10.0	9.9	9.8	9.7	9.5
	70.00	9.8	9.8	9.6	9.5	9.4	9.2
	80.00	9.4	9.3	9.2	9.0	8.9	8.7
	90.00	9.1	8.9	8.8	8.6	8.4	8.3
	100.00	8.8	8.6	8.5	8.3	8.1	7.8
	110.00	8.5	8.3	8.1	7.9	7.7	7.5
	120.00	8.2	8.1	7.9	7.7	7.5	7.2
	130.00	8.0	7.8	7.6	7.4	7.2	7.0
	140.00	7.8	7.6	7.4	7.2	7.0	6.7

atmospheric and at high pressure over a wide range of temperatures. Isothermal compressibility and isobaric expansivity were also obtained.

Acknowledgements

This paper is part of the Doctoral Thesis of N. Muñoz-Rujas.

N. Muñoz-Rujas acknowledges financial support for this research from the University of Burgos (Pre-Doctoral Grants 2014).

List of symbols

AAD	absolute Average Deviation
a_i	coefficients of isobaric thermal expansivity correlation
A_i, B_i, C	coefficients of density correlation
Bias	average Deviation
Calc	calculated
Exp	experimental
i	constituent identification
lit	literature
MD	maximum Deviation
N_P	number of experimental data points which are in our p, T ranges
P	pressure
p_0	reference pressure
RMSD	root Mean Square Deviation
T	temperature
V^E	excess molar volume

Greek letters

σ	standard deviation
α_p	isobaric thermal expansivity
ρ	density
ρ_0	density at a reference pressure p_0
κ_T	isothermal compressibility

Appendix A. Supplementary data

Supplementary data related to this article can be found at http://dx.doi.org/10.1016/j.fluid.2016.09.014.

References

[1] W.T. Tsai, J. Hazard. Mater 119 (2005) 69–78.
[2] 3M™ Novec™ Engineered Fluids. http://solutions.3m.com/wps/portal/3M/en_US/3MNovec/Home.
[3] P. Tuma, S. Paul, L. Tousignant, Earth 16 (2010).
[4] J.B. Durkee II, Cleaning with Solvents: Science and Technology, first ed., Elsevier B.V, Oxford, 2014.
[5] F.E.M. Alaoui, E.A. Montero, G. Qiu, F. Aguilar, J. Wu, J. Chem. Thermodyn. 65 (2013) 174–183.
[6] M.J.P. Comuñas, J. Bazile, A. Baylaucq, C. Boned, J. Chem. Eng. Data 53 (2008) 986–994.
[7] H. Lagourette, B. Boned, C. Saint-Guirons, H. Xans, P. Zhou, Meas. Sci. Technol. 3 (1992) 699–703.
[8] W. Wagner, A. Pruß, J. Phys. Chem. Ref. Data 31 (2002), 387–535.
[9] Expression of the Uncertainty of Measurement in Calibration, European Cooperation for Accreditation, EA-4/02, 1999.
[10] I. Cibulka, L. Hnedkovsky, T. Takagi, J. Chem. Eng. Data 42 (1997) 415–433.
[11] H. Kubota, Y. Tanaka, T. Makita, Int. J. Thermophys. 8 (1987) 47–70.
[12] I.F. Golubev, T.N. Vasil'Kovskaya, V.S. Zolin, J. Eng. Phys. Thermophys. 38 (1980) 399–401 (Translation of: Inzh.-Fiz. Zh. 38 (1980) 668-670).
[13] M. Dakkach, F. Aguilar, F.E.M. Alaoui, E.A. Montero, J. Chem. Thermodyn. 80 (2015) 135–141.
[14] M. Dakkach, F. Aguilar, F.E.M. Alaoui, E.A. Montero, J. Chem. Thermodyn. 89 (2015) 278–285.
[15] T. Minamihounoki, T. Takigawa, K. Tamura, S. Murakami, J. Chem. Thermodyn. 33 (2001) 189–203.
[16] G. Marchionni, P. Maccone, G. Pezzin, J. Fluor. Chem. 118 (2002) 149–155.
[17] M.H. Rausch, L. Kretschmer, S. Will, A. Leipertz, A.P. Fröba, J. Chem. Eng. Data 60 (2015) 3759–3765.
[18] M.M. Piñeiro, D. Bessières, J.L. Legido, H. Saint-Guirons, Int. J. Thermophys. 24 (2003) 1265–1276.
[19] H. Qi, D. Fang, X. Meng, J. Wu, J. Chem. Thermodyn. 77 (2014) 131–136.
[20] J.L. Hales, J.H. Ellender, J. Chem. Thermodyn. 8 (1976) 1177–1184.
[21] T.M. Aminabhavi, M.I. Aralaguppi, S.B. Harogoppad, R.H. Balundgi, J. Chem. Eng. Data 38 (1993) 31–39.
[22] C.A. Cerdeiriña, C.A. Tovar, J. Troncoso, E. Carballo, L. Romaní, Fluid Phase Equilib. 157 (1999) 93–102.
[23] B. González, A. Domínguez, J. Tojo, J. Chem. Thermodyn. 35 (2003) 939–953.
[24] M.I. Aralaguppi, J.G. Baragi, J. Chem. Thermodyn. 38 (2006) 434–442.
[25] B. González, A. Domínguez, J. Tojo, J. Chem. Thermodyn. 38 (2006) 1172–1185.
[26] M.M.H. Bhuiyan, J. Ferdaush, M.H. Uddin, J. Chem. Thermodyn. 39 (2007) 675–683.
[27] F.M. Pang, C.E. Seng, T.T. Teng, M.H. Ibrahim, J. Mol. Liq. 136 (2007) 71–78.
[28] Q.S. Li, M.G. Su, S. Wang, J. Chem. Eng. Data 52 (2007) 1141–1145.
[29] H.A. Zarei, F. Jalili, J. Chem. Thermodyn. 39 (2007) 55–66.
[30] A.M. Awwad, H.M. Alsyouri, M.A. Abu-Daabes, K.A. Jbara, J. Chem. Thermodyn. (2008) 592–598.
[31] H.A. Zarei, S. Asadi, H. Iloukhani, J. Mol. Liq. 141 (2008) 25–30.
[32] G.P. Dubey, M. Sharma, J. Chem. Thermodyn. 41 (2009) 115–122.
[33] Y.C. Kao, C.H. Tu, J. Chem. Thermodyn. 43 (2011) 216–226.
[34] E. Vercher, A.V. Orchillés, F.J. Llopis, V. González-Alfaro, A. Martínez-Andreu, J. Chem. Eng. Data 56 (2011) 4633–4642.
[35] F. Kermanpour, H.Z. Niakan, J. Chem. Thermodyn. 54 (2012) 10–19.
[36] M. Almasi, J. Chem. Eng. Data 57 (2012) 2992–2998.
[37] S. Singh, M. Aznar, N. Deenadayalu, J. Chem. Thermodyn. 57 (2013) 238–247.
[38] A. Pal, H. Kumar, B. Kumar, R. Gaba, J. Mol. Liq. 187 (2013) 278–286.
[39] E.J. González, P.F. Requejo, A. Domínguez, E.A. Macedo, J. Solut. Chem. 42 (2013) 746–763.
[40] E.J. González, B. González, E.A. Macedo, J. Chem. Eng. Data 58 (2013)

1440–1448.
[41] M. Almasi, Phys. B Condens. Matter 412 (2013) 100–105.
[42] S.S. Sastry, S. Babu, T. Vishwam, H.S. Tiong, J. Therm. Anal. Calorim. 116 (2014) 923–935.
[43] F.M.R. Mesquita, F.X. Feitosa, M. Aznar, H.B. De Sant'Ana, R.S. Santiago-Aguiar, J. Chem. Eng. Data 59 (2014) 2196–2206.
[44] Y.-F. Lin, C.-H. Tu, J. Taiwan Inst. Chem. Eng. 45 (2014) 2194–2204.
[45] M. Almasi, Thermochim. Acta 591 (2014) 75–80.
[46] R. Yaginuma, T. Nakajima, H. Tanaka, M. Kato, J. Chem. Eng. Data 47 (1997) 814–816.
[47] M. Moha-Ouchane, C. Boned, A. Allal, M. Benseddik, Int. J. Thermophys. 19 (1998) 161–189.
[48] C. Boned, M. Moha-Ouchane, J. Jose, Phys. Chem. Liq. 38 (2000) 113–136.
[49] A. Zúñiga-Moreno, L.A. Galicia-Luna, J. Chem. Eng. Data 47 (2002) 155–160.
[50] P. Stringari, G. Scalabrin, A. Valtz, D. Richon, J. Chem. Thermodyn. 41 (2009) 683–688.
[51] F.E.M. Alaoui, E.A. Montero, J.P. Bazile, F. Aguilar, C. Boned, J. Chem. Thermodyn. 54 (2012) 358–365.
[52] H. Nourozieh, M. Kariznovi, J. Abedi, J. Chem. Thermodyn. 65 (2013) 191–197.
[53] P. Gómez-Álvarez, D. González-Salgado, J.P. Bazile, D. Bessieres, F. Plantier, Fluid Phase Equilib. 358 (2013) 7–26.
[54] C.A. Cerdeiriña, C.A. Tovar, D. González-Salgado, E. Carballo, L. Romaní, Phys. Chem. Chem. Phys. 3 (2001) 5230–5236.
[55] J. Troncoso, D. Bessières, C.A. Cerdeiriña, E. Carballo, L. Romaní, Fluid Phase Equilib. 208 (2003) 141–154.
[56] J. Jacquemin, P. Husson, V. Mayer, I. Cibulka, J. Chem. Eng. Data 52 (2007) 2204–2211, 2007.
[57] Y. Miyake, A. Baylaucq, F. Plantier, D. Bessières, H. Ushiki, C. Boned, J. Chem. Thermodyn. 40 (2008) 836–845.
[58] G. Watson, T. Lafitte, C.K. Zéberg-Mikkelsen, A. Baylaucq, D. Bessieres, C. Boned, Fluid Phase Equilib. 247 (2006) 121–134.

J. Chem. Thermodynamics 112 (2017) 52–58

Contents lists available at ScienceDirect

J. Chem. Thermodynamics

journal homepage: www.elsevier.com/locate/jct

Speed of sound and derivative properties of hydrofluoroether fluid HFE-7500 under high pressure

Natalia Muñoz-Rujas [a,b], Jean Patrick Bazile [a], Fernando Aguilar [b], Guillaume Galliero [a], Eduardo Montero [b,*], Jean Luc Daridon [a]

[a] Laboratoire des Fluides Complexes et leurs Réservoirs, CNRS-TOTAL, UMR 5150, Université de Pau, BP 1155, 64013 Pau Cedex, France
[b] Departamento de Ingeniería Electromecánica, Escuela Politécnica Superior, Universidad de Burgos, E-09006 Burgos, Spain

ARTICLE INFO

Article history:
Received 1 December 2016
Received in revised form 30 March 2017
Accepted 15 April 2017
Available online 18 April 2017

Keywords:
Hydrofluoroethers
Speed of sound
Density
High pressure
Isentropic compressibility

ABSTRACT

The speed of sound of hydrofluoroether fluid HFE-7500 has been measured at pressures up to 100 MPa along isotherms ranging from (293.15 to 353.15) K. The measurements were carried out using a pulse echo technique operating at 3 MHz. Additional high pressure density data were measured up to 140 MPa with temperatures from (293.15 to 393.15) K in order to evaluate isentropic compressibility using speed of sound measurements. A correlation was then proposed to describe both density and speed of sound within their estimated uncertainties and used to evaluate the density and its derivatives.

1. Introduction

Many manufacturing processes require dielectric heat transfer liquids to maintain process or components temperature, such as physical vapor deposition and chemical vapor deposition. Other processes need to use fluids as heat transfer media to cool electronic components in direct contact single or two phase cooling of supercomputers, reactors and military electronics among others. Perfluorocarbons (PFCs) and perfluoropolyethers (PFPEs) have been used for these applications [1] but their high global warming potentials, and long atmospheric lifetimes have led to search for other fluids with the same properties but with low environmental impact to substitute them.

Because of this fact, many alternatives were proposed in order to replace these fluorocarbons, such as HFCs with lower global warming potentials, hydrofluoroolefins (HFOs), hydrofluoroethers (HFEs), and so on. Hydrofluoroethers, which were introduced by mid of '90s, are a class of ethers having a mixture of alkyl and fluorinated alkyl substituents. The C–H bonds in the hydrofluoroether molecule lead to an increase in the reaction with the OH radicals present in the troposphere, thus giving shorter atmospheric lifetimes. HFEs have a high vapor pressure, being volatile and insoluble in water [2]. This kind of fluids share many of the properties of CFCs, HCFCs, PFCs and PFPEs, they are also non-flammable fluids with very low overall toxicity [3], zero ozone depletion potential (ODP), low global warming potential (GWP), and have any significant environmental hazard [4], being also compatible with most of the common metals and polymers. These fluids are intended to be used in many applications such as refrigerants, blowing agents, cleaning solvents, dry etching agents, as heat transfer fluids, etc.

HFE-7500 is being a viable option for replace PFCs and PFPEs in a wide range of applications. Its physical properties make it a good choice to use in heat transfer applications; semiconductor manufacturing processes, to cool high voltage transformers and power electronics, and in pharmaceutical processes such as freeze drying.

The knowledge of thermophysical properties, such as speed of sound and density is necessary to correctly design the equipment that will be used in chemical and industrial applications. Many industrial applications require accurate data at high pressures, data that are also needed in order to develop modelling for scientific and engineering purposes.

In this work, speed of sound and density measurements of hydrofluoroether fluid HFE-7500 were carried out in a wide range of pressure and temperature. The determination of the derivative properties, that is, the isentropic compressibility, isothermal compressibility and isobaric expansion, which can lead to valuable information on the dependence of the volumetric properties on temperature and pressure, have also been carried out.

* Corresponding author.
E-mail address: emontero@ubu.es (E. Montero).

http://dx.doi.org/10.1016/j.jct.2017.04.007
0021-9614/

2. Experimental section

2.1. Materials

Hydrofluoroether fluid HFE-7500, also known by its chemical name, 2-trifluoromethyl-3-ethoxydodecafluorohexane or 3-ethoxy-1,1,1,2,3,4,4,5,5,6,6,6-dodecafluoro-2-trifluoromethylhexane (CAS No.: 297730-93-9, molar mass 414.11 g·mol^{-1}) was obtained from the 3M company with a stated mass fraction purity greater than 0.995 determined by gas chromatography. The fluid was subject to no further purification.

2.2. Speed of sound measurement

The method employed to measure the speed of sound at high pressure is based on a pulse echo technique working in transmission mode. The apparatus, which has been described in detail previously [5] consists of an acoustic probe made of two 3 MHz piezoelectric discs facing each other at both ends of a stainless steel cylindrical support with a fixed path length. One of the transducers acts as a transmitter, and the other receives the echoes from the ultrasonic wave. The speed of sound was then determined from the measurement of the time delay between the transmitted pulse and the first echo by using an oscilloscope. A calibration with two reference fluids with a known speed of sound, in this case water [6,7] and heptane [8] at different pressures and temperatures was carried out in order to give the path length that will be necessary to calculate the speeds of sound of HFE-7500. The uncertainty given by this calibration is less than 0.06%.

The entire acoustic probe was immersed into the liquid sample within a high pressure cell closed at one end by a plug in which three electrical feedthroughs were machined in order to allow connecting the piezoelectric elements to a high voltage ultrasonic pulser-receiver device. The pressure into the liquid was generated thanks to a high pressure volumetric pump and then transmitted to the cell. The cell is fully immersed in a thermo-regulated bath filled with silicone oil with a stability of 0.02 K in the temperature range investigated. The temperature is measured with a Pt100 probe housed in a metal finger in order to isolate it from pressure with an uncertainty of ±0.1 K. A pressure gauge calibrated up to 100 MPa was used to measure the pressure in order to give an uncertainty lower than 0.01 MPa. Then, the overall expanded uncertainty of speed of sound in the pressure range measured (0.1–100) MPa is estimated to be less than 0.2% using the law of propagation of standard uncertainties [9].

2.3. Density measurement

High pressure density measurements were carried out in the range (0.1–140) MPa for the pressure and (293.15–393.15) K for the temperature. To perform these measurements, a vibrating tube densitometer Anton Paar DMA HPM was used. The principle of the apparatus is to measure the period of oscillation of a U-shape tube and to deduce the density which is related to the square of the period by a linear law. The calibration of the densitometer was performed according to the procedure described by Comuñas et al. [10] by using vacuum and both water [11] and decane [12]. The temperature of the densitometer is regulated by an external circulating fluid using a thermostatic bath and measured thanks to a Pt 100 probe with an uncertainty of ±0.1 K in the temperature range investigated (293.15 to 393.15) K. Concerning the pressure measurement, a volumetric pump was used in order to increase the pressure inside the cell by the liquid itself. A HBM pressure gauge located between the pump to the U-tube circuit is responsible to give the pressure values. Then the uncertainty given by the HBM pressure gauge is estimated to be 0.1% for the pressure interval investigated (0.1–140) MPa. Considering both uncertainties in temperature and in pressure, the density of the reference fluid as well as the error in the measurements of the period of oscillation for the vacuum, the two reference fluids and the studied liquid, the overall experimental uncertainty in density values is estimated to be ±0.5 kg·m^{-3} (0.06%) between (0.1 and 140) MPa.

3. Results and discussion

Speed of sound measurements were undertaken along isotherms spaced out 10 K from (293.15 to 353.15) K in the pressure range from 0.1 to 100 MPa using 20 MPa steps. The data are listed in Table 1. The experimental data were correlated using a rational function which correlates $1/c^2$ as a function of pressure and temperature by considering nine adjustable parameters:

$$\frac{1}{c^2} = \frac{A + BP + CP^2 + DP^3}{1 + ET + FP} \tag{1}$$

in which:

$$A = A_0 + A_1 T + A_2 T^2 + A_3 T^3 \tag{2}$$

The values obtained for the nine parameters are listed in Table 2 along with the average deviation (AD%), absolute deviation (AAD%) and maximum deviation (MD%). These deviations show that the correlation leads to a good interpolation for the speed of sound data. It can be seen that the value for the maximum deviation between experimental and calculated data is lower than the estimated experimental uncertainty. The speed of sound of HFE-7500 fluid was measured previously by our team [13] in the pressure range (0.1–100) MPa and in the temperature range (283.15–373.15) K covering our pressure and temperature ranges. The present article shows a new set of measurements of speed of sound performed with a recently renovated speed of sound probe in the apparatus, which means that a new setup and calibration was necessary. The comparison between these measurements shows a good agreement within the combined uncertainty, with an AD = −0.01%, an AAD = 0.07% and a MD = 0.27%.

Density was calculated by integration of speed of sound data in the full pressure range (0.1 to 100) MPa by using a method which rests on the Newton-Laplace relationships [14] between the speed of sound and the isentropic compressibility, κ_S.

With the high pressure speed of sound and density data, and assuming that the ultrasonic speed is identical with the speed of sound within the limit of zero frequencies, C_0, we can evaluate both the isentropic compressibility and the isothermal compressibility by using the following equations:

$$\kappa_S = \frac{1}{\rho c^2} \tag{3}$$

and

$$\kappa_T = \kappa_S + \frac{T\alpha_p^2}{\rho C_p} \tag{4}$$

where ρ, α_P, κ_S, κ_T, and C_p are, respectively, the density, the isobaric expansion, the isentropic and isothermal compressibilities, and the isobaric heat capacity. Then the combination of Eqs. (3) and (4) can lead to a relation that connects the speed of sound to the thermodynamic properties:

$$\frac{v^2}{c^2} = v\kappa_T - \frac{T v^2 \alpha_p^2}{C_p} \tag{5}$$

The heat capacity data can be estimated by integration of the following thermodynamic relationship when values at a reference pressure are known [15]:

Table 1
Experimental values of speed of sound, c, at temperatures T and pressures P for the liquid HFE-7500[a]

P/MPa	T/K	c/m·s^{-1}	P/MPa	T/K	c/m·s^{-1}
0.1	293.15	673.7	60.0	323.15	878.6
20.0	293.15	781.1	80.0	323.15	945.6
40.0	293.15	865.8	100.0	323.15	1004.9
60.0	293.15	938.1	0.1	333.15	561.4
80.0	293.15	1001.8	20.0	333.15	688.4
100.0	293.15	1058.0	40.0	333.15	783.3
0.1	303.15	643.7	60.0	333.15	861.5
20.0	303.15	755.3	80.0	333.15	929.1
40.0	303.15	842.8	100.0	333.15	989.3
60.0	303.15	916.9	0.1	343.15	534.8
80.0	303.15	981.3	20.0	343.15	667.7
100.0	303.15	1038.5	40.0	343.15	765.0
0.1	313.15	616.7	60.0	343.15	844.9
20.0	313.15	732.2	80.0	343.15	913.5
40.0	313.15	822.0	100.0	343.15	974.0
60.0	313.15	897.4	0.1	353.15	509.0
80.0	313.15	963.0	20.0	353.15	647.6
100.0	313.15	1021.7	40.0	353.15	747.5
0.1	323.15	588.4	60.0	353.15	828.9
20.0	323.15	709.6	80.0	353.15	898.5
40.0	323.15	802.1	100.0	353.15	960.3

[a] Standard uncertainties u are $u(T) = 0.1$ K, $u(P) = 0.01$ MPa. The combined expanded uncertainty U_c (level of confidence = 0.95) is $U_c(c) = 0.002c$.

Table 2
Parameters of Eqs. (1) and (2) for HFE-7500.

Parameters	HFE-7500
A_0	$-7.10290\cdot10^{-7}$
A_1	$7.73670\cdot10^{-9}$
A_2	$-8.11420\cdot10^{-12}$
A_3	$-1.82570\cdot10^{-15}$
B	$6.35416\cdot10^{-9}$
C	$-3.57310\cdot10^{-11}$
D	$1.18674\cdot10^{-13}$
E	$-2.15449\cdot10^{-3}$
F	$9.85184\cdot10^{-3}$
Deviations[a]	
AD%	$4.28\cdot10^{-4}$
AAD%	$4.23\cdot10^{-2}$
MD%	$1.21\cdot10^{-1}$

[a] AD = average deviation; AAD = absolute average deviation; MD = maximum deviation.

$$\left(\frac{\partial C_p}{\partial P}\right)_T = -T\left(\frac{\partial^2 v}{\partial T^2}\right)_P \tag{6}$$

where:

$$C_p(T) = C_{p,ref}(T) - T\frac{\partial^2}{\partial T^2}\int_{Pref}^{P} v\,dP \tag{7}$$

In this work, the values of $C_{p,ref}$ were measured at atmospheric pressure by using a SETARAM Micro DSC 7 evo calorimeter and were expressed as a linear function of temperature in the range investigated:

$$C_{p,ref}/\mathrm{J\cdot K^{-1}\cdot kg^{-1}} = 8.169\times10^{2} + 0.458T + 1.942\times10^{-3}T^{2} \tag{8}$$

Eq. (5) can be transformed into Eq. (9), which relates the square of the ratio of both properties, speed of sound and density to the derivatives of the volume with respect to temperature and pressure:

$$\left(\frac{v}{c}\right)^2 = -\left(\frac{\partial v}{\partial P}\right)_T - \frac{T}{C_p}\left(\frac{\partial v}{\partial T}\right)_P^2 \tag{9}$$

The square of the ratio of the volume to the speed of sound was used to adjust the parameters of an equation of state function defined by the volume at atmospheric pressure and the change in volume with respect to pressure:

$$v_{ref} = v_0 + v_1T + v_2T^2 + v_3T^3 \tag{10}$$

$$\left(\frac{\partial v}{\partial P}\right)_T = -\frac{a+dP}{b+P} \tag{11}$$

where d is constant and a and b are expressed as a function of temperature by means of the following polynomials:

$$a = a_0 + a_1T + a_2T^2 + a_3T^3 \tag{12}$$

$$b = b_0 + b_1T + b_2T^2 \tag{13}$$

By integrating and or deriving this equation, the volume, its derivatives and all of the thermophysical properties, that is, the density, the heat capacity, isobaric expansion, isothermal compressibility, isentropic compressibility and speed of sound can be obtained. All the details concerning the various stages in the calculation of these properties are discussed in a previous paper [16].

In order to adjust parameters, it is necessary to evaluate the parameter of v_{ref} from atmospheric density data and then to estimate the coefficients a, b and d by minimizing the following objective function:

$$OF = \sum_{i}^{N_{exp}} - \left(\left(\frac{\partial v}{\partial P}\right)_T^{cal} - \frac{T}{C_p^{cal}}\left(\frac{\partial v}{\partial T}\right)_P^{2,cal} - \left(\frac{v_i^{exp}}{c_i^{exp}}\right)^2\right)^2 \tag{14}$$

Listed in Table 3 are the values of the densities, ρ, calculated from the integration of speed of sound measurements.

According to the density calculations, the quality of this correlation was checked by comparison with the survey of literature data [13,17–20]. Ref. [17] provides values for comparison only at atmospheric pressure, and the rest of the references provide values at high pressure covering our entire pressure and temperature ranges. We observed a typographical error in density table of Ref. [13]. There is a lag between pressure column and density columns of this table. The value 2.5 MPa was put instead of 10 MPa and therefore all the above pressures are shifted one place. This mistake was corrected before performing comparison with the present measurements. Table 4 gathers the comparisons between the literature values and those from our correlation as well as the devia-

Table 3
Values of densities, ρ, at temperatures T and at pressures P determined from the integration of speed of sound measurements in liquid HFE-7500[a]

P/MPa	T/K	ρ/g·cm^{-3}	P/MPa	T/K	ρ/g·cm^{-3}	P/MPa	T/K	ρ/g·cm^{-3}
0.1	293.15	1.6303	40.0	313.15	1.6784	80.0	333.15	1.7102
10.0	293.15	1.6541	50.0	313.15	1.6946	90.0	333.15	1.7230
20.0	293.15	1.6747	60.0	313.15	1.7095	100.0	333.15	1.7350
30.0	293.15	1.6929	70.0	313.15	1.7232	0.1	343.15	1.5237
40.0	293.15	1.7091	80.0	313.15	1.7360	10.0	343.15	1.5593
50.0	293.15	1.7239	90.0	313.15	1.7479	20.0	343.15	1.5879
60.0	293.15	1.7376	100.0	313.15	1.7593	30.0	343.15	1.6119
70.0	293.15	1.7502	0.1	323.15	1.5674	40.0	343.15	1.6328
80.0	293.15	1.7621	10.0	323.15	1.5975	50.0	343.15	1.6513
90.0	293.15	1.7732	20.0	323.15	1.6226	60.0	343.15	1.6680
100.0	293.15	1.7838	30.0	323.15	1.6442	70.0	343.15	1.6833
0.1	303.15	1.6096	40.0	323.15	1.6631	80.0	343.15	1.6974
10.0	303.15	1.6353	50.0	323.15	1.6801	90.0	343.15	1.7106
20.0	303.15	1.6573	60.0	323.15	1.6956	100.0	343.15	1.7230
30.0	303.15	1.6765	70.0	323.15	1.7098	0.1	353.15	1.5012
40.0	303.15	1.6937	80.0	323.15	1.7231	10.0	353.15	1.5399
50.0	303.15	1.7092	90.0	323.15	1.7355	20.0	353.15	1.5705
60.0	303.15	1.7234	100.0	323.15	1.7471	30.0	353.15	1.5958
70.0	303.15	1.7366	0.1	333.15	1.5458	40.0	353.15	1.6176
80.0	303.15	1.7489	10.0	333.15	1.5785	50.0	353.15	1.6369
90.0	303.15	1.7605	20.0	333.15	1.6053	60.0	353.15	1.6543
100.0	303.15	1.7715	30.0	333.15	1.6280	70.0	353.15	1.6701
0.1	313.15	1.5886	40.0	333.15	1.6479	80.0	353.15	1.6847
10.0	313.15	1.6165	50.0	333.15	1.6657	90.0	353.15	1.6983
20.0	313.15	1.6400	60.0	333.15	1.6818	100.0	353.15	1.7110
30.0	313.15	1.6603	70.0	333.15	1.6965			

[a] Standard uncertainties u are $u(T) = 0.1$ K, $u(P) = 0.01$ MPa. The combined expanded uncertainty U_c (level of confidence = 0.95) is $U_c(\rho) = 0.001\rho$.

Table 4
Deviations between density from literature data and values interpolated by Eqs. (9) to (13), ([ρ(cal) − ρ(lit)]/ρ(cal)), and deviations between density from literature and the correlation data given by Eqs. (15) to (17), ([ρ(Tait) − ρ(lit)]/ρ(Tait))[a]

			[ρ(cal) − ρ(lit)]/ρ(cal)			[ρ(Tait) − ρ(lit)]/ρ(Tait)		
Ref.	T range/K	P range/MPa	AD%	AAD%	MD%	AD%	AAD%	MD%
[13]	(293.15–343.15)	(0.1–100)	0.01	0.02	0.05	−0.01	0.02	0.08
[17]	(293.15–363.15)	(0.1)	−0.03	0.03	0.07	$2.2\cdot10^{-3}$	0.02	0.05
[18]	(308–350)	(1.2858–19.786)	−0.08	0.08	0.12	0.09	0.09	0.12
[19]	(289.85–389.85)	(0.5–50)	−0.03	0.03	0.09	$1.6\cdot10^{-3}$	0.02	0.04
[20]	(293.05–362.60)	(0.1–100)	0.05	0.09	0.32	−0.09	0.13	0.42

[a] AD = average deviation; AAD = absolute average deviation; MD = maximum deviation.

tions observed, showing a good agreement for almost all the references, whose AAD% and AD% are lower or very close to the expanded uncertainty, except for Ref. [20], which exhibits a MD % = 0.32, while its AD% = 0.05 and its AAD% = 0.09. A graphical comparison between these deviations can be observed in Fig. 1.

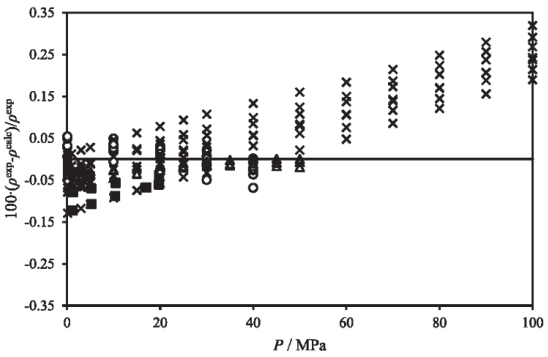

Fig. 1. Percentage deviations between literature density data and calculated densities from the integration of speed of sound measurements versus pressure in liquid HFE-7500. ○, Ref. [13]; ◇, Ref. [17]; ■, Ref. [18]; Δ, Ref. [19]; ×, Ref. [20].

Table 5 lists the coefficients obtained by using this procedure along with the AD, AAD, and the MD both for the speed of sound and for the density. The deviations reveal that the function

Table 5
Parameters of Eqs. (10) to (13) and deviations for sound speed and density.

Parameters	HFE-7500
v_0	$2.74730\cdot10^{-4}$
v_1	$2.25791\cdot10^{-6}$
v_2	$-6.23490\cdot10^{-9}$
v_3	$8.43737\cdot10^{-12}$
a_0	$-4.08850\cdot10^{-5}$
a_1	$5.70071\cdot10^{-7}$
a_2	$-1.35510\cdot10^{-9}$
a_3	$1.29408\cdot10^{-12}$
b_0	$2.15883\cdot10^{2}$
b_1	$-8.19201\cdot10^{-1}$
b_2	$7.80994\cdot10^{-4}$
d	$3.82412\cdot10^{-8}$
Deviations[a]	
AD% for ρ	$5.43\cdot10^{-4}$
AAD% for ρ	$3.56\cdot10^{-3}$
MD% for ρ	$1.12\cdot10^{-2}$
AD% for c	$-3.58\cdot10^{-3}$
AAD% for c	$1.28\cdot10^{-1}$
MD% for c	$3.88\cdot10^{-1}$

[a] AD = average deviation; AAD = absolute average deviation; MD = maximum deviation.

Table 6
Values of isentropic compressibility κ_s at temperatures T and at pressures P for HFE-7500[a]

P/MPa	T/K	κ_s/GPa^{-1}	P/MPa	T/K	κ_s/GPa^{-1}
0.1	293.15	1.351	60.0	323.15	0.764
20.0	293.15	0.979	80.0	323.15	0.649
40.0	293.15	0.780	100.0	323.15	0.566
60.0	293.15	0.654	0.1	333.15	2.053
80.0	293.15	0.565	20.0	333.15	1.315
100.0	293.15	0.500	40.0	333.15	0.989
0.1	303.15	1.499	60.0	333.15	0.801
20.0	303.15	1.057	80.0	333.15	0.677
40.0	303.15	0.831	100.0	333.15	0.588
60.0	303.15	0.690	0.1	343.15	2.295
80.0	303.15	0.593	20.0	343.15	1.413
100.0	303.15	0.523	40.0	343.15	1.046
0.1	313.15	1.655	60.0	343.15	0.839
20.0	313.15	1.137	80.0	343.15	0.705
40.0	313.15	0.881	100.0	343.15	0.611
60.0	313.15	0.726	0.1	353.15	2.571
80.0	313.15	0.621	20.0	353.15	1.518
100.0	313.15	0.544	40.0	353.15	1.106
0.1	323.15	1.843	60.0	353.15	0.879
20.0	323.15	1.224	80.0	353.15	0.735
40.0	323.15	0.934	100.0	353.15	0.633

[a] Standard uncertainties u are $u(T) = 0.1$ K, $u(P) = 0.01$ MPa. The combined expanded uncertainty U_c (level of confidence = 0.95) is $U_c(\kappa_s) = 0.005\kappa_s$.

provides a very good representation of both density and speed of sound with a MD about 0.4% for the speed of sound and a MD = 0.01% for the density.

It can be seen also in Table 6 the values of the isentropic compressibility, κ_S obtained by using Eq. (3).

Concerning the isothermal compressibility and the isobaric expansion, a correlation has been stablished by employing equations (10) to (13). The deviations obtained between the calculated values and those given by the correlation are quite good showing an AD = 0.00%, an AAD = 0.22% and a MD = 0.63 for the isothermal compressibility data, and an AD = 0.01%, an AAD = 0.23% and a MD = 0.74% for the isobaric expansion. These comparisons can be seen in Figs. 2 and 3.

Density was measured with the U-tube densitometer along 11 isotherms ranging from (293.15 to 393.15) K and in the pressure range from atmospheric to 140 MPa. The experimental data obtained are reported in Table 7. The range of pressure and temperature on experimental density measurements has been broaden with respect to our previous publication [13], from (0.1 to 40 MPa) and (283.15 to 343.15 K), up to 140 MPa and (293.15 to 393.15 K) in the present article. In order to compare our experimental density data with those of the literature, a Tait-like equation, which has been used in our previous work

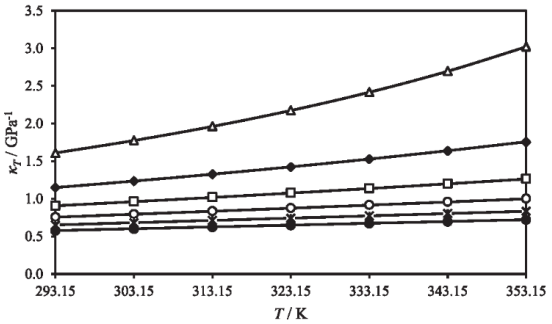

Fig. 2. Values of isothermal compressibility κ_T as a function of temperature T at: Δ, 0.1 MPa, ◆, 20 MPa; □, 40 MPa; ○, 60 MPa; ж, 80 MPa; ●, 100 MPa. The solid line represents the correlation for κ_T given by Eqs. (10) to (13).

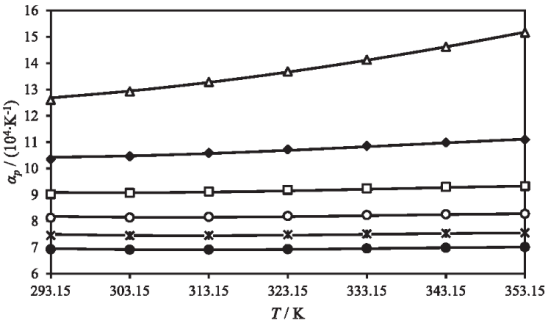

Fig. 3. Values of isobaric expansion α_p as a function of temperature T at: Δ, 0.1 MPa, ◆, 20 MPa; □, 40 MPa; ○, 60 MPa; ж, 80 MPa; ●, 100 MPa. The solid line represents the correlation for α_p given by Eqs. (10) to (13).

[21], was employed to correlate the values over the entire pressure and temperature ranges.

$$\rho(T,p) = \frac{\rho_0(T)}{1 - C\ln\left(\frac{B(T)+p}{B(T)+0.1\ \text{MPa}}\right)} \tag{15}$$

where:

$$\rho_0(T) = A_0 + A_1T + A_2T^2 + A_3T^3 \tag{16}$$

$$B(T) = B_0 + B_1T + B_2T^2 \tag{17}$$

In Eqs. (15) to (17), the parameters A_i, B_i and C were determined by correlating the experimental density values versus pressure and temperature. The values of these parameters together with their deviations (AD%, AAD%, and MD%) are listed in Table 8. The deviations obtained from the comparison between the experimental density data, and the values from the five literature references are shown in Table 4. It can be observed that in all cases the AD %, AAD% and MD% are lower than the experimental uncertainty, being Ref. [20] the only one which exceeds this value, with an AAD% = 0.13 and MD% = 0.42.

A comparison of the density behaviour with pressure evaluated from speed of sound measurements with respect to the density

Table 7
Values of experimental densities, ρ, at temperatures T and at pressures P measured in liquid HFE-7500 by using a U-tube densimeter[a]

P/MPa	T/K	ρ/kg·m^{-3}	P/MPa	T/K	ρ/kg·m^{-3}	P/MPa	T/K	ρ/kg·m^{-3}
0.1	293.15	1630.2	100.0	323.15	1748.7	50.0	363.15	1623.4
10.0	293.15	1654.0	110.0	323.15	1760.0	60.0	363.15	1641.7
20.0	293.15	1674.8	120.0	323.15	1770.6	70.0	363.15	1658.3
30.0	293.15	1693.3	130.0	323.15	1780.7	80.0	363.15	1673.6
40.0	293.15	1709.8	140.0	323.15	1790.5	90.0	363.15	1687.9
50.0	293.15	1724.9	0.1	333.15	1545.6	100.0	363.15	1701.2
60.0	293.15	1738.8	10.0	333.15	1578.4	110.0	363.15	1713.7
70.0	293.15	1751.7	20.0	333.15	1605.3	120.0	363.15	1725.3
80.0	293.15	1763.9	30.0	333.15	1628.1	130.0	363.15	1736.6
90.0	293.15	1775.4	40.0	333.15	1648.2	140.0	363.15	1747.3
100.0	293.15	1786.2	50.0	333.15	1666.2	0.1	373.15	1454.4
110.0	293.15	1796.5	60.0	333.15	1682.6	10.0	373.15	1500.9
120.0	293.15	1806.3	70.0	333.15	1697.7	20.0	373.15	1535.8
130.0	293.15	1815.8	80.0	333.15	1711.6	30.0	373.15	1564.2
140.0	293.15	1824.9	90.0	333.15	1724.6	40.0	373.15	1588.4
0.1	303.15	1609.7	100.0	333.15	1736.9	50.0	373.15	1609.6
10.0	303.15	1635.5	110.0	333.15	1748.2	60.0	373.15	1628.5
20.0	303.15	1657.8	120.0	333.15	1759.3	70.0	373.15	1645.8
30.0	303.15	1677.3	130.0	333.15	1769.7	80.0	373.15	1661.7
40.0	303.15	1694.6	140.0	333.15	1779.5	90.0	373.15	1676.4
50.0	303.15	1710.4	0.1	343.15	1523.6	100.0	373.15	1689.9
60.0	303.15	1724.9	10.0	343.15	1559.1	110.0	373.15	1702.8
70.0	303.15	1738.4	20.0	343.15	1587.8	120.0	373.15	1714.7
80.0	303.15	1750.9	30.0	343.15	1611.9	130.0	373.15	1726.2
90.0	303.15	1762.8	40.0	343.15	1633.0	140.0	373.15	1737.1
100.0	303.15	1773.9	50.0	343.15	1651.7	0.1	383.15	1430.4
110.0	303.15	1784.5	60.0	343.15	1668.7	10.0	383.15	1481.2
120.0	303.15	1794.5	70.0	343.15	1684.2	20.0	383.15	1518.4
130.0	303.15	1804.2	80.0	343.15	1698.6	30.0	383.15	1548.4
140.0	303.15	1813.4	90.0	343.15	1712.0	40.0	383.15	1573.8
0.1	313.15	1588.6	100.0	343.15	1724.4	50.0	383.15	1595.9
10.0	313.15	1616.6	110.0	343.15	1736.5	60.0	383.15	1615.5
20.0	313.15	1640.2	120.0	343.15	1747.8	70.0	383.15	1633.3
30.0	313.15	1660.7	130.0	343.15	1758.4	80.0	383.15	1649.6
40.0	313.15	1678.9	140.0	343.15	1768.6	90.0	383.15	1664.6
50.0	313.15	1695.4	0.1	353.15	1501.6	100.0	383.15	1678.5
60.0	313.15	1710.5	10.0	353.15	1540.0	110.0	383.15	1691.6
70.0	313.15	1724.6	20.0	353.15	1570.5	120.0	383.15	1704.0
80.0	313.15	1737.1	30.0	353.15	1596.0	130.0	383.15	1715.7
90.0	313.15	1749.7	40.0	353.15	1618.0	140.0	383.15	1726.8
100.0	313.15	1761.2	50.0	353.15	1637.6	0.1	393.15	1405.6
110.0	313.15	1772.2	60.0	353.15	1655.2	10.0	393.15	1461.3
120.0	313.15	1782.5	70.0	353.15	1671.3	20.0	393.15	1500.9
130.0	313.15	1792.5	80.0	353.15	1686.2	30.0	393.15	1532.5
140.0	313.15	1802.0	90.0	353.15	1700.0	40.0	393.15	1559.0
0.1	323.15	1567.3	100.0	353.15	1712.9	50.0	393.15	1581.9
10.0	323.15	1597.6	110.0	353.15	1724.9	60.0	393.15	1602.2
20.0	323.15	1622.7	120.0	353.15	1736.6	70.0	393.15	1620.6
30.0	323.15	1644.3	130.0	353.15	1747.4	80.0	393.15	1637.1
40.0	323.15	1663.4	140.0	353.15	1757.8	90.0	393.15	1652.8
50.0	323.15	1680.6	0.1	363.15	1478.1	100.0	393.15	1667.1
60.0	323.15	1696.4	10.0	363.15	1520.4	110.0	393.15	1680.5
70.0	323.15	1710.9	20.0	363.15	1553.0	120.0	393.15	1693.2
80.0	323.15	1724.2	30.0	363.15	1579.9	130.0	393.15	1705.1
90.0	323.15	1736.8	40.0	363.15	1603.0	140.0	393.15	1716.3

[a] Standard uncertainties u are $u(T) = 0.1$ K, $u(P) = 0.01$ MPa. The combined expanded uncertainty U_c (level of confidence = 0.95) is $U_c(\rho) = 0.5$ kg·m^{-3}.

Table 8
Parameters of Eqs. (15) to (17) for HFE-7500.

Parameters	HFE-7500
A_0	2.159054
A_1	$-1.871408\cdot10^{-3}$
A_2	$1.234302\cdot10^{-6}$
A_3	$-3.418435\cdot10^{-9}$
B_0	295.0642
B_1	−1.188985
B_2	$1.225459\cdot10^{-3}$
C	0.08144405
Deviations[a]	
AD%	$4.46\cdot10^{-6}$
AAD%	$1.55\cdot10^{-2}$
MD%	$5.41\cdot10^{-2}$

[a] AD = average deviation; AAD = absolute average deviation; MD = maximum deviation.

measured from the U-tube densitometer is plotted in Fig. 4. This comparison shows a satisfactory agreement with an AD of −0.05%, an AAD of 0.05% and a MD of 0.14%. These deviations reflect the consistency between the density correlation from speed of sound measurements and the U-tube measurements, confirming that the acoustic technique is a viable option to measure density under high pressure.

It can be seen on Fig. 5 the deviations of density and speed of sound of HFE-7500 between its experimental measurements and the calculations. The density reveals a dependence on pressure, although the values of the deviations are quite small, about 0.05% in the worst case. For the speed of sound the deviations do not increase systematically with pressure, showing values of below ±0.25% in all the cases.

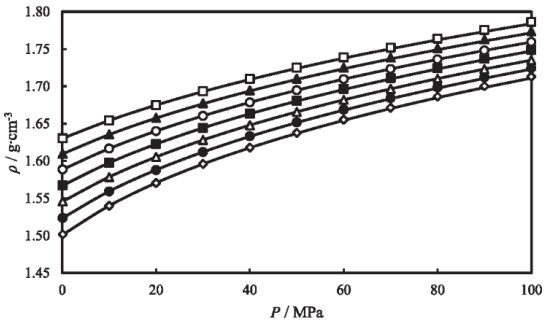

Fig. 4. Comparison between densities of HFE-7500 evaluated from speed of sound integration (line) and measured from a U-tube densimeter. □, 293.15 K, ▲, 303.15 K; ○, 313.15 K; ■, 323.15 K; Δ, 333.15 K; ●, 343.15 K; ◇, 353.15 K.

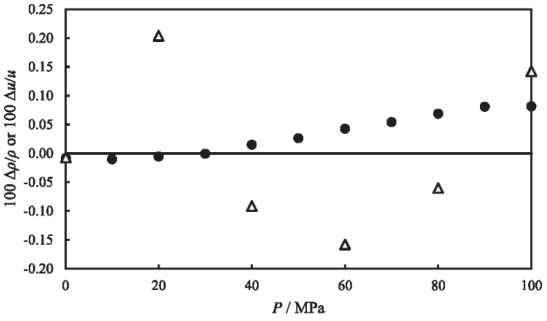

Fig. 5. Relative deviations between measurements and calculation for HFE-7500 at 343.15 K. ●, density deviation: $\Delta\rho/\rho = [\rho(\text{exp}) - \rho(\text{cal})]/\rho(\text{exp})$; Δ, speed of sound deviation: $\Delta c/c = [c(\text{exp}) - c(\text{cal})]/c(\text{exp})$.

4. Conclusions

Speeds of sound of liquid HFE-7500 were measured over a pressure range between (0.1–100) MPa with temperature ranging from (293.15 to 353.15) K. Density was determined between atmospheric pressure and 100 MPa by integration of speed of sound data, and was also measured thanks to a U-tube densimeter in the pressure range (0.1–140) MPa and in the temperature range (293.15–393.15) K. A correlation was proposed to represent both density and speed of sound data within their experimental uncertainty. The good agreement observed between both properties confirm the reliability of the experimental measurements. The evaluation carried out through speed of sound and density measurements of an equation of state provides a predictive tool to determine other derivative properties such as isothermal compressibility and isobaric expansion in the same *P*, *T* conditions than speed of sound measurements.

Acknowledgements

Natalia Muñoz-Rujas acknowledges support for this research to the University of Burgos, for the funding of her doctoral grant, and to the University of Pau for the funding of a five months research period in 2015.

This paper is part of the doctoral thesis of Natalia Muñoz-Rujas.

References

[1] P. Tuma, L. Tousignant, SEMI Technical Symposium, 2001, http://multimedia.3m.com/mws/media/1223810/reducing-emissions-of-pfc-heat-transfer-fluids.pdf?fn=tech_pfc.pdf.
[2] W.-T. Tsai, J. Hazard. Mater. 119 (2005) 69–78.
[3] M™ Novec™ Engineered Fluids, http://multimedia.3m.com/mws/media/654960/3mtm-novectm-7500-engineered-fluid.pdf.
[4] M. Goto, Y. Inoue, M. Kawasaki, A.G. Guschin, L.T. Molina, M.J. Molina, T.J. Wallington, M.D. Hurley, Environ. Sci. Technol. 36 (2002) 2395–2402.
[5] E.H.I. Ndiaye, D. Nasri, J.L. Daridon, J. Chem. Eng. Data 57 (2012) 2667–2676.
[6] W.D. Wilson, J. Acoust. Soc. Am. 31 (1959) 1067–1072, W.D..
[7] E.H. Baltasar, M. Taravillo, V.G. Baonza, P.D. Sanz, B. Guignon, J. Chem. Eng. Data 56 (2011) 4800–4807.
[8] J.L. Daridon, A. Lagrabette, B. Lagourette, J. Chem. Thermodyn. 30 (1998) 607–623.
[9] B.N. Taylor, C.E. Kuyatt, Guidelines for Evaluating and Expressing the Uncertainty of NIST Measurements Results, NIST Technical Note 1297, National Institute of Standards and Technology, Gaithersburg, MD, 1994.
[10] M.J.P. Comuñas, J.P. Bazile, A. Baylaucq, C. Boned, J. Chem. Eng. Data 53 (2008) 986–994.
[11] W. Wagner, A. Pruß, J. Phys. Chem. Ref. Data 31 (2002) 387–535.
[12] TRC Thermodynamic Tables; Texas A&M University: College Station, TX, 1996.
[13] T. Lafitte, F. Plantier, M.M. Piñeiro, J.L. Daridon, D. Bessières, Ind. Eng. Chem. Res. 46 (2007) 6998–7007.
[14] J.L. Daridon, B. Lagourette, J.P. Grolier, Int. J. Thermophys. 19 (1998) 145–160.
[15] J.S. Rowlinson, F.L. Swinton, Liquid and Liquid Mixtures, 3rd ed., Butterworth Scientific, London, 1982.
[16] E.H.I. Ndiaye, M. Habrioux, J.A.P. Coutinho, M.L.L. Paredes, J.L. Daridon, J. Chem. Eng. Data. 58 (2013) 1371–1377.
[17] M.H. Rausch, L. Kretschmer, S. Will, A. Leipertz, A.P. Fröba, J. Chem. Eng. Data 60 (2015) 3759–3765.
[18] M.O. McLinden, C. Lösch-Will, J. Chem. Thermodyn. 39 (2007) 507–530.
[19] S.L. Outcalt, J. Chem. Eng. Data 59 (2014) 2087–2094.
[20] D. Fang, Y. Li, X. Meng, J. Wu, J. Chem. Thermodyn. 69 (2014) 36–42.
[21] N. Muñoz-Rujas, F. Aguilar, J.-P. Bazile, E.A. Montero, Fluid Phase Equilib. 429 (2016) 281–292.

JCT 16-928

Fluid Phase Equilibria 449 (2017) 148–155

Contents lists available at ScienceDirect

Fluid Phase Equilibria

journal homepage: www.elsevier.com/locate/fluid

Speed of sound, density and derivative properties of diisopropyl ether under high pressure

Natalia Muñoz-Rujas [a, b], Jean Patrick Bazile [a], Fernando Aguilar [b], Guillaume Galliero [a], Eduardo Montero [b, *], Jean Luc Daridon [a]

[a] Laboratoire des Fluides Complexes et Leurs Réservoirs, CNRS-TOTAL, UMR 5150, Université de Pau, BP 1155, 64013 Pau Cedex, France
[b] Departamento de Ingeniería Electromecánica, Escuela Politécnica Superior, Universidad de Burgos, E-09006 Burgos, Spain

ARTICLE INFO

Article history:
Received 3 May 2017
Received in revised form
19 June 2017
Accepted 24 June 2017
Available online 30 June 2017

Keywords:
Diisopropyl ether
Density
Speed of sound
High pressure

ABSTRACT

Accurate knowledge of physical and acoustical properties is of importance in many fields of science and engineering. In this work, density and speed of sound measurements of diisopropyl ether (DIPE) are reported. The speed of sound has been measured up to 100 MPa and in the temperature range (293.15–353.15) K by using an apparatus based on a pulse echo technique working in transmission mode, and a correlation for this property was proposed. By using a procedure which rests on the Newton-Laplace relationships, density and its derivatives were determined. To show the reliability of this method, high pressure density measurements were carried out up to 140 MPa and within the temperature interval (293.15–393.15) K with an Anton Paar densitometer.

1. Introduction

Nowadays, industrial applications require environmentally friendly fluids to develop all the processes involving cleaning, refrigeration, solvent extraction, e.g. Ethers play an important role in solvents industry due to its stability, high volatility, and solubility similar to that of the alcohols. Ethers in general are of very low chemical reactivity, and exhibit relatively low boiling points due to they are unable to form hydrogen bonds. Dialkyl ethers as dimethyl ether and diethyl ether are used as solvents while ethyl ether is used too as solvent and as a starter fuel for diesel engines [1]. Tertiary alkyl ethers, as tert-amyl methyl ether (TAME), methyl tert-butyl ether (MTBE), and ethyl tert-butyl ether (ETBE), are being widely used as oxygenate gasoline additives due to its ability to increase the octane number and to raise the oxygen content in gasoline, offering sometimes equal or greater benefits than other commonly used additives such as ethanol.

The use of some of these ethers, as is the case of MTBE, has generated controversy because of its contamination of groundwater [2] and soils, and also due to its toxicity, which have led to search for other substitutes. While ETBE and TAME are still being used due to its favorable environmental properties, diisopropyl ether (DIPE), a dialkyl ether, was introduced as an oxygenate additive for gasolines due to its non-polluting profile [3], and also due to its physical properties, such as the relatively high boiling point [4]. Diisopropyl ether is a secondary ether obtained as a by-product in the production of 2-propanol but a great advantage is that it can be simply produced from the base olefin, propylene and water [5]. Diisopropyl ether has a favorable blending Reid vapor pressure and low solubility in water compared with other ethers, being a good choice as oxygenate gasoline additive. Other uses of diisopropyl ether include solvent for paints, waxes and resins, as solvent in the recovery of phenol in the plastics industry, an extraction agent in metallurgy as it can extract gold from a nitric acid solution. Diisopropyl ether can also be used as solvent in gas chromatography (GC) and in liquid chromatography (LC) analysis.

As diisopropyl ether is a very useful compound in the industry, the availability of reliable scientific data concerning its physical properties as well as its acoustic properties is needed to well develop all the processes involved in the utilization of this compound. High pressure speed of sound measurements in the ranges (0.1–100) MPa for the pressure and (293.15–353.15) K for the temperature have been carried out, broadening the speed of sound data ranges published previously in the literature [6–13]. High pressure density measurements in the ranges (0.1–140) MPa for the pressure and (293.15–393.15) K for the temperature in liquid

* Corresponding author.
E-mail address: emontero@ubu.es (E. Montero).

http://dx.doi.org/10.1016/j.fluid.2017.06.024
0378-3812/

diisopropyl ether were carried out and compared with the literature data available [4,14–21]. An evaluation of the volume and its derivatives has been conducted from an equation of state that represents both the density and the speed of sound.

2. Experimental section

2.1. Materials

Diisopropyl ether, also known as 2,4-dimethyl-3-oxapentane ($C_6H_{14}O$, molar mass: 102.17 $g \cdot mol^{-1}$, CAS No. 108-20-3), was supplied by Sigma-Aldrich with a mole fraction purity greater than 0.995 certified by gas chromatography by the supplier. The liquid was stored over molecular sieves type 0.4 to avoid any moisture and was used without any further purification except careful degassing before use.

2.2. Speed of sound measurement

High pressure speed of sound data were determined experimentally with a previously described apparatus [22] which consists of an acoustic sensor composed of two piezoelectric transducers facing each other at both ends of a stainless steel cylindrical support and in direct contact with the fluid. The device uses a pulse-echo technique operating at 3 MHz with a fixed path length equal to $L_0 = 30$ mm working in transmission mode to determine the time delay between a transmitted pulse and the first echo of the ultrasonic wave.

The acoustic sensor is fully immersed in the studied liquid within a stainless-steel high-pressure vessel closed at one end by a plug in which three electric feedthroughs were machined.

The temperature inside the cell is regulated thanks to a thermostatic bath and is measured in the liquid by means of a Pt100 probe housed in a metal finger. The uncertainty in temperature measurement is of ±0.1 K. A volumetric pump ensures the compression of the fluid in the whole circuit, being able to reach pressures up to 100 MPa. A pressure gauge capable of measuring up to 100 MPa was used to capture the pressure data. This pressure gauge leads to a pressure measurement with an uncertainty of 0.01 MPa.

As a calibration is needed in order to bring the path length for calculating speed of sound, two reference fluids whose speeds of sounds were measured at different temperatures and pressures were used to this purpose: purified water [23,24] and heptane [25], giving an uncertainty in speed of sound of 0.06%. Taking into account the standard uncertainties in temperature, pressure, the uncertainty in the speed of sound for the calibration and according to the law of propagation of standard uncertainties [26] the expanded uncertainty for the speed of sound in the temperature and pressure ranges measured is estimated to be 0.2%.

2.3. Density measurement

To carry out high pressure density measurements, ρ, in liquid diisopropyl ether, an Anton Paar DMA HPM vibrating tube densitometer connected to a high pressure volumetric pump was used. In such kind of densitometer, the determination of the density is carried out by the measurement of vibration period of the fluid located inside a hollow U-tube. There is a drive element that makes tube vibrate harmonically and a pick-up element for measuring the vibration period [27]. The vibrating tube densitometer utilized allowed us to measure densities in a range of pressures from (0.1–140) MPa every 10 MPa steps with an estimated uncertainty of ±0.015 MPa (Presens Precise Gold Plus pressure transmitter). The temperature measurements were performed in the interval from (293.15–393.15) K. The circulation of a fluid controlled by a thermostatic bath ensures a constant temperature inside the apparatus while a Pt probe located inside the densitometer measures the temperature, giving an uncertainty of ±0.01 K.

Before each campaign of measurements, a calibration was performed according to the procedure described by Comuñas et al. [28] which is a modification of the procedure previously proposed by Lagourette et al. [29]. In this procedure vacuum, and as calibration fluids, water [30] and decane [31] were used due to their known densities. In this way, considering the uncertainties in temperature, in pressure, the uncertainty in measurements of oscillation period, the density of the reference fluids used in the calibration, the overall expanded uncertainty in the experimental density values is estimated to be ±0.5 $kg \cdot m^{-3}$.

3. Results and discussion

High pressure speed of sound measurements in liquid diisopropyl ether were carried out in the temperature interval (293.15–353.15) K along seven isotherms separated by 10 K for pressures ranging from (0.1–100) MPa every 20 MPa. Due to the low boiling temperature of diisopropyl ether under atmospheric pressure (341.66 K) [32], no measurements were done at 343.15 K and at 353.15 K at atmospheric pressure, avoiding the vapor phase and ensuring all the measurements were done in liquid state. The experimental data of speed of sound for diisopropyl ether can be seen in Table 1. To correlate speed of sound measurements, a rational function with nine adjustable parameters was considered:

$$\frac{1}{c^2} = \frac{A_0 + A_1 T + A_2 T^2 + A_3 T^3 + BP + CP^2 + DP^3}{1 + ET + FP} \quad (1)$$

The values of the nine parameters, together with their deviations (AD%, AAD% and MD%) are included in Table 2. It can be observed in Fig. 1 the comparison between the experimental and calculated speed of sound values from equation (1).

The experimental speed of sound values were compared with data reported in the literature. Seven references report speed of sound data at atmospheric pressure for diisopropyl ether [6–13], and were compared with calculated data by interpolation of our

Table 1
Experimental values of speed of sound, c, at temperatures T and pressures P for diisopropyl Ether.[a]

P/MPa	T/K	c/m·s^{-1}	P/MPa	T/K	c/m·s^{-1}
0.1	293.15	1019.71	60.0	323.15	1278.96
20.0	293.15	1161.24	80.0	323.15	1368.68
40.0	293.15	1274.50	100.0	323.15	1448.65
60.0	293.15	1369.29	0.1	333.15	847.29
80.0	293.15	1454.22	20.0	333.15	1017.78
100.0	293.15	1528.73	40.0	333.15	1146.81
0.1	303.15	974.32	60.0	333.15	1252.38
20.0	303.15	1122.56	80.0	333.15	1343.16
40.0	303.15	1240.38	100.0	333.15	1423.50
60.0	303.15	1337.63	0.1	343.15	
80.0	303.15	1423.43	20.0	343.15	984.53
100.0	303.15	1501.88	40.0	343.15	1117.79
0.1	313.15	930.24	60.0	343.15	1226.40
20.0	313.15	1086.83	80.0	343.15	1318.72
40.0	313.15	1207.91	100.0	343.15	1400.75
60.0	313.15	1308.13	0.1	353.15	
80.0	313.15	1396.71	20.0	353.15	953.14
100.0	313.15	1474.97	40.0	353.15	1090.71
0.1	323.15	887.83	60.0	353.15	1200.36
20.0	323.15	1051.90	80.0	353.15	1294.59
40.0	323.15	1177.10	100.0	353.15	1378.37

[a] Standard uncertainties u are $u(T) = 0.1$ K, $u(P) = 0.01$ MPa. The combined expanded uncertainty U_c (level of confidence = 0.95) is $U_c(c) = 0.002c$.

Table 2
Parameters of equation (1) for diisopropyl ether.

Parameters	Diisopropyl Ether
A_0	$-5.49090 \cdot 10^{-7}$
A_1	$5.65860 \cdot 10^{-9}$
A_2	$-1.09040 \cdot 10^{-11}$
A_3	$7.08795 \cdot 10^{-15}$
B	$2.43691 \cdot 10^{-9}$
C	$-1.01400 \cdot 10^{-11}$
D	$2.78237 \cdot 10^{-14}$
E	$-2.17061 \cdot 10^{-3}$
F	$8.54005 \cdot 10^{-3}$
deviations[a]	
AD%	$4.39 \cdot 10^{-4}$
AAD%	$5.01 \cdot 10^{-2}$
MD%	$1.28 \cdot 10^{-1}$

[a] AD = average deviation; AAD = absolute average deviation; MD = maximum deviation.

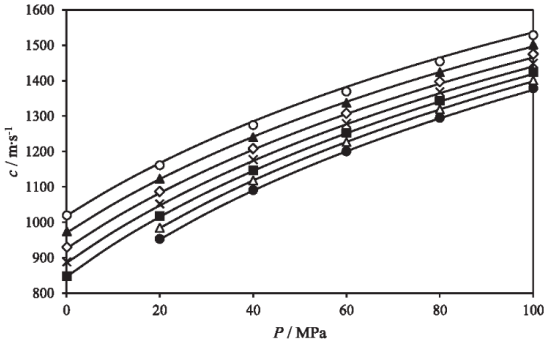

Fig. 1. Comparison between experimental and calculated sound velocities, c of diisopropyl ether vs. the pressure, P. ○; 293.15 K, ▲; 303.15 K, ◊; 313.15 K, x; 323.15 K, ■; 333.15 K, Δ; 343.15 K, ●; 353.15 K. The solid line represents the calculated data by using equation (1).

measures at only P = 0.1 MPa. Table 3 shows the values for the deviations between the literature and the calculated speed of sound data. For references [6and7] the values of the deviations are lower than our uncertainty in speed of sound (±0.2%), with a maximum MD% = 0.13 for reference [7]. The worst values were founded for reference [9], which reports only one value at 303 K with an AD% = −2.57 and an AAD% = MD% = 2.57. Reference [10] also gives high deviation values, with an AD% = −1.05 and an AAD% = MD% = 1.05 for the comparison with the only one point which is given at 303.15 K. However, references [9and10] do not report uncertainty of their measurements.

For the rest of references [8,11and12], the values of the deviations are slightly higher than the uncertainty in speed of sound, with a MD% = 0.25 for reference [12], a MD% = 0.27 for reference [8] and a MD% = 0.26 for reference [11]. Only references [11and12] provide uncertainty of the respective apparatus. However, the uncertainty of 0.01 $m \cdot s^{-1}$ claimed by Ref. [11] should be discussed, as the supplier of the apparatus reported for the speed of sound measure (Anton Paar, model DSA 5000) declares an accuracy of 0.5 $m \cdot s^{-1}$, and then the uncertainty should be a greater value. Though a negative deviation can be observed for all the AD% values, most part of deviations obtained in the comparison with the atmospheric literature data [6–8,11,12] are lower or slightly higher than the estimated uncertainty of our measurements.

The only reference of speed of sound found at high pressure [13] shows a set of 77 points in the range of temperatures (302.28–353.81) K and at pressures from atmospheric to 10 MPa. The comparison between these data and the obtained from our correlation shows quite high deviations, with a MD% = 3.58, an AD% = −0.95 and an AAD% = 1.02. Such a bad agreement should take into consideration the fact that the comparison concerns the pressure range 0–10 MPa [13], a range in which our work do not have experimental points as the measurements are every 20 MPa.

High pressure density was measured experimentally by using a U-tube densitometer in the temperature range from (293.15–393.15) K every 10 K steps and in the pressure range (0.1–140) MPa every 10 MPa. In the same way as it was done for the speed of sound, measurements at atmospheric pressure at temperatures 343.15 K and above were not carried out due to in these conditions diisopropyl ether would be in vapor phase. Experimental density data are listed in Table 4. By integration of speed of sound data in the full pressure range using a method which rests on the Newton–Laplace relationships between the speed of sound and the isentropic compressibility, κ_S [33], high pressure density values were obtained. These density values are showed in Table 5. As can be seen in Fig. 2, the density trend with pressure for the density values obtained by integration of speed of sound measurements has a good match with those obtained experimentally with the U-tube densitometer.

In addition, derivative properties of density, that is, the isentropic compressibility, κ_S, the isothermal compressibility, κ_T, and the isobaric expansion, α_P where determined. To conduct all the calculations, we have that for the isentropic compressibility:

Table 3
Deviations between speed of sound data from literature and values calculated from equation (1) for liquid diisopropyl ether.[a]

Reference	N_P	T range/K	P range/MPa	AD%	AAD%	MD%	Speed of sound uncertainty
At atmospheric pressure							
[6]	1	298.15	0.1	−0.08	0.08	0.08	–
[7]	1	303.15	0.1	−0.13	0.13	0.13	–
[8]	26	(298.150–323.151)	0.1	−0.24	0.24	0.27	–
[9]	1	303	0.1	−2.57	2.57	2.57	–
[10]	1	303.15	0.1	−1.05	1.05	1.05	–
[11]	5	(293.15–313.15)	0.1	−0.18	0.18	0.26	±0.01 $m \cdot s^{-1}$
[12]	3	(303.15–323.15)	0.1	−0.23	0.23	0.25	1 $m \cdot s^{-1}$
At high pressure							
[13]	77	(302.38–353.81)	(1.00–10.00)	−0.95	1.02	3.58	0.0138 $m \cdot s^{-1}$

N_P Number of data points which are in our P, T ranges.
[a] AD = average deviation; AAD = absolute average deviation; MD = maximum deviation.

Table 4
Values of experimental densities, ρ, at temperatures T and at pressures P measured in liquid diisopropyl ether by using a U-tube densimeter.[a]

P/MPa	T/K	ρ/g·cm^{-3}	P/MPa	T/K	ρ/g·cm^{-3}	P/MPa	T/K	ρ/g·cm^{-3}
0.1	293.15	0.7235	100.0	323.15	0.7795	50.0	363.15	0.7171
10.0	293.15	0.7346	110.0	323.15	0.7850	60.0	363.15	0.7261
20.0	293.15	0.7445	120.0	323.15	0.7903	70.0	363.15	0.7344
30.0	293.15	0.7533	130.0	323.15	0.7952	80.0	363.15	0.7420
40.0	293.15	0.7613	140.0	323.15	0.8000	90.0	363.15	0.7490
50.0	293.15	0.7686	0.1	333.15	0.6806	100.0	363.15	0.7555
60.0	293.15	0.7754	10.0	333.15	0.6963	110.0	363.15	0.7617
70.0	293.15	0.7817	20.0	333.15	0.7093	120.0	363.15	0.7675
80.0	293.15	0.7876	30.0	333.15	0.7205	130.0	363.15	0.7730
90.0	293.15	0.7932	40.0	333.15	0.7303	140.0	363.15	0.7783
100.0	293.15	0.7985	50.0	333.15	0.7391	0.1	373.15	
110.0	293.15	0.8035	60.0	333.15	0.7471	10.0	373.15	0.6559
120.0	293.15	0.8084	70.0	333.15	0.7545	20.0	373.15	0.6733
130.0	293.15	0.8130	80.0	333.15	0.7614	30.0	373.15	0.6874
140.0	293.15	0.8174	90.0	333.15	0.7678	40.0	373.15	0.6994
0.1	303.15	0.7129	100.0	333.15	0.7738	50.0	373.15	0.7099
10.0	303.15	0.7252	110.0	333.15	0.7794	60.0	373.15	0.7193
20.0	303.15	0.7359	120.0	333.15	0.7848	70.0	373.15	0.7280
30.0	303.15	0.7453	130.0	333.15	0.7899	80.0	373.15	0.7357
40.0	303.15	0.7538	140.0	333.15	0.7947	90.0	373.15	0.7431
50.0	303.15	0.7615	0.1	343.15		100.0	373.15	0.7498
60.0	303.15	0.7685	10.0	343.15	0.6860	110.0	373.15	0.7562
70.0	303.15	0.7751	20.0	343.15	0.7000	120.0	373.15	0.7622
80.0	303.15	0.7812	30.0	343.15	0.7118	130.0	373.15	0.7678
90.0	303.15	0.7870	40.0	343.15	0.7222	140.0	373.15	0.7731
100.0	303.15	0.7924	50.0	343.15	0.7314	0.1	383.15	
110.0	303.15	0.7976	60.0	343.15	0.7397	10.0	383.15	0.6453
120.0	303.15	0.8025	70.0	343.15	0.7473	20.0	383.15	0.6640
130.0	303.15	0.8073	80.0	343.15	0.7544	30.0	383.15	0.6790
140.0	303.15	0.8118	90.0	343.15	0.7610	40.0	383.15	0.6918
0.1	313.15	0.7022	100.0	343.15	0.7672	50.0	383.15	0.7028
10.0	313.15	0.7155	110.0	343.15	0.7732	60.0	383.15	0.7125
20.0	313.15	0.7269	120.0	343.15	0.7786	70.0	383.15	0.7214
30.0	313.15	0.7369	130.0	343.15	0.7840	80.0	383.15	0.7295
40.0	313.15	0.7457	140.0	343.15	0.7889	90.0	383.15	0.7370
50.0	313.15	0.7538	0.1	353.15		100.0	383.15	0.7439
60.0	313.15	0.7611	10.0	353.15	0.6762	110.0	383.15	0.7504
70.0	313.15	0.7681	20.0	353.15	0.6912	120.0	383.15	0.7566
80.0	313.15	0.7743	30.0	353.15	0.7037	130.0	383.15	0.7624
90.0	313.15	0.7803	40.0	353.15	0.7146	140.0	383.15	0.7679
100.0	313.15	0.7860	50.0	353.15	0.7242	0.1	393.15	
110.0	313.15	0.7915	60.0	353.15	0.7330	10.0	393.15	0.6348
120.0	313.15	0.7964	70.0	353.15	0.7409	20.0	393.15	0.6549
130.0	313.15	0.8014	80.0	353.15	0.7482	30.0	393.15	0.6707
140.0	313.15	0.8059	90.0	353.15	0.7551	40.0	393.15	0.6840
0.1	323.15	0.6915	100.0	353.15	0.7614	50.0	393.15	0.6954
10.0	323.15	0.7060	110.0	353.15	0.7673	60.0	393.15	0.7056
20.0	323.15	0.7180	120.0	353.15	0.7730	70.0	393.15	0.7148
30.0	323.15	0.7285	130.0	353.15	0.7784	80.0	393.15	0.7229
40.0	323.15	0.7378	140.0	353.15	0.7835	90.0	393.15	0.7308
50.0	323.15	0.7462	0.1	363.15		100.0	393.15	0.7380
60.0	323.15	0.7539	10.0	363.15	0.6661	110.0	393.15	0.7446
70.0	323.15	0.7610	20.0	363.15	0.6823	120.0	393.15	0.7509
80.0	323.15	0.7675	30.0	363.15	0.6956	130.0	393.15	0.7568
90.0	323.15	0.7737	40.0	363.15	0.7070	140.0	393.15	0.7623

[a] Standard uncertainties u are $u(T) = 0.1$ K, $u(P) = 0.01$ MPa. The combined expanded uncertainty U_c (level of confidence = 0.95) is $U_c(\rho) = 0.5$ kg·m^{-3}.

$$\kappa_S = \frac{v}{c^2} \tag{2}$$

where v is the volume per unit of mass, and c is the speed of sound. The values of isentropic compressibility, κ_S obtained by using equation (2) are listed in Table 6. Isothermal compressibility, κ_T, can then be evaluated by using the equation:

$$\kappa_T = \kappa_S + \frac{T v \alpha_p^2}{C_p} \tag{3}$$

where α_p and C_p are, respectively the isobaric expansion and the isobaric heat capacity. The combination of the above equations (2) and (3) lead to equation (4), which connects the speed of sound to the isothermal compressibility, κ_T, the isobaric expansion, α_p and the heat capacity, C_p:

$$\frac{v^2}{c^2} = v\kappa_T - \frac{T v^2 \alpha_p^2}{C_p} \tag{4}$$

Equation (5) allows to estimate the heat capacity data needed:

$$\left(\frac{\partial C_p}{\partial P}\right)_T = -T\left(\frac{\partial^2 v}{\partial T^2}\right)_P \tag{5}$$

where:

Table 5
Values of densities, ρ, at temperatures T and at pressures P determined from the integration of speed of sound measurements in liquid diisopropyl ehter.[a]

P/MPa	T/K	ρ/g·cm-3	P/MPa	T/K	ρ/g·cm-3	P/MPa	T/K	ρ/g·cm-3
0.1	293.15	0.7235	40.0	313.15	0.7463	80.0	333.15	0.7622
10.0	293.15	0.7351	50.0	313.15	0.7544	90.0	333.15	0.7687
20.0	293.15	0.7452	60.0	313.15	0.7619	100.0	333.15	0.7748
30.0	293.15	0.7542	70.0	313.15	0.7688	0.1	343.15	
40.0	293.15	0.7623	80.0	313.15	0.7752	10.0	343.15	0.6864
50.0	293.15	0.7697	90.0	313.15	0.7813	20.0	343.15	0.7006
60.0	293.15	0.7765	100.0	313.15	0.7870	30.0	343.15	0.7126
70.0	293.15	0.7828	0.1	323.15	0.6915	40.0	343.15	0.7230
80.0	293.15	0.7887	10.0	323.15	0.7061	50.0	343.15	0.7324
90.0	293.15	0.7943	20.0	323.15	0.7184	60.0	343.15	0.7408
100.0	293.15	0.7996	30.0	323.15	0.7291	70.0	343.15	0.7486
0.1	303.15	0.7129	40.0	323.15	0.7386	80.0	343.15	0.7558
10.0	303.15	0.7254	50.0	323.15	0.7471	90.0	343.15	0.7625
20.0	303.15	0.7362	60.0	323.15	0.7548	100.	343.15	0.7688
30.0	303.15	0.7457	70.0	323.15	0.7620	0.1	353.15	
40.0	303.15	0.7542	80.0	323.15	0.7687	10.0	353.15	0.6763
50.0	303.15	0.7619	90.0	323.15	0.7750	20.0	353.15	0.6915
60.0	303.15	0.7691	100.0	323.15	0.7809	30.0	353.15	0.7042
70.0	303.15	0.7757	0.1	333.15	0.6805	40.0	353.15	0.7152
80.0	303.15	0.7818	10.0	333.15	0.6964	50.0	353.15	0.7250
90.0	303.15	0.7877	20.0	333.15	0.7096	60.0	353.15	0.7338
100.0	303.15	0.7932	30.0	333.15	0.7209	70.0	353.15	0.7419
0.1	313.15	0.7022	40.0	333.15	0.7308	80.0	353.15	0.7493
10.0	313.15	0.7157	50.0	333.15	0.7397	90.0	353.15	0.7562
20.0	313.15	0.7273	60.0	333.15	0.7478	100.0	353.15	0.7627
30.0	313.15	0.7373	70.0	333.15	0.7553			

[a] Standard uncertainties u are $u(T) = 0.1$ K, $u(P) = 0.01$ MPa. The combined expanded uncertainty U_c (level of confidence = 0.95) is $U_c(\rho) = 0.001\rho$.

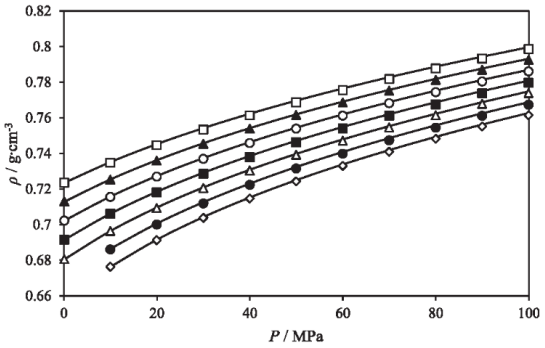

Fig. 2. Comparison between densities, ρ of diisopropyl ether evaluated from speed of sound integration (line) and measured from a U-tube densimeter vs. the pressure, P. □; 293.15 K, ▲; 303.15 K, ○; 313.15 K, ■; 323.15 K, Δ; 333.15 K, ●; 343.15 K, ◊; 353.15 K.

$$C_p(T) = C_{p,ref}(T) - T\frac{\partial^2}{\partial T^2}\int_{Pref}^{P} v\,dP \quad (6)$$

Therefore, experimental values of $C_{p,ref}$ at atmospheric pressure, P_{ref}, are needed. To this purpose, a SETARAM Micro DSC 7 evo calorimeter was used to perform the measurements at temperatures below the boiling point of diisopropyl ether. The data obtained from these measurements are listed in Table 7. With these data, a quadratic function of temperature was stablished:

$$C_{p,ref}\Big/\mathrm{J\cdot K^{-1}\cdot kg^{-1}} = 1.369\cdot 10^{3} + 9.123\cdot 10^{-1}T + 5.059\cdot 10^{-3}T^{2} \quad (7)$$

By using equation (7), a comparison between the heat capacity

Table 6
Values of isentropic compressibility κ_s at temperatures T and at pressures P for diisopropyl ether.[a]

P/MPa	T/K	κ_s/GPa^{-1}	P/MPa	T/K	κ_s/GPa^{-1}
0.1	293.15	1.333	60.0	323.15	0.810
20.0	293.15	0.995	80.0	323.15	0.695
40.0	293.15	0.809	100.0	323.15	0.612
60.0	293.15	0.687	0.1	333.15	2.054
80.0	293.15	0.601	20.0	333.15	1.363
100.0	293.15	0.536	40.0	333.15	1.043
0.1	303.15	1.481	60.0	333.15	0.854
20.0	303.15	1.078	80.0	333.15	0.728
40.0	303.15	0.863	100.0	333.15	0.637
60.0	303.15	0.727	0.1	343.15	
80.0	303.15	0.632	20.0	343.15	1.475
100.0	303.15	0.561	40.0	343.15	1.109
0.1	313.15	1.648	60.0	343.15	0.899
20.0	313.15	1.166	80.0	343.15	0.761
40.0	313.15	0.920	100.0	343.15	0.663
60.0	313.15	0.768	0.1	353.15	
80.0	313.15	0.663	20.0	353.15	1.597
100.0	313.15	0.586	40.0	353.15	1.179
0.1	323.15	1.837	60.0	353.15	0.946
20.0	323.15	1.260	80.0	353.15	0.795
40.0	323.15	0.980	100.0	353.15	0.690

[a] Standard uncertainties u are $u(T) = 0.1$ K, $u(P) = 0.01$ MPa. The combined expanded uncertainty U_c (level of confidence = 0.95) is $U_c(\kappa_s) = 0.005\ \kappa_s$.

data founded in the literature and those calculated was carried out. The six references founded [34–39] provide heat capacity data at atmospheric pressure, and were compared with the calculated data taking into account the temperature range of our experimental measurements. Table 8 lists the obtained deviations from this comparison. The comparison with reference [35], for which 7 values were compared, exhibit the lowest deviations, with an AAD % = 1.04 and a MD% = 1.29, while the worst values are founded for reference [34] with an AAD% = AD% = MD% = 2.10.

With the heat capacity data it is possible to relate the square of the ratio of both measured properties, the density, ρ, and the speed

Table 7
Liquid heat capacities for Diisopropyl ether at 0.1 MPa as a function of temperature, *T*, measured by using a SETARAM Micro DSC 7 evo calorimeter.

T/K	Cp/J·K^{-1}·kg^{-1}
290.50	2061
295.44	2079
300.38	2099
305.32	2119
310.26	2139
315.19	2159
320.13	2179
325.07	2199
330.01	2221
334.95	2242
339.89	2263

Standard uncertainty u is $u(T) = 0.01$ K. Expanded uncertainty, U_c (level of confidence = 0.95) is $U_c(Cp) = 0.5\%$.

of sound, c, to the derivative properties of the volume with respect to temperature and pressure by means of the following relation:

$$\left(\frac{v}{c}\right)^2 = -\left(\frac{\partial v}{\partial P}\right)_T - \frac{T}{C_p}\left(\frac{\partial v}{\partial T}\right)_P^2 \quad (8)$$

Since the speed of sound and density data are known, the parameters of an equation of state for the volume at atmospheric pressure and as a function of temperature can be determined:

$$v\left(P_{ref}, T\right) = v_0 + v_1 T + v_2 T^2 + v_3 T^3 \quad (9)$$

$$\left(\frac{\partial v}{\partial P}\right)_T = -\frac{a_0 + a_1 T + a_2 T^2 + a_3 T^3 + dP}{b_0 + b_1 T + b_2 T^2 + P} \quad (10)$$

where d is constant. Coefficients a_0, a_1, a_2, a_3, b_0, b_1, b_2 and d from equation (10) were determined by minimizing the following objective function:

$$OF = \sum_i^{N_{exp}} -\left(\left(\frac{\partial v}{\partial P}\right)_T^{cal} - \frac{T}{C_p^{cal}}\left(\frac{\partial v}{\partial T}\right)_P^{2,cal} - \left(\frac{v_i^{exp}}{c_i^{exp}}\right)^2\right)^2 \quad (11)$$

By following this procedure, it is possible to calculate the density, its derivatives, the heat capacity and the speed of sound. All the stages concerning this calculations are detailed in a previous paper [40]. Table 9 gathers the obtained coefficients from equations (9) and (10) along with their deviations for both the density and the speed of sound. It can be seen that the function provides a good representation for both properties, giving an AD% less than 0.05 and a MD% less than 0.10 for the density, while for the speed of sound the AD% is equal to $-5.30 \cdot 10^{-3}$ with a MD% = 0.94.

A survey of literature density data was conducted to make a comparison between the density values obtained with the above

Table 9
Parameters of equations (9) and (10) and deviations for sound speed and density.

Parameters	Diisopropyl ether
v_0	$-5.36220 \cdot 10^{-4}$
v_1	$1.59075 \cdot 10^{-5}$
v_2	$-4.85300 \cdot 10^{-8}$
v_3	$5.65895 \cdot 10^{-11}$
a_0	$-8.01520 \cdot 10^{-5}$
a_1	$9.58545 \cdot 10^{-7}$
a_2	$-1.12800 \cdot 10^{-9}$
a_3	$2.34625 \cdot 10^{-13}$
b_0	$1.59174 \cdot 10^{2}$
b_1	$-4.32337 \cdot 10^{-1}$
b_2	$1.47588 \cdot 10^{-4}$
d	$7.47004 \cdot 10^{-8}$
deviations[a]	
AD% for ρ	$4.87 \cdot 10^{-2}$
AAD% for ρ	$4.92 \cdot 10^{-2}$
MD% for ρ	$9.94 \cdot 10^{-2}$
AD% for c	$-5.30 \cdot 10^{-3}$
AAD% for c	$2.40 \cdot 10^{-1}$
MD% for c	$9.37 \cdot 10^{-1}$

[a] AD = average deviation; AAD = absolute average deviation; MD = maximum deviation.

mentioned correlation and the values of the references published in the literature. Nine references were found reporting high pressure density data [4,14–21]. Most of them provide density values at pressures below our pressure range, being references [4and21] the ones which overlap our pressure and temperature ranges. References [4,18–21] are in good agreement with the correlation data, with maximum values of AD% = −0.11, AAD% = 0.12 and MD % = 0.27 for reference [19], being reference [18] the one in which the values of deviations are the lowest, with an AD% = −0.03, an AAD% = 0.04, and a MD% = 0.10. The greater deviations were obtained for reference [15], showing a high MD% = 1.27, an AD % = −0.55 and an AAD% = 0.57. References [14,16and17] exhibit also high deviations, with a maximum MD% = 1.10 for references [16and17]. All the density references, together with the studied deviations are listed in Table 10. A graphical comparison of these deviations can be observed in Fig. 3.

Isothermal compressibility data, κ_T, determined from the above procedures were compared with the calculated values. Fig. 4 show the good fitting provided by the correlation.

4. Conclusions

As already stated, reliable data of thermophysical properties of solvents, as is the case of diisopropyl ether, is needed to well design the processes in which it is used. This works reports a complete set of experimental high pressure speed of sound data, in the temperature interval from (293.15–353.15) K and in the pressure range (0.1–100) MPa, and high pressure density data for diisopropyl ether in the temperature range from (293.15–393.15) K and in the

Table 8
Deviations between heat capacity data from literature and values calculated from equation (7) for liquid diisopropyl ether.[a,b]

Reference	N_P	*T* range/K	*P*/MPa	AD%	AAD%	MD%	Cp uncertainty
[34]	1	(293.1)	0.1	2.10	2.10	2.10	–
[35]	7	(290–340)	0.1	1.04	1.04	1.29	–
[36–38]	1	(298.15)	0.1	1.46	1.46	1.46	–
[39]	24	(291.17–337.14)	0.1	1.29	1.29	1.50	0.3%

N_P Number of data points which are in our *T* range.
[a] AD = average deviation; AAD = absolute average deviation; MD = maximum deviation.
[b] Expanded uncertainty, U_c (level of confidence = 0.95) is $U_c(Cp) = 0.5\%$.

Table 10
Deviations between density data from literature and values interpolated by equations (8) to (10).[a]

Reference	N_P	T range/K	P range/MPa	AD%	AAD%	MD%	Density uncertainty
[14]	4	(303.15–323.15)	(0.1–53.1)	0.20	0.41	1.09	–
[15]	40	(298.15–328.15)	(0.1–8.0)	−0.55	0.57	1.27	–
[16,17]	8	(298.15–323.15)	(0.1–60)	0.66	0.66	1.10	–
[18]	109	(293.21–353.15)	(0.356–39.909)	−0.03	0.04	0.10	±0.2 kg·m^{-3}
[19]	35	(293.15–353.15)	(0.1–21.49)	−0.11	0.12	0.27	±0.2%
[4]	94	(293.15–353.15)	(0.1–100)	0.07	0.07	0.16	±0.7 kg·m^{-3}
[20]	126	(293.15–333.15)	(0.1–65)	−0.07	0.07	0.17	±0.1 kg·m^{-3}
[21]	94	(293.15–353.15)	(0.1–100)	0.05	0.06	0.15	±0.7 kg·m^{-3}

N_P Number of data points which are in our P, T ranges.
[a] AD = average deviation; AAD = absolute average deviation; MD = maximum deviation.

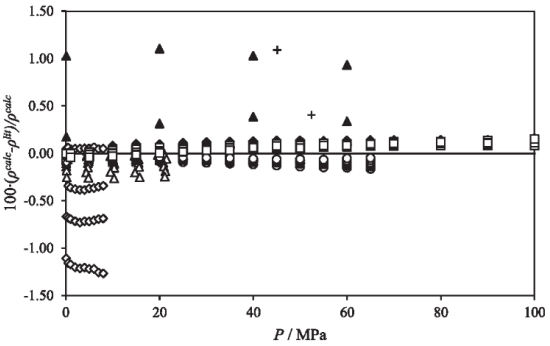

Fig. 3. Percentage deviations between literature density data and calculated densities from the integration of speed of sound measurements versus pressure in liquid diisopropyl ether. +; ref. [14], ◊; ref. [15], ▲; refs. [16,17], x; ref. [18], Δ; ref. [19], ◆; ref. [4], ○; ref. [20], □; ref. [21].

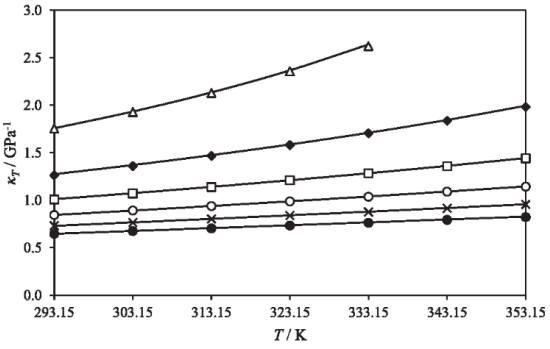

Fig. 4. Values of isothermal compressibility κ_T of diisopropyl ether as a function of temperature T at: Δ; 0.1 MPa, ◆; 20 MPa, □; 40 MPa, ○; 60 MPa, x; 80 MPa, ●; 100 MPa. The solid line represents the correlation for κ_T given by eqs (9) and (10).

pressure range from (0.1–140) MPa. Moreover, high pressure density data were determined from integration of speed of sound measurements in the same P, T ranges, as well as its derivative properties, that is, the isentropic compressibility, the isothermal compressibility and the isobaric expansion. All these speed of sound and density data were compared with the literature references available, showing in most cases low deviations.

Once this measurements have been taken, a correlation was stablished with which the speed of sound, the density and its derivatives were calculated, showing a good agreement between the calculated data, and those measured experimentally.

Acknowledgements

Natalia Muñoz-Rujas acknowledges support for this research to the University of Burgos, for the funding of her doctoral grant, and to the University of Pau for the funding of a five months research period in 2015.

This paper is part of the doctoral thesis of Natalia Muñoz-Rujas.

References

[1] N.P. Cheremisinoff, Industrial Solvents Handbook, second ed., Marcel Dekker Inc, New York, U.S.A, 2003.
[2] R. González-Olmos, M. Iglesias, Chemosphere 71 (2008) 2098–2105.
[3] National Institute for Occupational Safety and Health NIOSH, International Chemical Safety Cards, 1996.
[4] M. Dakkach, F. Aguilar, F.E.M. Alaoui, E.A. Montero, J. Chem. Thermodyn. 80 (2015) 135–141.
[5] F.P. Heese, M.E. Dry, K.P. Möller, Catal. Today 24 (1999) 327–335.
[6] A. Arce, A. Arce Jr., J. Marínez-Ageitos, O. Rodríguez, A. Soto, Fluid Phase Equilibria 170 (2000) 113–126.
[7] K.V.N. Suresh Reddy, G. Sankara Reddy, A. Krishnaiah, Thermochim. Acta 440 (2006) 43–50.
[8] R. González-Olmos, M. Iglesias, B.M.R.P. Santos, S. Mattedi, Phys. Chem. Liqs 46 (2008) 223–237.
[9] G. Nath, S. Sahu, R. Paikaray, Indian. J. Phys. 83 (2009) 429–436.
[10] G. Sankara Reddy, A. Subba Reddy, M. Venkata Subbaiah, K. Vasudha, A. Krishnaiah, J. Ind. Eng. Chem. 16 (2010) 941–946.
[11] D.F. Montaño, S. Martín, P. Cea, M.C. López, H. Artigas, J. Chem. Eng. Data 55 (2010) 5953–5959.
[12] V. Pandiyan, S.L. Oswall, N.I. Malek, P. Vasantharani, Thermochim. Acta 524 (2011) 140–150.
[13] Y. Zhang, X. Zheng, M. He, L. Liang, Y. Chen, J. Chem. Thermodyn. 104 (2017) 1–8.
[14] L.G. Schornack, C.A. Eckert, J. Phys. Chem. 74 (1970) 3014–3020.
[15] U.P. Govender, T.M. Lercher, S.K. Garg, J.C. Ahluwalia, J. Chem. Eng. Data 41 (1996) 147–150.
[16] P. Ulbig, M. Bubolz, C. Kornek, S. Schulz, J. Chem. Eng. Data 42 (1997) 449–452.
[17] P. Ulbig, H. Geyer, O. Gross, S. Schulz, J. Chem. Eng. Data 43 (1998) 175–177.
[18] E.C. Ihmels, J. Gmehling, J. Chem. Eng. Data 47 (2002) 1307–1313.
[19] X. Meng, J. Wu, Z. Liu, J. Chem. Eng. Data 54 (2009) 2353–2358.
[20] V. Antón, J. Muñoz-Embid, M. Artal, C. Lafuente, Fluid Phase Equilibria 417 (2016) 7–18.
[21] M. Dakkach, F. Aguilar, F.E.M. Alaoui, E.A. Montero, J. Chem. Thermodyn. 105 (2017) 123–132.
[22] E.H.I. Ndiaye, D. Nasri, J.L. Daridon, J. Chem. Eng. Data 57 (2012) 2667–2676.
[23] W.D. Wilson, J. Acoust. Soc. Am. 31 (1959) 1067–1072.
[24] E.H. Baltasar, M. Taravillo, V.G. Baonza, P.D. Sanz, B. Guignon, J. Chem. Eng. Data 56 (2011) 4800–4807.
[25] J.L. Daridon, A. Lagrabette, B. Lagourette, J. Chem. Thermodyn. 30 (1998) 607–623.
[26] B.N. Taylor, C.E. Kuyatt, Guidelines for Evaluating and Expressing the Uncertainty of NIST Measurements Results, NIST Technical Note 1297, National Institute of Standards and Technology, Gaithersburg, MD, 1994.
[27] E. Wilhem, T. Letcher, Volume Properties : Liquids, Solutions and Vapours, The Royal Society of Chemistry, Cambridge, U.K, 2015.
[28] M.J.P. Comuñas, J.P. Bazile, A. Baylaucq, C. Boned, J. Chem. Eng. Data 53 (2008) 986–994.
[29] B. Lagourette, C. Boned, H. Saint-Guirons, P. Xans, H. Zhou, Meas. Sci. Technol. 3 (1992) 699–703.
[30] W. Wagner, A. Pruß, J. Phys. Chem. Ref. Data 31 (2002) 387–535.
[31] TRC Thermodynamic Tables, Texas A&M University, College Station, TX, 1996.
[32] J.A. Riddick, W.B. Bunger, T.K. Sakano, Organic Solvents: Physical Properties and Methods of Purification, fourth ed., vol. II, Wiley, U.S, 1986.

[33] J.L. Daridon, B. Lagourette, J.P. Grolier, Int. J. Thermophys. 19 (1998) 145–160.
[34] G.S. Parks, H.M. Huffman, M. Barmore, J. Am. Chem. Soc. 55 (1933) 2733–2740.
[35] R.J.L. Andon, J.F. Counsell, D.A. Lee, J.F. Martin, J. Chem. Soc. 70 (1974) 1914–1916.
[36] J.-P.E. Grolier, G. Roux-Desgranges, M. Berkane, J. Chem. Thermodyn. 23 (1991) 421–429.
[37] J.-P.E. Grolier, G. Roux-Desgranges, M. Berkane, J. Chem. Thermodyn. 25 (1993) 41–50.
[38] J.-P.E. Grolier, G. Roux-Desgranges, M. Berkane, E. Wilhelm, J. Sol. Chem. 23 (1994) 153–166.
[39] R. Páramo, M. Zouine, F. Sobrón, C. Casanova, J. Chem. Eng. Data 49 (2004) 58–61.
[40] E.H.I. Ndiaye, M. Habrioux, J.A.P. Coutinho, M.L.L. Paredes, J.L. Daridon, J. Chem. Eng. Data 58 (2013) 1371–1377.

Speed of Sound, Density and Derivative Properties of Binary Mixtures HFE-7500 + Diisopropyl Ether under High Pressure

Natalia Muñoz-Rujas[1,2], Jean Patrick Bazile[1,], Fernando Aguilar[2], Guillaume Galliero[1], Eduardo Montero[2], Jean Luc Daridon[1]

[1]Laboratoire des Fluides Complexes et leurs Réservoirs, CNRS-TOTAL, UMR 5150, Université de Pau, BP 1155, 64013 Pau Cedex, France.

[2]Departamento de Ingeniería Electromecánica, Escuela Politécnica Superior, Universidad de Burgos, E-09006 Burgos, Spain.

[*] Corresponding author: Phone: +34947258916, Fax: +34947258916, e-mail: emontero@ubu.es

Abstract

Speeds of sound for the binary system HFE-7500 + diisopropyl ether have been measured at pressures up to 100 MPa and within a temperature interval from (293.15 to 353.15) K. High pressure density measurements were carried out by using a U-tube densimeter up to 140 MPa and at temperatures from (293.15 to 393.15) K. Additionally, the density and the isentropic compressibility were evaluated from integration of speed of sound data in the pressure range from (0.1 to 100) MPa and in the temperature interval from (293.15 to 353.15) K. This work also reports a correlation for both the density and the speed of sound within their estimated uncertainties to evaluate the volume and its derivatives with respect to pressure and temperature.

Keywords

Hydrofluoroethers, Diisopropyl ether, Speed of Sound, Density, High pressure, Compressibility.

1. Introduction

Since the decade of the ‘70s, concern on stratospheric ozone layer depletion [1] and later on climate change [2] has led to plan a phase-out of halogenated hydrocarbons by setting limits in emissions and production of these substances in order to reduce its impact on the atmosphere. Perfluorocarbons (PFCs) and perfluoropolyethers (PFPEs) were introduced as alternatives to ozone depleting substances and were intended to be used as propellants, cleaning solvents, lubricants, as refrigerants of some specialized refrigeration systems or as heat transfer media due to its stability, low viscosity, low surface tension and excellent dielectric properties. Although

these properties made them widely used in industry processes, PFCs were demonstrated to have extraordinary long atmospheric lifetimes and to be some of the most potent greenhouse gases [3]. The Kyoto Protocol, adopted on December 1997 implemented the objective to reduce these anthropogenic greenhouse gas emissions, stablishing a structure of emission reduction commitment periods, in which the first period included the PFCs as one of the fluids whose use and production had to be diminished during the period (2008 – 2012). The Paris Agreement, which was adopted on December 2015, and signed in April 2016, provided a proposal to mitigate the greenhouse gas emissions that will start in the year 2020, focusing high GWP substances on the spotlight. This situation urged to search environmentally friendly alternatives to these commonly used fluorocarbons but with the same or similar properties. Some fluids, as fluorinated ethers, fluoroamines, alcohols and sulphur compounds were proposed and investigated [4] but the knowledge about their thermophysical properties, toxicity and stability is sometimes scarce.

Hydrofluoroether fluids (HFEs) are a type of fluorinated ethers investigated since the decade of the ‘90s as substitutes of CFCs, HCFCs and PFCs among other fluorocarbons, due to their desirable environmental properties, that is, zero ozone depletion potential (ODP), low global warming potential (GWP) and short atmospheric lifetimes (ALT) and due to their thermophysical properties. HFEs show low toxicities, compatibility with a large range of materials including most metals and plastics, stability and low difussive and drag-out losses [5].

2-trifluoromethyl-3-ethoxydodecafluorohexane, known as HFE-7500, is proposed to be a good alternative to PFCs and PFPEs replacement because it is a dielectric fluid with low viscosity, high liquid density, low surface tension, being almost non-toxic and showing favorable environmental properties such as zero ODP, a very low GWP and an ALT of 2.2 years.

Diisopropyl ether (DIPE) is used in a wide variety of applications, for example it is used as solvent or as cleaning agent. The addition of the fluorinated compound HFE-7500 implies a reduction on the flammability of Diisopropyl ether, making this binary mixture a good option to be used in high precision cleaning, or as solvent as oil-based solutions dissolve in it.

In this work the physical properties speed of sound and density of the binary mixture x HFE-7500 + (1-x) Diisopropyl ether have been determined experimentally at high pressures and at high temperatures at five mole fractions, x = (0.250, 0.375, 0.500, 0.625 and 0.750). Density was also calculated by integration of speed of sound data, and the derivative properties isentropic compressibility, isothermal compressibility and isobaric expansion were also determined from speed of sound measurements.

2. Experimental Section

2.1 Materials

Hydrofluoroether fluid HFE-7500, also known by its chemical name, 2-trifluoromethyl-3-ethoxydodecafluorohexane or 3-ethoxy-1,1,1,2,3,4,4,5,5,6,6,6-dodecafluoro-2-trifluoromethylhexane (CAS: 297730-93-9) was obtained from the 3M company with a stated mass fraction purity greater than 0.995. Diisopropyl ether (DIPE), also known as 2,4-dimethyl-3-oxapentane, was supplied by Sigma-Aldrich (CAS: 108-20-3), with a purity greater than 0.995. Neither one of the fluids was subject to further purification. Table 1 shows the specifications of both chemicals.

Table 1. Sample description.

Compound	Source	Formula	Molar mass / $g \cdot mol^{-1}$	Stated purity[a]	CAS number
HFE-7500[b]	3M Company	$C_9H_5F_{15}O$	414.11	>99.5[c]	297730-93-9
Diisopropyl ether	Sigma-Aldrich	$C_6H_{14}O$	102.17	>99.5[d]	108-20-3

[a] Determined by gas chromatography (GC) by the supplier.
[b] HFE-7500 = 2-trifluoromethyl-3-ethoxydodecafluorohexane.
[c] Mass fraction purity / $g \cdot mol^{-1}$%.
[d] Mole fraction purity / mol%.

2.2 Speed of Sound Measurement

To determine the speed of sound at high pressure in compressed liquids, a cylindrical acoustic cell using a pulse-echo technique working in transmission mode was used. The operating principle is based on the determination of the time delay between the transmitted pulse and the first echo of an acoustic wave that spreads through the fluid. The apparatus, which has been described previously [6], was made to measure speeds of sound in liquids and was designed for working up to 210 MPa using a pulse-echo method working at 3 MHz with a path length fixed to L_0 = 30 mm. It has two electromechanical transducers in direct contact with the fluid facing each other inside a hollow cylindrical support in which one acts as a transmitter, and the other as the receiver. The acoustic sensor is placed inside a stainless-steel vessel closed at one end by a plug with three electric connectors. Prior to make the measurements, and in order to bring the path length needed for calculating speed of sound, the apparatus was calibrated with two reference fluids, purified water [7, 8] and heptane [9] at different pressures and temperatures.

To ensure a constant temperature, the acoustic cell is immersed in a thermoregulated bath filled with silicone oil so that the stability in temperature is of 0.02 K in the range investigated. The temperature is measured thanks to a Pt100 probe in contact with the liquid sample with an uncertainty of $\pm$ 0.1 K. With respect to the pressure, it is generated by a high pressure volumetric pump that reaches the cell by the liquid itself and is measured by using a pressure gauge calibrated between (0.1 and 100) MPa so the uncertainty is of 0.01 MPa in our pressure range. The expanded uncertainty for speed of sound in the pressure and temperature ranges investigated according to the law of propagation of standard uncertainties [10] is estimated to be 2 $m \cdot s^{-1}$.

2.3 Density Measurement

Since density is one of the most important physical properties because other important properties can be determined from its knowledge, high pressure densities for the binary mixture *x* HFE-7500 + (*1-x*) Diisopropyl ether were determined experimentally in this work. For this purpose, an Anton Paar DMA HPM vibrating tube densitometer operating in the ranges (293.15 to 393.15) K for the temperature and (0.1 to 140) MPa for the pressure was used. The density is determined by the oscillation period of a U-tube made of Hastelloy in the presence of damping and under an external periodic force. This oscillation period differs for each fluid and it depends also on temperature and on pressure, being density related to the square of the period by a linear law. The calibration of the vibrating-tube densitometer has been performed according to the procedure described by Comuñas *et al.* [11] using three reference fluids: vacuum, water [12] and decane [13], being decane the choice as reference liquid for temperatures higher than the boiling point of water (373.15 K) at 0.1 MPa.

The estimated uncertainty given in temperature by the Pt100 probe placed inside the densitometer was ± 0.1 K in the temperature range investigated, (293.15 – 393.15) K while the estimated uncertainty given in pressure by the HBM pressure gauge was 0.01 MPa for the pressure interval considered (0.1 – 140) MPa. The expanded uncertainty in density was then obtained from the uncertainties in temperature, in pressure, and taking into account the uncertainty in measurements of oscillation period, as well the error in the calibration method, giving an estimated value of ± 0.5 $kg \cdot m^{-3}$ (0.06%) in the pressure range investigated. The mixtures were prepared immediately before use by weighing the corresponding amount of each component for every mole fraction, filling stoppered bottles of 250 cm^3 in volume at atmospheric pressure using a high precision Sartorius balance with an uncertainty of ± 0.001 g. Taking into account the uncertainty of the balance, and considering a coverage factor k = 2, the expanded uncertainty in the composition of the mixtures results to be $6 \cdot 10^{-5}$ in mole fraction.

2.4 Micro Differential Scanning Calorimetry (μDSC)

In order to calculate high pressure density data from speed of sound measurements by following the procedure described on section 3. Results and Discussion, heat capacity values C_p, are needed. For this purpose, a SETARAM Micro DSC 7 evo calorimeter was used to measure this property at atmospheric pressure and in different temperature ranges for the pure compounds and for the five mole compositions of the binary mixture *x* HFE-7500 + (*1-x*) Diisopropyl ether. This calorimeter is based on the Calvet calorimetric principle, being the output signal given by the difference of the heat flux received by the flux meters located around the reference and measuring cells. To regulate the temperature, two stages of high sensitivity Peltier thermo elements are located around the measuring and the reference cells, and on the calorimetric block. Inside this block, the atmosphere is dried by using nitrogen gas with a volume purity $\geq$ 99.995%. The calibration of the apparatus was checked by measuring the heat capacity of *n*-dodecane (molar purity $\geq$ 99.0%) in the liquid state and comparing to the data obtained by the NIST [14], resulting in an average deviation of 0.40%. The differential heat flux, that is fixed to be ±0.005 mW, and the temperature versus time were monitored and analyzed by using a Calisto SETARAM software. To carry all the measurements, the SETARAM cylindrical standard batch vessels were used. The samples were weighed with an OHAUS Explorer E0RR80 balance, with a resolution of ±0.0001 g. Concerning the mixtures, the procedure of preparation was the one followed in Section 2.3, being the uncertainty in the composition of these mixtures is $6 \cdot 10^{-5}$ in mole fraction. After introducing the sample in the calorimeter, the heat capacity measurements were carried out using the scanning or continuous method with a constant heating rate of 0.2 $K \cdot min^{-1}$. The expanded uncertainty for the temperature was 0.01 K and 0.005 mW for the heat flux from calorimeter manufacturer estimation with a level of confidence of 95% (k = 2). The combined expanded uncertainty for the heat capacity measurements, considering the same level of confidence was estimated to be as 0.5%.

3. Results and Discussion

Speed of sound measurements for the binary system *x* HFE-7500 + (*1-x*) Diisopropyl ether were carried out for the five molar compositions x = (0.250, 0.375, 0.500, 0.625 and 0.750) in the pressure range from (0.1 to 100) MPa every 20 MPa, and in the range of temperatures from (293.15 to 353.15) K along isotherms spaced 10 K. Due to the low boiling point at atmospheric pressure for Diisopropyl ether (341.66 K), [15] vaporization at high temperatures was expected; then a limit in temperature for the mixtures was stablished. At x = 0.250, no measurements have been done at temperatures 343.15 K and higher. At x = 0.375, x = 0.500, and x = 0.625, no

measurements were taken at 353.15 K. At x = 0.750, all temperature points were measured. The experimental values of these measurements are listed in Table 2.

Table 2. Experimental values of speed of sound, c, at temperatures T and pressures P for the binary mixture x HFE-7500 + (*1-x*) Diisopropyl ether[a].

x	P / MPa	T / K						
		293.15	303.15	313.15	323.15	333.15	343.15	353.15
		c / m·s^{-1}						
0.250	0.1	802.0	763.8	729.6	693.3	659.8		
	20.0	930.1	898.1	870.2	841.6	816.0	792.6	767.9
	40.0	1029.9	1001.7	975.8	952.5	930.9	911.7	889.5
	60.0	1113.8	1089.1	1065.1	1043.6	1024.9	1007.3	986.5
	80.0	1187.2	1164.4	1141.4	1123.2	1106.8	1089.6	1069.1
	100.0	1254.0	1231.9	1209.6	1193.8	1180.2	1161.8	1142.6
0.375	0.1	756.1	717.2	687.0	650.0	617.9	588.0	
	20.0	879.0	848.7	821.7	794.7	769.7	745.6	724.5
	40.0	975.3	948.6	924.1	901.0	878.9	858.7	841.4
	60.0	1056.9	1032.1	1009.2	987.7	968.2	949.5	935.6
	80.0	1127.9	1104.0	1082.8	1063.0	1044.5	1026.7	1015.6
	100.0	1190.8	1170.1	1148.8	1129.2	1111.7	1095.1	1087.0
0.500	0.1	719.2	687.9	656.3	624.3	593.4	563.0	
	20.0	839.0	812.7	786.8	761.3	737.4	714.0	692.8
	40.0	933.0	909.1	885.6	862.9	842.0	822.8	804.5
	60.0	1012.2	989.8	967.9	946.9	927.8	911.0	894.0
	80.0	1081.1	1059.8	1039.3	1019.6	1001.6	987.0	971.0
	100.0	1143.0	1123.0	1102.9	1084.4	1067.2	1054.1	1039.1
0.625	0.1	701.5	670.9	641.2	609.9	579.9	550.5	
	20.0	818.1	793.7	769.5	745.2	720.8	697.6	676.5
	40.0	909.4	889.5	866.8	846.1	823.8	803.3	785.2
	60.0	988.0	969.5	946.8	927.8	907.5	889.2	872.6
	80.0	1056.3	1038.9	1017.4	998.6	980.0	963.1	947.8
	100.0	1116.9	1101.7	1079.9	1061.6	1043.9	1028.7	1014.4
0.750	0.1	686.9	656.0	626.5	597.4	568.6	540.2	512.6
	20.0	799.8	773.5	749.4	726.1	703.1	681.6	660.7
	40.0	888.3	864.7	843.3	822.8	802.8	783.8	765.7
	60.0	963.7	941.8	921.7	902.5	884.3	867.0	850.4

80.0	1029.1	1008.7	990.1	971.8	954.4	938.2	923.1
100.0	1088.5	1068.1	1050.9	1033.7	1016.8	1001.7	987.2

[a] Standard uncertainties u are $u(T) = 0.1$ K, $u(P) = 0.01$ MPa. The combined expanded uncertainty U_c (level of confidence = 0.95) is $U_c(c) = 2$ m·s^{-1}. The expanded uncertainty in the composition of the mixtures is $U_c(x) = 6 \cdot 10^{-5}$ in mole fraction.

A correlation has been stablished by using a rational function with nine adjustable parameters:

$$\frac{1}{c^2} = \frac{A_0 + A_1 T + A_2 T^2 + A_3 T^3 + BP + CP^2 + DP^3}{1 + ET + FP} \quad (1)$$

Table 3. Parameters of Equation (1) for the binary system *x* HFE-7500 + (*1*-*x*) Diisopropyl ether.

	x				
Parameters	0.250	0.375	0.500	0.625	0.750
A_0	$-2.95870 \cdot 10^{-6}$	$4.79791 \cdot 10^{-6}$	$7.03670 \cdot 10^{-6}$	$9.60725 \cdot 10^{-6}$	$7.01312 \cdot 10^{-7}$
A_1	$2.75208 \cdot 10^{-8}$	$-4.63690 \cdot 10^{-8}$	$-6.51540 \cdot 10^{-8}$	$-8.74990 \cdot 10^{-8}$	$-5.49450 \cdot 10^{-9}$
A_2	$-7.19940 \cdot 10^{-11}$	$1.63505 \cdot 10^{-10}$	$2.16839 \cdot 10^{-10}$	$2.81615 \cdot 10^{-10}$	$3.16993 \cdot 10^{-11}$
A_3	$6.43616 \cdot 10^{-14}$	$-1.84120 \cdot 10^{-13}$	$-2.33610 \cdot 10^{-13}$	$-2.94070 \cdot 10^{-13}$	$-4.13000 \cdot 10^{-14}$
B	$5.45921 \cdot 10^{-9}$	$5.76481 \cdot 10^{-9}$	$5.98172 \cdot 10^{-9}$	$7.38184 \cdot 10^{-9}$	$6.99274 \cdot 10^{-9}$
C	$-3.29050 \cdot 10^{-11}$	$-3.29120 \cdot 10^{-11}$	$-3.33960 \cdot 10^{-11}$	$-4.60160 \cdot 10^{-11}$	$-4.17890 \cdot 10^{-11}$
D	$1.11177 \cdot 10^{-13}$	$1.08329 \cdot 10^{-13}$	$1.05380 \cdot 10^{-13}$	$1.59685 \cdot 10^{-13}$	$1.41511 \cdot 10^{-13}$
E	$-2.22183 \cdot 10^{-3}$	$-2.21254 \cdot 10^{-3}$	$-2.20337 \cdot 10^{-3}$	$-2.15686 \cdot 10^{-3}$	$-2.16907 \cdot 10^{-3}$
F	$1.02215 \cdot 10^{-2}$	$1.02902 \cdot 10^{-2}$	$1.02092 \cdot 10^{-2}$	$1.11237 \cdot 10^{-2}$	$1.05069 \cdot 10^{-2}$
deviations[a]					
AD%	$1.42 \cdot 10^{-3}$	$-1.28 \cdot 10^{-4}$	$-5.16 \cdot 10^{-2}$	$9.61 \cdot 10^{-4}$	$-6.16 \cdot 10^{-4}$
AAD%	$8.78 \cdot 10^{-2}$	$7.08 \cdot 10^{-2}$	$7.02 \cdot 10^{-2}$	$6.31 \cdot 10^{-2}$	$3.51 \cdot 10^{-2}$
MD%	$3.49 \cdot 10^{-1}$	$3.68 \cdot 10^{-1}$	$2.14 \cdot 10^{-1}$	$2.34 \cdot 10^{-1}$	$1.14 \cdot 10^{-1}$

[a]AD = average deviation; AAD = absolute average deviation; MD = maximum deviation.

No experimental speed of sound data have been found in the literature for this binary mixture. Table 3 shows the values for the nine parameters for each of the mole fractions, together with its average deviation (AD%), absolute average deviation (AAD%) and maximum deviation (MD%). It can be seen that the AAD% and AD% values are lower than the expanded uncertainty, while the MD% values for almost all molar compositions are lower than this value (2 m·s^{-1}), being able to conclude that the correlation given by equation (1) leads to a good interpolation.

In Figure 1 are plotted the deviations between the experimental speeds of sound and the calculated values for the five mole fractions of the binary mixture vs. the pressure in the temperature range investigated. The highest deviation is showed at 0.1 MPa for the mole fraction x = 0.375 with a MD% = 0.37. It can be seen that the vast majority of the values are founded between the dashed lines which represent the uncertainty in speed of sound (0.2%), confirming that the correlation is able to predict the behavior of the speed of sound at high pressure.

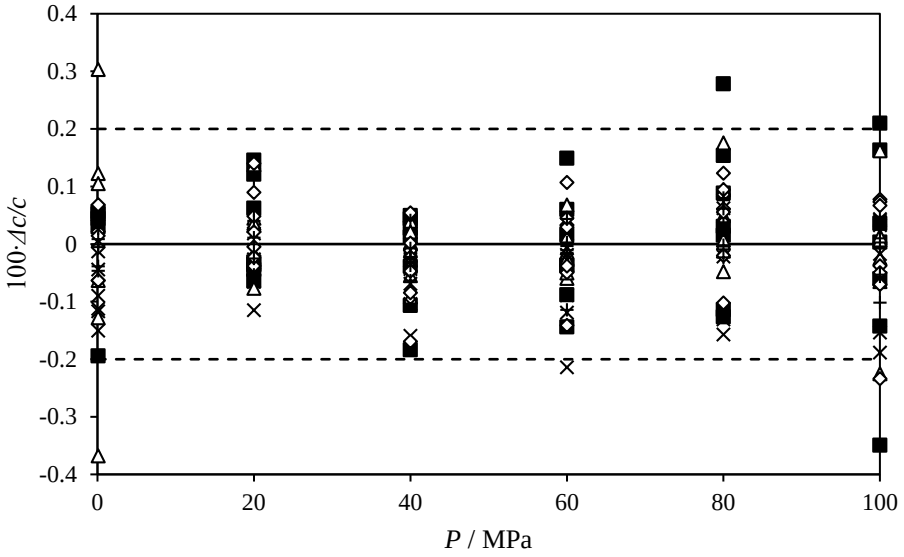

Figure 1. Deviations between the experimental speeds of sound and the calculated values, $\Delta c/c$ = [c(exp) – c(cal)]/c(exp) at different mole fractions for the binary mixture x HFE-7500 + (*1*-x) Diisopropyl ether in the temperature range (from 293.15 to 353.15) K. ■; x = 0.250, Δ; x = 0.375, x; x = 0.500, ◊; x = 0.625, +; x = 0.750. The dashed line represents the value of expanded uncertainty in speed of sound.

With the high pressure speed of sound data and by integration in the full pressure range (0.1 to 100), high pressure density values were obtained. The method used to carry out these calculations rests on the relationships between the speed of sound and the isentropic compressibility, κ_S [16]:

$$\kappa_S = \frac{1}{\rho c^2} \tag{2}$$

where ρ is the density and c is the speed of sound. The values of isentropic compressibility, κ_S obtained by using equation (2) are listed in Table 4.

Table 4. Values of isentropic compressibility, κ_S, at temperatures T and at pressures P for the binary mixture x HFE-7500 + (*1*-x) Diisopropyl ether[a].

x	P / MPa	T / K						
		293.15	303.15	313.15	323.15	333.15	343.15	353.15
		κ_S / GPa^{-1}						
0.250	0.1	1.477	1.652	1.847	2.067	2.321		
	20.0	1.066	1.154	1.247	1.344	1.449	1.561	1.683
	40.0	0.851	0.907	0.964	1.022	1.082	1.145	1.210
	60.0	0.713	0.753	0.793	0.833	0.873	0.914	0.957
	80.0	0.616	0.646	0.676	0.706	0.736	0.766	0.796
	100.0	0.545	0.570	0.593	0.617	0.640	0.663	0.685
0.375	0.1	1.488	1.664	1.865	2.094	2.354	2.650	
	20.0	1.064	1.153	1.249	1.351	1.458	1.569	1.681
	40.0	0.846	0.902	0.962	1.023	1.085	1.147	1.206
	60.0	0.707	0.748	0.790	0.832	0.874	0.915	0.952
	80.0	0.610	0.642	0.673	0.705	0.736	0.766	0.792
	100.0	0.540	0.565	0.590	0.615	0.640	0.662	0.682
0.500	0.1	1.500	1.665	1.858	2.082	2.340	2.638	
	20.0	1.069	1.152	1.244	1.344	1.452	1.565	1.682
	40.0	0.847	0.900	0.957	1.017	1.080	1.143	1.206
	60.0	0.707	0.745	0.785	0.827	0.869	0.911	0.951
	80.0	0.609	0.638	0.669	0.700	0.731	0.762	0.790
	100.0	0.538	0.561	0.585	0.610	0.634	0.658	0.679
0.625	0.1	1.462	1.617	1.801	2.017	2.267	2.554	2.883
	20.0	1.041	1.117	1.205	1.302	1.407	1.519	1.636
	40.0	0.824	0.873	0.927	0.986	1.048	1.112	1.176
	60.0	0.687	0.721	0.760	0.801	0.843	0.886	0.928
	80.0	0.591	0.618	0.647	0.678	0.709	0.741	0.771
	100.0	0.522	0.543	0.566	0.591	0.616	0.640	0.664
0.750	0.1	1.435	1.595	1.775	1.981	2.217	2.492	2.813
	20.0	1.028	1.109	1.196	1.290	1.390	1.498	1.614
	40.0	0.817	0.869	0.923	0.979	1.038	1.100	1.163
	60.0	0.683	0.719	0.758	0.797	0.837	0.878	0.920
	80.0	0.589	0.617	0.646	0.675	0.705	0.735	0.765
	100.0	0.520	0.543	0.566	0.589	0.613	0.636	0.659

[a] Standard uncertainties u are $u(T) = 0.1$ K, $u(P) = 0.01$ MPa. The combined expanded uncertainty U_c (level of confidence = 0.95) is $U_c(\kappa_s) = 0.005\ \kappa_s$. The expanded uncertainty in the composition of the mixtures is $U_c(x) = 6 \cdot 10^{-5}$ in mole fraction.

With both density and speed of sound data the calculation of the volume and its derivatives with respect to temperature and pressure can be done by employing a procedure of adjustment to a PVT equation, [17, 18] which rests on the Newton-Laplace relationships that relates the isothermal compressibility, κ_T to the isentropic compressibility, κ_S:

$$\kappa_T = \kappa_S + \frac{T\alpha_P^2}{\rho C_p} \tag{3}$$

where α_P, and C_p are, respectively the isobaric expansion and the isobaric heat capacity. By combining equation (3) with equation (2) it leads to a relation connecting the speed of sound to the thermodynamic properties:

$$\frac{v^2}{c^2} = v\kappa_T - \frac{Tv^2\alpha_P^2}{C_p} \tag{4}$$

In this equation, the heat capacity data were estimated by using the following thermodynamic relationship when values at reference pressure are known [19]:

$$\left(\frac{\partial C_p}{\partial P}\right)_T = -T\left(\frac{\partial^2 v}{\partial T^2}\right)_P \tag{5}$$

where:

$$C_p(T) = C_{p,ref}(T) - T\frac{\partial^2}{\partial T^2}\int_{\Pr ef}^{P} v dP \tag{6}$$

To determine $C_{p,ref}$ values, experimental measurements were carried out at atmospheric pressure by using a SETARAM Micro DSC 7 evo calorimeter. These experimental data were measured for the five mole fractions studied, and are showed as a quadratic function of temperature in the ranges investigated taking into account the boiling point of the mixtures. Table 5 lists the heat capacity values for the five mole fractions of the mixture x HFE-7500 + (*1*-x) Diisopropyl ether together with the values of the pure components. The polynomial equation employed to correlate the heat capacity values has the form:

$$C_{p,ref}/J \cdot K^{-1} \cdot kg^{-1} = A + BT + CT^2 \quad (7)$$

Table 5. Liquid heat capacities for the mixture *x* HFE-7500 + (*1-x*) Diisopropyl ether as a function of temperature, *T*, measured by using a SETARAM Micro DSC 7 evo calorimeter[a].

T / K	*x*						
	0	0.250	0.375	0.500	0.625	0.750	1
	Liquid heat capacity / $J \cdot K^{-1} \cdot kg^{-1}$						
290.50	2018	1518	1378	1296	1208	1196	
295.44	2038	1531	1390	1307	1217	1205	
297.91							1126
300.38	2058	1545	1402	1318	1227	1215	
305.32	2078	1559	1414	1330	1237	1224	
307.79							1142
310.26	2099	1574	1426	1341	1247	1233	
315.20	2119	1588	1439	1352	1257	1243	
317.66							1158
320.13	2139	1603	1452	1364	1268	1253	
325.07	2161	1619	1465	1377	1278	1263	
327.54							1175
330.01	2183	1635	1478	1389	1288	1273	
334.95	2206	1651	1491	1401	1298	1283	
337.42							1193
339.89	2229	1666	1504	1414	1308	1293	
344.82					1320	1304	
347.29							1209
349.76					1329	1314	
354.70						1324	
357.17							1228
359.64						1334	
367.05							1249
376.92							1265
386.80							1284

[a] Standard uncertainties *u* are $u(T) = 0.01$ K, $u(W) = 0.005$ mW. The combined expanded uncertainty U_c (level of confidence = 0.95) is $U_c(C_p) = 0.005\ C_p$. The expanded uncertainty in the composition of the mixtures is $U_c(x) = 6 \cdot 10^{-5}$ in mole fraction.

Parameters A, B, and C of equation (7) are given in table Table 6 for the five mole fractions and for the pure compounds together with their deviations. It can be seen that the AAD%, AD% and

MD% values are in all cases lower than the expanded uncertainty for heat capacity (0.5%), due to the simplicity of this equation.

Table 6. Parameters of equation (7) for the binary mixture *x* HFE-7500 + (*1*-*x*) Diisopropyl ether. Values for $x = 0$ were taken from reference [20], and values of $x = 1$ were taken from reference [21].

Parameter	*x*						
	0	0.250	0.375	0.500	0.625	0.750	1
A	$1.548 \cdot 10^{3}$	$1.259 \cdot 10^{3}$	$0.9647 \cdot 10^{3}$	$0.9992 \cdot 10^{3}$	$0.7319 \cdot 10^{3}$	$0.8069 \cdot 10^{3}$	$0.8169 \cdot 10^{3}$
B	$-6.277 \cdot 10^{-1}$	$-9.282 \cdot 10^{-1}$	$4.511 \cdot 10^{-1}$	$-1.438 \cdot 10^{-1}$	1.286	$7.986 \cdot 10^{-1}$	$4.581 \cdot 10^{-1}$
C	$7.736 \cdot 10^{-3}$	$6.259 \cdot 10^{-3}$	$3.344 \cdot 10^{-3}$	$4.013 \cdot 10^{-3}$	$1.208 \cdot 10^{-3}$	$1.859 \cdot 10^{-3}$	$1.942 \cdot 10^{-3}$
deviations[a]							
AD%	$-3.27 \cdot 10^{-3}$	$-9.24 \cdot 10^{-5}$	$-2.11 \cdot 10^{-3}$	$4.42 \cdot 10^{-4}$	$-9.58 \cdot 10^{-4}$	$2.68 \cdot 10^{-3}$	$4.90 \cdot 10^{-5}$
AAD%	0.02	0.02	0.01	0.02	0.02	0.02	0.05
MD%	0.05	0.04	0.04	0.05	0.04	0.05	0.19

[a]AD = average deviation; AAD = absolute average deviation; MD = maximum deviation.

The C_p values of the pure compounds were compared with the data available in the literature. No comparison was established with the values of the mixtures since no data was found. Table 7 gathers the deviations obtained for the pure HFE-7500 values with respect to those of the literature. Only reference [22] reports data points of heat capacities in the temperature range (304.12 – 353.38) while reference [23] reports an equation to determine C_p values; due to this, the data comparison with this reference was done in the same temperature range as our experimental heat capacity measurements were carried out (297.91 – 386.80). High deviations were found for reference [22], with an AAD% = 15.06, a Bias% = -13.09 and a MD% = 24.43. Indeed, when plotting our C_p values and the values of the two references versus the temperature, a big difference between both slopes is observed, as can be seen in Figure 2. We have to consider that reference [22] reports the utilization of a flow calorimeter with an expanded uncertainty in the heat capacity measurements of 2%, bigger than ours. The deviations obtained for the comparison with the equation provided by reference [23] show a better agreement, with values slightly higher than the expanded uncertainty (0.5%), with a MD% = 1.85, an AAD% = 0.72 and a Bias% = 0.66. For pure Diisopropyl ether, six references [24 - 29] were found in the literature. The lowest values of deviations are observed for reference [25], which provides 7 points with an AAD% = Bias% = 2.87, and a MD% = 3.30. The worst values are those which result from the comparison with reference [24], which provides only one point, with an AAD% = Bias% = MD% = 4.08. These results can be seen in Table 8.

Table 7. Values of deviations between the experimental C_p measurements and those from the literature by using equation (7) and the A, B, C parameters reported in Table 6 for HFE-7500.

Reference	Year	N_P	T_{min} (K)	T_{max} (K)	AAD (%)	MD (%)	Bias (%)
Zheng *et al.* [22]	2014	6	304.12	353.38	15.06	24.43	-13.09
3M[a] [23]	2008	10	297.91	386.80	0.72	1.85	0.66

[a]Equation provided on reference [3M] for calculating liquid specific heat of HFE-7500; C_p ($J \cdot kg^{-1} \cdot K^{-1}$) = 1.4982·T (ºC)+1091.

N_P Number of data points which are in our P, T ranges.

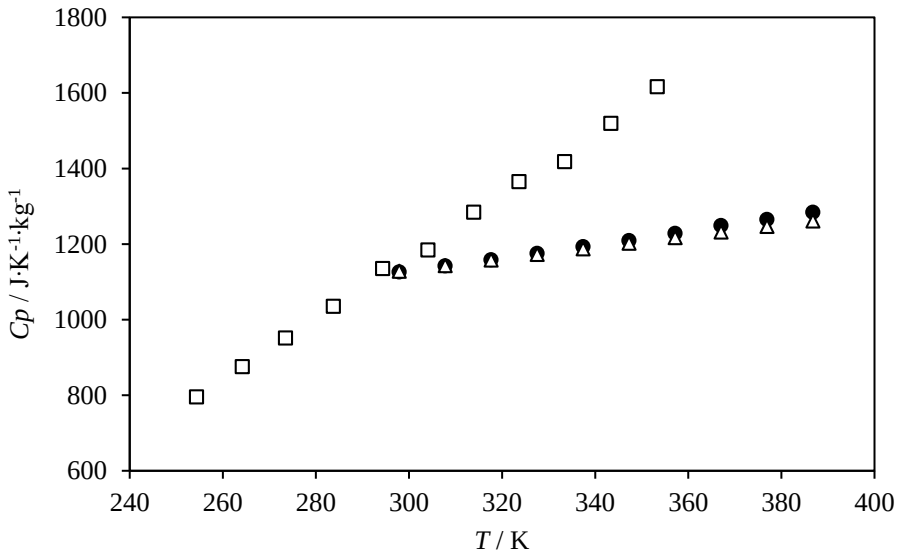

Figure 2. Heat capaciy data C_p, for the hydrofluoroether fluid HFE-7500 vs. the temperature. □; reference [22], Δ; reference [23], ●; experimental values.

Then, equation (4) can be transformed into equation (8), which relates the square of the ratio of the measured speeds of sound and densities to the derivatives of the volume with respect to temperature and pressure:

$$\left(\frac{v}{c}\right)^2 = -\left(\frac{\partial v}{\partial P}\right)_T - \frac{T}{C_p}\left(\frac{\partial v}{\partial T}\right)_P^2 \tag{8}$$

With the knowledge of speed of sound and density data, an adjustment of the parameters of an equation of state as a function of temperature which is defined by the volume at atmospheric pressure and the change in volume respect to pressure can be done:

$$v(P_0,T) = v_0 + v_1 T + v_2 T^2 + v_3 T^3 \tag{9}$$

$$\left(\frac{\partial v}{\partial P}\right)_T = -\frac{a_0 + a_1 T + a_2 T^2 + a_3 T^3 + dP}{b_0 + b_1 T + b_2 T^2 + P} \tag{10}$$

where d is constant. Equation (10) expresses the change in volume with respect to pressure in a rational form, and it enables to calculate speed of sound and density data within their experimental uncertainties. The parameters of equation (9), v_0, v_1, v_2 and v_3 were previously evaluated from atmospheric density data and coefficients a_0, a_1, a_2, a_3, b_0, b_1, b_2 and d from equation (10) were determined by minimizing the following objective function:

$$OF = \sum_i^{N_{\exp}} \left(-\left(\frac{\partial v}{\partial P}\right)_T^{cal} - \frac{T}{C_p^{cal}} \left(\frac{\partial v}{\partial T}\right)_P^{2,cal} - \left(\frac{v_i^{\exp}}{c_i^{\exp}}\right)^2 \right)^2 \tag{11}$$

Table 8. Deviations from literature values for heat capacity data C_p, by using equation (7) and the A, B, C parameters given in Table 6 at atmospheric pressure by using a SETARAM Micro DSC 7 evo calorimeter for pure Diisopropyl ether.

Reference	Year	N_P	$T_{\min}$ (K)	$T_{\max}$ (K)	AAD (%)	MD (%)	Bias (%)
Parks *et al.* [24]	1933	1	293.15	293.15	4.08	4.08	4.08
Andon *et al.* [25]	1974	7	290	340	2.87	3.30	2.87
Grolier *et al.* [26 - 28]	1991 - 1994	1	298.15	298.15	3.42	3.42	3.42
Páramo *et al.* [29]	2004	24	291.17	337.14	3.10	3.50	3.10

N_P Number of data points which are in our P, T ranges.

This procedure, which is described in detail in a previous paper, [30] allows to calculate the volume, the density and its derivatives, that is the isobaric expansion, isothermal compressibility and isentropic compressibility, as well as the heat capacity and the speed of sound. Table 9 lists the coefficients obtained by using the above mentioned procedure along with its AD%, AAD%, and the MD% both for the speed of sound and for the density. It can be seen the good

representation provided by the function due to the deviations given both for density and for speed of sound, with a MD that does not exceed 0.02% at x = 0.250, and with a MD about 0.6% at x = 0.500 for the speed of sound.

Table 9. Parameters of Equations (9) and (10) and deviations from sound speed and density of binary mixture x HFE-7500 + (*1*-x) Diisopropyl ether.

Parameters	x				
	0.250	0.375	0.500	0.625	0.750
v_0	$6.61026 \cdot 10^{-4}$	$2.97057 \cdot 10^{-4}$	$1.23910 \cdot 10^{-4}$	$5.36667 \cdot 10^{-4}$	$4.95955 \cdot 10^{-4}$
v_1	$1.27970 \cdot 10^{-6}$	$3.62769 \cdot 10^{-6}$	$4.92116 \cdot 10^{-6}$	$4.74912 \cdot 10^{-7}$	$6.11924 \cdot 10^{-7}$
v_2	$-3.26820 \cdot 10^{-9}$	$-9.66290 \cdot 10^{-9}$	$-1.45150 \cdot 10^{-8}$	$-2.87350 \cdot 10^{-10}$	$-9.41330 \cdot 10^{-10}$
v_3	$7.70669 \cdot 10^{-12}$	$1.26417 \cdot 10^{-11}$	$1.81140 \cdot 10^{-11}$	$2.68116 \cdot 10^{-12}$	$3.25320 \cdot 10^{-12}$
a_0	$-4.64460 \cdot 10^{-4}$	$-1.69790 \cdot 10^{-7}$	$1.08783 \cdot 10^{-4}$	$5.34912 \cdot 10^{-5}$	$-8.70930 \cdot 10^{-5}$
a_1	$4.89285 \cdot 10^{-6}$	$7.42210 \cdot 10^{-7}$	$-8.82410 \cdot 10^{-9}$	$2.35986 \cdot 10^{-7}$	$1.12309 \cdot 10^{-6}$
a_2	$-1.52620 \cdot 10^{-8}$	$-3.01660 \cdot 10^{-9}$	$-1.59760 \cdot 10^{-9}$	$-1.69380 \cdot 10^{-9}$	$-3.29510 \cdot 10^{-9}$
a_3	$1.64268 \cdot 10^{-11}$	$4.20008 \cdot 10^{-12}$	$3.59141 \cdot 10^{-12}$	$3.02230 \cdot 10^{-12}$	$3.54341 \cdot 10^{-12}$
b_0	$2.92765 \cdot 10^{2}$	$3.08150 \cdot 10^{2}$	$3.55633 \cdot 10^{2}$	$3.28908 \cdot 10^{2}$	$2.47196 \cdot 10^{2}$
b_1	-1.30970	-1.40472	-1.67653	-1.52498	-1.02535
b_2	$1.53830 \cdot 10^{-3}$	$1.67734 \cdot 10^{-3}$	$2.06594 \cdot 10^{-3}$	$1.85504 \cdot 10^{-3}$	$1.10066 \cdot 10^{-3}$
c	$6.22822 \cdot 10^{-8}$	$7.17546 \cdot 10^{-8}$	$5.71788 \cdot 10^{-8}$	$5.66787 \cdot 10^{-8}$	$4.66203 \cdot 10^{-8}$
deviations[a]					
AD% for ρ	$9.17 \cdot 10^{-4}$	$1.27 \cdot 10^{-3}$	$-2.21 \cdot 10^{-3}$	$-6.91 \cdot 10^{-4}$	$-2.84 \cdot 10^{-3}$
AAD% for ρ	$8.03 \cdot 10^{-3}$	$4.93 \cdot 10^{-3}$	$7.11 \cdot 10^{-3}$	$6.49 \cdot 10^{-3}$	$5.22 \cdot 10^{-3}$
MD% for ρ	$1.90 \cdot 10^{-2}$	$1.33 \cdot 10^{-2}$	$1.52 \cdot 10^{-2}$	$1.08 \cdot 10^{-2}$	$7.51 \cdot 10^{-3}$
AD% for c	$3.90 \cdot 10^{-2}$	$-1.92 \cdot 10^{-2}$	$8.95 \cdot 10^{-2}$	$1.48 \cdot 10^{-2}$	$3.95 \cdot 10^{-4}$
AAD% for c	$2.94 \cdot 10^{-1}$	$1.66 \cdot 10^{-1}$	$2.11 \cdot 10^{-1}$	$1.84 \cdot 10^{-1}$	$1.72 \cdot 10^{-1}$
MD% for c	$5.88 \cdot 10^{-1}$	$2.45 \cdot 10^{-1}$	$6.23 \cdot 10^{-1}$	$3.51 \cdot 10^{-1}$	$3.57 \cdot 10^{-1}$

[a]AD = average deviation; AAD = absolute average deviation; MD = maximum deviation.

The values of the densities, ρ, calculated from the integration of speed of sound measurements are listed in Table 10.

Table 10. Values of densities, ρ, at temperatures T and at pressures P determined from the integration of speed of sound measurements for the mixture x HFE-7500 + (*1*-x) Diisopropyl ether[a].

x	P / MPa	T / K						
		293.15	303.15	313.15	323.15	333.15	343.15	353.15
		ρ / g·cm^{-3}						
0.250	0.1	1.0532	1.0381	1.0226	1.0067	0.9905		
	10.0	1.0709	1.0573	1.0435	1.0294	1.0152	1.0008	0.9863
	20.0	1.0861	1.0736	1.0610	1.0482	1.0353	1.0222	1.0091
	30.0	1.0994	1.0878	1.0761	1.0642	1.0521	1.0401	1.0279
	40.0	1.1114	1.1005	1.0894	1.0782	1.0668	1.0555	1.0441
	50.0	1.1222	1.1119	1.1014	1.0907	1.0799	1.0691	1.0583
	60.0	1.1323	1.1224	1.1123	1.1021	1.0918	1.0814	1.0711
	70.0	1.1416	1.1321	1.1224	1.1126	1.1026	1.0927	1.0828
	80.0	1.1503	1.1412	1.1318	1.1223	1.1127	1.1031	1.0936
	90.0	1.1584	1.1497	1.1406	1.1314	1.1221	1.1128	1.1036
	100.0	1.1662	1.1577	1.1490	1.1400	1.1309	1.1219	1.1130
0.375	0.1	1.1784	1.1615	1.1446	1.1275	1.1104	1.0930	
	10.0	1.1982	1.1829	1.1677	1.1527	1.1377	1.1227	1.1077
	20.0	1.2154	1.2011	1.1871	1.1733	1.1597	1.1462	1.1327
	30.0	1.2304	1.2169	1.2037	1.1909	1.1782	1.1657	1.1532
	40.0	1.2439	1.2310	1.2185	1.2063	1.1943	1.1826	1.1708
	50.0	1.2562	1.2438	1.2317	1.2201	1.2087	1.1975	1.1864
	60.0	1.2675	1.2555	1.2439	1.2326	1.2217	1.2110	1.2003
	70.0	1.2781	1.2663	1.2551	1.2442	1.2336	1.2233	1.2130
	80.0	1.2880	1.2765	1.2655	1.2549	1.2447	1.2347	1.2248
	90.0	1.2973	1.2861	1.2753	1.2650	1.2551	1.2453	1.2358
	100.0	1.3062	1.2951	1.2846	1.2745	1.2648	1.2553	1.2460
0.500	0.1	1.2895	1.2715	1.2534	1.2350	1.2163	1.1971	
	10.0	1.3109	1.2946	1.2784	1.2622	1.2459	1.2295	1.2127
	20.0	1.3295	1.3142	1.2993	1.2845	1.2698	1.2550	1.2400
	30.0	1.3458	1.3313	1.3173	1.3035	1.2899	1.2763	1.2625
	40.0	1.3605	1.3466	1.3332	1.3201	1.3073	1.2946	1.2817
	50.0	1.3739	1.3604	1.3475	1.3350	1.3228	1.3107	1.2986
	60.0	1.3862	1.3730	1.3605	1.3485	1.3368	1.3253	1.3138
	70.0	1.3976	1.3848	1.3726	1.3609	1.3497	1.3386	1.3276

	80.0	1.4084	1.3957	1.3838	1.3725	1.3616	1.3509	1.3404
	90.0	1.4185	1.4061	1.3943	1.3833	1.3727	1.3624	1.3522
	100.0	1.4281	1.4158	1.4043	1.3934	1.3831	1.3732	1.3633
0.625	0.1	1.3913	1.3719	1.3522	1.3323	1.3121	1.2918	1.2712
	10.0	1.4139	1.3962	1.3785	1.3608	1.3432	1.3255	1.3079
	20.0	1.4334	1.4170	1.4006	1.3843	1.3682	1.3523	1.3365
	30.0	1.4506	1.4350	1.4196	1.4043	1.3894	1.3746	1.3599
	40.0	1.4660	1.4511	1.4363	1.4219	1.4077	1.3938	1.3801
	50.0	1.4801	1.4656	1.4514	1.4376	1.4241	1.4108	1.3978
	60.0	1.4930	1.4790	1.4652	1.4519	1.4389	1.4262	1.4137
	70.0	1.5051	1.4914	1.4780	1.4650	1.4524	1.4402	1.4283
	80.0	1.5164	1.5029	1.4899	1.4772	1.4650	1.4532	1.4417
	90.0	1.5270	1.5138	1.5010	1.4887	1.4768	1.4653	1.4542
	100.0	1.5371	1.5241	1.5115	1.4994	1.4878	1.4767	1.4659
0.750	0.1	1.4784	1.4586	1.4385	1.4181	1.3974	1.3764	1.3551
	10.0	1.5015	1.4836	1.4656	1.4475	1.4293	1.4111	1.3929
	20.0	1.5215	1.5049	1.4884	1.4718	1.4552	1.4388	1.4225
	30.0	1.5390	1.5235	1.5080	1.4925	1.4771	1.4618	1.4468
	40.0	1.5546	1.5400	1.5253	1.5107	1.4961	1.4818	1.4677
	50.0	1.5689	1.5549	1.5409	1.5269	1.5131	1.4995	1.4861
	60.0	1.5820	1.5686	1.5551	1.5417	1.5285	1.5154	1.5026
	70.0	1.5942	1.5812	1.5683	1.5554	1.5426	1.5300	1.5177
	80.0	1.6056	1.5931	1.5805	1.5680	1.5556	1.5435	1.5316
	90.0	1.6163	1.6042	1.5920	1.5798	1.5678	1.5560	1.5445
	100.0	1.6265	1.6147	1.6028	1.5910	1.5793	1.5678	1.5566

[a] Standard uncertainties u are $u(T) = 0.1$ K, $u(P) = 0.01$ MPa. The combined expanded uncertainty U_c (level of confidence = 0.95) is $U_c(\rho) = 0.001\rho$.

For the compressibilities, that is, the isentropic compressibility, κ_S, and the isothermal compressibility, κ_T, a comparison between the calculated values and those given by the correlation established by equations (9) and (10) have been carried out for all the molar compositions, and adding the two pure compounds with reference to our previous papers [20 and 21] since they were measured previously. Figure 3 shows the good agreement between the isentropic compressibility values given by the correlation, and those calculated from experimental speed of sound data. As expected, watching the two graphs in which (a) gives values at 293.15 K and (b) shows the comparison at 353.15 K, isentropic compressibility values increase when increasing temperature. Both graphs offer data at pressures equal to 0.1, 20, 40, 60, 80 and 100 MPa to study the effect of

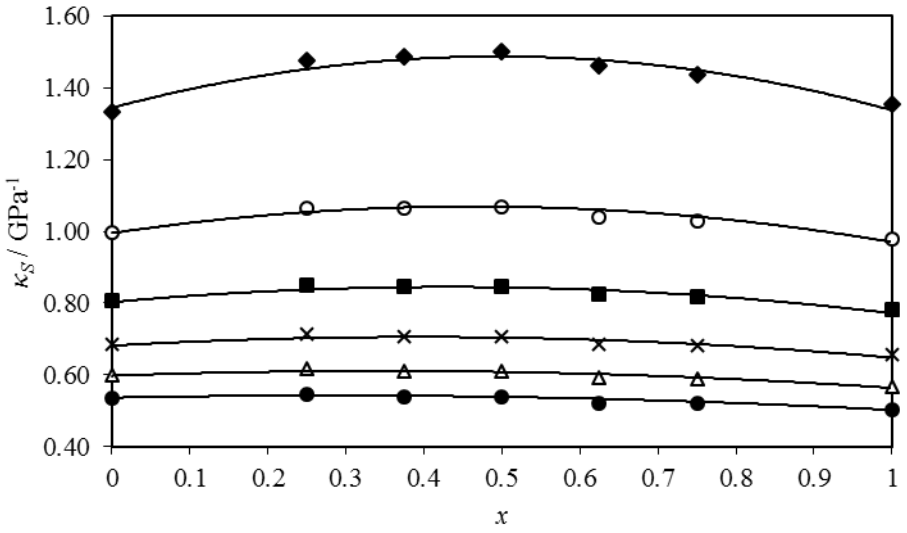

(a)

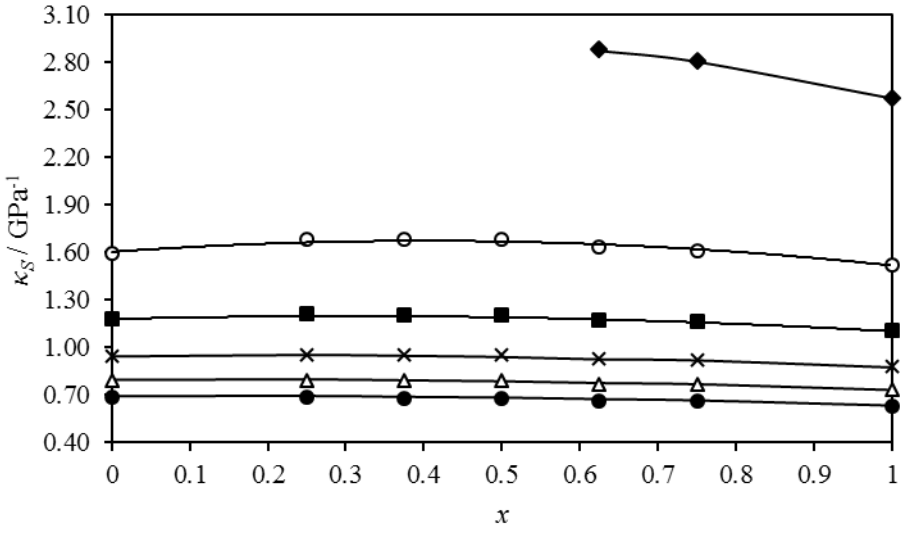

(b)

Figure 3. Values of isentropic compressibilities, κ_S for different mole fractions of x HFE-7500 + (*1*-x) Diisopropyl ether at (a) 293.15 K and (b) at 353.15 K. ♦; P = 0.1 MPa, ○; P = 20 MPa, ■; P = 40 MPa, ×; P = 60 MPa, Δ; P = 80 MPa, ●; P = 100 MPa. The solid line represents the correlation for κ_S given by equations (13) and (14) Mole fraction x = 0 comes from reference [20], and mole fraction x = 1 comes from reference [21].

pressure on isentropic compressibility. Taking a look to them, we may then assert than regardless of the temperature, isentropic compressibility values are higher at low pressures, so for our measurements, the higher values of isentropic compressibility are founded at 0.1 MPa. The

maximum deviations founded for the comparison show a MD% = 0.13 for Diisopropyl ether (x = 0) at 20 MPa and at 293.15 K, and a MD% = 0.12 also for Diisopropyl ether at 20 MPa at 353.15 K.

Table 11 shows the values of isothermal compressibility, κ_T calculated by using equations (9) and (10).

Table 11. Values of isothermal compressibility, κ_T at temperatures T and at pressures P calculated from equations (9) and (10) for the mixture x HFE-7500 + (*1*-x) Diisopropyl ether[a].

x	P / MPa	T / K						
		293.15	303.15	313.15	323.15	333.15	343.15	353.15
		κ_T / GPa^{-1}						
0.250	0.1	1.848	2.062	2.300	2.569	2.872		
	20.0	1.306	1.412	1.523	1.640	1.763	1.893	2.033
	40.0	1.024	1.090	1.157	1.225	1.295	1.369	1.447
	60.0	0.850	0.897	0.943	0.990	1.037	1.087	1.139
	80.0	0.733	0.768	0.803	0.838	0.873	0.909	0.948
	100.0	0.648	0.676	0.704	0.731	0.759	0.787	0.818
0.375	0.1	1.857	2.053	2.280	2.541	2.840	3.180	
	20.0	1.314	1.405	1.504	1.612	1.728	1.851	1.980
	40.0	1.033	1.087	1.144	1.204	1.269	1.336	1.406
	60.0	0.861	0.897	0.935	0.975	1.017	1.062	1.108
	80.0	0.745	0.771	0.799	0.828	0.858	0.891	0.925
	100.0	0.662	0.681	0.702	0.725	0.749	0.774	0.800
0.500	0.1	1.832	2.020	2.244	2.508	2.816	3.170	
	20.0	1.304	1.389	1.484	1.591	1.710	1.839	1.978
	40.0	1.027	1.074	1.128	1.187	1.253	1.324	1.400
	60.0	0.856	0.886	0.921	0.959	1.002	1.049	1.100
	80.0	0.740	0.761	0.785	0.812	0.843	0.878	0.916
	100.0	0.656	0.671	0.689	0.710	0.734	0.761	0.791
0.625	0.1	1.791	1.976	2.192	2.443	2.730	3.057	3.421
	20.0	1.272	1.358	1.452	1.556	1.668	1.789	1.917
	40.0	1.001	1.051	1.105	1.163	1.226	1.293	1.363
	60.0	0.835	0.868	0.903	0.942	0.983	1.027	1.074
	80.0	0.722	0.746	0.771	0.799	0.829	0.861	0.896
	100.0	0.641	0.659	0.678	0.699	0.722	0.748	0.775

0.750	0.1	1.727	1.911	2.119	2.356	2.627	2.938	3.297
	20.0	1.222	1.314	1.411	1.514	1.624	1.741	1.866
	40.0	0.959	1.016	1.074	1.135	1.197	1.262	1.330
	60.0	0.798	0.838	0.878	0.919	0.961	1.004	1.048
	80.0	0.688	0.718	0.749	0.779	0.810	0.841	0.873
	100.0	0.609	0.633	0.657	0.681	0.705	0.729	0.754

[a] Standard uncertainties u are $u(T) = 0.1$ K, $u(P) = 0.01$ MPa. The combined expanded uncertainty U_c (level of confidence = 0.95) is $U_c(\kappa_T) = 0.02\ \kappa_T$.

The comparison between the calculated values of κ_T and those given by the correlation has been represented in Figure 4. In Figure 4 (a) the κ_T values for all the compositions and at different pressures are shown for the temperature 293.15 K while in Figure 4 (b) the κ_T values at different pressures for the seven molar compositions are given at the temperature 353.15 K. Figure 4 (a) exhibits lower values of κ_T compared with Figure 4 (b) at the same pressures. According to the pressure, it can be seen for both graphs (a) and (b) that the higher values for κ_T are found at lower pressures, being the increase in the κ_T values higher when the lower pressures are reached. The higher deviations are found for pure Diisopropyl ether ($x = 0$) at 20 MPa for both temperatures, with a MD% = $1.29 \cdot 10^{-2}$ at 293.15 K and a MD% = $1.18 \cdot 10^{-2}$ at 353.15 K, values which are in all cases below the combined expanded uncertainty (0.02 κ_T). For the isobaric expansion, α_P the values given by the correlation established employing equations (9) and (10) and the comparison from calculated values lead to a MD% = 4.72 at 293.15 K and at 100 MPa for a mole composition $x = 0.250$, and a MD% = 2.34 at 353.15 K. and at 100 MPa for a $x = 0.625$. These comparisons can be observed in Figure 5.

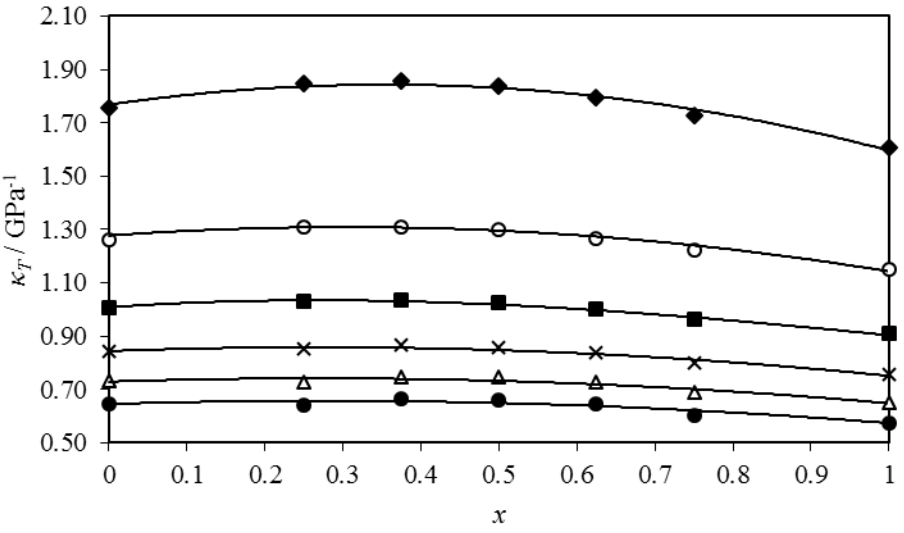

(a)

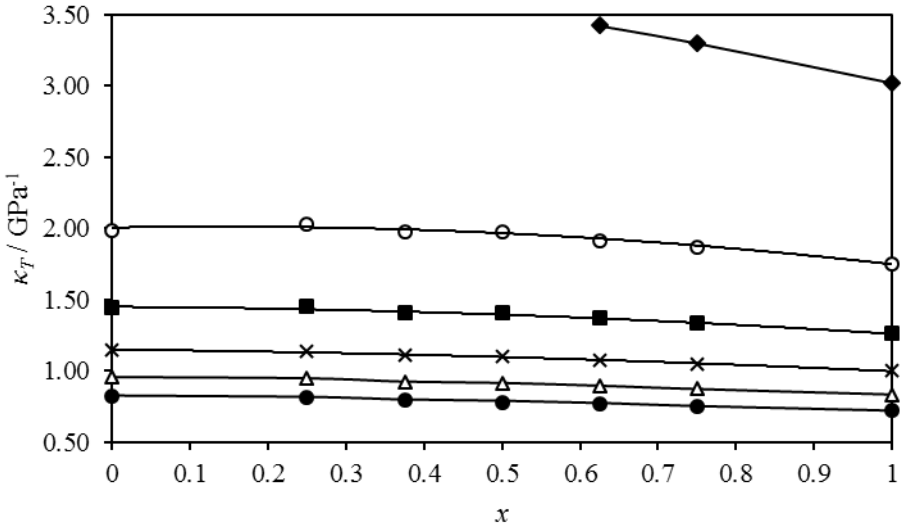

(b)

Figure 4. Values of isothermal compressibilities, κ_T for different mole fractions of x HFE-7500 + (*1-x*) Diisopropyl ether at (a) 293.15 K and (b) at 353.15 K. ♦; P = 0.1 MPa, ○; P = 20 MPa, ■; P = 40 MPa, ×; P = 60 MPa, Δ; P = 80 MPa, ●; P = 100 MPa. The solid line represents the correlation for κ_T given by equations (13) and (14) Mole fraction x = 0 comes from reference [20], and mole fraction x = 1 comes from reference [21].

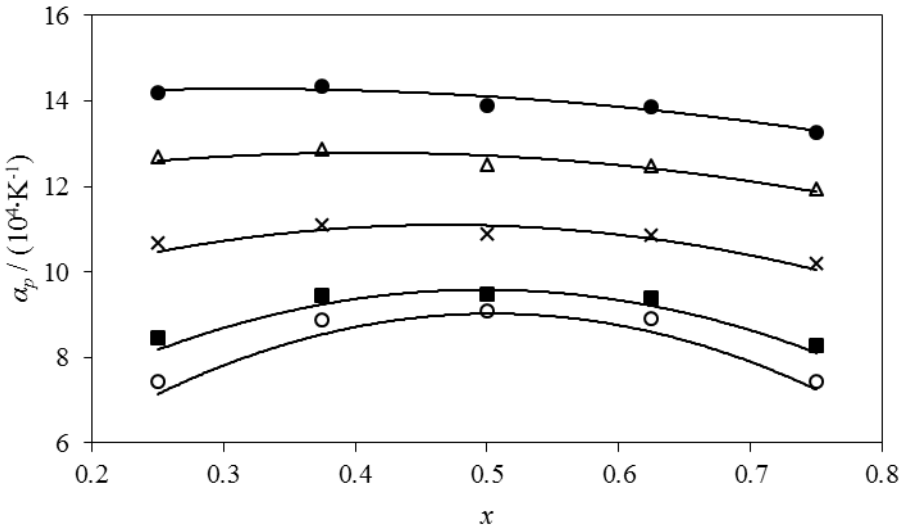

(a)

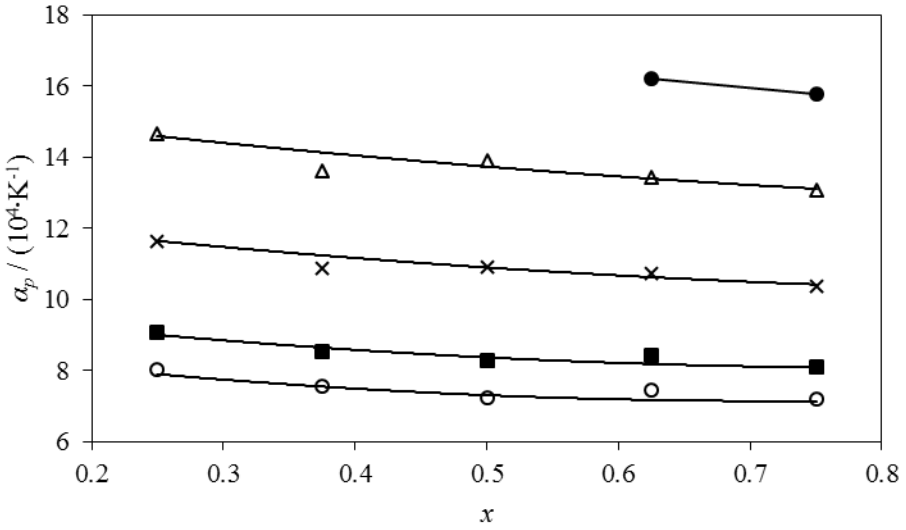

(b)

Figure 5. Values of isobaric expansion α_p as a function of molar compositions, x_1 at (a) 293.15 K and (b) 353.15 K of binary mixtures *x* HFE-7500 + (*1*-*x*) Diisopropyl ether. ●; 0.1 MPa, Δ; 10 MPa, x; 30 MPa, ■; 70 MPa, ○; 100 MPa. The solid line represents the correlation for α_p given by eqs (13) and (14).

The speed of sound data obtained by employing the correlation given by equations (9) and (10) are plotted in Figure 6 together with the speed of sound values obtained experimentally so that the good fitting provided from the calculated data to the experimental ones can be observed. In this figure, values of speed of sound, *c*, versus the mole fraction at different pressures are plotted at 293.15 K (a), and at 353.15 K (b). At a first sight it can be stated that speed of sound values are lower at low pressures. The speed of sound in the liquid has an inversely proportional dependence on density and on isentropic compressibility, so when temperature increases, the values of speed of sound decrease. This statement can be observed in Figure 6 by comparing graphs (a) and (b).

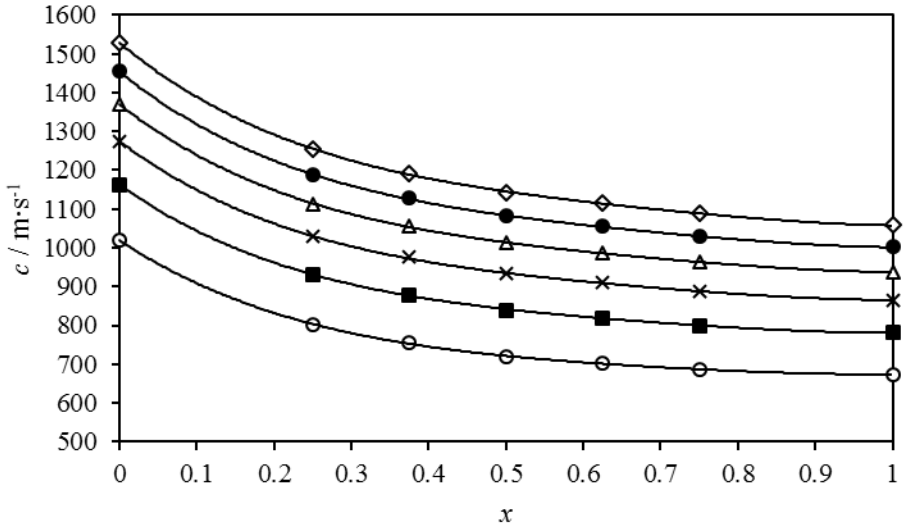

(a)

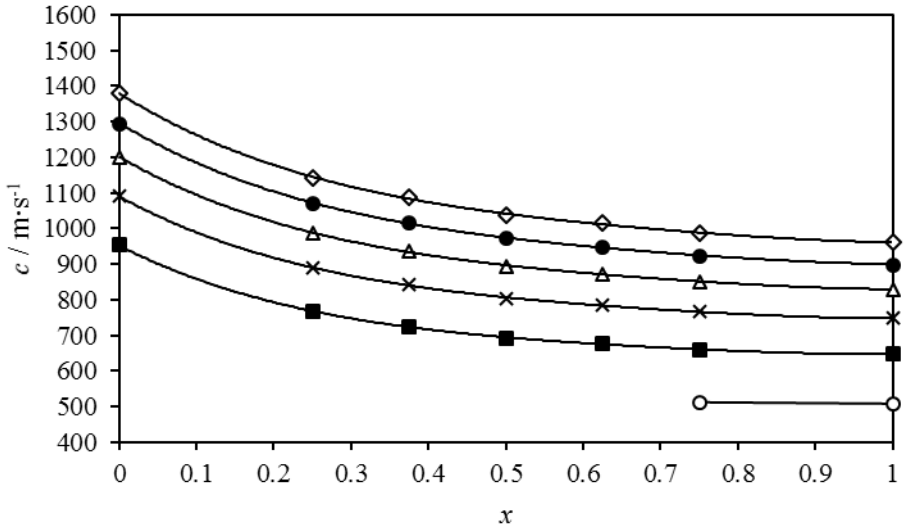

(b)

Figure 6. Comparison between sound velocities, *c* for different mole fractions of *x* HFE-7500 + (*1-x*) Diisopropyl ether evaluated from equation (1), (line) and values from experimental measurements vs. the mole fraction, *x* at (a) 293.15 K and (b) at 353.15 K. ○; *P* = 0.1 MPa, ■; *P* = 20 MPa, ×; *P* = 40 MPa, Δ; *P* = 60 MPa, ●; *P* = 80 MPa, ◊; *P* = 100 MPa. Mole fraction *x* = 0 comes from reference [20], and mole fraction *x* = 1 comes from reference [21].

Experimental density measurements using a U-tube densitometer were carried out for the five mole fractions along 11 isotherms in the temperature interval from (293.15 to 393.15) K and in the pressure range from (0.1 to 140) MPa at every 10 MPa. These density data are listed in Table 12. In the same way at it was done for speed of sound measurements, a limit in temperature was fixed in order to ensure liquid state for all the molar compositions. Due to this, no density

measurements were performed at temperatures 343.15 K or higher at x = 0.250, no measurements were carried out at temperatures 353.15 K and above for the mole fractions x = 0.375 and x = 0.500, and no measurements were done at temperatures 363.15 K and higher at x = 0.625 and at x = 0.750. No experimental density data were found in the literature for this binary mixture. A comparison between those values of density given by the integration of speed of sound and the experimental ones vs. the pressure at 293.15 K and at 353.15 K for all the mole fractions considered and for the two pure compounds can be seen in Figure 7.

Table 12. Values of densities, ρ, at temperatures T and at pressures P measured by using a U-tube densitometer for the mixture x HFE-7500 + (*1*-x) Diisopropyl ether[a].

x	P / MPa	T / K					
		293.15	303.15	313.15	323.15	333.15	343.15
		ρ / g·cm^{-3}					
0.250	0.1	1.0532	1.0383	1.0224	1.0067	0.9905	
	10.0	1.0710	1.0572	1.0429	1.0290	1.0149	1.0006
	20.0	1.0861	1.0736	1.0603	1.0475	1.0347	1.0219
	30.0	1.0994	1.0877	1.0753	1.0633	1.0515	1.0396
	40.0	1.1112	1.1003	1.0885	1.0772	1.0662	1.0552
	50.0	1.1221	1.1117	1.1005	1.0897	1.0793	1.0688
	60.0	1.1321	1.1221	1.1114	1.1010	1.0911	1.0811
	70.0	1.1415	1.1318	1.1215	1.1115	1.1019	1.0924
	80.0	1.1502	1.1408	1.1309	1.1211	1.1120	1.1028
	90.0	1.1584	1.1493	1.1397	1.1302	1.1214	1.1125
	100.0	1.1662	1.1573	1.1480	1.1388	1.1303	1.1215
	110.0	1.1735	1.1649	1.1560	1.1469	1.1385	1.1301
	120.0	1.1807	1.1721	1.1633	1.1545	1.1464	1.1382
	130.0	1.1874	1.1788	1.1704	1.1617	1.1539	1.1459
	140.0	1.1938	1.1854	1.1772	1.1687	1.1609	1.1533
0.375	0.1	1.1783	1.1618	1.1445	1.1272	1.1095	1.0914
	10.0	1.1979	1.1830	1.1677	1.1523	1.1370	1.1213
	20.0	1.2149	1.2012	1.1872	1.1730	1.1592	1.1451
	30.0	1.2298	1.2170	1.2039	1.1905	1.1779	1.1648
	40.0	1.2431	1.2311	1.2186	1.2061	1.1942	1.1821
	50.0	1.2552	1.2438	1.2320	1.2200	1.2088	1.1973
	60.0	1.2663	1.2554	1.2441	1.2326	1.2220	1.2109
	70.0	1.2768	1.2662	1.2550	1.2442	1.2340	1.2234

	80.0	1.2864	1.2761	1.2654	1.2550	1.2449	1.2349
	90.0	1.2955	1.2855	1.2753	1.2651	1.2554	1.2457
	100.0	1.3043	1.2943	1.2844	1.2745	1.2651	1.2558
	110.0	1.3124	1.3028	1.2932	1.2835	1.2742	1.2653
	120.0	1.3203	1.3108	1.3013	1.2919	1.2829	1.2742
	130.0	1.3278	1.3184	1.3094	1.2999	1.2912	1.2827
	140.0	1.3351	1.3259	1.3168	1.3077	1.2990	1.2907
0.500	0.1	1.2895	1.2716	1.2534	1.2350	1.2165	1.1970
	10.0	1.3106	1.2945	1.2783	1.2620	1.2459	1.2292
	20.0	1.3289	1.3141	1.2992	1.2842	1.2698	1.2547
	30.0	1.3449	1.3311	1.3172	1.3032	1.2900	1.2759
	40.0	1.3593	1.3463	1.3331	1.3199	1.3075	1.2944
	50.0	1.3724	1.3600	1.3474	1.3349	1.3232	1.3108
	60.0	1.3844	1.3726	1.3605	1.3485	1.3373	1.3254
	70.0	1.3956	1.3842	1.3726	1.3610	1.3503	1.3389
	80.0	1.4061	1.3951	1.3838	1.3725	1.3623	1.3513
	90.0	1.4160	1.4052	1.3943	1.3834	1.3735	1.3628
	100.0	1.4253	1.4148	1.4042	1.3937	1.3840	1.3735
	110.0	1.4341	1.4239	1.4137	1.4032	1.3939	1.3838
	120.0	1.4426	1.4326	1.4224	1.4124	1.4032	1.3933
	130.0	1.4507	1.4408	1.4310	1.4211	1.4121	1.4025
	140.0	1.4583	1.4487	1.4390	1.4294	1.4205	1.4112
0.625	0.1	1.3912	1.3724	1.3518	1.3322	1.3123	1.2918
	10.0	1.4136	1.3966	1.3781	1.3608	1.3433	1.3256
	20.0	1.4328	1.4173	1.4001	1.3842	1.3685	1.3524
	30.0	1.4499	1.4353	1.4192	1.4043	1.3898	1.3748
	40.0	1.4651	1.4513	1.4360	1.4219	1.4084	1.3944
	50.0	1.4790	1.4658	1.4511	1.4376	1.4249	1.4117
	60.0	1.4917	1.4792	1.4649	1.4520	1.4399	1.4273
	70.0	1.5037	1.4914	1.4777	1.4651	1.4537	1.4414
	80.0	1.5147	1.5028	1.4896	1.4773	1.4664	1.4546
	90.0	1.5251	1.5136	1.5007	1.4888	1.4784	1.4668
	100.0	1.5350	1.5237	1.5111	1.4996	1.4894	1.4782
	110.0	1.5443	1.5333	1.5212	1.5098	1.4999	1.4891
	120.0	1.5532	1.5424	1.5306	1.5195	1.5097	1.4993
	130.0	1.5618	1.5512	1.5395	1.5287	1.5192	1.5091

	140.0	1.5699	1.5595	1.5481	1.5374	1.5281	1.5182
0.750	0.1	1.4784	1.4587	1.4384	1.4181	1.3975	1.3763
	10.0	1.5014	1.4837	1.4654	1.4474	1.4293	1.4111
	20.0	1.5214	1.5051	1.4881	1.4717	1.4553	1.4388
	30.0	1.5390	1.5238	1.5078	1.4925	1.4773	1.4620
	40.0	1.5548	1.5404	1.5253	1.5107	1.4966	1.4823
	50.0	1.5692	1.5555	1.5410	1.5272	1.5138	1.5003
	60.0	1.5824	1.5693	1.5554	1.5422	1.5294	1.5165
	70.0	1.5948	1.5821	1.5687	1.5559	1.5437	1.5313
	80.0	1.6063	1.5940	1.5811	1.5687	1.5569	1.5449
	90.0	1.6171	1.6052	1.5926	1.5806	1.5693	1.5576
	100.0	1.6273	1.6158	1.6035	1.5919	1.5809	1.5695
	110.0	1.6371	1.6258	1.6140	1.6025	1.5918	1.5808
	120.0	1.6464	1.6353	1.6236	1.6125	1.6021	1.5914
	130.0	1.6553	1.6444	1.6330	1.6221	1.6119	1.6016
	140.0	1.6638	1.6531	1.6419	1.6313	1.6212	1.6112

Table 12. (Continuation).

x	P / MPa	T / K				
		353.15	363.15	373.15	383.15	393.15
		ρ / g·cm^{-3}				
0.250	0.1					
	10.0	0.9865	0.9722	0.9575	0.9428	0.9279
	20.0	1.0093	0.9968	0.9838	0.9713	0.9584
	30.0	1.0282	1.0168	1.0050	0.9938	0.9821
	40.0	1.0444	1.0338	1.0228	1.0126	1.0018
	50.0	1.0587	1.0487	1.0384	1.0289	1.0187
	60.0	1.0716	1.0620	1.0523	1.0432	1.0337
	70.0	1.0833	1.0741	1.0648	1.0562	1.0472
	80.0	1.0942	1.0852	1.0763	1.0681	1.0593
	90.0	1.1041	1.0955	1.0869	1.0790	1.0708
	100.0	1.1134	1.1051	1.0969	1.0892	1.0813
	110.0	1.1221	1.1142	1.1061	1.0987	1.0910
	120.0	1.1304	1.1227	1.1148	1.1077	1.1003
	130.0	1.1383	1.1307	1.1231	1.1161	1.1089
	140.0	1.1456	1.1384	1.1308	1.1242	1.1170

0.375	0.1					
	10.0	1.1056	1.0896	1.0740	1.0580	1.0416
	20.0	1.1312	1.1171	1.1036	1.0896	1.0757
	30.0	1.1523	1.1393	1.1272	1.1147	1.1022
	40.0	1.1702	1.1581	1.1471	1.1356	1.1240
	50.0	1.1860	1.1748	1.1643	1.1536	1.1427
	60.0	1.2003	1.1896	1.1797	1.1695	1.1593
	70.0	1.2133	1.2030	1.1937	1.1840	1.1743
	80.0	1.2252	1.2155	1.2064	1.1972	1.1877
	90.0	1.2362	1.2270	1.2183	1.2093	1.2004
	100.0	1.2466	1.2375	1.2292	1.2206	1.2119
	110.0	1.2563	1.2475	1.2396	1.2312	1.2228
	120.0	1.2654	1.2571	1.2493	1.2413	1.2330
	130.0	1.2742	1.2659	1.2583	1.2506	1.2426
	140.0	1.2824	1.2746	1.2670	1.2596	1.2516
0.500	0.1					
	10.0	1.2129	1.1964	1.1796	1.1626	1.1451
	20.0	1.2401	1.2256	1.2109	1.1963	1.1812
	30.0	1.2627	1.2493	1.2360	1.2230	1.2094
	40.0	1.2819	1.2695	1.2572	1.2454	1.2327
	50.0	1.2988	1.2873	1.2758	1.2647	1.2528
	60.0	1.3142	1.3031	1.2922	1.2818	1.2705
	70.0	1.3281	1.3175	1.3072	1.2972	1.2865
	80.0	1.3409	1.3308	1.3208	1.3113	1.3008
	90.0	1.3527	1.3431	1.3335	1.3243	1.3144
	100.0	1.3638	1.3545	1.3453	1.3363	1.3268
	110.0	1.3742	1.3653	1.3562	1.3476	1.3384
	120.0	1.3841	1.3754	1.3666	1.3583	1.3494
	130.0	1.3935	1.3850	1.3764	1.3681	1.3597
	140.0	1.4024	1.3942	1.3857	1.3779	1.3693
0.625	0.1	1.2712				
	10.0	1.3082	1.2903	1.2723	1.2542	1.2359
	20.0	1.3370	1.3212	1.3053	1.2897	1.2738
	30.0	1.3608	1.3464	1.3318	1.3178	1.3034
	40.0	1.3812	1.3678	1.3542	1.3415	1.3280
	50.0	1.3992	1.3866	1.3738	1.3619	1.3491

	60.0	1.4155	1.4034	1.3912	1.3799	1.3680
	70.0	1.4303	1.4186	1.4070	1.3963	1.3851
	80.0	1.4439	1.4326	1.4215	1.4114	1.4003
	90.0	1.4565	1.4456	1.4350	1.4250	1.4147
	100.0	1.4682	1.4578	1.4474	1.4378	1.4280
	110.0	1.4792	1.4691	1.4591	1.4498	1.4401
	120.0	1.4897	1.4798	1.4701	1.4612	1.4516
	130.0	1.4997	1.4900	1.4805	1.4718	1.4625
	140.0	1.5090	1.4997	1.4904	1.4819	1.4729
0.750	0.1	1.3551				
	10.0	1.3930	1.3744	1.3558	1.3367	1.3178
	20.0	1.4227	1.4062	1.3898	1.3731	1.3567
	30.0	1.4474	1.4321	1.4173	1.4020	1.3873
	40.0	1.4685	1.4543	1.4405	1.4265	1.4128
	50.0	1.4873	1.4738	1.4608	1.4476	1.4348
	60.0	1.5042	1.4912	1.4789	1.4664	1.4542
	70.0	1.5195	1.5070	1.4953	1.4833	1.4717
	80.0	1.5337	1.5215	1.5103	1.4988	1.4875
	90.0	1.5468	1.5349	1.5243	1.5131	1.5024
	100.0	1.5590	1.5474	1.5372	1.5264	1.5160
	110.0	1.5704	1.5593	1.5494	1.5388	1.5287
	120.0	1.5814	1.5704	1.5608	1.5507	1.5407
	130.0	1.5917	1.5809	1.5716	1.5617	1.5521
	140.0	1.6014	1.5910	1.5818	1.5723	1.5627

[a] Standard uncertainties u are $u(T) = 0.1$ K, $u(P) = 0.01$ MPa. The combined expanded uncertainty U_c (level of confidence = 0.95) is $U_c(\rho) = 0.5$ kg·m^{-3}. The expanded uncertainty in the composition of the mixtures is $U_c(x) = 6 \cdot 10^{-5}$ in mole fraction.

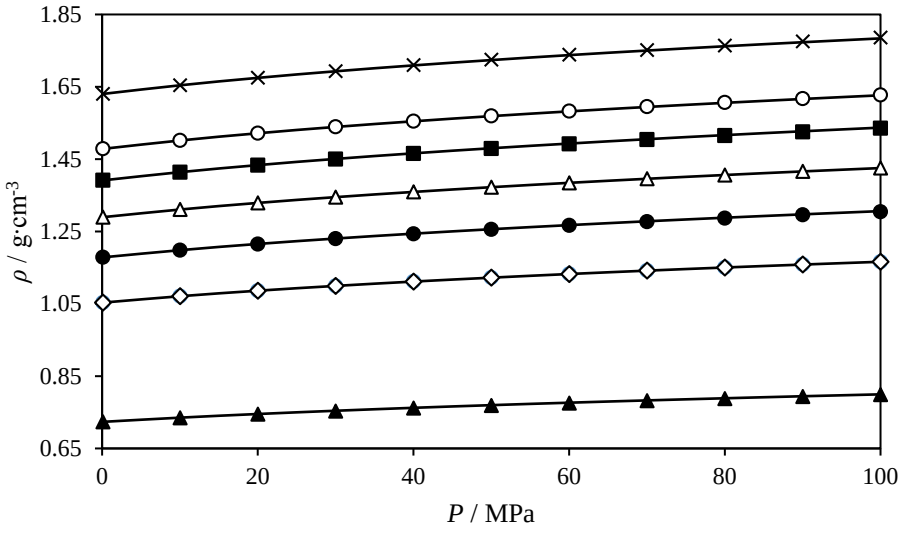

(a)

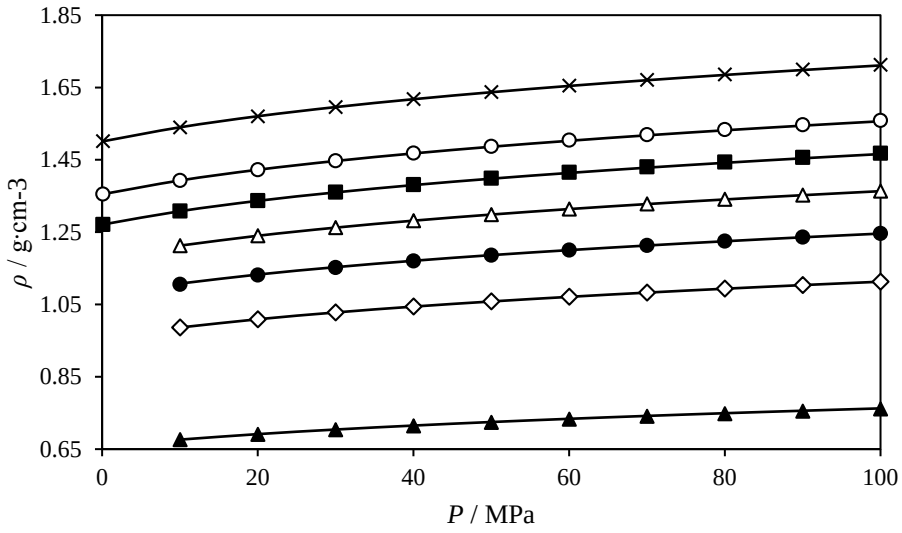

(b)

Figure 7. Comparison between densities, ρ for different mole fractions of x HFE-7500 + (*1-x*) Diisopropyl ether evaluated from speed of sound integration (line) and measured from a U-tube densimeter vs. the pressure, P at (a) 293.15 K and (b) at 353.15 K. ▲; x = 0 (from reference [20]), ◊; x = 0.250, ●; x = 0.375, Δ; x = 0.500, ■; x = 0.625, ○; x = 0.750, ×; x = 1 (from reference [21]).

Figure 8 shows the deviations between the values of density measured with the vibrating tube densitometer and the density data calculated from the integration of speed of sound measurements in the range of pressures from (0.1 to 100) MPa and at 353.15 K for the five molar compositions. While a dependence in pressure can be observed, there is a good consistency between the

experimental data and the calculations since the worst deviation datum at 293.15 K has a MD = 0.20% at 100 MPa for the mole fraction x = 0.500, and a maximum deviation MD = -0.19% at 10 MPa for the mole fraction x = 0.375 is given.

Complementary to these calculations, the experimental high pressure density values were correlated over the entire pressure and temperature ranges by means of a Tait-like equation, which was used in our previous works [21] and [31 and 32]:

$$\rho(T,p) = \frac{\rho_0(T)}{1 - C\ln\left(\frac{B(T) + p}{B(T) + 0.1\ \mathrm{MPa}}\right)} \tag{12}$$

where:

$$\rho_0(T) = A_0 + A_1 T + A_2 T^2 + A_3 T^3 \tag{13}$$

$$B(T) = B_0 + B_1 T + B_2 T^2 \tag{14}$$

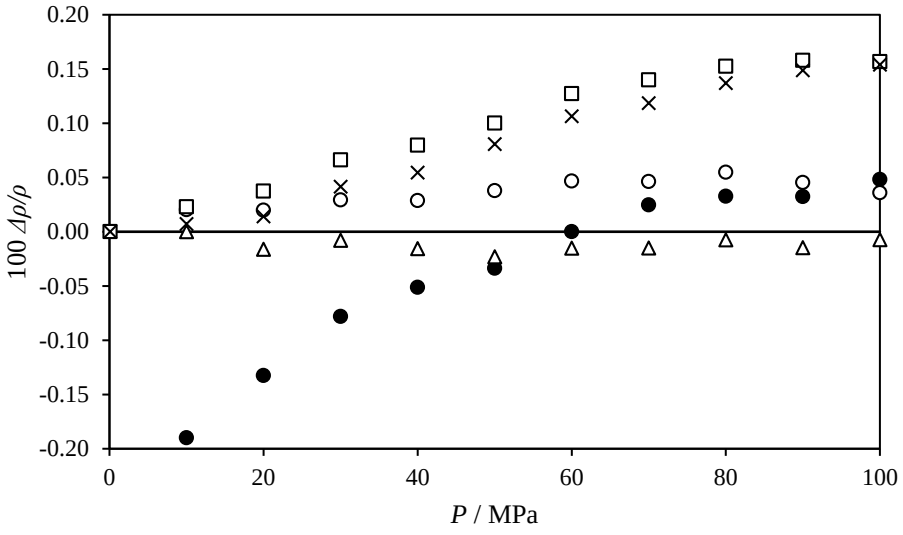

Figure 8. Deviations between the measured densities and the calculated values, $\Delta\rho/\rho$ = [ρ(exp) – ρ(cal)]/ρ(exp) at different mole fractions for the binary system x HFE-7500 + (*1-x*) Diisopropyl ether at 353.15 K. ○; x = 0.250, ●; x = 0.375, Δ; x = 0.500, □; x = 0.625, x; x = 0.750.

By correlating the experimental density values, the eight adjustable parameters of the Tait equation were then obtained. These A_i, B_i and C parameters and their deviations (AD%, AAD% and MD%) for the five molar compositions and for the pure components are listed in Table 13. Two graphs in which the experimental density values and those calculated by the Tait-like equation versus the pressure, P, at 293.15 K (a) and at 393.15 K (b) can be seen in Figure 9. In the same way, Figure 9 shows also two graphs with the experimental density values and the values obtained by the correlation, versus the temperature, T, at 10 MPa (c) and at 140 MPa (d). For all the representations, it can be stated that the Tait-like equation matches perfectly the experimental high pressure density values for the studied mixture.

Table 13. Obtained parameters and deviations for density correlation by using equations (12) to (14) for x HFE-7500 + (1-x) Diisopropyl ether.

Parameters	x				
	0.250	0.375	0.500	0.625	0.750
A_0 / g cm^{-3}	1.552196	1.740680	1.876771	2.238997	2.069813
A_1 / g cm^{-3} K^{-1}	$-2.396749\cdot10^{-3}$	$-2.800415\cdot10^{-3}$	$-2.834359\cdot10^{-3}$	$-4.890069\cdot10^{-3}$	$-2.563328\cdot10^{-3}$
A_2 / g cm^{-3} K^{-2}	$4.106381\cdot10^{-6}$	$5.124040\cdot10^{-6}$	$4.836268\cdot10^{-6}$	$1.038079\cdot10^{-5}$	$3.489773\cdot10^{-6}$
A_3 / g cm^{-3} K^{-3}	$-5.908088\cdot10^{-9}$	$-7.199597\cdot10^{-9}$	$-6.823930\cdot10^{-9}$	$-1.214350\cdot10^{-8}$	$-5.546330\cdot10^{-9}$
B_0 / MPa	299.1508	289.9261	284.6317	287.9135	294.0110
B_1 / MPa K^{-1}	-1.232389	-1.185106	-1.160436	-1.171328	-1.201497
B_2 / MPa K^{-2}	$1.290638\cdot10^{-3}$	$1.229045\cdot10^{-3}$	$1.204028\cdot10^{-3}$	$1.212723\cdot10^{-3}$	$1.255013\cdot10^{-3}$
C	0.08690060	0.08594350	0.08479067	0.08407787	0.08316717
AAD /(%)	0.02	0.02	0.02	0.02	0.02
MD /(%)	0.05	0.07	0.08	0.07	0.05
Bias /(%)	$-5.04\cdot10^{-5}$	$-6.94\cdot10^{-4}$	$-4.48\cdot10^{-5}$	$-4.27\cdot10^{-4}$	$-4.61\cdot10^{-5}$
σ /(g·cm^{-3})	$2.09\cdot10^{-1}$	$2.47\cdot10^{-1}$	$2.64\cdot10^{-1}$	$3.68\cdot10^{-1}$	$2.88\cdot10^{-1}$
RMSD /(g·cm^{-3})	$2.03\cdot10^{-1}$	$2.41\cdot10^{-1}$	$2.57\cdot10^{-1}$	$3.58\cdot10^{-1}$	$8.48\cdot10^{-2}$

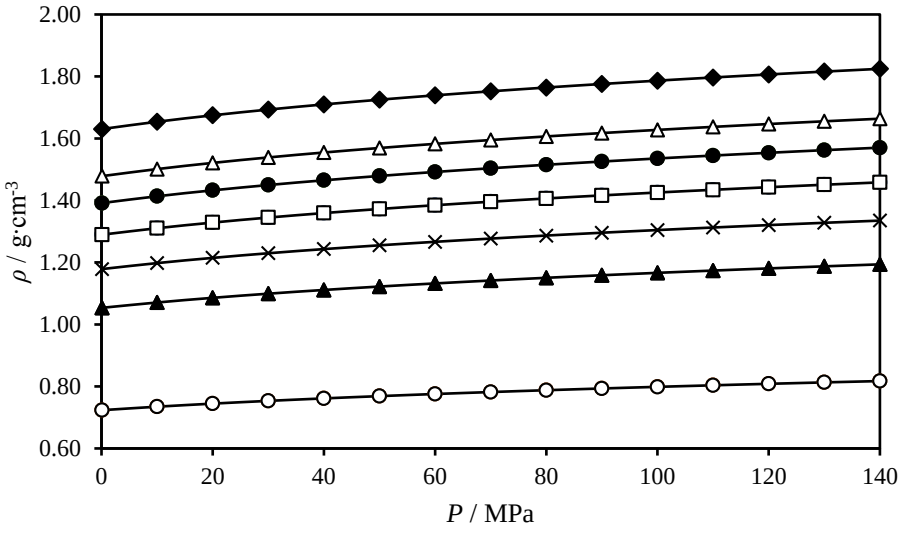
2.00
1.80
1.60
1.40
1.20
1.00
0.80
0.60
ρ / g·cm-3
0
20
40
60
80
100
120
140
P / MPa

(a)

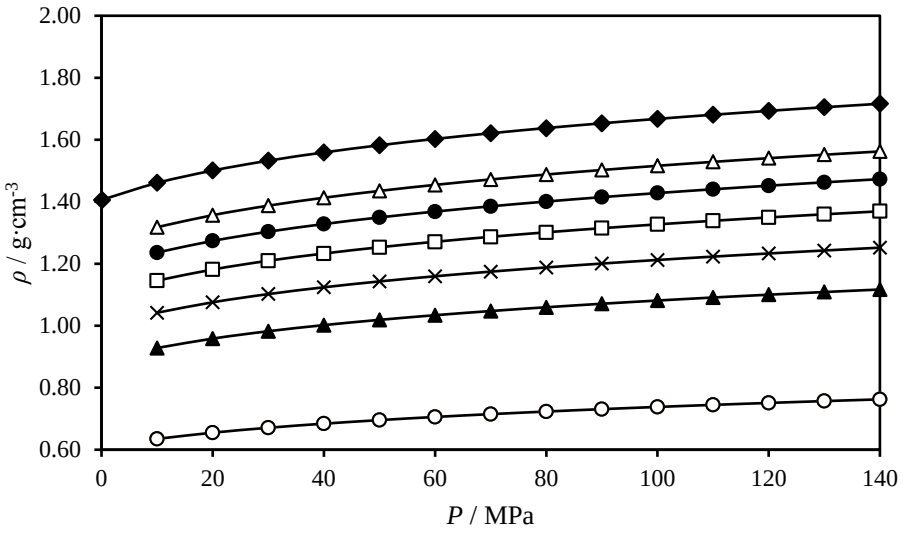
2.00
1.80
1.60
1.40
1.20
1.00
0.80
0.60
ρ / g·cm-3
0
20
40
60
80
100
120
140
P / MPa

(b)

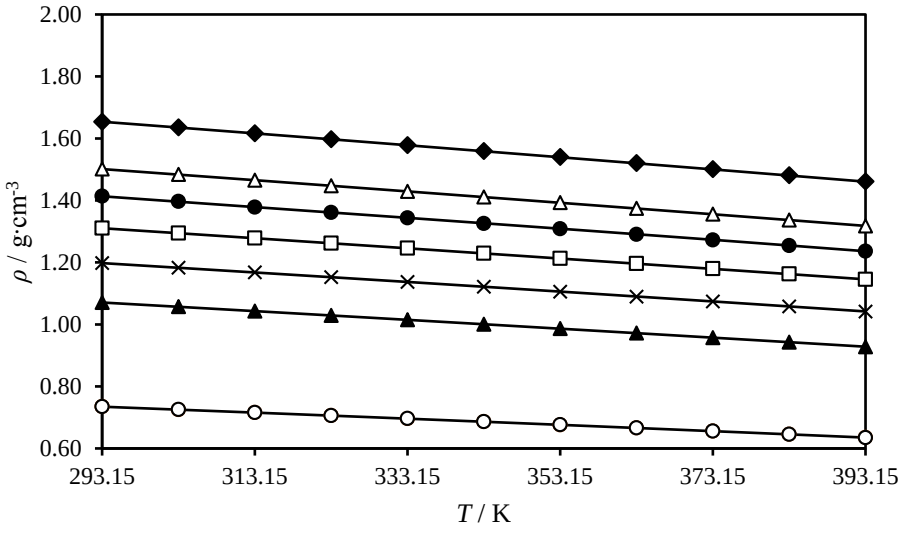

(c)

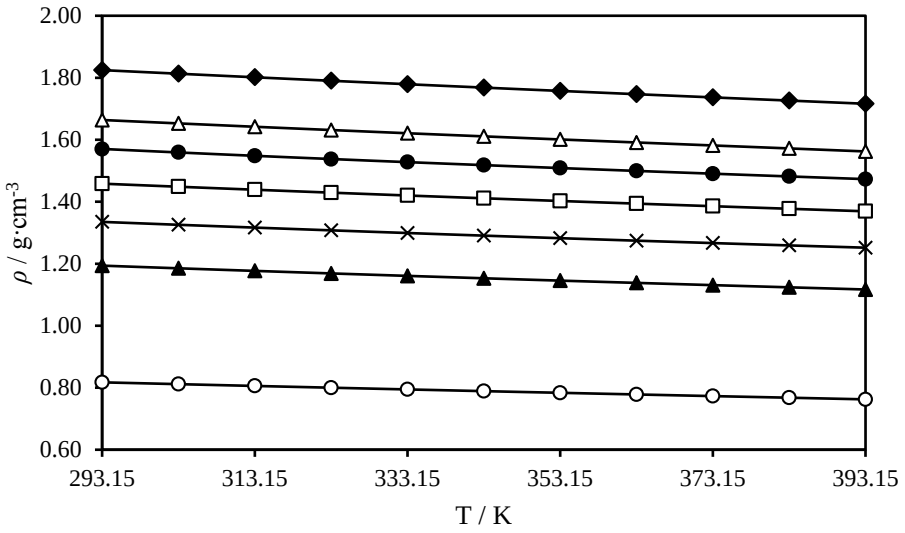

(d)

Figure 9. Experimental values of densities, ρ, for different mole fractions of x HFE-7500 + (*1-x*) Diisopropyl ether vs. (a) the pressure, P at 293.15 K and (b) the pressure, P at 393.15 K, (c) the temperature, T at 10 MPa and (d) the temperature, T at 140 MPa. ○; $x = 0$, ▲; $x = 0.250$, ×; $x = 0.375$, □; $x = 0.500$, ●; $x = 0.625$, Δ; $x = 0.750$, ♦; $x = 1$, (−); Tait equation (). Mole fraction $x = 0$ comes from reference [20], and mole fraction $x = 1$ comes from reference [21].

Excess molar volumes were calculated in order to determine the effects of pressure and temperature in the mixture. Equation (15) was employed for this purpose:

$$V^E = \sum_{i=1}^{n} x_i M_i \left[\left(1/\rho \right) - \left(1/\rho_i \right) \right] \tag{15}$$

Figure 10 shows the values obtained for the excess volumes considering the five molar compositions studied and the pure compounds. In this figure, graph (a) shows results at 1 MPa and at temperatures from (293.15 to 393.15) K spaced 20 K while graph (b) shows excess volumes at 50 MPa at the same temperatures. For both pressures the values of the excess volumes are always positive, which can be explained as a volume expansion that is a result of the interaction between two molecules with very different sizes, being the HFE molecule the higher one. Being both compounds ethers, no strong interaction between them will take place, so the values of the excess volumes will be relatively high. By comparing graphs (a) and (b), it can be stated that a dependency in pressure takes place. When the higher the pressure is, the lower the values of the excess volumes are for all the temperatures considered, which is a result of a better packing effect promoted by the increase in pressure.

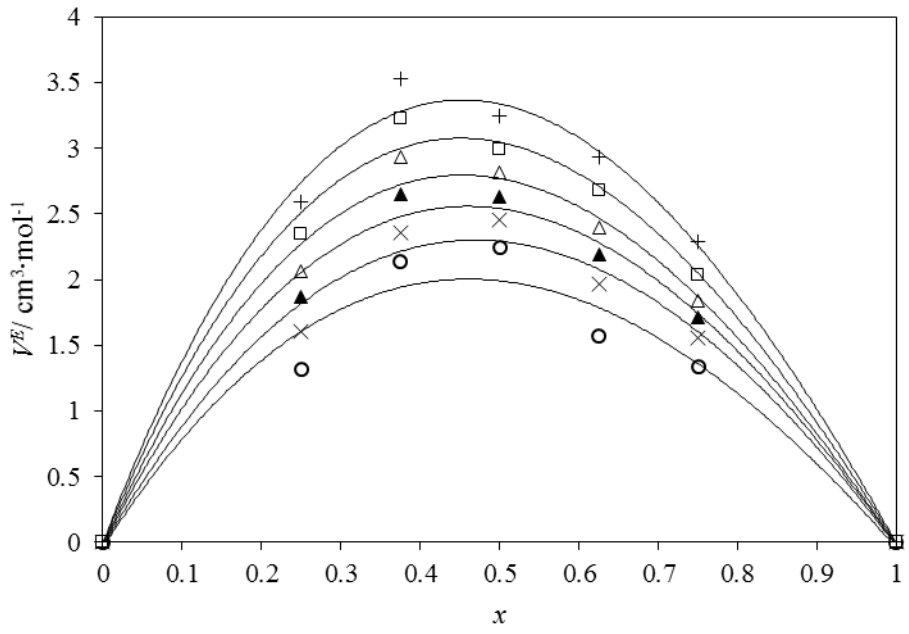

(a)

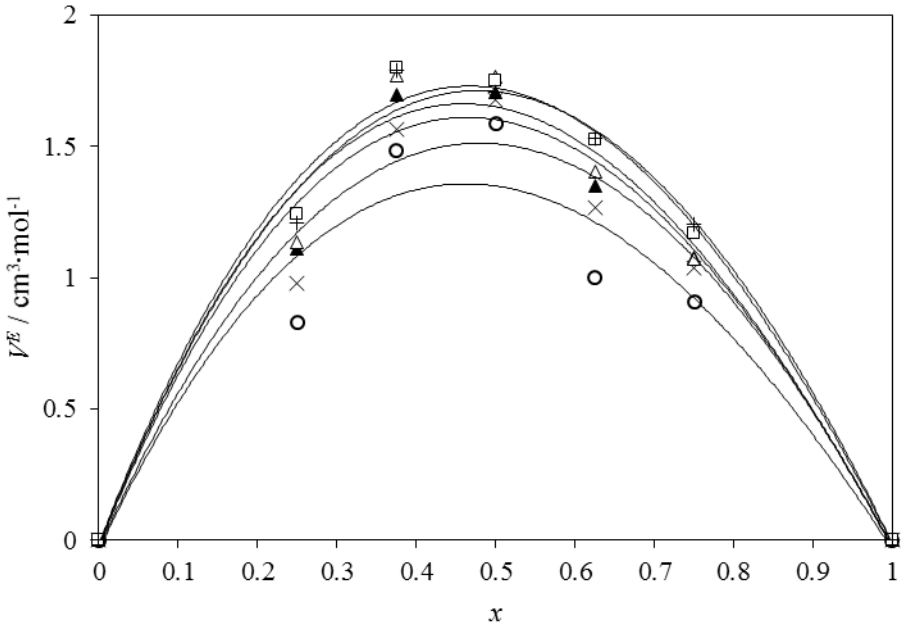
2
1.5
1
0.5
0
V^E / cm^3·mol^{-1}
0
0.1
0.2
0.3
0.4
0.5
0.6
0.7
0.8
0.9
1
x

(b)

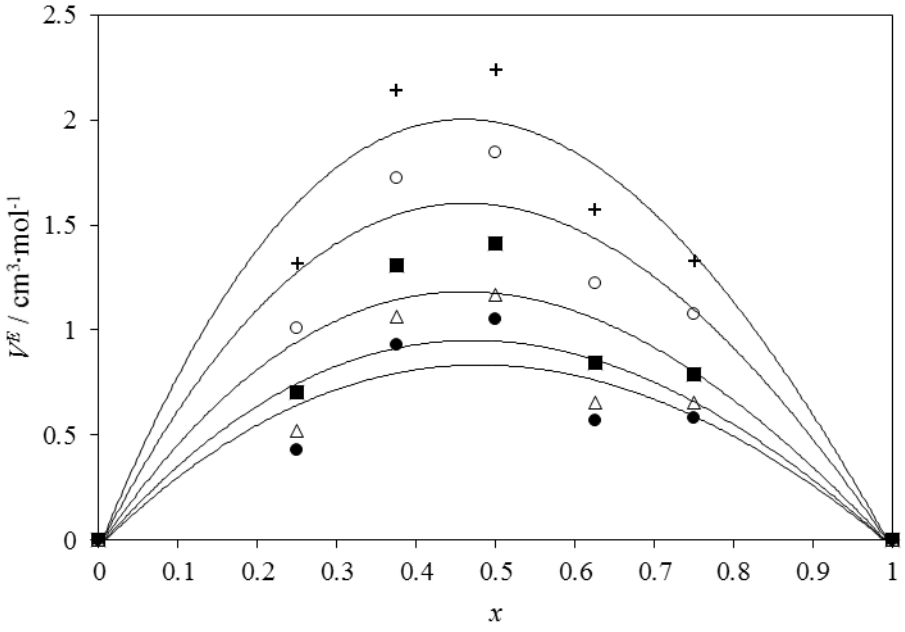
2.5
2
1.5
1
0.5
0
V^E / cm^3·mol^{-1}
0
0.1
0.2
0.3
0.4
0.5
0.6
0.7
0.8
0.9
1
x

(c)

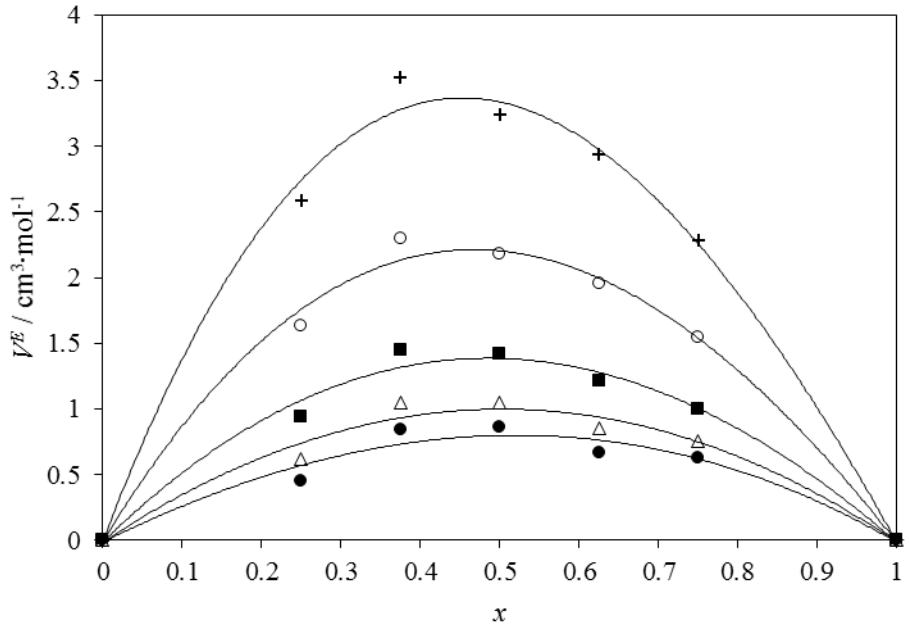

(d)

Figure 10. Experimental values of excess molar volumes for the binary mixtures x HFE-7500 + (1-x) diisopropyl ether as a function of the mole fraction at different temperatures, (a) at P = 1 MPa, (b) at P = 50 MPa, where: ○, 293.15 K; ×, 313.15 K; ▲, 333.15 K; Δ, 353.15 K; □, 373.15 K; +, 393.15 K and (c) at T = 298.15 K and (d) at T = 393.15 K at various pressures, where: +, 1 MPa; ○, 30 MPa; ■, 70 MPa; Δ, 110 MPa; ●, 140 MPa. (─), Redlich-Kister's equation (16).

In Figure 10, Graphs (c) and (d) show the different excess volume values for different pressures at a certain temperature. Graph (c) provides values at 293.15 K while graph (d) provides data at 393.15 K. For both temperatures, the pressures considered are 1 MPa, 30 MPa, 70 MPa, 110 MPa and 140 MPa, a broad enough range of pressures to study the temperature effect on excess volume. Comparing both graphs, as is the case for graphs (a) and (b), the values of excess volumes are always positive. It can be observed that when the higher the temperature is, the higher the excess volume values, considering the same pressure datum. These results are reasonable because an increase in temperature promotes an intermolecular spacing, deriving this in an increase in the value of excess volume. It can be said also that this increase on excess volume values is greater at high pressures at 393.15 K than the increase observed at high pressures but at 293.15 K.

For all the excess volume values of the four graphs, a fitting to a Redlich-Kister equation (16) was done.

$$V^E = x(1-x)\sum_i z_i (2x-1)^{i-1} \tag{16}$$

In Table 14 are listed the values of the adjustable parameters, z_i, and the standard deviations at different pressures for the temperatures 293.15 K and 393.15 K, and at different temperatures for the pressures 1 MPa, 50 MPa, 110 MPa, and 140 MPa.

Table 14. Values of parameters z_i of equation (16) and the corresponding standard deviation, σ, for binary mixtures at 293.15 K and 393.15 K for different pressures, and at 1.00 MPa, 50.00 MPa, 110.00 MPa and 140.00 MPa for all the temperatures measured.

	z_1	z_2	z_3	$\sigma\,(V^E)$/ cm^3·mol^{-1}
P / MPa		(T = 293.15 K)		
1.00	8.5988	-1.3071	-6.5478	0.14
30.00	6.9769	-0.9570	-6.1415	0.13
70.00	5.2340	-0.7670	-5.4742	0.13
110.00	4.2881	-0.4655	-5.1196	0.12
140.00	3.8095	-0.2804	-4.9264	0.12
P / MPa		(T = 393.15 K)		
1.00	13.4764	-2.5746	-1.3169	0.11
30.00	8.9708	-1.1561	-1.6449	0.07
70.00	5.7485	-0.3205	-2.1805	0.06
110.00	4.1981	0.0522	-2.1386	0.06
140.00	3.4056	0.2679	-2.2173	0.06
T / K		(P = 1.00 MPa)		
293.15	8.5988	-1.3071	-6.5478	0.14
313.15	9.6686	-1.1475	-5.1631	0.08
333.15	10.5473	-1.6744	-3.9579	0.08
353.15	11.4735	-2.1549	-4.0494	0.14
373.15	12.4127	-2.4655	-2.3761	0.10
393.15	13.4764	-2.5746	-1.3169	0.09
T / K		(P = 50.00 MPa)		
293.15	5.9498	-0.8569	-5.7060	0.13
313.15	6.4978	-0.5018	-4.7307	0.08
333.15	6.7756	-0.9492	-3.8128	0.07
353.15	7.0566	-1.1211	-4.6888	0.07
373.15	7.1501	-0.9346	-2.7355	0.06

393.15	7.0403	-0.6304	-2.1595	0.06
T / K		(P = 110.00 MPa)		
293.15	4.2881	-0.4655	-5.1196	0.12
313.15	4.7375	-0.1757	-4.7779	0.08
333.15	4.8037	-0.6745	-4.0297	0.08
353.15	4.8215	-0.6251	-4.9948	0.07
373.15	4.6884	-0.2813	-2.7801	0.04
393.15	4.1981	0.0522	-2.1386	0.06
T / K		(P = 140.00 MPa)		
293.15	3.8095	-0.2804	-4.9264	0.12
313.15	4.2032	0.0528	-4.5403	0.08
333.15	4.2665	-0.4365	-3.8980	0.08
353.15	4.2109	-0.5085	-4.6514	0.07
373.15	4.1939	-0.6629	-4.1744	0.06
393.15	3.4056	0.2679	-2.2173	0.06

4. Conclusions

Experimental measurements of speed of sound have been carried out in the pressure range from (0.1 to 100) MPa and in the temperature interval from (293.15 to 353.15) K for the binary mixture HFE-7500 + Diisopropyl ether. High pressure density data were determined by integration of speed of sound data in the same pressure and temperature ranges. This property was also measured experimentally by using a U-tube densitometer over a pressure range between (0.1 – 140) MPa and in the temperature range from (293.15 to 393.15) K.

The measurements were used to determine the isentropic and isothermal compressibilities as well as the isobaric expansion data in the same P, T range than speed of sound measurements. A correlation representing density and speed of sound data was proposed, showing a good agreement between the experimental and the calculated data. Therefore, it is proved that the correlation stablished for both properties is a viable option to represent density, speed of sound and its derivatives.

Acknowledgements

Natalia Muñoz-Rujas acknowledges support for this research to the University of Burgos, for the funding of her doctoral grant, and to the University of Pau for the funding of a five months research period in 2015.
This paper is part of the doctoral thesis of Natalia Muñoz-Rujas.

References

[1] M.J. Molina, F.S. Rowland, Nature 249 (1974) 810-812.

[2] J.C. Farman, B.G. Gardiner, J.D. Shanklin, Nature 315 (1985) 207-210.

[3] M.A.K. Khalil, R.A. Rasmussen, J.A. Culbertson, J.M. Prins, E.P. Grismund, M.J. Shearer, Environ. Sci. Technol. 37 (2003) 4358-4361.

[4] D.B. Bivens, B.H. Minor, Int. J. Refrig. 21 (1998) 567-576.

[5] J. Kehren, http://www.solvents.net.au/index_htm_files/71IPA%20Engineered%20Fluid.pdf. Last access: 03/02/2017.

[6] E.H.I. Ndiaye, D. Nasri, J.L. Daridon, J. Chem. Eng. Data 57 (2012) 2667-2676.

[7] W.D. Wilson, J. Acoust. Soc. Am. 31 (1959) 1067-1072.

[8] E.H. Baltasar, M. Taravillo, V.G. Baonza, P.D. Sanz, B. Guignon, J. Chem. Eng. Data 56 (2011) 4800-4807.

[9] J.L. Daridon, A. Lagrabette, B. Lagourette, J. Chem. Thermodyn. 30 (1998) 607-623.

[10] B.N. Taylor, C.E. Kuyatt, Guidelines for Evaluating and Expressing the Uncertainty of NIST Measurements Results, NIST Technical Note 1297; National Institute of Standards and Technology: Gaithersburg, MD, 1994.

[11] M.J.P. Comuñas, J.P. Bazile, A. Baylaucq, C. Boned, J. Chem. Eng. Data 53 (2008) 986-994.

[12] W. Wagner, A. Pruβ, J. Phys. Chem. Ref. Data 31 (2002) 387-535.

[13] TRC Thermodynamic Tables; Texas A&M University: College Station, TX, 1996.

[14] E.W. Lemmon, M.O. McLinden, D.G. Friend, Thermophysical Properties of Fluid Systems in WebBook of Chemistry NIST. In: P.J. Linstrom, W.G. Mallard, editors. Standard Reference Database NIST number 69 (2013).

[15] J.A. Riddick, W.B. Bunger, T.K. Sakano, Organic Solvents: Physical Properties and Methods of Purification, vol. II, 4th ed. Wiley: U.S., 1986.

[16] J.L. Daridon, B. Lagourette, J.P. Grolier, Int. J. Thermophys. 19 (1998) 145-160.

[17] R.L. Mills, D.H. Lienbenberg, J.C. Bronson, J. Chem. Phys. 68 (1978) 2663-2668.

[18] J.L. Daridon, B. Lagourette, P. Labes, Int. J. Thermophys. 17 (1996) 851-871.

[19] J.S. Rowlinson, F.L. Swinton, Liquid and Liquid Mixtures, 3rd ed. Butterworth Scientific: London, 1982.

[20] N. Muñoz-Rujas, J.P. Bazile, F. Aguilar, G. Galliero, E. Montero, J.L. Daridon, J. Chem. Thermodyn. 112 (2017) 52-58.

[21] N. Muñoz-Rujas, J.P. Bazile, F. Aguilar, G. Galliero, E. Montero, J.L.Daridon, Fluid Phase Equilib. 449 (2017)148-155.

[22] Y. Zheng, H. Gao, Q. Chen, X. Meng, J. Wu, Fluid Phase Equilib. 372 (2014) 56-62.

[23] 3M™ Novec™ Engineered Fluids: http://multimedia.3m.com/mws/media/65496O/3mtm-novectm-7500-engineered-fluid.pdf

[24] G.S. Parks, H.M. Huffman, M. Barmore, J. Am. Chem. Soc. 55 (1993) 2733-2740.

[25] R.J.L. Andon, J.F. Counsell, D.A. Lee, J.F. Martin, J. Chem. Soc. 1 (1974) 1914-1916.

[26] J-P.E. Grolier, G. Roux-Desgranges, M. Berkane, E. Wilhem, J. Chem. Thermodyn. 23 (1991) 421-429.

[27] J-P.E. Grolier, G. Roux-Desgranges, M. Berkane, E. Jiménez, E. Wilhem, J. Chem. Thermodyn. 25 (1993) 41-50.

[28] J-P.E. Grolier, G. Roux-Desgranges, M. Berkane, E. Wilhem, J. Sol. Chem. 23 (1994) 153-166.

[29] R. Páramo, M. Zouine, F. Sobrón, C. Casanova, J. Chem. Eng. Data 49 (2004) 58-61.

[30] E.H.I. Ndiaye, M. Habrioux, J.A.P. Coutinho, M.L.L. Paredes, J.L. Daridon, J. Chem. Eng. Data 58 (2013) 1371-1377.

[31] N. Muñoz-Rujas, F. Aguilar, J-P. Bazile, E.A. Montero, Fluid Phase Equilib. 429 (2016) 281-292.

[32] A. Srhiyer, N. Muñoz-Rujas, F. Aguilar, J.J. Segovia, E.A. Montero, J. Chem. Thermodyn. 113 (2017) 213-218.

High Pressure Density and Speed of Sound of Hydrofluoroether Fluid 1,1,1,2,2,3,4,5,5,5-decafluoro-3-methoxy-4-(trifluoromethyl)-pentane (HFE-7300).

Natalia Muñoz-Rujas[a], Fernando Aguilar[a], Jesús M. García-Alonso[a], Eduardo A. Montero[a,]*

[a] Departamento de Ingeniería Electromecánica, Escuela Politécnica Superior, Universidad de Burgos, E-09006 Burgos, Spain

emontero@ubu.es

Abstract

High pressure density measurements were carried out for the hydrofluoroether fluid HFE-7300. A total of 159 points have been measured in the pressure range from 0.1 to 140 MPa and along seven isotherms within the temperature interval (293.15 - 393.15) K. To perform these measurements, an Anton Paar vibrating tube densitometer was used. The experimental high pressure density data were correlated to a Tait-like equation and compared with the available literature. By deriving the Tait-like equation, the isothermal compressibility and isothermal compressibility were also determined in the same *P* and *T* ranges. The speed of sound measurements were performed along six isotherms from 293.15 to 333.15 K at atmospheric pressure. The isentropic compressibilities were also calculated from speed of sound and density data by means of the Laplace equation.

Keywords

Hydrofluoroethers, Density, Isobaric Expansion, Isothermal Compressibility, Speed of Sound.

1. Introduction

Industry needs a broad range of fluids to meet their requirements on heat transfer, cleaning applications, lubricant deposition and electronics applications such as cooling, front end semiconductor wafer processing and back end integrated circuit packaging [1 - 3].

Over time, a wide variety of compounds (mineral oils, silicone oils, perfluorocarbons (PFC), perfluoropolyethers (PFPE), etc.) have been used for these purposes due to their desirable physicochemical properties, but often without taking into account their environmental impact.

PFC liquids are used because they are chemically inert and non-flammable, they have high dielectric strength and electrical resistivity, and they evaporate cleanly [4]. Amongst the drawbacks, they exhibits long atmospheric lifetimes and high global warming potentials (GWP), which are non-desirable properties for the environment, even they are non-ozone depleting agents. Something similar occurs for PFPE: their physicochemical properties are of interest for the aforementioned purposes, but their high GWP and large atmospheric lifetimes require search for other environmentally friendly fluids.

Segregated hydrofluoroethers (HFEs) are a class of fluids synthesized since the ‘90s. In its structure a perfluorocarbon segment is separated from an hydrocarbon segment by an ether oxygen, which brings environmentally desirable properties such as short atmospheric lifetimes, in the order of 3 years or less. Also, these kind of compounds have zero or near-zero ozone depletion potential (ODP) and low global warming potential. The variety of HFEs synthesized offer a wide useful temperature ranges, a relatively high thermal capacity, low viscosity and high liquid density, being also non-flammable, inert to common metals and polymers, and exhibiting very low overall toxicity [5].

1,1,1,2,2,3,4,5,5,5-decafluoro-3-methoxy-4-(trifluoromethyl)-pentane, also known as HFE-7300, is a segregated hydrofluoroether which can be used in heat transfer applications, cleaning applications, and in lubricant deposition. The properties knowledge about this fluid is scarce. Some papers report its environmental properties: reference [6] reports the low contribution of HFE-7300 to the atmospheric warming even though this compound is highly fluorinated. This reference also states that HFE-7300 is effective at mitigating the aggressiveness and the flammability of solvents, so this fluid can be used as pure compound or in mixture with other fluids. Some patent [7] propose several mixtures of HFE-7300 with other flammable compounds to be used as electronics cleaning agents, lubricants, and heat transfer fluids.

This work provides experimental density data for pure HFE-7300 in the pressure range (0.1 – 140) MPa and in the temperature interval (293.15 – 393.15) K. Correlation of data was performed by using a Tait-like equation, and also the derived properties, that is, the isothermal compressibility, κ_T, and the isobaric expansion, α_P were calculated. A comparison of density data was done with the only reference found at atmospheric pressure, being no high pressure density data available in the literature. Speed of sound was measured at 0.1 MPa and at temperatures (293.15 – 333.15) K. Isentropic compressibility was determined in the same temperature range.

2. Experimental

2.1 Materials

The hydrofluoroether fluid 1,1,1,2,2,3,4,5,5,5-decafluoro-3-methoxy-4-(trifluoromethyl)-pentane, known as HFE-7300, ($C_7H_3F_{13}O$, molar mass 350 g·mol^{-1}, CAS number 132182-92-4) was supplied by the 3M Company (Novec Engineered Fluids) with a mass purity greater than 0.995. No further purification method was carried out before using, only careful degassing with an ultrasound bath to prevent bubbles formation.

2.2. Apparatus and procedure

To carry out the high pressure density measurements with HFE-7300, a vibrating tube densitometer Anton Paar, model DMA HPM, was used. With this apparatus, the measurements were performed from 0.1 MPa up to 140 MPa, with 5 MPa intervals from 0.1 MPa to 65 MPa, and at every 10 MPa from 70 MPa to 140 MPa for the pressure *P*. For the temperature *T*, a thermostatic bath connected with the densitometer allows to set a wide range of temperatures, being the measurements performed along seven isotherms (293.15, 298.15, 313.15, 333.15, 353.15, 373.15 and 393.15) K. The experimental setup was described previously [8]. The calibration of the densitometer was performed according to the procedure described by Comuñas *et al.* [9] which is a modification of the procedure previously proposed by Lagourette *et al.* [10]. Two reference fluids were used in order to perform the calibrations, vacuum and water. These fluids were selected because there is vast knowledge about their properties. For water, although there are lots of data concerning density values, we took those from the equation of state (EoS) reported by Wagner and Pruss [11].

The sample was prepared by filling a stoppered bottle of 21 cm^3 and degassing it with an ultrasound bath PSelecta, model Ultrasons H, to prevent bubbles formation and consequently an air intake in the densitometer. When vacuum is done inside the densitometer, the sample enters the system by suction. After closing the fluid inlet valve, and when the sample reaches the thermal and mechanical equilibrium, the density measurement starts. The DMA HPM measuring cell is connected to the Anton Paar mPDS 2000V3 evaluation unit, which evaluates the oscillation period from the measuring cell filled with the sample. Depending on the mass of the sample, the temperature and the pressure, the oscillation period of the cell changes. Then, it is possible to determine the density values from the given values of period. In this way, a total of 159 points were measured within the pressure and temperature ranges established.

Concerning the uncertainties, the Pt 100 probe that is directly inserted into the densitometer leads to an expanded uncertainty in temperature of 0.03 K. For the pressure, the expanded

uncertainty is 0.04 MPa (pressure transducer WIKA CPH 6000). Then, the estimated expanded uncertainty (k = 2) in density, calculated following the EA-4/02 document [12], taking into account the accuracy of the temperature, the pressure, the period of oscillation measurement for water, vacuum, the studied system, and the water density accuracy, is estimated to be $0.7 \cdot 10^{-3}$ g·cm^{-3} (*i.e*, around 0.07 % for density close to water density).

The speed of sound, c, in pure HFE-7300 was measured by using an Anton Paar DSA 5000 vibrating tube densitometer and sound analyzer automatically thermostatted within ±0.01 K. The measurements were performed at atmospheric pressure and at temperatures: 293.15, 298.15, 303.15, 313.15, 323.15 and 333.15 K. The calibration of this apparatus, performed once a week and every time a new temperature was set, was made with ambient air and Millipore quality water following the manufacturer's instructions. The results of the calibrations were compared with those of references [11] for water, and [13] for air. Prior to make any measurement, the samples were degassed for at least 15 minutes in an ultrasonic bath PSelecta model Ultrasons H. The accuracy for the speed of sound measurements is 0.5 m·s^{-1}, being the expanded uncertainty 1 m·s^{-1}. In order to calculate the isentropic compressibility, κ_S, densities were also measured with the same apparatus due to the high pressure density measurements do not include the points at atmospheric pressure and at temperatures 303.15 and 323.15 K. The accuracy for the density is $5 \cdot 10^{-6}$ g·cm^{-3} while the expanded uncertainty in density is $1 \cdot 10^{-5}$ g·cm^{-3}.

3. Results and Discussion

3.1. Experimental density data

High pressure density measurements of pure HFE-7300 fluid were performed along seven isotherms ranging from 293.15 K to 393.15 K and along 23 isobars from 0.1 MPa up to 140 MPa. Due to the boiling point of HFE-7300 at 0.1 MPa is 371.15 K [5], no measurements were performed at 373.15 K and at 393.15 K at this pressure to avoid gaseous state and to ensure all the measurements were performed in liquid state. Table 1 shows the density values measured experimentally with the high pressure densitometer.

3.2. Tait representation

A Tait-like equation was used to correlate the experimental high pressure density data in order to be able to interpolate values at different pressures or temperatures within our pressure and temperature ranges. The Tait-like equation proposed was used in our previous works [14 - 16].

Table 1. Density values ρ, for the hydrofluoroether fluid HFE-7300 at several pressures and temperatures[a].

P / MPa	T / K						
	293.15	298.15	313.15	333.15	353.15	373.15	393.15
				ρ / g·cm^{-3}			
0.10	1.6682	1.6567	1.6213	1.5727	1.5217		
1.00	1.6708	1.6594	1.6245	1.5765	1.5265	1.4735	1.4172
5.00	1.6819	1.6710	1.6377	1.5923	1.5456	1.4971	1.4469
10.00	1.6948	1.6844	1.6527	1.6099	1.5665	1.5219	1.4767
15.00	1.7066	1.6966	1.6663	1.6257	1.5847	1.5431	1.5014
20.00	1.7176	1.7080	1.6788	1.6398	1.6010	1.5615	1.5228
25.00	1.7279	1.7186	1.6904	1.6530	1.6158	1.5783	1.5415
30.00	1.7377	1.7286	1.7014	1.6652	1.6295	1.5937	1.5584
35.00	1.7469	1.7381	1.7116	1.6765	1.6421	1.6077	1.5738
40.00	1.7556	1.7471	1.7212	1.6873	1.6537	1.6204	1.5880
45.00	1.7640	1.7556	1.7305	1.6975	1.6648	1.6325	1.6010
50.00	1.7720	1.7638	1.7392	1.7070	1.6752	1.6439	1.6133
55.00	1.7797	1.7717	1.7476	1.7161	1.6851	1.6546	1.6249
60.00	1.7870	1.7793	1.7555	1.7247	1.6945	1.6647	1.6358
65.00	1.7941	1.7865	1.7633	1.7331	1.7035	1.6743	1.6460
70.00	1.8009	1.7934	1.7707	1.7410	1.7121	1.6834	1.6558
80.00	1.8140	1.8067	1.7848	1.7561	1.7281	1.7006	1.6741
90.00	1.8263	1.8191	1.7979	1.7702	1.7431	1.7165	1.6909
100.00	1.8378	1.8310	1.8102	1.7833	1.7570	1.7313	1.7065
110.00	1.8488	1.8420	1.8220	1.7956	1.7701	1.7451	1.7210
120.00	1.8593	1.8527	1.8329	1.8073	1.7825	1.7581	1.7347
130.00	1.8693	1.8628	1.8435	1.8185	1.7941	1.7703	1.7475
140.00	1.8788	1.8725	1.8535	1.8291	1.8052	1.7820	1.7597

[a] *Estimated expanded uncertainty (k=2): temperature U(T) = 0.03 K, pressure U(P) = 0.04 MPa, density U(ρ) = 0.0007 g·cm^{-3}.*

$$\rho(T,p) = \frac{\rho_0(T)}{1 - C\ln\left(\frac{B(T) + p}{B(T) + 0.1\ \mathrm{MPa}}\right)} \tag{1}$$

where

$$\rho_0(T) = A_0 + A_1 T + A_2 T^2 + A_3 T^3 \tag{2}$$

$$B(T) = B_0 + B_1 T + B_2 T^2 \tag{3}$$

The A_i, B_i and C parameters values were determined by correlating simultaneously all the experimental densities values versus pressure and temperature.

To compare the experimental density values with those obtained with the correlation considered in this work, we have used the Absolute Average Deviation (AAD%), the Maximum Deviation (MD%), and the Average Deviation (AD%), which are defined as follows:

$$\mathrm{AAD} = \frac{100}{\mathrm{N}} \sum_{\mathrm{i}=1}^{\mathrm{N}} \left| \frac{\rho_{\mathrm{i}}^{\mathrm{exp}} - \rho_{\mathrm{i}}^{\mathrm{calc}}}{\rho_{\mathrm{i}}^{\mathrm{exp}}} \right| \tag{4}$$

$$\mathrm{MD} = \mathrm{Max}\left(100 \left| \frac{\rho_{\mathrm{i}}^{\mathrm{exp}} - \rho_{\mathrm{i}}^{\mathrm{calc}}}{\rho_{\mathrm{i}}^{\mathrm{exp}}} \right| \right) \tag{5}$$

$$\mathrm{AD} = \frac{100}{N} \sum_{i=1}^{N} \frac{\rho_i^{\mathrm{exp}} - \rho_i^{\mathrm{calc}}}{\rho_i^{\mathrm{exp}}} \tag{6}$$

$$\sigma = \sqrt{\frac{\sum_{\mathrm{i}=1}^{\mathrm{N}} (\rho_{\mathrm{i}}^{\mathrm{exp}} - \rho_{\mathrm{i}}^{\mathrm{calc}})^2}{\mathrm{N\text{-}m}}} \tag{7}$$

$$\mathrm{RMSD} = \sqrt{\frac{\sum_{\mathrm{i}=1}^{\mathrm{N}} (\rho_{\mathrm{i}}^{\mathrm{exp}} - \rho_{\mathrm{i}}^{\mathrm{calc}})^2}{\mathrm{N}}} \tag{8}$$

where N is the number of experimental data (N = 159) and m is the number of parameters (m = 8).

The eight A_i, B_i and C calculated parameters of the Tait-like equation and the statistical values obtained with this correlation are given in Table 2 for HFE-7300.

Table 2. Obtained parameters and deviations for density correlation by using equations (1) to (3) for liquid HFE-7300.

A_0 / g cm^{-3}	2.323585
A_1 / g cm^{-3} K^{-1}	$-2.839676 \cdot 10^{-3}$
A_2 / g cm^{-3} K^{-2}	$4.253851 \cdot 10^{-6}$
A_3 / g cm^{-3} K^{-3}	$-7.473361 \cdot 10^{-9}$
B_0 / MPa	296.9519
B_1 / MPa K^{-1}	-1.226653
B_2 / MPa K^{-2}	$1.287132 \cdot 10^{-3}$
C	0.08208861
AAD /(%)	0.01
MD /(%)	0.05
AD /(%)	$-8.41 \cdot 10^{-5}$
σ /(g·cm^{-3})	$2.65 \cdot 10^{-4}$
RMSD /(g·cm^{-3})	$2.59 \cdot 10^{-4}$

In this work, it has to be noted that all the fitting deviations (the AAD%, MD%, AD%, the standard deviation σ and the RMSD) are lower than the experimental uncertainty in density (±0.07%). This fact can be also verified in Figure 1 (a) where the average deviations are plotted versus the pressure considering all the temperatures measured, and in Figure 1 (b) where the deviations are showed against the temperature for several pressure values.

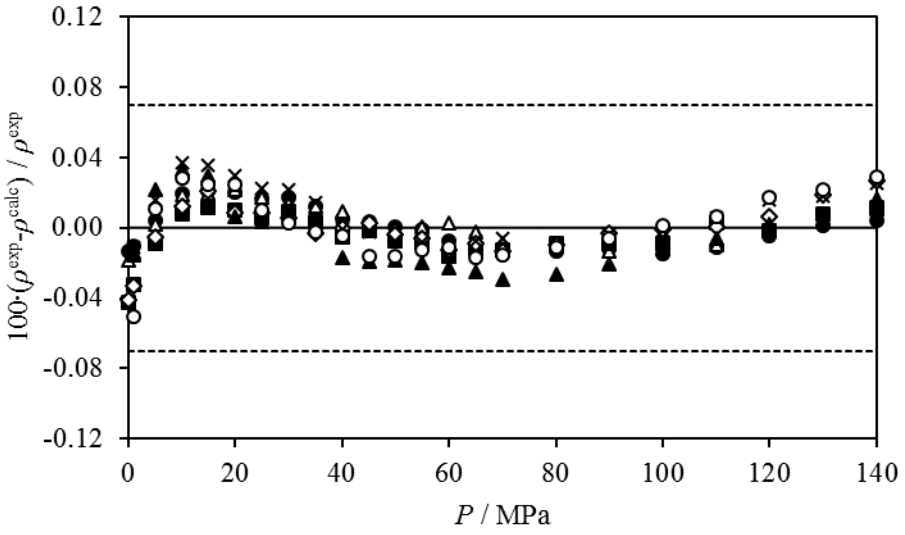

(a)

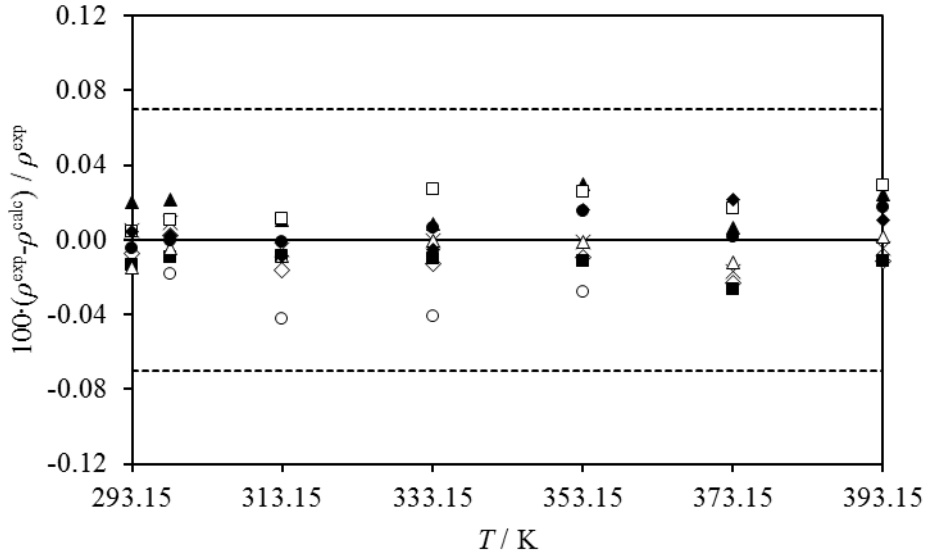

(b)

Figure 1. Deviations between the experimental high pressure density data and those calculated by using the Tait-like equation for HFE-7300 (a) versus the pressure, where: ●; 293.15 K, Δ;

298.15 K, ■; 313.15 K, ◊; 333.15 K, ×; 353.15 K, ▲; 373.15 K, ○; 393.15 K, and (b) versus the temperature, where: ○; 0.1 MPa, ♦; 5 MPa, ▲; 20 MPa, ×; 40 MPa, ◊; 60 MPa, ■; 80 MPa, Δ; 100 MPa, ●; 120 MPa, □; 140 MPa. The dashed lines represent the value of the expanded uncertainty (0.07% g·cm^{-3}).

Figure 2 (a) shows a comparison between the experimental density values ρ, and those obtained with the correlation equations (1 – 3) versus the pressure, for the seven isotherms measured. It can be seen the non-linear behaviour of the density versus the pressure, particularly at high temperatures. The shape of this curves is compatible with the logarithmic relationship used in the Tait-like equation used to model the influence of pressure on density.

It can be stated also that for all the temperatures the values of density increase when increasing the pressure. In the same manner, the lower the temperature, the higher the values of density, being the maximum at 293.15 K and at 140 MPa with a value in density of 1.8788 g·cm^{-3}.

Figure 2 (b) presents the obtained deviations between the experimental densities and the obtained ones with the correlation equations versus the temperature for eight isobars (0.1, 20, 40, 60, 80, 100, 120 and 140) MPa. It can be stated that at low pressures the density values are lower than for the higher pressures. Considering the temperature, density values decrease when increasing temperature, as expected.

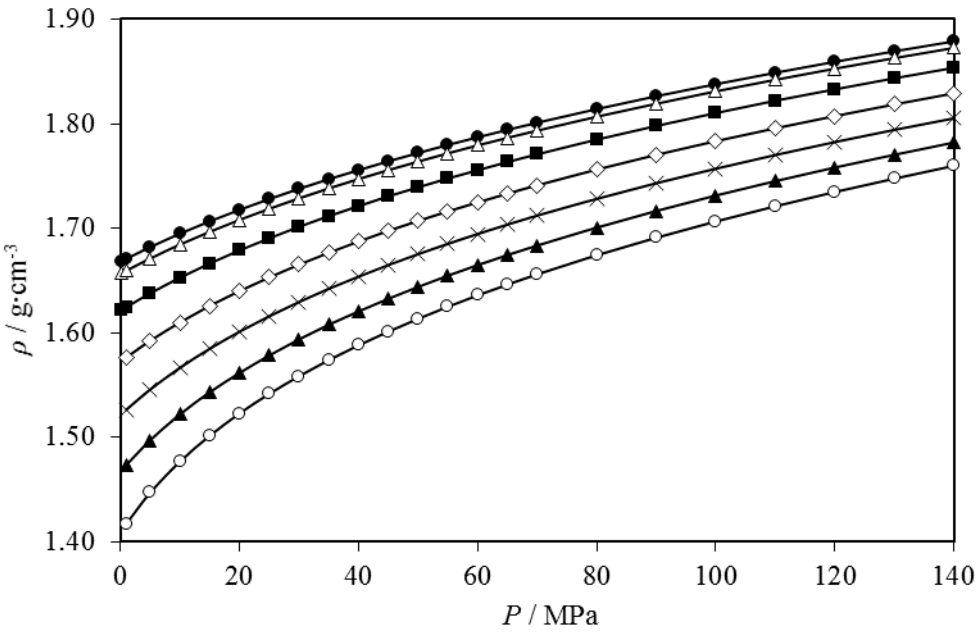

(a)

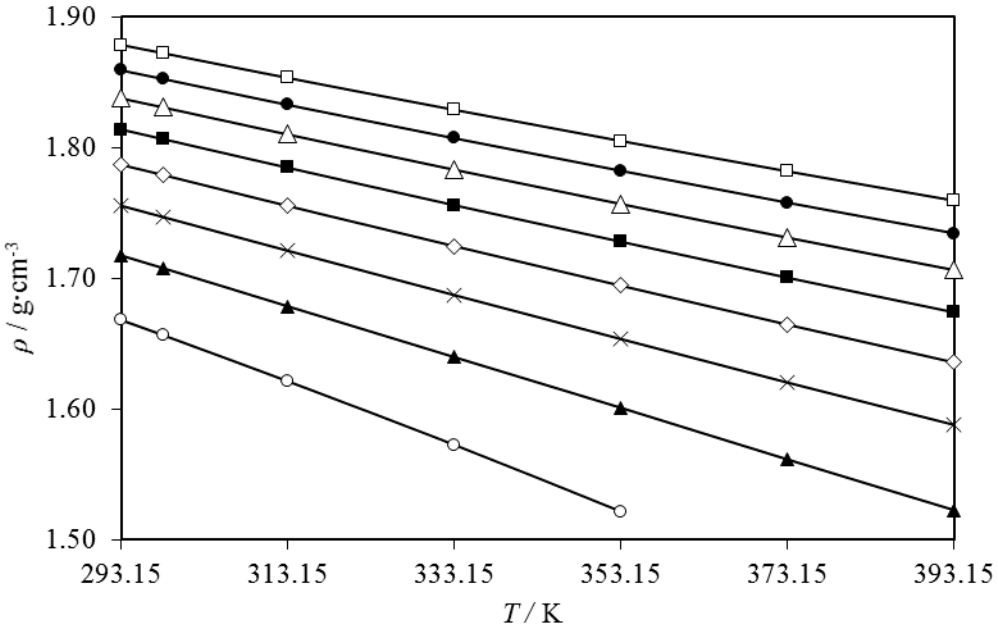

(b)

Figure 2. Comparison between experimental density values ρ, and those obtained by the correlation proposed by the Tait-like equation for HFE-7300 (a) versus the pressure at different temperatures, and (b) versus the temperature at several pressures. For (a): ●; 293.15 K, Δ; 298.15 K, ■; 313.15 K, ◊; 333.15 K, ×; 353.15 K, ▲; 373.15 K, ○; 393.15 K. For (b): ○; 0.1 MPa, ▲; 20 MPa, ×; 40 MPa, ◊; 60 MPa, ■; 80 MPa, Δ; 100 MPa, ●; 120 MPa, □; 140 MPa. The solid line represents the values calculated by equations (1) to (3).

3.3. Comparison with literature data

For HFE-7300, only one reference which provides density data at atmospheric pressure was found [17]. This reference gives 19 points in our temperature range, from (293.15 – 363.15) K at every 5 K. In order to compare our data with those given by this reference, due to the temperature values are not exactly the same, equations (1) to (3) were used.

The results of the comparison show an AD% = -0.01, an AAD% = 0.03 and a MD% = 0.04, being all the deviation values lower than the combined expanded uncertainty (±0.07%). Figure 3 shows the results of this comparison.

3.4. The derived thermodynamic properties.

The derived properties isothermal compressibility and isobaric expansion data allow the determination of the ability of a given equation not only to correlate PVT data but also to yield the derivatives of V with respect to T or P. Isothermal compressibility, κ_T, describes the effect of

pressure on density at a fixed temperature. By differentiating equation (1) respect to the pressure, then equation (9) provides the way to calculate this property:

$$\kappa_T = \left(\frac{1}{\rho}\right)\left(\frac{\partial \rho}{\partial p}\right)_T = \frac{C}{\left(1 - C\ln\left(\frac{B(T)+p}{B(T)+0.1MPa}\right)\right)\left(B(T)+p\right)} \tag{9}$$

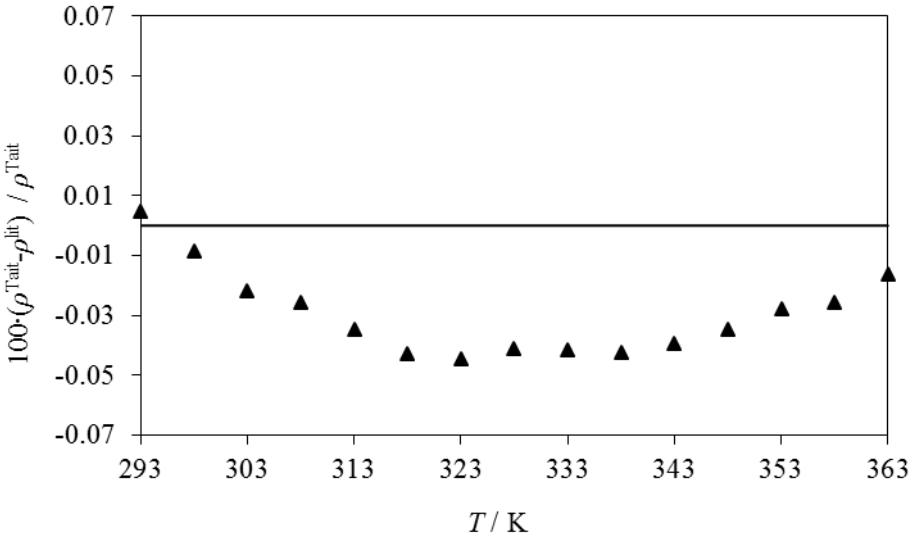

Figure 3. Percentage deviations between the density data obtained in the literature [17], and the values calculated using the Tait-like equation at atmospheric pressure and at several temperatures for the pure fluid HFE-7300.

Table 3 gathers the isothermal compressibility values calculated by using equation (9) in the pressure and temperature ranges considered. Also, Figure 4 shows the κ_T values versus the pressure for the seven isotherms evaluated. It can be stated that for all the isotherms measured, the values of κ_T are increases when the pressure decreases. This statement is in accordance with the assumption that at low pressures the molecules of the fluid are wider apart, so then compressibility takes higher values than when the molecules of the fluid are under pressure, being in this case the molecules closer to each other.

The second derivative property, the isobaric expansion, α_p, which explains how a change in temperature promotes a change in density at a fixed pressure, could also be obtained by differentiating equation (1) taking into account the temperature dependence of $\rho_0(T)$ and $B(T)$:

$$\alpha_P = -\left(\frac{1}{\rho}\right)\left(\frac{\partial \rho}{\partial T}\right)_p \tag{10}$$

Table 3. Values of isothermal compressibility, κ_T, for HFE-7300 at several pressures and temperatures[a].

P / MPa	T / K						
	293.15	298.15	313.15	333.15	353.15	373.15	393.15
				$\kappa_T \cdot 10^4$/ MPa^{-1}			
0.10	17.1	17.9	21.0	26.3	33.7		
1.00	16.8	17.6	20.5	25.6	32.6	42.4	56.4
5.00	15.6	16.3	18.8	23.0	28.5	35.7	45.2
10.00	14.4	15.0	17.1	20.4	24.6	29.9	36.3
15.00	13.3	13.9	15.6	18.4	21.7	25.8	30.5
20.00	12.4	12.9	14.4	16.7	19.5	22.7	26.3
25.00	11.6	12.1	13.4	15.4	17.7	20.3	23.2
30.00	11.0	11.3	12.5	14.2	16.2	18.4	20.8
35.00	10.4	10.7	11.7	13.2	14.9	16.8	18.8
40.00	9.8	10.1	11.0	12.4	13.9	15.5	17.2
45.00	9.3	9.6	10.4	11.6	13.0	14.4	15.9
50.00	8.9	9.1	9.9	11.0	12.2	13.4	14.8
55.00	8.5	8.7	9.4	10.4	11.5	12.6	13.8
60.00	8.1	8.3	9.0	9.9	10.8	11.9	12.9
65.00	7.8	8.0	8.6	9.4	10.3	11.2	12.2
70.00	7.5	7.7	8.2	9.0	9.8	10.6	11.5
80.00	7.0	7.1	7.6	8.2	8.9	9.7	10.4
90.00	6.5	6.6	7.1	7.6	8.2	8.9	9.5
100.00	6.1	6.2	6.6	7.1	7.6	8.2	8.7
110.00	5.8	5.9	6.2	6.6	7.1	7.6	8.1
120.00	5.4	5.5	5.8	6.2	6.7	7.1	7.6
130.00	5.2	5.3	5.5	5.9	6.3	6.7	7.1
140.00	4.9	5.0	5.2	5.6	5.9	6.3	6.7

[a] *Estimated expanded uncertainty (k=2): temperature U(T) = 0.03 K, pressure U(P) = 0.04 MPa, isothermal compressibility U(κ_T) = 0.001 κ_T.*

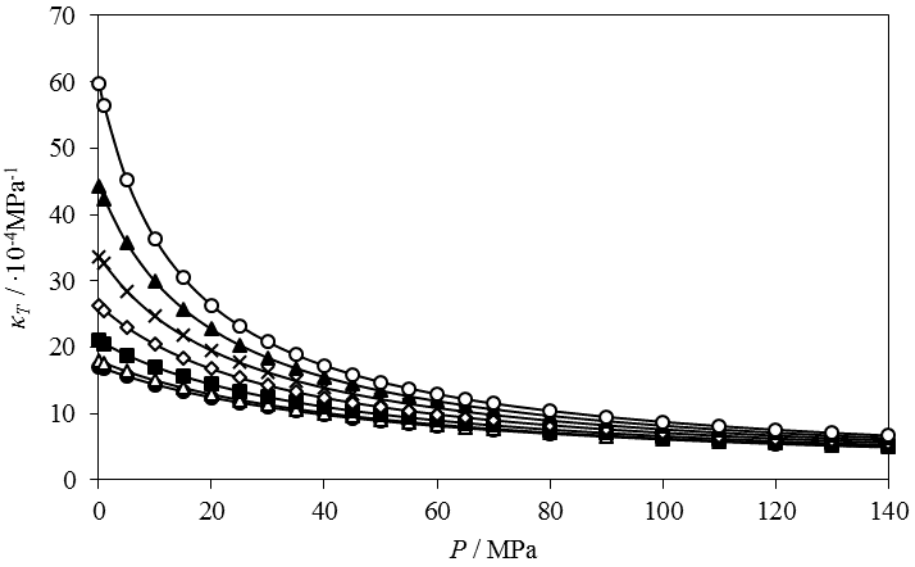

Figure 4. Values of isothermal compressibility κ_T, versus the pressure for the fluid HFE-7300. ●; 293.15 K, Δ; 298.15 K, ■; 313.15 K, ◊; 333.15 K, ×; 353.15 K, ▲; 373.15 K, ○; 393.15 K.

Due to the dependence with respect to the temperature of $\rho_0(T)$, some authors [18] and [19] recommend to derive the isobaric expansion from the isobaric densities.

Also, Jaquemin *et al*. [20] reports that differences sometimes found for the values of isobaric expansion in the literature are due not only to differences in density values but also to the fitting equations. Taking this into account, we suppose at each pressure that $\rho_p(T) = a_0+a_1T+a_2T^2$ and consequently $(\partial\rho/\partial T)_p = a_1 + 2a_2T$. For each pressure we get a set (a_0, a_1, a_2).

By inserting the differentiated density and the calculated densities $\rho_p(T)$ into $\alpha_p = -(1/\rho(\partial\rho/\partial T)_p$ the isobaric expansion at the different *T*, *p* conditions has been derived:

$$\alpha_P = -\frac{a_1 + 2a_2T}{a_0 + a_1T + a_2T^2} \tag{11}$$

The isobaric expansion values, α_p, in the pressure and temperature ranges investigated are reported in Table 4. Figure 5 shows the variation of α_p versus the temperature for some isobars (0.1, 30, 60, 90, 120 and 140) MPa. It can be seen that when the pressure increases, the values of α_p decreases. Therefore, considering an isobar, the isobaric expansion values at low or medium pressures (0.1 and 30 MPa) are higher when the temperature increases, but at high pressures (from 60 to 140 MPa), when the temperature increases, the values of α_p decrease slightly.

By following these procedures, the isothermal compressibility, κ_T, and the isobaric thermal expansion, α_p, were calculated. Following the EA-4/02 document [13], the estimated uncertainty is 1% for the isothermal compressibility κ_T, and in the order of 3% for the isobaric expansion α_p, as previously reported on similar papers [8], [21, 22] that have used the same methods.

3.5. Speed of sound measurements

Speed of sound, *c*, is a basic acoustic property. Besides, other thermodynamics properties, such as isentropic compressibility, heat capacity, virial coefficient, and other properties can be derived from it [23]. Table 5 presents the results of the experimental speed of sound measurements, the density values and the isentropic compressibility, κ_S, obtained by means of the Laplace equation (12).

$$\kappa_S = \rho^{-1} \cdot c^{-2} \tag{12}$$

Table 4. Values of isobaric expansion, α_P, for HFE-7300 at differrent pressures and temperatures[a].

P / MPa	*T* / K						
	293.15	298.15	313.15	333.15	353.15	373.15	393.15
				$\alpha_P \cdot 10^4$/ K^{-1}			
0.10	13.7	14.0	14.7	15.8	17.0		
1.00	13.3	13.6	14.4	15.6	17.0	18.4	20.0
5.00	12.8	13.0	13.6	14.5	15.4	16.4	17.5
10.00	12.3	12.4	12.8	13.4	14.0	14.7	15.4
15.00	11.7	11.8	12.1	12.6	13.0	13.5	14.0
20.00	11.3	11.4	11.6	11.9	12.2	12.5	12.8
25.00	11.0	10.9	11.1	11.3	11.5	11.8	12.0
30.00	10.5	10.5	10.6	10.8	11.0	11.1	11.3
35.00	10.2	10.2	10.3	10.4	10.5	10.6	10.7
40.00	9.9	9.9	9.9	10.0	10.1	10.1	10.2
45.00	9.6	9.6	9.6	9.7	9.7	9.8	9.8
50.00	9.3	9.3	9.3	9.4	9.4	9.4	9.4
55.00	9.2	9.2	9.3	9.3	9.3	9.3	9.3
60.00	8.9	8.9	8.9	8.9	8.8	8.8	8.8
65.00	8.7	8.7	8.7	8.6	8.6	8.6	8.5
70.00	8.5	8.5	8.5	8.4	8.4	8.3	8.3
80.00	8.2	8.2	8.1	8.1	8.0	7.9	7.9
90.00	8.0	7.8	7.8	7.7	7.7	7.6	7.5
100.00	7.6	7.6	7.5	7.5	7.4	7.3	7.2
110.00	7.4	7.3	7.3	7.2	7.1	7.0	6.9
120.00	7.2	7.2	7.1	7.0	6.9	6.8	6.7
130.00	7.0	7.0	6.9	6.8	6.7	6.6	6.5
140.00	6.8	6.8	6.7	6.6	6.5	6.4	6.3

[a] *Estimated expanded uncertainty (k=2): temperature U(T) = 0.03 K, pressure U(P) = 0.04 MPa, isobaric expansion U(α_P) = 0.003 α_P.*

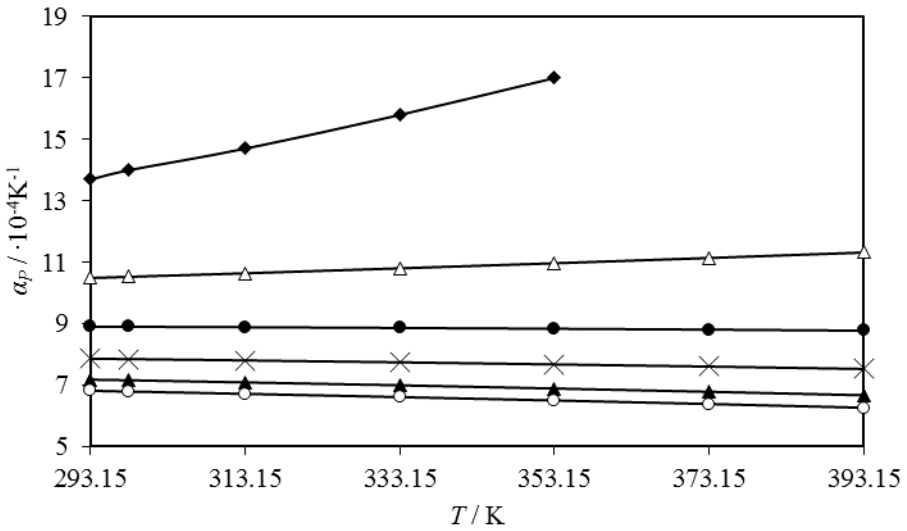

Figure 5. Values of isobaric expansion α_P, versus the temperature for the hydrofluoroether fluid HFE-7300. ♦; 0.1 MPa, Δ; 30 MPa, ●; 60 MPa, ×; 90 MPa, ▲; 120 MPa, ○; 140 MPa.

Table 5. Experimental speed of sound, c, and density, ρ, obtained by using the Anton Paar DSA 5000 density and speed of sound meter, calculated isentropic compressibility, κ_S, and average deviations between experimental density data and literature values [17] for HFE-7300[a].

T / K	c / m·s^{-1}	ρ / g·cm^{-3}	κ_S / TPa^{-1}	AD%
293.15	644.50	1.66843	1443	$1.85 \cdot 10^{-3}$
298.15	629.44	1.65679	1523	$1.54 \cdot 10^{-3}$
303.15	614.76	1.64511	1608	$1.78 \cdot 10^{-3}$
313.15	585.65	1.62435	1795	-0.18
323.15	557.04	1.59704	2018	0.02
333.15	529.01	1.57280	2272	-0.01

[a] *Estimated expanded uncertainty (k = 2): temperature U(T) = 0.01 K, speed of sound U(c) = 1 m·s^{-1}, density U(ρ) = 1·10^{-5} g·cm^{-3}, isentropic compressibility U(κ_S) = 0.50 κ_S.*

These results can be seen also in Figure 6. As can be observed, the speed of sound can be represented as a linear function in which its value decreases with increasing temperature. On the other hand, isentropic compressibility values increase with increasing temperature. In this case, the function that represents this property is not linear due to the influence of the density, whose change with temperature is also non-linear.

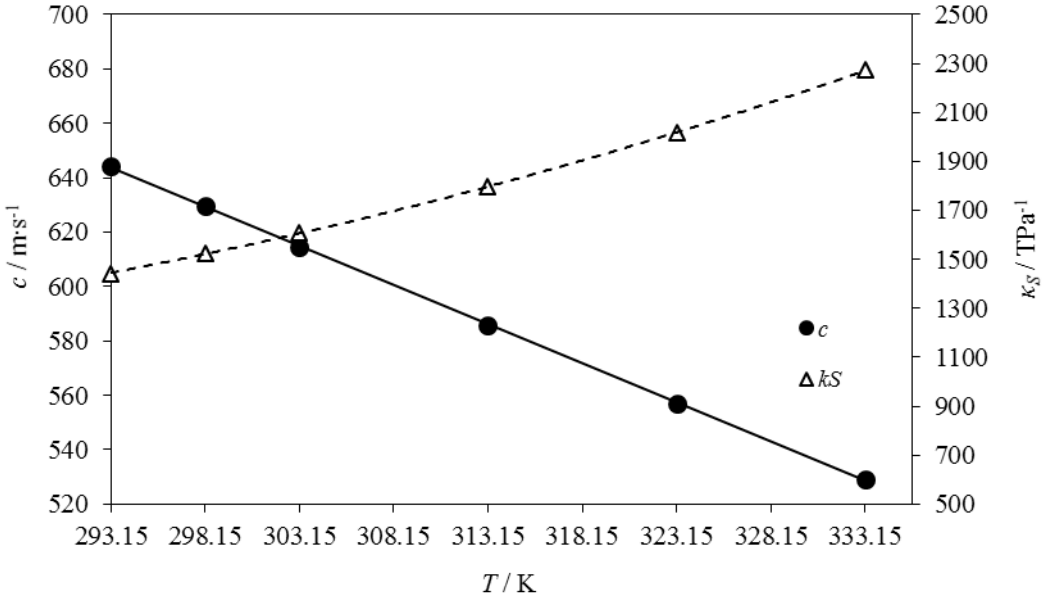

Figure 6. Speeds of sound c, and isentropic compressibilites κ_S, at 0.1 MPa and at several temperatures for the hydrofluoroether fluid HFE-7300.

4. Conclusions

A total of 159 experimental high pressure density points were measured for the liquid HFE-7300 within a temperature range (293.15 – 393.15) and in the pressure range (0.1 – 140) MPa. These density measurements suppose a new contribution of data that broadens the scarce

physical properties data base available for this fluid. By correlation with a Tait-like equation, the good agreement between the experimental high pressure density data and those calculated was checked, obtaining a maximum deviation MD = 0.05%, being all deviation values below the expanded uncertainty (0.07%). The derived properties, isothermal compressibility and isobaric expansion, were also calculated from the Tait-like equation in the same *P*, *T* ranges. Speed of sound at 0.1 MPa and at temperatures from 293.15 to 333.15 K was also measured. Isentropic compressibility was determined from density and speed of sound data.

List of symbols

AAD	Absolute Average Deviation
AD	Average Deviation
a_i	coefficients of isobaric thermal expansivity correlation
A_i, B_i, C	coefficients of density correlation
lit	literature
MD	Maximum Deviation
N	number of experimental data points which are in our *P*, *T* ranges
P	pressure
T	temperature

Greek letters

σ	Standard deviation
α_p	isobaric thermal expansivity
ρ	density
κ_S	isentropic compressibility
κ_T	isothermal compressibility

Aknowledgements

This paper is part of the Doctoral Thesis of N. Muñoz-Rujas.

N. Muñoz-Rujas acknowledges support for this research to the University of Burgos, for the funding of her doctoral grant (Pre-Doctoral Grants 2014).

References

[1] P. Clark, L. Zazzera, Advanced Semiconductor Manufacturing Conference (2006) 296-300. http://ieeexplore.ieee.org/document/1638772/

[2] J. Kehren, Data Storage (2001). http://www.solvents.net.au/index_htm_files/71IPA%20Engineered%20Fluid.pdf

[3] P.G. Clark, E. D. Olson, H. Kofuse, International Conference on Soldering and Reliability (2009) http://multimedia.3m.com/mws/media/591010O/the-use-of-segregated-hydrofluoroethers-as-cleaning-agents.pdf

[4] P. Tuma, L. Tousignant, SEMI Technical Symposium (2001) http://multimedia.3m.com/mws/media/122381O/reducing-emissions-of-pfc-heat-transferfluids.pdf?fn=tech_pfc.pdf.

[5] 3M™ Novec™ Engineered Fluids. http://multimedia.3m.com/mws/media/338713O/3mtm-novectm-7300-engineered-fluid.pdf

[6] A. Rodríguez, D. Rodríguez, A. Moraleda, I. Bravo, E. Moreno, A. Notario, Atmospheric Environment 96 (2014) 145-153.

[7] J.G. Owens, Patent: US/12/557,610 (2012).

[8] F.E.M. Alaoui, E.A. Montero, G. Qiu, F. Aguilar, J. Wu, J. Chem. Thermodyn. 65 (2013) 174-183.

[9] M.J.P. Comuñas, J. Bazile, A. Baylaucq, C. Boned, J. Chem. Eng. Data 53 (2008) 986-994.

[10] H. Lagourette, B. Boned, C. Saint-Guirons, H. Xans, P. Zhou, Meas. Sci. Technol. 3 (1992) 699-703.

[11] W. Wagner, A. Pruß, J. Phys. Chem. Ref. Data 31 (2002) 387-535.

[12] Expression of the Uncertainty of Measurement in Calibration, European Cooperation for Accreditation, EA-4/02, 1999.

[13] TRC, Thermodynamic Tables, Texas A & M University, College Station, 1996.

[14] N. Muñoz-Rujas, F. Aguilar, J.-P. Bazile, E.A. Montero, Fluid Phase Equilib. 429 (2016) 281–292.

[15] N. Muñoz-Rujas, J.-P. Bazile, F. Aguilar, G. Galliero, E.A. Montero, J.L. Daridon, J. Chem. Thermodyn. 112 (2017) 52-58.

[16] A. Srhiyer, N. Muñoz-Rujas, F. Aguilar, J.J. Segovia, E.A. Montero, J. Chem. Thermodyn. 113 (2017) 213-218.

[17] M.H. Rausch, L. Kretschmer, S. Will, A. Leipertz, A.P. Fröba, J. Chem. Eng. Data 60 (2015) 3759–3765.

[18] C. A. Cerdeiriña, C. A. Tovar, D. González-Salgado, E. Carballo, L. Romaní, Phys. Chem. Chem. Phys. 3(2001) 5230–5236.

[19] J. Troncoso, D. Bessières, C. A. Cerdeiriña, E. Carballo, L. Romaní, Fluid Phase Equilib. 208 (2003) 141-154.

[20] J. Jacquemin, P. Husson, V. Mayer, I. Cibulka, J. Chem. Eng. Data 52 (2007) 2204-2211.

[21] Y. Miyake, A. Baylaucq, F. Plantier, D. Bessières, H. Ushiki, C. Boned, J. Chem. Thermodyn. 40 (2008) 836–845.

[22] G. Watson, T. Lafitte, C.K. Zéberg-Mikkelsen, A. Baylaucq, D. Bessieres, C. Boned, Fluid Phase Equilib. 247 (2006) 121-134.

[23] J. P. M. Trusler, Physical Acoustics and Metrology of Fluids, Adam Hilger, Bristol, 1991.

(P, V^E, T) Measurements of Mixtures Methyl Nonafluorobutyl Ether (HFE-7100) + 1-Propanol at Pressures up to 70 MPa and Temperatures from 298.15 K to 393.15 K.

Natalia Muñoz-Rujas[a], Fernando Aguilar[a], Eduardo A. Montero[a,]*

(a) Departamento de Ingeniería Electromecánica, Escuela Politécnica Superior, Universidad de Burgos, E-09006 Burgos, Spain

[*]Corresponding author: Phone: +34947258916, Fax: +34947258916, e-mail: emontero@ubu.es

Abstract

Nowadays thermophysical properties characterization of new environmentally friendly fluids, as is the case of HFEs and its mixtures with other compounds, is necessary in order to well design the machinery and piping networks involved on its utilization. Indeed, scarce data concerning those kind of fluids is actually available. In this work, new experimental high pressure density data (742 points) for the binary system *x* HFE-7100 + (*1-x*) 1-propanol are presented. This property was measured by using an Anton Paar vibrating tube densitometer in the temperature range (298.15 – 393.15) K and in the pressure interval (0.1 – 70) MPa. A comparison between our experimental high pressure density data and those found in the literature was carried out only for the pure compounds since no density data for the binary mixture were available. To perform this comparison, we used a Tait-like equation in order to correlate our results to those of the literature. With the experimental density data the derivative properties isothermal compressibility, κ_T, and isobaric expansion, α_P, were determined in the same pressure and temperature ranges. Excess molar volumes of the binary system were also determined and compared with the ones of the mixture *x* HFE-7100 + (*1-x*) 2-propanol published in our previous work [1].

Keywords

Methyl Nonafluorobutyl Ether, 1-Propanol, High Pressure, Derivative Properties, Excess Volumes.

1. Introduction

HCFCs and HFCs are being widely used for common purposes such as refrigerant fluids, heat transfer media, as precision cleaning fluids or in aerosol applications among others. Although HFCs emerged as an alternative to the CFCs and HCFCs phase out proposal at expense of the

Montreal Protocol, in 1987, some of these fluorocarbons show high ozone depletion potentials (ODP), high global warming potentials (GWP) and also large atmospheric lifetimes (ALT). Due to this, many researchers led efforts to search for new fluids with the same properties as CFCs, HCFCs and HFCs but with zero or near zero ODP, low GWP and short atmospheric lifetimes.

Hydrofluoroether fluids (HFEs) were found as an alternative to these fluids since they have similar properties, so they are capable to substitute CFCs, HCFCs and HFCs in a wide array of applications [2]. HFEs have low GWP and short atmospheric lifetimes, properties which are provided by the oxygen atom of the ether in the molecule. HFEs also show zero ODP. HFEs are non-flammable fluids, and they are compatible with most metals and hard polymers [3]. With respect to the toxicity, HFEs briefly exhibit relatively low toxicity from the results of acute toxicity tests [4].

Methyl nonafluorobutyl ether, known as HFE-7100, possess some desirable properties such as high latent heat of vaporization, a high liquid density and low viscosity, properties that make it ideal to be used as CFC, HCFC, and HFC replacement as pure component or in mixture with other compounds such as ethers or alkanols.

Low molecular weight alcohols are acceptable rinsing and cleaning agents however they are flammable, so the addition of fluorinated compounds to the mixture will reduce or eliminate the flammability [5].

The binary mixture HFE-7100 + 1- propanol is a viable option in the replacement of some fluorocarbons. This binary mixture forms an azeotrope at a weight concentration of HFE-7100 of 97.90% that can be considered as a good replacement for HCFC-225ca/cb [6], a mixture of isomers primarily used in vapor degreasing and in aerosol applications.

Density is the most important physical property, and its determination as a function of temperature and pressure gives other valuable properties such as isothermal compressibility and isobaric expansion. With the molar mass, excess volumes can also be determined. In this work, densities for six mole fractions, x = (0.1502, 0.3258, 0.5010, 0.6754, 0.8495 and 0.9184) of the binary mixture x HFE-7100 + (1-x) 1-propanol have been measured within the temperature range from 298.15 to 393.15 K and in the pressure range from 0.1 to 70 MPa by using an Anton Paar U-tube densitometer with an uncertainty of + 0.7 $kg \cdot m^{-3}$ for the density. The derivative properties, that is, the isothermal compressibility and the isobaric expansion are also reported in the same pressure and temperature ranges.

2. Experimental

2.1 Materials

Methyl nonafluorobutyl ether or 1-methoxy-nonafluorobutane was obtained from the 3M Company. This fluid, also known as HFE-7100, ($C_5H_3F_9O$, molar mass 250.06 g·mol^{-1}) consists of two inseparable isomers with essentially identical properties (CAS 163702-08-7/163702-07-6). The supplier certifies a mass purity for HFE-7100 greater than 0.995. 1-propanol (C_3H_8O, molar mass 60.096 g·mol^{-1}, CAS 71-23-8), was obtained from Sigma-Aldrich with mole fraction purity of 0.998 and stored over molecular sieves type 0.4 to avoid any moisture. The two fluids were subject to no further purification method except careful degassing before the use. The specifications of both two fluids are reflected in Table 1.

Table 1. Description of the chemicals.

Compound	Source	Formula	Molar mass / g·mol^{-1}	Stated purity[a] / mol%	CAS number
HFE-7100[b]	3M Company	$C_5H_3F_9O$	250.06	>99.5[c]	163702-08-7 / 163702-07-6[d]
1-Propanol	Sigma-Aldrich	C_3H_8O	60.096	>99.8[e, f]	71-23-8

[a] Determined by gas chromatography (GC) by the supplier.
[b] HFE-7100 = 1,1,1,2,2,3,3,4,4-nonafluoro-4-methoxybutane.
[c] Mass fraction purity, g·mol^{-1}%
[d] Binary mixture of two isomers with mass ratio 0.5.
[e] The water content was checked to be less than 0.01% by titration method.
[f] Mole fraction purity, mol%.

2.2. Measurement technique. Experimental procedure

To determine high pressure density values of the binary system *x* HFE-7100 + (*1-x*) 1-propanol, an Anton Paar DMA HPM high pressure vibrating tube densitometer was employed. This technique belongs to the direct methods to determine the density of a fluid, and is based on the determination of the vibration period of the U-tube which is located inside the apparatus, and contains the sample. Then, the vibration period will depend on the mass of the fluid that is contained inside the U-tube; with this datum, the calibration constants A and B, the sample mass and the inner U-tube volume, density can be easily obtained.

By using this apparatus densities were determined in the pressure range (0.1 – 70) MPa at every 5 MPa steps, and along six isotherms (298.15, 313.15, 333.15, 353.15, 373.15 and 393.15) K. The experimental setup was described in one of our previous papers [7]. Concerning the calibration of the densitometer, the followed procedure was that described by Comuñas *et al.* [8] which is a modification of the procedure previously proposed by Lagourette *et al.* [9]. The

calibration was performed by using two reference fluids: vacuum and water, and taking the density values of water from the equation of state (EoS) reported by Wagner and Pruss [10]. Due to no measurements were done at temperatures over the boiling point of water (373.15 K) at 0.1 MPa, it was not necessary to consider other fluid to perform the calibrations at temperatures higher than 373.15 K and at 0.1 MPa.

Prior to make any measurement, it was necessary to ensure that all the circuit was completely clean in order not to contaminate the sample, so vacuum was done during almost one hour. All the samples were degassed prior to be introduced in the densitometer by using an ultrasonic bath PSelecta, model Ultrasons-H. The mixtures were prepared immediately before measuring, by weighing in glass vials sealed to prevent evaporation. For weighing, a Mettler Toledo balance model MS 204S has been used, with resolution of 10^{-4} g, and an uncertainty equal to ±0.0001 g. The estimated expanded uncertainty in the composition of the mixture is $\pm 4 \cdot 10^{-5}$ in mole fraction. Therefore, the excess molar volume should be accurate to within ±0.004 $cm^3 \cdot mol^{-1}$.

After preparing the mixtures and degassing, the densitometer was filled with the sample, and brought to the desired temperature by means of the thermostatic bath, and to the desired pressure by using the step by step engine. Considering the thermostatic bath, the estimated expanded uncertainty of the measured temperature was ±0.03 K (Pt 100 calibrated probe). For the pressure, we have that the estimated expanded uncertainty of the measured pressure was ±0.04 MPa (pressure transducer WIKA CPH 6000). Both temperature and pressure sensors were periodically calibrated before and after the measurement campaign. As mentioned above, the technique leads to determine the vibration period of the U-tube, then, in order to bring this datum, the DMA HPM measuring cell is connected to the Anton Paar mPDS 2000V3 evaluation unit, which evaluates the oscillation period from the measuring cell filled with the sample. The estimated expanded uncertainty (k = 2) is ±0.7 $kg \cdot m^{-3}$, and was calculated by using the recommended document EA-4/02 [11], taking into account the accuracy of the temperature, the pressure, the period of oscillation measurement for water, vacuum, and the studied systems, and the water density accuracy.

3. Results and Discussion

3.1. Density

High pressure densities were measured along six isotherms from 298.15 K to 393.15 K and in the pressure range from 0.1 MPa to 70 MPa at every 5 MPa. To have a good representation of the density behaviour in the whole composition range, eight mole compositions of the mixture *x* HFE-7100 + (*1*-*x*) 1-propanol were measured: (*x* = 0.0000, *x* = 0.1502, *x* = 0.3258, *x* = 0.4963, *x* = 0.6754, *x* = 0.8495, *x* = 0.9184 and *x* = 1.0000), where the mole fraction *x* = 0.9184

corresponds to the azeotropic composition of the binary mixture [6]. For the mole composition x = 1.000, the density data are referred to our previous work [1]. Table 2 gathers the data of the experimental measurements obtained by using the vibrating tube densitometer. The boiling points at 0.1 MPa for the pure components determine the boiling point for the different molar fractions of the mixture at 0.1 MPa. Taking this into account we have that for HFE-7100 its boiling temperature T_b = 332.85 K [2], and for the pure 1-propanol T_b = 370.26 K [12], then it was estimated that for the mole compositions x = 0.0000 and x = 0.1502 no measurements should be done at 0.1 MPa and at 373.15 K and 393.15 K due to the mixture will be in vapour phase. The same occurs for the mole compositions x = 0.3258, x = 0.4963, x = 0.6754 at 0.1 MPa and at 353.15, 373.15 and 393.15 K, and for the mole compositions x = 0.8495, x = 0.9184 and x = 1.0000, for which measurements at 0.1 MPa and at temperatures 333.15, 353.15, 373.15 and 393.15 K shouldn't be done. Following these estimations, no measurements were done at the aforementioned pressures and temperatures for the different mole compositions that finally results in a total amount of 742 density points.

Table 2. Experimental values of density ρ, at temperatures T and pressures P for the binary mixture x HFE-7100 + (*1*-x) 1-propanol[a].

x	P / MPa	T / K					
		298.15	313.15	333.15	353.15	373.15	393.15
		ρ / g·cm^{-3}					
0.0000	0.10	0.7996	0.7873	0.7703	0.7522		
	1.00	0.8003	0.7880	0.7712	0.7532	0.7335	0.7117
	5.00	0.8035	0.7915	0.7751	0.7577	0.7386	0.7177
	10.00	0.8073	0.7955	0.7796	0.7628	0.7445	0.7245
	15.00	0.8108	0.7994	0.7839	0.7675	0.7500	0.7308
	20.00	0.8142	0.8031	0.7880	0.7720	0.7550	0.7366
	25.00	0.8176	0.8067	0.7918	0.7764	0.7598	0.7421
	30.00	0.8207	0.8099	0.7955	0.7804	0.7644	0.7471
	35.00	0.8237	0.8133	0.7991	0.7844	0.7686	0.7518
	40.00	0.8267	0.8164	0.8024	0.7881	0.7727	0.7564
	45.00	0.8297	0.8194	0.8057	0.7915	0.7766	0.7606
	50.00	0.8324	0.8224	0.8089	0.7950	0.7803	0.7647
	55.00	0.8351	0.8252	0.8119	0.7983	0.7839	0.7686
	60.00	0.8378	0.8279	0.8149	0.8014	0.7873	0.7724
	65.00	0.8404	0.8307	0.8178	0.8046	0.7907	0.7761
	70.00	0.8429	0.8333	0.8207	0.8076	0.7939	0.7796
0.1502	0.10	0.9994	0.9804	0.9523	0.9242		
	1.00	1.0005	0.9816	0.9541	0.9261	0.8961	0.8632
	5.00	1.0058	0.9876	0.9609	0.9340	0.9055	0.8748
	10.00	1.0119	0.9944	0.9687	0.9430	0.9160	0.8874

	15.00	1.0175	1.0007	0.9760	0.9511	0.9255	0.8985
	20.00	1.0226	1.0066	0.9827	0.9587	0.9340	0.9083
	25.00	1.0276	1.0122	0.9889	0.9657	0.9420	0.9174
	30.00	1.0323	1.0173	0.9949	0.9722	0.9495	0.9257
	35.00	1.0367	1.0224	1.0005	0.9786	0.9562	0.9334
	40.00	1.0410	1.0269	1.0057	0.9843	0.9628	0.9405
	45.00	1.0451	1.0315	1.0109	0.9898	0.9688	0.9472
	50.00	1.0490	1.0359	1.0157	0.9952	0.9746	0.9536
	55.00	1.0529	1.0400	1.0203	1.0003	0.9802	0.9596
	60.00	1.0566	1.0440	1.0248	1.0051	0.9854	0.9655
	65.00	1.0602	1.0480	1.0292	1.0098	0.9905	0.9710
	70.00	1.0636	1.0517	1.0334	1.0144	0.9953	0.9763
0.3267	0.10	1.1572	1.1324	1.0978			
	1.00	1.1589	1.1344	1.1002	1.0637	1.0237	0.9789
	5.00	1.1662	1.1427	1.1100	1.0756	1.0383	0.9977
	10.00	1.1748	1.1521	1.1210	1.0886	1.0539	1.0168
	15.00	1.1827	1.1608	1.1311	1.1002	1.0676	1.0331
	20.00	1.1900	1.1689	1.1402	1.1106	1.0797	1.0472
	25.00	1.1970	1.1765	1.1488	1.1204	1.0907	1.0598
	30.00	1.2035	1.1836	1.1567	1.1293	1.1009	1.0713
	35.00	1.2098	1.1904	1.1643	1.1377	1.1101	1.0817
	40.00	1.2158	1.1967	1.1712	1.1455	1.1189	1.0914
	45.00	1.2216	1.2029	1.1780	1.1528	1.1270	1.1003
	50.00	1.2270	1.2088	1.1844	1.1599	1.1347	1.1087
	55.00	1.2324	1.2144	1.1905	1.1665	1.1419	1.1167
	60.00	1.2375	1.2198	1.1964	1.1729	1.1488	1.1243
	65.00	1.2425	1.2251	1.2020	1.1790	1.1555	1.1315
	70.00	1.2472	1.2301	1.2075	1.1848	1.1618	1.1383
0.5004	0.10	1.2817	1.2530	1.2118			
	1.00	1.2838	1.2556	1.2150	1.1706	1.1223	1.0663
	5.00	1.2931	1.2663	1.2282	1.1868	1.1430	1.0936
	10.00	1.3037	1.2785	1.2429	1.2043	1.1644	1.1202
	15.00	1.3136	1.2896	1.2561	1.2197	1.1826	1.1419
	20.00	1.3226	1.2998	1.2679	1.2335	1.1983	1.1605
	25.00	1.3312	1.3093	1.2789	1.2460	1.2127	1.1768
	30.00	1.3392	1.3182	1.2890	1.2574	1.2257	1.1914
	35.00	1.3469	1.3267	1.2985	1.2680	1.2377	1.2048
	40.00	1.3542	1.3345	1.3075	1.2777	1.2483	1.2170
	45.00	1.3611	1.3421	1.3160	1.2871	1.2586	1.2282
	50.00	1.3676	1.3493	1.3239	1.2958	1.2683	1.2388
	55.00	1.3740	1.3562	1.3315	1.3041	1.2773	1.2487
	60.00	1.3802	1.3627	1.3387	1.3120	1.2859	1.2581
	65.00	1.3861	1.3691	1.3457	1.3195	1.2940	1.2669
	70.00	1.3917	1.3752	1.3524	1.3268	1.3017	1.2754

0.6757	0.10	1.3772	1.3427	1.2942			
	1.00	1.3797	1.3456	1.2980	1.2469	1.1905	1.1267
	5.00	1.3906	1.3582	1.3133	1.2661	1.2153	1.1602
	10.00	1.4031	1.3722	1.3301	1.2865	1.2404	1.1919
	15.00	1.4144	1.3850	1.3451	1.3041	1.2615	1.2173
	20.00	1.4249	1.3967	1.3586	1.3197	1.2796	1.2386
	25.00	1.4348	1.4076	1.3709	1.3339	1.2959	1.2573
	30.00	1.4440	1.4176	1.3823	1.3467	1.3105	1.2738
	35.00	1.4526	1.4271	1.3929	1.3586	1.3237	1.2887
	40.00	1.4609	1.4359	1.4027	1.3696	1.3361	1.3023
	45.00	1.4688	1.4444	1.4121	1.3799	1.3475	1.3148
	50.00	1.4763	1.4525	1.4210	1.3896	1.3582	1.3266
	55.00	1.4835	1.4601	1.4293	1.3989	1.3681	1.3375
	60.00	1.4904	1.4675	1.4374	1.4075	1.3776	1.3479
	65.00	1.4970	1.4746	1.4450	1.4159	1.3867	1.3576
	70.00	1.5033	1.4814	1.4524	1.4239	1.3952	1.3668
0.8495	0.10	1.4558	1.4178				
	1.00	1.4586	1.4211	1.3687	1.3128	1.2515	1.1822
	5.00	1.4708	1.4353	1.3863	1.3350	1.2806	1.2218
	10.00	1.4848	1.4512	1.4054	1.3584	1.3093	1.2583
	15.00	1.4975	1.4655	1.4223	1.3782	1.3332	1.2870
	20.00	1.5091	1.4786	1.4373	1.3958	1.3536	1.3108
	25.00	1.5200	1.4906	1.4511	1.4116	1.3717	1.3315
	30.00	1.5302	1.5017	1.4638	1.4259	1.3879	1.3499
	35.00	1.5397	1.5122	1.4755	1.4391	1.4026	1.3662
	40.00	1.5489	1.5220	1.4859	1.4513	1.4162	1.3813
	45.00	1.5575	1.5313	1.4963	1.4626	1.4287	1.3951
	50.00	1.5656	1.5402	1.5061	1.4733	1.4405	1.4078
	55.00	1.5736	1.5486	1.5154	1.4834	1.4515	1.4198
	60.00	1.5811	1.5566	1.5243	1.4930	1.4618	1.4311
	65.00	1.5883	1.5643	1.5328	1.5021	1.4717	1.4417
	70.00	1.5952	1.5718	1.5409	1.5109	1.4810	1.4518
0.9184	0.10	1.4835	1.4445				
	1.00	1.4865	1.4481	1.3944	1.3372	1.2751	1.2049
	5.00	1.4992	1.4629	1.4128	1.3605	1.3054	1.2462
	10.00	1.5137	1.4794	1.4326	1.3848	1.3353	1.2840
	15.00	1.5268	1.4941	1.4502	1.4054	1.3600	1.3136
	20.00	1.5389	1.5077	1.4657	1.4235	1.3811	1.3382
	25.00	1.5502	1.5201	1.4799	1.4399	1.3998	1.3596
	30.00	1.5606	1.5316	1.4930	1.4546	1.4165	1.3784
	35.00	1.5705	1.5425	1.5052	1.4683	1.4316	1.3953
	40.00	1.5799	1.5526	1.5163	1.4808	1.4457	1.4107
	45.00	1.5888	1.5622	1.5271	1.4925	1.4585	1.4249

	50.00	1.5972	1.5713	1.5371	1.5035	1.4706	1.4380
	55.00	1.6053	1.5800	1.5465	1.5139	1.4819	1.4502
	60.00	1.6131	1.5882	1.5556	1.5237	1.4925	1.4618
	65.00	1.6206	1.5962	1.5642	1.5331	1.5026	1.4727
	70.00	1.6276	1.6038	1.5726	1.5421	1.5122	1.4831
1.0000	0.10	1.5155	1.4759				
	1.00	1.5186	1.4796	1.4253	1.3677	1.3048	1.2339
	5.00	1.5318	1.4950	1.4444	1.3918	1.3361	1.2766
	10.00	1.5468	1.5120	1.4649	1.4169	1.3670	1.3153
	15.00	1.5603	1.5273	1.4830	1.4381	1.3924	1.3457
	20.00	1.5728	1.5413	1.4991	1.4568	1.4141	1.3710
	25.00	1.5844	1.5542	1.5138	1.4736	1.4333	1.3929
	30.00	1.5952	1.5660	1.5273	1.4888	1.4505	1.4122
	35.00	1.6054	1.5772	1.5397	1.5029	1.4660	1.4295
	40.00	1.6151	1.5876	1.5513	1.5157	1.4804	1.4453
	45.00	1.6243	1.5975	1.5623	1.5277	1.4936	1.4598
	50.00	1.6329	1.6068	1.5725	1.5390	1.5060	1.4732
	55.00	1.6413	1.6158	1.5822	1.5497	1.5175	1.4858
	60.00	1.6492	1.6242	1.5916	1.5597	1.5284	1.4977
	65.00	1.6569	1.6324	1.6005	1.5693	1.5388	1.5088
	70.00	1.6642	1.6403	1.6090	1.5786	1.5486	1.5194

[a] Estimated expanded uncertainties (k = 2) are: temperature, $U(T)$ = ± 0.03 K; pressure, $U(P)$ = ±0.04 MPa; mole fraction, $U(x)$ = ±0.00004; density, $U(\rho)$ = ±0.7 kg·m^{-3}.
Data at mole compostion x = 1.000 come from reference [1].

3.2. Tait representation

Due to experimental measurements give density points at a fixed pressure P, and temperature T, it is necessary to establish a correlation in order to better determine the behaviour of density over the whole pressure and temperature ranges. In our case, we have used a Tait-like equation for this purpose, and also to obtain the derivative properties. This equation was used in some of our previous works [1], [13, 14]. The equation is as follows:

$$\rho(T,p) = \frac{\rho_0(T)}{1 - C\ln\left(\frac{B(T) + p}{B(T) + 0.1\ \mathrm{MPa}}\right)} \quad (1)$$

Where:

$$\rho_0(T) = A_0 + A_1 T + A_2 T^2 + A_3 T^3 \quad (2)$$

$$B(T) = B_0 + B_1 T + B_2 T^2 \quad (3)$$

To obtain the A_i, B_i and C parameters values is necessary to correlate simultaneously all the experimental densities values versus pressure and temperature. The obtained parameters for the mixture *x* HFE-7100 + (*1-x*) 1-propanol are listed in Table 3 along with its deviations (Average Absolute Deviation AAD%, Maximum Deviation MD%, Average Deviation AD%, Standard Deviation σ, and Root Mean Square Deviation RMSD). In Figure 1 can be seen different plots for density versus temperature / pressure representations for the eight mole compositions. Graph (a) presents high pressure density data vs. temperature at 1 MPa while graph (b) shows density vs. temperature at the maximum pressure measured, 70 MPa. For all the compositions, density decreases when increasing temperature, following the principle that an increase in temperature promotes the molecular agitation and its separation, deriving in a decrease on density values. Comparing graphs (a) and (b), it can be seen that the highest density values are found at 70 MPa; it is a result of the approximation of the molecules due to the increase of pressure.

When comparing density values versus pressure, graphs (c) and (d) are indicative of the influence of temperature on density. At lower temperatures, that is the case of graph (c), (298.15 K) the values of density are quite high than those of graph (d), at 393.15 K considering the same mole composition. As abovementioned, an increase on temperature promotes a decrease on density. Figure 1 shows also the representation given by the Tait-like equation, becoming clear the good agreement provided by this equation to correlate the density values.

Table 3. Parameters and deviations for density correlation by using equations (1) to (3) for the mixture *x* HFE-7100 + (*1-x*) 1-Propanol.

Parameters	*x*			
	0.0000	0.1502	0.3267	0.5004
A_0 / g cm^{-3}	1.331097	0.920369	2.251629	1.839532
A_1 / g cm^{-3} K^{-1}	$-3.788955\cdot10^{-3}$	$2.295496\cdot10^{-3}$	$-7.921889\cdot10^{-3}$	$-3.211469\cdot10^{-3}$
A_2 / g cm^{-3} K^{-2}	$1.020614\cdot10^{-5}$	$-8.634220\cdot10^{-6}$	$2.170865\cdot10^{-5}$	$8.793464\cdot10^{-6}$
A_3 / g cm^{-3} K^{-3}	$-1.165938\cdot10^{-8}$	$6.126779\cdot10^{-9}$	$-2.498247\cdot10^{-8}$	$-1.441912\cdot10^{-8}$
B_0 / MPa	300.6631	403.4429	285.9509	325.6063
B_1 / MPa K^{-1}	-0.8549343	-1.649344	-1.091895	-1.377304
B_2 / MPa K^{-2}	$4.930723\cdot10^{-4}$	$1.731205\cdot10^{-3}$	$1.027191\cdot10^{-3}$	$1.469064\cdot10^{-3}$
C	0.08897226	0.08394413	0.08433540	0.0854712
AAD /(%)	0.01	0.03	0.01	0.02
MD /(%)	0.03	0.09	0.03	0.08
Bias /(%)	$-2.10\cdot10^{-5}$	$9.91\cdot10^{-4}$	$-1.08\cdot10^{-5}$	$1.44\cdot10^{-5}$
σ /(g·cm^{-3})	$9.61\cdot10^{-5}$	$3.43\cdot10^{-4}$	$1.27\cdot10^{-4}$	$3.65\cdot10^{-4}$
RMSD /(g·cm^{-3})	$9.32\cdot10^{-5}$	$3.28\cdot10^{-4}$	$1.22\cdot10^{-4}$	$3.49\cdot10^{-4}$

Parameters	*x*			
	0.6757	0.8495	0.9184	1.0000
A_0 / g cm^{-3}	2.967275	3.116687	3.044518	2.931883
A_1 / g cm^{-3} K^{-1}	$-1.177863\cdot10^{-2}$	$-1.211537\cdot10^{-2}$	$-1.110597\cdot10^{-2}$	$-9.745889\cdot10^{-3}$
A_2 / g cm^{-3} K^{-2}	$3.299252\cdot10^{-5}$	$3.362117\cdot10^{-5}$	$3.040079\cdot10^{-5}$	$2.621836\cdot10^{-5}$
A_3 / g cm^{-3} K^{-3}	$-3.814353\cdot10^{-8}$	$-3.913635\cdot10^{-8}$	$-3.592223\cdot10^{-8}$	$-3.173991\cdot10^{-8}$
B_0 / MPa	289.0735	291.1874	289.0501	290.3497
B_1 / MPa K^{-1}	-1.208301	-1.248919	-1.247116	-1.256549
B_2 / MPa K^{-2}	$1.261910\cdot10^{-3}$	$1.343254\cdot10^{-3}$	$1.350916\cdot10^{-3}$	$1.367948\cdot10^{-3}$
C	0.08441107	0.08419121	0.0840422	0.08490464
AAD /(%)	0.01	0.01	0.01	0.01
MD /(%)	0.03	0.05	0.05	0.12
Bias /(%)	$4.86\cdot10^{-5}$	$-4.74\cdot10^{-5}$	$-4.31\cdot10^{-5}$	$4.13\cdot10^{-5}$
σ /(g·cm^{-3})	$1.67\cdot10^{-4}$	$2.19\cdot10^{-4}$	$1.98\cdot10^{-4}$	$2.99\cdot10^{-4}$
RMSD /(g·cm^{-3})	$1.60\cdot10^{-4}$	$2.09\cdot10^{-4}$	$1.89\cdot10^{-4}$	$2.90\cdot10^{-4}$

N is the number of experimental data points and *m* is the number of parameters.

[a]Absolute Average Deviation: $\mathrm{AAD} = \frac{100}{\mathrm{N}} \sum_{\mathrm{i=1}}^{\mathrm{N}} \left| \frac{\rho_{\mathrm{i}}^{\mathrm{exp}} - \rho_{\mathrm{i}}^{\mathrm{calc}}}{\rho_{\mathrm{i}}^{\mathrm{exp}}} \right|$

[b]Maximum deviation: $\mathrm{MD} = \mathrm{Max}\left(100 \left| \frac{\rho_{\mathrm{i}}^{\mathrm{exp}} - \rho_{\mathrm{i}}^{\mathrm{calc}}}{\rho_{\mathrm{i}}^{\mathrm{exp}}} \right| \right)$

[c]Average Deviation: $\mathrm{Bias} = \frac{100}{\mathrm{N}} \sum_{\mathrm{i=1}}^{\mathrm{N}} \frac{\rho_{\mathrm{i}}^{\mathrm{exp}} - \rho_{\mathrm{i}}^{\mathrm{calc}}}{\rho_{\mathrm{i}}^{\mathrm{exp}}}$

[d]Standard Deviation: $\sigma = \sqrt{\frac{\sum_{\mathrm{i=1}}^{\mathrm{N}} (\rho_{\mathrm{i}}^{\mathrm{exp}} - \rho_{\mathrm{i}}^{\mathrm{calc}})^2}{\mathrm{N\text{-}m}}}$

[e]Root Mean Square Deviation: $\mathrm{RMSD} = \sqrt{\frac{\sum_{\mathrm{i=1}}^{\mathrm{N}} (\rho_{\mathrm{i}}^{\mathrm{exp}} - \rho_{\mathrm{i}}^{\mathrm{calc}})^2}{\mathrm{N}}}$

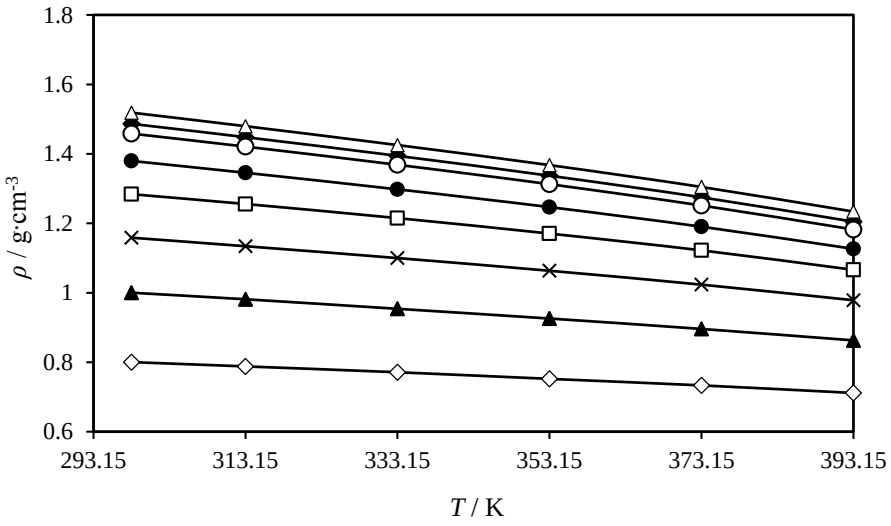
1.8
1.6
1.4
1.2
1
0.8
0.6
ρ / g·cm-3
293.15
313.15
333.15
353.15
373.15
393.15
T / K

(a)

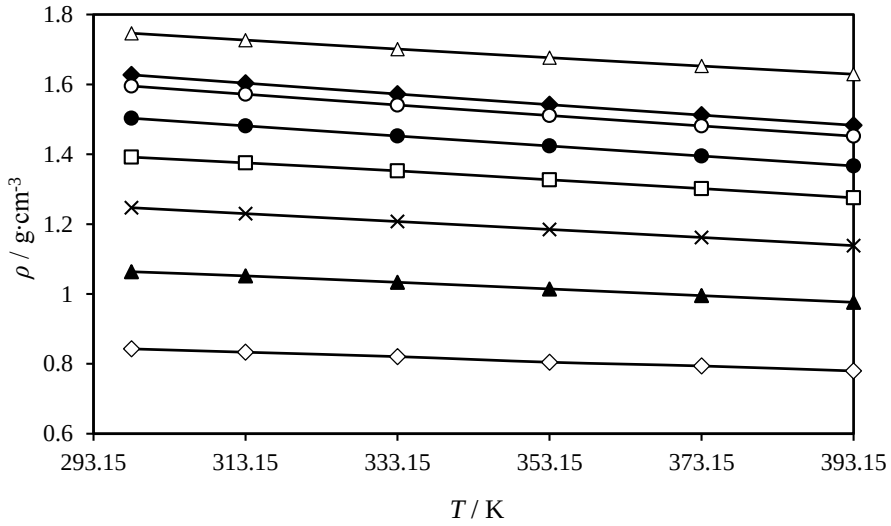
1.8
1.6
1.4
1.2
1
0.8
0.6
ρ / g·cm-3
293.15
313.15
333.15
353.15
373.15
393.15
T / K

(b)

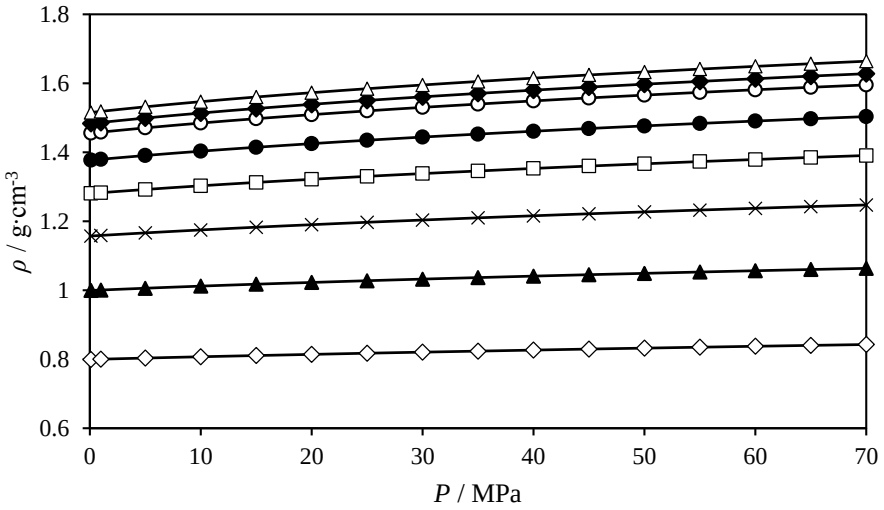

(c)

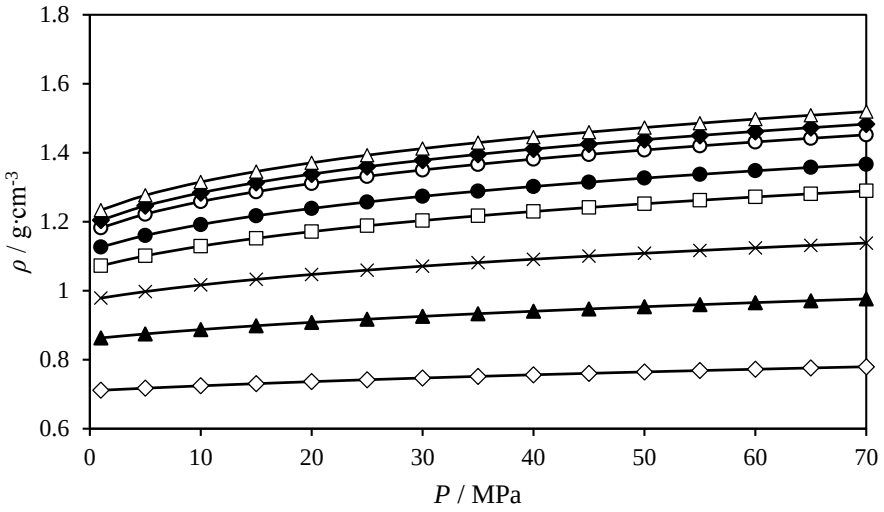

(d)

Figure 1. Experimental values of densities, ρ, for different mole fractions of x HFE-7100 + (1-x) 1-propanol vs. (a) the temperature, T at 1 MPa, (b) the temperature, T at 70 MPa, (c) the pressure, P at 298.15 K and (d) the pressure, P at 393.15 K: ◊; x = 0.0000, ▲; x = 0.1502, ×; x = 0.3258, □; x = 0.4963, ●; x = 0.6754, ○; x = 0.8495, ♦; x = 0.9184, Δ; x = 1.0000, (—); equations (1) to (3).

3.3. Comparison with literature data

Due to the density of both two pure fluids was previously measured by some authors, a comparison between our values and those found in the literature was carried out. When making that comparisons, the experimental high pressure density data were correlated by using

equations (1) to (3) due to some of the published data are not in the same *P*, *T* sets than ours. For pure HFE-7100 scarce density data was available. Only two references report data at high pressure [15, 16] while three references give density data at 0.1 MPa [17 - 19]. At atmospheric pressure, the three references give density values at 298.15 K, being only reference [19] the one that brings more than one point and in the temperature interval (298.15 – 363.15) K. The highest deviation is found for reference [18], with an AAD% = MD% = Bias% = 1.35. For the two references at high pressure, [16] is the one which provides data at pressures higher than the measured by us (100 MPa), with a total of 116 points in our *P*, *T* ranges, and with a MD% = 0.25. For reference [15], the total of 60 points provide better deviations, with a MD% = 0.08. These results can be seen in Figure 2.

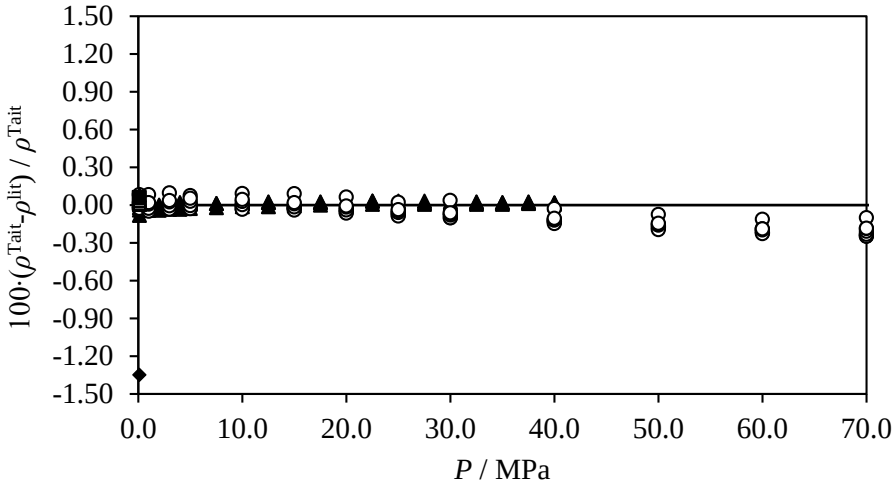

Figure 2. Deviations between the experimental values of densities and those obtained in the literature for pure HFE-7100. ■; reference [17], ♦; reference [18], Δ; reference [19], ▲; reference [15], ○; reference [16].

For pure 1-propanol several authors report high pressure density data. A set of 16 references [20 - 36], were found in the literature in different pressure and temperature ranges. Most of them report data at pressures lower than those measured by us, being references [20 and 36] the ones that bring a set of data at higher pressures, with values of 139.0 and 140.0 MPa respectively. To respect to the temperatures, only reference [31] provides density values at higher temperatures, although we have considered only those that fit our temperature range. Concerning the deviations, the results are quite satisfactory. The better results were found for reference [28], with an AAD% = 0.01, a Bias% = 0.01 and a MD% = 0.03 while the worst values are those of reference [34], with an AAD% = Bias% = 0.12, and a MD% = 0.21. Very few references have values of average deviations (AD%) higher than the expanded uncertainty (±0.07 %), being only two of them [25 and 34] above that value with an AD% = 0.08 and 0.12 respectively. Table

4 presents the summary of the references, along with its deviations, and the number of points which are in our *P, T* ranges. No data were found in the literature for the mixture *x* HFE-7100 + (*1-x*) 1-propanol to compare with.

Table 4. Comparison between the values generated by using the Tait-like equation at exactly the same experimental *P, T* sets given for 1-propanol for several literature references.

Reference	Year	N_P	T_{min} / K	T_{max} / K	P_{min} / MPa	P_{max} / MPa	AAD / %	MD / %	Bias / %	Density uncertainty
Kubota *et al.* [20]	1987	27	298.15	348.15	0.1	139.0	0.06	0.13	-0.05	±0.8 kg·m^{-3}
Ormanoudis *et al.* [21]	1991	11	298.15	308.15	0.1	33.8	0.04	0.06	-0.04	±10^{-4} g·cm^{-3}
Papaioannou *et al.* [22]	1993	10	298.15	298.15	0.1	33.9	0.05	0.07	-0.05	±10^{-4} g·cm^{-3}
Papaioannou and Panayiotou [23]	1995	10	298.15	298.15	0.1	33.9	0.06	0.09	-0.06	±10^{-4} g·cm^{-3}
Yaginuma *et al.* [24]	1998	12	313.15	313.15	0.1	9.8	0.07	0.10	0.04	±0.1 kg·m^{-3}
Zúñiga-Moreno and Galicia-Luna [25]	2002	164	298.07	362.77	0.1	25.090	0.08	0.12	0.08	<0.05%
Kitajima *et al.* [26]	2003	16	315.15	390.15	5.12	27.0	0.03	0.04	-0.03	±0.16%
Gil-Hernández *et al.* [27]	2005	20	298.15	308.15	0.1	19.7	0.05	0.14	-0.04	0.1 kg·m^{-3}
Zéberg-Mikkelsen and Andersen [28]	2005	28	303.15	333.15	0.1	30.0	0.01	0.03	0.01	±0.05%
Watson *et al.* [29 and 30]	2006	84	303.15	353.15	0.1	65.0	0.04	0.09	3.41·10^{-3}	±0.5 kg·m^{-3}
Abdulagatov *et al.* [31]	2008	36	298.15	373.15	0.11	39.95	0.04	0.11	0.04	±0.02%
Torcal *et al.* [32]	2010	15	298.15	328.15	0.1	20.0	0.03	0.09	-0.02	±0.5 kg·m^{-3}
Torcal *et al.* [33]	2010	15	298.15	328.15	20.0	60.0	0.04	0.09	0.04	±0.5 kg·m^{-3}
Dávila *et al.* [34]	2012	98	298.15	358.15	0.1	60.0	0.12	0.21	0.12	±0.0012 g·cm^{-3}
Kariznovi *et al.* [35]	2013	22	303.2	323.2	0.1	10.0	0.07	0.12	-0.02	0.1 kg·m^{-3}
Alaoui *et al.* [36]	2014	60	293.15	353.15	0.1	140.0	0.02	0.08	-1.54·10^{-3}	±0.05% g·cm^{-3}

N_P Number of data points which are in our *P, T* ranges.

3.4. Excess Molar Volumes

To well determine the difference in volume of the mixture between the theoretical results of mixing the two pure compounds and the experimental ones, the excess molar volumes V^E, were determined. These data were calculated by using equation (4):

$$V^E = \sum_{i=1}^{n} x_i M_i \left[\left(1/\rho \right) - \left(1/\rho_i \right) \right] \tag{4}$$

In this equation n is the number of components, x_i is the mole fraction of component i in the mixture, M_i is the molar mass of component i, ρ and ρ_i are the measured densities of the mixture and pure component i, respectively.

Figure 3 shows different representations of excess volumes V^E, vs. the composition x, considering a fixed temperature and evaluating what happens when pressure changes, as is the case of plots (a) at 298.15 K, and (b) at 393.15 K, or considering a fixed value in pressure evaluating temperature changes, as can be seen in plots (c) at P = 1 MPa and (d) at P = 70 MPa.

A comparison has been carried out between the obtained excess molar volumes for the mixture x HFE-7100 + (*1*-x) 1-propanol and the previously studied mixture x HFE-7100 + (*1*-x) 2-propanol [1] considering the same temperatures and the same pressures, and at practically the same mole compositions (x = 0.000, x = 0.1490, x = 0.3255, x = 0.4996, x = 0.6758, x = 0.7940, x = 0.8497 and x = 1.0000). Then, for all graphs, (a), (b), (c) and (d) the solid figures represent the excess volumes for the binary mixture x HFE-7100 + (*1*-x) 1-propanol while the hollow figures correspond to the excess volumes for the mixture x HFE-7100 + (*1*-x) 2-propanol.

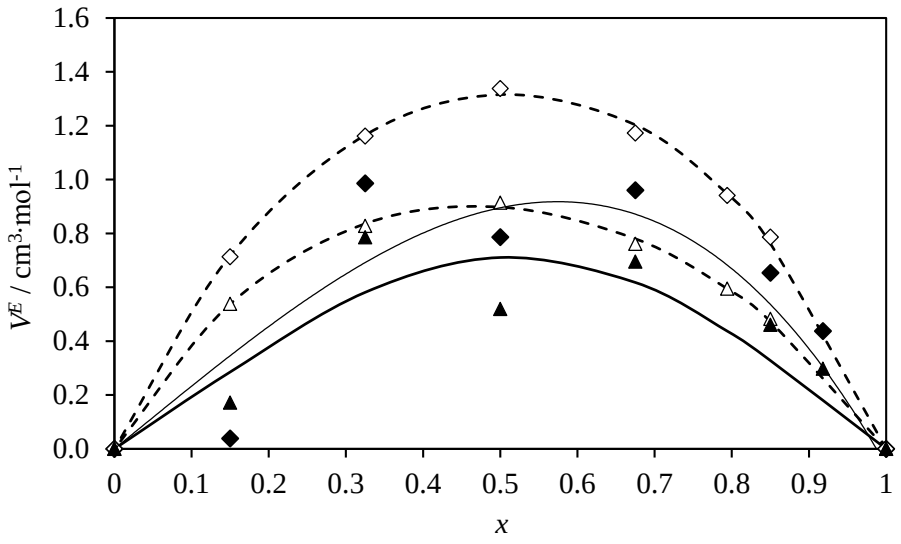

(a)

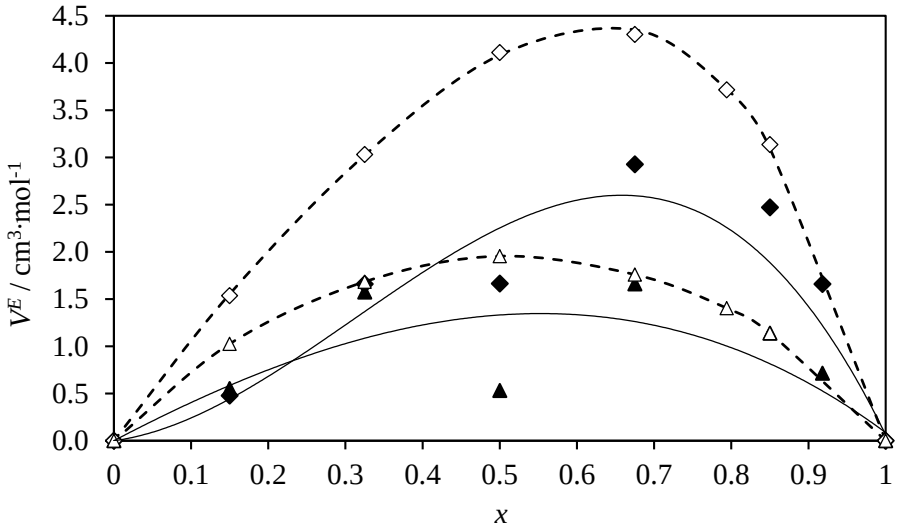
4.5
4.0
3.5
3.0
2.5
2.0
1.5
1.0
0.5
0.0
V^E / cm^3·mol^{-1}
0
0.1
0.2
0.3
0.4
0.5
0.6
0.7
0.8
0.9
1
x

(b)

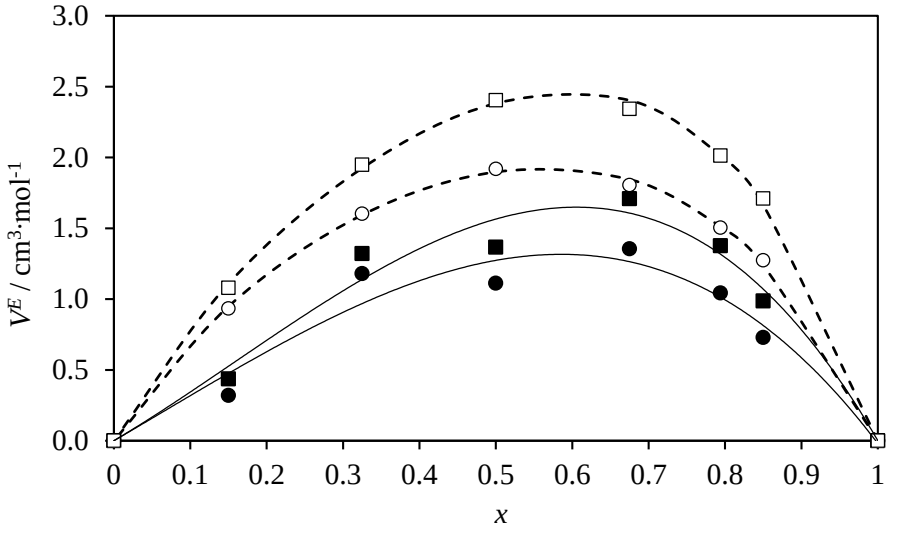
3.0
2.5
2.0
1.5
1.0
0.5
0.0
V^E / cm^3·mol^{-1}
0
0.1
0.2
0.3
0.4
0.5
0.6
0.7
0.8
0.9
1
x

(c)

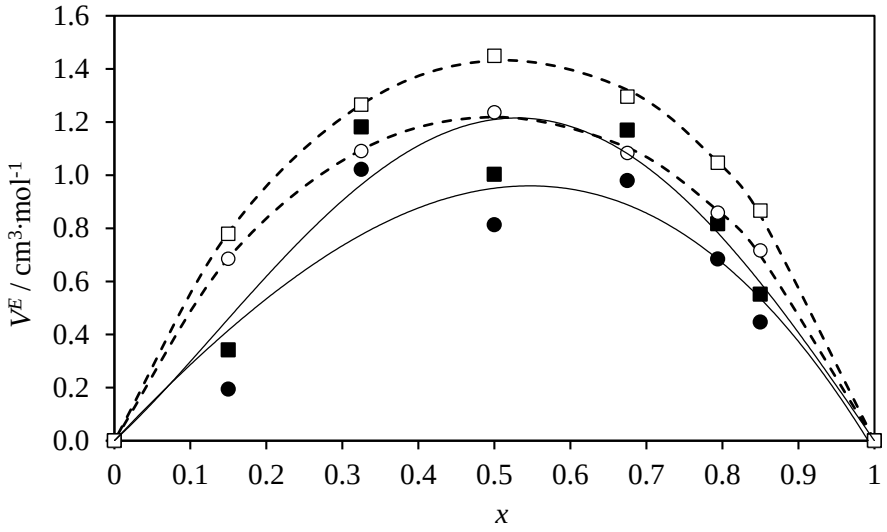

(d)

Figure 3. Comparison between the experimental values for excess volumes obtained for the binary mixture *x* HFE-7100 + (1-*x*) 1-propanol and the values of excess volumes for the system *x* HFE-7100 + (1-*x*) 2-propanol, reference [1] as a function of the mole fraction and at different pressures, (a) at 298.15 K, (b) at 393.15 K, where: ♦; 1 MPa, ▲; 70 MPa (for the mixture *x* HFE-7100 + (1-*x*) 1-propanol), ◊; 1 MPa, Δ; 70 MPa (for the mixture *x* HFE-7100 + (1-*x*) 2-propanol) and (c) at *P* = 1 MPa and (d) at *P* = 70 MPa at various temperatures, where: ●; 333.15 K, ■; 353.15 K (for the mixture *x* HFE-7100 + (1-*x*) 1-propanol), ○; 333.15 K, □; 353.15 K (for the mixture *x* HFE-7100 + (1-*x*) 2-propanol). (—), Redlich-Kister's equation (*x* HFE-7100 + (1-*x*) 1-propanol), (- -), Redlich-Kister's equation (*x* HFE-7100 + (1-*x*) 2-propanol).

In all the cases the excess volumes show a positive trend at the different temperatures and pressures measured. The size of the HFE-7100 molecules is much higher than the size of the 1-propanol molecules, so the approximation of both two types of molecules generates an expansion that takes place in the mixture, resulting in positive values of V^E. The low polarity of the HFE compared to that of the alkanol leads to a low packing effect, contributing to the relatively high values of excess volumes. The same positive tendency is observed for the mixture *x* HFE-7100 + (*1-x*) 2-propanol, being the values of excess volumes higher in the case of this mixture when comparing with the system *x* HFE-7100 + (*1-x*) 1-propanol.

In plots (a) and (b) can be seen that the differences in the V^E values become higher when the temperature increases; both plots show what occurs at different pressures, 1 MPa and 70 MPa considering a fixed temperature, 298.15 K for (a) and 393.15 K for (b). If we evaluate the pressure, at 1 MPa the excess volumes are higher in both cases (a) and (b) than for 70 MPa. When evaluating the temperature, the when the higher the temperature is, the higher the values of excess volumes, so we have a maximum value of V^E = 2.47 cm^3·mol^{-1} at *P* = 1 MPa and at *T* = 393.15 K for the mole composition *x* = 0.6757.

As described above, the V^E results for the compared mixture, *x* HFE-7100 + (*1-x*) 2-propanol, show higher values than for the mixture studied in this work in all cases. The different sizes between the two alkanol molecules promote the difference in excess volumes. The maximum value of V^E is found at the same mole composition, pressure and temperature than for the mixture *x* HFE-7100 + (*1-x*) 1-propanol; x = 0.6757, P = 1 MPa and at T = 393.15 K with a value of V^E = 4.30 $cm^3 \cdot mol^{-1}$.

By studying graphs (c) and (d), where a value of pressure is fixed and the changes in temperature are showed, it can be seen that for (c), at P = 1 MPa the values of V^E are higher than for (d), at P = 70 MPa for the two temperatures studied, 333.15 K and 353.15 K. Considering the temperature, the lower values are found when the lower the temperature is, then, for both graphs, values at 333.15 K are lower than values at 353.15 K, which is a consequence of the approximation of the molecules promoted by the decrease in temperature. In this case, the maximum value of V^E is found for the mole composition x = 0.6757 at P = 1 MPa and at T = 353.15 K with a V^E = 1.71 $cm^3 \cdot mol^{-1}$.

For the binary system *x* HFE-7100 + (*1-x*) 2-propanol, the tendency remains the same, being its V^E values higher than those of the mixture *x* HFE-7100 + (*1-x*) 1-propanol for all the pressures and all the temperatures. For this mixture, the higher value of V^E is found at the same pressure and temperature than for the mixture *x* HFE-7100 + (*1-x*) 1-propanol, (P = 1 MPa and T = 353.15 K) but for a different mole composition, x = 0.4996, with a V^E = 2.40 $cm^3 \cdot mol^{-1}$.

In addition, Figure 3 also shows the fitting curves obtained for both the two binary systems by using a Redlich-Kister polynomial of the type:

$$V^E = x(1-x)\sum_i z_i (2x-1)^{i-1} \tag{5}$$

In equation (5) z_i are the adjustable parameters, and x is the mole fraction of HFE-7100. Then, for the mixture studied in this work, *x* HFE-7100 + (*1-x*) 1-propanol, the solid line represents the fitting curve to the experimental data while for the previously studied system, *x* HFE-7100 + (*1-x*) 2-propanol, the dashed line corresponds to the fitting to the Redlich-Kister polynomial.

Table 5 reports the values of the adjustable parameters, z_i, and the standard deviations obtained by using equation (5) for different pressures at T = 298.15 K and at T = 393.15 K and also for all the temperatures measured at 1.0 MPa, 35.0 MPa and 70.0 MPa.

Table 5. Values of parameters z_i of equation (5) and the corresponding standard deviation, σ, for the binary system x HFE-7100 + (1-x) 1-propanol at 298.15 K and 393.15 K for different pressures, and at 1.0 MPa, 35.0 MPa and 70.0 MPa for all the temperatures measured.

	z_1	z_2	z_3	$\sigma(V^E)$/ $cm^3 \cdot mol^{-1}$
P / MPa		(T = 298.15 K)		
0.10	4.0445	1.3620	-3.0917	0.14
1.00	4.0492	1.3356	-3.0521	0.14
35.00	3.4601	0.6956	-2.2125	0.13
50.00	3.1758	0.4345	-1.5798	0.12
70.00	2.8412	0.2379	-0.8906	0.11
P / MPa		(T = 393.15 K)		
1.00	8.5461	7.8258	3.0543	0.27
35.00	6.6186	1.3842	3.4652	0.33
50.00	5.6358	1.0185	3.8922	0.34
70.00	4.6790	0.9201	4.2242	0.35
T / K		(P = 1.00 MPa)		
298.15	4.0492	1.3356	-3.0521	0.14
313.15	4.5102	1.7289	-2.6695	0.14
333.15	5.2403	1.9771	-0.9525	0.12
353.15	6.2577	3.0492	0.0167	0.11
373.15	6.4842	4.8158	3.7563	0.25
393.15	8.5461	7.8258	3.0543	0.27
T / K		(P = 35.00 MPa)		
298.15	3.4601	0.6956	-2.2125	0.13
313.15	4.0224	1.0967	-2.7305	0.14
333.15	4.7810	0.9683	-1.8112	0.12
353.15	5.7896	1.0307	-1.1828	0.12
373.15	5.0855	1.1341	4.3957	0.32
393.15	6.6186	1.3842	3.4652	0.33
T / K		(P = 70.00 MPa)		
298.15	2.8412	0.2379	-0.8906	0.11
313.15	3.3671	0.7735	-1.9915	0.13
333.15	4.0912	0.8366	-1.8719	0.13
353.15	4.8389	0.7572	-1.4379	0.12
373.15	3.6801	0.7984	4.6316	0.32
393.15	4.6790	0.9201	4.2242	0.35

3.5. The derived thermodynamic properties.

From experimental density data it is possible to obtain other properties of importance that will give valuable information on the dependence of the volumetric properties on temperature and pressure. This are the so called derivative properties, which are the isothermal compressibility κ_T, and the isobaric expansion α_P. The isothermal compressibility gives information about the effect of pressure on the density when the temperature remains constant, and it can be expressed as:

$$\kappa_T = \left(\frac{1}{\rho}\right)\left(\frac{\partial\rho}{\partial p}\right)_T = \frac{C}{\left(1 - C\ln\left(\frac{B(T)+p}{B(T)+0.1MPa}\right)\right)\left(B(T)+p\right)} \tag{6}$$

Table 6 gathers the values of isothermal compressibility for all the measured compositions of the binary mixture *x* HFE-7100 + (*1*-*x*) 1-propanol. Figure 4 shows a representation of κ_T versus the mole composition at (a) 298.15 K and (b) at 393.15 K. For the two plots the studied pressures are *P* = 1 MPa, 20 MPa, 40 MPa and 70 MPa. It can be seen both for plots (a) and (b) that for this property, when the higher the content of HFE-7100 in the mixture is, the higher the value of κ_T, with the exception of the case at 393.15 K and at 1 MPa, for which the value of κ_T at *x* = 1.0000 is slightly lower than for the precedent mole composition (*x* = 0.9184). Moreover, an increase in temperature promotes an increase on the values of isothermal compressibility, but therefore, when pressure increases κ_T decreases, being the mole composition *x* = 0.0000 at 298.15 and at 70.0 MPa the one with the lowest values of κ_T = 5.9 MPa^{-1}.

Table 6. Values of isothermal compressibility $\kappa_T \cdot 10^4$, for *x* HFE-7100 + (1-*x*) 1-propanol as function of pressure *P*, and at different temperatures T^a.

x	*P* / MPa	*T* / K					
		298.15	313.15	333.15	353.15	373.15	393.15
		$\kappa_T.10^4$ / MPa^{-1}					
0.0000	0.10	9.9	10.9	12.6			
	1.00	9.8	10.8	12.4	14.5	17.4	21.3
	5.00	9.5	10.4	11.8	13.7	16.2	19.6
	10.00	9.0	9.8	11.2	12.8	15.0	17.9
	15.00	8.6	9.4	10.6	12.1	13.9	16.4
	20.00	8.3	9.0	10.0	11.4	13.0	15.2
	25.00	7.9	8.6	9.6	10.8	12.3	14.1
	30.00	7.6	8.2	9.1	10.2	11.6	13.2
	35.00	7.4	7.9	8.7	9.7	10.9	12.4

	40.00	7.1	7.6	8.4	9.3	10.4	11.7
	45.00	6.9	7.3	8.1	8.9	9.9	11.1
	50.00	6.6	7.1	7.7	8.5	9.4	10.6
	55.00	6.4	6.8	7.5	8.2	9.0	10.1
	60.00	6.2	6.6	7.2	7.9	8.7	9.6
	65.00	6.0	6.4	7.0	7.6	8.3	9.2
	70.00	5.9	6.2	6.7	7.3	8.0	8.8
0.1502	0.10	12.8	14.8				
	1.00	12.6	14.6	17.8	22.2	28.0	35.7
	5.00	12.0	13.7	16.6	20.3	25.0	30.9
	10.00	11.2	12.8	15.2	18.3	22.0	26.6
	15.00	10.6	11.9	14.1	16.7	19.7	23.3
	20.00	10.0	11.2	13.1	15.3	17.9	20.8
	25.00	9.5	10.6	12.2	14.2	16.4	18.8
	30.00	9.1	10.0	11.5	13.2	15.1	17.2
	35.00	8.7	9.5	10.9	12.4	14.0	15.8
	40.00	8.3	9.1	10.3	11.6	13.1	14.7
	45.00	7.9	8.7	9.8	11.0	12.3	13.7
	50.00	7.6	8.3	9.3	10.4	11.6	12.8
	55.00	7.3	8.0	8.9	9.9	11.0	12.1
	60.00	7.1	7.7	8.5	9.4	10.4	11.4
	65.00	6.8	7.4	8.2	9.0	9.9	10.8
	70.00	6.6	7.1	7.8	8.6	9.4	10.3
0.3267	0.10	16.3	18.8				
	1.00	16.0	18.5	22.7	28.7	37.5	51.5
	5.00	15.0	17.1	20.7	25.6	32.3	42.2
	10.00	13.9	15.7	18.6	22.5	27.6	34.6
	15.00	12.9	14.5	17.0	20.1	24.1	29.4
	20.00	12.1	13.4	15.6	18.2	21.5	25.6
	25.00	11.4	12.6	14.4	16.7	19.4	22.7
	30.00	10.7	11.8	13.4	15.4	17.7	20.4
	35.00	10.2	11.1	12.6	14.3	16.2	18.6
	40.00	9.7	10.5	11.8	13.3	15.0	17.0
	45.00	9.2	10.0	11.1	12.5	14.0	15.8
	50.00	8.8	9.5	10.6	11.8	13.1	14.7
	55.00	8.4	9.1	10.0	11.1	12.3	13.7
	60.00	8.1	8.7	9.6	10.5	11.6	12.9
	65.00	7.8	8.3	9.1	10.0	11.0	12.2
	70.00	7.5	8.0	8.7	9.6	10.5	11.5
0.5004	0.10	18.7	22.2				
	1.00	18.4	21.8	27.8	36.6	49.9	70.6
	5.00	17.1	19.9	24.9	31.7	41.2	54.5
	10.00	15.6	18.0	22.0	27.2	34.0	42.6

	15.00	14.5	16.5	19.8	23.9	29.0	35.2
	20.00	13.5	15.2	17.9	21.3	25.3	30.0
	25.00	12.6	14.1	16.4	19.2	22.5	26.2
	30.00	11.8	13.1	15.2	17.6	20.3	23.3
	35.00	11.2	12.3	14.1	16.2	18.5	21.0
	40.00	10.6	11.6	13.2	15.0	17.0	19.2
	45.00	10.0	11.0	12.4	14.0	15.7	17.6
	50.00	9.5	10.4	11.7	13.1	14.7	16.3
	55.00	9.1	9.9	11.1	12.3	13.7	15.2
	60.00	8.7	9.4	10.5	11.7	12.9	14.2
	65.00	8.4	9.0	10.0	11.1	12.2	13.4
	70.00	8.0	8.7	9.5	10.5	11.6	12.7
0.6757	0.10	20.5	24.4				
	1.00	20.1	23.9	30.7	40.9	56.9	84.4
	5.00	18.5	21.6	27.1	34.8	45.8	62.2
	10.00	16.9	19.4	23.7	29.4	37.0	47.2
	15.00	15.5	17.6	21.1	25.5	31.1	38.2
	20.00	14.3	16.1	19.0	22.6	26.9	32.2
	25.00	13.3	14.9	17.3	20.3	23.7	27.9
	30.00	12.5	13.8	15.9	18.4	21.3	24.6
	35.00	11.7	12.9	14.7	16.9	19.3	22.1
	40.00	11.1	12.1	13.7	15.6	17.7	20.0
	45.00	10.5	11.4	12.9	14.5	16.3	18.4
	50.00	9.9	10.8	12.1	13.5	15.1	17.0
	55.00	9.5	10.3	11.4	12.7	14.2	15.8
	60.00	9.0	9.8	10.8	12.0	13.3	14.7
	65.00	8.7	9.3	10.3	11.4	12.5	13.8
	70.00	8.3	8.9	9.8	10.8	11.9	13.0
0.8495	0.10	22.0	26.4				
	1.00	21.5	25.7	33.5	45.3	64.2	96.6
	5.00	19.7	23.1	29.3	37.9	50.4	68.6
	10.00	17.8	20.6	25.3	31.6	39.9	50.8
	15.00	16.3	18.6	22.4	27.2	33.2	40.5
	20.00	15.0	16.9	20.1	23.9	28.5	33.9
	25.00	13.9	15.6	18.2	21.3	25.0	29.2
	30.00	13.0	14.4	16.7	19.3	22.3	25.7
	35.00	12.2	13.4	15.4	17.6	20.1	22.9
	40.00	11.4	12.6	14.3	16.2	18.4	20.8
	45.00	10.8	11.8	13.3	15.0	16.9	19.0
	50.00	10.3	11.2	12.5	14.0	15.7	17.5
	55.00	9.8	10.6	11.8	13.1	14.6	16.2
	60.00	9.3	10.1	11.2	12.4	13.7	15.2
	65.00	8.9	9.6	10.6	11.7	12.9	14.2
	70.00	8.5	9.2	10.1	11.1	12.2	13.4

0.9184	0.10	22.5	27.0				
	1.00	22.0	26.3	34.4	46.6	66.1	99.2
	5.00	20.1	23.6	30.0	38.8	51.5	69.9
	10.00	18.1	21.0	25.8	32.2	40.6	51.5
	15.00	16.5	18.9	22.8	27.6	33.7	41.0
	20.00	15.2	17.2	20.4	24.2	28.8	34.2
	25.00	14.1	15.8	18.4	21.6	25.2	29.4
	30.00	13.1	14.6	16.9	19.5	22.5	25.8
	35.00	12.3	13.6	15.5	17.8	20.3	23.1
	40.00	11.6	12.7	14.4	16.4	18.5	20.9
	45.00	10.9	12.0	13.5	15.2	17.0	19.1
	50.00	10.4	11.3	12.6	14.1	15.8	17.6
	55.00	9.9	10.7	11.9	13.3	14.7	16.3
	60.00	9.4	10.2	11.3	12.5	13.8	15.2
	65.00	9.0	9.7	10.7	11.8	13.0	14.3
	70.00	8.6	9.2	10.2	11.2	12.3	13.5
1.0000	0.10	22.7	27.3				
	1.00	22.2	26.6	34.7	46.8	66.0	97.6
	5.00	20.3	23.9	30.2	39.1	51.6	69.3
	10.00	18.3	21.2	26.1	32.5	40.8	51.3
	15.00	16.7	19.1	23.0	27.8	33.8	41.0
	20.00	15.4	17.4	20.6	24.4	29.0	34.2
	25.00	14.2	16.0	18.6	21.8	25.4	29.5
	30.00	13.3	14.8	17.0	19.7	22.6	25.9
	35.00	12.4	13.7	15.7	17.9	20.4	23.2
	40.00	11.7	12.9	14.6	16.5	18.7	21.0
	45.00	11.1	12.1	13.6	15.3	17.2	19.2
	50.00	10.5	11.4	12.8	14.3	15.9	17.7
	55.00	10.0	10.8	12.0	13.4	14.8	16.4
	60.00	9.5	10.3	11.4	12.6	13.9	15.3
	65.00	9.1	9.8	10.8	11.9	13.1	14.4
	70.00	8.7	9.3	10.3	11.3	12.4	13.6

[a] *Estimated expanded uncertainty (k=2): temperature U(T) = ±0.03 K, pressure U(P) = ±0.04 MPa, isothermal compressibility* $U(\kappa_T) = \pm 0.001\,\kappa_T$.

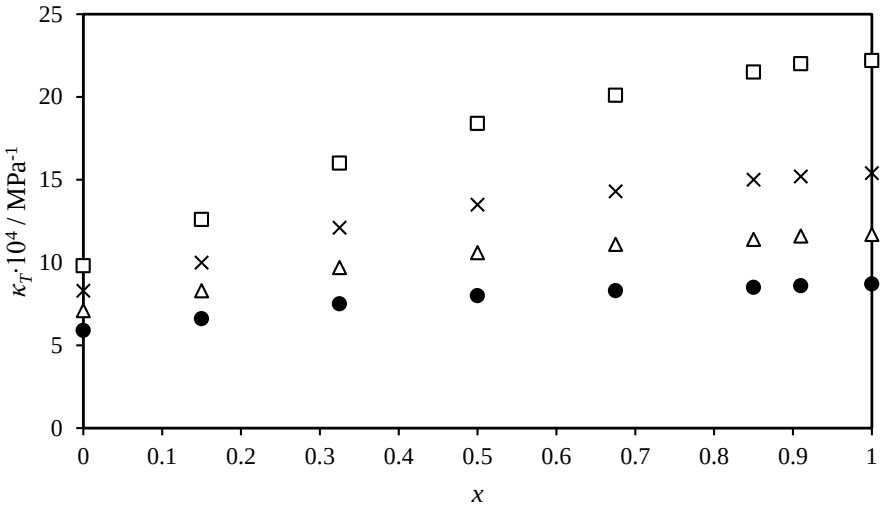

(a)

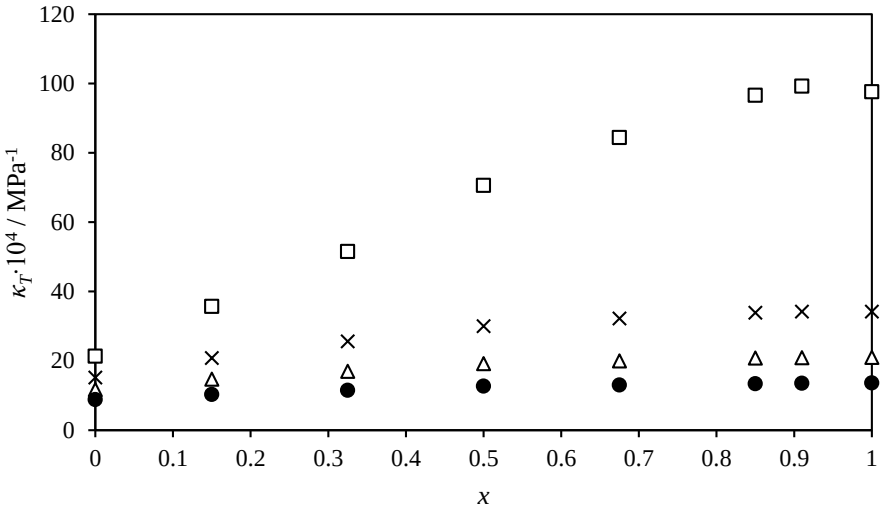

(b)

Figure 4. Isothermal compressibility κ_T, values for the binary mixture x HFE-7100 + (*1-x*) 1-propanol vs. the mole composition at different pressures P, and at (a) 298.15 K, and (b) 393.15 K. □; P = 1 MPa, ×; P = 20 MPa, Δ; P = 40 MPa, ●; P = 70 MPa.

In the same manner, the isobaric expansion α_P, could also be obtained by differentiating equation (1) taking into account the temperature dependence of $\rho_0(T)$ and $B(T)$:

$$\alpha_{\mathrm{p}} = -\left(\frac{1}{\rho}\right)\left(\frac{\partial \rho}{\partial T}\right)_{\mathrm{p}} \tag{7}$$

As some authors [37, 38] report the estimated isobaric expansion depends on the form of functions *B(T)* and $\rho_0(T)$. Also, Jaquemin *et al.* [39] have noticed that the differences that are sometimes found for α_P in the literature are due to the difference on density values, and also to the fitting equations. So as an alternative it was proposed to derive the isobaric expansion from the isobaric densities, and then at each pressure we suppose that $\rho_p(T) = a_0+a_1T+a_2T^2$ and consequently $(\partial\rho/\partial T)_p = a_1 + 2a_2T$. In this way we have that for each pressure we get a set (a_0, a_1, a_2).

By inserting the differentiated density and the calculated densities $\rho_p(T)$ into $\alpha_p = -(1/\rho(\partial\rho/\partial T)_p$ the isobaric expansion at the different *T, p* conditions has been derived:

$$\alpha_p = -\frac{a_1 + 2a_2T}{a_0 + a_1T + a_2T^2} \tag{8}$$

The estimated uncertainty following [11] is 1% for the isothermal compressibility and around 3% for the isobaric expansion, as recently indicated on similar high-pressure density studies [7, 8] and [29] with the same methods.

In Table 7 can be seen the values of isobaric expansion α_p for the binary mixture in the ranges of pressure at temperature measured experimentally, and for all the mole compositions studied. Figure 5 (a) and (b) show the values of isobaric expansion at 298.15 K and at 393.15 K respectively, and at different pressures. At 298.15 K (a), it can be observed that the values of α_p follow a tendency of decrease when increasing the pressure in all cases. When taking a look to the mole composition at a fixed pressure, α_p decreases when the higher the content of HFE-7100 is, except for the case of pure HFE-7100, whose value increases rapidly. Similarly as occurs at 298.15 K, at 393.15 K (b) the values of α_p are lower at high pressures when considering a fixed mole composition. Evaluating the mole compositions, the values of α_p are lower for the mixtures with less content in HFE-7100 up to a mole composition of x = 0.8495, then, the α_p values tend to decrease rapidly when increasing the HFE-7100 content. If we compare graphs (a) and (b), the values of isobaric expansion at 393.15 K are higher than for 298.15 K.

Table 7. Values of isobaric expansion $\alpha_P \cdot 10^4$, for x HFE-7100 + (1-x) 1-propanol as function of pressure P, and at different temperatures T^a.

x	P / MPa	T / K					
		298.15	313.15	333.15	353.15	373.15	393.15
				$\alpha_P.10^4$ / K^{-1}			
0.0000	0.10	10.1	10.7	11.5			
	1.00	9.7	10.5	11.5	12.6	13.8	15.1
	5.00	9.4	10.1	11.1	12.2	13.3	14.5
	10.00	9.0	9.7	10.7	11.7	12.8	14.0
	15.00	8.8	9.5	10.3	11.2	12.2	13.2
	20.00	8.6	9.2	10.0	10.8	11.7	12.6
	25.00	8.5	9.0	9.7	10.4	11.2	12.1
	30.00	8.3	8.7	9.4	10.1	10.9	11.6
	35.00	8.1	8.5	9.2	9.8	10.5	11.3
	40.00	8.0	8.4	9.0	9.6	10.2	10.8
	45.00	7.8	8.2	8.8	9.3	9.9	10.5
	50.00	7.7	8.1	8.6	9.1	9.7	10.2
	55.00	7.6	7.9	8.4	8.9	9.4	10.0
	60.00	7.5	7.8	8.2	8.7	9.2	9.7
	65.00	7.4	7.7	8.1	8.5	9.0	9.4
	70.00	7.2	7.5	7.9	8.4	8.8	9.3
0.1502	0.10	13.4	13.7				
	1.00	10.6	12.0	14.1	16.3	18.7	21.4
	5.00	10.0	11.4	13.3	15.4	17.7	20.3
	10.00	9.4	10.7	12.6	14.6	16.7	19.1
	15.00	8.9	10.1	11.9	13.8	15.9	18.1
	20.00	8.4	9.6	11.3	13.2	15.2	17.3
	25.00	8.0	9.2	10.9	12.7	14.6	16.6
	30.00	7.7	8.8	10.4	12.2	14.0	16.0
	35.00	7.4	8.5	10.1	11.8	13.6	15.5
	40.00	7.1	8.2	9.7	11.4	13.1	15.0
	45.00	6.8	7.9	9.4	11.0	12.7	14.6
	50.00	6.6	7.6	9.1	10.7	12.4	14.2
	55.00	6.3	7.4	8.9	10.4	12.1	13.8
	60.00	6.1	7.2	8.6	10.1	11.7	13.5
	65.00	5.9	7.0	8.4	9.9	11.5	13.2
	70.00	5.8	6.8	8.2	9.7	11.2	12.9
0.3267	0.10	14.9	15.3				
	1.00	11.2	13.0	15.7	18.5	21.7	25.3
	5.00	10.3	12.1	14.5	17.2	20.1	23.4
	10.00	9.5	11.1	13.4	15.9	18.7	21.7
	15.00	8.8	10.4	12.6	14.9	17.5	20.3
	20.00	8.3	9.8	11.9	14.1	16.6	19.3

	25.00	7.8	9.3	11.3	13.5	15.8	18.4
	30.00	7.4	8.8	10.8	12.9	15.2	17.7
	35.00	7.0	8.4	10.4	12.4	14.6	17.0
	40.00	6.7	8.1	10.0	12.0	14.1	16.5
	45.00	6.4	7.8	9.6	11.6	13.7	16.0
	50.00	6.2	7.5	9.3	11.3	13.3	15.6
	55.00	5.9	7.2	9.1	11.0	13.0	15.2
	60.00	5.7	7.0	8.8	10.7	12.7	14.8
	65.00	5.5	6.8	8.6	10.4	12.4	14.5
	70.00	5.3	6.6	8.4	10.2	12.1	14.2
0.5004	0.10	15.5	15.9				
	1.00	11.4	13.7	17.0	20.6	24.6	29.3
	5.00	10.2	12.3	15.3	18.7	22.3	26.5
	10.00	9.3	11.2	13.9	16.8	20.0	23.6
	15.00	8.7	10.5	13.1	15.9	18.9	22.3
	20.00	8.1	9.9	12.4	15.1	18.0	21.2
	25.00	7.2	8.9	11.3	13.8	16.5	19.4
	30.00	6.8	8.4	10.7	13.1	15.7	18.6
	35.00	6.3	7.9	10.1	12.5	15.0	17.8
	40.00	6.0	7.5	9.7	12.0	14.5	17.1
	45.00	5.6	7.2	9.3	11.6	14.0	16.6
	50.00	5.3	6.9	8.9	11.1	13.5	16.0
	55.00	5.1	6.6	8.6	10.8	13.1	15.6
	60.00	4.6	6.1	8.3	10.6	13.0	15.6
	65.00	4.4	5.9	8.1	10.3	12.7	15.2
	70.00	4.1	5.7	7.8	10.0	12.3	14.9
0.6757	0.10	17.2	17.7				
	1.00	12.3	14.8	18.4	22.3	26.8	32.0
	5.00	10.7	13.1	16.5	20.2	24.4	29.2
	10.00	9.4	11.7	14.8	18.2	22.1	26.4
	15.00	8.5	10.6	13.6	16.8	20.4	24.4
	20.00	7.8	9.8	12.7	15.8	19.2	22.9
	25.00	7.2	9.2	11.9	14.9	18.1	21.7
	30.00	6.7	8.6	11.3	14.2	17.3	20.7
	35.00	6.3	8.1	10.8	13.6	16.6	19.9
	40.00	5.9	7.7	10.3	13.0	16.0	19.2
	45.00	5.5	7.4	9.9	12.6	15.4	18.6
	50.00	5.2	7.0	9.5	12.1	15.0	18.0
	55.00	5.0	6.7	9.2	11.8	14.6	17.6
	60.00	4.7	6.5	8.9	11.5	14.2	17.1
	65.00	4.5	6.2	8.6	11.1	13.8	16.7
	70.00	4.3	6.0	8.4	10.9	13.5	16.4

0.8495	0.10	17.9	18.4				
	1.00	12.3	15.0	18.9	23.3	28.3	34.1
	5.00	10.7	13.2	16.8	20.7	25.1	30.2
	10.00	9.3	11.6	15.0	18.6	22.6	27.1
	15.00	8.3	10.5	13.7	17.0	20.8	25.0
	20.00	7.5	9.7	12.7	15.9	19.4	23.4
	25.00	6.9	9.0	11.9	15.0	18.3	22.1
	30.00	6.4	8.4	11.2	14.2	17.5	21.0
	35.00	5.9	7.9	10.7	13.6	16.7	20.2
	40.00	5.5	7.5	10.2	13.0	16.1	19.4
	45.00	5.1	7.0	9.7	12.5	15.5	18.7
	50.00	4.9	6.8	9.4	12.1	15.1	18.3
	55.00	4.6	6.5	9.0	11.7	14.6	17.8
	60.00	4.4	6.2	8.7	11.4	14.2	17.3
	65.00	4.1	6.0	8.5	11.1	13.9	17.0
	70.00	3.9	5.7	8.2	10.8	13.6	16.6
0.9184	0.10	18.0	18.5				
	1.00	12.4	15.1	18.9	23.2	28.1	33.7
	5.00	10.8	13.2	16.7	20.5	24.8	29.8
	10.00	9.4	11.7	14.9	18.4	22.3	26.6
	15.00	8.4	10.5	13.6	16.8	20.4	24.5
	20.00	7.7	9.8	12.7	15.9	19.3	23.2
	25.00	7.0	9.0	11.8	14.7	18.0	21.6
	30.00	6.4	8.4	11.1	14.0	17.1	20.6
	35.00	6.0	7.9	10.5	13.3	16.4	19.7
	40.00	5.6	7.4	10.0	12.8	15.7	19.0
	45.00	5.2	7.1	9.6	12.3	15.2	18.4
	50.00	4.9	6.7	9.2	11.9	14.7	17.8
	55.00	4.7	6.4	8.9	11.5	14.3	17.3
	60.00	4.4	6.2	8.6	11.2	13.9	16.9
	65.00	4.2	5.9	8.3	10.9	13.6	16.5
	70.00	4.0	5.7	8.1	10.6	13.3	16.1
1.0000	0.10	16.0	19.3				
	1.00	15.8	17.4	19.8	22.5	25.4	28.8
	5.00	15.4	16.4	18.0	19.6	21.5	23.5
	10.00	14.6	15.3	16.3	17.4	18.5	19.8
	15.00	13.9	14.4	15.1	15.8	16.6	17.4
	20.00	13.3	13.6	14.1	14.6	15.1	15.7
	25.00	12.7	13.0	13.3	13.7	14.1	14.5
	30.00	12.4	12.5	12.7	12.8	13.0	13.2
	35.00	11.9	12.0	12.1	12.2	12.3	12.4
	40.00	11.6	11.6	11.6	11.7	11.7	11.7
	45.00	11.2	11.2	11.2	11.2	11.2	11.2
	50.00	10.9	10.9	10.8	10.8	10.7	10.7

55.00	10.6	10.6	10.5	10.4	10.3	10.2
60.00	10.3	10.3	10.2	10.1	10.0	9.8
65.00	10.1	10.0	9.9	9.8	9.7	9.5
70.00	9.8	9.8	9.6	9.5	9.4	9.2

[a] *Estimated expanded uncertainty (k=2): temperature U(T) = ±0.03 K, pressure U(P) = ±0.04 MPa, isobaric expansion U(α_P) = ±0.003 α_P.*

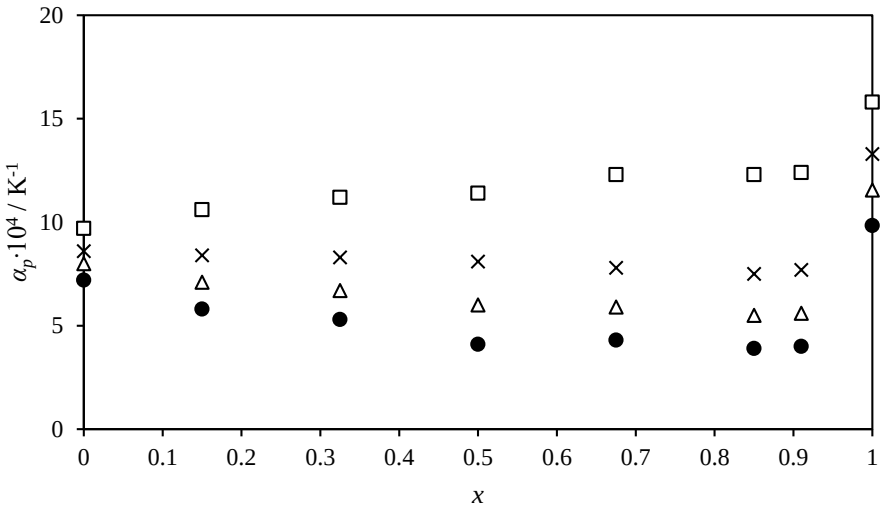

(a)

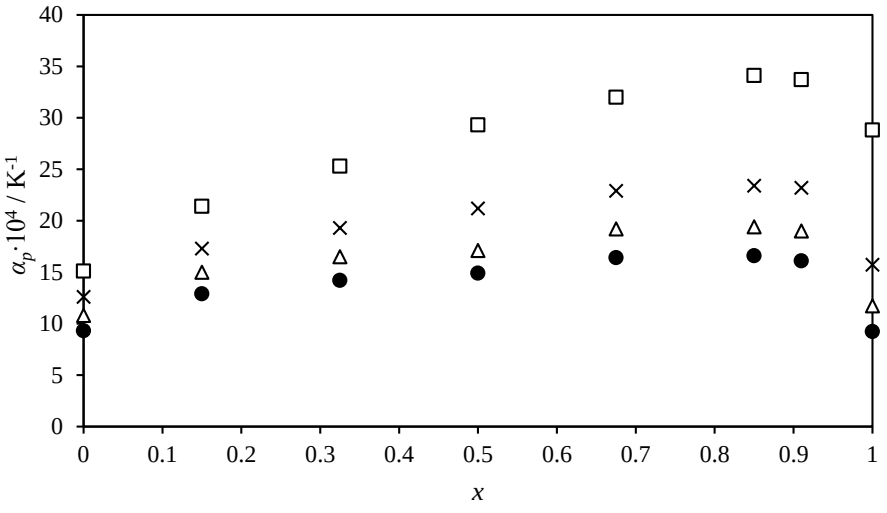

(b)

Figure 5. Isobaric expansion α_P, values for the binary mixture *x* HFE-7100 + (*1-x*) 1-propanol vs. the mole composition at different pressures *P*, and at (a) 298.15 K, and (b) 393.15 K. □; *P* = 1 MPa, ×; *P* = 20 MPa, Δ; *P* = 40 MPa, ●; *P* = 70 MPa.

4. Conclusions

Experimental determination of (ρ, V^E, T) values for the binary system x HFE-7100 + (1-x) 1-propanol was carried out by employing a vibrating tube densitometer in the pressure range from 0.1 to 70 MPa and along six isotherms ranging from 298.15 K to 393.15 K. The experimental high pressure density data were fitted to a Tait-like equation in order to well correlate the density values over the entire P, T ranges, showing the low deviations obtained between the experimental data and the calculated. A survey to compare the experimental density data and the values obtained in the literature was carried out both for pure HFE-7100 and for 1-propanol. No data was found in the literature for the binary mixture. On the basis of the experimental density measurements, excess volumes, V^E were obtained, and a comparison between these values and those measured previously concerning the binary mixture x HFE-7100 + (1-x) 2-propanol was conducted. Finally, by differentiating the Tait-like equation, isobaric expansion α_P, and isothermal compressibilities κ_T, were determined.

List of symbols

AAD	Absolute Average Deviation
a_i	coefficients of isobaric thermal expansivity correlation
A_i, B_i, C	coefficients of density correlation
Bias	Average Deviation
exp	experimental
i	constituent identification
lit	literature
MD	Maximum Deviation
N_P	number of experimental data points which are in our p, T ranges
P	pressure
P_0	reference pressure
RMSD	Root Mean Square Deviation
T	temperature
V^E	excess molar volume

Greek letters

σ	Standard deviation
α_p	isobaric expansion
ρ	density
ρ_0	density at a reference pressure P_0
κ_T	isothermal compressibility

Aknowledgements

This paper is part of the Doctoral Thesis of N. Muñoz-Rujas.
N. Muñoz-Rujas acknowledges support for this research to the University of Burgos, for the funding of her doctoral grant (Pre-Doctoral Grants 2014).

References

[1] N. Muñoz-Rujas, F. Aguilar, J-P. Bazile, E.A. Montero, Fluid Phase Equilib. 429 (2016) 281-292.

[2] 3M™ Novec™ Engineered Fluids. http://solutions.3m.com/wps/portal/3M/en_US/3MNovec/Home.

[3] P. Tuma, S. Paul, L. Tousignant, Earth 16 (2010).

[4] W-T. Tsai, J. Hazard. Matter. 119 (2005) 69-78.

[5] K. Doyel, and M. Bixenman, Patent US 7288511 B2 (2007).

[6] J. B. Durkee II, Cleaning with Solvents: Science and Technology, first ed., Elsevier B. V., Oxford (2014).

[7] F. E. M. Alaoui, E. A. Montero, G. Qiu, F. Aguilar, J. Wu, J. Chem. Thermodyn. 65 (2013) 174–183.

[8] M. J. P. Comuñas, J. Bazile, A. Baylaucq, C. Boned, J. Chem. Eng. Data 53 (2008) 986–994.

[9] H. Lagourette, B. Boned, C. Saint-Guirons, H. Xans, P. Zhou, Meas. Sci. Technol. 3 (1992) 699–703.

[10] W. Wagner, A. Pruß, J. Phys. Chem. Ref. Data 31 (2002) 387–535.

[11] Expression of the Uncertainty of Measurement in Calibration, European Cooperation for Accreditation, EA-4/02, 1999.

[12] J.A. Riddick, W.B. Bunger, T.K. Sakano, Organic Solvents: Physical Properties and Methods of Purification, fourth ed., Wiley, New York (1986).

[13] N. Muñoz-Rujas, J-P. Bazile, F. Aguilar, G. Galliero, E. Montero, J.L. Daridon, J. Chem. Thermodyn. 112 (2017) 52-48.

[14] A. Srhiyer, N. Muñoz-Rujas, F. Aguilar, J.J. Segovia, E.A. Montero, J. Chem. Thermodyn. 113 (2017) 213-218.

[15] M. M. Piñeiro, D. Bessières, J. L. Legido, H. Saint-Guirons, Int. J. Thermophys. 24 (2003) 1265–1276.

[16] H. Qi, D. Fang, X. Meng, J. Wu, J. Chem. Thermodyn. 77, (2014) 131–136.

[17] T. Minamihounoki, T. Takigawa, K. Tamura, S. Murakami, J. Chem. Thermodyn. 33 (2001) 189–203.

[18] G. Marchionni, P. Maccone, G. Pezzin, J. Fluor. Chem. 118, (2002) 149–155.

[19] M. H. Rausch, L. Kretschmer, S. Will, A. Leipertz, A. P. Fröba, J. Chem. Eng. Data 60 (2015) 3759-3765.

[20] H. Kubota, Y. Tanaka, T. Makita, Int. J. Thermophys. 8 (1987) 47-70.

[21] C. Ormanoudis, C. Dakos, C. Panayiotou, J. Chem. Eng. Data 36 (1991) 39-42.

[22] D. Papaioannou, M. Bridakis, C.G. Panayiotou, J. Chem. Eng. Data 38 (1993) 370-378.

[23] D. Papaioannou, C.G. Panayiotou, J. Chem. Eng. Data 40 (1995) 202-209.

[24] R. Yaginuma, T. Nakajima, H. Tanaka, M. Kato, Fluid Phase Equilib. 114 (1998) 203-210.

[25] A. Zúñiga-Moreno, L.A. Galicia-Luna, J. Chem. Eng. Data 47 (2002) 155-160.

[26] H. Kitajima, N. Kagawa, H. Endo, S. Tsuruno, J.W. Magee, J. Chem. Eng. Data 47 (2003) 1583-1586.

[27] V. Gil-Hernández, P. García-Giménez, J. Muñoz Embid, M. Artal, I. Velasco, Phys. Chem. Liq. 43 (2005) 523-533.

[28] C.K. Zéberg-Mikkelsen, S. I. Andersen, J. Chem. Eng. Data 50 (2005) 524-528.

[29] G. Watson, T. Lafitte, C.K. Zéberg-Mikkelsen, A. Baylaucq, D. Bessieres, C. Boned, Fluid Phase Equilib. 247 (2006) 121-134.

[30] G. Watson, T. Lafitte, C.K. Zéberg-Mikkelsen, A. Baylaucq, D. Bessieres, C. Boned, Fluid Phase Equilib. 253 (2007) 80.

[31] I.M. Abdulagatov, J.T. Safarov, F.Sh. Aliyev, M.A. Talibov, A.N. Shahverdiyev, E.P. Hassel, Fluid Phase Equilib. 268 (2008) 21-33.

[32] M. Torcal, M.I. Teruel, J. García, J.S. Urieta, A.M. Mainar, J. Chem. Eng. Data 55 (2010) 5332-5339.

[33] M. Torcal, S. García-Abarrio, J.I. Pardo, A.M. Mainar, J.S. Urieta, J. Chem. Eng. Data 55 (2010) 5932-5940.

[34] M. J. Dávila, R. Alcalde, M. Atilhan, S. Aparicio, J. Chem. Thermodyn. 47 (2012) 241-259.

[35] M. Kariznovi, H. Nourozieh, J. Abedi, J. Chem. Thermodyn. 57 (2013) 408-415.

[36] F.E.M. Alaoui, E.A. Montero, J-P. Bazile, F. Aguilar, C. Boned, Fluid Phase Equilib. 363 (2014) 131-148.

[37] C. A. Cerdeiriña, C. A. Tovar, D. González-Salgado, E. Carballo, L. Romaní, Phys. Chem. Chem. Phys. 3(2001) 5230–5236.

[38] J. Troncoso, D. Bessières, C. A. Cerdeiriña, E. Carballo, L. Romaní, Fluid Phase Equilib. 208 (2003) 141-154.

[39] J. Jacquemin, P. Husson, V. Mayer, I. Cibulka, J. Chem. Eng. Data 52 (2007) 2204–2211, 2007.

Thermodynamics of Binary Mixtures 1-ethoxy-1,1,2,2,3,3,4,4,4-nonafluorobutane (HFE-7200) + 2-Propanol: High Pressure Density, Speed of Sound and Derivative Properties.

Natalia Muñoz-Rujas[a], Fernando Aguilar[a], Eduardo A. Montero[a,]*

(a) Departamento de Ingeniería Electromecánica, Escuela Politécnica Superior, Universidad de Burgos, E-09006 Burgos, Spain

[*]Corresponding author: Phone: +34947258916, Fax: +34947258916, e-mail: emontero@ubu.es

Abstract

Awareness about environmental impact of greenhouse gas emissions has lead to search for other alternatives which can cover the same utility range of wellknown CFCs, HCFCs and PFCs but without their undesirable effects on the planet. Since Hydrofluoroether fluids (HFEs) have emerged as a good alternative, it is necessary to characterize their thermophysical properties in order to bring reliable data to the industry. Density and speed of sound are two of the most important physical properties because of the amount of information that they provide in the design of the machinery involved in the utilization of these fluids as well as data for the parametrization of equations of state. This paper reports a set of new data concerning high pressure density ρ, for the binary mixture x HFE-7200 + (1-x) 2-Propanol in a broad range of pressures (0.1 – 140 MPa), and at several temperatures (from 293.15 to 393.15 K). Density values were correlated by employing a Tait-like equation in the same P, T ranges, and the derivative properties, that is, the isothermal compressibility κ_T, and the isobaric expansion α_P, were determined. Excess molar volumes V^E, which bring information about the change in volume observed in the mixture were also calculated for the eight mole fractions investigated. Speeds of sound c, at atmospheric pressure were measured experimentally by means of an Anton Paar DSA 5000 density and sound velocity analyzer, as well as the densities, in the temperature range (293.15 – 333.15 K). By using the Laplace equation, isentropic compressibilities κ_S, were calculated from density and sound velocity values.

Keywords

1-ethoxy-1,1,2,2,3,3,4,4,4-nonafluorobutane, 2-Propanol, Density, Derivative Properties, Excess Volumes.

1. Introduction

Segregated hydrofluoroethers (HFEs) are a class of fluids which were introduced in 1996 as an environmentally acceptable alternative to commonly used CFCs and HCFCs [1]. Unlike these two kind of fluids, HFEs have no chlorine atoms in its molecule, which lead to a favorable environmental profile. In the same manner, the presence of fluorine atoms impart characteristics of stability and nonflammability [2], and the ether structure promotes an increase of reaction with –OH radicals in the lower atmosphere. HFEs exhibit a good balance between safety, performance, and environmental properties, due to its low toxicity, nonflammability, compatibility with other materials, stability, zero ODP, short atmospheric lifetimes (ALT), low global warming potentials (GWP), and low solubility in water among others [3] .

1-Ethoxy-1,1,2,2,3,3,4,4,4-nonafluorobutane, or HFE-7200 exhibits low viscosity, low surface tension, high density, no flash point and higher boiling point than most CFCs, HCFCs and HFCs, properties which make it useful as heat transfer fluid besides rinsing agent for vapor degreasing, aerosol cleaning, wipe cleaning, lubricant carrier, CFC, HCFC, HFC and PFC replacement agent. Particularly it is indicated to be a good substitute of HCFC-225 ca/cb, HCFC-141b. Due to its dielectric nature, it can also be used for electronic cooling, and its mixture formulations are being considered for thermal management systems in the electronics industry [4].

Particularly interesant is its mixture with 2-Propanol because at a weight composition of 87% of HFE-7200 an azeotrope is formed with a minimun boiling point at 338.15 K. This binary azeotrope is viable to replace HCFC-225ca/cb for solvent cleaning operations [5]. The cleaning processes that use azeotropes require a stronger solvent mixture, and the mechanism of cleaning with an azeotrope system is almost exclussively via dissolving the soil [6], being able to clean many oils, waxes and greases. Though isopropanol is a flammable agent, the addition of the HFE leads the mixture to be nonflammable, and the equipment in which this azeotrope can be used does not differ from the conventionally used with other azeotropes.

Due to the applications of the binary mixture x HFE-7200 + (1-x) 2-Propanol, the thermophysical characterization of its properties is of importance. Density provides information about the change in volume that takes place when changes in pressure P, and in temperature T, occur in the mixture, and from its knowledge, derivative properties such as isobaric expansion α_P, and isothermal compressibility κ_T, which are also of importance, can be determined. Obtaining high pressure and high temperature density data will provide the industry valuable information concerning this mixture. This paper reports 1264 points of density at several pressures (from 0.1 to 140 MPa) and at different temperatures (from 293.15 to 393.15 K) for eight mole fractions of the binary system x HFE-7200 + (1-x) 2-Propanol. Isothermal

compressibilities κ_T, and isobaric expansion values α_P, were also determinded as well as the excess volumes in the temperature and pressure ranges considered. Speeds of sound at atmospheric pressure and in the temperature range (293.15 – 333.15) were determined and isentropic compressibilities were calculated from these data.

2. Experimental

2.1 Materials

Hydrofluoroether fluid 1-ethoxy-1,1,2,2,3,3,4,4,4-nonafluorobutane, also known as HFE-7200, (CAS: 163702-06-5 / 163702-05-4), which consists of a mixture of two inseparable isomers with identical properties was supplied by the 3M Company with a mass fraction purity greater than 99.5%.

2-Propanol (CAS: 67-63-0) was obtained from Sigma-Aldrich with mole fraction purity greater than 99.8%. This fluid was stored over molecular sieves type 0.4 to prevent any moisture. Both the two fluids were degassed prior any measurement in order to avoid air bubbles in the sample. None of the fluids was subject to further purtification method. The data list concerning the pure compounds can be seen in Table 1.

Table 1. Related data for the studied chemicals.

Compound	Source	Formula	Molar mass / g·mol^{-1}	Stated purity[a]	CAS number
HFE-7200[b]	3M Company	$C_6H_5F_9O$	264.09	>99.5[c]	163702-06-5 / 163702-05-4[d]
2-Propanol	Sigma-Aldrich	C_3H_8O	60.096	>99.8[e, f]	67-63-0

[a] Determined by gas chromatography (GC) by the supplier.
[b] HFE-7200 = 1-ethoxy-1,1,2,2,3,3,4,4,4-nonafluorobutane.
[c] Mass fraction purity, g·mol^{-1}%
[d] Binary mixture of two isomers with mass ratio 0.5.
[e] The water content was checked to be less than 0.01% by titration method.
[f] Mole fraction purity, mol%.

2.2. Measurement technique. High pressure density

Various techniques are available to determine density data: piezometers, pycnometers, isochoric methods, densitometers based on vibrating elements, *etc*. One of the most widely used methods corresponds to vibrating tube densitometers (VTD), which used has increased due to its main advantages: simple operation, high accuracy and small sample requirement among others [7].

In our case, we used an Anton Paar vibrating tube densitometer model DMA HPM to determine high pressure density values. The description and operation of this densitometer was addressed in a previous paper [8]. The ranges in which the measurements were carried out are (0.1 – 140) for the pressure and (293.15 – 393.15 K) for the temperature. The pressure inside the measuring cell is generated by a step by step engine while the Anton Paar mPDS 2000V3 evaluation unit controls the oscillation period from the measuring cell which is filled with the sample. The estimated expanded uncertainty of the measured pressure was ±0.04 MPa (pressure transducer WIKA CPH 6000). The temperature inside the densitometer is ensured by means of a silicone oil circulating fluid which is heated or cooled in a thermosthatic bath Julabo F25 HE. A Pt 100 probe directly inserted in the measuring cell measures the temperature of the sample with an uncertainty of ±0.03 K. Both temperature and pressure sensors were periodically calibrated before and after the measurement campaign.

Densitometer calibrations were performed according to the procedure described by Comuñas *et al.* [9] which is a modification of the procedure previously proposed by Lagourette *et al.* [10]. Taking this into account, two reference fluids were used, vacuum and water. The density values of water were taken from the equation of state (EoS) reported by Wagner and Pruss [11]. Because of the boiling points of the pure components (T_b = 349.15 K for HFE-7200, reference [12], and T_b = 355.39 K for 2-Propanol, reference [13]), no measurements were carried out at temperatures 353.15 K and higher at atmospheric pressure for all the compositions in order to ensure liquid state.

Concerning the expanded uncertainty, taking into account the accuracy of the temperature, the pressure, the period of oscillation measurement for water, vacuum, and the studied systems, and the water density accuracy, the estimated expanded density uncertainty (k = 2) is ±0.7 kg·m^{-3} (*i.e*, around ±0.07 % for density close to water density), following the EA-4/02 document [14].

To prevent any bubble formation inside the sample, a degasification procedure was carried out before introducing the sample in the densitometer. An ultrasonic bath PSelecta, model Ultrasons-H was employed for this purpose. The mixtures were prepared by weighing amounts of the pure components with a Mettler Toledo model MS 204S with resolution of 10^{-4} g, and uncertainty ±0.0001 g. The estimated expanded uncertainty in the composition of the mixture is $\pm 4 \cdot 10^{-5}$ in mole fraction. Then the expanded uncertainty for the excess volumes is stated to be ±0.004 cm^3·mol^{-1}.

2.3. Measurement technique. Speed of sound

Speeds of sound at atmospheric pressure were measured by using an Anton Paar DSA 5000 density and sound velocity meter in the temperature ranges (293.15 – 333.15). The temperatures

differ from those considered for high pressure density measurements due to the limit in temperature stablished of the manufacturer of the apparatus. Speed of sound in a fluid is obtained by measuring the travelling time, *t* that a wave needs to pass across the fluid at a determined distance. This property provides information on transport coefficients, thermodynamic properties as well as relaxation processes [7]. The sound velocity analyzer employed allows us also to calculate the density of the sample; a vibrating tube made of glass located inside the apparatus is filled with the sample, being the operating principle the one of a vibrating tube densitometer. Then the two properties, speed of sound and density can be determined simultaneously with the same sample. The density and sound velocity analyzer is provided with a built-in thermostat, being the accuracy in temperature ±0.01 K. The uncertainty in speed of sound is estimated to be ±0.1 $m \cdot s^{-1}$ while the uncertainty in density is ±1·10^{-5} $g \cdot cm^{-3}$. The instrument is calibrated once a week following the instructions of the manufacturer with two fluids: ambient air and Millipore quality water or *n*-decane. The accuracy of the sound velocity can not be validated as there are no certified liquid standards for speed of sound available. Then, the calibration method involves the comparison with a reference value, and it is only possible to do this procedure for the density. During the calibration procedure, three measurements with each fluid were made in order to calculate an average of the period of vibration for the sample. With these data it is possible to determine the two constants, *a* and *b* of the following calibration equation:

$$\rho = a + \tau^2 \cdot b \tag{1}$$

Where τ corresponds to the period of oscillation of the vibrating tube with the sample. The results of the calibrations were compared with those of [11] in the case of water, and with reference [15] in the cases of air and *n*-decane. The choice of *n*-decane was subject to the bubbles formation inside the glass tube at high temperatures (323.15 K and 333.15 K), which lead to bad values of density in the case of water. In those cases, calibration was realized with ambient air and *n*-decane. The mixtures were prepared by weighing amounts of each compound by using a Mettler Toledo balance model MS 204S with resolution of 10^{-4} g, and uncertainty ±0.0001 g. The components were placed in stoppered bottles of 14 cm^3 and degassed during at least 15 minutes prior to any measurement with an ultrasonic bath PSelecta, model Ultrasons-H.

3. Results and Discussion

3.1. Density

For the purpose of bringing an adequate representation of density along the different compositions in the mixture, eight mole fractions were studied (x = 0.0000, x = 0.1520, x = 0.3275, x = 0.5019, x = 0.6053, x = 0.6777, x = 0.8526 and x = 1.0000). Since an azeotrope is described to appear at a weight composition of 87% [5], the corresponding mole fraction, x = 0.6053 was added in order to characterize the density at this point. Density of each of the mole fractions was determined along 23 isobars from 0.1 MPa to 140 MPa at every 5 MPa (from 0.1 to 65 MPa), and at every 10 MPa (from 70 to 140 MPa), and along seven isotherms (293.15 K, 298.15 K, 313.15 K, 333.15 K, 353.15 K, 373.15 K and 393.15 K). All the density values at each P, T sets are gathered in Table 2. As mentioned in the previous section, no measurements were carried out at atmospheric pressure and at temperatures 353.15 K and over due to the boiling point of the pure compounds is lower or close to 353.15 K.

Table 2. Experimental high pressure densities ρ, at temperatures T and at pressures P for the binary mixture x HFE-7200 + (*1-x*) 2-Propanol[a].

x	P/ MPa	T / K						
		293.15	298.15	313.15	333.15	353.15	373.15	393.15
		ρ / g·cm^{-3}						
0.0000	0.10	0.7854	0.7814	0.7682	0.7494			
	1.00	0.7862	0.7821	0.7691	0.7505	0.7298	0.7066	0.6804
	5.00	0.7896	0.7856	0.7730	0.7549	0.7350	0.7128	0.6882
	10.00	0.7936	0.7898	0.7774	0.7600	0.7410	0.7199	0.6967
	15.00	0.7974	0.7937	0.7818	0.7649	0.7465	0.7263	0.7044
	20.00	0.8011	0.7973	0.7857	0.7693	0.7517	0.7320	0.7114
	25.00	0.8045	0.8009	0.7895	0.7736	0.7565	0.7377	0.7176
	30.00	0.8079	0.8043	0.7933	0.7777	0.7610	0.7429	0.7235
	35.00	0.8112	0.8077	0.7969	0.7815	0.7654	0.7478	0.7290
	40.00	0.8142	0.8108	0.8001	0.7853	0.7693	0.7522	0.7342
	45.00	0.8172	0.8138	0.8034	0.7889	0.7733	0.7566	0.7390
	50.00	0.8201	0.8167	0.8065	0.7923	0.7770	0.7607	0.7435
	55.00	0.8229	0.8197	0.8096	0.7956	0.7806	0.7647	0.7479
	60.00	0.8256	0.8225	0.8125	0.7987	0.7840	0.7686	0.7521
	65.00	0.8282	0.8252	0.8154	0.8018	0.7874	0.7721	0.7561
	70.00	0.8308	0.8276	0.8182	0.8048	0.7906	0.7756	0.7600
	80.00	0.8358	0.8328	0.8234	0.8105	0.7967	0.7823	0.7672
	90.00	0.8405	0.8375	0.8285	0.8159	0.8026	0.7885	0.7739
	100.00	0.8450	0.8423	0.8331	0.8209	0.8080	0.7944	0.7802
	110.00	0.8494	0.8464	0.8378	0.8258	0.8132	0.7999	0.7862
	120.00	0.8535	0.8508	0.8421	0.8304	0.8181	0.8053	0.7918
	130.00	0.8576	0.8548	0.8464	0.8348	0.8228	0.8102	0.7972

	140.00	0.8612	0.8587	0.8504	0.8392	0.8273	0.8151	0.8023
0.1520	0.10	0.9747	0.9686	0.9495	0.9222			
	1.00	0.9760	0.9699	0.9509	0.9239	0.8943	0.8614	0.8246
	5.00	0.9813	0.9754	0.9571	0.9312	0.9030	0.8721	0.8384
	10.00	0.9875	0.9819	0.9642	0.9395	0.9128	0.8839	0.8527
	15.00	0.9933	0.9879	0.9709	0.9471	0.9216	0.8942	0.8651
	20.00	0.9988	0.9934	0.9770	0.9540	0.9297	0.9033	0.8761
	25.00	1.0040	0.9988	0.9827	0.9606	0.9371	0.9120	0.8858
	30.00	1.0090	1.0039	0.9884	0.9668	0.9440	0.9199	0.8947
	35.00	1.0137	1.0088	0.9936	0.9725	0.9506	0.9273	0.9031
	40.00	1.0183	1.0134	0.9985	0.9781	0.9565	0.9339	0.9106
	45.00	1.0225	1.0179	1.0033	0.9834	0.9624	0.9403	0.9178
	50.00	1.0267	1.0221	1.0079	0.9884	0.9679	0.9465	0.9244
	55.00	1.0308	1.0263	1.0123	0.9932	0.9731	0.9522	0.9307
	60.00	1.0347	1.0303	1.0165	0.9977	0.9782	0.9577	0.9368
	65.00	1.0385	1.0341	1.0206	1.0022	0.9830	0.9630	0.9425
	70.00	1.0421	1.0377	1.0246	1.0064	0.9877	0.9680	0.9480
	80.00	1.0492	1.0449	1.0321	1.0145	0.9963	0.9774	0.9583
	90.00	1.0558	1.0517	1.0392	1.0222	1.0046	0.9862	0.9678
	100.00	1.0621	1.0582	1.0459	1.0293	1.0123	0.9945	0.9767
	110.00	1.0682	1.0641	1.0524	1.0362	1.0196	1.0023	0.9849
	120.00	1.0740	1.0702	1.0584	1.0426	1.0264	1.0097	0.9926
	130.00	1.0796	1.0757	1.0643	1.0489	1.0330	1.0166	1.0000
	140.00	1.0847	1.0812	1.0699	1.0549	1.0392	1.0233	1.0071
0.3275	0.10	1.1263	1.1184	1.0937	1.0587			
	1.00	1.1280	1.1201	1.0958	1.0612	1.0238	0.9824	0.9361
	5.00	1.1352	1.1277	1.1043	1.0714	1.0362	0.9981	0.9565
	10.00	1.1436	1.1364	1.1140	1.0828	1.0498	1.0146	0.9770
	15.00	1.1513	1.1444	1.1229	1.0932	1.0619	1.0289	0.9941
	20.00	1.1585	1.1518	1.1311	1.1025	1.0728	1.0412	1.0090
	25.00	1.1654	1.1589	1.1388	1.1113	1.0827	1.0527	1.0219
	30.00	1.1719	1.1655	1.1461	1.1194	1.0918	1.0632	1.0337
	35.00	1.1780	1.1719	1.1529	1.1270	1.1004	1.0728	1.0445
	40.00	1.1839	1.1778	1.1594	1.1342	1.1081	1.0814	1.0543
	45.00	1.1894	1.1836	1.1656	1.1411	1.1158	1.0898	1.0634
	50.00	1.1949	1.1890	1.1714	1.1475	1.1229	1.0976	1.0721
	55.00	1.2001	1.1944	1.1772	1.1537	1.1296	1.1050	1.0801
	60.00	1.2050	1.1996	1.1824	1.1595	1.1360	1.1121	1.0879
	65.00	1.2098	1.2044	1.1878	1.1652	1.1422	1.1187	1.0951
	70.00	1.2145	1.2091	1.1928	1.1707	1.1481	1.1251	1.1020
	80.00	1.2234	1.2182	1.2023	1.1810	1.1591	1.1371	1.1149
	90.00	1.2317	1.2267	1.2113	1.1906	1.1696	1.1481	1.1267
	100.00	1.2396	1.2348	1.2197	1.1997	1.1791	1.1585	1.1378
	110.00	1.2473	1.2423	1.2278	1.2082	1.1884	1.1681	1.1480

	120.00	1.2544	1.2497	1.2354	1.2162	1.1969	1.1772	1.1577
	130.00	1.2613	1.2567	1.2427	1.2241	1.2051	1.1859	1.1668
	140.00	1.2678	1.2634	1.2496	1.2315	1.2128	1.1941	1.1755
0.5019	0.10	1.2352	1.2260	1.1972	1.1567			
	1.00	1.2373	1.2281	1.1998	1.1598	1.1167	1.0691	1.0158
	5.00	1.2460	1.2373	1.2102	1.1724	1.1322	1.0889	1.0421
	10.00	1.2561	1.2477	1.2220	1.1864	1.1490	1.1093	1.0676
	15.00	1.2654	1.2574	1.2327	1.1988	1.1636	1.1267	1.0885
	20.00	1.2740	1.2663	1.2425	1.2101	1.1767	1.1416	1.1062
	25.00	1.2821	1.2747	1.2517	1.2206	1.1885	1.1553	1.1217
	30.00	1.2898	1.2825	1.2604	1.2302	1.1994	1.1677	1.1356
	35.00	1.2971	1.2900	1.2685	1.2391	1.2095	1.1791	1.1483
	40.00	1.3039	1.2971	1.2760	1.2477	1.2187	1.1893	1.1599
	45.00	1.3105	1.3038	1.2833	1.2557	1.2276	1.1991	1.1706
	50.00	1.3168	1.3102	1.2901	1.2633	1.2359	1.2082	1.1805
	55.00	1.3229	1.3164	1.2969	1.2705	1.2438	1.2168	1.1899
	60.00	1.3286	1.3224	1.3031	1.2773	1.2513	1.2250	1.1989
	65.00	1.3342	1.3281	1.3092	1.2840	1.2584	1.2327	1.2072
	70.00	1.3396	1.3334	1.3151	1.2902	1.2653	1.2401	1.2152
	80.00	1.3500	1.3440	1.3262	1.3022	1.2781	1.2540	1.2300
	90.00	1.3596	1.3539	1.3365	1.3134	1.2901	1.2667	1.2436
	100.00	1.3686	1.3632	1.3462	1.3237	1.3012	1.2786	1.2563
	110.00	1.3775	1.3719	1.3555	1.3337	1.3117	1.2898	1.2680
	120.00	1.3857	1.3805	1.3643	1.3429	1.3216	1.3001	1.2790
	130.00	1.3936	1.3884	1.3727	1.3518	1.3310	1.3100	1.2894
	140.00	1.4011	1.3961	1.3806	1.3603	1.3398	1.3188	1.2993
0.6053	0.10	1.2869	1.2770	1.2465	1.2034			
	1.00	1.2892	1.2794	1.2493	1.2067	1.1610	1.1108	1.0547
	5.00	1.2986	1.2893	1.2606	1.2205	1.1781	1.1326	1.0838
	10.00	1.3096	1.3007	1.2734	1.2358	1.1965	1.1551	1.1117
	15.00	1.3196	1.3111	1.2850	1.2493	1.2124	1.1739	1.1343
	20.00	1.3289	1.3207	1.2957	1.2615	1.2266	1.1900	1.1535
	25.00	1.3376	1.3297	1.3055	1.2728	1.2393	1.2048	1.1702
	30.00	1.3459	1.3381	1.3149	1.2832	1.2510	1.2181	1.1851
	35.00	1.3537	1.3462	1.3235	1.2928	1.2619	1.2302	1.1986
	40.00	1.3611	1.3538	1.3316	1.3019	1.2717	1.2412	1.2110
	45.00	1.3680	1.3610	1.3395	1.3105	1.2813	1.2517	1.2224
	50.00	1.3748	1.3678	1.3468	1.3186	1.2902	1.2615	1.2331
	55.00	1.3813	1.3745	1.3539	1.3263	1.2986	1.2707	1.2430
	60.00	1.3875	1.3809	1.3606	1.3336	1.3066	1.2794	1.2526
	65.00	1.3934	1.3870	1.3672	1.3407	1.3142	1.2876	1.2614
	70.00	1.3992	1.3927	1.3734	1.3475	1.3216	1.2955	1.2699
	80.00	1.4102	1.4040	1.3853	1.3602	1.3351	1.3101	1.2856
	90.00	1.4205	1.4144	1.3962	1.3721	1.3479	1.3237	1.3000

	100.00	1.4301	1.4244	1.4066	1.3831	1.3597	1.3363	1.3133
	110.00	1.4395	1.4336	1.4165	1.3935	1.3709	1.3481	1.3258
	120.00	1.4482	1.4427	1.4257	1.4034	1.3813	1.3592	1.3375
	130.00	1.4567	1.4512	1.4347	1.4129	1.3912	1.3696	1.3484
	140.00	1.4645	1.4593	1.4431	1.4218	1.4006	1.3795	1.3588
0.6777	0.10	1.3188	1.3086	1.2768	1.2322			
	1.00	1.3212	1.3110	1.2797	1.2358	1.1886	1.1369	1.0794
	5.00	1.3311	1.3215	1.2917	1.2503	1.2066	1.1599	1.1102
	10.00	1.3426	1.3334	1.3052	1.2663	1.2259	1.1836	1.1395
	15.00	1.3531	1.3443	1.3173	1.2805	1.2426	1.2033	1.1631
	20.00	1.3628	1.3543	1.3284	1.2932	1.2574	1.2203	1.1831
	25.00	1.3719	1.3637	1.3388	1.3050	1.2708	1.2356	1.2006
	30.00	1.3805	1.3725	1.3485	1.3159	1.2830	1.2495	1.2161
	35.00	1.3887	1.3810	1.3575	1.3259	1.2943	1.2622	1.2302
	40.00	1.3963	1.3888	1.3659	1.3354	1.3046	1.2736	1.2430
	45.00	1.4036	1.3963	1.3741	1.3445	1.3146	1.2845	1.2548
	50.00	1.4106	1.4034	1.3817	1.3528	1.3237	1.2947	1.2659
	55.00	1.4174	1.4103	1.3892	1.3608	1.3325	1.3041	1.2762
	60.00	1.4238	1.4170	1.3961	1.3685	1.3408	1.3132	1.2860
	65.00	1.4300	1.4233	1.4029	1.3759	1.3487	1.3217	1.2952
	70.00	1.4360	1.4293	1.4094	1.3828	1.3564	1.3299	1.3040
	80.00	1.4474	1.4409	1.4217	1.3960	1.3704	1.3452	1.3202
	90.00	1.4580	1.4518	1.4331	1.4083	1.3837	1.3591	1.3352
	100.00	1.4681	1.4622	1.4438	1.4197	1.3960	1.3722	1.3490
	110.00	1.4777	1.4717	1.4541	1.4306	1.4074	1.3844	1.3618
	120.00	1.4868	1.4811	1.4636	1.4408	1.4183	1.3958	1.3739
	130.00	1.4955	1.4899	1.4729	1.4506	1.4286	1.4066	1.3852
	140.00	1.5037	1.4983	1.4816	1.4599	1.4382	1.4169	1.3960
0.8526	0.10	1.3851	1.3737	1.3404	1.2931			
	1.00	1.3877	1.3764	1.3436	1.2970	1.2476	1.1940	1.1355
	5.00	1.3986	1.3879	1.3567	1.3130	1.2675	1.2195	1.1691
	10.00	1.4112	1.4009	1.3714	1.3307	1.2886	1.2453	1.2008
	15.00	1.4226	1.4127	1.3848	1.3462	1.3069	1.2668	1.2264
	20.00	1.4331	1.4236	1.3969	1.3600	1.3230	1.2850	1.2478
	25.00	1.4430	1.4338	1.4080	1.3728	1.3374	1.3016	1.2665
	30.00	1.4524	1.4434	1.4186	1.3846	1.3506	1.3166	1.2830
	35.00	1.4612	1.4524	1.4284	1.3954	1.3629	1.3302	1.2981
	40.00	1.4694	1.4609	1.4375	1.4057	1.3739	1.3424	1.3118
	45.00	1.4773	1.4690	1.4463	1.4154	1.3846	1.3541	1.3244
	50.00	1.4849	1.4767	1.4546	1.4244	1.3946	1.3649	1.3362
	55.00	1.4922	1.4842	1.4625	1.4330	1.4039	1.3752	1.3472
	60.00	1.4990	1.4913	1.4700	1.4413	1.4128	1.3849	1.3577
	65.00	1.5057	1.4981	1.4773	1.4491	1.4213	1.3939	1.3674
	70.00	1.5121	1.5045	1.4843	1.4566	1.4295	1.4027	1.3767

	80.00	1.5244	1.5170	1.4975	1.4708	1.4446	1.4189	1.3941
	90.00	1.5359	1.5286	1.5098	1.4840	1.4587	1.4338	1.4098
	100.00	1.5465	1.5397	1.5212	1.4962	1.4717	1.4477	1.4245
	110.00	1.5569	1.5499	1.5322	1.5078	1.4841	1.4607	1.4381
	120.00	1.5666	1.5601	1.5425	1.5187	1.4956	1.4729	1.4510
	130.00	1.5759	1.5693	1.5523	1.5292	1.5065	1.4844	1.4629
	140.00	1.5847	1.5784	1.5617	1.5391	1.5169	1.4953	1.4743
1.0000	0.10	1.4339	1.4228	1.3884	1.3407			
	1.00	1.4366	1.4256	1.3918	1.3448	1.2952	1.2421	1.1839
	5.00	1.4482	1.4377	1.4056	1.3616	1.3161	1.2684	1.2183
	10.00	1.4613	1.4515	1.4211	1.3801	1.3381	1.2951	1.2508
	15.00	1.4734	1.4639	1.4351	1.3963	1.3571	1.3173	1.2770
	20.00	1.4845	1.4754	1.4478	1.4108	1.3739	1.3362	1.2991
	25.00	1.4948	1.4862	1.4595	1.4242	1.3889	1.3533	1.3183
	30.00	1.5047	1.4961	1.4706	1.4364	1.4026	1.3688	1.3354
	35.00	1.5139	1.5057	1.4808	1.4478	1.4153	1.3829	1.3509
	40.00	1.5225	1.5145	1.4903	1.4585	1.4268	1.3956	1.3651
	45.00	1.5308	1.5230	1.4995	1.4686	1.4379	1.4077	1.3781
	50.00	1.5387	1.5311	1.5081	1.4780	1.4482	1.4188	1.3902
	55.00	1.5463	1.5388	1.5164	1.4870	1.4579	1.4294	1.4016
	60.00	1.5535	1.5463	1.5243	1.4955	1.4672	1.4395	1.4124
	65.00	1.5605	1.5534	1.5319	1.5037	1.4759	1.4489	1.4225
	70.00	1.5672	1.5602	1.5392	1.5115	1.4845	1.4579	1.4321
	80.00	1.5800	1.5732	1.5529	1.5263	1.5002	1.4747	1.4500
	90.00	1.5919	1.5854	1.5657	1.5400	1.5148	1.4902	1.4662
	100.00	1.6031	1.5969	1.5776	1.5527	1.5283	1.5045	1.4815
	110.00	1.6139	1.6076	1.5890	1.5647	1.5411	1.5179	1.4955
	120.00	1.6240	1.6180	1.5997	1.5760	1.5530	1.5305	1.5087
	130.00	1.6337	1.6278	1.6100	1.5868	1.5643	1.5423	1.5211
	140.00	1.6428	1.6372	1.6197	1.5972	1.5751	1.5537	1.5321

[a] Estimated expanded uncertainties (k = 2) are: temperature, $U(T)$ = ± 0.03 K; pressure, $U(P)$ = ±0.04 MPa; mole fraction, $U(x)$ = ±0.00004; density, $U(\rho)$ = ±0.7 kg·m^{-3}.

3.2. Tait representation

Correlation equations are necessary to be employed with experimental data due to with its utilization density points which have not been measured at a determined *P* or *T* can be obtained. In our case we have used a Tait-like equation to correlate the high pressure density values measured experimentally. The Tait equation, which was firstly used to fit the results on the compressibility of fresh water and seawater at different pressures, has demonstrated to bring a great accuracy in reproducing high pressure density data for liquids [16]. This equation was used in some of our previous works [17 - 20], and is as follows:

$$\rho(T,p) = \frac{\rho_0(T)}{1 - C\ln\left(\frac{B(T) + p}{B(T) + 0.1\ \text{MPa}}\right)} \quad (2)$$

Where:

$$\rho_0(T) = A_0 + A_1 T + A_2 T^2 + A_3 T^3 \quad (3)$$

$$B(T) = B_0 + B_1 T + B_2 T^2 \quad (4)$$

The A_i, B_i and C parameters are obtained by correlating simultaneously all the experimental densities values versus pressure and temperature. Table 3 shows the eight parameters for the eight mole fractions along with its deviations: AAD% (Average Absolute Deviation), MD% (Maximum Deviation), Bias% (Average Deviation), σ (Standard Deviation), and RMSD (Root Mean Square Deviation). It can be seen that for all the mole fractions the AAD% and the Bias% are lower than the experimental uncertainty. Evaluating the MD%, mole fractions x = 0.5019, x = 0.6053, x = 0.6777, x = 0.8526 and x = 1.0000 slightly exceed this value, with a maximum MD% = 0.10 for the compositions x = 0.8526 and x = 1.0000.

Figure 1 reports some representations of experimental densities with the correlation given by the Tait equation vs. the temperature T, in cases (a) and (b), and vs. the pressure for graphs (c) and (d). Graphs (a) and (b) show data at each mole composition at 1 MPa (a) and at 140 MPa (b). Regardless of pressure, a decrease in the value of density is observed when the temperature increases. Considering the different pressures, the density values are higher at 140 MPa than at 1 MPa when comparing the same composition at the same temperature, with a maximum value of density = 1.6428 g·cm^{-3} at a molar fraction x = 1.000. Graphs (c) and (d) report density data at 293.15 K and at 393.15 K respectively. In both two graphs the shape of the curves is concave, which is related to the negative second order derivative, being this appearance compatible with the logarithmic relationship used in the Tait-like equation. Following this trend of the curves, it can be stated that when the pressure increases, the density also increases in a logarithmic form regardless of the temperature. The highest values of density are found at 293.15 K (graph (c)), due to at lower temperatures the molecules in the fluid have less energy than at high temperature, resulting in an approximation of them and hence in lower values of density.

Table 3. Parameters and deviations for density correlation by using equations (2) to (4) for the mixture *x* HFE-7200 + (*1*-*x*) 2-Propanol.

Parameters	*x*			
	0.0000	0.1520	0.3275	0.5019
A_0 / g cm^{-3}	1.238217	1.590277	1.921285	2.163775
A_1 / g cm^{-3} K^{-1}	$-3.279986\cdot10^{-3}$	$-4.287405\cdot10^{-3}$	$-5.470008\cdot10^{-3}$	$-6.360817\cdot10^{-3}$
A_2 / g cm^{-3} K^{-2}	$9.436122\cdot10^{-6}$	$1.196245\cdot10^{-5}$	$1.498874\cdot10^{-5}$	$1.729270\cdot10^{-5}$
A_3 / g cm^{-3} K^{-3}	$-1.198655\cdot10^{-8}$	$-1.533770\cdot10^{-8}$	$-1.902113\cdot10^{-8}$	$-2.181810\cdot10^{-8}$
B_0 / MPa	309.7820	314.6991	306.3666	296.5245
B_1 / MPa K^{-1}	-0.978167	-1.165526	-1.213514	-1.211458
B_2 / MPa K^{-2}	$6.718266\cdot10^{-4}$	$1.051842\cdot10^{-3}$	$1.194813\cdot10^{-3}$	$1.236862\cdot10^{-3}$
C	0.08744809	0.08685676	0.08656384	0.08636395
AAD /(%)	0.01	0.01	0.01	0.01
MD /(%)	0.04	0.04	0.06	0.08
Bias /(%)	$5.52\cdot10^{-5}$	$2.09\cdot10^{-5}$	$1.32\cdot10^{-6}$	$-2.02\cdot10^{-5}$
σ /(g·cm^{-3})	0.11	0.16	0.20	0.22
RMSD /(g·cm^{-3})	0.11	0.16	0.20	0.22

Parameters	*x*			
	0.6053	0.6777	0.8526	1.0000
A_0 / g cm^{-3}	2.232172	2.262014	2.184386	2.222441
A_1 / g cm^{-3} K^{-1}	$-6.344043\cdot10^{-3}$	$-6.197039\cdot10^{-3}$	$-4.623221\cdot10^{-3}$	$-4.364889\cdot10^{-3}$
A_2 / g cm^{-3} K^{-2}	$1.699920\cdot10^{-5}$	$1.632308\cdot10^{-5}$	$1.099809\cdot10^{-5}$	$9.763048\cdot10^{-6}$
A_3 / g cm^{-3} K^{-3}	$-2.167670\cdot10^{-8}$	$-2.099945\cdot10^{-8}$	$-1.544841\cdot10^{-8}$	$-1.380877\cdot10^{-8}$
B_0 / MPa	293.2964	292.0680	286.8810	276.3470
B_1 / MPa K^{-1}	-1.215491	-1.220966	-1.215997	-1.168877
B_2 / MPa K^{-2}	$1.262329\cdot10^{-3}$	$1.281457\cdot10^{-3}$	$1.299226\cdot10^{-3}$	$1.248849\cdot10^{-3}$
C	0.08624520	0.08620237	0.08597850	0.08572617
AAD /(%)	0.01	0.01	0.02	0.01
MD /(%)	0.09	0.09	0.10	0.10
Bias /(%)	$-5.67\cdot10^{-5}$	$1.89\cdot10^{-5}$	$-4.48\cdot10^{-5}$	$-4.59\cdot10^{-4}$
σ /(g·cm^{-3})	0.23	0.23	0.31	0.27
RMSD /(g·cm^{-3})	0.22	0.23	0.30	0.26

N is the number of experimental data points and *m* is the number of parameters.

[a]Absolute Average Deviation: $\mathrm{AAD} = \frac{100}{\mathrm{N}} \sum_{\mathrm{i}=1}^{\mathrm{N}} \left| \frac{\rho_{\mathrm{i}}^{\mathrm{exp}} - \rho_{\mathrm{i}}^{\mathrm{calc}}}{\rho_{\mathrm{i}}^{\mathrm{exp}}} \right|$

[b]Maximum deviation: $\mathrm{MD} = \mathrm{Max}\left(100 \left| \frac{\rho_{\mathrm{i}}^{\mathrm{exp}} - \rho_{\mathrm{i}}^{\mathrm{calc}}}{\rho_{\mathrm{i}}^{\mathrm{exp}}} \right| \right)$

[c]Average Deviation: $\mathrm{Bias} = \frac{100}{\mathrm{N}} \sum_{\mathrm{i}=1}^{\mathrm{N}} \frac{\rho_{\mathrm{i}}^{\mathrm{exp}} - \rho_{\mathrm{i}}^{\mathrm{calc}}}{\rho_{\mathrm{i}}^{\mathrm{exp}}}$

[d]Standard Deviation: $\sigma = \sqrt{\frac{\sum_{\mathrm{i}=1}^{\mathrm{N}} (\rho_{\mathrm{i}}^{\mathrm{exp}} - \rho_{\mathrm{i}}^{\mathrm{calc}})^2}{\mathrm{N\text{-}m}}}$

[e]Root Mean Square Deviation: $\mathrm{RMSD} = \sqrt{\frac{\sum_{\mathrm{i}=1}^{\mathrm{N}} (\rho_{\mathrm{i}}^{\mathrm{exp}} - \rho_{\mathrm{i}}^{\mathrm{calc}})^2}{\mathrm{N}}}$

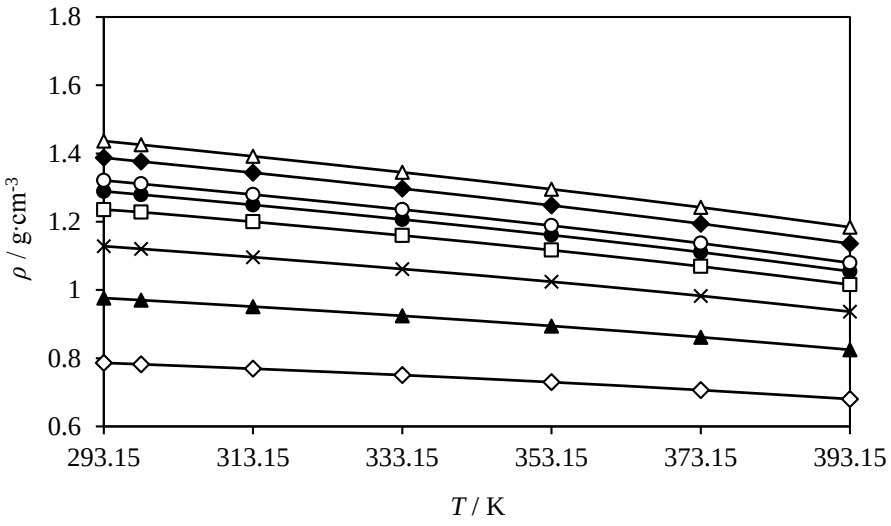
1.8
1.6
1.4
1.2
1
0.8
0.6
ρ / g·cm-3
293.15
313.15
333.15
353.15
373.15
393.15
T / K

(a)

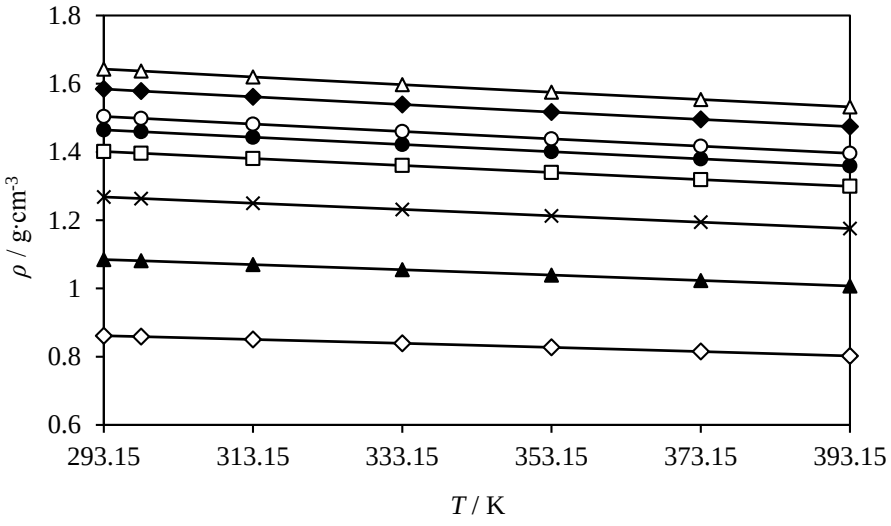
1.8
1.6
1.4
1.2
1
0.8
0.6
ρ / g·cm-3
293.15
313.15
333.15
353.15
373.15
393.15
T / K

(b)

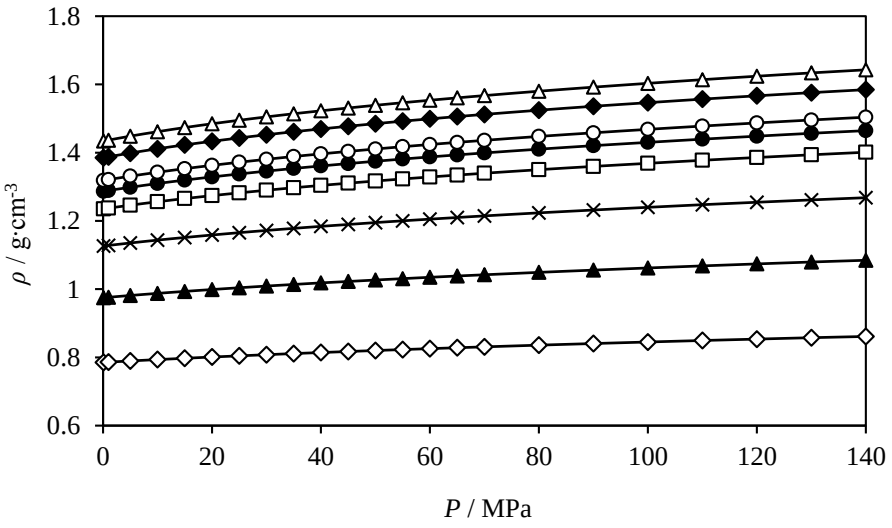

(c)

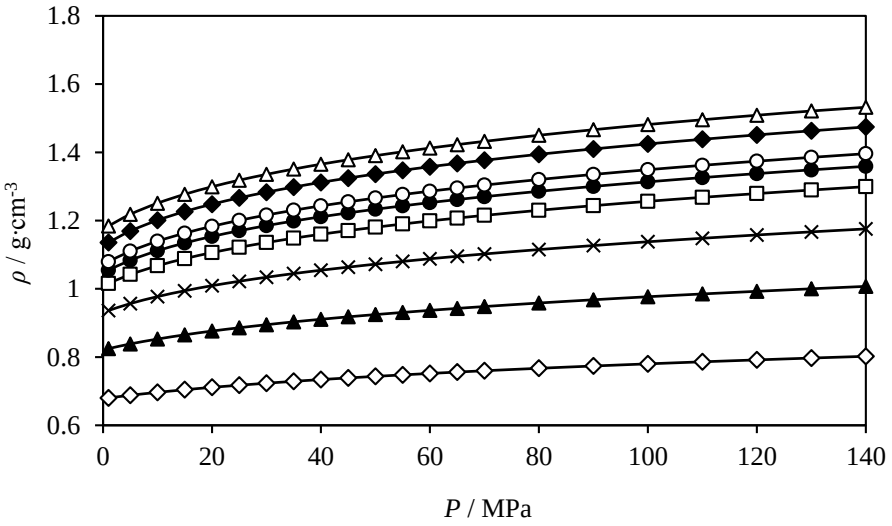

(d)

Figure 1. Experimental values of densities, ρ, for different mole fractions of x HFE-7200 + (1-x) 2-propanol vs. (a) the temperature, T at 1 MPa, (b) the temperature, T at 140 MPa, (c) the pressure, P at 293.15 K and (d) the pressure, P at 393.15 K: ◊, x = 0.0000; ▲, x = 0.1502; x, x = 0.3258; □, x = 0.4963; ●, x = 0.6754; ○, x = 0.8495; ♦, x = 0.9184; Δ, x = 1.0000; (─), Tait equation (2) to (4).

3.3. Comparison with literature data

There was possible to compare our density values for the two pure compounds with the literature data available, but concerning the mixture, no data was found to compare with. Due to

some of the published data are not in the same *P*, *T* sets than ours, we used equations (2) to (4) to establish a correlation that would allow to compare our data with those from the literature. Three references [4], [21 and 22] at atmospheric pressure were found for pure HFE-7200, while references [23 and 24] report 126 points at high pressure in the interval (0.1 – 100 MPa). Only reference [22] reports deviations lower than the expanded uncertainty, with a MD% = 0.06, an AAD% = 0.04 and a Bias% = -0.04. For the reference at high pressure, the reported MD% = 0.38 while the AAD% and the Bias% return data slightly higher than the uncertainty, 0.13 and -0.13 respectively. The worst datum is given by reference [21], with a MD% = AAD% = 0.75 and a Bias% = -0.75. Table HFE-lit gathers all the information concerning the comparisons done for pure HFE-7200.

Table 4. Literature comparison between the values generated using the Tait-like equation at exactly the same experimental *P*, *T* sets given for HFE-7200 for several literature references.

Reference	Year	N_P	T_{min} / K	T_{max} / K	P_{min} / MPa	P_{max} / MPa	AAD / %	MD / %	Bias / %
At Atmospheric Pressure									
Murata *et al.* [21]	2002	1	296.15	296.15	0.1	0.1	0.75	0.75	-0.75
Warrier and Teja [4]	2011	2	297.80	298.20	0.1	0.1	0.44	0.47	-0.44
Rausch *et al.* [22]	2015	15	293.15	363.15	0.1	0.1	0.04	0.06	-0.04
At High Pressure									
Fang *et al.* [23 and 24]	2014 - 2015	126	293.33	362.72	0.10	100.00	0.13	0.38	-0.13

N_P Number of data points which are in our *p*, *T* ranges.

Several references were found for 2-Propanol; in this work we have considered those which contain data at high pressure. Figure 2 shows graphically the deviations obtained when comparing with the 11 references found [17], [25 - 34].

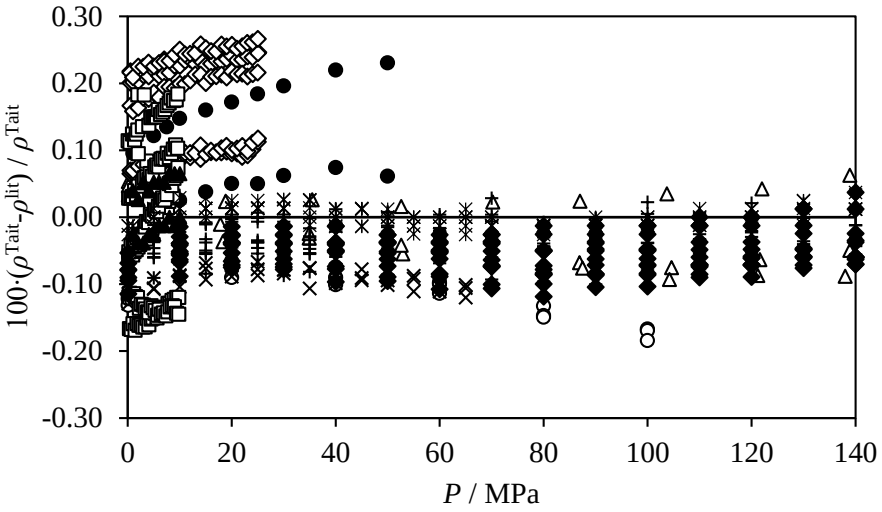

Figure 2. Obtained deviations between the values from the literature and the values generated by our correlation (Equation (to)) at the same *P*, *T* sets. ●; reference [25], Δ; reference [26], ▼; reference [27], ○; reference [28], ×; reference [29], ◊; reference [30], □; reference [31], ♦; reference [32], ▲; reference [33], +; reference [34], Ж; reference [17].

Most of the references report density data at pressures lower than 70 MPa, being references [26], [32], [34] and [17] the ones which have measured up to 140 MPa (up to 138.9 in the case of reference [26]. According to the temperature intervals, no reference overlaps our lower limit (293.15 K), since the lowest temperature value measured is 293.15 K for reference [32]. The upper limit in temperature (393.15 K) is overtaken by references [26] and [34], with 400.00 and 403.15 K respectively. For the deviations between the literature values and those obtained by our correlation, the best values are those found in the comparison with our previous paper [17], with a MD% = 0.04, and AAD% = 0.01 and a Bias% = $-8.30 \cdot 10^{-6}$. References [26], [27], [32 and 33], report maximum deviations MD close to the experimental uncertainty, with values of 0.09%, 0.09%, 0.12% and 0.06% respectively. The worst value correspond to the comparison with reference [30], which reports 156 points with an AAD% = 0.18, a MD% = 0.27 and a Bias% = 0.18.

3.4. Excess Molar Volumes

The excess volume V^E, can be defined as the difference between the real change in volume on the mixture and the ideal change of volume on mixing. Excess volumes provide reliable information so its determination from experimental high pressure density data is reported in this section. From the aforementioned definition one can determine the equation of calculation for excess volume:

$$V^E = \sum_{i=1}^{n} x_i M_i \left[\left(1/\rho \right) - \left(1/\rho_i \right) \right] \tag{5}$$

Where n is the number of components, x_i is the mole fraction of component i in the mixture, M_i is the molar mass of component i, ρ and ρ_i are the measured densities of the mixture and pure component i, respectively.

Figure 3 shows representations of excess volumes V^E, vs. the composition x, at different pressures and at (a) 293.15 K and (b) at 393.15 K and at different temperatures, where (c) shows excess volumes at 1 MPa, and (d) at 140 MPa. In all cases excess volumes show a positive trend and relatively high values, which is a result of the low packing effect between the molecules of HFE-7200 and 2-Propanol. When comparing graph (a) with (b) a big difference in the values of excess volumes is observed. At higher temperatures, as is the case of (b), the packing effect is less effective than at lower temperatures, being the V^E values much higher at 393.15 K (b) than at 293.15 K (a). At 293.15 K the highest value of excess volume is found at the lowest pressure (1 MPa) and at a molar composition of x = 0.5019 being this trend the same for the rest of the pressures. In the case of 393.15 K (b), the highest value of VE is found also at 1 MPa, but for a mole composition of x = 0.6777. In graphs (c) and (d) the difference in the excess volumes values is much higher at low pressures (1 MPa, case (c)) than at high pressures (case (d), 140 MPa). The highest value of V^E is observed at 1 MPa, at the temperature of 393.15 K and at the mole composition x = 0.6053 with an excess volume of 4.16 $cm_3 \cdot mol^{-1}$.

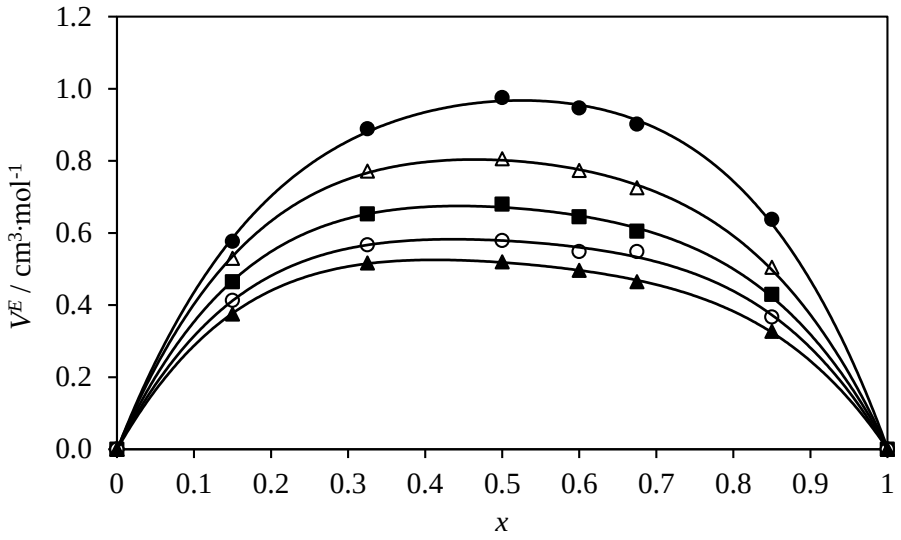

(a)

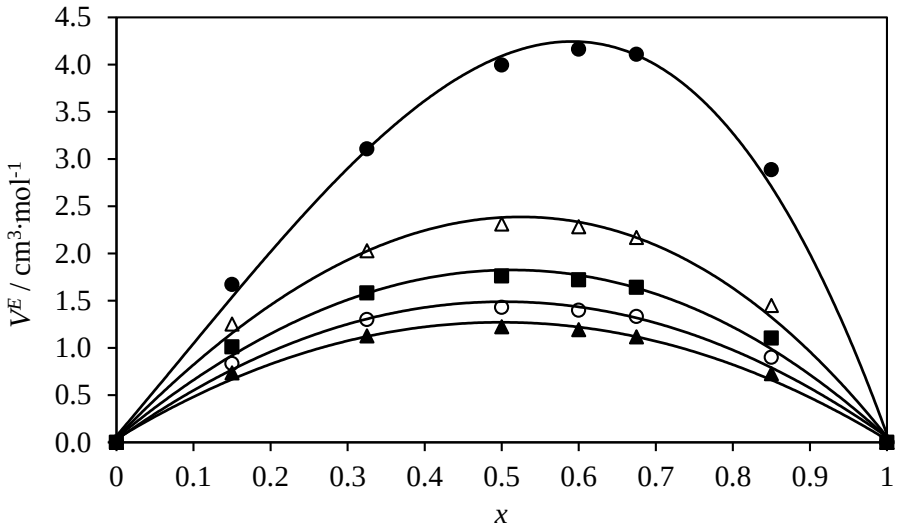
4.5
4.0
3.5
3.0
2.5
2.0
1.5
1.0
0.5
0.0
V^E / cm^3·mol^{-1}
0
0.1
0.2
0.3
0.4
0.5
0.6
0.7
0.8
0.9
1
x

(b)

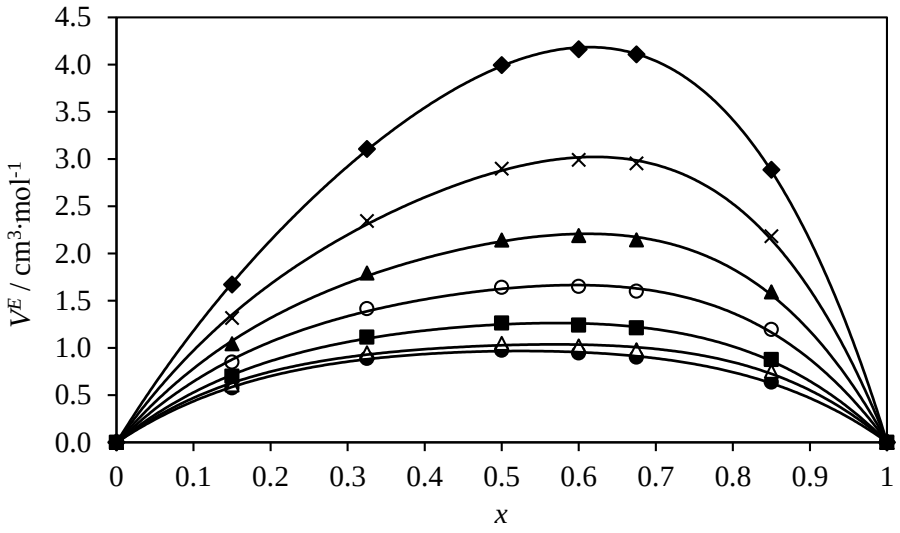
4.5
4.0
3.5
3.0
2.5
2.0
1.5
1.0
0.5
0.0
V^E / cm^3·mol^{-1}
0
0.1
0.2
0.3
0.4
0.5
0.6
0.7
0.8
0.9
1
x

(c)

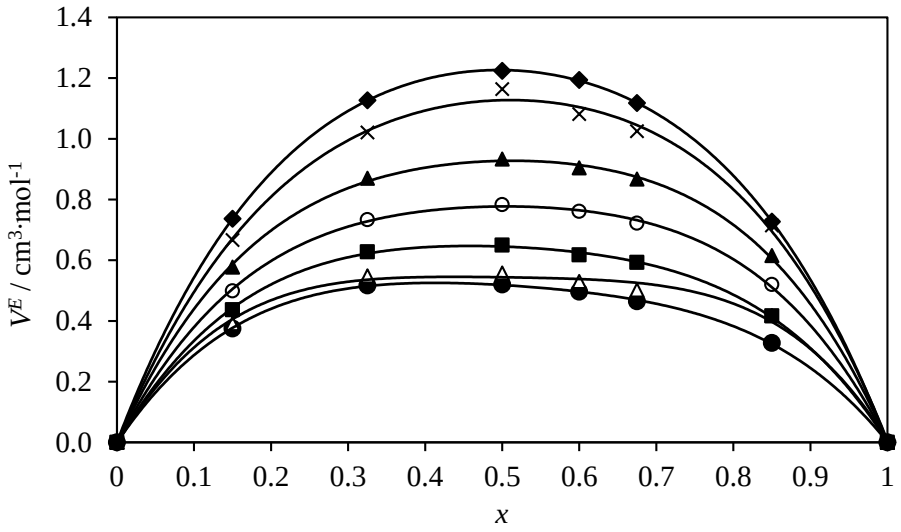

(d)

Figure 3. Experimental values for excess volumes obtained for the binary mixture *x* HFE-7200 + (1-*x*) 2-propanol as a function of the mole fraction and at different pressures *P*, (a) at 293.15 K, (b) at 393.15 K, where: ●; 1 MPa, Δ; 35 MPa, ■; 70 MPa, ○; 110 MPa, ▲; 140 MPa, and at different temperatures *T*, (c) at *P* = 1 MPa and (d) at *P* = 140 MPa where: ●; 293.15 K, Δ; 298.15 K, ■; 313.15 K, ○; 333.15 K, ▲; 353.15 K, ×; 373.15 K, ♦; 393.15 K. (─); Redlich-Kister's equation.

Figure 3 also shows the fitting curves obtained for both the two binary systems by using a Redlich-Kister polynomial of the type:

$$V^E = x(1-x)\sum_i z_i (2x-1)^{i-1} \tag{6}$$

In equation (6) z_i are the adjustable parameters, and *x* is the mole fraction of HFE-7200. Then, for the mixture studied in this work, *x* HFE-7200 + (*1*-*x*) 2-Propanol, the solid line represents the fitting curve to the experimental data. Table 5 reports the values of the adjustable parameters, z_i, and the standard deviations obtained by using equation (6) for the pressures 0.10 MPa and at temperatures from 293.15 K to 333.15 K, and at 1.00 MPa, 70 MPa, 110 MPa and 140 MPa all at temperatures from 293.15 K to 393.15 K.

Table 5. Values of parameters z_i of equation (6) and the corresponding standard deviation, σ, for the binary system x HFE-7200 + (*1*-x) 2-propanol for all the temperatures measured T, at different pressures P.

	z_1	z_2	z_3	$\sigma\,(V^E)$/ $cm^3 \cdot mol^{-1}$
T / K		(P = 0.10 MPa)		
293.15	3.9066	0.2586	1.8454	0.01
298.15	4.2365	0.8903	2.7890	0.02
313.15	5.1291	1.3157	2.7740	0.04
333.15	6.6412	2.2488	3.6086	0.06
T / K		(P = 1.00 MPa)		
293.15	3.8644	0.2162	1.8120	0.01
298.15	4.1922	0.8662	2.7045	0.04
313.15	5.0660	1.2628	2.9083	0.04
333.15	6.5910	2.1445	3.6355	0.05
353.15	8.5969	3.3976	4.5572	0.06
373.15	11.6002	5.3423	5.7151	0.08
393.15	16.0255	8.0954	6.0922	0.12
T / K		(P = 70.00 MPa)		
293.15	2.6680	0.0000	1.6825	0.02
298.15	2.8787	0.2371	2.3223	0.01
313.15	3.4175	0.2678	2.2462	0.03
333.15	4.1804	0.5302	2.5789	0.03
353.15	5.0716	0.8184	2.7855	0.04
373.15	6.0799	1.0669	3.1775	0.06
393.15	7.1293	1.2353	3.4803	0.07
T / K		(P = 110.00 MPa)		
293.15	2.2786	0.0000	1.5878	0.02
298.15	2.4436	0.1205	2.2456	0.01
313.15	2.8939	0.1297	1.9117	0.02
333.15	3.4994	0.3855	2.3211	0.03
353.15	4.2129	0.5966	2.5047	0.04
373.15	4.9713	0.7401	2.8253	0.05
393.15	5.8006	0.9295	2.9419	0.06
T / K		(P = 140.00 MPa)		
293.15	2.0536	0.0000	1.4306	0.02
298.15	2.1714	0.0000	1.9986	0.01
313.15	2.5687	0.0000	1.5985	0.01
333.15	3.1085	0.0285	1.7880	0.01
353.15	3.7093	0.0983	1.9751	0.01
373.15	4.5080	0.1267	1.7365	0.02
393.15	4.9025	0.0000	1.7151	0.01

3.5. The derived thermodynamic properties.

The derived thermodynamic properties, that is, the isothermal compressibility κ_T, and isobaric expansion α_p, can give valuable information on the dependence of the volumetric properties on temperature and pressure. The isothermal compressibility, κ_T, describes the effect of pressure on the density based on the equation:

$$\kappa_T = \left(\frac{1}{\rho}\right)\left(\frac{\partial \rho}{\partial p}\right)_T = \frac{C}{\left(1 - C\ln\left(\frac{B(T)+p}{B(T)+0.1MPa}\right)\right)\left(B(T)+p\right)} \quad (7)$$

Table 6 gathers the values of isothermal compressibility for all the measured compositions of the binary mixture *x* HFE-7200 + (*1-x*) 2-Propanol. It can be seen that the values of κ_T are higher for HFE-7200 than for any of the mixtures and for pure 2-Propanol, and in the same way κ_T increases when increasing the temperature but taking into account the pressure, it promotes an effect of decrease when the higher the pressure is.

Table 6. Values of isothermal compressibility $\kappa_T \cdot 10^4$, for the system *x* HFE-7200 + (1-*x*) 2-propanol as function of pressure *P*, and at different temperatures T^a.

x	*P* / MPa	*T* / K						
		293.15	298.15	313.15	333.15	353.15	373.15	393.15
		$\kappa_T.10^4$ / MPa^{-1}						
0.0000	0.10	10.8	11.2	12.6	14.9			
	1.00	10.7	11.1	12.4	14.7	17.8	22.3	29.2
	5.00	10.2	10.6	11.8	13.9	16.6	20.4	26.0
	10.00	9.7	10.1	11.2	12.9	15.3	18.5	23.0
	15.00	9.3	9.6	10.5	12.1	14.2	16.9	20.6
	20.00	8.8	9.1	10.0	11.4	13.2	15.6	18.7
	25.00	8.5	8.7	9.5	10.8	12.4	14.4	17.1
	30.00	8.1	8.3	9.1	10.3	11.7	13.5	15.8
	35.00	7.8	8.0	8.7	9.8	11.0	12.6	14.7
	40.00	7.5	7.7	8.3	9.3	10.5	11.9	13.7
	45.00	7.2	7.4	8.0	8.9	10.0	11.3	12.9
	50.00	7.0	7.1	7.7	8.5	9.5	10.7	12.1
	55.00	6.7	6.9	7.4	8.2	9.1	10.2	11.5
	60.00	6.5	6.7	7.1	7.9	8.7	9.7	10.9
	65.00	6.3	6.5	6.9	7.6	8.4	9.3	10.4
	70.00	6.1	6.3	6.7	7.3	8.0	8.9	9.9

	80.00	5.8	5.9	6.3	6.8	7.5	8.2	9.1
	90.00	5.5	5.6	5.9	6.4	7.0	7.6	8.4
	100.00	5.2	5.3	5.6	6.0	6.5	7.1	7.8
	110.00	5.0	5.0	5.3	5.7	6.2	6.7	7.3
	120.00	4.7	4.8	5.1	5.4	5.8	6.3	6.8
	130.00	4.5	4.6	4.8	5.2	5.5	6.0	6.5
	140.00	4.3	4.4	4.6	4.9	5.3	5.7	6.1
0.1520	0.10	13.7	14.3	16.4	20.1			
	1.00	13.5	14.1	16.1	19.7	24.7	32.0	43.5
	5.00	12.8	13.3	15.1	18.2	22.4	28.2	36.8
	10.00	12.0	12.4	14.0	16.6	20.1	24.6	31.0
	15.00	11.3	11.7	13.1	15.3	18.2	21.9	26.8
	20.00	10.7	11.0	12.3	14.2	16.7	19.7	23.7
	25.00	10.1	10.4	11.5	13.3	15.4	18.0	21.3
	30.00	9.6	9.9	10.9	12.4	14.3	16.5	19.3
	35.00	9.2	9.4	10.3	11.7	13.4	15.3	17.7
	40.00	8.8	9.0	9.8	11.1	12.5	14.3	16.3
	45.00	8.4	8.6	9.4	10.5	11.8	13.3	15.1
	50.00	8.1	8.3	9.0	10.0	11.2	12.6	14.2
	55.00	7.8	8.0	8.6	9.5	10.6	11.9	13.3
	60.00	7.5	7.7	8.2	9.1	10.1	11.2	12.5
	65.00	7.2	7.4	7.9	8.7	9.6	10.7	11.9
	70.00	7.0	7.1	7.6	8.4	9.2	10.2	11.3
	80.00	6.5	6.7	7.1	7.8	8.5	9.3	10.2
	90.00	6.1	6.3	6.7	7.2	7.9	8.6	9.4
	100.00	5.8	5.9	6.3	6.8	7.3	8.0	8.7
	110.00	5.5	5.6	5.9	6.4	6.9	7.4	8.1
	120.00	5.2	5.3	5.6	6.0	6.5	7.0	7.5
	130.00	5.0	5.1	5.3	5.7	6.1	6.6	7.1
	140.00	4.8	4.8	5.1	5.4	5.8	6.2	6.7
0.3275	0.10	16.2	17.0	19.8	24.9			
	1.00	16.0	16.7	19.5	24.3	31.2	41.6	58.2
	5.00	15.0	15.6	18.0	22.1	27.6	35.4	46.9
	10.00	13.9	14.5	16.5	19.8	24.2	30.0	37.9
	15.00	12.9	13.5	15.2	18.0	21.5	26.1	31.9
	20.00	12.1	12.6	14.1	16.5	19.4	23.1	27.6
	25.00	11.4	11.8	13.1	15.2	17.7	20.7	24.4
	30.00	10.8	11.2	12.3	14.1	16.3	18.8	21.9
	35.00	10.2	10.6	11.6	13.2	15.1	17.3	19.8
	40.00	9.7	10.0	11.0	12.4	14.1	16.0	18.2
	45.00	9.3	9.6	10.4	11.7	13.2	14.8	16.8
	50.00	8.9	9.1	9.9	11.1	12.4	13.9	15.6
	55.00	8.5	8.7	9.5	10.5	11.7	13.0	14.6
	60.00	8.2	8.4	9.0	10.0	11.1	12.3	13.7

	65.00	7.9	8.1	8.7	9.6	10.5	11.7	12.9
	70.00	7.6	7.7	8.3	9.1	10.1	11.1	12.2
	80.00	7.1	7.2	7.7	8.4	9.2	10.1	11.0
	90.00	6.6	6.7	7.2	7.8	8.5	9.2	10.1
	100.00	6.2	6.3	6.7	7.3	7.9	8.5	9.3
	110.00	5.9	6.0	6.3	6.8	7.4	8.0	8.6
	120.00	5.6	5.7	6.0	6.4	6.9	7.4	8.0
	130.00	5.3	5.4	5.7	6.1	6.5	7.0	7.5
	140.00	5.0	5.1	5.4	5.8	6.2	6.6	7.1
0.5019	0.10	18.1	19.0	22.4	28.5			
	1.00	17.8	18.7	21.9	27.7	36.2	49.0	70.0
	5.00	16.5	17.3	20.1	24.9	31.4	40.7	54.3
	10.00	15.2	15.9	18.2	22.0	27.0	33.7	42.6
	15.00	14.1	14.7	16.6	19.8	23.8	28.8	35.2
	20.00	13.2	13.7	15.3	18.0	21.2	25.2	30.1
	25.00	12.3	12.8	14.2	16.5	19.2	22.5	26.3
	30.00	11.6	12.0	13.3	15.2	17.6	20.3	23.4
	35.00	11.0	11.3	12.5	14.2	16.2	18.5	21.2
	40.00	10.4	10.7	11.7	13.3	15.0	17.0	19.3
	45.00	9.9	10.2	11.1	12.5	14.0	15.8	17.7
	50.00	9.4	9.7	10.5	11.8	13.1	14.7	16.4
	55.00	9.0	9.2	10.0	11.1	12.4	13.8	15.3
	60.00	8.6	8.8	9.5	10.6	11.7	13.0	14.4
	65.00	8.3	8.5	9.1	10.1	11.1	12.2	13.5
	70.00	8.0	8.1	8.7	9.6	10.6	11.6	12.8
	80.00	7.4	7.6	8.1	8.8	9.6	10.5	11.5
	90.00	6.9	7.0	7.5	8.2	8.9	9.6	10.5
	100.00	6.5	6.6	7.0	7.6	8.2	8.9	9.6
	110.00	6.1	6.2	6.6	7.1	7.7	8.3	8.9
	120.00	5.8	5.9	6.2	6.7	7.2	7.7	8.3
	130.00	5.5	5.6	5.9	6.3	6.7	7.2	7.8
	140.00	5.2	5.3	5.6	6.0	6.4	6.8	7.3
0.6053	0.10	18.9	20.0	23.6	30.2			
	1.00	18.6	19.6	23.1	29.4	38.5	52.5	75.3
	5.00	17.2	18.1	21.0	26.1	33.2	43.1	57.4
	10.00	15.8	16.5	19.0	23.0	28.3	35.3	44.5
	15.00	14.6	15.2	17.3	20.6	24.8	30.0	36.5
	20.00	13.6	14.1	15.9	18.6	22.0	26.1	31.1
	25.00	12.7	13.2	14.7	17.1	19.9	23.2	27.1
	30.00	11.9	12.4	13.7	15.7	18.1	20.9	24.0
	35.00	11.3	11.6	12.8	14.6	16.7	19.0	21.7
	40.00	10.7	11.0	12.0	13.6	15.4	17.4	19.7
	45.00	10.1	10.4	11.4	12.8	14.4	16.1	18.1
	50.00	9.7	9.9	10.8	12.0	13.5	15.0	16.8

	55.00	9.2	9.5	10.2	11.4	12.7	14.1	15.6
	60.00	8.8	9.0	9.8	10.8	12.0	13.2	14.6
	65.00	8.5	8.7	9.3	10.3	11.3	12.5	13.7
	70.00	8.1	8.3	8.9	9.8	10.8	11.8	13.0
	80.00	7.5	7.7	8.2	9.0	9.8	10.7	11.7
	90.00	7.0	7.2	7.6	8.3	9.0	9.8	10.6
	100.00	6.6	6.7	7.1	7.7	8.3	9.0	9.8
	110.00	6.2	6.3	6.7	7.2	7.8	8.4	9.0
	120.00	5.9	6.0	6.3	6.8	7.3	7.8	8.4
	130.00	5.6	5.7	6.0	6.4	6.8	7.3	7.9
	140.00	5.3	5.4	5.7	6.0	6.5	6.9	7.4
0.6777	0.10	19.4	20.5	24.3	31.2			
	1.00	19.1	20.1	23.7	30.3	39.9	54.5	78.1
	5.00	17.7	18.5	21.6	26.9	34.2	44.4	59.0
	10.00	16.2	16.9	19.4	23.6	29.1	36.2	45.5
	15.00	14.9	15.5	17.6	21.1	25.3	30.7	37.2
	20.00	13.9	14.4	16.2	19.0	22.5	26.6	31.6
	25.00	12.9	13.4	15.0	17.4	20.2	23.6	27.5
	30.00	12.1	12.6	13.9	16.0	18.4	21.2	24.4
	35.00	11.4	11.8	13.0	14.8	16.9	19.3	21.9
	40.00	10.8	11.2	12.2	13.8	15.6	17.7	19.9
	45.00	10.3	10.6	11.5	13.0	14.6	16.3	18.3
	50.00	9.8	10.1	10.9	12.2	13.6	15.2	16.9
	55.00	9.3	9.6	10.4	11.5	12.8	14.2	15.8
	60.00	8.9	9.2	9.9	10.9	12.1	13.4	14.7
	65.00	8.6	8.8	9.4	10.4	11.5	12.6	13.9
	70.00	8.2	8.4	9.0	9.9	10.9	11.9	13.1
	80.00	7.6	7.8	8.3	9.1	9.9	10.8	11.8
	90.00	7.1	7.2	7.7	8.4	9.1	9.9	10.7
	100.00	6.7	6.8	7.2	7.8	8.4	9.1	9.8
	110.00	6.3	6.4	6.7	7.3	7.8	8.4	9.1
	120.00	5.9	6.0	6.4	6.8	7.3	7.9	8.5
	130.00	5.6	5.7	6.0	6.4	6.9	7.4	7.9
	140.00	5.3	5.4	5.7	6.1	6.5	7.0	7.5
0.8526	0.10	20.4	21.5	25.6	33.0			
	1.00	20.0	21.1	25.0	32.0	42.1	57.5	81.5
	5.00	18.4	19.4	22.6	28.2	35.8	46.3	60.9
	10.00	16.8	17.6	20.2	24.6	30.2	37.5	46.6
	15.00	15.5	16.1	18.3	21.8	26.2	31.6	37.9
	20.00	14.3	14.9	16.7	19.7	23.2	27.3	32.1
	25.00	13.4	13.8	15.4	17.9	20.8	24.1	27.9
	30.00	12.5	12.9	14.3	16.4	18.9	21.6	24.7
	35.00	11.8	12.1	13.4	15.2	17.3	19.6	22.2
	40.00	11.1	11.5	12.5	14.2	16.0	18.0	20.1

	45.00	10.5	10.8	11.8	13.3	14.9	16.6	18.5
	50.00	10.0	10.3	11.2	12.5	13.9	15.4	17.1
	55.00	9.5	9.8	10.6	11.8	13.0	14.4	15.9
	60.00	9.1	9.3	10.1	11.1	12.3	13.5	14.9
	65.00	8.7	8.9	9.6	10.6	11.6	12.8	14.0
	70.00	8.4	8.6	9.2	10.1	11.1	12.1	13.2
	80.00	7.8	7.9	8.5	9.2	10.0	10.9	11.9
	90.00	7.2	7.4	7.8	8.5	9.2	10.0	10.8
	100.00	6.8	6.9	7.3	7.9	8.5	9.2	9.9
	110.00	6.4	6.5	6.8	7.4	7.9	8.5	9.2
	120.00	6.0	6.1	6.4	6.9	7.4	8.0	8.5
	130.00	5.7	5.8	6.1	6.5	7.0	7.5	8.0
	140.00	5.4	5.5	5.8	6.2	6.6	7.0	7.5
1.0000	0.10	20.9	22.0	26.1	33.4			
	1.00	20.4	21.5	25.4	32.4	42.4	57.2	79.7
	5.00	18.8	19.7	23.0	28.5	36.0	46.1	59.8
	10.00	17.1	17.9	20.5	24.8	30.3	37.3	45.9
	15.00	15.7	16.4	18.5	22.0	26.3	31.4	37.5
	20.00	14.5	15.1	16.9	19.8	23.2	27.2	31.7
	25.00	13.5	14.0	15.6	18.0	20.8	24.0	27.6
	30.00	12.7	13.1	14.5	16.5	18.9	21.5	24.4
	35.00	11.9	12.3	13.5	15.3	17.3	19.6	22.0
	40.00	11.2	11.6	12.6	14.2	16.0	17.9	20.0
	45.00	10.6	10.9	11.9	13.3	14.9	16.5	18.3
	50.00	10.1	10.4	11.2	12.5	13.9	15.4	16.9
	55.00	9.6	9.9	10.7	11.8	13.0	14.4	15.8
	60.00	9.2	9.4	10.1	11.2	12.3	13.5	14.7
	65.00	8.8	9.0	9.7	10.6	11.6	12.7	13.9
	70.00	8.4	8.6	9.2	10.1	11.0	12.0	13.1
	80.00	7.8	8.0	8.5	9.2	10.0	10.9	11.8
	90.00	7.3	7.4	7.9	8.5	9.2	9.9	10.7
	100.00	6.8	6.9	7.3	7.9	8.5	9.2	9.8
	110.00	6.4	6.5	6.9	7.4	7.9	8.5	9.1
	120.00	6.0	6.1	6.5	6.9	7.4	7.9	8.5
	130.00	5.7	5.8	6.1	6.5	7.0	7.4	7.9
	140.00	5.4	5.5	5.8	6.2	6.6	7.0	7.5

[a] *Estimated expanded uncertainty (k=2): temperature U(T) = ±0.03 K, pressure U(P) = ±0.04 MPa, isothermal compressibility U(κ_T) = ±0.001 κ_T.*

In a similar way, the isobaric expansion α_p, could also be obtained by differentiating equation (2) taking into account the temperature dependence of $\rho_0(T)$ and $B(T)$:

$$\alpha_{\mathrm{p}} = -\left(\frac{1}{\rho}\right)\left(\frac{\partial \rho}{\partial T}\right)_{\mathrm{p}} \tag{8}$$

Nevertheless, the estimated isobaric expansion depends on the form of functions $B(T)$ and $\rho_0(T)$ as pointed out by references [35, 36]. Then, it is better to derive the isobaric thermal expansivity from the isobaric densities. So at each pressure we suppose that $\rho_p(T) = a_0+a_1T+a_2T^2$ and consequently $(\partial\rho/\partial T)_p = a_1 + 2a_2T$. For each pressure we get a set (a_0, a_1, a_2).

By inserting the differentiated density and the calculated densities $\rho_p(T)$ into $\alpha_p = -(1/\rho(\partial\rho/\partial T)_p$ the isobaric thermal expansivity at the different T, p conditions has been derived:

$$\alpha_p = -\frac{a_1 + 2a_2T}{a_0 + a_1T + a_2T^2} \tag{9}$$

As mentioned, the method used to evaluate the isobaric thermal expansion coefficient may affect the accuracy of the values. The differences sometimes found for the values of this coefficient from the literature are due not only to differences in density values but also to the fitting equations, as stated in [37].

The isobaric expansion, α_p, and the isothermal compressibility, κ_T, were calculated from the above procedures. The estimated uncertainty following [14] is 1% for the isothermal compressibility and around 3% for the isobaric expansion, as recently indicated on similar high-pressure density studies [8, 9] and [38] with the same methods.

Table 7 reports the isobaric expansion, α_p. Similarly as it occurs with the isothermal compressibility, the highest values of α_p are found for HFE-7200, and the values of α_p increase with increasing temperature and decrease with increasing pressure.

Table 7. Values of isobaric expansion $\alpha_P \cdot 10^4$, for the binary mixture x HFE-7200 + (1-x) 2-propanol as function of pressure P, and at different temperatures T^a.

x	P / MPa	T / K						
		293.15	298.15	313.15	333.15	353.15	373.15	393.15
				$\alpha_P.10^4$ / K^{-1}				
0.0000	0.10	9.90	10.33	11.66	13.53			
	1.00	9.78	10.20	11.51	13.36	15.35	17.52	19.91
	5.00	9.51	9.89	11.06	12.72	14.49	16.42	18.52
	10.00	9.44	9.77	10.79	12.22	13.76	15.42	17.22
	15.00	9.18	9.48	10.40	11.70	13.09	14.58	16.19
	20.00	8.99	9.26	10.09	11.25	12.50	13.83	15.26
	25.00	8.77	9.02	9.78	10.86	12.00	13.22	14.53

	30.00	8.54	8.77	9.49	10.49	11.55	12.68	13.89
	35.00	8.37	8.58	9.25	10.19	11.18	12.23	13.35
	40.00	8.26	8.46	9.06	9.91	10.81	11.76	12.77
	45.00	8.08	8.27	8.85	9.65	10.51	11.41	12.36
	50.00	7.92	8.10	8.65	9.41	10.22	11.07	11.98
	55.00	7.84	8.00	8.51	9.21	9.94	10.72	11.55
	60.00	7.73	7.88	8.36	9.01	9.70	10.43	11.20
	65.00	7.55	7.70	8.17	8.81	9.49	10.21	10.97
	70.00	7.43	7.57	8.01	8.63	9.28	9.95	10.67
	80.00	7.20	7.33	7.74	8.30	8.89	9.50	10.15
	90.00	6.98	7.10	7.48	8.01	8.56	9.13	9.74
	100.00	6.84	6.95	7.29	7.77	8.26	8.78	9.32
	110.00	6.67	6.77	7.09	7.52	7.97	8.45	8.94
	120.00	6.51	6.60	6.91	7.32	7.75	8.20	8.67
	130.00	6.32	6.41	6.70	7.10	7.52	7.95	8.40
	140.00	6.21	6.30	6.57	6.94	7.33	7.73	8.15
0.1520	0.10	11.95	12.40	13.81	15.82			
	1.00	11.74	12.18	13.56	15.53	17.67	20.03	22.66
	5.00	11.02	11.43	12.73	14.56	16.55	18.73	21.14
	10.00	10.30	10.69	11.90	13.62	15.47	17.48	19.69
	15.00	9.71	10.09	11.23	12.85	14.59	16.48	18.55
	20.00	9.27	9.63	10.74	12.30	13.97	15.77	17.74
	25.00	8.79	9.13	10.18	11.67	13.25	14.96	16.81
	30.00	8.50	8.83	9.87	11.32	12.87	14.54	16.34
	35.00	8.07	8.39	9.38	10.77	12.25	13.83	15.54
	40.00	7.83	8.15	9.13	10.49	11.94	13.49	15.17
	45.00	7.51	7.82	8.77	10.09	11.49	12.99	14.59
	50.00	7.26	7.56	8.49	9.79	11.16	12.62	14.19
	55.00	7.21	7.51	8.45	9.76	11.14	12.61	14.19
	60.00	6.86	7.16	8.07	9.34	10.68	12.11	13.63
	65.00	6.65	6.94	7.84	9.07	10.38	11.76	13.24
	70.00	6.42	6.71	7.59	8.81	10.10	11.46	12.91
	80.00	6.12	6.40	7.25	8.44	9.69	11.00	12.40
	90.00	5.80	6.08	6.93	8.10	9.32	10.62	11.99
	100.00	5.54	5.81	6.64	7.79	9.00	10.26	11.61
	110.00	5.30	5.57	6.39	7.53	8.71	9.96	11.28
	120.00	5.09	5.36	6.18	7.30	8.47	9.70	11.00
	130.00	4.90	5.16	5.97	7.08	8.24	9.45	10.74
	140.00	4.71	4.97	5.77	6.87	8.01	9.21	10.48
0.3275	0.10	14.29	14.67	15.87	17.58			
	1.00	14.15	14.53	15.71	17.41	19.26	21.32	23.62
	5.00	13.22	13.57	14.65	16.20	17.90	19.76	21.82
	10.00	12.53	12.86	13.87	15.32	16.89	18.61	20.51
	15.00	11.93	12.24	13.20	14.56	16.04	17.64	19.40

	20.00	11.41	11.70	12.61	13.90	15.29	16.80	18.45
	25.00	10.93	11.21	12.08	13.30	14.62	16.04	17.59
	30.00	10.50	10.77	11.59	12.76	14.01	15.36	16.82
	35.00	10.10	10.36	11.15	12.26	13.45	14.73	16.12
	40.00	9.74	9.99	10.74	11.81	12.95	14.17	15.49
	45.00	9.39	9.63	10.36	11.38	12.47	13.64	14.89
	50.00	9.07	9.30	10.00	10.98	12.03	13.14	14.34
	55.00	8.83	9.05	9.73	10.68	11.69	12.77	13.93
	60.00	8.48	8.69	9.35	10.26	11.22	12.25	13.34
	65.00	8.21	8.41	9.04	9.92	10.85	11.84	12.89
	70.00	7.95	8.15	8.76	9.60	10.50	11.45	12.46
	80.00	7.46	7.65	8.22	9.01	9.85	10.73	11.66
	90.00	7.07	7.25	7.79	8.54	9.32	10.15	11.03
	100.00	6.81	6.98	7.50	8.22	8.97	9.76	10.60
	110.00	6.59	6.75	7.25	7.95	8.67	9.44	10.24
	120.00	6.38	6.54	7.02	7.70	8.40	9.13	9.91
	130.00	6.19	6.35	6.82	7.47	8.15	8.86	9.61
	140.00	6.02	6.17	6.63	7.26	7.92	8.61	9.33
0.5019	0.10	14.81	15.20	16.40	18.13			
	1.00	13.86	14.36	15.91	18.15	20.63	23.39	26.52
	5.00	13.56	13.93	15.09	16.76	18.58	20.59	22.82
	10.00	13.04	13.32	14.20	15.46	16.82	18.30	19.93
	15.00	12.57	12.79	13.48	14.45	15.51	16.64	17.88
	20.00	12.11	12.29	12.85	13.65	14.50	15.42	16.42
	25.00	11.66	11.82	12.30	12.97	13.69	14.46	15.29
	30.00	11.19	11.33	11.77	12.39	13.04	13.75	14.50
	35.00	10.76	10.89	11.29	11.86	12.46	13.10	13.78
	40.00	10.40	10.52	10.89	11.42	11.98	12.57	13.20
	45.00	10.06	10.18	10.53	11.02	11.54	12.09	12.68
	50.00	9.77	9.88	10.21	10.67	11.16	11.68	12.23
	55.00	9.70	9.81	10.15	10.63	11.14	11.68	12.24
	60.00	9.24	9.34	9.64	10.06	10.50	10.96	11.45
	65.00	9.04	9.13	9.42	9.83	10.26	10.71	11.18
	70.00	8.80	8.89	9.16	9.55	9.95	10.37	10.82
	80.00	8.42	8.50	8.76	9.12	9.50	9.90	10.31
	90.00	8.08	8.16	8.41	8.75	9.10	9.48	9.87
	100.00	7.77	7.85	8.08	8.41	8.74	9.10	9.47
	110.00	7.50	7.58	7.80	8.12	8.44	8.79	9.14
	120.00	7.27	7.34	7.56	7.86	8.18	8.51	8.86
	130.00	7.04	7.11	7.33	7.62	7.93	8.26	8.59
	140.00	6.84	6.91	7.13	7.42	7.73	8.04	8.38
0.6053	0.10	15.04	15.45	16.74	18.59			
	1.00	14.24	14.73	16.28	18.51	20.98	23.73	26.86
	5.00	13.90	14.26	15.39	17.00	18.77	20.73	22.90

	10.00	13.08	13.41	14.46	15.95	17.58	19.36	21.33
	15.00	12.39	12.70	13.68	15.07	16.58	18.23	20.04
	20.00	12.05	12.28	12.99	13.99	15.08	16.25	17.52
	25.00	11.51	11.73	12.39	13.32	14.33	15.41	16.58
	30.00	11.03	11.23	11.85	12.72	13.65	14.65	15.74
	35.00	10.59	10.77	11.36	12.17	13.04	13.98	14.98
	40.00	10.18	10.36	10.91	11.67	12.49	13.36	14.30
	45.00	9.80	9.97	10.49	11.21	11.97	12.79	13.66
	50.00	9.45	9.61	10.10	10.78	11.50	12.26	13.07
	55.00	9.22	9.38	9.85	10.51	11.20	11.94	12.72
	60.00	8.85	8.99	9.43	10.04	10.69	11.38	12.11
	65.00	8.55	8.69	9.11	9.69	10.30	10.94	11.63
	70.00	8.32	8.45	8.85	9.41	10.00	10.62	11.28
	80.00	7.94	8.07	8.45	8.99	9.55	10.14	10.77
	90.00	7.60	7.72	8.09	8.61	9.14	9.71	10.31
	100.00	7.30	7.42	7.78	8.28	8.80	9.34	9.92
	110.00	7.03	7.15	7.50	7.98	8.49	9.02	9.58
	120.00	6.79	6.90	7.24	7.72	8.21	8.73	9.28
	130.00	6.57	6.68	7.02	7.49	7.98	8.50	9.03
	140.00	6.39	6.50	6.83	7.30	7.78	8.28	8.81
0.6777	0.10	14.88	15.38	16.97	19.26			
	1.00	14.46	14.94	16.47	18.67	21.10	23.82	26.91
	5.00	14.13	14.47	15.56	17.12	18.82	20.70	22.80
	10.00	13.54	13.79	14.58	15.69	16.90	18.22	19.67
	15.00	12.98	13.17	13.77	14.61	15.52	16.51	17.58
	20.00	12.47	12.62	13.09	13.75	14.46	15.22	16.03
	25.00	11.99	12.12	12.50	13.03	13.60	14.21	14.86
	30.00	11.56	11.66	11.98	12.43	12.90	13.41	13.94
	35.00	11.22	11.30	11.56	11.92	12.30	12.70	13.12
	40.00	10.88	10.96	11.17	11.47	11.79	12.12	12.47
	45.00	10.51	10.57	10.78	11.06	11.36	11.67	11.99
	50.00	10.25	10.31	10.47	10.70	10.94	11.19	11.45
	55.00	10.23	10.28	10.45	10.68	10.92	11.17	11.43
	60.00	9.76	9.80	9.93	10.10	10.27	10.46	10.65
	65.00	9.52	9.56	9.67	9.83	9.99	10.16	10.33
	70.00	9.30	9.34	9.44	9.58	9.72	9.87	10.02
	80.00	8.94	8.97	9.04	9.15	9.25	9.36	9.48
	90.00	8.60	8.62	8.68	8.77	8.85	8.94	9.03
	100.00	8.32	8.34	8.38	8.44	8.50	8.56	8.62
	110.00	8.04	8.05	8.09	8.14	8.20	8.25	8.30
	120.00	7.82	7.83	7.86	7.89	7.92	7.95	7.98
	130.00	7.59	7.59	7.62	7.65	7.68	7.71	7.75
	140.00	7.39	7.40	7.41	7.43	7.45	7.47	7.49
0.8526	0.10	15.48	15.88	17.11	18.90			

	1.00	14.85	15.29	16.67	18.66	20.87	23.32	26.09
	5.00	14.44	14.74	15.68	17.03	18.50	20.12	21.92
	10.00	13.78	13.99	14.64	15.56	16.55	17.63	18.81
	15.00	13.14	13.30	13.77	14.43	15.15	15.91	16.74
	20.00	12.60	12.71	13.06	13.56	14.09	14.65	15.25
	25.00	12.10	12.19	12.46	12.83	13.23	13.65	14.09
	30.00	11.64	11.71	11.93	12.23	12.54	12.87	13.22
	35.00	11.25	11.30	11.47	11.70	11.94	12.19	12.45
	40.00	10.92	10.96	11.08	11.26	11.43	11.62	11.81
	45.00	10.55	10.58	10.69	10.84	11.00	11.16	11.33
	50.00	10.26	10.29	10.37	10.49	10.61	10.73	10.85
	55.00	10.55	10.55	10.55	10.53	10.52	10.49	10.46
	60.00	9.75	9.76	9.81	9.87	9.93	9.99	10.05
	65.00	9.52	9.53	9.57	9.61	9.66	9.70	9.75
	70.00	9.27	9.28	9.31	9.36	9.40	9.44	9.48
	80.00	8.92	8.92	8.93	8.93	8.94	8.94	8.94
	90.00	8.55	8.55	8.56	8.56	8.56	8.56	8.55
	100.00	8.27	8.26	8.25	8.23	8.21	8.18	8.15
	110.00	7.97	7.97	7.96	7.94	7.91	7.89	7.86
	120.00	7.78	7.77	7.73	7.69	7.64	7.59	7.53
	130.00	7.52	7.51	7.49	7.45	7.41	7.37	7.32
	140.00	7.31	7.30	7.28	7.24	7.20	7.15	7.10
1.0000	0.10	15.42	15.75	16.79	18.28			
	1.00	10.55	11.33	13.74	17.19	20.99	25.27	30.17
	5.00	9.01	9.76	12.10	15.41	19.04	23.07	27.65
	10.00	8.14	8.83	10.93	13.90	17.11	20.66	24.63
	15.00	7.30	7.95	9.95	12.77	15.81	19.13	22.82
	20.00	6.63	7.26	9.20	11.91	14.81	17.97	21.46
	25.00	6.11	6.72	8.59	11.20	13.98	17.00	20.32
	30.00	5.62	6.22	8.06	10.61	13.33	16.26	19.48
	35.00	5.22	5.81	7.61	10.11	12.75	15.60	18.72
	40.00	4.87	5.45	7.22	9.67	12.26	15.04	18.07
	45.00	4.57	5.14	6.88	9.29	11.83	14.56	17.52
	50.00	4.29	4.85	6.57	8.95	11.45	14.12	17.02
	55.00	4.25	4.82	6.55	8.93	11.44	14.13	17.04
	60.00	3.81	4.36	6.05	8.36	10.80	13.39	16.19
	65.00	3.61	4.16	5.82	8.12	10.53	13.09	15.84
	70.00	3.41	3.96	5.61	7.89	10.27	12.80	15.52
	80.00	3.07	3.61	5.24	7.48	9.81	12.29	14.95
	90.00	2.78	3.31	4.93	7.14	9.44	11.88	14.49
	100.00	2.51	3.04	4.64	6.82	9.10	11.50	14.06
	110.00	2.28	2.80	4.39	6.56	8.81	11.18	13.71
	120.00	2.07	2.59	4.17	6.32	8.55	10.89	13.39
	130.00	1.88	2.40	3.97	6.10	8.31	10.64	13.11
	140.00	1.73	2.25	3.81	5.93	8.13	10.44	12.90

[a] *Estimated expanded uncertainty (k=2): temperature U(T) = ±0.03 K, pressure U(P) = ±0.04 MPa, isobaric expansion U(α_P) = ±0.003 α_P.*

3.6. Speed of Sound

Speeds of sound *c*, of binary mixtures *x* HFE-7200 + (1-*x*) 2-Propanol were determined at atmospheric pressure and in the range of temperatures (293.15 – 333.15 K) by using an Anton Paar DSA 5000 density and sound velocity meter. Densities ρ, at atmospheric pressure in the same temperature range were also determined, and isentropic compressibilities κ_S, were calculated from these experimental data by means of the Laplace equation (10)

$$\kappa_S = \rho^{-1} \cdot c^{-2} \tag{10}$$

The obtained data are showed in Table 8. It can be seen that the higher values of speed of sound are found for pure 2-Propanol (x = 0.0000), and it can be stated also that the sound velocity values decrease when increasing the temperature. By contrast, isentropic compressibilities show the highest values at the mole fraction x = 1.0000 (pure HFE-7200), and these values increase when increasing temperature. This fact is due to the densities for HFE-7200 are quite higher than those of 2-Propanol, and its values decrease in the same way as the temperature increases.

Table 8. Experimental speeds of sound *c*, densities ρ, and calculated isentropic compressibilities κ_S, at different temperatures and at atmospheric pressure for the binary system *x* HFE-7200 + (1-*x*) 2-Propanol.

T / K	x	c / m·s^{-1}	ρ / g·cm^{-3}	κ_S / TPa^{-1}
293.15	0.0000	1157.54	0.78546	950
	0.1517	931.61	0.97447	1182
	0.3270	802.01	1.12622	1380
	0.5016	729.80	1.23522	1520
	0.6055	700.59	1.28720	1583
	0.6762	684.39	1.31853	1619
	0.8505	654.40	1.38484	1686
	1.0000	637.83	1.43427	1714
298.15	0.0000	1139.71	0.78127	985
	0.1518	913.88	0.96845	1236
	0.3511	772.59	1.13518	1476

	0.4975	714.45	1.22380	1601
	0.6057	683.91	1.27742	1674
	0.6994	663.41	1.31768	1724
	0.8484	638.73	1.37317	1785
	1.0000	622.13	1.42306	1816
303.15	0.0000	1122.56	0.77700	1021
	0.1520	896.39	0.96232	1293
	0.3281	767.25	1.11099	1529
	0.5027	696.29	1.21713	1695
	0.6068	667.45	1.26787	1770
	0.6772	651.84	1.29814	1813
	0.8510	622.54	1.36284	1893
	1.0000	606.46	1.41162	1926
313.15	0.0000	1087.2	0.76821	1101
	0.1526	861.01	0.94996	1420
	0.3288	733.22	1.09477	1699
	0.5017	663.82	1.19732	1895
	0.606	635.32	1.24692	1987
	0.6757	620.05	1.27628	2038
	0.8498	591.35	1.33989	2134
	1.0000	575.75	1.38853	2173
323.15	0.0000	1051.78	0.75907	1191
	0.1518	827.09	0.93593	1562
	0.3268	700.69	1.07643	1892
	0.5036	630.75	1.17833	2133
	0.6054	603.51	1.22564	2240
	0.6776	588.19	1.25528	2303
	0.8492	560.51	1.31658	2418
	1.0000	545.46	1.36515	2462
333.15	0.0000	1015.29	0.74942	1294
	0.1501	794.18	0.92030	1723
	0.3275	667.60	1.05879	2119
	0.5007	599.56	1.15645	2406
	0.6047	572.22	1.20354	2538
	0.6738	557.64	1.23131	2612
	0.8499	529.89	1.29295	2755
	1.0000	515.64	1.34102	2805

[a] *Uncertainties: temperature U(T) = ±0.01 K, speed of sound U(c) = ±0.1 m·s^{-1}, density U(ρ) = ± 1·10^{-5} g·cm^{-3}, isentropic compressibility U(κ_S) = ±0.50 κ_S.*

Figure 4. shows the deviations between the isentropic compressibility values calculated from the pure compounds, and those calculated from the experimental speeds of sounds and densities

obtained at every mole fraction. In all the cases the highest values are found at compositions approximately x = 0.5000, and as occurs for isentropic compressibility, the deviations are higher when the higher the temperatures are.

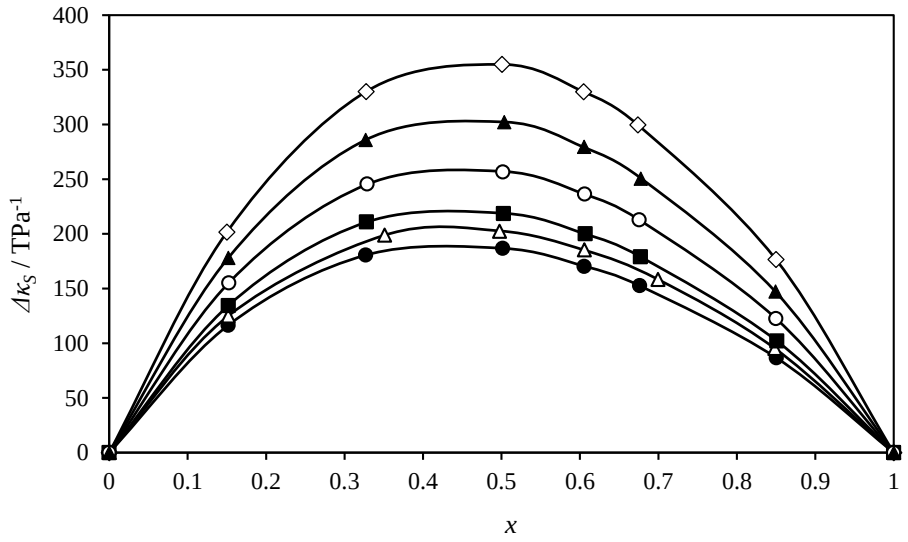

Figure 4. Deviations from isentropic compressibility $\Delta\kappa_S$, vs. the mole fraction at different temperatures for the binary mixture x HFE-7200 + (1-x) 2-Propanol. ●; 293.15 K, Δ; 298.15 K, ■; 303.15 K, ○; 313.15 K, ▲; 323.15 K, ◊; 333.15 K.

4. Conclusions

High pressure densities ρ, were determined by using a vibrating tube densitometer for the binary system x HFE-7200 + (*1*-x) 2-Propanol. The densities were determined along 23 isobars ranging from 0.1 to 140 MPa and in the temperature interval from 293.15 to 393.15 K for eight mole fractions. A Tait-like equation was employed to correlate the density values over the entire pressure and temperature ranges, showing a good agreement between the experimental data and the calculated ones. Isothermal compressibility κ_T, and isobaric expansion α_P, data was determined by deriving the Tait-like equation A literature comparison for the densities of both the two pure fluids was carried out since no data for the binary mixture was found in the literature. Excess volumes V^E, were also determined from the high pressure density data of the pure compounds and of the mixtures. Speeds of sound c, and densities ρ, at atmospheric pressure were measured by using an Anton Paar DSA 5000 density and sound velocity meter along six isotherms from 293.15 K to 333.15 K, and isentropic compressibilities κ_S, were calculated from these data sets.

List of symbols

AAD	Absolute Average Deviation
a_i	coefficients of isobaric thermal expansivity correlation
A_i, B_i, C	coefficients of density correlation
Bias	Average Deviation
exp	experimental
i	constituent identification
lit	literature
MD	Maximum Deviation
N_P	number of experimental data points which are in our p, T ranges
P	pressure
P_0	reference pressure
RMSD	Root Mean Square Deviation
T	temperature
V^E	excess molar volume

Greek letters

σ	Standard deviation
α_p	isobaric expansion
ρ	density
ρ_0	density at a reference pressure P_0
κ_S	isentropic compressibility
κ_T	isothermal compressibility

Aknowledgements

This paper is part of the Doctoral Thesis of N. Muñoz-Rujas.

N. Muñoz-Rujas acknowledges support for this research to the University of Burgos, for the funding of her doctoral grant (Pre-Doctoral Grants 2014).

References

[1] F. Govaerts, D.D. Keane, Medical Device Technol. (2001). http://solutions.3mbelgie.be/3MContentRetrievalAPI/BlobServlet?lmd=1360239440000&locale=nl_BE&assetType=MMM_Image&assetId=1319247019271&blobAttribute=ImageFile

[2] J. Kehren, Datatech. http://www.solvents.net.au/index_htm_files/71IPA%20Engineered%20Fluid.pdf

[3] D.B. Bivens, B.H. Minor, Int. J. Refrig. 21 (1998) 567-576.

[4] P. Warrier, A.S. Teja, J. Chem. Eng. Data 56 (2011) 4291-4294.

[5] J. B. Durkee II, Cleaning with Solvents: Science and Technology, 1st ed. Elsevier B.V., Oxford (2014).

[6] B. Kanegsberg, E. Kanegsberg, Handbook for Critical Cleaning: Cleaning Agents and Systems, 2nd ed. CRC Press, New York (2011).

[7] E. Wilhem, T. Letcher, Volume Properties, Liquids, Solutions and Vapours, 1st ed. Royal Society of Chemistry, Cambridge (2015).

[8] F. E. M. Alaoui, E. A. Montero, G. Qiu, F. Aguilar, J. Wu, J. Chem. Thermodyn. 65 (2013) 174–183.

[9] M. J. P. Comuñas, J. Bazile, A. Baylaucq, C. Boned, J. Chem. Eng. Data 53 (2008) 986–994.

[10] H. Lagourette, B. Boned, C. Saint-Guirons, H. Xans, P. Zhou, Meas. Sci. Technol. 3 (1992) 699–703.

[11] W. Wagner, A. Pruß, J. Phys. Chem. Ref. Data 31 (2002) 387–535.

[12] 3M™ Novec™ Engineered Fluids. https://multimedia.3m.com/mws/media/199819O/3mtm-novectm-7200-engineered-fluid.pdf

[13] J.A. Riddick, W.B. Bunger, T.K. Sakano, Organic Solvents: Physical Properties and Methods of Purification, 4th ed., Wiley, New York (1986).

[14] Expression of the Uncertainty of Measurement in Calibration, European Cooperation for Accreditation, EA-4/02 (1999).

[15] TRC, Thermodynamic Tables, Texas A&M University, College Station (1996).

[16] J.H. Dymond, R. Malhotra, Int. J. Thermophys. 9 (1988) 942-951.

[17] N. Muñoz-Rujas, F. Aguilar, J-P. Bazile, E.A. Montero, Fluid Phase Equilib. 429 (2016) 281-292.

[18] N. Muñoz-Rujas, J-P. Bazile, F. Aguilar, G. Galliero, E. Montero, J.L. Daridon, J. Chem. Thermodyn. 112 (2017) 52-48.

[19] A. Srhiyer, N. Muñoz-Rujas, F. Aguilar, J.J. Segovia, E.A. Montero, J. Chem. Thermodyn. 113 (2017) 213-218.

[20] A. Srhiyer, N. Muñoz-Rujas, F. Aguilar, J.J. Segovia Puras, E.A. Montero, J. Chem. Eng. Data 113 (2017) 213-218.

[21] J. Murata, S. Yamashita, M. Akiyama, J. Chem. Eng. Data 47 (2002) 911-915.

[22] M. H. Rausch, L. Kretschmer, S. Will, A. Leipertz, A. P. Fröba, J. Chem. Eng. Data 60 (2015) 3759-3765.

[23] D. Fang, Y. Li, X. Meng, J. Wu, J. Chem. Thermodyn. 69 (2014) 36-42.

[24] D. Fang, Y. Li, X. Meng, J. Wu, J. Chem. Thermodyn. 83 (2015) 123-125.

[25] I. F. Golubev, T. N. Vasil'Kovskaya, V. S. Zolin, J. Eng. Phys. Thermophys. 38 (1980) 399–401. (Translation of: Inzh.-Fiz. Zh. 38 (1980) 668-670).

[26] H. Kubota, Y. Tanaka, T. Makita, Int. J. Thermophys. 8 (1987) 47–70.

[27] R. Yaginuma, T. Nakajima, H. Tanaka, M. Kato, J. Chem. Eng. Data 47 (1997) 814–816.

[28] M. Moha-Ouchane, C. Boned, A. Allal, M. Benseddik, Int. J. Thermophys. 19 (1998) 161-189.

[29] C. Boned, M. Moha-Ouchane, J. Jose, Phys. Chem. Liq. 38 (2000) 113–136.

[30] A. Zúñiga-Moreno, L. A. Galicia-Luna, J. Chem. Eng. Data 47 (2002) 155–160.

[31] P. Stringari, G. Scalabrin, A. Valtz, D. Richon, J. Chem. Thermodyn. 41 (2009) 683–688.

[32] F. E. M. Alaoui, E. A. Montero, J. P. Bazile, F. Aguilar, C. Boned, J. Chem. Thermodyn. 54 (2012) 358–365.

[33] H. Nourozieh, M. Kariznovi,J. Abedi, J. Chem. Thermodyn. 65 (2013) 191–197.

[34] P. Gómez-Álvarez, D. González-Salgado, J. P. Bazile, D. Bessières, F. Plantier, Fluid Phase Equilib. 358 (2013) 7–26.

[35] C. A. Cerdeiriña, C. A. Tovar, D. González-Salgado, E. Carballo, L. Romaní, Phys. Chem. Chem. Phys. 3(2001) 5230–5236.

[36] J. Troncoso, D. Bessières, C. A. Cerdeiriña, E. Carballo, L. Romaní, Fluid Phase Equilib. 208 (2003) 141-154.

[37] J. Jacquemin, P. Husson, V. Mayer, I. Cibulka, J. Chem. Eng. Data 52 (2007) 2204–2211.

[38] G. Watson, T. Lafitte, C. K. Zéberg-Mikkelsen, A. Baylaucq, D. Bessieres, C. Boned, Fluid Phase Equilib. 247 (2006) 121–134.

High Pressure Viscosity Measurements for the Binary Mixture HFE-7500 + Diisopropyl ether

Natalia Muñoz-Rujas[1,2], Jean Patrick-Bazile[1], Fernando Aguilar[2], Guillaume Galliero[1], Eduardo Montero[2] and Christian Boned[1]

[1] Laboratoire des Fluides Complexes et leurs Réservoirs, CNRS-TOTAL, UMR 5150, Université de Pau, BP 1155, 64013 Pau Cedex, France.

[2] Departamento de Ingeniería Electromecánica, Escuela Politécnica Superior, Universidad de Burgos, Burgos, E-09006, Spain.

[1*] Tel: +34 947 258 916, E-mail: emontero@ubu.es

Abstract

In this work, high pressure viscosity measurements for seven compositions of the binary mixture (*x*) HFE-7500 + (1-*x*) Diisopropyl ether were carried out. A set of 163 points have been measured covering the range (293.15 – 353.15) K for the temperature and up to 100 MPa for the pressure by using a falling body viscometer with an experimental uncertainty of ±2%. At 0.1 MPa the viscosity determinations were conducted by using an Ubbelohde capillary viscometer with an uncertainty of ±1%. The experimental high pressure viscosity data were also correlated as a function of pressure and temperature by employing a Vogel-Fulcher-Tamman (VFT) equation.

Keywords: Hydrofluoroethers, Viscosity, High Pressure, Falling Body Viscometer.

1. Introduction

Perfluorocarbons (PFCs) and perfluoropolyethers (PFPEs) have been used as heat transfer fluids, in semiconductor manufacturing processes, and to maintain process or components temperatures among other utilities [1] due to its chemically inert and non-flammable properties. Their high global warming potentials, and long atmospheric lifetimes urged to search at the expense of the Kyoto Protocol (1997), and of the Agreement of Paris (2015), industry fluids with lower GWPs in order to replace PFCs and PFPEs with similar properties.

Hydrofluoroether fluids (HFEs) have been developed to replace CFCs, HCFCs, PFCs and PFPEs in applications such as carrier fluids for lubricant deposition, heat transfer agents and high precision cleaning solvents for electronic equipment. HFEs have low GWP, zero ozone depletion potential (ODP) and short atmospheric lifetimes being also non-flammable fluids, with very low overall toxicity [2] and with any significant environmental hazard [3]. Their properties and utilities

can vary widely so some of them are desirable for refrigerant applications, others can act as working fluids in Organic Rankine Cycles (ORC), high precision cleaning for electronic components, light-duty cleaning and heat transfer fluids, etc.

At this point, HFE-7500 shares many desirable properties to be used as cleaning solvent or in electronics cooling, i.e. non flammability, an adequate wetting index, and a low dielectric constant among others.

Mixing with other solvents enhances cleaning performance, so in this case Diisopropyl ether (DIPE) was the choice due to some of its non desirable safety properties, as is the case of flammability, is reduced.

Viscosity is a transport property whose knowledge has a lot of importance in the design of transport networks, pumps, storage tanks, and most of the equipment that will be used in chemical and industrial applications. It is also a variable with strong influence in fluid flow measurements, and an important property in the establishment of process conditions.

High pressure viscosity was determined in this work at seven molar compositions of the binary mixture *x* HFE-7500 + (1-*x*) Diisopropyl ether by using a falling body viscometer giving a total of 163 points in the pressure range from 0.1 to 100 MPa and at temperatures 293.15, 313.15, 333.15 and 353.15 K.

2. Experimental Section

2.1 Materials

Hydrofluoroether fluid HFE-7500, also known by its chemical name, 2-trifluoromethyl-3-ethoxydodecafluorohexane or 3-ethoxy-1,1,1,2,3,4,4,5,5,6,6,6-dodecafluoro-2-trifluoromethylhexane (CAS: 297730-93-9, molar mass 414.11 g·mol^{-1}) was obtained from the 3M company with a stated mass fraction purity greater than 0.995. Diisopropyl Ether (DIPE) was supplied by Sigma-Aldrich (CAS: 108-20-3, molar mass 102.17 g·mol^{-1}) with a purity greater than 0.995. Table 1 shows the sample description for HFE-7500 and for Diisopropyl ether. Both fluids were not subject to further purification.

Table 1. Sample description.

Compound	Source	Formula	Molar mass / g·mol^{-1}	Stated purity[a] / mol%	CAS number
HFE-7500[b]	3M Company	$C_9H_5F_{15}O$	414.11	>99.5	297730-93-9
Diisopropyl ether	Sigma-Aldrich	$C_6H_{14}O$	102.17	>99.5	108-20-3

[a] Determined by gas chromatography (GC).
[b] HFE-500 = 2-trifluoromethyl-3-ethoxydodecafluorohexane.

2.2 Falling body viscometer

The measuring technique was carried out by using a falling body viscometer, which is based in the measure of the falling time that a body with a known density employs to fall trough a tube vertically placed, which contains the fluid with the unknown density. The apparatus has been described in detail previously [4]. It consists on a cylindrical measuring cell filled with the fluid and the falling body that will move vertically into it.

The pressure in the measuring cell is obtained by means of a supplementary cell fitted with a piston. This cell is in communication with the measuring cell in order to make an increase or a decrease in pressure. The pressure in the fluid is generated by the oil contained at the top of the pressure cell, and the O-rings fitted in the piston avoid its leakage. The pressure is measured thanks to a HBM-P3M manometer connected between the two cells, ensuring to give a real data of pressure. The uncertainty in the measure of pressure is of 0.2 MPa.

A Pt-100 probe, directly inserted into the measuring cell and coupled with a temperature meter, allows to obtain temperature data with an uncertainty of ±0.05 K. The temperature of the sample remains constant due to a silicone oil which circulates along the whole apparatus. In the same way, the measuring cell and the pressure cell were both placed inside a thermoregulated cell which ensures homogeneous temperature on the surroundings of the system.

When the piston is moved to the top of the cell and vacuum has been done, the filling of the measuring cell with the liquid sample free of bubbles is done by gravity once opening the valve connected at the top of the cell.

The measuring procedure is based in the falling of a metallic cylindrical sinker with hemispherical ends with a known density. In this case the density was approximately eight times the density of the fluid. The determination of the falling time from the top to the bottom of the cell is carried out by the detection of the sinker passing through four pairs of electrical coils fitted on the tube. The inductance of the first pair of coils increases when the sinker passes through them, starting an electronic timer so that when the sinker passes through the other three pairs, the timer switches off.

Both the measuring and the pressure cells are able to rotate 180º thanks to a pneumatic pump in order to make the measurements ensuring the same temperature in the whole fluid.

Taking into account the error in temperature, pressure, and falling time measurements as well as the uncertainty in the reference values, the overall experimental uncertainty in the viscosity measured by this technique is estimated to be ± 2 %.

For the viscosity data calculation in this type of viscometer, and taking into account that the viscosity of the fluid at 0.1 MPa and 298.15 K is higher than 0.1 mPa·s, Daugé *et al.* [4] emphasize that an equation of the type (1) should be used:

$$\eta = K(\rho_S - \rho_L)\Delta t \tag{1}$$

This equation relates the dynamic viscosity, η, with the difference in densities of the metallic sinker (ρ_S), and the liquid fluid density (ρ_L), and the falling time between two detections (Δt). In this work Δt corresponds to the average value between six measurements done for the fluid. K is a characteristic parameter which depends on the viscometer and on the metallic sinker. In this work two different stainless steel sinkers with hemispherical ends were used. Both them were similar in shape but with different material density, ρ_S because the differences in density for the two fluids was very high; since the density at 293.15 K and at 0.1 MPa for pure HFE-7500 is of 1.6302 g·cm^{-3} [5], the density in the same conditions for Diisopropil ether is 0.7235 g·cm^{-3} [6]. Then the density of the plug used with pure HFE-7500 and at x = 0.750 was equal to 7.753 g·cm^{-3}, and the one used with the pure Diisopropil ether and when x = 0.250, x = 0.375, x = 0.500, and x = 0.625 had a density of 7.777 g·cm^{-3}.

The calibration procedure of the apparatus is described in detail in the paper of Zéberg-Mikkelsen *et al*. [7]. It has been done by using toluene and decane as reference fluids in order to quantify the parameter K as a function of pressure and temperature taking into account the viscosity of the reference fluid. The values of viscosity and density for toluene were estimated from those obtained from Assael *et al*. [8]. In the case of decane, the values of both density and viscosity were estimated from the values reported by Huber *et al.* [9]. The overall uncertainty for the calculated viscosity is of 2%.

3. Results and Discussion

A set of seven molar compositions, (x = 0.000, x = 0.250, x = 0.375, x = 0.500, x = 0.625, x = 0.750 and x = 1.000) was prepared by weighing the required amounts of each pure liquid at every mole fraction and putting them into stoppered bottles of 250 cm^3. The viscosity measurements were performed along four isotherms spaced at 20 K intervals from 293.15 K to 353.15 K. According to the pressure, it has been measured from atmospheric to 100 MPa every 20 MPa steps. The values of the viscosities obtained for the seven mole fractions are listed in Table 2. It has to be pointed out that at atmospheric pressure the dynamic viscosity was obtained from the kinematic viscosity measured with a classical capillary viscometer (Ubbelohde). For this purpose several tubes connected to an AVS350 Schott Geräte Analyzer have been used. The temperature of the fluid is controlled within 0.1 K using a thermostatic bath. When multiplying the kinematic viscosity by the density, the dynamic viscosity is then obtained with an uncertainty less than 1%. The values of density used in these calculations were determined experimentally and reported in

our previous papers [5, 6] and [10]. Due to the low boiling point of Diisopropyl ether at 0.1 MPa (341.66 K), [11], at 353.15 K and for mole fractions with high content of this component, the vaporization of the mixture is expected. Then at molar compositions of x = 0.250, x = 0.375, x = 0.500, x = 0.625 and for pure Diisopropyl ether no measurements were performed at 353.15 K.

Table 2. Experimental values of viscosity, η measured with falling body viscometer at temperatures T and pressures P for the binary mixture x HFE-7500 + (*1*-x) Diisopropyl ether[a].

T/K	P/ MPa	η / MPa						
		x = 0.000	x = 0.250	x = 0.375	x = 0.500	x = 0.625	x = 0.750	x = 1.000
293.15	0.1	0.330	0.483	0.573	0.685	0.818	0.985	1.369
293.15	20	0.410	0.627	0.766	0.939	1.106	1.305	1.942
293.15	40	0.470	0.766	0.953	1.217	1.425	1.741	2.687
293.15	60	0.540	0.924	1.175	1.521	1.821	2.285	3.649
293.15	80	0.620	1.104	1.442	1.857	2.311	2.968	4.892
293.15	100	0.712	1.310	1.760	2.230	2.922	3.828	6.507
313.15	0.1	0.270	0.386	0.441	0.526	0.617	0.735	0.983
313.15	20	0.360	0.492	0.593	0.689	0.802	0.959	1.425
313.15	40	0.408	0.600	0.747	0.893	1.056	1.289	1.943
313.15	60	0.462	0.720	0.917	1.123	1.347	1.676	2.583
313.15	80	0.524	0.853	1.106	1.383	1.678	2.129	3.373
313.15	100	0.595	1.002	1.313	1.675	2.054	2.656	4.353
333.15	0.1	0.225	0.311	0.356	0.416	0.486	0.574	0.739
333.15	20	0.332	0.432	0.499	0.561	0.646	0.737	1.110
333.15	40	0.365	0.506	0.610	0.709	0.829	0.984	1.504
333.15	60	0.404	0.591	0.737	0.878	1.039	1.265	1.975
333.15	80	0.450	0.690	0.883	1.069	1.280	1.585	2.539
333.15	100	0.506	0.807	1.051	1.286	1.554	1.948	3.215
353.15	0.1						0.465	0.576
353.15	20	0.304	0.369	0.415	0.442	0.500	0.579	0.871
353.15	40	0.338	0.437	0.514	0.577	0.660	0.774	1.174
353.15	60	0.372	0.511	0.621	0.724	0.836	0.996	1.522
353.15	80	0.405	0.591	0.736	0.878	1.025	1.240	1.923
353.15	100	0.440	0.678	0.857	1.037	1.223	1.506	2.387

[a]Standard uncertainties u are u(T) = 0.05 K, u(P) = 0.2 MPa, and the combined expanded uncertainties U_c (level of confidence = 0.95) is $U_c(\eta) = 0.02\eta$.

The experimental data of viscosity were correlated by employing a modified Vogel-Fulcher-Tamman (VFT) equation, which is known to be suitable at high pressure viscosity values. In this case we have used six parameters, employing a second-degree polynomial in pressure as follows (2):

$$\eta = A\exp\left(a_1\Delta P + \frac{B + b_1\Delta P + b_2\Delta P^2}{T - C}\right) \quad (2)$$

where $\Delta P = P - P_{ref}$. Mylona *et al*. [12] have used this equation recently, as well as Comuñas *et al*. [13]. In Eq (2) we use 0.1 MPa as reference pressure, so when P is equal to 0.1 MPa, this equation reduces to:

$$\eta = A\exp\left(\frac{B}{T-C}\right) \tag{3}$$

To assess the performance of the correlations, the average absolute percentage deviation, AAD, the maximum absolute percentage deviation, MD, and the average percentage deviation, Bias, are defined as follows,

$$AAD\,(\%) = \frac{100}{N}\sum_{i=1}^{N}\left|\frac{\eta_i^{exp} - \eta_i^{calc}}{\eta_i^{exp}}\right| \tag{4}$$

$$MD\,(\%) = Max\left(100\left|\frac{\eta_i^{exp} - \eta_i^{calc}}{\eta_i^{exp}}\right|\right) \tag{5}$$

$$Bias\,(\%) = \frac{100}{N}\sum_{i=1}^{N}\frac{\eta_i^{exp} - \eta_i^{calc}}{\eta_i^{exp}} \tag{6}$$

The obtained coefficients of equation (2) and the statistical values are summarized in Table 3.

Figure 1 shows a set of graphs with the experimental values of viscosity at different pressures and at different temperatures. In addition, the calculated values obtained with equations (2) and (3) are shown as a solid line. Diagrams (a) and (b) show the obtained values of viscosity versus the pressure at the minimum and maximum temperatures measured (293.15 and 353.15 K). The trend of both experimental data and those given by the correlation is exponential, as expected for this property. The maximum values are reached at the lower temperature and for the pure HFE-7500, with a maximum value of 6.507 at 100 MPa while the minimum value of viscosity is given for the pure Diisopropyl ether at 20 MPa and at 353.15 K.

Diagrams (c) and (d) provide the viscosity data for the seven molar compositions at 0.1 and 100 MPa respectively. The increase in pressure of the mixture results in an approximation of the molecules, thus giving higher values of viscosity at 100 MPa than at 0.1 MPa. In the same way,

the values of viscosity are higher for pure HFE-7500, and then its value decrease in the same way as the mole fraction does.

Table 3. Parameters of equation (VFT) for the binary system *x* HFE-7500 + (*1-x*) Diisopropyl ether.

Parameters	*x*						
	0.000	0.250	0.375	0.500	0.625	0.750	1.000
A / mPa·s	$1.3830 \cdot 10^{-2}$	$1.2303 \cdot 10^{-2}$	$1.0897 \cdot 10^{-2}$	$1.0779 \cdot 10^{-2}$	$1.0496 \cdot 10^{-2}$	$3.2152 \cdot 10^{-2}$	$1.52349 \cdot 10^{-2}$
a_1 / MPa^{-1}	$4.7490 \cdot 10^{-2}$	$3.0488 \cdot 10^{-2}$	$3.0077 \cdot 10^{-2}$	$7.1501 \cdot 10^{-3}$	$1.3318 \cdot 10^{-2}$	$6.5887 \cdot 10^{-3}$	$3.0552 \cdot 10^{-2}$
a_2 / MPa^{-2}	$-3.8795 \cdot 10^{-4}$	$-2.3935 \cdot 10^{-4}$	$-2.1414 \cdot 10^{-4}$	$9.2155 \cdot 10^{-6}$	$-1.0172 \cdot 10^{-4}$	$-1.8614 \cdot 10^{-5}$	$-2.4380 \cdot 10^{-4}$
B / K	930.01	1075.7	1161.3	1217.2	1276.7	729.90	1132.2
b_1 / MPa^{-1}·K	-9.7553	-4.0221	-3.8876	2.7423	0.32166	1.3552	-2.8447
b_2 / MPa^{-2}·K	$6.7229 \cdot 10^{-2}$	$2.0683 \cdot 10^{-2}$	$2.7007 \cdot 10^{-2}$	$-2.1959 \cdot 10^{-2}$	$2.4308 \cdot 10^{-2}$	$1.5249 \cdot 10^{-2}$	$4.6045 \cdot 10^{-2}$
b_3 / MPa·K^{-3}	$2.8024 \cdot 10^{-4}$	$3.0206 \cdot 10^{-4}$	$1.9361 \cdot 10^{-4}$	$5.4222 \cdot 10^{-5}$	$9.7064 \cdot 10^{-6}$	$-1.0344 \cdot 10^{-4}$	$6.7238 \cdot 10^{-5}$
C / K	0	0	0	0	0	79.885	41.473
AAD /(%)	1.13	1.74	1.06	0.88	1.09	1.12	1.20
MD /(%)	2.16	3.89	2.17	2.36	2.48	2.18	2.47
Bias /(%)	-0.23	-0.21	-0.41	0.10	0.15	0.55	-0.49

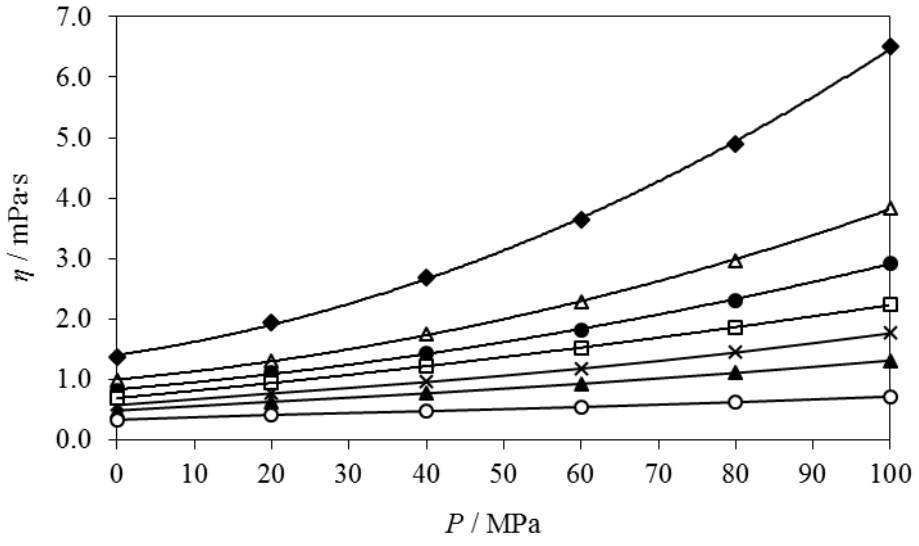

(a)

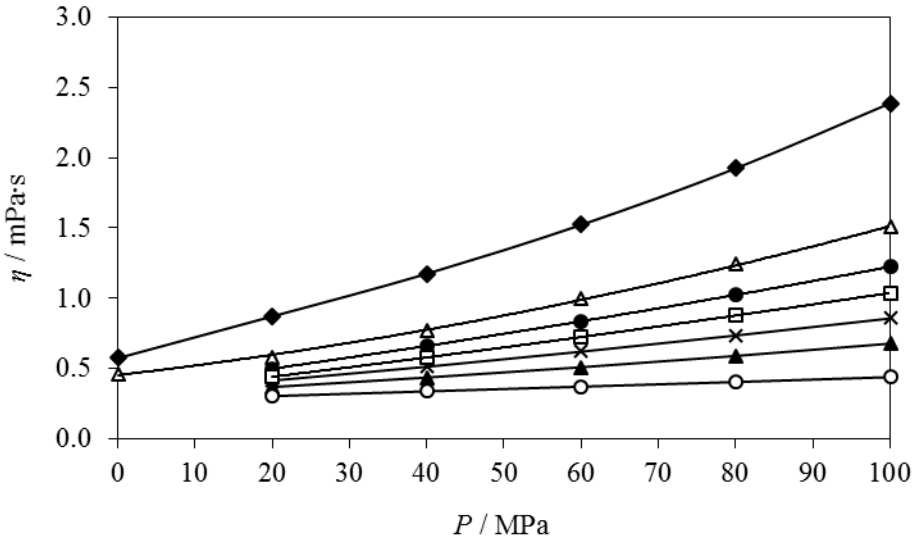
3.0
2.5
2.0
1.5
1.0
0.5
0.0
η / mPa·s
0
10
20
30
40
50
60
70
80
90
100
P / MPa

(b)

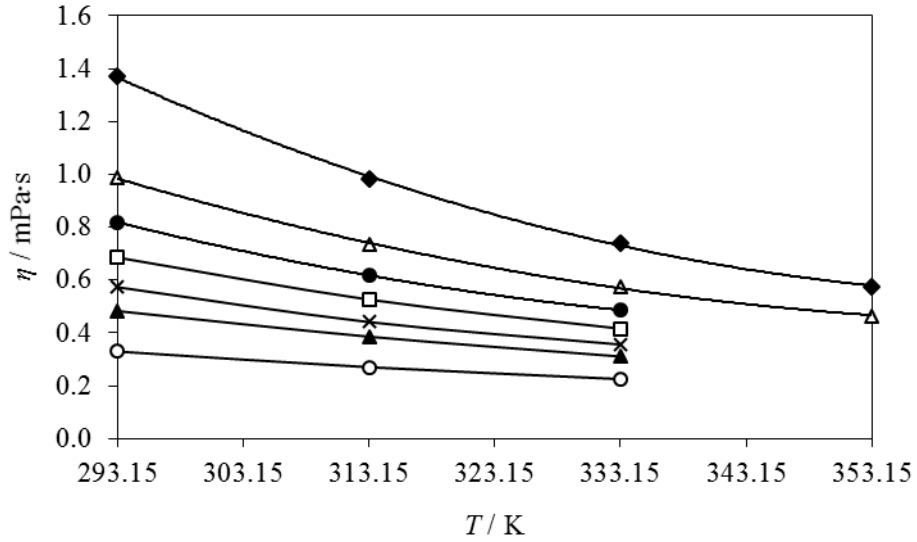
1.6
1.4
1.2
1.0
0.8
0.6
0.4
0.2
0.0
η / mPa·s
293.15
303.15
313.15
323.15
333.15
343.15
353.15
T / K

(c)

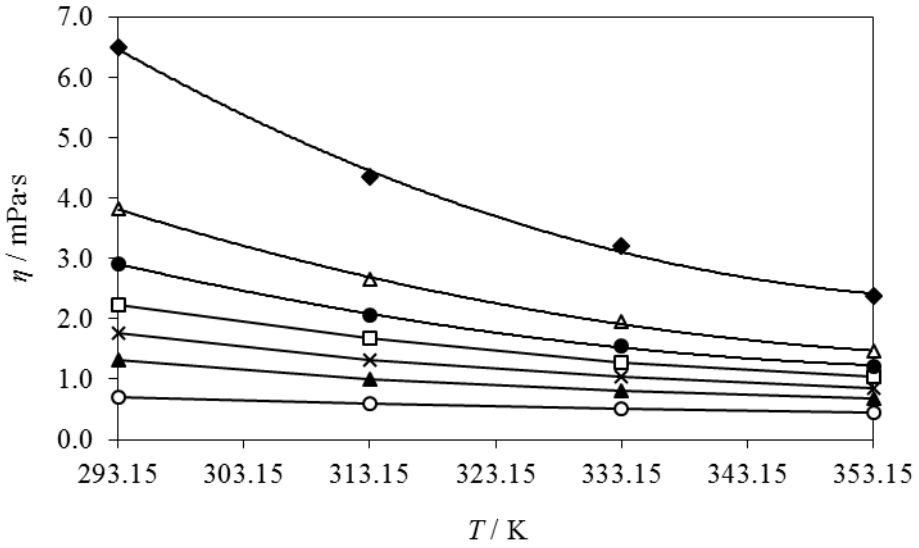

(d)

Figure 1. Experimental values of viscosities, η, for different mole fractions of the binary system x HFE-7500 + (1-x) Diisopropyl ether versus (a) the pressure, at 293.15 K, (b) the pressure at 353.15 K, (c) the temperature at 0.1 MPa, and (d) the temperature at 100 MPa. ○; x = 0.000, ▲; x = 0.250, ×; x = 0.375, □; x = 0.500, ●; x = 0.625, Δ; x = 0.750, ♦; x = 1.000. The solid line represents the values of dynamic viscosity calculated by using the VFT equation.

Figure 2 shows a comparison in which the viscosity versus the mole fraction is represented at 0.1 MPa and at 100 MPa, confirming the aforementioned statements.

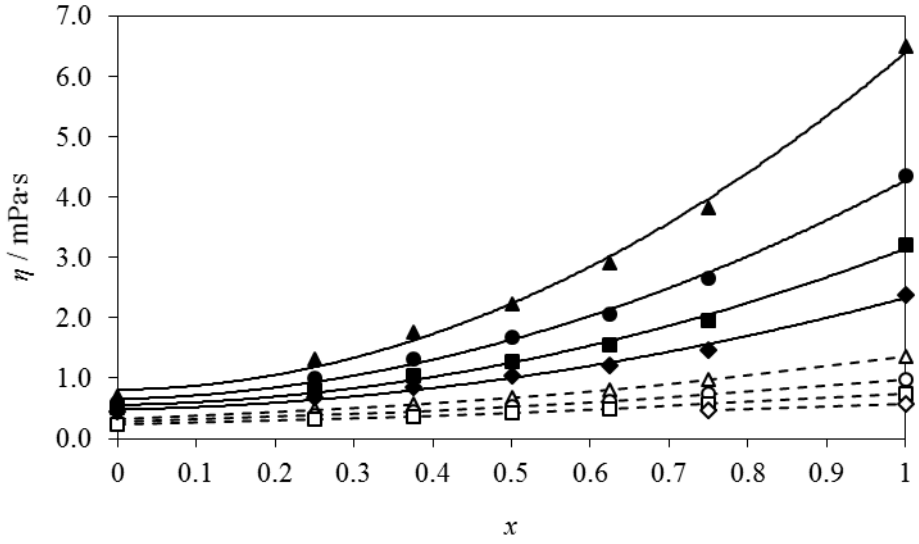

Figure 2. Experimental values of viscosities, η, versus the mole fraction, x, at different pressures for the binary mixture x HFE-7500 + (1-x) Diisopropyl ether. At 0.1 MPa: Δ; T = 293.15 K, ○; T = 313.15 K, □; T = 333.15 K, ◊; T = 353.15 K. The dashed line represents the calculated values using equations (2) and (3). At 100 MPa: ▲; T = 293.15 K, ●; T = 313.15 K, ■; T = 333.15 K, ♦; T = 353.15 K. The solid line represents the calculated values using equations (2) and (3).

The relative deviations between the experimental values and the viscosity data obtained by using the VFT equation are shown in Figure 3. Most of the deviation values are lower than the expanded uncertainty in viscosity (±2%), demonstrating that the VFT equation is a viable option to correlate the dynamic viscosity values. However, at $x = 0.250$ some of the deviation values are greater than the uncertainty, with a maximum value, MD = 3.89% founded at 313.15 K and at 40 MPa. No dependence in pressure was found since the deviation values are distributed similarly for the six pressure points considered (0.1, 20, 40, 60, 80 and 100 MPa).

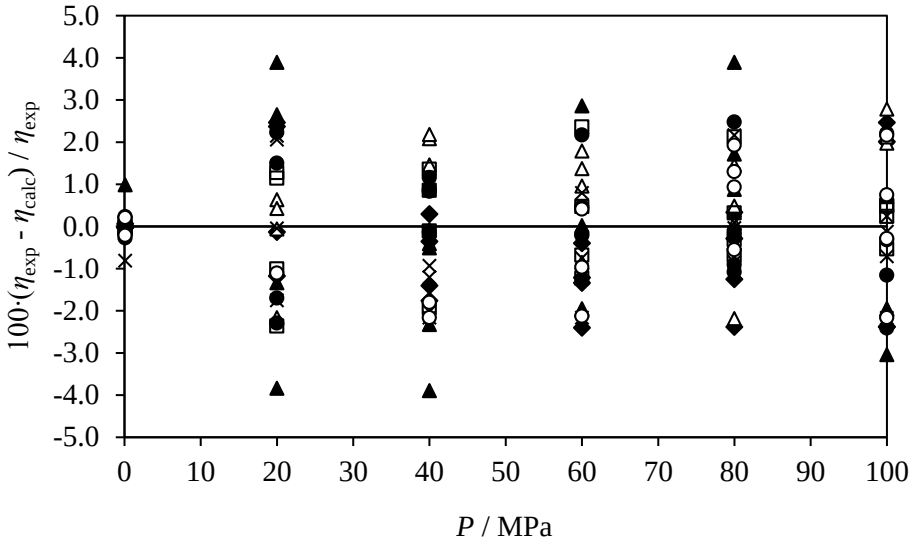

Figure 3. Deviations between the viscosity values measured experimentally and those calculated with equations (2) and (3). ○; $x = 0.000$, ▲; $x = 0.250$, ×; $x = 0.375$, □; $x = 0.500$, ●; $x = 0.625$, Δ; $x = 0.750$, ♦; $x = 1.000$.

A comparison has been stablished between the viscosity values determined by the correlation proposed in equations (2) and (3) and those obtained in the literature. This comparison could only be conducted for the pure components HFE-7500 and Diisopropyl ether while no references were found for the binary mixture. For pure HFE-7500, only two references were found, and only one of them reports viscosity data at high pressure. At 0.1 MPa, and in the temperature range (293.15 to 353.15) K, reference [14] provides an AAD% = 2.46, a MD% = 6.55 and a Bias% = -1.93. Reference [15], which reports viscosity data up to 30 MPa and in the temperature interval (293.190 to 353.221) K gives similar deviations, with an AAD% = 0.77, a MD% = 3.84 and a Bias% = -0.53. These comparisons can be seen in Table 4. According to Diisopropyl ether, nine references were found [16 - 24], most of them with viscosity data only at 0.1 MPa, being reference [24] the only one which reports data under high pressure. Table 5 shows the literature comparisons together with their deviations. At 0.1 MPa, no reference reaches the temperature of 353.15 K, being reference [21] the one with the wider range of temperatures measured (293.15 to 313.15) K, giving deviations of 0.98 for the AAD%, an MD% = 1.38 and a Bias = 0.98. The highest

deviations are found in reference [22], with AAD% = 15.20, a MD% = 19.19 and a Bias = 15.20. Regarding the reference at high pressure [24], the temperature interval reported covers our entire temperature range (293.15 to 353.15) K, being its highest pressure datum of 21.49 MPa. This reference provides an AAD% = 3.55, a MD% = 9.53, and a Bias = -3.50 for a total of 35 points.

Table 4. Comparison between the values generated by the Vogel-Fulcher-Tamman (VFT) equation and the literature values for pure HFE-7500.

Reference	Year	N_P	T_{min} (K)	T_{max} (K)	p_{min} (MPa)	p_{max} (MPa)	AAD (%)	MD (%)	Bias (%)	Viscosity uncertainty
At atmospheric pressure										
Rausch *et al.* [14]	2015	7	293.15	353.15	0.1	0.1	2.46	6.55	-1.93	±0.03mPa·s
At high pressure										
Hu *et al.* [15]	2015	48	293.19	353.22	0.1	30	0.77	3.84	-0.53	2%

N_P Number of data points which are in our *p, T* ranges.
AD = average deviation; AAD = absolute average deviation; MD = maximum deviation.

Table 5. Comparison between the calculated values using the VFT equation and the literature values for pure Diisopropyl ether (DIPE).

Reference	Year	N_P	T_{min} (K)	T_{max} (K)	p_{min} (MPa)	p_{max} (MPa)	AAD (%)	MD (%)	Bias (%)	Viscosity uncertainty
At atmospheric pressure										
Peng and Tu [16]	2002	2	298.15	308.15	0.1	0.1	0.28	0.45	-0.28	±0.8%
George and Sastry [17]	2003	2	298.15	308.15	0.1	0.1	9.06	17.53	9.06	±0.002 mPa·s
Ye and Tu [18]	2005	2	298.15	308.15	0.1	0.1	0.12	0.13	0.12	±0.5%
Chen and Tu [19]	2006	2	298.15	308.15	0.1	0.1	0.04	0.07	0.04	±0.006 mPa·s
Suresh Reddy *et al.* [20]	2006	1	303.15	303.15	0.1	0.1	14.94	14.94	14.94	-
Montaño *et al.* [21]	2010	5	293.15	313.15	0.1	0.1	0.98	1.38	0.98	-
Palani and Balakrishnan [22]	2010	3	303	313	0.1	0.1	15.20	19.19	15.20	-
Gómez Marigliano and Medina Naessens [23]	2015	3	293.15	303.15	0.1	0.1	3.70	4.77	-3.70	±0.3%
At high pressure										
Meng *et al.* [24]	2009	35	293.15	353.15	0.1	21.49	3.55	9.53	-3.50	±2.0%

N_P Number of data points which are in our *p, T* ranges.
AD = average deviation; AAD = absolute average deviation; MD = maximum deviation.

4. Conclusions

Viscosities in the compressed liquid state for the binary mixture HFE-7500 + Diisopropyl ether were determined by using a falling body viscometer at temperatures between 293.15 K to 353.15 K and at pressures up to 100 MPa. The experimental viscosity data were correlated with a Volgel-Fulcher-Tamman (VFT) equation, with the viscosity expressed as a function of pressure and temperature. The correlation shows a good agreement with data published in the literature for both pure fluids since there was no data in the literature for the binary mixture.

Acknowledgements

Natalia Muñoz-Rujas acknowledges support for this research to the University of Burgos, for the funding of her doctoral grant and to the University of Pau for the funding of a five months research period in 2015. This work is part of the doctoral thesis of Natalia Muñoz-Rujas.

References

[1] P. Tuma, S. Paul, L. Tousignant, Reducing Emissions of PFC Heat Transfer Fluids, Earth, 2010, 16: 1-8.

[2] 3M™ Novec™ Engineered Fluids, http://solutions.3m.com/wps/portal/3M/en_US/3MNovec/Home. Last access: 22-Jan-2016.

[3] M. Goto, Y. Inoue, M. Kawasaki, A G. Guschin, L. T. Molina, M. J. Molina, *et al.*, Atmospheric chemistry of HFE-7500 in-C3F7CF(OC2H5)CF(CF3)2]: reaction with OH radicals and Cl atoms and atmospheric fate of n-C3F7CF(OCHO*)CF(CF3)2 and n-C3F7CF(OCH2CH2O9)CF(CF3)2 radicals, Environmental Science and Technology, 2002, 11: 2395–2402.

[4] P. Daugé, A. Baylaucq, L. Marlin, C. Boned, Development of an isobaric transfer viscometer operating up to 140 Mpa. Application to a methane + decane system, Journal of Chemical and Engineering Data, 2001, 46: pp. 823–830, 2001.

[5] N. Muñoz-Rujas, J.P. Bazile, F. Aguilar, G. Galliero, E. Montero, J.L. Daridon, J. Chem. Thermodyn. 112 (2017) 52-58.

[6] N. Muñoz-Rujas, J.P. Bazile, F. Aguilar. G. Galliero, E. Montero, J.L. Daridon, Fluid Phase Equilibria 449 (2017) 148-155.

[7] C. K. Zéberg-Mikkelsen, A. Baylaucq, G. Watson, C. Boned, High-pressure viscosity measurements for the ethanol + toluene binary system, International Journal of Thermophysics, 2005, 26: 1289–1302.

[8] M. J. Assael, J. H. Dymond, M. Papadaki, P. M. Patterson, Correlation and prediction of dense fluid transport coefficients, Fluid Phase Equilibria, 1992, 75: 245–255.

[9] M. L. Huber, A. Laesecke, H.W. Xiang, Fluid Phase Equilibria 224 (2004) 263-270.

[10] N. Muñoz-Rujas, J.P. Bazile, F. Aguilar, G. Galliero, E. Montero, J.L. Daridon, J. Chem. Thermodyn. (in revision).

[11] J.A. Riddick, W.B. Bunger, T.K. Sakano, Organic Solvents: Physical Properties and Methods of Purification, 4th ed. Wiley: U.S. 1986.

[12] S. K. Mylona, M. J. Assael, M. J. P. Comuñas, X. Paredes, F. M. Gaciño, J. Fernández *et al.*, Reference correlations for the density and viscosity of squalane from 273 to 473 K at pressures to 200 MPa, Journal of Physical and Chemical Reference Data, 2014, 43: 0-11.

[13] M. J. P. Comuñas, X. Paredes, F. M. Gaciño, J. Fernández, J. P. Bazile, C. Boned *et al.*, Reference correlation of the viscosity of squalane from 273 to 373 K at 0.1 MPa, Journal of Physical and Chemical Reference Data, 2013, 42: 0–6.

[14] M.H. Rausch, L. Kretschmer, S. Will, A. Leipertz, A.P. Fröba, J. Chem. Eng. Data 60 (2015) 3759-3765.

[15] X. Hu, X. Meng, K. Wei, W. Li, J. Wu, J. Chem. Eng. Data 60 (2015) 3562-3570.

[16] I-H. Peng, C-H. Tu, J. Chem. Eng. Data 47 (2002) 1457-1461.

[17] J. George, N.V. Sastry, Int. J. Thermophys. 24 (2003) 1697-1719.

[18] J-D. Ye, C-H. Tu, J. Chem. Eng. Data 50 (2005) 1060-1067.

[19] H-W. Chen, C-H. Tu, J. Chem. Eng. Data 51 (2006) 261-267.

[20] K.V.N. Suresh Reddy, G. Sankara Reddy, A. Krishnaiah, Thermochimica Acta 440 (2006) 43-50.

[21] D. Montaño, H. Guerrero, I. Bandrés, M.C. López, C. Lafuente, Int. J. Thermophys. 31 (2010) 488-501.

[22] R. Palani, S. Balakrishnan, Indian J.Pure App. Phys. 48 (2010) 644-650.

[23] A.C. Gómez Marigliano, R.N. Medina Naessens, J. Phys. Chem. Biophys. 5 (2015).

[24] X. Meng, J. Wu, Z. Liu, J. Chem. Eng. Data 54 (2009) 2353-2358.

Isobaric Vapor-Liquid Equilibrium at 50.0, 101.3 and 200.0 kPa, Density and Speed of Sound at 298.15 K of Binary Mixtures HFE-7100 + 2-Propanol

Natalia Muñoz-Rujas, Adil Srhiyer, Eduardo Montero, Fernando Aguilar

Departamento de Ingeniería Electromecánica, Escuela Politécnica Superior, Universidad de Burgos, E-09006, Burgos, Spain.

The isobaric vapor-liquid equilibrium (VLE) at 50.0, 101.3 and 200.0 kPa, densities, and speeds of sound at 298.15 K have been measured for the binary system methyl nonafluorobutyl ether (HFE-7100) + 2-propanol. Excess molar volumes, isentropic compresibilities and deviation in isentropic compressibility have been calculated from these experimental data. The excess properties upon mixing were correlated by the Redlich-Kister polynomial satisfactorily. Vapor-liquid equilibrium data have been correlated by means of Wilson, NRTL and UNIQUAC equations. Thermodynamic consistency was checked applying the Wisniak point to point and area test, and the Fredenslund point to point test. The binary system shows positive azeotropes at every measured pressure.

---

1. Introduction

Hydrofluoroether fluids (HFEs) are being used as third generation alternatives to replace CFCs (chlorofluorocarbons), HCFCs (hydrochlorofluorocarbons) and PFCs (perflurocarbons) because of their nearly zero ozone depletion (ODP), relatively low global warming potential (GWP) and short atmospheric lifetimes [1]. In addition, they may be industrially used as cleaning solvents in the electronic components, protective gas used in melting of alloys, decontamination of fluids and heat transfer fluids in the heat exchangers [2].

Though a variety of HFEs have been synthesized, their performance and environmental properties and hence their utility can vary widely. For example, 1-methoxy-nonafluorobutane, also known as HFE-7100, has zero ozone depletion potential and other favorable environmental properties. The high boiling point and low surface tension of HFE-7100 fluid make it ideal for use as cleaner fluid as pure component or in mixtures with other solvents. Moreover, its chemical and thermal stability, non-flammability and low toxicity make it useful for many other

industrial uses, such as high-GWP refrigerants replacement, as heat transfer fluid and in organic Rankine Cycles (ORC).

This paper reports experimental densities and speeds of sound at 298.15 K and at atmospheric pressure for the binary system HFE-7100 + 2-propanol. Vapor-liquid equilibrium (VLE) at 50.0, 101.3 and 200.0 kPa is also reported in this work. Vapor-liquid equilibrium have been measured with an isobaric ebullometer. No data were found in the literature for the vapor-liquid equilibrium of this system.

2. Experimental Section

2.1 Materials.

HFE-7100 (Novec 7100 Engineered Fluid, I.D. No. 98-0211-8941-4, Lot. No. 25007), consists of two inseparable isomers with essentially identical properties: 1-methoxynonafluoroisobutane $(CF_3)_2CFCF_2$-O-CH_3, HFOC-449mmzxEγδ, CAS registry no. 163702-08-7, and 1-methoxynonafluorobutane $CF_3CF_2CF_2CF_2$-O-CH_3, HFOC-449Eδ€, CAS registry no. 163702-07-6. The purity of the hydrofluoroether is > 99.5%. 2-Propanol puriss. p.a. was supplied by Sigma-Aldrich, with a purity > 99.8%. The chemicals were recently acquired, kept stored in the absence of air and light and degassed in an ultrasound bath. 2- propanol was stored over freshly activated molecular sieves Type 0.4 nm supplied by Fluka for at least 72 hours before using.

2.2 Apparatus and Procedure.

The density and the speed of sound of the pure liquids and mixtures were measured with an Anton Paar DSA 5000M densimeter and sound analyzer with a precision of $\pm 5 \cdot 10^{-5}$ g·cm^3 and ±0.5 m/s. Before each series of measurements, these instruments were calibrated with Millipore quality water and degassed and ambient air. The accuracy in the calculation of excess volumes, and deviation of isentropic compressibilities were estimated as better than 10^{-2} cm^3·mol^{-1}, and 2 TPa^{-1}, respectively. The mixtures were prepared by weighing amounts of the pure liquids by syringing into stoppered vials to prevent evaporation and reducing possible errors in mole fraction calculations. A Mettler Toledo MS-204S balance was used with a precision of$\pm 1 \cdot 10^{-4}$ g, covering the whole composition range of the mixture. Table 1 gathers some of the experimental properties for the pure compounds measured with the Anton Paar density and sound velocity analyzer and the values for these properties found in the literature.

Table 1. Density ρ, and speed of sound u, at 298.15 K, of the pure components

	ρ / g cm $^{-3}$		u / (m s^{-1})	
Component	experimental	literature	experimental	literature
HFE-7100	1.51589	1.52 [a]	600.25	600.2 [d]
		1.51650 [b]		
		1.5153 [c]		
2-propanol	0.78127	0.78126[e]	1139.7	1139[f]
		0.78087[f]		1138.71[g]
		0.78112[g]		1138.87[h]
		0.780824[h]		

[a] From ref [2]. [b] From ref [3]. [c] From ref [4]. [d] From ref [5]. [e] From ref [6]. [f] From ref [7]. [g] From ref [8]. [h] From ref [9].

A glass Fischer Labodest VLE apparatus model 602S was used in the equilibrium determinations. The equilibrium vessel is a dynamic recirculating still, and it is equipped with a Cottrell circulation pump. The equilibrium temperature was measured with a digital thermometer, with a four wire Pt100 with an accuracy of ±0.02 K. A digital pressure controller Wika Mensor CPC3000 with an accuracy of ±0.001 kPa and an operation range of 0.1-300 KPa and 273.15-523.15 K was used for the pressure measurement. The cold water necessary for the vapor phase condensation is provided at the required temperature by a circulating bath Julabo, model F12-ED.

Inside the ebulliometer, the fluid is heated at isobaric condition by an electrical heater installed in the apparatus. The heater is controlled at a desirable value to make about 2 drops per second of condensed vapor phase. A part of the liquid mixture is evaporated due to the heat produced. This vapors transport some drops of boiling liquid which are removed from vapor phase in a separation chamber so that the vapor phase is condensed in a separate condenser. When temperature remains constant for 30 minutes or longer, the condition of equilibrium is assumed, and then liquid and vapor samples are taken for analysis. Liquid and vapor-phase composition were determined indirectly by measure of density and speed of sound.

3. Results and Discussion.

3.1 Physical properties

The measured densities, ρ, refractive indices, n_D, speeds of sound, u, calculated values of excess molar volumes, V^E_m, isentropic compressibility, κ_S, and isentropic compressibility changes of mixing, $\Delta\kappa_S$, were listed in Table 2 and calculated by means of the following expressions.

Excess molar volumes, V^E_m:

$$V_m^E = \sum_{i=1}^{N} x_i M_i (\rho^{-1} - \rho^{o\,-1}_i) \quad (1)$$

where x_i and M_i are the mole fraction and molar mass of component i in the mixture, ρ is the density of the mixture, and ρ^o_i is the density of the pure component *i*.

The isentropic compressibility changes of mixing, $\Delta\kappa_S$:

$$\Delta k_S = k_S - \sum_{i=1}^{N} x_i k_{Si} \quad (2)$$

where the isentropic compressibility, κ_S was calculated by means of the Laplace equation:

$$k_S = \rho^{-1} u^{-2} \quad (3)$$

where *u* is the speed of sound.

Excess molar volume values and isentropic compressibility changes of mixing were fitted with a Redlich-Kister-type equation:

$$\Delta Q_{ij} = x_i x_j \sum_{p=0}^{M} Ap(x_i - x_j)^p \quad (4)$$

where ΔQ_{ij} is the excess property, x_i is the molar fraction of component *i*, *Ap* is the fitting parameter and *M* is the degree of the polynomial expansion. The degree of this equation was optimized by applying the F-test [10]. The correlation parameters calculated by using equation (4) are shown in Table 3 together with the root-mean-square deviations σ, calculated applying the following expression:

$$\sigma = (\sum_{i}^{N} (Z_{\exp} - Z_{calc})^2 / N - m)^{1/2} \quad (5)$$

where property values are represented by *Z*, *N* is the number of experimental data, and *m* is the number of parameters.

Table 2. Densities ρ, speeds of sound u, excess molar volumes V^E, isentropic compressibilities κ_S, and isentropic compressibility changes of mixing $\Delta\kappa_S$, for the binary mixture HFE-7100 (1) + 2-propanol (2) at 298.15 K and atmospheric pressure.

x_1	ρ (g·cm^{-3})	u (m·s^{-1})	V^E(cm^3·mol^{-1})	κ_S (TPa^{-1})	$\Delta\kappa_S$ (TPa^{-1})
0	0.78129	1139.7	0	985	0
0.0509	0.85342	1044.3	0.343	1074	46
0.1008	0.91728	970.5	0.593	1157	87
0.1506	0.97536	911.9	0.770	1233	120
0.2026	1.02999	861.8	0.955	1307	151
0.2493	1.07543	824.9	1.044	1367	170
0.3018	1.12245	789.6	1.123	1429	188
0.3508	1.16254	761.9	1.210	1482	200
0.4058	1.20391	734.8	1.298	1538	210
0.4535	1.23787	716.0	1.292	1576	207
0.5001	1.26872	698.8	1.294	1614	206
0.5518	1.30055	682.0	1.302	1653	201
0.5987	1.32784	668.7	1.274	1684	193
0.6509	1.35644	655.5	1.230	1716	180
0.7002	1.38192	644.5	1.166	1742	165
0.7539	1.40826	633.7	1.068	1768	146
0.8034	1.43148	624.9	0.935	1789	124
0.8517	1.45295	617.5	0.806	1805	100
0.9015	1.47427	610.4	0.627	1821	73
0.9490	1.49416	605.0	0.397	1828	41
1	1.51579	600.3	0	1831	0

Figure 1 shows the calculated excess molar volumes plotted against the mole fraction of HFE-7100. As shown, the excess molar volumes are positive over the whole composition range, with a maximum around $x_1 = 0.55$. The magnitude and sign of excess molar volumes indicates the type of interactions taking place in the mixture. There is a destruction of the dipolar interaction in the pure ether which contributes to have positive values. The hydrogen bonds of the alkanol remain unbroken so that the excess molar volume values were reduced.

Isentropic compressibility changes of mixing values are positive for the entire composition range, with a maximum at $x_1 = 0.40$.

Table 3. Parameters Ap of equation (4) and standard root-mean square deviations σ for the binary system HFE-7100 (1) + 2-propanol (2).

	A_0	A_1	A_2	A_3	A_4	σ
V^E(cm^3·mol^{-1})	5.2448	0.0392	1.0200	0.4028	2.1934	0.004
$\Delta\kappa_S$ (TPa^{-1})	827.4	-156.8	86.6	108.6		0.3

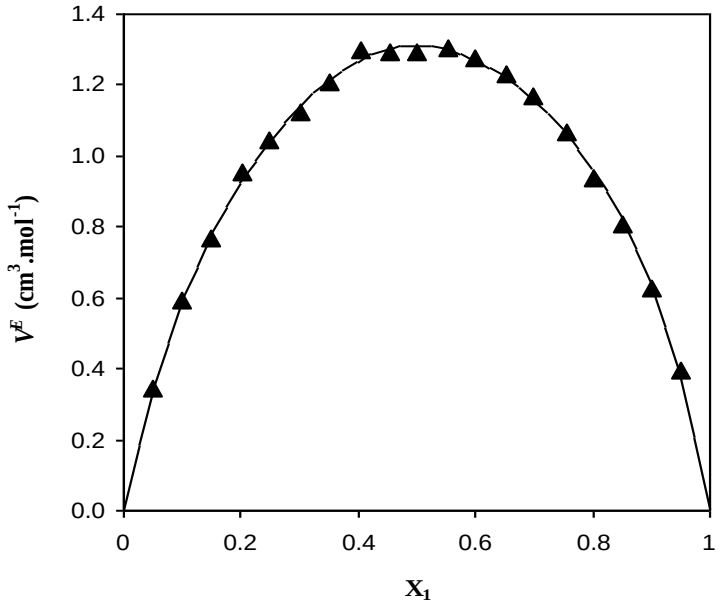

Figure 1. Excess molar volumes at 298.15 K and atmospheric pressure against mole fraction, x_1 of the binary mixture HFE-7100 (1) + 2-propanol (2). ▲ Experimental values. The solid line represents the data fitting to eq. 4.

3.2 Vapor-liquid equilibrium

Boiling temperatures, Tb, molar fractions of HFE-7100 in liquid phase (x_1) and in vapor phase (y_1), activity coefficients (γ_1) and (γ_2) for the isobaric vapor-liquid equilibrium at the pressures of 50.0, 101,3 and 200.0 kPa are presented in Table 4. The three binary systems form positive azeotropes. The azeotropic data, determined on the basis of the experimental VLE data, are shown in Table 5. It can be seen also that the azeotrope moves to the left when pressure increases. No data were found in the literature for the binary system.

Vapor pressures of HFE-7100 from 25 to 290 kPa and of 2-propanol from 6 to 280 kPa were obtained with the ebulliometer. The T vs. P^o_i pairs were correlated to the Antoine equation:

$$\ln P_i^0 = A - \frac{B}{T(K) + C} \qquad (6)$$

The Antoine constants of the pure components are listed in Table 6.

Table 4. Isobaric Vapor-Liquid Equilibrium data at 50.0, 101.3 and 200.0 kPa for the binary system HFE-7100 (1) + 2-propanol (2).

x_1	y_1	*Tb*/K	γ_1	γ_2
		50.0 kPa		
0.0000	0.0000	338.82		0.998
0.0161	0.3290	333.05	10.491	0.883
0.0197	0.3953	330.92	11.016	0.883
0.0255	0.4523	328.75	10.453	0.892
0.0370	0.5213	326.38	8.969	0.885
0.0561	0.5699	323.95	7.019	0.915
0.1230	0.6644	319.00	4.427	0.989
0.1800	0.7473	314.92	3.941	0.990
0.2420	0.7711	313.26	3.215	1.062
0.3947	0.8012	311.78	2.165	1.254
0.5410	0.8114	311.15	1.638	1.625
0.6813	0.8230	310.76	1.339	2.246
0.7108	0.8267	310.69	1.293	2.433
0.7360	0.8285	310.65	1.253	2.643
0.7763	0.8323	310.59	1.196	3.061
0.8052	0.8365	310.57	1.160	3.433
0.8719	0.8479	310.55	1.086	4.867
0.8964	0.8565	310.60	1.065	5.664
0.9122	0.8598	310.65	1.049	6.509
0.9448	0.8785	310.93	1.023	8.849
0.9575	0.8861	311.07	1.013	10.703
0.9731	0.9049	311.45	1.003	13.839
1.0000	1.0000	313.45	1.000	

x_1	y_1	*Tb*/K	γ_1	γ_2
		101.3 kPa		
0.0000	0.0000	355.49		1.000
0.0386	0.4361	343.95	8.209	0.936
0.0595	0.5244	340.87	6.977	0.922
0.0698	0.5382	340.00	6.259	0.940
0.0967	0.6026	337.47	5.445	0.933
0.1332	0.6517	335.10	4.590	0.949
0.1635	0.6714	334.07	3.976	0.973
0.1684	0.6802	333.65	3.961	0.971
0.1707	0.6839	333.58	3.938	0.966
0.2060	0.7053	331.77	3.560	1.023
0.2484	0.7145	331.00	3.065	1.086
0.2904	0.7210	330.97	2.647	1.126
0.3532	0.7372	330.11	2.287	1.213
0.4048	0.7480	329.60	2.058	1.295
0.4230	0.7464	329.90	1.946	1.326
0.4945	0.7594	329.25	1.729	1.481
0.5493	0.7643	329.15	1.571	1.636
0.6220	0.7732	328.99	1.411	1.892
0.7464	0.7901	328.80	1.208	2.638
0.7795	0.7963	328.80	1.166	2.945
0.8082	0.8019	328.80	1.133	3.295
0.8709	0.8193	328.89	1.070	4.451
0.9102	0.8372	329.09	1.040	5.715

0.9260	0.8469	329.23	1.029	6.488
0.9359	0.8552	329.38	1.023	7.036
0.9736	0.9074	330.60	1.002	10.371
1.0000	1.0000	332.83	1.002	

x_1	y_1	Tb/K	γ_1	γ_2
		200.0 kPa		
0.0000	0.0000	373.51		1.007
0.0043	0.0810	371.21	13.192	1.003
0.0574	0.4180	360.80	6.334	0.972
0.0810	0.4741	358.15	5.416	0.996
0.1167	0.5255	356.18	4.370	1.009
0.1557	0.5723	354.18	3.748	1.030
0.1809	0.5940	353.33	3.419	1.043
0.2473	0.6298	352.07	2.737	1.089
0.3078	0.6536	350.99	2.346	1.158
0.3768	0.6706	350.22	2.005	1.263
0.4051	0.6786	349.87	1.905	1.310
0.4796	0.6935	349.41	1.664	1.456
0.5094	0.6994	349.26	1.586	1.525
0.5811	0.7108	348.97	1.423	1.740
0.7391	0.7439	348.77	1.176	2.502
0.7522	0.7468	348.78	1.160	2.604
0.7693	0.7509	348.79	1.140	2.752
0.8649	0.7884	349.09	1.055	3.958
0.8894	0.8038	349.39	1.037	4.436
0.9622	0.8851	351.39	0.999	7.087
0.9782	0.9269	352.55	0.998	7.497
1.0000	1.0000	354.53	1.000	

Table 5. Azeotropic data for the system HFE-7100 (1) + 2-propanol (2) at 50.0, 101.3 and 200.0 kPa.

Pressure	Azeotropic temperature	Azeotropic composition
50 kPa	310.56	0.8383
101.32 kPa	328.80	0.7941
200 kPa	348.77	0.7393

Table 6. Antoine constants A, B and C for equation (7).

Compound	A	B	C	D
HFE-7100	6.15555[a]	1171.368[a]	-50.618[a]	
	22.415[b]	36.41.9[b]	2.29859[b]	26.410[b]
2-propanol	6.88209[a]	1377.649[a]	-72.985[a]	
	6.86618[c]	1360.131[c]	-75.558[c]	
	6.87294[d]	1365.38[d]	-70.04[d]	

[a] This work. [b] From ref [11]. [c] From ref [6]. [d] From ref [12].

Activity coefficients (γ_1) and (γ_2) were calculated by using the Tsonopoulos method [13], which employs the Pitzer-Curl correlation for nonpolar compounds in a modified form. This method allows to get the second virial coefficients (B_{11}), (B_{22}) and (B_{12}), which represent the interaction between two molecules for calculating the activity coefficients of the vapor-liquid equilibrium equation (7) from them.

$$\ln \gamma_i = \ln \frac{y_i \cdot P}{x_i \cdot P_{sat}} + \frac{(B_{ii} - V_i^L) \cdot (P - P_{sat})}{R \cdot T} + \frac{P}{R \cdot T} \cdot (1 - y_i)^2 \delta_{ji} \quad (7)$$

where the term

$$\frac{(B_{ii} - V_i^L) \cdot (P - P_{sat})}{R \cdot T} + \frac{P}{R \cdot T} \cdot (1 - y_i)^2 \delta_{ji} = \ln \phi_i \quad (8)$$

allows to calculate the fugacity coefficients (ϕ_1) y (ϕ_2).

B_{ii} is the second virial coefficient, V_i^L is the molar volume in the liquid phase, calculated with the Rackett equation, P is the total pressure, P_{sat} is the vapor pressure of the component at temperature T obtained from the Antoine equation (6), R is the molar gas constant, x_i and y_i are the molar fractions of component i, and δ_{ji} is the second virial cross coefficient calculated from the second virial coefficients (B_{11}), (B_{22}) and (B_{12}).

Critical properties for HFE-7100 were estimated with different methods due to the scarce available data. Only one reference of critical temperature and critical pressure data was found in the literature [2]. Critical properties of HFE-7100 and 2-propanol are presented in Table 7.

Table 7. Critical properties of HFE-7100 and of 2-propanol

	T_c/K	P_c/kPa	V_c(cc/mol)	ρ_c(g/cc)
HFE-7100	469.67[a]	2288.63[b]	413.87[c]	0.6042
	468.15[d]	2230[d]		
2-propanol	508.3	4761	223	0.27317

[a] Estimated, method of Wilson and Jasperson, from ref [14] [b] Estimated, Antoine equation. [c] Estimated, method of Grigoras, from ref [14]. [d] From ref [2].

The experimental data of this work were verified to evaluate the thermodynamic consistency by using the point-to-point test proposed by Fredenslund et al [15], and the point-to-point test and area tests proposed by Wisniak [16].

The method of Fredenslund et al is based on the phase rule. Taking into account the general form of the Gibbs-Duhem equation (9),

$$\sum x_k d\ln\gamma_k = -\frac{V^E}{RT}dP + \frac{H^E}{RT^2}dT \qquad (9)$$

The experimental data can be considered as thermodynamically consistent when the average absolute deviation of the vapor phase composition (AADy) is less than 0.01. The test uses the third-order Legendre polynomials, expressed as:

$$\ln\gamma_1 = g + x_2 g' \qquad g \equiv G^E/RT$$
$$\ln\gamma_2 = g + x_1 g' \qquad g' \equiv (dg/dx_1)_\sigma \qquad (10)$$

$$g = \frac{G^E}{RT} = x_1(1-x_1)\sum^{k} a_k L_k(x_1) \qquad k = 0,1,\ldots,n \qquad (11)$$

$$L_k(x_1) = \{(2k-1)(2x_1-1)L_k\text{-}1(x_1)-(k-1)L_{k-2}(x_1)\}/k$$
$$L_0(x_1) = 1$$
$$L_1(x_1) = 2x_1\text{-}1 \qquad (12)$$

where the subscript σ denotes "along the saturation line", $L_k(x_1)$ is the expression for the Legendre polynomials, n is the polynomial order used, and a_k is the parameter of Legendre polynomials.

It can be seen that for an isobaric case the term $V^E/RT\ dT$ in eq (9) can be neglected. In addition, we neglect the term $H^E/RT^2\ dT$ in the Gibbs-Duhem equation due to the difficulty in measuring the excess enthalpy. The results of the average deviation of pressure (AADP) and the AADy are presented in Table 8. The AADy values were 0.021, 0.014 and 0.036 at the pressures of 50.0, 101.3 and 200.0 respectively, which are evaluated as not good. The fact of neglecting the term $H^E/RT^2\ dT$ may have caused more than 0.01 AADy. Also, it has to be considered that in the mixture, the ether group has strong association with the –OH group of the alkanol.

Table 8. Average absolute deviations in pressure and in vapor-phase composition for the consistency test of Fredenslund.

P (kPa)	AADP	AADy
50.0	0.867	0.0207
101.3	0.829	0.0143
200.0	1.328	0.0366

Due to this fact, we have to apply another thermodynamic consistency test which considers temperature dependence. In order to this, we performed an additional test proposed by Wisniak. It links the excess of the Gibbs function of a mixture, G^E, with its boiling point, applying the Clausius-Clapeyron equation (13).

$$\ln \frac{P}{Pi^{o}} = \frac{\Delta H_i{}^{o}(T_i{}^{o} - T)}{RT_i{}^{o}T} = \frac{\Delta S_i{}^{o}(T_i{}^{o} - T)}{RT} \tag{13}$$

The strength of the Wisniak test is that can be performed as an area test, or a point-to-point test. The test is thermodynamically consistent when the values of D_W are less than 3-5. The higher limit is proposed for the case where the heats of vaporization are not available and must be estimated. The test is expressed as

$$D_W = 100\frac{|L - W|}{L + W} \tag{14}$$

where L and W are defined as

$$L = \int_0^1 L_n dx_i = \int_0^1 W_n dx_i = W \tag{15}$$

$$L_n = \frac{T^{o}{}_i\, x_{i,n}\Delta S^{o}{}_{i,n} + T^{o}{}_j\, x_{j,n}\Delta S^{o}{}_{j,n}}{x_{i,n}\Delta S^{o}{}_{i,n} + x_{j,n}\Delta S^{o}{}_{j,n}} - T_n \tag{16}$$

$$W_n = \frac{RT_n\left[\left(x_{i,n}\ln\gamma_{i,n} + x_{j,n}\ln\gamma_{j,n}\right) - w_n\right]}{x_{i,n}\Delta S^{o}{}_{i,n} + x_{j,n}\Delta S^{o}{}_{j,n}} \tag{17}$$

where T_n is the experimental temperature at each data point, T_i^o and T_j^o are the boiling points of components *i* and *j*, and $\Delta S^o_{i,n}$ and $\Delta S^o_{j,n}$ are entropy of vaporization of pure components *i* and *j*.

w_n and $\Delta S^o_{i,n}$ are defined as follows

$$w_n = \sum x_{i,n} \ln(y_{i,n} / x_{i,n}) \quad (18)$$

$$\Delta S^o{}_{i,n} = \frac{\Delta H^o{}_i}{T^o{}_i} \quad (19)$$

In our case, the heats of vaporization of HFE-7100 have been estimated due to the lack of these data. Also, data for 2-propanol at 50.0 and 200.0 kPa had to be estimated. The values of heat of vaporization are listed in Table 9 together with the Wisniak consistency test results.
It can be seen that both area and point-to-point tests are thermodynamically consistent, with values lower than 3.

Table 9. Heats of vaporization and the results of the Wisniak consistency test.

P (kPa)	ΔH_i^o (kJ/mol)		Wisniak point test		Wisniak area test		
	HFE-7100	2-propanol	min. D_{wi}	max. D_{wi}	L	W	D_w
50.0	30.566[a]	42.570[a]	0.029	0.932	13.682	13.766	0.307
101.3	29.059[a]	39.85[b]	0.810	2.604	13.355	14.006	2.378
200.0	27.124[a]	38.524[a]	0.842	2.774	13.231	13.925	2.555

[a] Estimated. Method of Haggenmacher, from ref [14]. [b] From ref [17]

3.3 VLE data correlation

The liquid-phase activity coefficients for the binary systems were correlated with the non-random two-liquid (NRTL) model [18], the Wilson [19] model and the Universal-Quasi-Chemical (UNIQUAC) [20] model. The interaction parameters were obtained by the simplex method, by using the minimization of the objective function (OF) (20).The binary interaction parameters and standard deviations are listed for each activity coefficient model in Table 10. The parameter α_{12} in the NRTL equation was set to 0.3 for the system at the three pressures in this work.

Table 10. Binary interaction parameters for the binary system HFE-7100 (1) + 2-propanol (2) at 50.0, 101.3 and 200.0 kPa.

Model	Parameters (J/mol)		
			σ_y
	50.0 kPa		
NRTL	γ_{12}-γ_{22} = 3725.44	γ_{21}-γ_{11} = 3438.04	0.05
Wilson	Λ_{12} = 2527.49	Λ_{21} = 6713.68	0.03
UNIQUAC	a_{12} = 1809.53	a_{21} = -170.46	0.03
	101.3 kPa		
NRTL	γ_{12}-γ_{22} = 3930.27	γ_{21}-γ_{11} = 3023.57	0.03
Wilson	Λ_{12} = 2077.51	Λ_{21} = 6604.47	0.01
UNIQUAC	a_{12} = 1264.00	a_{21} = -172.88	0.01
	200.0 kPa		
NRTL	γ_{12}-γ_{22} = 3154.30	γ_{21}-γ_{11} = 3692.03	0.02
Wilson	Λ_{12} = 2882.26	Λ_{21} = 5528.12	0.01
UNIQUAC	a_{12} = 1140.72	a_{21} = -175.07	0.01

The structural parameters for the pure components r, q and q´used in the UNIQUAC model calculations are shown in Table 11. The three models show a good fitting to the experimental data. Figure 2 shows the experimental activity coefficients and the correlation given by the Wilson model versus the composition at the three pressures investigated. The good fitting to the experimental data can be observed for all pressures.

$$OF = \sum_{j=1}^{np} \sum_{i=1}^{nc} \left[\frac{\gamma_{ij}^{\exp} - \gamma_{ij}^{calc}}{\gamma_{ij}^{\exp}} \right]^2 \tag{20}$$

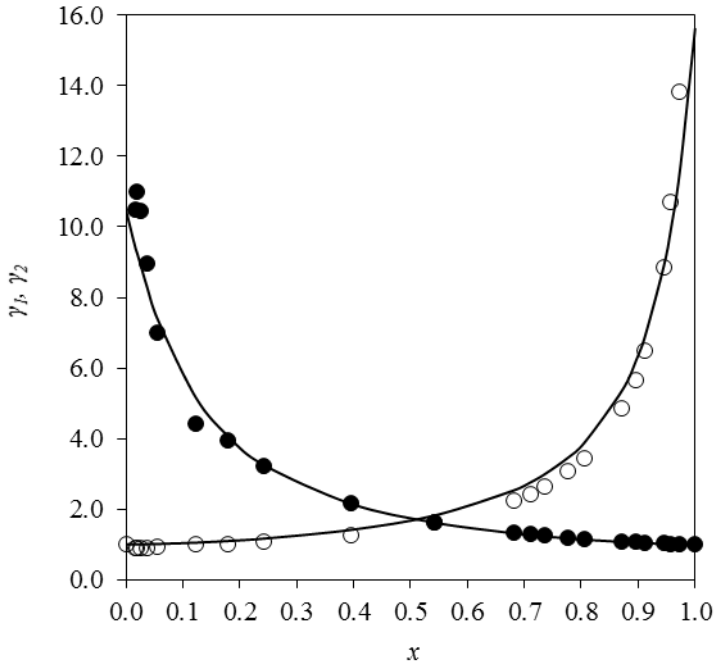

(a)

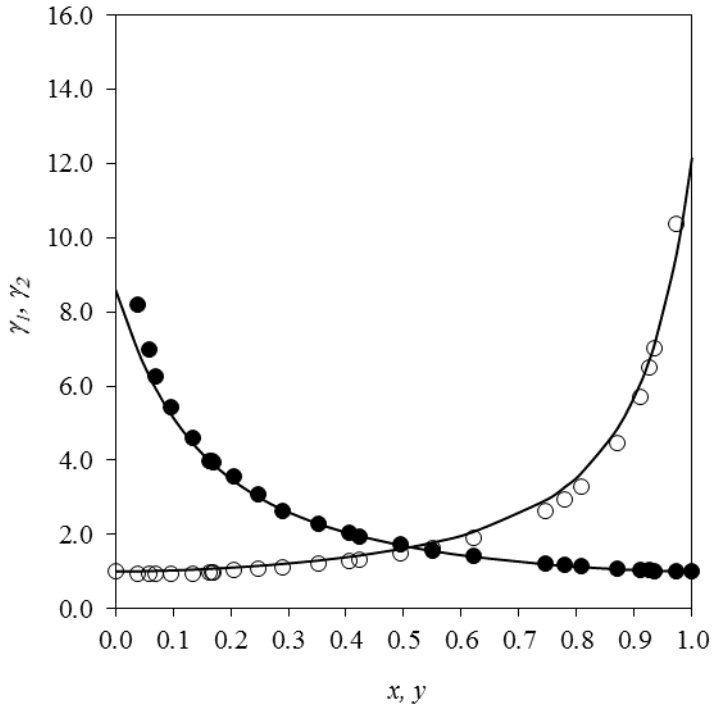

(b)

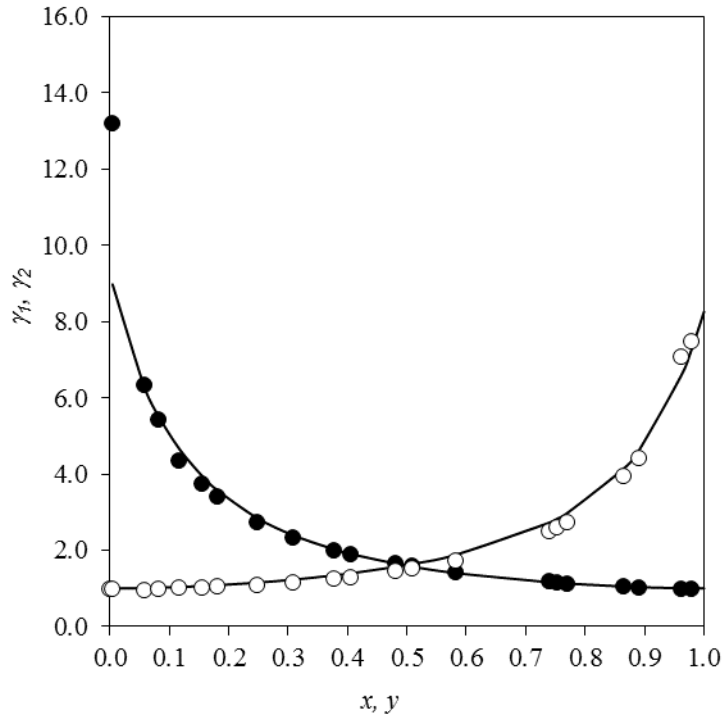

(c)

Figure 2. Experimental activity coefficients γ_1 and γ_2 vs. the mole fraction of the binary system (1) HFE-7100 + (2) 2-propanol at (a) 50.0 kPa, (b) 101.3 kPa, and (c) 200.0 kPa. ●; experimental γ_1, ○; experimental γ_2. The solid line represents the correlation to the Wilson model.

In Figure 3 the *x*, *y* experimental compositions and the fitting to the Wilson model are represented versus the temperature. The shift of the azeotrope considering the different pressures can be observed. When pressure increases, the azeotrope moves to the left according to lower HFE-7100 compositions, and also the highest temperatures for the azeotrope were found at the highest pressure.

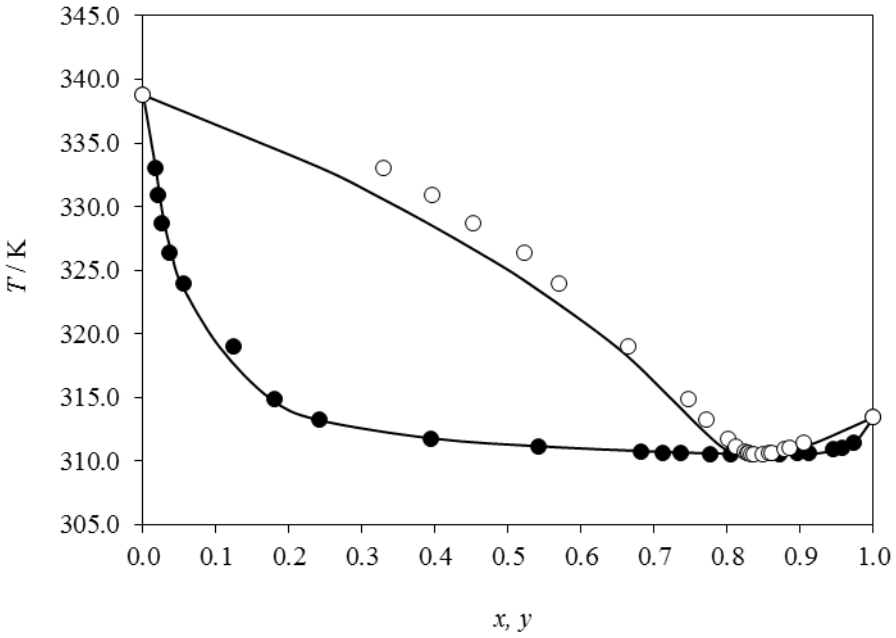

(a)

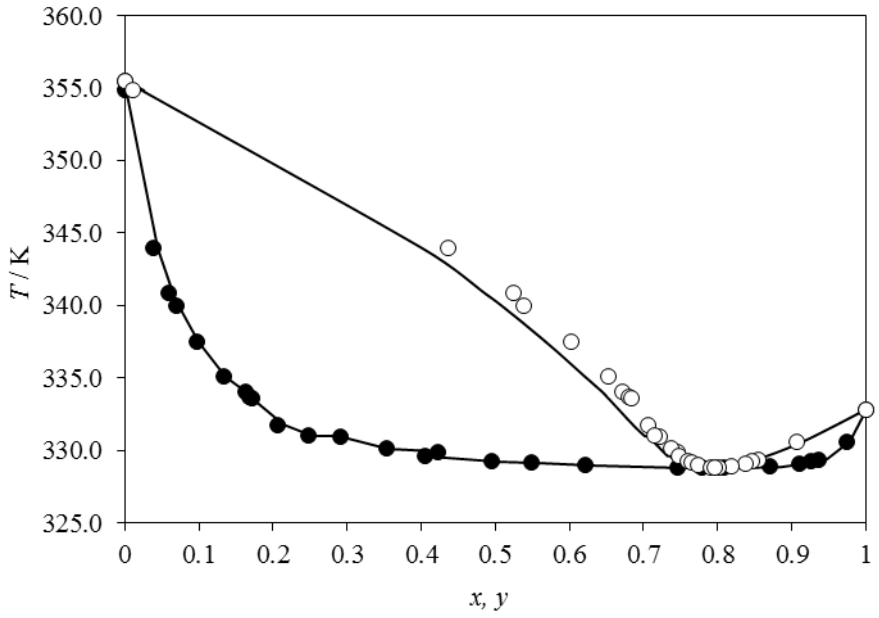

(b)

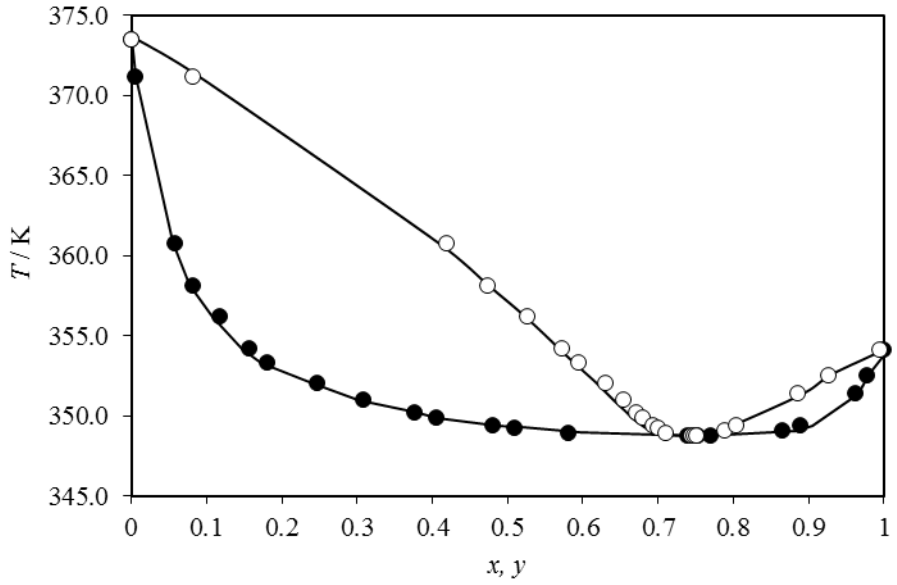

(c)

Figure 3. Experimental *x, y* data versus the temperature, *T* for the (1) HFE-7500 + (2) Diisopropyl ether binary system at (a) 50.0 kPa, (b) 101.3 kPa, and (c) 200.0 kPa. ●; experimental x_1, ○; experimental y_1. The solid line represents the calculated values by using the Wilson model.

Table 11. UNIQUAC structural parameters of pure compounds.

component	r	q	q´
HFE-7100	5.58[a]	5.22[a]	5.22[a]
2-propanol	2.78[b]	2.51[b]	0.89[b]

[a] Calculated from UNIFAC, ref [22]. [b] From ref [21]

4. Conclusions

Density, speed of sound, excess molar volume, isentropic compressibilities and isentropic compressibility changes of mixing were evaluated at 298.15 K and atmospheric pressure for the binary mixture HFE-7100 + 2-propanol. The effects of mixing on these properties were determined. The excess molar volume was positive over the whole composition range. Isentropic compressibility changes of mixing were positive over the whole composition range. The property changes of mixing were correlated by the Redlich-Kister polynomial.

Vapor-liquid equilibria for the system at the pressures of 50.0, 101.3 and 200.0 kPa were determined. The measured data were verified by the Fredenslund point-to-point test, and by the Wisniak point-to-point and area tests. According to the Fredenslund method the data are not consistent because the AADy values exceed 1%. The Wisniak test, which considers the

temperature dependency, was carried out and showed that all the data are thermodynamically consistent.

The measured systems were correlated using the second virial equation for the vapor phase and the NRTL, Wilson and UNIQUAC activity coefficient models for the liquid phase. The deviations show that these models are suitable for correlating the VLE data.

Aknowledgements

Natalia Muñoz-Rujas acknowledges support for this research to the University of Burgos, for the funding of her doctoral grant. This work is part of the doctoral thesis of Natalia Muñoz-Rujas.

References

[1] W. Ts*ai*, J. Hazard. Mater. 119 (2005) 69–78.

[2] 3M™ Novec™ Engineered Fluids, http://solutions.3m.com/wps/portal/3M/en_US/3MNovec/Home.

[3] Minamihonoki T, Ogawa H, Murakami S, Nomura H. Excess molar enthalpies and volumes of binary mixtures of nonafluorobutylmethylether with ketones at T = 298.15 K. Journal of Chemical Thermodynamics 38 (2006) 1254–1259.

[4] Piñeiro M.M., Bessières D, Legido J.L., Saint-Guirons H. *Pρt* measurements of Nonafluorobutyl Methyl Ether and Nonafluorobutyl Ethyl Ether between 283.15 and 323.15 K at pressures up to 40 MPa. International Journal of Thermophysics 24 (2003) 1265–1276.

[5] Piñeiro M.M., Plantier F, Bessières D, Legido J.L., Daridon JL. High-pressure speed of sound measurements in methyl nonafluorobutyl ether and ethyl nonafluorobutyl ether. Fluid Phase Equilibria 222 (2004) 297–302.

[6] Riddick, J. A., Bunger, W.B., Sakano, T.K. Organic solvents physical properties and methods of purification, 4th ed.; vol. II, Wiley, New York (1986).

[7] González B, Domínguez Á, Tojo J. Viscosity, density, and speed of sound of methylcyclopentane with primary and secondary alcohols at T = (293.15, 298.15, and 303.15) K. Journal of Chemical Thermodynamics 38 (2006) 1172–1185.

[8] Singh S, Aznar M, Deenadayalu N. Densities, speeds of sound, and refractive indices for binary mixtures of 1-butyl-3-methylimidazolium methyl sulphate ionic liquid with alcohols at T = (298.15, 303.15, 308.15, and 313.15) K. Journal of Chemical Thermodynamics 57 (2013) 238–247

[9] Zafarani-Moattar M.T., Sadeghi R., Sarmad S. Measurement and modeling of densities and sound velocities of the systems {poly(propylene glycol) + methanol, +ethanol, +1-propanol, +2-propanol and +1-butanol} at T = 298.15 K. Journal of Chemical Thermodynamics 38 (2006) 257–263.

[10] Bevington, P. Data reduction and error analysis for the physical sciences. McGraw-Hill, New York (1969).

[11] Shiflett M.B., Yokozeki A. Liquid-liquid equilibria of hydrofluoroethers and ionic liquid 1-ethyl-3-methylimidazolium bis(trifluoromethvlsulfonvl)imide. Journal of Chemical and Engineering Data 52 (2007) 2413–2418.

[12] González C., Ortega J., Hernández P., Galván S. Experimental determination of densities and isobaric vapor-liquid equilibria of binary mixtures formed by a propyl alkanoate (methanoate to butanoate) + an alkan-2-ol (C3, C4). Journal of Chemical and Engineering Data 44 (1999) 772–783.

[13] Tsonopoulos, C. An empirical correlation of second virial coefficients. AIChE Journal 20 (1974) 263-272.

[14] Polling, B.E., Prausnitz, J.M., O´Connell, J.P. The properties of gases and liquids, 5th ed. McGraw-Hill, New York (2001).

[15] Fredenslund, A., Gmehling, J., Rasmussen P. Vapor-liquid equilibria using UNIFAC. ed. Elsevier, Amsterdam (1977).

[16] Wisniak, J. A new test for the thermodynamic consistency of vapor-liquid equilibrium. Industrial and Engineering Chemistry Research 32 (1993) 1531–1533.

[17] Majer, V. Svoboda, V. Uchytilová, V. Finke, M. Enthalpies of vaporization of aliphatic C5 and C6 alcohols. Fluid Phase Equilibria 20 (1985) 111-118.

[18] Renon, H., Prausnitz, J.M. Local compositions in thermodynamic excess functions for liquid mixtures. AIChE J. 14 (1968) 135-144.

[19] Wilson, G.M. Vapor-liquid equilibrium. XI. A New expression for the excess free energy of mixing. Journal of the American Chemical Society. 86 (1964) 127-130.

[20] Abrams D.S., Prausnitz J.M. Statistical thermodynamics of liquid mixtures: A new expression for the excess Gibbs energy of partly or completely miscible systems, AIChE J. 21 (1975) 116-128.

[21] Chen, Y., Wang, H., Tang, Y., Zeng, J. Ternary (liquid + liquid) equilibria for (water + 2-propanol + α-pinene, or β-pinene) mixtures at four temperatures. J. Chem. Thermodynamics 51 (2012) 144-149

[22] Fredenslund, A., Jones, R.L., Prausnitz, J.M. AIChE J. 21 (1975) 1086-1100.

Isobaric Vapor-Liquid Equilibrium at 50.0 and at 101.3 kPa, Density and Speed of Sound at 298.15 K of Binary Mixtures HFE-7500 + Diisopropyl Ether (DIPE).

Natalia Muñoz-Rujas[a], Adil Srhiyer[a], Eduardo Montero[a], Fernando Aguilar[a]

[a] Departamento de Ingeniería Electromecánica, Escuela Politécnica Superior, Universidad de Burgos, E-09006, Burgos, Spain.

Abstract

Isobaric vapor-liquid equilibria (VLE) at 50.0 and at 101.3 were measured for the binary system *x* HFE- 7500 + (1-*x*) Diisopropyl ether (DIPE) by employing a glass Fischer Labodest VLE 602S ebullometer. Activity coefficients were determined by employing the Tsonopoulos method, as well as the Gibbs free energy on mixing. Several models were employed to correlate the experimental data, and the thermodynamic consistency was checked by means of the Fredenslund and Wisniak point to point and area tests. Densities, and speeds of sound at 298.15 K have been measured by using an Anton Paar DAS 5000 density and sound velocity analyzer. Excess molar volumes, isentropic compresibilities and deviation in isentropic compressibility have been calculated from these experimental data. The excess properties upon mixing were correlated by the Redlich-Kister polynomial satisfactorily.

1. Introduction

Whith increasingly more and more awareness about the impact of greenhouse gas emissions on climate change, there is now a greater concern with introducing new substances without negative impact on the atmosphere. Ozone depleting substances, such as chlorofluorocarbons (CFCs) and hydrochlorofluorocarbons (HCFCs) production and utilization were gradually banned since the signature of the Montreal Protocol in 1978. These substances were widely employed in domestic and mobil air conditioning, electronic components cleaning, in isolating materials production, etc. The Kyoto Protocol (1997) focused on greenhouse substances such as CO_2, hydrofluorocarbons (HFCs), sulphur hexafluoride (SF_6) and perfluorocarbons (PFCs), and determined to reduce the consumption of these substances. In the same direction, the Paris Agreement, signed by most of the parties in 2016, introduced considerations concerning greenhouse effect mitigation. During decades, lots of efforts were carried out in order to find

non-ozone depleting and low global warming substances to substitute commonly used fluorocarbons.

One of these propoded alternatives are the hydrofluoroether fluids (HFEs). A variety of them are being synthesized, exhibiting different properies that cover the range of many CFCs, HCFCs, HFCs and PFCs utilizations. These fluids have zero ozone depletion potentials (ODP), low global warming potentials (GWP), short atmospheric lifetimes (ALT), they have very low-overall toxicity and are non-flammable [1].

Electronics industry is one of the many in which heat transfer fluids are widely used. This industry is characterised by highly-packed electronics in which heat is confined in smaller spaces, and the requirements of non-flammable and high dielectric strenght fluids place HFEs in the view point. Due to its boiling point (T_b = 401.15 K), high density, low viscosity and low latent heat of vaporization [1], HFE-7500 is a good option to cover these range of applications. The properites of HFE-7500 allow also to conduct two-phase immersion cooling of supercomputers, in which the liquid phase evaporates at the boiling point of the fluid, and after it condenses, returning to its liquid phase. These properties can help reduce component bulk and weight, and allow to use less floor space [2]. HFE-7500 has many applications also in medical industry; this fluid does not support biological growth, the parts cleaned with it have less chance of corrosion, it can be used as inert media to separate samples going for diagnostic analysis, and it can also be a coating for blood bags in order to prevent blood clots formation [3]. Other utilizations of HFE-7500 can include cleaning or coating sensitive materials in aerosol formulations, and to act as carrier solvent for lubricant deposition.

Diisopropyl ether has many applications; it can be used as additive in gasolines due to its anti-knocking effect, it is used in solvents industry for paints and also in cleaning processes. However, diisopropyl ether is a flammable solvent, so the addition of a non-flammable substance, as is the case of HFE-7500, improves its utilizations.

The knowledge of vapor-liquid equilibrium (ELV) data brings information about the boiling point of the mixture depending on the (x, y) compositions of each component, allowing to the prediction of equilibrium diagrams and allowing also to design equipment and industrial plants.

In this work, the VLE determinations for the binary mixture x HFE- 7500 + (1-x) Diisopropyl ether were performed by using an isobaric ebullometer at pressures 50.0 kPa and 101.3 kPa. The experimental data were correlated to several models (NRTL, Wilson, UNIQUAC), and the UNIFAC predictive model was also used. Densities and speeds of sound of the mixtures at atmospheric pressure and at 298.15 K were also carried out by using an Anton

Paar DSA density and sound velocity meter. Isentropic compressibilities were also determined from density and speed of sound data.

2. Experimental Section

2.1 Materials.

Hydrofluoroether fluid HFE-7500, also known by its chemical name, 2-trifluoromethyl-3-ethoxydodecafluorohexane or 3-ethoxy-1,1,1,2,3,4,4,5,5,6,6,6-dodecafluoro-2-trifluoromethylhexane (CAS No.: 297730-93-9) was obtained from the 3M company with a stated mass fraction purity greater than 0.995. Diisopropyl ether (DIPE), also known as 2,4-dimethyl-3-oxapentane, was supplied by Sigma-Aldrich (CAS: 108-20-3), with a purity greater than 0.995. Neither one of the fluids was subject to further purification. Table 1 shows the specifications of both chemicals.

Table 1. Description and related purity of chemicals.

Compound	Source	Formula	Molar mass / g·mol^{-1}	Stated purity[a]	CAS number
HFE-7500[b]	3M Company	$C_9H_5F_{15}O$	414.11	>99.5[c]	297730-93-9
Diisopropyl ether	Sigma-Aldrich	$C_6H_{14}O$	102.17	>99.5[d]	108-20-3

[a] Determined by gas chromatography (GC) by the supplier.
[b] HFE-7500 = 2-trifluoromethyl-3-ethoxydodecafluorohexane.
[c] Mass fraction purity / g·mol^{-1}%.
[d] Mole fraction purity / mol%.

2.3 Density and Speed of Sound Measurements

To determine the density ρ, and the speed of sound c, of the pure liquids and mixtures, an Anton Paar DSA 5000 density and sound velocity meter was used. This apparatus has a precision of ±5·10-5 g·cm^3 on its density measurementsand ±0.5 m/s of precision for the speed of sound measurements. Before each series of measurements, the density and sound velocity analyzer was calibrated with Millipore quality water and ambient air. The mixtures were prepared by weighing amounts of the pure liquids by syringing into stoppered vials of 14 cm^3 of volume to prevent evaporation and reducing possible errors in mole fraction calculations. A Mettler Toledo MS-204S balance was used with a precision of ±1·10^{-4} g, covering the whole composition range of the mixture. The accuracy in the calculation of excess volumes, and deviation of isentropic compressibilities κ_S, were estimated to be as better than 10^{-2} cm^3·mol^{-1},

and 2 TPa^{-1}, respectively. Table 2 gathers the density and sound velocity values obtained experimentally at 298.15 K and at 0.1 MPa, as well as some density values found in the literature.

Table 2. Density ρ, and Speed of Sound c, at 298.15 K, of the pure components.

	ρ / g cm^{-3}		c / (m s^{-1})
Component	experimental	literature	experimental
HFE-7500	1.62013	1.614 [a]	658.85
		1.61992 [b]	
Diisopropyl ether	0.71842	0.71854[c]	998.39
		0.7178[d]	
		0.7183[e]	

[a] From reference [1]. [b] From reference [4]. [c] From reference [5].
[d] From reference [6]. [e] From reference [7].

2.2 Vapor Liquid Equilibria Measurements

To carry out the VLE measurements, a glass Fischer Labodest VLE apparatus model 602S was used. The equilibrium vessel is a dynamic recirculating still, and it is equipped with a Cottrell circulation pump. The equilibrium temperature was measured with a digital thermometer, equipped with a four wire Pt100 with an accuracy of ±0.02 K and an uncertainty of ±0.03 K. A digital pressure controller Wika Mensor CPC3000 with an accuracy of ±0.001 kPa and an operation range of 0.1-300 kPa and 273.15-523.15 K was used for the pressure measurement with an uncertainty of ±0.025%. The cold water necessary for the vapor phase condensation is provided at the required temperature by a circulating bath Julabo, model F12-ED.

At least 75 cm^3 of fluid were introduced in the ebullometer. Then, with the valves closed, the fluid is heated at isobaric condition by an electrical heater installed in the apparatus while the pressure controller helps the pressure to remain constant inside the cell. The heater is controlled at a desirable value to make about 2 drops per second of condensed vapor phase. A part of the liquid mixture is evaporated due to the heat produced. This vapors transport some drops of boiling liquid which are removed from vapor phase in a separation chamber so that the vapor phase is condensed in a separate condenser. When temperature remains constant for 30 minutes or longer, the condition of equilibrium is assumed, and then liquid and vapor samples are taken for analysis. Both the two samples (liquid and vapor) have a maximum amount of 3 cm^3 for each phase. Liquid and vapor-phase compositions were determined indirectly by measure of density by using Anton Paar DSA 5000 density and sound velocity meter.

3. Results and Discussion.

3.1 Physical properties

Densities, ρ, and speeds of sound, c, were determined experimentally by employing an Anton Paar DSA 5000 density and sound velocity analyzer at atmospheric pressure and at 298.15 K. 21 mole fractions of the binary mixture x HFE-7500 + (1-x) Diisopropyl ether were prepared and studied with this apparatus. From density measurements excess volumes, V^E were calculated by using equation (1), and with density and speed of sound values isentropic compressibility, κ_S was also determined by means of the Laplace equation (2). Isentropic compressibility changes of mixing, $\Delta\kappa_S$, were calculated using equation (3). Table 3 shows the experimental densities, sound velocities, isentropic compressibilities, changes on isentropic compressibility on mixing and excess volumes for all the studied compositions.

$$V_m^E = \sum_{i=1}^{N} x_i M_i (\rho^{-1} - \rho^{o\,-1}_i) \tag{1}$$

Where x_i and M_i are the mole fraction and molar mass of component i in the mixture, ρ is the density of the mixture, and ρ^o_i is the density of the pure component i.
The equation of Laplace to calculate isentropic compressibility, κ_S is as follows:

$$k_S = \rho^{-1} c^{-2} \tag{2}$$

Equation (3) allows to calculate the changes on isentropic compressibility:

$$\Delta k_S = k_S - \sum_{i=1}^{N} x_i k_{Si} \tag{3}$$

Excess molar volume values and isentropic compressibility changes of mixing were fitted with a Redlich-Kister-type equation:

$$\Delta Q_{ij} = x_i x_j \sum_{p=0}^{M} Ap(x_i - x_j)^p \tag{4}$$

Where ΔQ_{ij} is the excess property, x_i is the molar fraction of component i, Ap is the fitting parameter and M is the degree of the polynomial expansion. The degree of this equation was optimized by applying the F-test [8]. The correlation parameters calculated by using equation

(4) are shown in Table 4 together with the root-mean-square deviations σ, calculated applying the following expression:

$$\sigma = (\sum_{i}^{N} (Z_{\exp} - Z_{calc})^2 / N - m)^{1/2} \quad (5)$$

Where property values are represented by *Z*, *N* is the number of experimental data, and *m* is the number of parameters.

Table 3. Densities ρ, sound velocities *c*, excess molar volumes V^E, isentropic compressibilities κ_S, and isentropic compressibility changes of mixing $\Delta\kappa_S$, for the binary mixture *x* HFE-7500 + (1-*x*) Diisopropyl ether at 298.15 K and at atmospheric pressure.

x	ρ / g·cm^{-3}	*c* / m·s^{-1})	V^E / cm^3·mol^{-1}	κ_S / TPa^{-1})	$\Delta\kappa_S$ / TPa^{-1}
0.0000	0.71842	998.4	0.000	1396	0
0.0496	0.79147	934.1	0.797	1448	50
0.1005	0.86111	883.9	1.444	1487	87
0.1511	0.92573	844.2	1.937	1516	115
0.2019	0.98628	811.9	2.340	1538	136
0.2525	1.04291	785.6	2.646	1554	150
0.3013	1.09452	764.3	2.839	1564	159
0.3513	1.14451	745.9	2.966	1570	163
0.3990	1.18936	731.5	3.100	1571	163
0.4504	1.23612	717.8	3.031	1570	160
0.5015	1.27972	706.6	3.003	1565	153
0.5492	1.31852	697.3	2.929	1560	146
0.5992	1.35760	689.6	2.777	1549	134
0.6476	1.39359	682.7	2.622	1540	123
0.6964	1.42913	677.2	2.316	1526	108
0.7492	1.4652	672.0	2.065	1511	92
0.7986	1.49792	668.5	1.746	1494	73
0.8470	1.52874	665.1	1.407	1478	56
0.8981	1.56041	662.6	0.962	1460	36
0.9474	1.58980	660.4	0.517	1442	17
1.0000	1.62013	658.8	0.000	1427	0

In Figure 1 a plot for the excess volumes V^E and its fitting to equation (4) can be observed. As shown, the excess molar volumes are positive over the whole composition range, with a maximum at *x* = 0.3990 with a value of 3.100 cm^3·mol^{-1}. The magnitude and sign of excess molar volumes indicates the type of interactions taking place in the mixture. There is a

destruction of the dipolar interaction in the pure ether molecules which contributes to have positive values.

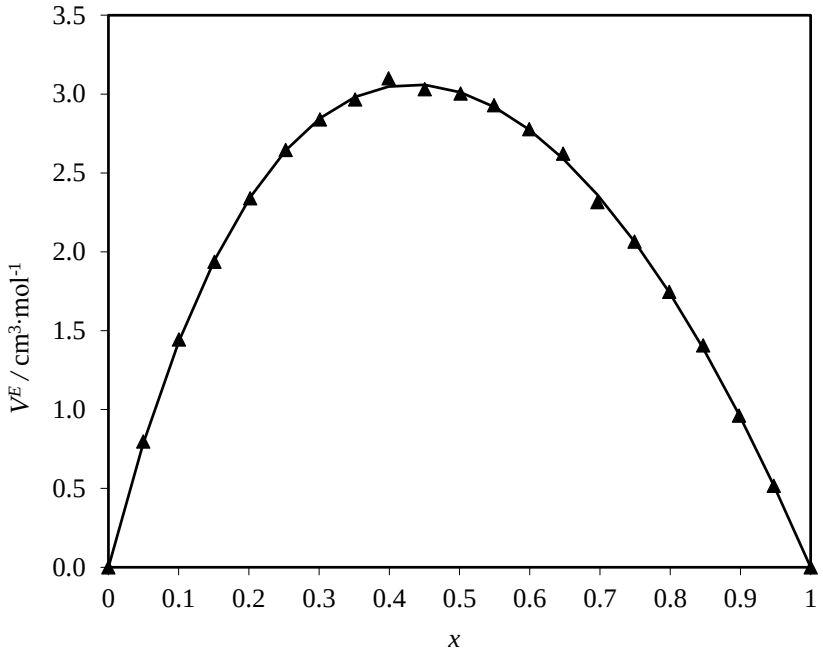

Figure 1. Excess molar volumes at 298.15 K and at atmospheric pressure versus the mole fraction, x of the binary mixture x HFE-7500 + (1-x) Diisopropyl ether. ▲ Experimental values. The solid line represents the data fitting to equation (4).

Table 4. Parameters A_p of equation (4) and standard root-mean square deviations σ for excess volumes and deviations on isentropic compressibility for the binary system x HFE-7500 + (1-x) Diisopropyl ether.

	A_0	A_1	A_2	A_3	σ
V^E / cm^3·mol^{-1}	12.0540	-2.8543	1.8219	-0.7358	0.02
$\Delta\kappa_S$ (TPa^{-1})	616.4	-282.6	96.0	-123.5	0.68

3.2 Vapor-liquid equilibrium

With a fixed pressure, boiling temperatures, T_b and mole fractions of HFE-7500 in liquid phase (x) and in vapor phase (y) were determined. By using the Tsonopoulos method [9], the second virial coefficients (B_{11}), (B_{22}) and (B_{12}), which represent the interaction between the two different molecules, were determined. Then, from these data it is possible to calculate the activity coefficients of the vapor-liquid equilibrium equation (6):

$$\ln \gamma_i = \ln \frac{y_i \cdot P}{x_i \cdot P_{sat}} + \frac{(B_{ii} - V_i^L) \cdot (P - P_{sat})}{R \cdot T} + \frac{P}{R \cdot T} \cdot (1 - y_i)^2 \delta_{ji} \quad (6)$$

Where the term:

$$\frac{(B_{ii} - V_i^L) \cdot (P - P_{sat})}{R \cdot T} + \frac{P}{R \cdot T} \cdot (1 - y_i)^2 \delta_{ji} = \ln \phi_i \quad (7)$$

allows to calculate the fugacity coefficients (ϕ1) y (ϕ2).

B_{ii} is the second virial coefficient, V_i^L is the molar volume in the liquid phase, calculated with the Rackett equation, P is the total pressure, P_{sat} is the vapor pressure of the component at the temperature T obtained from the Antoine equation (8), R is the molar gas constant, x_i and y_i are the molar fractions of component i, and δ_{ji} is the second virial cross coefficient calculated from the second virial coefficients (B_{11}), (B_{22}) and (B_{12}).

Table 5 presents the values for both the liquid and vapor compositions (x and y), the boiling temperatures, T_b and the activity coefficients, γ_1 and γ_2 obtained at 50.0 kPa and at 101.325 kPa.

In order to determine the molar volumes V_i^L, and the second virial coefficients it is necessary to have critical properties data. In this case, some these properties were determined due to the absence of data in the literature, that is the case of HFE-7500. Table 6 shows the values of the critical properties for both the two pure components.

Table 5. Isobaric Vapor-Liquid Equilibrium data at 50.0 and 101.3 kPa for the binary system x HFE-7500 (1) + (1-x) Diisopropyl ether.

x	y	T_b / K	γ_1	γ_2
		50.0 kPa		
0.0000	0.0000	321.01	-	1.0001
0.0144	0.0050	321.17	3.4064	1.0040
0.0588	0.0163	321.89	2.6449	1.0136
0.1650	0.0336	323.39	1.8086	1.0656
0.2310	0.0415	324.25	1.5340	1.1141
0.3073	0.0499	325.47	1.3104	1.1762
0.3839	0.0553	326.15	1.1254	1.2850
0.4621	0.0679	327.83	1.0638	1.3728
0.5647	0.0858	331.27	0.9442	1.4863
0.6203	0.1005	333.57	0.9106	1.5577
0.7433	0.1404	339.50	0.8258	1.8321
0.7943	0.1836	344.10	0.8366	1.8941

0.8340	0.2254	347.75	0.8459	2.0054
0.8547	0.2662	350.78	0.8660	1.9942
0.8860	0.3262	355.15	0.8670	2.0741
0.9125	0.3823	358.45	0.8731	2.2706
0.9373	0.4746	363.30	0.8859	2.3808
0.9527	0.5502	366.11	0.9151	2.5232
0.9679	0.6489	370.03	0.9285	2.6413
0.9798	0.7566	373.35	0.9568	2.6940
0.9995	0.9840	379.70	0.9931	6.3206
1.0000	1.0000	380.02	0.9987	-
		101.3 kPa		
0.0000	0.0000	341.66	-	0.9980
0.0230	0.0081	341.85	2.6769	1.0075
0.0880	0.0251	342.83	2.0669	1.0310
0.2485	0.0516	345.15	1.3709	1.1386
0.3198	0.0622	346.39	1.2229	1.2009
0.4811	0.0893	350.22	1.0076	1.3742
0.5735	0.1148	353.70	0.9525	1.4794
0.6462	0.1408	356.99	0.9186	1.5872
0.7648	0.2019	365.01	0.8369	1.8123
0.7865	0.2310	367.06	0.8676	1.8312
0.8020	0.2355	367.59	0.8518	1.9377
0.8108	0.2778	370.97	0.8868	1.7697
0.8378	0.3115	373.55	0.8837	1.8542
0.8688	0.3601	376.75	0.8879	1.9834
0.8823	0.3731	378.24	0.8638	2.0955
0.8945	0.3968	379.65	0.8667	2.1805
0.9196	0.4543	382.92	0.8715	2.4165
0.9253	0.5131	385.60	0.9013	2.1932
0.9476	0.5871	389.16	0.9052	2.4680
0.9560	0.6286	390.93	0.9120	2.5542
0.9633	0.6492	392.46	0.8942	2.8014
0.9649	0.6935	393.28	0.9312	2.5207
0.9797	0.7891	396.67	0.9477	2.8218
0.9977	0.9740	402.05	0.9907	2.8271
1.0000	1.0000	402.64	0.9989	-

Table 6. Critical properties of HFE-7500 and of Diisopropyl ether.

	T_c / K	P_c / kPa	V_c / $cm^3 \cdot mol^{-1}$	ρ_c / $g \cdot cm^{-3}$
HFE-7500	522.53[a]	1425.52[b]	866.22[c]	0.4781[c]
Diisopropyl ether	500.32[d]	2832[d]	386[d]	0.2647[d]

[a] Estimated, method of Wilson and Jasperson, from reference [10], [b] Estimated, Antoine equation. [c] Estimated, method of Grigoras, from reference [10]. [d] From reference [10].

Vapor pressures of HFE-7500 from 2.5 to 260 kPa and of Diisopropyl ether from 15 to 285 kPa were obtained with the ebulliometer. The T vs. P^oi pairs were correlated to the Antoine equation:

$$\ln P_i^0 = A - \frac{B}{T(K) + C} \tag{8}$$

The Antoine constants of the pure components are listed in Table 7.

Table 7. Antoine constants *A*, *B* and *C* for equation (8).

Compound	*A*	*B*	*C*
HFE-7500	6.6490[a]	1694.9503[a]	-37.5647[a]
Diisopropyl ether	5.9976[a]	1151.0268[a]	-53.2110[a]
	5.9768[b]	1143.0730[b]	-53.8100[b]

[a] This work. [b] From reference [5].

Different tests were used to verify the thermodynamic consistency of the experimental data: the Fredenslund [11] test and the Wisniak point-to-point and area tests [12].

The method of Fredenslund et al is based on the phase rule. Taking into account the general form of the Gibbs-Duhem equation (9):

$$\sum x_k d \ln \gamma_k = -\frac{V^E}{RT} dP + \frac{H^E}{RT^2} dT \tag{9}$$

The experimental data can be considered as thermodynamically consistent when the average absolute deviation of the vapor phase composition (AAD_y) is less than 0.01. The test uses the third-order Legendre polynomials, expressed as:

$$\ln \gamma_1 = g + x_2 g' \qquad g \equiv G^E/RT$$
$$\ln \gamma_2 = g + x_1 g' \qquad g' \equiv (dg / dx_1)_\sigma \tag{10}$$

$$g = \frac{G^E}{RT} = x_1(1-x_1)\sum^{k} a_k L_k(x_1) \qquad k = 0,1,\ldots,n \tag{11}$$

$$L_k(x_1) = \{(2k-1)(2x_1-1)L_k\text{-}1(x_1)-(k-1)L_{k-2}(x_1)\}/k$$
$$L_0(x_1) = 1$$
$$L_1(x_1) = 2x_1\text{-}1 \tag{12}$$

where the subscript σ denotes "along the saturation line", $L_k(x_1)$ is the expression for the Legendre polynomials, n is the polynomial order used, and a_k is the parameter of Legendre polynomials.

The term $V^E/RT\ dT$ in eq (9) can be neglected in the isobaric case. In addition, we neglect the term $H^E/RT^2\ dT$ in the Gibbs-Duhem equation due to the difficulty in measuring the excess enthalpy. Table 8 gathers the results for the average absolute deviations (AAD_P and AAD_y) obtained at the two measured pressures (50.0 and 101.3 kPa). In both cases the AAD_P values are high while the AAD_y results show that the data are consistent, being the value in the two cases equal to 0.01.

Table 8. Average absolute deviations in pressure and in vapor-phase composition for the consistency test of Fredenslund.

P / kPa	AAD_P	AAD_y
50.0	0.91	0.01
101.3	2.52	0.01

Although the AAD_y values for the Fredenslund's consistency test show that the data are consistent, other test was applied in order to evaluate the consistency. The Wisniak consistency test [12], which considers temperature dependence, links the excess of the Gibbs function of a mixture, G^E, with its boiling point, applying the Clausius-Clapeyron equation (13):

$$\ln\frac{P}{Pi^{o}} = \frac{\Delta H_i{}^{o}(T_i{}^{o}-T)}{RT_i{}^{o}T} = \frac{\Delta S_i{}^{o}(T_i{}^{o}-T)}{RT} \tag{13}$$

The strength of the Wisniak test is that can be performed as an area test, or a point-to-point test. The test is thermodynamically consistent when the values of D_W are less than 3-5. The higher limit is proposed for the case where the heats of vaporization are not available and must be estimated. The test is expressed as:

$$D_W = 100\frac{|L-W|}{L+W} \tag{14}$$

where L and W are defined as:

$$L = \int_0^1 L_n dx_i = \int_0^1 W_n dx_i = W \tag{15}$$

$$L_n = \frac{T^o{}_i\ x_{i,n}\Delta S^o{}_{i,n} + T^o{}_j\ x_{j,n}\Delta S^o{}_{j,n}}{x_{i,n}\Delta S^o{}_{i,n} + x_{j,n}\Delta S^o{}_{j,n}} - T_n \tag{16}$$

$$W_n = \frac{RT_n\left[\left(x_{i,n}\ln\gamma_{i,n} + x_{j,n}\ln\gamma_{j,n}\right) - w_n\right]}{x_{i,n}\Delta S^o{}_{i,n} + x_{j,n}\Delta S^o{}_{j,n}} \tag{17}$$

where T_n is the experimental temperature at each data point, T_i^o and T_j^o are the boiling points of components i and j, and $\Delta S^o_{i,n}$ and $\Delta S^o_{j,n}$ are entropy of vaporization of pure components i and j. w_n and $\Delta S^o_{i,n}$ are defined as follows:

$$w_n = \sum x_{i,n}\ln(y_{i,n}/x_{i,n}) \tag{18}$$

$$\Delta S^o{}_{i,n} = \frac{\Delta H^o{}_i}{T^o{}_i} \tag{19}$$

Due to the lack of enthalpies of vaporization for the HFE-7500 fluid, these data have been estimate by using the method of Haggenmacher proposed in reference [10]. In the case of Diisopropyl ether, we used also the estimated data by employing the same method to perform the Wisniak consistency test. The values of heats of vaporization are listed in Table 9 together with the Wisniak consistency test results.

It can be seen that both area and point-to-point tests are thermodynamically consistent, with values lower than 5.

Table 9. Heats of vaporization and the results of the Wisniak consistency test

P / kPa	ΔH_V / kJ·mol^{-1}		Wisniak point test		Wisniak area test		
	HFE-7500	Diisopropyl ether	min. D_{wi}	max. D_{wi}	L	W	D_w
50.0	37.93[a]	30.46[a]	0.56	2.81	16.38	16.98	1.81
101.3	36.12[a]	29.01[a]	0.21	3.96	15.97	16.46	1.52

[a] Estimated. Method of Haggenmacher, from reference [10].

3.3 VLE data correlation

Several local composition models were employed to correlate the experimental *T,x,y* data and also the liquid-phase activity coefficient data of the vapor-liquid equilibria. The non-random two-liquid (NRTL) model [13], the Wilson [14] model and the Universal-Quasi-Chemical (UNIQUAC) [15] model were used for this purpose. The interaction parameters were obtained by minimizing the objective function expressed in equation (20). The binary interaction parameters and standard deviations are listed for each activity coefficient model in Table 10. The parameter α_{12} in the NRTL equation was set to 0.3 for the system at all the pressures measured.

Table 10. Binary interaction parameters and deviations for the employed local composition models.

Model	Parameters (J/mol)		ΔT/K	Δy
	50.0 kPa			
NRTL	γ_{12}-γ_{22} = 2819.51	γ_{21}-γ_{11} = 1470.78	1.11	0.01
Wilson	Λ_{12} = 5899.14	Λ_{21} = 4436.63	0.74	0.01
UNIQUAC	a_{12} = 204.28	a_{21} = -91.61	1.35	0.01
	101.3 kPa			
NRTL	γ_{12}-γ_{22} = 3848.18	γ_{21}-γ_{11} = 769.75	0.97	$3.52\cdot10^{-3}$
Wilson	Λ_{12} = 5582.66	Λ_{21} = 5004.44	1.47	$2.20\cdot10^{-3}$
UNIQUAC	a_{12} = 166.19	a_{21} = -70.10	1.10	$4.46\cdot10^{-3}$

The structural parameters for the pure components r, q and q´ used in the UNIQUAC model calculations are shown in Table 11. The three models show good correlation to the experimental data.

A correlation was also established by using the predictive model of UNIFAC [16] for the binary system at the two pressures measured by using the structural parameters reported in Table 11.

Figure 2 shows the experimental activity coefficients, its correlation to the NRTL model, and also its correlation to the predictive UNIFAC model versus the composition. The good

agreement between the fittings can be observed for both pressures, (a) at 50.0 kPa, and (b) at 101.3 kPa.

$$OF = \sum_{j=1}^{np} \sum_{i=1}^{nc} \left[\frac{\gamma_{ij}^{\exp} - \gamma_{ij}^{calc}}{\gamma_{ij}^{\exp}} \right]^2 \tag{20}$$

Table 11. UNIQUAC structural parameters of pure compounds.

Component	r	q	q´
HFE-7500	9.30[a]	8.53[a]	8.53[a]
Diisopropyl ether	4.74[a]	4.09[a]	4.09[a]

[a] Calculated from UNIFAC, reference [16].

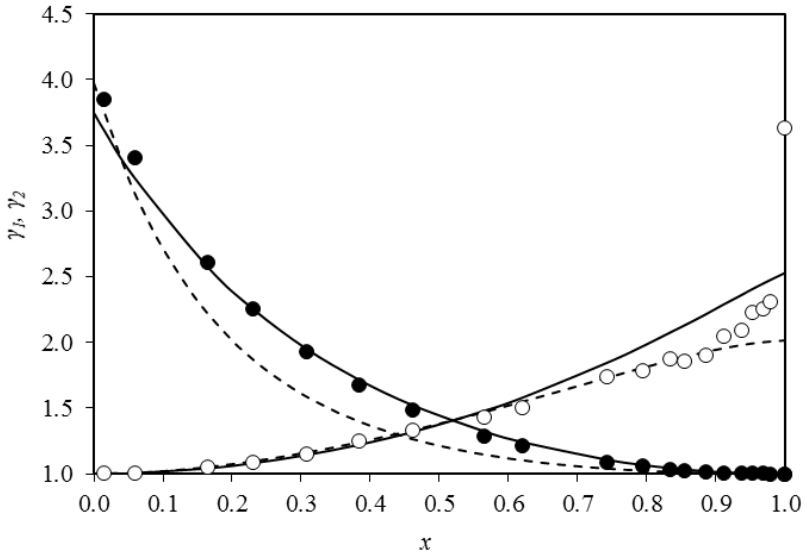

(a)

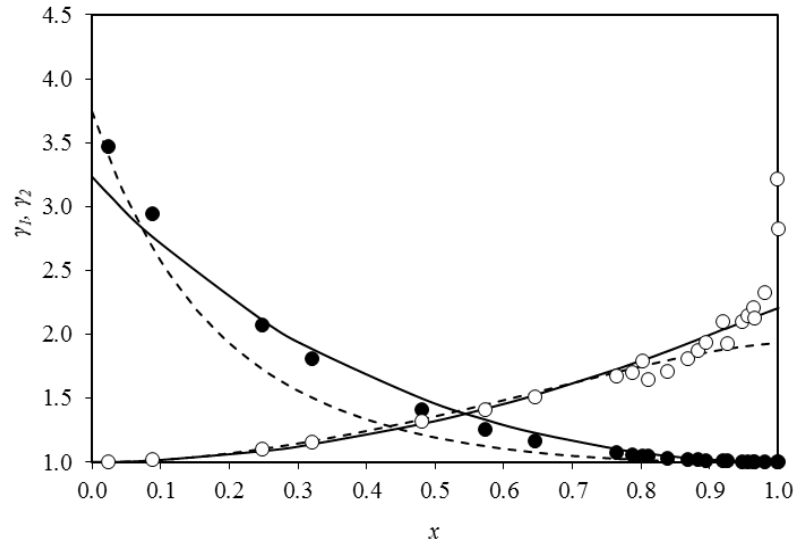

(b)

Figure 2. Activity coefficients γ_1 and γ_2 vs. the mole fraction of the binary mixture x HFE-7500 + (1-x) Diisopropyl ether at (a) 50.0 kPa and at (b) 101.3 kPa. ●; experimental γ_1, ○; experimental γ_2. The solid line represents the correlation to the NRTL model while the dashed line represents the predicted values using the UNIFAC model with binary parameters.

In Figure 3 can be seen the *T,x,y* diagrams at (a) 50.0 kPa and (b) 101.3 kPa. The fitting to the NRTL and UNIFAC models can also be observed. The effect of pressure in the mixture determines the boiling point at each mole composition, so that at 50.0 kPa the boiling temperatures are lower than at 101.3 kPa taking into account the same *x, y* compositions. The non-ideality of the mixture can be observed particularly at low HFE-7500 compositions.

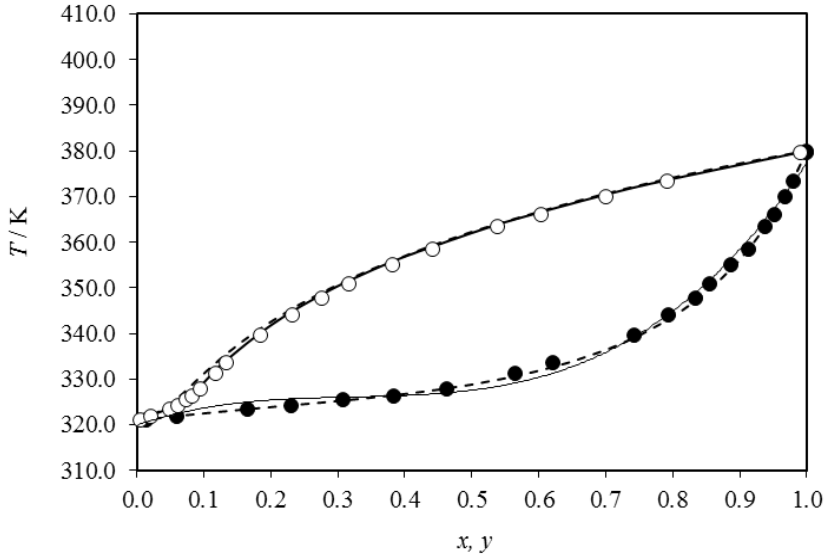

(a)

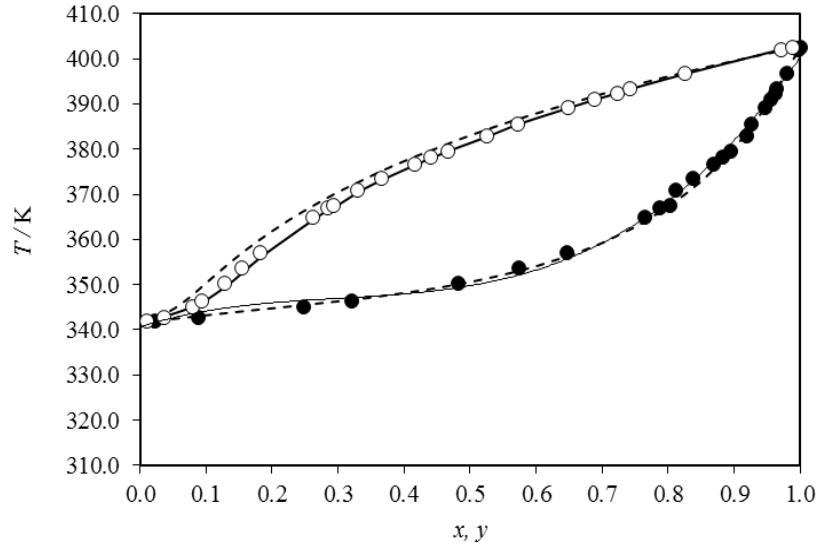

(b)

Figure xi. VLE data for the *x* HFE-7500 + (1-*x*) Diisopropyl ether binary system at (a) 50.0 kPa and at (b) 101.3 kPa. ●; experimental *x*, ○; experimental *y*. The solid line represents the calculated values by using the NRTL model. The dashed line represents the predicted values using the UNIFAC model with binary parameters.

4. Conclusions

Density, speeds of sound, excess molar volumes, isentropic compressibilities and isentropic compressibility changes on mixing were evaluated at 298.15 K and atmospheric pressure for the binary mixture *x* HFE-7500 + (1-*x*) Diisopropyl ether. The effects of mixing on these properties were determined. The obtained values of the excess molar volume were positive over the whole composition range. Isentropic compressibility changes of mixing were positive over the whole composition range. The property changes of mixing were correlated by the Redlich-Kister polynomial.

VLE determinations at 50.0 and at 101.3 kPa were carried out for the binary mixture *x* HFE-7500 + (1-*x*) Diisopropyl ether. The experimental data obtained were evaluated to be consistent by using the Fredenslund and the Wisniak point-to-point and area tests. Several models (NRTL, Wilson, UNIQUAC) were used to correlate the experimental *T,x,y* data and the activity coefficients, and the UNIFAC predictive model was also employed.

Aknowledgements

Natalia Muñoz-Rujas acknowledges support for this research to the University of Burgos, for the funding of her doctoral grant. This work is part of the doctoral thesis of Natalia Muñoz-Rujas.

References

[1] 3M™ Novec™ Engineered Fluids. https://multimedia.3m.com/mws/media/65496O/3mtm- novectm-7500-engineered-fluid.pdf

[2] 3M™ Novec™ Engineered Fluids. https://multimedia.3m.com/mws/media/569860O/3mtm-thermal-management-fluids-for-military-aerospace-apps.pdf

[3] 3M™ Novec™ Engineered Fluids. https://multimedia.3m.com/mws/media/480559O/3mtm-novectm-engineered-fluids-medical-applications.pdf

[4] M.H. Rausch, L. Kretschmer, S. Will, A. Leipertz, A.P. Fröba, J. Chem. Eng. Data 60 (2015) 3759-3765.

[5] J.A. Riddick, W.B. Bunger, T.K. Sakano, Organic Solvents: Physical Properties and Methods of Purification, vol. II, 4th ed. Wiley: U.S., 1986.

[6] U.P. Govender, T.M. Lercher, S.K. Garg, J.C. Ahluwalia, J. Chem. Eng. Data 41 (1996) 147-150.

[7] M. Dakkach, F. Aguilar, F.E.M. Alaoui, E.A. Montero, J. Chem. Thermodyn. 80 (2015) 135-141.

[8] Bevington, P. Data reduction and error analysis for the physical sciences. McGraw-Hill, New York (1969).

[9] Tsonopoulos, C. An empirical correlation of second virial coefficients. AIChE Journal 20 (1974) 263-272.

[10] Polling, B.E., Prausnitz, J.M., O´Connell, J.P. The properties of gases and liquids, 5th ed. McGraw-Hill, New York (2001).

[11] Fredenslund, A., Gmehling, J., Rasmussen P. Vapor-liquid equilibria using UNIFAC. ed. Elsevier, Amsterdam (1977).

[12] Wisniak, J. A new test for the thermodynamic consistency of vapor-liquid equilibrium. Industrial and Engineering Chemistry Research 32 (1993) 1531–1533.

[13] Renon, H., Prausnitz, J.M. Local compositions in thermodynamic excess functions for liquid mixtures. AIChE J. 14 (1968) 135-144.

[14] Wilson, G.M. Vapor-liquid equilibrium. XI. A New expression for the excess free energy of mixing. Journal of the American Chemical Society. 86 (1964) 127-130.

[15] Abrams D.S., Prausnitz J.M. Statistical thermodynamics of liquid mixtures: A new expression for the excess Gibbs energy of partly or completely miscible systems, AIChE J. 21 (1975) 116-128.

[16] Fredenslund, A., Jones, R.L., Prausnitz, J.M. AIChE J. 21 (1975) 1086-1100.

Anexo II

Contribuciones a congresos nacionales e internacionales

Isobaric vapor-liquid equilibrium of binary mixtures HFE-7100 + 2-propanol

Natalia Muñoz[1], Adil Srhiyer[1], Eduardo Montero[1], Fernando Aguilar[1*]
[1]*Department of Electromechanical Engineering, University of Burgos, Spain*
**faguilar@ubu.es*

Hydrofluoroether fluids (HFEs) are being used as third generation alternatives to replace CFCs (chlorofluorocarbons), HCFCs (hydrochlorofluorocarbons) and PFCs (perflurocarbons) because of their nearly zero ozone depletion, relatively low global warming potential and short atmospheric lifetimes [1]. In addition, they may be industrially used as cleaning solvents in the electronic components, protective gas used in melting of alloys, decontamination of fluids and heat transfer fluids in the heat exchangers [2].

Though a variety of HFEs have been synthesized, their performance and environmental properties and hence their utility can vary widely. For example, 1-methoxy-nonafluorobutane, also known as HFE 7100, has zero ozone depletion potential and other favorable environmental properties. The high boiling point and low surface tension of HFE 7100 fluid make it ideal for use as cleaner fluid as pure component or in mixtures with other solvents. Moreover, its chemical and thermal stability, non-flammability and low toxicity make it useful for many other industrial uses, such as high-GWP refrigerants replacement and as heat transfer fluid.

Experimental vapor-liquid equilibrium of the binary system HFE7100 + 2-propanol at 50, 101.325 and 200 kPa are reported in this work. Vapor-liquid equilibrium (VLE) have been measured with an isobaric ebullometer. Pressure stability is better than 0.06 kPa and temperature uncertainty is ±0.2 K. Composition of vapor and liquid phase is estimated by means of density and refractive index measurements. No data were found in the literature for this binary mixture.

Acknowledgements: N. Muñoz acknowledges support for this research to the University of Burgos, for the funding of her doctoral grant. This work is part of the Doctoral Thesis of N. Muñoz.

[1] W. Tsai, *J. Hazard. Mater. A* 2005, 119, 69–78.

[2] 3M™ Novec™ Engineered Fluids, http://solutions.3m.com/wps/portal/3M/en_US/3MNovec/Home (last visit 08/04/2014)

Isobaric vapor-liquid equilibrium of binary mixtures HFE 7500 + di-isopropyl ether

Natalia Muñoz[1], Adil Srhiyer[1], Eduardo Montero[1], Fernando Aguilar[1*]
[1]*Department of Electromechanical Engineering, University of Burgos, Spain*
[*]*faguilar@ubu.es*

Scientific topic: Measurement of Thermodynamic Properties. Phase Equilibria and Chemical Equilibria.

Keywords: Hydrofluoroether, di-isopropyl ether, vapor-liquid equilibrium.

Introduction

Hydrofluoroether fluids (HFEs) are being used as third generation alternatives to replace CFCs (chlorofluorocarbons), HCFCs (hydrochlorofluorocarbons) and PFCs (perflurocarbons) because of their nearly zero ozone depletion, relatively low global warming potential and short atmospheric lifetimes [1]. In addition, they may be industrially used as cleaning solvents in the electronic components, protective gas used in melting of alloys, decontamination of fluids and heat transfer fluids in the heat exchangers [2].
Though a variety of HFEs have been synthesized, their performance and environmental properties and hence their utility can vary widely. For example, 2-trifluoromethyl-3-ethoxydodecafluorohexane, also known as HFE 7500, has zero ozone depletion potential and other favorable environmental properties. The high boiling point and low surface tension of HFE 7500 fluid make it ideal for use as cleaner fluid as pure component or in mixtures with other solvents. Moreover, its chemical and thermal stability, non-flammability and low toxicity make it useful for many other industrial uses, such as high-GWP refrigerants replacement and as heat transfer fluid.

Experimental Section

Experimental isobaric vapor-liquid equilibrium of the binary system HFE7500 + di-isopropyl ether are reported in this work. A glass i-Fischer VLE apparatus model 602 S was used in the equilibrium determinations. Pressure stability is better than 0.06 kPa and temperature uncertainty is ±0.04 K. Composition of vapor and liquid phase is estimated by means of density and speed of sound measurements with an Anton Paar DSA-5000 digital vibrating tube densimeter and sound velocity meter, with a precision of $\pm 10^{-5}$ g cm^{-3}, ± 0.1 m·s^{-1}. No data were found in the literature for this binary mixture.

Results and Discussion

Experimental VLE data are determined for the binary systems HFE7500 + di-isopropyl ether at the constant pressures of 50 and 101.325 kPa. Thermodynamical consistency of the experimental VLE data reported in this work has been checked out by means of different tests, the point-to-point Fredeslund's and Wisniak's consistency tests and the Wisniak's L–W test for the binary system.

Conclusions

Results shown that $G^E>0$ for the full composition range. Several equations and models have been used to correlate experimental VLE data: Redlich-Kister, Margules, Wilson, Van Laar, NRTL and UNIQUAC. In relation with the equations, better correlation results have been obtained for Wilson than for Margules and Van Laar equations. Concerning models, UNIQUAC model presents better results than NRTL model.

References

[1] W. Tsai, J. Hazard. Mater. A 2005, 119, 69–78.
[2] 3M™ Novec™ Engineered Fluids,
http://solutions.3m.com/wps/portal/3M/en_US/3MNovec/Home (last visit 03/12/2014)

Acknowledgments
N. Muñoz acknowledges support for this research to the University of Burgos, for the funding of her doctoral grant. This work is part of the Doctoral Thesis of N. Muñoz.

Density and speed of sound for the binary system HFE-7500 + di-isopropyl ether.

Natalia Muñoz-Rujas[1], Adil Srhiyer[1], Eduardo Montero[1], Fernando Aguilar[1]

[1] Departamento de Ingeniería Electromecánica, Universidad de Burgos, Avda. Cantabria s/n E-09006, Burgos, Spain

Hydrofluoroether fluids (HFEs) are being used as third generation alternatives to replace CFCs (chlorofluoro-carbons), HCFCs (hydrochlorofluorocarbons) and PFCs (perflurocarbons) because of their nearly zero Ozone Depletion, relatively low Global Warming Potential and short atmospheric lifetimes[1]. A variety of HFEs have been synthesized, their performance and environmental properties and hence their utility can vary widely[2].

2-trifluoromethyl-3-ethoxydodecafluorohexane, known as HFE-7500, is a nonflammable fluid with very low global warming potential for use in heat transfer applications. In addition, it may be industrially used to cool high voltage transformers and power electronics, to cool semiconductor thermal shock and test equipment and as an alternative to commonly used fluids in pharmaceutical and chemical manufacturing processes, such as freeze drying and reactor cooling. To some extent, it can be used in mixture with other solvents.

Experimental densities and speeds of sound for the binary system HFE-7500 + di-isopropyl ether have been measured at 298.15 K and at atmospheric pressure. The excess molar volumes and the deviations in isentropic compressibility upon mixing have been correlated by the Redlich-Kister polynomial. No data were found in the literature for this binary mixture.

N. Muñoz acknowledges support for this research to the University of Burgos, for the funding of her doctoral grant.

[1] W. Tsai, J. Hazard. Mater. A, 119, (2005), 69–78.
[2] 3M™ Novec™ Engineered Fluids.

High-Pressure Viscosity Measurements for the Hydrofluoroether Fluid HFE-7500

Natalia Muñoz-Rujas[1,2*], Jean-Patrick Bazile[1], Fernando Aguilar[2], Guillaume Galliero[1], Eduardo Montero[2] and Christian Boned[1]

[1]*Laboratoire des Fluides Complexes et leurs Réservoirs, CNRS-TOTAL, UMR 5051, Université de Pau, BP 1155, 64013 Pau Cedex, France*

[2]*Departamento de Ingeniería Electromecánica, Escuela Politécnica Superior, Universidad de Burgos, E-09006 Burgos, Spain*

**Corresponding/Presenting author: nmrujas@ubu.es*

Scientific topic: Thermodynamics and Transport Properties

Keywords: Hydrofluoroethers, Viscosity, Density.

Abstract

Hydrofluoroether fluids (HFEs) have low GWP, zero ozone depletion potential (ODP) and short atmospheric lifetimes. HFEs are also non-flammable fluids, have very low overall toxicity [1] and have any significant environmental hazard [2]. Since HFEs are being introduced at the end of the 20th century, they have been considered as a good alternative to the CFCs, HCFCs, PFCs and PFPEs replacement. Their properties and utilities can vary widely so some of them are desirable for refrigerant applications, others can act as working fluids in Organic Rankine Cycles (ORC), high precision for electronic components cleaning, light-duty cleaning and heat transfer fluids, etc.

Hydrofluoroether fluid HFE-7500 shares many of the properties of the PFCs and PFPEs, being a viable option for replace them in a wide range of applications. Their physical properties and boiling point make it ideal to use it in heat transfer applications; semiconductor manufacturing processes, to cool semiconductor thermal shock, in electronics cooling, and as an alternative to commonly used fluids in chemical and pharmaceutical manufacturing processes.

In this work, high pressure viscosity measurements for the fluid HFE-7500 were carried out in the ranges (0.1 – 100) MPa for the pressure and (293.15 – 353.15) K for the temperature. The determination of the dynamic viscosity has been carried out with the supplementary high pressure density measurements in the range (0.1 – 140) MPa for pressure and (293.15 – 393.15) K for the temperature in order to calculate the high pressure dynamic viscosity data.

References

[1] 3M™ Novec™ Engineered Fluids, http://solutions.3m.com/wps/portal/3M/en_US/3M Novec/Home. (last visit: 09/18/15)

[2] M. Goto, Y. Inoue, M. Kawasaki, A. G. Guschin, L. T. Molina, M. J. Molina, T. J. Wallington, M. D. Hurley "Atmospheric Chemistry of HFE-7500 [n-C3F7CF(OC2H5)CF(CF3)2]: Reaction with OH Radicals and Cl Atoms and Atmospheric Fate of n-C3F7CF(OCHO·)CF(CF3)2 and n-C3F7CF(OCH2CH2O·)CF(CF3)2 Radicals" Environ. Sci. Technol. 2002, 36: 2395-2402.

Acknowledgements

N. Muñoz-Rujas acknowledges support for this research to the University of Burgos, for the funding of her doctoral grant. This work is part of the doctoral thesis of N. Muñoz-Rujas.

Speed of Sound and Derivative Properties of Hydrofluoroether Fluid HFE-7500 under High Pressure

Natalia Muñoz-Rujas[1,2], Jean Patrick-Bazile[1], Fernando Aguilar[2], Guillaume Galliero[1], Eduardo Montero[2] and Jean-Luc Daridon[1]

[1] Laboratoire des Fluides Complexes et leurs Réservoirs, CNRS-TOTAL, UMR 5150, Université de Pau, BP 1155, 64013 Pau Cedex, France.
[2] Departamento de Ingeniería Electromecánica, Escuela Politécnica Superior, Universidad de Burgos, Burgos, E-09006, Spain.
[1*] Tel: +34 947 258 916, E-mail: nmrujas@ubu.es

HFE-7500 is a fluid with low global warming potential (GWP) and zero ozone depletion potential (ODP) that can be used in heat transfer applications and in chemical and pharmaceutical manufacturing processes among others, being a viable option for the replacement of perfluorocarbons (PFCs) and perfluoropolyethers (PFPEs) [1].

The speed of sound at high pressure for the fluid HFE-7500 was measured in the ranges of pressure (0.1 – 100) MPa and from (293.15 to 353.15) K for the temperature. The determination of the derivative properties, that is, the isentropic compressibility and thermal expansivity have also been carried out.

Acknowledgment

N. Muñoz-Rujas acknowledges support for this research to the University of Burgos, for the funding of her doctoral grant, and to the University of Pau for the funding of a five months research period in 2015.

This paper is part of the doctoral thesis of N. Muñoz-Rujas.

References

1. 3M™ Novec™ Engineered Fluids, http://solutions.3m.com/wps/portal/3M/en_US/3MNovec/Home.

Viscosity and Density for the binary mixture HFE-7500 + diisopropyl ether under High Pressure

Natalia Muñoz-Rujas[1,2], Jean Patrick-Bazile[1], Fernando Aguilar[2], Guillaume Galliero[1], Eduardo Montero[2] and Christian Boned[1]

[1] Laboratoire des Fluides Complexes et leurs Réservoirs, CNRS-TOTAL, UMR 5150, Université de Pau, BP 1155, 64013 Pau Cedex, France.
[2] Departamento de Ingeniería Electromecánica, Escuela Politécnica Superior, Universidad de Burgos, Burgos, E-09006, Spain.
[1*] Tel: +34 947 258 916, E-mail: nmrujas@ubu.es

HFE-7500 is considered as a good alternative to the PFCs and PFPEs replacement in a wide range of applications. Their physical properties and boiling point make it ideal to use it in heat transfer applications; semiconductor manufacturing processes, in electronics cooling and in other chemical processes [1].

The viscosity at high pressure for the mixture HFE-7500 + diisopropyl ether was measured in the ranges of pressure (0.1 – 100) MPa and from (293.15 to 353.15) K for the temperature while density was measured in the range (0.1 – 140) MPa for the pressure and (293.15 – 393.15) K for the temperature.

Acknowledgment

N. Muñoz-Rujas acknowledges support for this research to the University of Burgos, for the funding of her doctoral grant, and to the University of Pau for the funding of a five months research period in 2015.

This paper is part of the doctoral thesis of N. Muñoz-Rujas.

References

1. 3M™ Novec™ Engineered Fluids, http://solutions.3m.com/wps/portal/3M/en_US/3MNovec/Home.

DENSITY OF THE BINARY SYSTEM HFE-7100 + 1-PROPANOL AT TEMPERATURES FROM 298.15 K TO 393.15 K AND AT PRESSURES UP TO 70 MPA.

Natalia Muñoz-Rujas[1*], Fernando Aguilar[1], Eduardo A. Montero[1]

[1]Departamento de Ingeniería Electromecánica, Escuela Politécnica Superior, Universidad de Burgos, E-09006, Burgos, Spain
[*]nmrujas@ubu.es

ABSTRACT

HCFCs and HFCs are being widely used for common purposes such as refrigerant fluids, heat transfer media, as precision cleaning fluids or in aerosol applications among others. Although HFCs emerged as an alternative to the CFCs and HCFCs phase out proposal at expense of the Montreal Protocol, in 1987, some of these fluorocarbons show high ozone depletion potentials (ODP), high global warming potentials (GWP) and also large atmospheric lifetimes (ALT). Due to this, many researchers led efforts to search for new fluids with the same properties as CFCs, HCFCs and HFCs but with zero or near zero ODP, low GWP and short atmospheric lifetimes.

Hydrofluoroether fluids (HFEs) were found as an alternative to these fluids since they have similar properties, so they are capable to substitute CFCs, HCFCs and HFCs in a wide array of applications [1]. HFEs have low GWP and short atmospheric lifetimes, properties which are provided by the oxygen atom of the ether in the molecule. HFEs also show zero ODP. HFEs are non flammable fluids, and they compatible with most metals and hard polymers [2]. With respect to the toxicity, HFEs briefly exhibit relatively low toxicity from the results of acute toxicity tests [3].

Methyl nonafluorobutyl ether, known as HFE-7100, posess some desirable properties such as high latent heat of vaporization, a high liquid density and low viscosity, properties that make it ideal to be used as CFC, HCFC, and HFC replacement as pure component or in mixture with other compounds such as ethers or alkanols.

Low molecular weight alcohols are acceptable rinsing and cleaning agents however they are flammable, so the addition of fluorinated compounds to the mixture will reduce or eliminate the flammability [4].

The binary mixture HFE-7100 + 1- propanol is a viable option in the replacement of some fluorocarbons. This binary mixture forms an azeotrope at a weight concentration of HFE-7100 of 97.90% that can be considered as a good replacement for HCFC-225ca/cb [5], a mixture of isomers primarily used in vapor degreasing and in aerosol applications.

Density is the most important physical property, and its determination as a function of temperature and pressure gives other valuable properties such as isothermal compressibility and isobaric expansion. With the molar mass, excess volumes can also be determined. In this work, densities of six mole fractions, x_1= (0.1502, 0.3258, 0.5010, 0.6754, 0.8495 and 0.9184) of the binary mixture HFE-7100 + 1-propanol have been measured within the temperature range from 298.15 to 393.15 K and in the pressure range from 0.1 to 70 MPa by using an Anton Paar U-tube densitometer with an uncertainty of $\pm$ 0.7 kg·m^{-3} for the density. The derivative properties, that is, the isothermal compressibility and the isobaric expansion are also reported in the same pressure and temperature ranges.

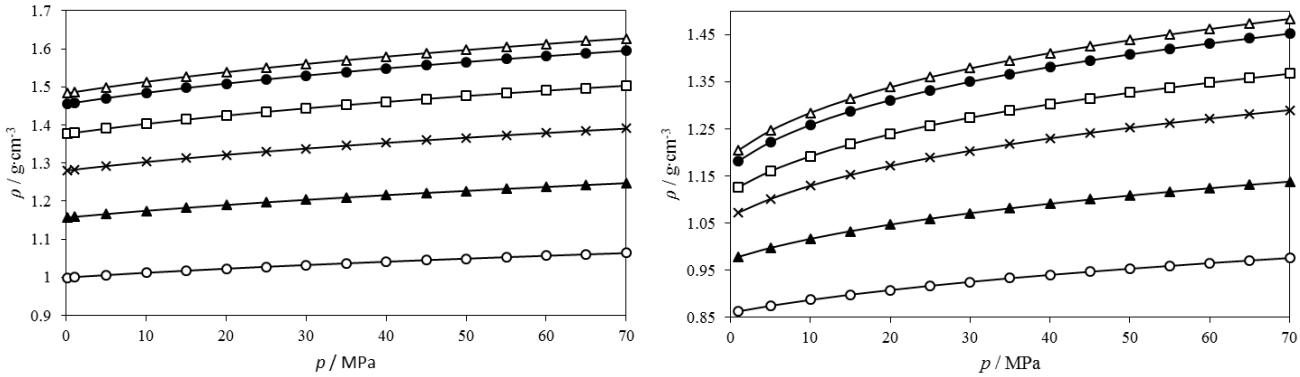

Figure 1: Experimental values of densities, ρ, for different mole fractions of x HFE-7100 + (*1*-x) 1-propanol vs. pressure, p, at (a) 298.15 K and (b) at 393.15 K: ○; x = 0.150, ▲; x = 0.325, x; x = 0.500, □; x = 0.675, ●; x = 0.850, Δ; x = 0.918, (−); Tait correlation.

REFERENCES

[1] 3M™ Novec™ Engineered Fluids. http://solutions.3m.com/wps/portal/3M/en_US/3MNovec/Home.
[2] P. Tuma, S. Paul, L. Tousignant, Earth, 16, 2010.
[3] W-T. Tsai, Environmental Risk Assessment of Hydrofluoroethers (HFEs), *J. Hazardous Matter.*, vol. 119, pp. 69-8, 2005.
[4] K. Doyel, and M. Bixenman, Cleaning Compositions Containing Dichloroethylene and Six Carbon Alkoxy Substituted Perfluoro Compounds, Patent US 7288511 B2, 2007.
[5] J. B. Durkee II, Cleaning with Solvents: Science and Technology, chapter 8, Elsevier B. V., Oxford, 2014.

JUNIO 2017

Density and speed of sound at 298.15 K and at atmospheric pressure for the binary mixture HFE-7200 + 2-propanol

Natalia Muñoz-Rujas[1], Fernando Aguilar[1], Eduardo A. Montero[1]

[1]Departamento de Ingeniería Electromecánica, Escuela Politécnica Superior, Universidad de Burgos, E-09006, Burgos, Spain. Phone: 34-947258916, e-mail: nmrujas@ubu.es ; faguilar@ubu.es ; emontero@ubu.es

1. Introduction

Many efforts have been carried out in the protection of the planet from the harmful effects of CFCs, HCFCs, and PFCs due to its impact in the ozone layer and in the global warming. New fluids with similar properties but with much lower ozone depletion potentials (ODP), global warming potentials (GWP) and with shorter atmospheric lifetimes (ALT) were investigated as potential alternatives to the replacement of the commonly used fluorocarbons.

Hydrofluoroether fluids (HFEs) are being studied since the decade of the ‘90s as third generation alternatives to replace CFCs, HCFCs and PFCs because of their nearly zero ODP, relatively low GWP and short atmospheric lifetimes [1]. HFE-7200 shares many of the properties of CFCs and HCFCs, which make it ideal for use in vapor degreasing and cold cleaning applications among others, being a substance with zero ODP, very low GWP, and with an ALT less than a year [2]. Due to its physico-chemical properties, the binary mixture HFE-7200 + 2-propanol is a viable option to substitute HCFC-225ca/cb in solvent cleaning operations [3].

2. Materials and method

Hydrofluoroether fluid HFE-7200, also known as ethoxy-nonafluorobutane, consists of two inseparable isomers (CAS No.: 163702-06-5 and CAS No.: 163702-05-4). It was obtained from the 3M company with a stated mass fraction purity greater than 0.995. 2- propanol (CAS No.: 67-63-0) was obtained from Sigma-Aldrich with 0.998 mole fraction purity.

The density and the speed of sound at 298.15 K and at atmospheric pressure of binary mixtures x HFE-7200 + (1-x) 2-propanol were measured with an Anton Paar DSA 5000M densimeter and sound analyzer with a precision of ±5·10-5 g·cm3 and ±0.5 m/s. Before each series of measurements, these instruments were calibrated with Millipore quality water previously degassed and with ambient air. The accuracy in the calculation of excess volumes, and deviation of isentropic compressibilities were estimated as better than 10-2 cm3·mol-1, and 2 TPa-1, respectively. The mixtures were prepared by weighing amounts of the pure liquids by syringing into stoppered vials to prevent evaporation and reducing possible errors in mole fraction calculations. A Mettler Toledo MS-204S balance was used with a precision of ±1·10-4 g, covering the whole composition range of the mixture.

3. Results and discussion

The experimental values of density and speed of sound for the binary mixture x HFE-7200 + (1-x) 2-propanol for 21 molar compositions are shown in Figure 1 together with the isentropic compressibility, which was calculated by means of the equation of Laplace, kS = ρ-1·u-2. All

the data were fitted to a polynomial equation. The excess molar volumes were also calculated and fitted to a Redlich-Kister type equation. These data can be seen in Figure 2. The positive deviation observed for the excess molar volumes show that the high size of the HFE molecule leads to a less effective packing effect than normal for an ether + alkanol mixture.

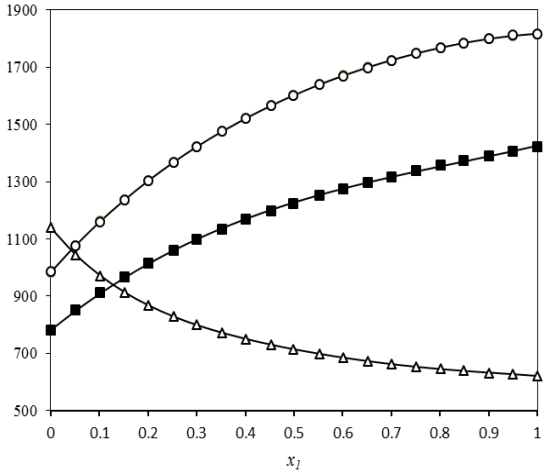

Figure 1. Density ρ, speed of sound u, and isentropic compressibility k_S, vs. mole fraction at 298.15 K and at atmospheric pressure for the binary system x HFE-7200 + (*1*-x) 2-propanol. ■; density, ρ (kg/m^{-3}), Δ; speed of sound, u (m/s) ○; isentropic compressibility, k_S (TPa^{-1}). The solid line represents the values obtained by using the polynomial equation.

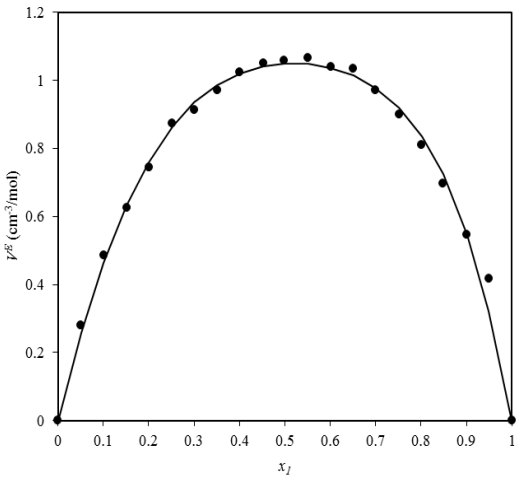

Figure 2. Excess molar volumes for the mixture x HFE-7200 + (*1*-x) 2-propanol at 298.15 K and at atmospheric pressure. ●; experimental values. The solid line represents the correlation to the Redlich-Kister equation.

4. Conclusions

Density and speed of sound of binary mixtures x HFE-7200 + (1-x) 2-propanol have been measured at 298.15 K and at atmospheric pressure. Isentropic compressibilities and excess molar volumes were also determined. The experimental data were fitted to a polynomial equation and to a Redlich-Kister equation respectively showing a good agreement.

5. Acknowledgements

This paper is part of the Doctoral Thesis of N. Muñoz-Rujas.

N. Muñoz-Rujas acknowledges financial support for this research from the University of Burgos (Pre-Doctoral Grants 2014).

6. References

[1] W. Tsai, J. Hazard. Mater. 119 (2005) 69-78.

[2] 3M™ Novec™ Engineered Fluids. http://solutions.3m.com/wps/portal/3M/en_US/3M Novec/Home.

[3] J.B. Durkee II, Cleaning with solvents : science and technology, 1st ed. Elsevier B.V. Oxford, 2014.

SPEED OF SOUND OF HYDROFLUOROETHER FLUID HFE-7500 + DIPE UNDER HIGH PRESSURE

N. Muñoz-Rujas[1,2], J. P. Bazile[1], F. Aguilar[2], G. Galliero[1], E. A. Montero[2], J. L. Daridon[1]
[1] *Laboratoire des Fluides Complexes et leurs Réservoirs CNRS-TOTAL, Université de Pau, France*
[2] *Department of Electromechanical Engineering, University of Burgos, Spain*
e-mail: emontero@ubu.es

Hydrofluoroether fluids (HFEs) are a type of fluorinated ethers investigated since the decade of the '90s as substitutes of CFCs, HCFCs and PFCs among other fluorocarbons, due to their desirable environmental properties, that is, zero ozone depletion potential, low global warming potential and short atmospheric lifetimes, and due to their thermophysical properties. 2-trifluoromethyl-3-ethoxydodecafluorohexane, known as HFE-7500, is proposed to be a good alternative to PFCs and PFPEs replacement because it is a dielectric fluid with low viscosity, high liquid density and low surface tension.

Diisopropyl ether (DIPE) is used in a wide variety of applications, for example it is used as solvent or as cleaning agent. The addition of the fluorinated compound HFE-7500 implies a reduction on the flammability of Diisopropyl ether, making this binary mixture a good option to be used in high precision cleaning, or as solvent as oil-based solutions dissolve in it.

In this work the physical properties speed of sound and density of the binary mixture x HFE-7500 + (1-x) Diisopropyl ether have been determined experimentally at pressures up to 100 MPa and at temperatures from (293.15 to 353.15) K for the speed of sound, and at pressures up to 140 MPa and in the temperature range (293.15 to 393.15) for the density at five mole fractions, x = (0.250, 0.375, 0.500, 0.625 and 0.750). The derivative properties isentropic compressibility, isothermal compressibility and isobaric expansion were also determined from speed of sound measurements.

N. Muñoz-Rujas acknowledges support for this research to the University of Burgos, for the funding of her doctoral grant, and to the University of Pau for the funding of a five months research stay in 2015. This paper is part of the doctoral thesis of N. Muñoz-Rujas.

Anexo III

Contrato Fundación General Universidad de Burgos

UNIVERSIDAD DE BURGOS

Referencia: PUE14- 215

PROGRAMA DE COOPERACIÓN EDUCATIVA ENTRE LA UNIVERSIDAD DE BURGOS Y FUNDACION GENERAL UNIVERSIDAD DE BURGOS

D. Alfonso Murillo Villar, Rector Magnífico de la Universidad de Burgos y D.Luis Javier Fierro Lopez, Gerente de Fundacion General Universidad De Burgos, suscriben el presente Convenio de Cooperación Educativa al amparo de la legislación vigente.

1. Alumna seleccionada por la entidad colaboradora: **NATALIA MUÑOZ RUJAS**
   Titulación: **Doctorado Tecnologías Industriales** DNI: **70249989P**
   Modalidad de práctica: **Extracurricular** Teléfono: **677766873**
   E-mail: **misiano_misiano@hotmail.com**

2. Tutor empresarial: **MONICA RAMOS PEREZ** Teléfono: **947258055**
   E-mail: **mperez@ubu.es**

3. Tutora Académica: **EDUARDO MONTERO** Teléfono: **630025406**
   E-mail: **emontero@ubu.es**

4. Objetivos del programa: Complementos de su formación mediante prácticas en la empresa.
   Proyecto Formativo. Breve descripción de las tareas a realizar por la alumna: **INVESTIGACIÓN EN TERMODINÁMICA**

5. Lugar dónde se desarrollará: **FUNDACION GENERAL UNIVERSIDAD DE BURGOS**
   DEPARTAMENTO INGENIERÍA ELECTROMECÁNICA
   CALLE HOSPITAL DEL REY S/N
   9001 BURGOS-BURGOS

6. Duración del programa:
   La duración máxima de este programa no podrá exceder el 50% del tiempo integro que constituye un curso académico (1 septiembre de 2013 al 31 de agosto de 2014)

   Fechas de realización de las prácticas: **07/01/2014 AL 06/07/2014**

UNIVERSIDAD DE BURGOS

Horario: **8 HORAS HORARIO FLEXIBLE**

Indicar si se trata de una renovación: Si ☐ No ☒

7. Bolsa de ayuda: En concepto de bolsa de ayuda al estudio, **FUNDACION GENERAL UNIVERSIDAD DE BURGOS** concederá a la alumna participante una ayuda mensual de **700 €**.

8. Seguro: El alumno menor de 28 años pertenece al Régimen de Seguro Escolar, el resto de estudiantes dispone de un seguro de Accidentes durante todo el periodo de prácticas. Con el fin de colaborar en la gestión del Programa, **FUNDACION GENERAL UNIVERSIDAD DE BURGOS** ingresará **36 €** por transferencia bancaria a CaixaBank C.C. 2100/9168/61/2200031866, indicando la referencia del presente convenio.
No se requiere el ingreso cuando sea una renovación en el mismo curso académico.

9. Obligaciones:

9.1. Es obligación de la Alumna:

- Cumplir los horarios y seguir las normas fijadas por la empresa.
- Aplicarse a las tareas que se le encomiendan.
- Mantener contacto con sus tutores en la forma en que éstos establezcan.
- Guardar el secreto profesional durante su estancia en la empresa y después de finalizado el periodo de prácticas.
- En el plazo de un mes, concluidas las prácticas, la alumna debe presentar a la tutora académica un informe del trabajo que ha realizado.

9.2. Es obligación del Tutor Empresarial:

- Fijar el plan de trabajo de la alumna.
- Orientarle y ayudarle en sus dudas y dificultades.
- Evaluar la actividad de la alumna en la empresa.

UNIVERSIDAD DE BURGOS

9.3. Es obligación de la Tutora Académica:

- Orientar y ayudar en sus dudas y dificultades a la alumna.
- Evaluar la estancia de la alumna en la empresa.

10. La suscripción por parte de **FUNDACION GENERAL UNIVERSIDAD DE BURGOS** del presente Programa de Cooperación no supondrá la adquisición de más compromiso que los estipulados en el mismo, y en ningún caso se derivarán obligaciones propias de un contrato laboral ya que la relación que se establezca entre la Alumna y la empresa no tendrá ese carácter.

11. En cualquier momento, si concurrieran causas que así lo aconsejasen, se podrá rescindir el convenio por iniciativa de cualquiera de las dos partes.

Burgos, a 19 de diciembre de 2013

POR LA UNIVERSIDAD DE BURGOS

D. Alfonso Murillo Villar

RECTOR

POR FUNDACION GENERAL UNIVERSIDAD DE BURGOS

Fundación Universidad de Burgos

D. Luis Javier Fierro Lopez

GERENTE

ALUMNA UNIVERSIDAD DE BURGOS

Dª. Natalia Muñoz Rujas

Anexo IV

Contrato Predoctoral

MINISTERIO DE EMPLEO
Y SEGURIDAD SOCIAL

CONTRATO PREDOCTORAL (PERSONAL INVESTIGADOR PREDOCTORAL EN FORMACIÓN)

Código de contrato

. Tiempo Completo | 4 | 0 | 1 |

POR LA EMPRESA

Código de Cuenta Cotización a la Seguridad Social	Régimen	Cód. prov.	Número	Dig. contr.
Q 0968272 E	01	11	09 1005265	59

Don/ª	D.N.I.	En concepto de (1)
ALFONSO MURILLO VILLAR	13098904J	RECTOR

Nombre o Razón Social	CIF/NIF	Actividad económica
UNIVERSIDAD DE BURGOS	Q 0968272 E	ENSENANZA

Domicilio Social	Localidad	C. Postal	Nº total de trab. en plantilla
Plaza de la Infanta Doña Elena s/n	BURGOS	09001	

Domicilio del centro de trabajo	Localidad	C. Postal	Nº trab. Centro de trabajo

EL TRABAJADOR/A

Don/ª	Nº afiliación S.S.	Nivel de estudios Terminados Código
NATALIA MUÑOZ RUJAS		MÁSTER

Fecha de nacimiento	D.N.I. (PASAPORTE)	Domicilio	Nacionalidad
22 de julio de 1983	70249989P	C/ Jerez, Nº 12- 1ºB (09006) BURGOS	ESPAÑOLA

DECLARAN

Que el empleador es Universidad Pública, perceptora de fondos cuyo destino incluya la contratación de personal investigador o para el desarrollo de los programas propios de I+D+I.

Que el trabajador está en posesión de: Título de Licenciado, ingeniero, arquitecto, graduado universitario con grado de al menos 300 créditos o master universitario o equivalente y hayan sido admitidos a un programa de doctorado. (1)

Que reúnen los requisitos exigidos para la celebración del presente contrato y, en consecuencia acuerdan formalizarlo con arreglo a las siguientes:

CLÁUSULAS

Primera: La persona contratada prestará sus servicios como (2) **INVESTIGADOR** contratado, al haber sido seleccionado de acuerdo con las Bases Reguladoras y Convocatoria de Ayudas para financiar contratos predoctorales de la Universidad de Burgos (Tablón Oficial de la Universidad de Burgos de 24 de julio de 2013) y Resolución Rectoral de 12 de febrero de 2014 (Registro de Salida Registro General 201400000493) por la que se estima recurso de reposición concediendo a la interesada una ayuda de la convocatoria mencionada. Incluido en el grupo profesional/categoría/nivel profesional (3) PERSONAL INVESTIGADOR (00074).

Segunda: La jornada de trabajo será:

☒ **A tiempo completo**: la jornada de trabajo será de 37 horas y 30 minutos semanales, prestadas de acuerdo con el régimen de horarios, permisos y licencias establecidos para el resto de los trabajadores del Centro de Trabajo.

Tercera: La duración del presente contrato se extenderá desde el **7 de marzo de 2014** hasta el **6 de marzo de 2015,** ver cláusula adicional 3ª.
Se establece un periodo de prueba de (4) SEIS MESES, respetándose lo establecido en el artículo 14 del Estatuto de los Trabajadores.

Cuarta: El trabajador percibirá una retribución bruta anual de 16.630 € distribuidos en 14 mensualidades. Esta cantidad podrá ser actualizada en posteriores resoluciones. Los costes laborales serán imputados inicialmente a la aplicación presupuestaria 12PR00-461AA-691.01. Las retribuciones íntegras devengadas por el investigador quedarán sujetas a las deducciones y retenciones que legalmente procedan en cada momento, de acuerdo con las disposiciones de aplicación en materia de Impuesto sobre la Renta de las Personas Físicas y cotización al Régimen General de la Seguridad Social.

1) Deberá acompañar el escrito de admisión al programa de doctorado expedido por la unidad responsable de dicho programa o por la escuela de doctorado o postgrado en su caso.
2) Indicar la profesión
3) Señalar el grupo profesional y la categoría o nivel profesional que corresponda, según el sistema de clasificación profesional vigente en la empresa.
4) Respetándose lo establecido en el artículo 14.1 del Texto Refundidos de la Ley del Estatuto de los Trabajadores, aprobado por el Real Decreto Legislativo 1/1995, de 24 de marzo.

Quinta: Las vacaciones anuales serán de (5) veintidós días hábiles de vacaciones por cada año completo de servicios o la parte proporcional que corresponda por el tiempo de servicios prestado.

Sexta: El contrato de trabajo se celebra para la realización de tareas de investigación en el ámbito de un proyecto específico y novedoso (6) **"Investigación sobre propiedades de nuevos fluidos industriales de bajo impacto ambiental como sustitutivos de gases fluorados para reducción del cambio climático"**.

Para el desarrollo de la actividad investigadora se estará a lo estipulado en las bases de la convocatoria por la que se seleccionó al trabajador/a, respetando en todo momento las normas de funcionamiento del centro y departamento al que se adscribe. Adscribiéndose a estos efectos al **Departamento de INGENIERÍA ELECTROMECÁNICA, Área de Conocimiento de MÁQUINAS Y MOTORES TÉRMICOS, ESCUELA POLITÉCNICA SUPERIOR.**

Séptima: Que el investigador conoce las obligaciones que se derivan de la normativa de incompatibilidades establecida en la Ley 53/1984, de 26 de diciembre y Real Decreto 598/1985, de 30 de abril, y no se halla incurso en ninguna de las incompatibilidades que en dicha normativa se contemplan. Que tampoco ha sido separado del servicio mediante expediente disciplinario de ninguna de las Administraciones Públicas. El presente contrato será incompatible con el disfrute de cualquier otro contrato laboral.

Dadas las características de la relación de empleo y del alcance de las actividades, programas y proyectos del Organismo, el investigador se compromete expresamente a realizar los desplazamientos necesarios para el desarrollo de los mismos o convenientes para la experiencia científica del investigador, según criterio de la Dirección del proyecto, con derecho a percibir las correspondientes indemnizaciones por razón del servicio.

Los derechos de propiedad intelectual e industrial que le correspondan o pudieran corresponderle por el trabajo para el que es contratado se regirán por lo establecido en la Resolución de 29 de marzo de 2012, de la Secretaría General de la Universidad de Burgos, por la que se ordena la publicación de la Normativa sobre Propiedad Industrial e Intelectual de la Universidad de Burgos (B.O.C. y L. de 12 de abril de 2012).

Octava: Este contrato dará derecho a una reducción del 30% de la cuota empresarial por contingencias comunes durante la duración del contrato.

Novena: A la finalización del contrato no se recibirá indemnización por tratarse de un contrato en prácticas.

Décima: En lo no previsto en este contrato se estará a la legislación vigente que resulte de aplicación y, particularmente, por los artículos 15 del Estatuto de los Trabajadores, por la Ley 14/2011 de 1 de junio, artículo 21 y Real Decreto 2.720/1998, de 18 de diciembre (BOE de 8 de enero) por el que se desarrolla el citado art. 15 del Estatuto de los Trabajadores. De acuerdo con lo establecido en los artículos 4.2 y 11 del Convenio Colectivo del Personal Docente e Investigador de las Universidades de Castilla y León, no le será de aplicación el sistema selectivo, carrera profesional, jornada laboral, régimen de vacaciones y retribuciones establecidas en el mismo. Los Estatutos de la Universidad de Burgos, aprobados mediante acuerdo 262/03 de 26 de diciembre de la Junta de Castilla y León, por el que se aprueban los Estatutos de la Universidad de Burgos (B.O.C. y L. 251 de 29 de diciembre de 2003).

Undécima: El contenido del presente contrato se comunicará a la Oficina de Empleo de BURGOS en el plazo de los 10 días siguientes a su concertación.(7)

Duodécima: Ambas partes se comprometen a comunicar el fin de la relación laboral a los Servicios Públicos de Empleo cuando ésta se produzca, de conformidad con lo establecido en el Art. 42.3 de la Ley 51/1980, de 8 de octubre, Básica de Empleo.

CLAUSULAS ADICIONALES

1ª. Este contrato está sometido a la condición suspensiva de existencia de crédito adecuado y suficiente.

2ª. Se consideran cláusulas adicionales al presente contrato lo dispuesto en la convocatoria indicada en la cláusula primera "Bases Reguladoras y Convocatoria de ayudas para financiar contratos predoctorales de la Universidad de Burgos".

3ª. El presente contrato se prorrogará anualmente, previo informe favorable de la Comisión Académica del Programa de Doctorado, hasta un máximo de tres años, no pudiendo exceder del **6 de marzo de 2017**. La obtención del título de Doctor conllevará la finalización del contrato según lo establecido en la convocatoria.

En Burgos, a 6 de marzo de 2014

El/la trabajador/a,

Firmado: NATALIA MUÑOZ RUJAS

El/la representante de la empresa,

Firmado: ALFONSO MURILLO VILLAR

5) Mínimo: 30 días naturales.
6) Identifíquese claramente el proyecto específico de investigación.
7) PROTECCIÓN DE DATOS- Los datos consignados en el presente modelo tendrán la protección derivada de Ley Orgánica 15/1999, de 13 de diciembre (BOE de 14 de diciembre).

UNIVERSIDAD DE BURGOS

C.I.F.: Q-0968272-E

MODELO 5R | **Y**

ANEXO AL CONTRATO PREDOCTORAL

TIPO DE RELACIÓN DE SERVICIO: PERSONAL LABORAL DOCENTE O INVESTIGADOR DE UNIVERSIDADES

DE UNA PARTE EL SR. RECTOR MAGFCO. DE LA UNIVERSIDAD DE BURGOS Y DE OTRA LA INTERESADA, CUYOS DATOS FIGURAN A CONTINUACIÓN, AMBOS CON PLENA CAPACIDAD PARA CELEBRAR EL PRESENTE CONTRATO, ACUERDAN LA CONTRATACIÓN DE LOS SERVICIOS DE ESTA ÚLTIMA EN LA FUNCIÓN QUE SE INDICA, DE CONFORMIDAD CON LA NORMATIVA VIGENTE Y LAS CLÁUSULAS GENERALES Y PARTICULARES QUE SE ESPECIFICAN EN ESTE CONTRATO.

Fecha: 6 de Marzo de 2014
POR LA UNIVERSIDAD

Fdo.: Alfonso Murillo Villar

EL/LA CONTRATADO/A

Fdo.: NATALIA MUÑOZ RUJAS

DATOS PERSONALES

N.I.P.	D.N.I. ☒ PASAPORTE ☐ N.I.E ☐ OTRO ☐
70249989	70249989P

PRIMER APELLIDO	SEGUNDO APELLIDO	NOMBRE
MUÑOZ	RUJAS	NATALIA

SEXO	PAÍS NACIONALIDAD				FECHA DE NACIMIENTO		
					DÍA	MES	AÑO
HOMBRE ☐ MUJER ☒	España	7	2	4	22	07	1983

Lugar de nacimiento PROVINCIA O EXTRANJERO			PAÍS			Localidad PAÍS O LOCALIDAD		
Segovia	4	0	España	7	2	4	SEGOVIA	0	0	1

DATOS DE LA RELACIÓN DE SERVICIOS

FECHA DE INICIO DEL CONTRATO			FECHA FIN DEL CONTRATO		
DÍA	MES	AÑO	DÍA	MES	AÑO
07	03	2014	06	03	2015

CONVENIO				
Personal fuera de convenio	0	S	C	0

FIGURA DOCENTE / CATEGORÍA					
PERSONAL CON CONTRATO PREDOCTORAL	0	1	1	7	0

TÍTULO ACADÉMICO APORTADO					LEGISLACIÓN APLICABLE
Máster en Ingeniería Térmica y de Fluidos	1	0	7	3	Ley 14/2011 de 1 de junio

DATOS DEL PUESTO /DESTINO

UNIVERSIDAD					
Universidad de Burgos	1	7	6	6	

ÁREA DE CONOCIMIENTO			
MAQUINAS Y MOTORES TERMICOS	5	9	0

DEPARTAMENTO DOCENTE				
INGENIERIA ELECTROMECANICA	V	1	1	7

CENTRO DOCENTE DE DESTINO				
ESCUELA POLITECNICA SUPERIOR	1	V	0	6

DEDICACIÓN			
Tiempo Completo	C	0	1

PROVINCIA DEL CENTRO DOCENTE			LOCALIDAD DEL CENTRO DOCENTE			
Burgos	0	9	Burgos	0	0	1

DATOS ECONÓMICOS

RETRIBUCIÓN MENSUAL
SUELDO BASE: 1.045,00
COMPLEMENTOS:
TOTAL: 1.045,00
RÉGIMEN DE SEGURIDAD SOCIAL: GENERAL
Nº CUENTA DE COTIZACIÓN: 09/100526559

PAGAS EXTRAORDINARIAS
NÚMERO: 2
IMPORTE: 1.045,00
APLICACIÓN PRESUPUESTARIA: 12PR00-461AA-691.01

ACTIVIDADES RETRIBUIDAS EN OTROS ENTES PÚBLICOS O PRIVADOS

Ejerce otras actividades en este u otro Ente Público o privado: Sí ☐ No ☒

MODELO 5R – SEGUNDA HOJA

D.N.I. ☒ PASAPORTE ☐ N.I.E. ☐ OTRO ☐

70249989P

APELLIDOS Y NOMBRE

MUÑOZ RUJAS, NATALIA

FECHA INICIO CONTRATO

DÍA		MES		AÑO			
0	7	0	3	2	0	1	4

CLÁUSULAS GENERALES DEL CONTRATO

PRIMERA.- Este documento es un anexo al contrato de trabajo a efectos de anotación en el Registro Central de Personal.

CLÁUSULAS PARTICULARES Y OBSERVACIONES

En prueba del consentimiento por ambas partes, se extiende el presente contrato en quintuplicado ejemplar.

Fecha: 6 de Marzo de 2014
POR LA UNIVERSIDAD

Fdo.: Alfonso Murillo Villar

EL/LA CONTRATADO/A

Fdo.: NATALIA MUÑOZ RUJAS

HOJA DE SERVICIOS

de Da. NATALIA MUÑOZ RUJAS

CONTRATADA LABORAL con fecha 07 de MARZO de 2014

y con Número de Registro de Personal 7024998957 Y002800121

sujeta al Convenio

C.C. DEL PERSONAL LABORAL DOCENTE E INVESTIGADOR DE LAS UNIVERSIDADES PUBLICAS DE CASTILLA Y LEON

con la siguiente clasificación profesional

categoría / actividad

PERSONAL INVESTIGADOR EN FORMACION

con tipo de relación de servicios PERSONAL LABORAL DOCENTE O INVESTIGADOR DE UNIVERSIDADES DE DURACION DETERMINADA

En su virtud expido la presente Hoja de Servicios que acredita su relación de trabajo con la Universidad.

Firmado en Burgos a 19 JUN. 2014

por

EL VICERRECTOR DE PROFESORADO Y DE PERSONAL DE ADMINISTRACIÓN Y SERVICIOS

P.D.: Alfredo Bol Arreba

LTL *70249989 *07032014

MINISTERIO DE HACIENDA Y ADMINISTRACIONES PÚBLICAS

Según los datos que constan en el nombramiento del/de la titular de la presente Hoja de Servicios, ha sido destinado/a al puesto de trabajo que a continuación se indica, quedando inscrito/a en el Registro Central de Personal

1. DATOS DEL TRABAJADOR/A

NIP: 70249989 **D.N.I./N.I.E./PASAPORTE/OTRO:** **N.R.P.:** 7024998957 Y002800121

APELLIDOS Y NOMBRE: MUÑOZ RUJAS NATALIA

TIPO DE RELACIÓN DE SERVICIOS: PERSONAL LABORAL DOCENTE O INVESTIGADOR DE UNIVERSIDADES DE DURACION DETERM

JORNADA: A TIEMPO COMPLETO

SITUACIÓN LABORAL: SERVICIO ACTIVO

MODALIDAD: OCUPANDO PLAZA O PUESTO

2. DATOS DEL PUESTO DE TRABAJO O PLAZA

UNIVERSIDAD: UNIVERSIDAD DE BURGOS

FACULTAD / CENTRO DOCENTE:

DEPARTAMENTO: INGENIERIA ELECTROMECANICA

ÁREA O ASIGNATURA: MAQUINAS Y MOTORES TERMICOS

DEDICACIÓN: TIEMPO COMPLETO

PROVINCIA: BURGOS **LOCALIDAD:** BURGOS

CONVENIO: C.C. DEL PERSONAL LABORAL DOCENTE E INVESTIGADOR DE LAS UNIVERSIDADES PUBLICAS DE C

GRUPO PROFESIONAL: **AREA FUNCIONAL:**

CATEGORÍA / ACTIVIDAD: PERSONAL INVESTIGADOR EN FORMACION

ESPECIALIDAD:

3. DATOS DEL CONTRATO

FECHA DE CONTRATACION:	07 DE MARZO DE 2014
FECHA FIN DE CONTRATO:	06 DE MARZO DE 2015

Madrid, 6 de junio de 2014

La Subdirectora General de Gestión Instrumental de los Recursos Humanos

Fdo.: Celia Tenés García

En cumplimiento del artículo 5 de la Ley Orgánica 15/1999, sus datos personales serán incorporados en el Registro Central de Personal, que es un registro de actos administrativos regulado por los Reales Decretos 1405/1986 y 2073/1999, cuya finalidad es la inscripción del personal de su ámbito competencial, en el que se anotan preceptivamente los actos que afecten a su vida administrativa y cuyos datos pueden ser cedidos en los términos previstos en su regulación. Su gestión corresponde a la Subdirección General de Gestión Instrumental de los Recursos Humanos, con sede en María de Molina, 50 de Madrid, donde podrá ejercer los derechos de acceso, rectificación, cancelación y oposición en los términos fijados en el artículo 16 del Real Decreto 2073/1999, así como en las Oficinas Delegadas del Registro Central de Personal.

RCM - FNMT

INFORMACIÓN ADMINISTRATIVA

El presente documento corresponde a la hoja de su título administrativo de funcionario de carrera (o su hoja de servicios para el resto del personal) es fiel reflejo del acto administrativo correspondiente firmado por la autoridad competente.

Este documento está realizado con papel tipo moneda y con la marca al agua del escudo nacional, además de ser producto de una ajustada programación y automatización en la emisión del mismo por parte del Registro Central de Personal.

Esta hoja del título debe ser conservada por usted junto con su acreditación inicial y el resto de los impresos, lo que conforma su expediente personal al igual que el que se conserva en el Registro Central de Personal a través del conjunto de las anotaciones preceptivas que realiza.

Con el presente sistema implantado por el Reglamento del Registro Central de Personal de 1986, se pretende ofrecer un mejor servicio a todo el personal de la Administración del Estado, al mismo tiempo que clarificar, homogeneizar y agilizar los procesos administrativos.

La existencia de la información respecto a su expediente en el Registro Central de Personal supone, además de una norma de obligado cumplimiento, una garantía frente a cualquier tipo de incidencia, pérdida o destrucción de información.

Anexo V

Estancia de investigación en la Universidad de Pau (Francia)

Pau, January 5, 2015

LFC-R

Laboratoire des Fluides Complexes
et leurs Réservoirs
TOTAL - CNRS
UMR 5150

Doctor E. MONTERO-GARCIA
University of Burgos
High Polytechnic School
Dpto Ingeniera Electromecanica
Escuela Polytechnica
Avda. Cantabria s/n
09006 BURGOS (Spain)

Dear Doctor Montero

Following your visit at the LFC-R laboratory on Friday 10 october 2014, we would like to confirm you that we agree to receive, Ms Natalia MUNOZ, one of your students, during the period February - June 2015 for an extended stay in the LFC-R laboratory in Pau for 5 months as a doctoral student

During this period of time, Ms MUNOZ will perform measurements on the high-pressure devices on the LFC-R. This will be an efficient way to pursue the collaboration between our two research groups.

I really hope that Ms MUNOZ will have the opportunity to stay in Pau as a doctoral student.

Yours sincerely.

Pr DARIDON Jean-Luc

LABORATOIRE DES FLUIDES COMPLEXES ET LEURS RÉSERVOIRS
LFC-R - UMR 5150
UNIVERSITÉ DE PAU ET DES PAYS DE L'ADOUR
B.P. 1155 - 64013 PAU CEDEX (France)
Tél. 05 59 40 76 93 - Fax 05 59 40 76 95

Pr GALLIERO Guillaume

LABORATOIRE DES FLUIDES COMPLEXES ET LEURS RÉSERVOIRS
LFC-R - UMR 5150
UNIVERSITÉ DE PAU ET DES PAYS DE L'ADOUR
B.P. 1155 - 64013 PAU CEDEX (France)
Tél. 05 59 40 76 93 - Fax 05 59 40 76 95

Adresse : BP 1155 64013 PAU Cedex (France)
Tél. : 05 59 40 76 93
Fax : 05 59 40 76 95

9 July 2015

Prof. Guillaume GALLIERO
Laboratoire des Fluides Complexes et leurs Réservoirs
UMR 5150 TOTAL-CNRS-UPPA
Université de Pau et des Pays de l'Adour, FRANCE
Tel : +33 5 59 40 7704
email : guillaume.galliero@univ-pau.fr

Certificate of research stay in Pau University: Ms. Natalia Mũnoz Rujas

From the 1st of February 2015 to the 30th of June 2015
on
"Measurements of HFE thermophysical properties under high pressures"

To whom it concerns,

I, hereby, confirm that Ms. Natalia Mũnoz Rujas stayed in our research lab (LFC-R) in the University of Pau (France) from the beginning of February 2015 to the end of June 2015.

During her research stay in Pau she has performed numerous measurements of thermophysical properties of HydroFluoEthers under high pressures conditions.

If you need further information feel free to contact me.

Yours sincerely,

Prof. G. GALLIERO
University of Pau, France

Anexo VI

Formación impartida en la École Nationale des Sciences Appliquées d'El Jadida (Marruecos)

ENSA
École Nationale des Sciences Appliquées d'El Jadida

UNIVERSITÉ CHOUAIB DOUKKALI
ÉCOLE NATIONALE DES SCIENCES
APPLIQUÉES D'EL JADIDA

جامعة شعيب الدكالي
Université Chouaïb Doukkali

El Jadida, 19 Octobre 2016

Attestation

Le Directeur de l'Ecole Nationale des Sciences Appliquées d'El Jadida (ENSA-J) de l'Université de Chouaib Doukkali d'El Jadida, certifie par la presente que Mme. Natalia Muñoz Rujas, professeur du Département d'Ingenierie Electromécanique de l'Université de Burgos, a animé à l'Ecole Nationale des Sciences Appliquées pendant la période de 12 à 19 d'Octobre les formations suivantes:

- Cours sur : **« L'apprentissage par recherche dans l'enseignement de l'ingénierie: application aux travaux de laboratoire de thermodynamique et froid industriel »**, 4 heures, adressé aux étudiants de master et de doctorat, spécialité: génie énergétique.

- Cours sur : **« New refrigerant fluids : characteristics and environmental impact »**, 2 heures, adressé aux étudiants de master et de doctorat, spécialité: génie énergétique.

Par ailleurs, Mme. Natalia Muñoz Rujas a assité à une réunion du travail avec le coordinateur de la filière et des professeurs pour la future coopération scientifique dans le cadre de la convention signée entre l'Université Chouaib Doukkali et l'Université de Burgos.

La présente attestation est délivrée à l'intéressé, sur sa demande, pour servir et valoir ce que de droit.